NEW WATER-SOLUBLE PORPHYRINS FOR OXYGEN SENSING IN PROTEIN-BASED MATERIALS

ALESSANDRO POZZOLI

A thesis submitted in partial fulfilment of the requirements of Liverpool John Moores University for the degree of Doctor of Philosophy

This research programme was carried out in collaboration with University of Hull and University of Nottingham

January 2018

Acknowledgments

"I have no special talent. I am only passionately curious."

Albert Einstein

Table of Contents

Abstract

Oxygen is a vital molecule for life and its precise quantification is pivotal to ensure correct functioning of cells. Instruments able to quantify accurately the oxygen levels are extremely important to understand cells behaviour especially in a three-dimension (3D) environment, where uneven distribution of oxygen can occur leading to zones of low cell viability. Optical oxygen sensing is a relatively recent method to monitor oxygen concentration. This approach exploits the emissive behaviour of a broad family of molecules (organic species and organometallic complexes), for which the luminescence emission is proportional to the quantity of oxygen present in the environment. Unlike methods based on the use of electrodes, optical oxygen sensing allows monitoring of oxygen levels without causing oxygen depletion in the observed sample and can be more easily applied in miniaturised devices.

Metalloporphyrins are widely employed as optical oxygen sensors thanks to their favourable physico-chemical properties. The aim of this project was to synthesise a library of oxygen-sensing porphyrins to monitor variation of oxygen in 3D cell cultures. For this specific application, the chromophore needed to (1) be a platinum or palladium complex to ensure oxygen response, (2) present a suitable functional group to allow conjugation to a support (*e.g.*, a biomacromolecule supporting the 3D cell construct) to avoid leaching and cell uptake, and (3) water-solubility to allow conjugation in aqueous solutions.

We first focused our attention on the synthesis of tetra *meso*-substituted porphyrins bearing a carboxylic group as the conjugatable function on one of the *beta*-positions of the macrocycle. This approach was overall successful in terms of yield and reaction conditions, but the side-chain proved insufficiently stable to allow further manipulation of the species. Attention was then directed to the synthesis of asymmetric porphyrin A_3B, bearing the conjugable group on one of the *meso*-substituted aryl ring. Novel positively and negatively charged water-soluble conjugatable porphyrins were developed during this work, obtained from a single high-value intermediate. The new species presented overall good yields employing relatively mild reaction conditions, *via* a synthetic procedure with gram-scale applicability. In addition, in this work the synthesis of two known water-soluble conjugatable porphyrin was improved and scaled-up. Platinum (II) and palladium (II) insertion in the water-soluble macrocycles was achieved employing a microwave-assisted reaction, which ensured reaction completion in short times. Finally, a high potential purification approach based on ion exchange was developed for cationic and anionic water-soluble derivatives. This method allows obtaining highly pure compounds employing cheap reagents and without the use of expensive purification instruments. The conjugation of the species to the proteins chosen as matrices for hydrogels (silk fibroin and collagen) was performed *via* N-hydroxysuccinimide chemistry.

Oxygen response of the complexes synthesised was tested both in aqueous solution and supported on protein-based hydrogels. Most species showed oxygen-dependent fluorescence and linear Stern-Volmer plot supported on solid support, indicating their suitability to monitor the oxygen levels in a heterogeneous system such as a hydrogel. To the best of our knowledge, this work represents the first example of optical oxygen measurements in silk fibroin hydrogels.

The objectives of this work were: (1) to synthesise and characterise a library of platinum (II) and palladium (II) complexes of water-soluble and conjugatable porphyrins, (2) to test their responsiveness to oxygen both as stand-alone probes and as protein conjugates in hydrogel materials.

INTRODUCTION

Oxygen, together with water, is one of the key molecules for existence of life as we know it. It allows cells to release energy through respiration. Not only the presence of oxygen is fundamental for life, but its concentration also plays a crucial role. The Earth's atmosphere contains 20.8 % of oxygen, and if this value drops below 17 %, asphyxia can occur leading to death. For few months a picture circulated on social media showing a piece of iron covered in rust, with the sentence: "This is rust. It is called oxidation and it is caused by oxygen. We breathe oxygen every day. If it can do that to a metal pipe, imagine what it can do to your lungs and health. Share to help raise awareness about the danger of oxygen".[1]

THIS IS RUST. IT'S CAUSED BY OXYGEN AND CALLED OXIDATION

WE BREATHE OXYGEN EVERYDAY. IF IT CAN DO THIS TO A CHAIN, JUST IMAGINE WHAT CAN IT DO TO YOUR LUNGS. SHARE TO HELP RAISE AWARENESS ABOUT THE DANGER OF OXYGEN.
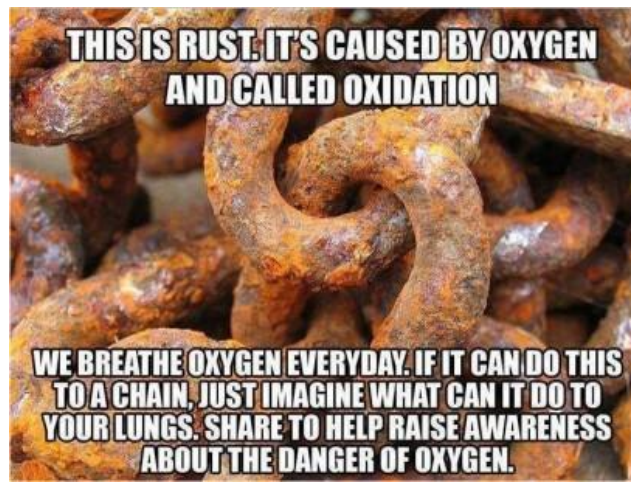
Image credit from reference 1

Obviously, this was merely a pun aimed at making fun of the recent unfortunate spreading of alarmist crusades void of any scientific bases and common sense, but despite the apocalyptic tones of the sentence above, excess of oxygen is indeed dangerous for life. Hyperoxia (a state characterised by excessive supply of oxygen to tissues and organs) is highly toxic to cells and can be exploited for specific therapeutic applications.[2,3]

Monitoring the oxygen levels in cultured cells and artificial tissues is a tool of the trade in biotechnology and in regenerative medicine. To ensure successful growth of a functional tissue from a 3D aggregate of cells, from a spheroid or from cells seeded in a matrix, the supply of oxygen needs to be carefully monitored and kept constant between appropriate values, which are dictated by the cell type and by their metabolic status.[4] Areas in which the oxygen tension is too low (hypoxic zones), which can arise from a non-uniform distribution of the cells within the scaffold, are incompatible with cell growth and differentiation. Similarly, cell proliferation is prevented in areas where the oxygen tension is too high, leading to cell damage through oxidative burst.[4] Ensuring that the supply of oxygen is sufficient and constant throughout a scaffold hosting a 3D cell culture is pivotal for the viability of

the cells.[5] Oxygen, like nutrients, can have a relatively low diffusion rate within cells construct, and if the oxygen consumed by the cells is not replaced efficiently, zones of lower oxygen tension can arise determining a different behaviour to the cells in the core of the construct compared to those close to the surface.[5] Therefore, oxygen tension must be constantly monitored to assess the suitability of a material for cell growth and proliferation, and ultimately if the material could be employed as scaffold in tissue engineering.

Traditional methods for oxygen measurement are based on titration,[6] amperometry,[7] chemiluminescence[8] and thermoluminescence.[9] For many years, Winkler titration has been considered the standard method for oxygen measurement (*Figure 1*). [6,10] This approach involves the addition of two solutions to the oxygen-containing sample, the first one containing manganese (II) sulphate and the second one potassium iodide, sodium hydroxide and sodium azide to suppress the nitrite present, that otherwise would react with the iodide interfering with the analysis. In the presence of oxygen, Mn^{2+} is oxidised to Mn^{3+} causing a precipitate of manganese (III) hydroxide. Sulphuric acid is then added, leading to the oxidation of iodide ions by Mn^{3+} to molecular iodine, later titrated with a thiosulfate solution. The iodine concentration is directly proportional to the amount of oxygen dissolved. Therefore, titrating the iodine allows determining the concentration of oxygen in the sample.

The method, however, presents non-negligible disadvantages. For instance, the result is strictly dependent on how the sample is handled and how well the system is sealed, because any oxygen that is introduced in the sample once the analysis has started will alter the result. In addition, the sample should not contain any oxidising or reducing agent that can interfere with iodine or manganese ions, changing the amount of oxygen detected.
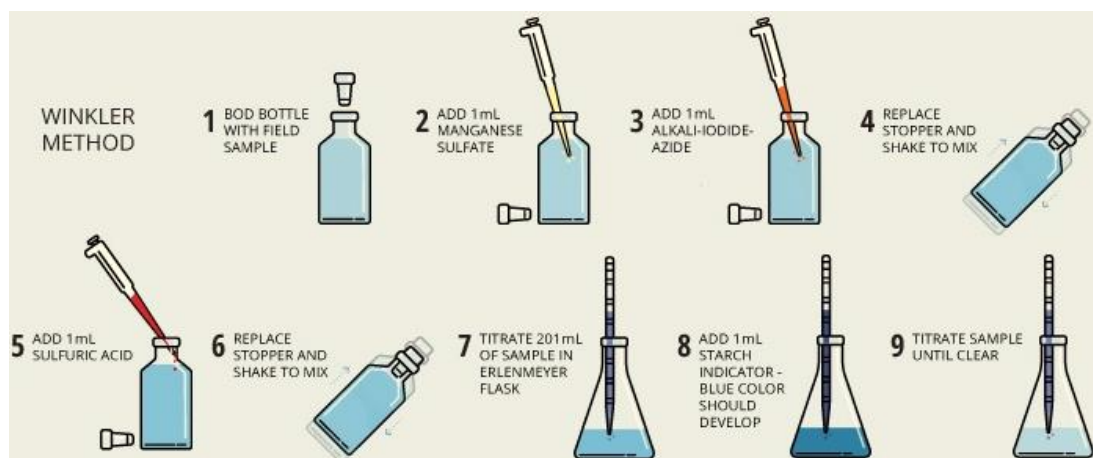
Figure 1: Winkler's titration example [10]

Despite its overall popularity, the Winkler titration has been replaced by approaches based on the use of Clark-type electrodes.[7] The Clark-type electrode employs a platinum cathode, where the oxygen is reduced producing an electric current proportional to the partial pressure of oxygen (*Figure 2*).[11]
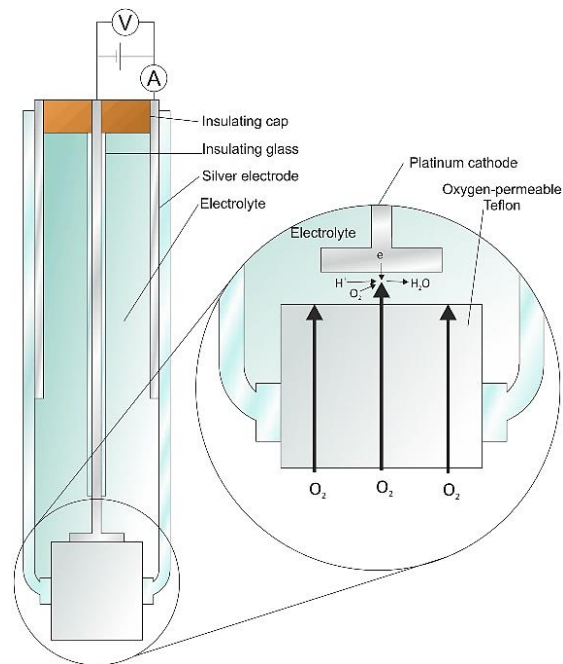
Figure 2: Clark's electrode [11]

Clark electrode is a very robust and popular approach for oxygen detection, but it presents several major disadvantages that limit its applicability to measurement in cells and tissues. Despite considerable efforts invested in the miniaturisation of the electrode, its bulkiness makes it unsuitable for measurements in cells or spheroids. As with most electrodes, the detection of low levels of oxygen in microscale samples can be affected by electrical interferences, but the most serious issue associated to the use of Clark electrode is determined by the fact that the measurement causes oxygen depletion in the sample under observation, thereby potentially affecting its behaviour.[12] Thus, especially for applications in regenerative medicine, new and improved techniques for monitoring oxygen levels are highly desirable.

1.1 Optical Oxygen Sensors

A technique suitable to measure oxygen in microscale biological samples should be non-invasive, highly specific for oxygen to avoid interferences with other analytes and it should show sensitivity and responsiveness in biologically relevant oxygen concentration range. The possibility to report real-time variations in oxygen concentrations and to carry out parallel measurements and multi-sample analysis would be highly desirable features.[13] The approach that better combines all the above features is

called optical oxygen sensing. Optical oxygen sensing (OOS) is a relatively recent oxygen sensing strategy but thanks to its features, it gained fast popularity and it is replacing the traditional polarographic methods. Optical oxygen sensors present faster response to changing concentrations of oxygen, they are less prone to electrical interferences and they only cause a transient limited oxygen consumption in the sample during the analysis.[14] In addition, optical oxygen sensors are relatively cheap, simple to use and can be easily incorporated in miniaturised devices.

1.2 How does an optical oxygen sensor work?

In 1985 a new optical method to monitor oxygen concentration in biological samples was developed, based on the collisional quenching of the excited state of pyrene butyric acid by molecular oxygen.[15] Excited states of molecules are generated following the absorption of electromagnetic radiation (hv, *Figure 3*). In the absence of a quencher, the excited species can follow two main pathways to lose energy and decay back to the ground state: it can dissipate the energy through vibrations (non-radiative decay) or it can emit photons by photoluminescence, which includes fluorescence and phosphorescence. Fluorescence (F) is the radiative transition between electronic states that possess the same electron spin multiplicity ($S_1 \rightarrow S_0$), while phosphoresce (P) is the radiative decay from the triplet excited state to the ground state ($T_1 \rightarrow S_0$), involving intersystem crossing (ISC) as shown in *Figure 3*. Since ISC is a forbidden transition according to the selection rules (triplet-to-singlet),[16] triplet state lifetimes and phosphorescence are typically longer than excited singlet lifetimes and fluorescence (10^{-6} to 10^2 s *vs.* 10^{-9} to 10^{-7} s).
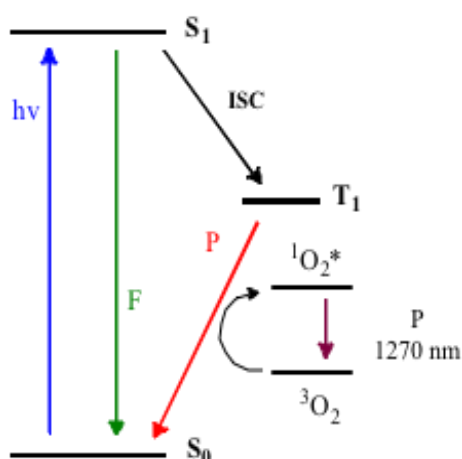
Figure 3: simplified Jablonski diagram showing the quenching of the excited triplet state by energy transfer to oxygen

In the presence of the quencher, the excited state can also be deactivated through collisions with quencher molecules. This additional pathway for decay reduces the luminescence intensity. Molecular oxygen is a very efficient quencher of excited states for most organic molecules. The reason for this is

still matter of intense debate, but it was suggested that paramagnetic oxygen induces ISC in the excited species, reducing the extent of luminescence decay. Collisional quenching can be static or dynamic: in static quenching the excited species associates with the quencher forming a complex that is non-emissive, whereas in dynamic quenching the collision results in an energy or electron transfer between the two species. For the purpose of this work, only dynamic quenching will be discussed.

Dynamic oxygen quenching is described by the Stern-Volmer equation (*Equation 1*), which states that the ratio between luminescence intensity (or triplet lifetime) in the absence and presence of the quencher is proportional to the concentration of the quencher. In *Equation 1*, I_o and I are the luminescence intensities, and τ_0 and τ are the triplet lifetimes in the absence and in the present of oxygen, respectively. $[O_2]$ is the concentration of oxygen, while k_q is the bimolecular quenching rate constant.

$$I_0/I = \tau_0/\tau = 1 + k_q\tau_0[O_2]$$

Equation 1: Stern-Volmer equation

The Stern-Volmer equation is the equation of a straight line, which can be used to determine graphically the constant rate of the quenching ($K_{SV} = k_q\tau_0$). Intensity-based measurement and lifetime-based measurement can be used interchangeably to obtain the Stern-Volmer equation if purely dynamic quenching occurs in the system under observation. When the lifetimes are measured, the luminescence quenching is followed in time-resolved domain,[17] whereas steady-state measurements follow the changes in luminescence intensity.[15,18] Time-resolved measurements are generally more reliable, as they are not influenced by the background fluorescence and less affected by changes in emission intensity caused by non-specific environmental parameters. On the other hand, steady-state measurements can be carried out with simpler and cheaper instrumentation.[19]

Figure 3 shows the quenching of an excited triplet state (T_1) by molecular oxygen leading to energy transfer between the two species, which results in the non-radiative decay of the molecule to the ground state (S_0) and the excitation of ground state oxygen (triplet, $^3O_2$) to its triplet state (singlet oxygen, $^1O_2^*$). It is important to note that molecular oxygen quenches excited singlet states as efficiently as triplet states, but the longer lifetime of triplet state allows the excited species to interact with oxygen present in a larger diffusion range. Crucially, the decay from triplet state is significantly slower than the collisional quenching rate: this makes phosphors with long triplet lifetimes useful oxygen sensors because the efficiency of the process is limited by the diffusion of oxygen in the sample.[12]

1.3 Chromophores for Optical Oxygen Sensing

A striking variety of chromophores for OOS has been developed over the last few decades. In some cases, the chromophores have been conceived to be used in oxygen measurements inside cells,[20] but most commonly they have been associated to different supports to obtain oxygen sensing materials for a wide range of applications (*e.g.*, industrial, technological and biomedical). Considering the relevance to this work, only the latter case will be discussed. Developing oxygen-sensing materials presents an additional challenge, because the performance of the final sensor does not solely depend on the efficiency of quenching of the excited chromophore but also on the characteristics of the matrix (*i.e.*, its permeability to oxygen, interaction with the chromophore etc.).

The most important and essential part of an optical oxygen sensor, however, is the chromophore, as it provides oxygen responsiveness. The many different chromophores employed as oxygen sensors can be divided in two main categories: organic and organometallic species.

1.3.1   Organic optical oxygen sensors

This class of sensors includes species presenting extended conjugated π systems, responsible for their oxygen sensitive properties. These species were employed in the early days of the OOS development, but their use has now declined. The non-negligible disadvantages of organic sensors are the need to use UV light for their excitation and their small Stokes shift. The latter causes a strong background noise and limit their applicability especially in biological samples. In addition, they display low brightness, long decay times and poor solubility in most polymeric matrices. For the above reasons, new and improved molecules presenting better stability and sensing properties have slowly replaced organic species. Two main sub-categories of organic optical oxygen sensors are worth mentioning:

- Polycyclic aromatic hydrocarbons (PAHs): this class of organic dyes was instrumental to develop the very technique of optical oxygen sensing. They were mostly dissolved and incorporated in polymer matrices. The structures of most popular PAHs are shown in *Figure 4*. Pyrene[21] **1** and its anchorable derivate pyrenebutyric acid **2** were successfully employed as probes for oxygen dissolved in bio systems,[22–24] as were perylene,[25] perylene dibutyrate (respectively **3** and **4**),[19] benzoperylene **5**[26] and decacyclene (DCY) **6**.[27–29] **6** has a good photostability, a large Strokes shift and the possibility to be excited with visible light, compared to other UV-excitable PAHs.

- C_{60} and C_{70} fullerenes (**7** and **8** in *Figure 4*) have been employed in OOS. Thanks to their extended conjugated system they display excellent delayed fluorescence, and have been exploited to build sensors capable of detecting oxygen at concentrations of the order of ppb.[30,31] C_{70} fullerene resulted in a more sensitive sensor compared to C_{60}.[32]
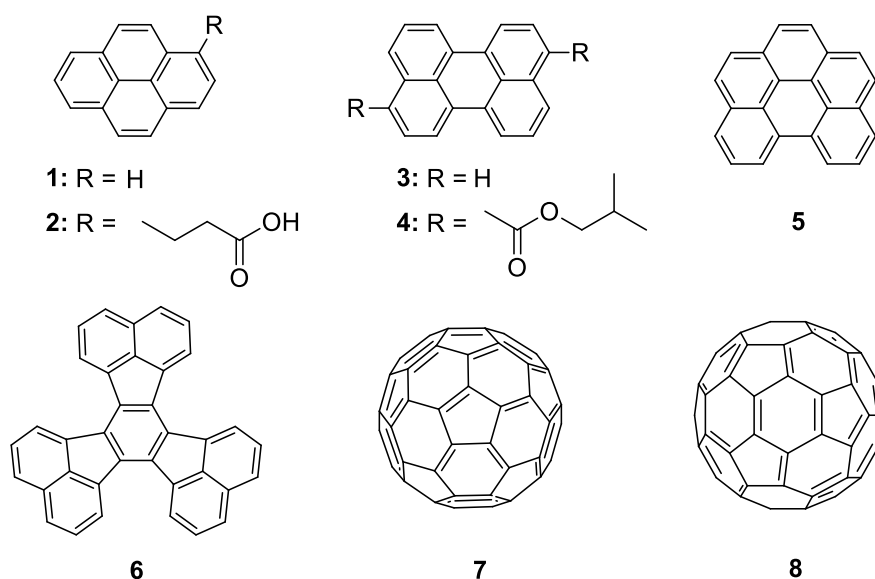
Figure 4: most commonly employed organic dyes with relative structure

1.3.2   Organometallic optical oxygen sensors

Organometallic complexes have nowadays replaced almost completely the organic PAHs.[33] These species show strong luminescence with long lifetimes, good photostability, absorption in the visible region and large Stokes shifts, so that no interactions with the exciting light occurs, which is important especially for biological applications. In this class of fluorophores, the triplet lifetime is increased thanks to metal-ligand charge transfer (MLCT), allowing enough time for the excited state to be quenched at low concentrations of oxygen, affording high sensitivity of the probe. It has been shown that the physico-chemical properties of these species, such as excitation and emission wavelengths, can be tuned by structural modifications to obtain materials with optimal features for the required application. Oxygen-sensing organometallic complexes can be divided into three main categories: polypyridyl complexes, cyclometalated complexes and metalloporphyrins.[12]

Polypyridyl complexes

This category comprises polypyridyl complexes with different metal ions coordinated, *i.e.*, ruthenium (II), osmium (II) and rhenium (I).

Ruthenium (II) polypyridyl complexes are characterized by absorption in the visible region of the spectrum, more specifically in the blue region, around 400-450 nm. They display long lifetimes with relatively large Stokes shifts, showing a response to oxygen measurable both in steady state and in time-resolved fashion. Their photophysical properties, such as excitation and emission wavelengths

or triplet quantum yield, can be tuned by modification of the ligands. These species are characterized by net charges, which make them soluble in hydrophilic polymers. By changing the counter ions from chlorides to more lipophilic ones, such as dodecyl sulphate, the solubility in organic polymers such as silicon rubbers (the most employed polymer matrix) notably improves.[34] A more homogeneous distribution of the chromophore in the matrix usually results in improved brightness of the sensors. The most common ruthenium (II) polypyridyl complexes are shown in *Figure 5*, many of which are commercially available or are straightforward to synthesise.
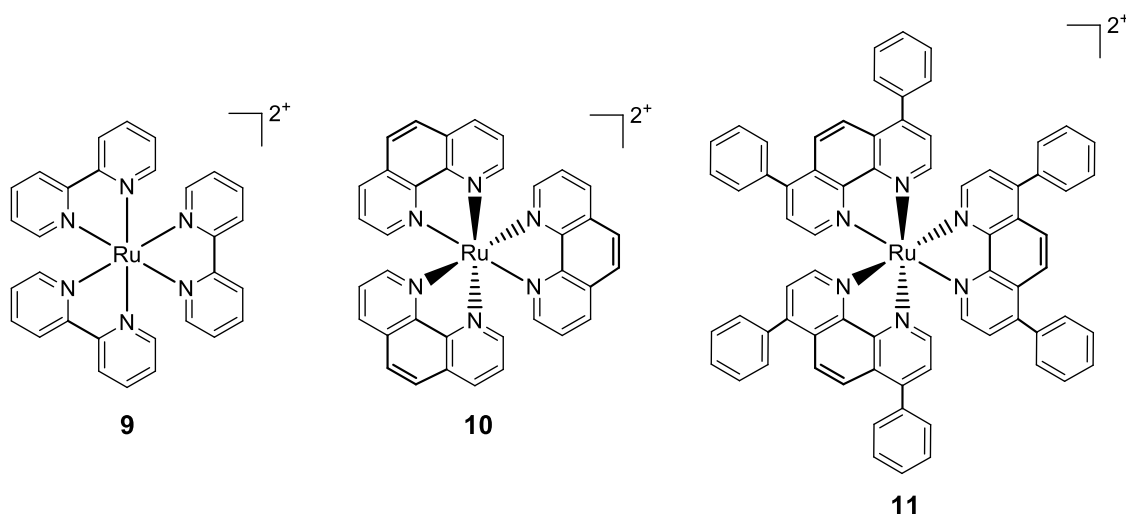
Figure 5: most common employed ruthenium (II) polypyridyl complexes

- Ruthenium (II) *tris*(bipyridine) dichloride **9** presents good properties, such as excitation in the visible region with light emitting diodes (LEDs) sources and large Stokes shift emitting in the red visible region.[35]

- Ruthenium (II) *tris*(1,10-phenanthroline) dichloride **10** (*Figure 5*) similarly to **9** possesses excitation and emission wavelengths in the visible spectra, but slightly larger molar absorption.[36,37] **10** has been employed also as temperature optical sensor.[38] Variation in the temperature and in oxygen concentration can be followed by monitoring the changes in lifetimes of the excited-state of the complex.[38]

- The last complex shown in *Figure 5*, ruthenium (II) tris(4,7'-diphenyl-1,10-phenanthroline) **11** is the most employed among the ruthenium polypyridyl complexes.[13,39] **11** presents better photostability, longer luminescence lifetimes, higher brightness and quantum yield compared to the other two ruthenium (II) complexes.[40]

These chromophores were modified to obtain conjugatable oxygen probes that were covalently linked to a polymer matrix to circumvent leaching. **10** has been provided with acrylamide groups to allow its polymerisation within the polymer matrix.[41] **9** has been covalently linked to sol-gel[42] and ormosil[43]

films employing triethoxysilane groups as a anchoring moieties. Conjugation of the dyes to the polymer matrix remarkably improves the stability of the sensors, preventing the leaching and preserving the probe for a longer time. Some ruthenium-phenanthroline complexes, crystallized with hydrophobic counterions such as PF_6^-, showed oxygen response in solid state.[44,45] The detection was possible because enough empty space is present in the crystal structure, as confirmed from a lower oxygen response of a crystal grown from a racemic mixture, compared to the enantiomerically pure one.[46] The crystal shows linear trend of oxygen response and good stability. The fact they can be directly employed as solid-state probe is an enormous advantage as no polymeric matrix is required. A further advantage arises from the fact that the dimensions of the crystal determine the size of the probe.

Osmium (II) polypyridyl complexes have been employed as oxygen probe to obtain optical oxygen sensors. Compared to the ruthenium analogues, these species have the advantage of being excitable in the red region of the visible spectrum.[47] This advantage is essential for *in vivo* applications, due to the better penetration of the red light in the tissue, compared to the blue light required to excite ruthenium complexes. Osmium (II) polypyridyl complexes present better photostability than the ruthenium ones, despite the shorter lifetime that limits their use only in highly oxygen-permeable polymers.[48] Importantly, osmium (II) complexes are extremely toxic and they must be covalently linked to the polymer matrix to avoid leaching and subsequent toxicity to cells. As in the case of ruthenium (II) complexes, the main ligands resulted to be α-diimine, such as bipyridine and 1,10-phenanthroline (see *Figure 5* for ligands).[49]

Rhenium (I) polypyridyl complexes are sensors that coordinate only one polypyridyl ligand, in addition to carbonyl ligands needed to enhance their luminescence.[50] They display large Stoke shift, high luminescence and long lifetimes, despite their poor photostability.[51] The photophysical properties of these complexes depend strictly on the ligand nature.[52] The most common complexes (**12** and **13**) are shown in *Figure 6*.

Optical oxygen sensors have been built employing also other less common and more expensive metals complexed with polypyridyl complexes, such as europium,[53] terbium[54] and gadolinium.[55]
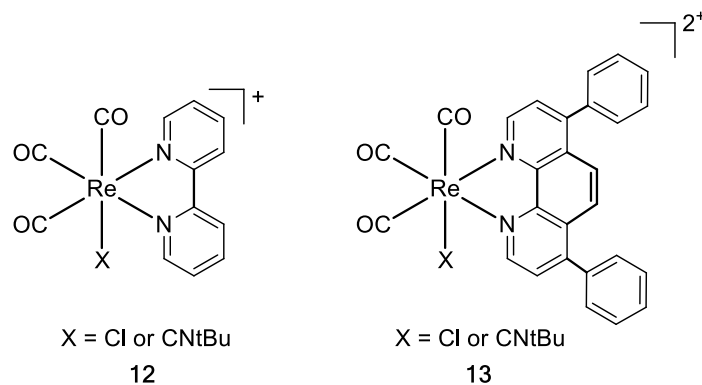
Figure 6: most common employed rhenium (I) polypyridyl complexes

Cyclometalated complexes

Cyclometalated complexes of iridium (III) and platinum (II) have also been employed as probes for OOS. They generally display strong luminescence with high quantum yield, large Stokes shifts and good photostability. They differ from the class of polypyridyl complexes because they present metal-carbon bonds with the ligands.

Iridium (III) cyclometalated complexes gained popularity over the recent years, mostly thanks to development of a cheap and versatile light source: Light Emitting Diodes (LEDs).[33]

- Ir(ppy) (**14**, *Figure 7*) displays a green luminescence trapped in a fluorinated polymer,[56] and its sensitivity proved to be dependent by the matrix employed.[57]
- Ir(ppy-NPh$_2$)$_3$ **15** displays better solubility in organic polymers,[58] thanks to the additional phenyl rings, and better photostability compared to **14**. The complex can be excited with red light.

Iridium (III) complexes with coumarin ligands bearing different heteroatoms have been synthesised.[59] A general structure is shown in *Figure 7*, where X can be either N-methyl (**16**), oxygen (**17**) or sulphur (**18**). Their main advantage, compared to complexes **14** and **15**, is the higher molar absorption coefficient in the blue part of the spectrum, responsible for their strong brightness. The photophysical properties of the sensors can be tuned changing the substituent X, showing a red shift in the order N > O > S.[59]

Example of iridium (III) cyclometalated complexes covalently bound to the matrix have been reported. Complex **14** was bound to the polymer matrix after replacement of one phenylpyridyl ligand for a 4-vinylpyridine and a chloride.[60] The vinyl moiety was exploited during the polymerization process to covalently link the dye to the polymer matrix. In a similar approach, **14** has been endowed with 2-(4-vinyl)-phenylpyridine, and **17** with a polymerizable allylacetoacetate group, replacing the acetylacetonate group (acac).[61]
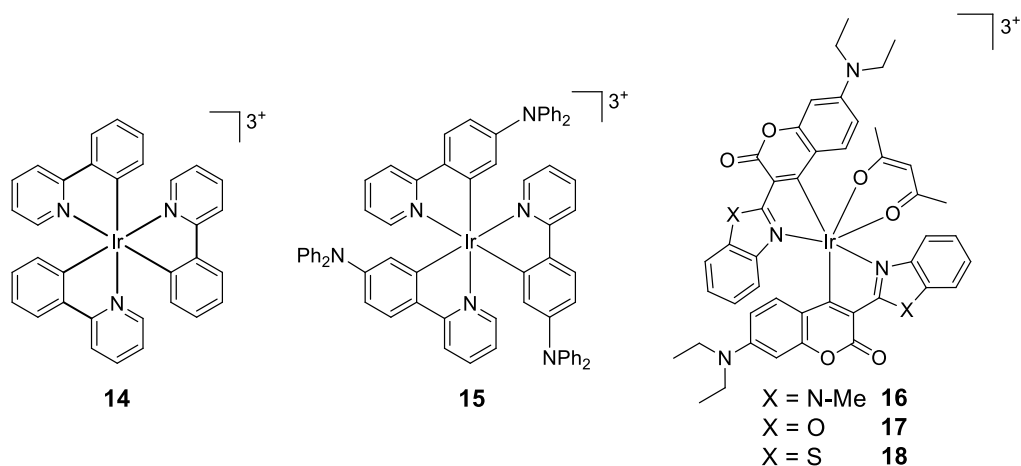
Figure 7: most common employed Iridium (III) cyclometalated complexes

Platinum (II) cyclometalated complexes have been employed as oxygen probes in OOS after the introduction of LEDs, as in the case of iridium (III) complexes. The main advantage of platinum (II) cyclometalated complexes compared to the iridium analogues is the absence of net charges. The neutral character of these molecules renders them insoluble in water, preventing possible leaching of the dye in aqueous environments. In parallel, their solubility in organic polymer is enhanced.

- Pt(thpy) (**19** *Figure 8*) was successfully trapped in a polydimethylsiloxane (PDMS) matrix, and it could be excited with blue LEDs, but it showed poor molar absorption.[62]

- Compound **20** and **21** presented dual emission: one fluorescence band not affected by oxygen, and a phosphorescence emission band sensitive to oxygen. Compound **21** showed a longer lifetime.[63]

- Compound **22** is one of many differently R-substituted compounds synthesised as oxygen probe, but the only one to display a near infrared (NIR) emission at 638 nm.[64]

- Compound **23** is one of few examples of charged platinum (II) cyclometalated complexes. It shows dual emission: fluorescence emission at 677 nm and phosphorescence at 732 nm.[65]
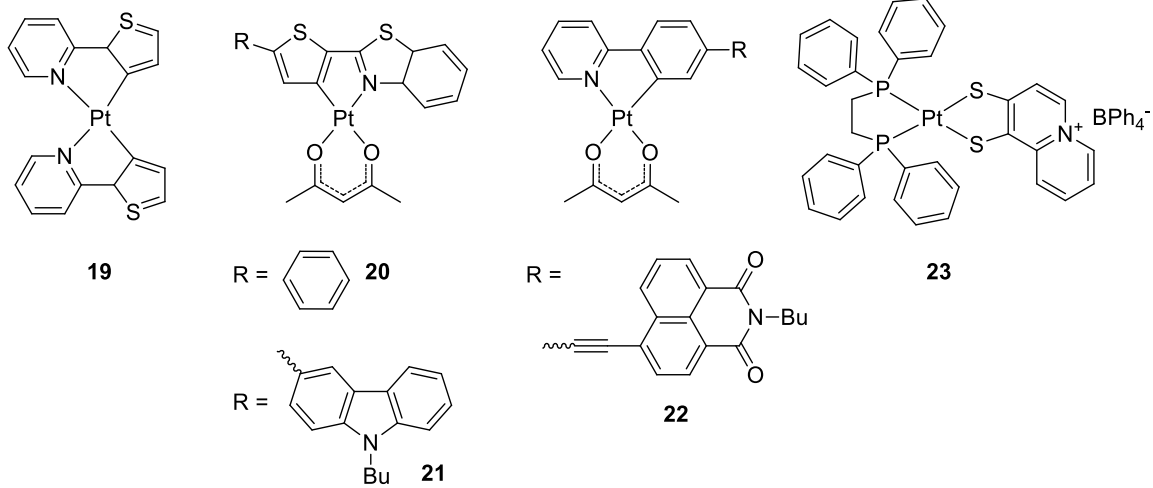
Figure 8: most common employed platinum (II) cyclometalated complexes

Metalloporphyrins

<u>Tetra-meso-substituted porphyrins</u>

The third group of organometallic optical oxygen sensors discussed here comprises platinum (II) and palladium (II) complexes of porphyrins. Thanks to their exceptional properties, this class of dyes became the most popular for obtaining optical oxygen sensors. These species show a very strong phosphorescence at room temperature, with high triplet quantum yield and long lifetime.[66] The triplet state of porphyrins is efficiently quenched by oxygen and the compounds generally show moderate to good photostability, enhanced by the presence of fluorine atoms.[67] Metalloporphyrins are characterized by a strong absorption band around 400 nm (Soret band), and weaker bands at wavelengths higher than 500 nm (Q-bands). Metalloporphyrins, as well as free porphyrins, show very large Stokes shifts, which eliminate the possibility of overlap between the excitation and the emission bands. The triplet lifetimes of metalloporphyrins are in the order of hundreds of nanoseconds, and in the case of palladium porphyrins they can reach microseconds, which make the latter species suitable to sense traces of oxygen.[68] On the other hand, platinum complexes show higher quantum yield compared to palladium complexes.

As in the case of the chromophores described above, the photophysical properties of metalloporphyrins can be tuned by structural modifications of the macrocycle to optimise the response to oxygen in the environment required by specific applications.[69] Platinum and palladium porphyrins are neutral complexes, allowing for a better solubility in organic polymers and limited leaching from the polymer into aqueous solutions. Similar to other oxygen sensing chromophores, porphyrins can be covalently linked to polymer matrices employing a wide array of chemistries. For instance, the nucleophilic substitution of the *para* fluorine atoms in *meso-tetrakis*(pentafluorophenyl)porphyrin (TFPP) and its derivatives (**79c**, **27** or **28**, *Figure 9*) has been widely explored, as well as the carboxylic groups of *meso-tetrakis*(4-carboxyphenyl)porphyrin (TCPP) and its derivatives (**30**, **31** or **32**, *Figure 9*).

Platinum (II) octaethylporphyrin (**25**) shown in *Figure 9*, is perhaps the most studied macrocycle as optical oxygen sensor.[70] **25** has been extensively employed as oxygen probe in association to various polymers, such as polystyrene,[71–73] poly(vinyl chloride) (PVC),[74] sol-gels[75,76] and many other different matrices.[70,77–80] **25** displays very strong phosphorescence at room temperature, with high triplet state quantum yield and long lifetime. Thanks to its remarkable brightness, it can be employed in small amounts to produce very thin films. **25** shows good solubility in most organic polymers and solvents, yielding a homogeneous distribution inside the matrix and therefore a uniform brightness.

M= 2H **24**, Pt **25**, Pd **26** M= 2H **33**, Pt **34**, Pd **35** M= 2H **36**, Pt **37**, Pd **38**

M= 2H **30**, Pt **31**, Pd **32** M= 2H **79c**, Pt **27**, Pd **28**
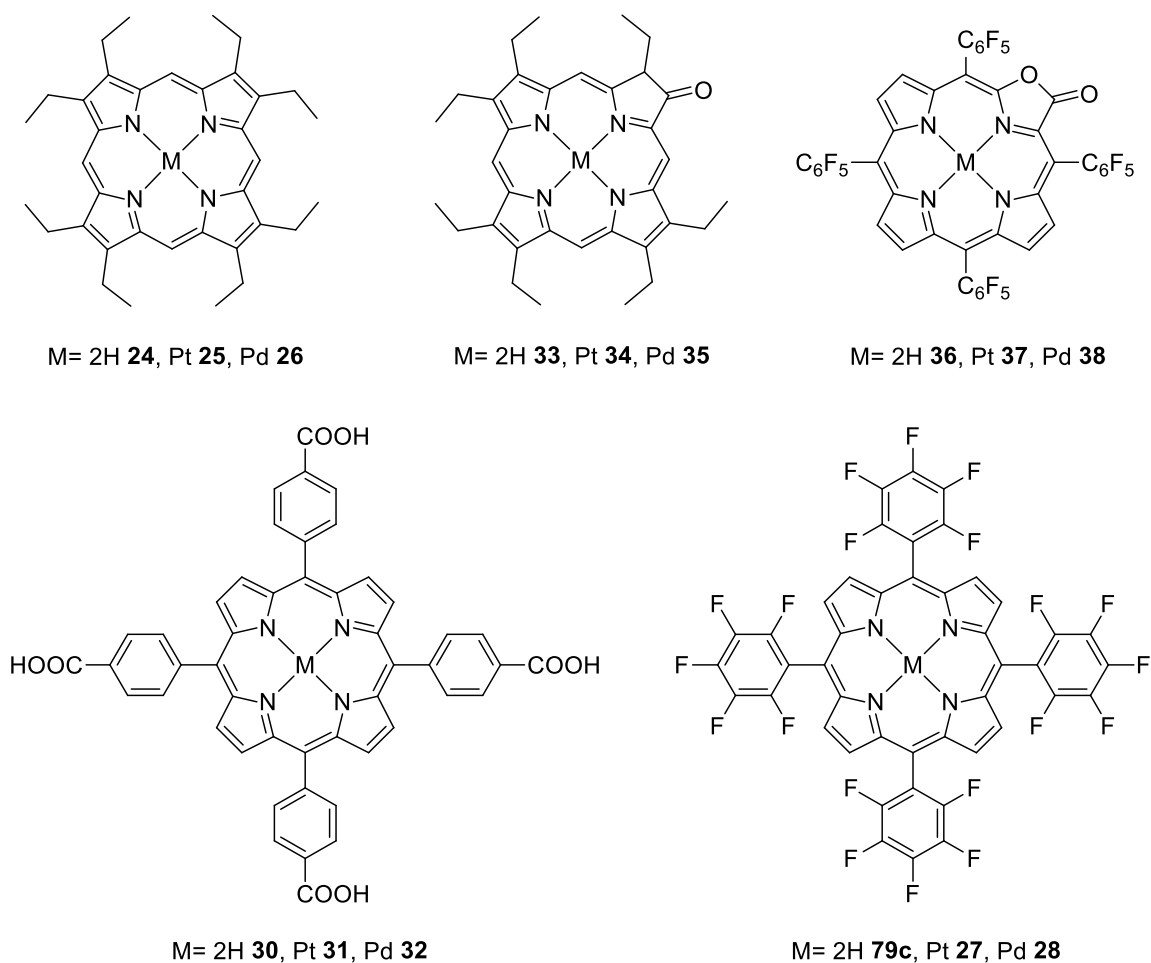
Figure 9: structures of oxygen-sensing metalloporphyrins

Further applications of **25** include its deposition as a solution on glass surfaces and its absorption into oxidized porous silicon layers to build oxygen sensing materials for application in microelectronics.[81] **25** has been embedded in a fibre-optic sensor to monitor the oxygen levels in the digestive tract mucosa.[82] The fibre-optic was coated with **25** dissolved in poly(ethyl methacrylate) (PEMA) yielding a sensitive probe that could withstand sterilisation and particularly suitable for mucosal measurements. **25** has been combined with 5-hexadecanoylamino-fluorescein, a pH sensitive molecule, and with quantum dots (QDs) to develop a ratiometric optical sensors to simultaneously monitor pH and oxygen concentrantion.[83] Exciting the sensor with a 405 nm LED source elicited emission at 650 nm (from oxygen-sensing **25**), at 520 nm (from pH-sensing fluorescein) and at 460 nm (reference signal from QDs), yielding simultaneous information on oxygen concentration and pH. In addition, **25** has been employed to build sensors to simultaneously monitor oxygen and carbon dioxide concentrations.[84] 8-Hydroxypyrene-1,3,6-trisulphonic acid trisodium salt (HPTS) and **25** were absorbed in PEMA, and when the sensor was excited by blue light at 470 nm, two fluorescent peaks were detected, one at 515 nm and one at 645 nm. The peak in the green part of the spectrum (515 nm) was relative to the

partial pressure of CO_2, while the peak in the red part (645 nm) corresponded to O_2.[84] The commercially availability of the dye contributed to its popularity and promoted its use as oxygen probe. However, **25** presents a non-negligible disadvantage: a marked photo-instability that drastically reduces the durability of the sensing device it is incorporated in.[75]

Palladium (II) octaethylporphyrin (**26**, *Figure 9*) has been less employed as oxygen probe compared to **25**. Palladium porphyrins display very long lifetimes thanks to the increased spin-orbit coupling,[66] and therefore they are suitable to detect trace levels of oxygen. However, their sensitivity is so high that they can be used to detect higher level of oxygen only if previously embedded in a polymer matrix with low gas permeability. **26** is commercially available, but it can be easily synthesised from the free base **24** (also commercially available) and a palladium source ($PdCl_2$ or $Pd(OAc)_2$).[79] **26** has been dissolved in many different matrices, such as PVC and ethyl cellulose,[74] fluoropolymers[78] and different fluorine-containing poly(aryl ether ketone)s.[79] **26** shows linear Stern–Volmer plots at low oxygen concentrations, and higher values of I_0/I compared to **25**.

As mentioned above, the photostability of metallo-octaethylporphyrin is very low due to the photo-oxidation caused by the singlet oxygen produced during the sensing process (*Figure 3*). The introduction of halogens atoms in the molecular structure reduces the electron density on the ring, rendering the molecule less prone to photo-oxidation.[67] However, the presence of halogens causes a reduction of the triplet quantum yield and lifetime. Amongst halogens, fluorine proved ideal as it increased notably the photostability of the porphyrin while leaving almost unaffected other photophysical properties.[33]

Derivatives of **79c** (*Figure 9*) are widely employed to obtain OOS materials. The strong electron withdrawing effect of the pentafluorophenyl rings causes a very low electron density on the ring, resulting in a reduced susceptibility to photo-oxidation by singlet oxygen.[67] Platinum complex **27** (*Figure 9*) trapped in a polystyrene matrix showed less than 10% degradation after 50 hours of continuous irradiation at 507 nm.[67] **27** displays high brightness and a long triplet lifetime, but its photostability made it particularly suitable for applications that require high light intensity and long exposure time, such as microscopy[85] and fibre-optic sensing.[86] **27** has been absorbed in polystyrene/poly(vinylpyrrolidone) core-shell particles, and employed with a temperature probe (**29**, *Figure 10*) incorporated in low gas permeability polyacrylonitrile (PAN) microparticles to build a new water-based fluorescent paint.[87] Oxygen pressure and temperature were detected simultaneously after excitation at 405 nm with a LED source, and the two emission signals (519 nm **29**, 658 nm **27**) were separated by almost 140 nm.[87] The paint was employed to monitor pressure and temperature in the aerospace industry.[87] **27** has been widely employed in pressure-sensitive paints,[88–90] but also embedded in sol-gels of different nature[86,91,92] and other matrices.[93,94] The brightness of this species

can be enhanced by light harvesting antennae, which are molecules that absorbs light and efficiently transfer it to the dye.[95] Palladium complex **28** (*Figure 9*), as in the case of octaethylporphyrin (OEP), has been less employed than its platinum analogue: its extremely long lifetime (in the order of milliseconds in solution) makes it suitable to measure nanomolar concentrations of oxygen.[96,97] Its emission is almost entirely quenched at atmospheric levels of oxygen.[68]

29
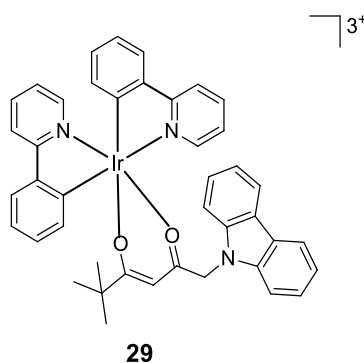
Figure 10: structure of Iridium 2-phenylpyridine carbazole

TCPP (**30** in *Figure 9*) is a further example of a porphyrin substrate to obtain oxygen sensors. The palladium complex **32** has been more frequently used than the platinum analogue **31**, probably due to its commercial availability and ease of metal insertion, which can be performed in mild reaction conditions with a palladium (II) salt such as $PdCl_2$.[98] **32** was bound to albumin through the carboxylic groups and the resulting complex was used to measure oxygen from air concentration to 0%.[99] In a similar approach, albumin conjugate of **32** was employed to simultaneously sense oxygen and as a photosensitizer.[100] **32** was also absorbed on different matrices, such as alumina plates,[101] silicon membranes to detect oxygen partial pressure in blood streams,[102] chitosan nanoparticles[103] and organically modified silicate made of TEOS/octyl-triEOS composite xerogel, showing linear detection in the 0-100 % oxygen range.

The platinum complex **31** was absorbed on alumina plates[101] and was also employed to build the first luminescent metal-organic frameworks (LMOFs).[104] It showed linear oxygen response, and it could be excited by UV light (365 nm) displaying a red emission (655 nm).[104]

Alongside the use of perfluorinated derivative mentioned above, an alternative approach to increase the photostability of oxygen sensing porphyrins consists in oxidising the macrocycle with osmium tetroxide (OsO_4) to obtain a porphyrin ketone.[105] Octaethylporphyrinketone (OEPK), **33** in *Figure 9*, is a highly photostable porphyrin. Derivative **34**, the corresponding platinum complex, was incorporated in matrices such as PVC and polystyrene (PS).[106,107] This species exhibit a bathochromic shift in the absorption (λ_{max} from *ca.* 400 nm to 570-600 nm) with a NIR emission peak. This property is particularly

useful for oxygen measurement in biological samples, due to reduced interferences from auto-fluorescence with the sample.[108] Compound **34** and **35** display good quantum yield and lifetime, despite the relatively poor brightness.

Meso-tetrakis(pentafluorophenyl)porphyrin lactone TFPPL (**36** in *Figure 9*) shows very weak photodegradation, even lower than **79c**, which has been attributed to the effect of the lactone group.[109] Similarly to **33**, this porphyrin displays a red-shifted emission. The dye can be synthesised starting from **79c**, reacted with silver nitrate and oxalic acid in refluxing acetic acid.[110] Interestingly, a derivative of **37** functionalised with polyethylene glycol (PEG) chains on the *para* position of the aryl rings, has been employed to measure the pH of water samples.[111] Crucially, comparable oxygen-sensing properties are displayed by the zinc (II) and the gallium (III) analogues. All the complexes were incorporated into a Nafion® membrane.[111]

<u>π-extended porphyrins</u>

M= 2H **39**, Pt **40**, Pd **41**   M= 2H **42**, Pt **43**, Pd **44**

Figure 11: structures of oxygen-sensing extended porphyrins

Meso-tetraphenyl-tetrabenzoporphyrins (TPTBP) are NIR emitting dyes characterized by an extended aromatic system condensed on the porphyrin structure which is responsible for a red shift in the emission,[112] and for enhanced brightness and photostability compared to porphyrins. TPTBP can be excited by both red and blue light, due to the very intense Soret band and the Q-bands that are only 3 times less intense than the Soret band.[113] Higher photostability is achieved by introducing fluorine atoms on the aryl rings, as shown in *Figure 11*.[113] The substitution on the *meso* position with aryl groups reduces the tendency of aggregation typical of these molecules.[108] As for other metal complexes, platinum benzoporphyrins are more suitable for oxygen detection on a broad concentration range, while palladium analogues are ideal for very low oxygen tensions.[114] **41** was

incorporated in PS nanoparticles together with a reference dye for *in vivo* ratiometric oxygen measurement.[115] **40** was embedded in differently substituted polystyrene matrices, such as poly(2,6-dichlorostyrene), poly(4-tert-butylstyrene) and poly(2,6-fluorostyrene).[116] Both metal complexes were incorporated in a silicon-glass micro-reactor for real-time measurement of oxygen tension in the reaction medium.[117] More specifically, **41** was employed for traces of oxygen (up to 2%) while **40** was suitable for low-to-ambient oxygen concentrations. The dyes were first embedded in a PS-silicon rubber matrix and then incorporated in the micro-reactors.[117] TPTBP are ideal for oxygen measurements in biological environment, in which a deep-penetrating light (red light) is required for the excitation and NIR emission is preferred to avoid interferences caused by background fluorescence.[118] **40** was also employed in organic solar concentrators for photovoltaics.[119] The stability of these compounds is considerably higher compared to the corresponding tetra-arylporphyrins, but their synthesis is much more challenging.

Further extension of the π-system of TPTBP results in meso-tetraphenyltetranaftoporphyrins such as species **42** (*Figure 11*), which determines a further red shift of the absorption peaks and an increased intensity ratio between Q-bands and Soret band.[112,120] However, these species present poor triplet quantum yields and lower photostability compared to benzoporphyrins.[121] Platinum complex **43** was encapsulated in phospholipid nanomicelles and employed to image anoxic tumours.[122] Its phosphorescence emission around 900 nm allowed to drastically reduce interferences from background autofluorescence.[122] **43** was also incorporated in poly(9-vinylcarbazole) and employed as dye in the construction of polymeric light emitting diodes (PLED).[123] In the class of π-extended porphyrins there are other compounds deriving from a mixture of benzo- and nafto-substituted porphyrins. These hybrids combine the properties of both dyes, affording an increased bathochromic shift in the emission but, on the other hand, a decrease in the quantum yield and a reduced photostability.[124]

Water-soluble porphyrins

Optical sensors designed for biological applications must display specific features to be suitable for use in an environment containing cells, namely:

- high triplet state quantum yield (higher the quantum yield results in a higher concentration of triplet state molecules, and potentially in a more intense signal)
- long triplet lifetime (the longer the lifetime, the higher the probability of intermolecular collisions even at low oxygen concentrations)
- high chemical- and photo-stability (to avoid the accidental production of species toxic to the cells)
- solubility in water (to maximise compatibility with living systems)

Water-soluble metalloporphyrins satisfy these criteria, and consequently they have been widely used for the detection of dissolved oxygen in aqueous solution. To ensure water solubility, most derivatives have either net charges or several polar groups.

Coproporphyrin (**45** *Figure 12*) is a water-soluble macrocycle in which the solubility in aqueous media is given by the four carboxylic groups. The palladium complex **47** was employed as oxygen probe immobilised on different polymeric matrices, such as PVC, poly(methyl methacrylate) (PMMA), PS and silicon rubber.[125] The optical oxygen sensors obtained by embedding the dye in PS was employed to measure the oxygen concentration in the gas phase, following excitation with a cheap flash lamp as light source.[125] The platinum complex **46** was employed as an albumin conjugate to measure the intracellular oxygen levels in mammalian cells.[126]

M= 2H **45**, Pt **46**, Pd **47**   M= 2H **48**, Pt **49**, Pd **50**
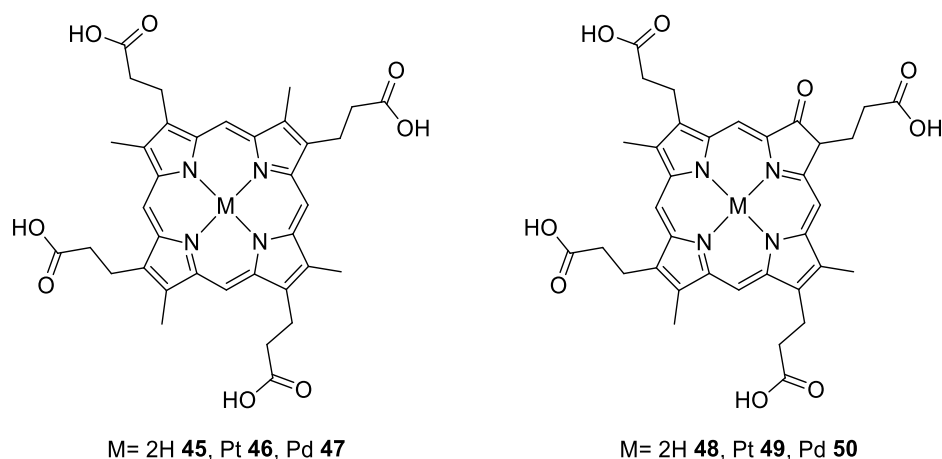
Figure 12: structure of oxygen-sensing coproporphyrins and coproporphyrin ketones

The photostability of coproporphyrins and their derivatives is rather poor, despite their otherwise good photophysical properties. To overcome this problem a new dye was synthesised bearing a ketone group on the macrocycle to give a coproporphyrin ketone (**48**, *Figure 12*)[127]. Both platinum and palladium complexes **49** and **50** were conjugated to serum albumin to detect intracellular oxygen.[127] As in the case of **24**, the introduction of the ketone group shifted the emission towards longer wavelengths in the NIR region and increased the intensity of the Q-bands.[127]

Other examples of water-soluble porphyrins employed as oxygen sensors include species bearing four charged groups on the *meso*-aryl substituents as shown in *Figure 13*.
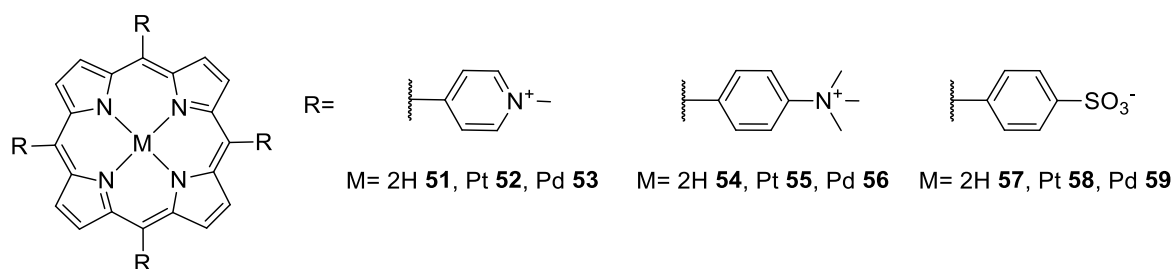
Figure 13: structure quadruple-charged free base, platinum (II) and palladium (II) species

Palladium complexes **53**, **56** and **59** (*Figure 13*) were tested both in aqueous solution and after incorporation on serum albumin, to detect oxygen concentrations from atmospheric levels down to the nanomolar range.[128] Platinum and palladium complexes **52,55** and **53,56** were embedded in a perfluorinated ion-exchange membranes (Nafion®) and the oxygen concentration was detected in the range 0-100%.[129] Linear Stern-Volmer plots, good sensitivity and photostability were observed in the whole concentration range. Compounds **52** and **53** were incorporated in synthetic clay (Sumecton SA®) to obtain a new hybrid material for oxygen sensing in aerobic conditions.[130] Clay minerals proved to be suitable matrices to host the metalloporphyrins, allowing fluorescence quenching by oxygen, while keeping the cost of the sensing material very low.

Second generation polyglutamic Pd-porphyrin-dendrimers (**60**) and tetrabenzoporphyrin-dendrimers (**61**) are further examples of water-soluble oxygen sensing porphyrins (*Figure 14*).[131]
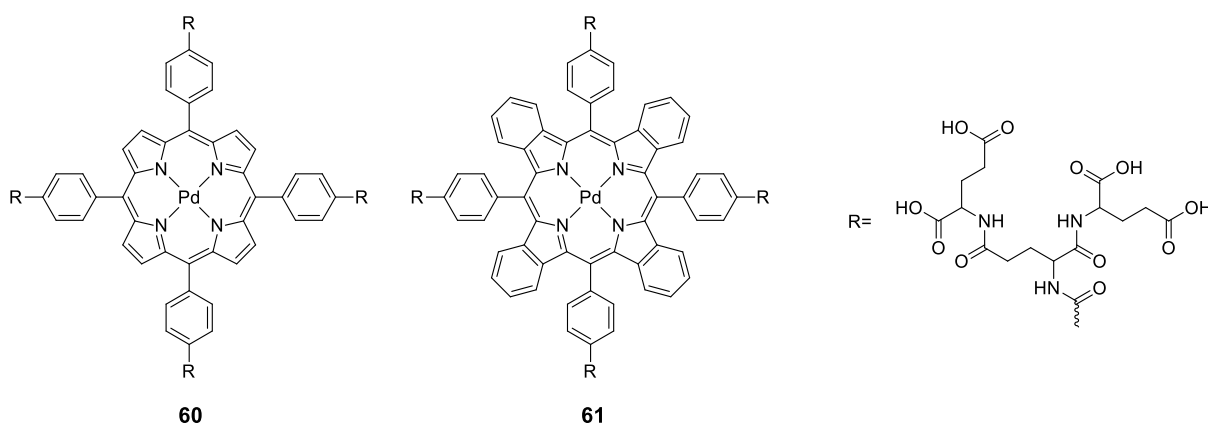
Figure 14: structure of oxygen-sensing glutamate-dendrimers

These complexes bear 16 carboxylate groups in the outer layer of the dendrimer, which are responsible for the good solubility in aqueous media. The size of the resulting molecule prevents it from crossing cell membranes.[131] Thanks to its red-shifted absorption and emission, compound **61** was employed as oxygen probe *in vivo* to measure the oxygen distribution in a subcutaneous tumour, after

incorporation in serum albumin.[131] Dendrimer **61** was also embedded in polyacrylamide hydrogels to monitor oxygen levels in cancer cells, both in aerobic and hypoxic conditions.[132] Despite their challenging synthesis, they soon became commercially available, fact that helped their use in the build of optical oxygen sensors.

A new class of porphyrins recently emerged as oxygen probes: iridium (III) octaethylporphyrin bearing different axial ligands (*Figure 15*). These dyes are characterized by a non-planar macrocycle, in which the central iridium ion can coordinate two ligands in the axial positions. The complexes are obtained from compound **62**[133] by ligand exchange. The different axial ligands influence the photophysical properties of the dye and play a key role in the solubility properties.[134] Compounds **63** and **64** bearing lipophilic ligands such as pyridines and *N*-butylimidazoles, respectively, are soluble in organic polymer and they were incorporated in PS matrices.
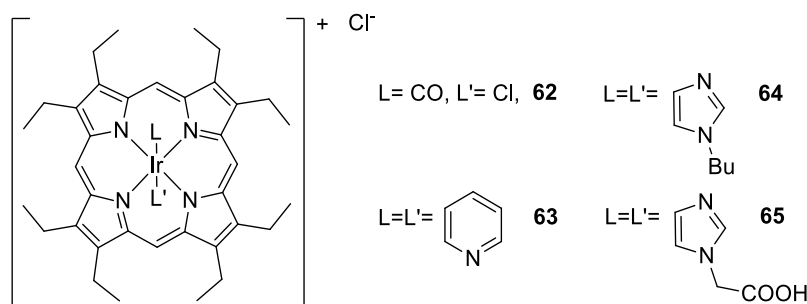
Figure 15: structure of iridium (III) octaethylporphyrin bearing different axial ligands

On the other hand, compound **65** bearing 1-imidazoleacetic acid as axial ligands is soluble in polar solvents.[134] Thanks to the carboxylic group on the ligand, this species can be covalently linked to a support: **65** was attached to bovine serum albumin and amino-modified silica gel allowing real time measurements in aqueous solutions.[134] Iridium (III) complexes with cell-penetrating and tumour-targeting peptides as axial ligands were also synthesised,[135] which showed linear Stern-Volmer plots and good solubility in aqueous media.[135]

Compound **65** introduced a new class of compounds, in which an axial ligand coordinated to central metal atom is exploited as anchoring moiety to covalently link the dye to the support. This was the first example of a conjugatable porphyrin complex attached to a support through an axial ligand.[134] Most frequently, the conjugation of the dye to a support is performed via a suitable functional group on the ring, or on the aryl substituents in the *meso*-positions. A covalent bond between the dye and the support is useful to prevent issues associated with leaching or uneven distribution of the dye in the environment where the measurement is taking place.[33,108]

Oxygen-sensing porphyrin monomers for radicalic polymerisation

For oxygen sensing in biological systems, the leakage of the dye must be prevented as much as possible to avoid toxicity in the sample. The most common approach to overcome this problem is to covalently link the dye to the polymeric matrix.[108] A number of porphyrins have been provided with a vinyl- or acryloyl-moiety and subsequently co-polymerised to obtain oxygen-sensing polymers (*Figure 17*). Porphyrin **66** (*Figure 17*) is an A$_3$B porphyrin in which a *meso*-substituent is different from the other three.[136] The carboxylic group on the starting porphyrin was esterified to provide the dye with polymerizable 2-methacryloyloxyethyl chain. The resulting species was co-polymerised with isobutyl methacrylate or 2,2,2-trifluoroethyl methacrylate.[137] The resulting oxygen sensitive material was employed for pressure sensitive paint in the aeronautical field. Compound **66** was also employed to obtain optical oxygen sensors capable of simultaneously sensing pH and oxygen.[138] In this case, poly(2-hydroxyethylmethacrylate)-co-poly(acrylamide) (PHEMA-co-PAM) was employed as matrix and **67** (Figure 16) was co-polymerised in the material *via* the same acryloyl moiety as pH sensor. The absence of toxicity, detected after 40 hours of incubation with HeLa cells on the material, confirmed that neither sensors leached from the polymer.[138] The favourable behaviour of **79c** (Figure 9) as an oxygen sensor encouraged researchers to explore different approaches to incorporate this species in various materials. The structure of **79c** is suitable for this purpose because the fluorine atoms in the *para* position on the aryl rings can be replaced *via* aromatic nucleophilic substitution. This strategy was widely pursued to introduce suitable groups to co-polymerise the dye in a matrix (Figure 17).

Four methacrylate groups were inserted on the *para* positions of the perfluorinated aryl rings of porphyrin **27** to obtain complex **68** (Figure 17) which was co-polymerised into two different polymers, namely a hydrophilic one made of poly(2-hydroxyethylmethacrylate)-co-polyacrylamide (PHEMA) and a hydrophobic one made of PS.[139] **68** showed negligible leaching from the polymer and higher photostability compared to the same polymer in which the porphyrin (**27**) was simply adsorbed.[139] Crucially, the sensors obtained with PHEMA proved ideal for applications in biological samples due to the biocompatibility of the material, a fast response, a high sensitivity to oxygen and no toxicity to human lung adenocarcinoma epithelial cells (A549).[139] The sensor made of **68** covalently linked to PHEMA was also employed to monitor the oxygen consumption of Escherichia coli.[140]

67
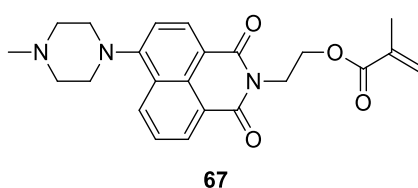
Figure 16: structure of 2-(1,3-dimethylene-6-(4-methylpiperazin-1-yl)-1H-benzo[de]isoquinolin-2(3H)-yl) ethyl methacrylate
67

Platinum complex **69** bearing four silyl groups (Figure 17) was used to covalently link the oxygen sensing species to silica gel. The resulting material showed a faster response and a higher ratio of fluorescence from environments without oxygen to oxygenated systems compared to **68** linked to PS and PHEMA.[140] Oxygen sensor **68**, pH sensor **67** (*Figure 16*) and a reference dye were copolymerized with PHEMA-co-PAM to obtain new ratiometric dual sensitive optical oxygen sensors.[141] Under excitation at 380 nm the sensor showed emission in the blue, green and red part of the visible spectrum, and it was employed to evaluate the photosynthetic activities of *Synechocystis sp.* PCC 6803.[141]
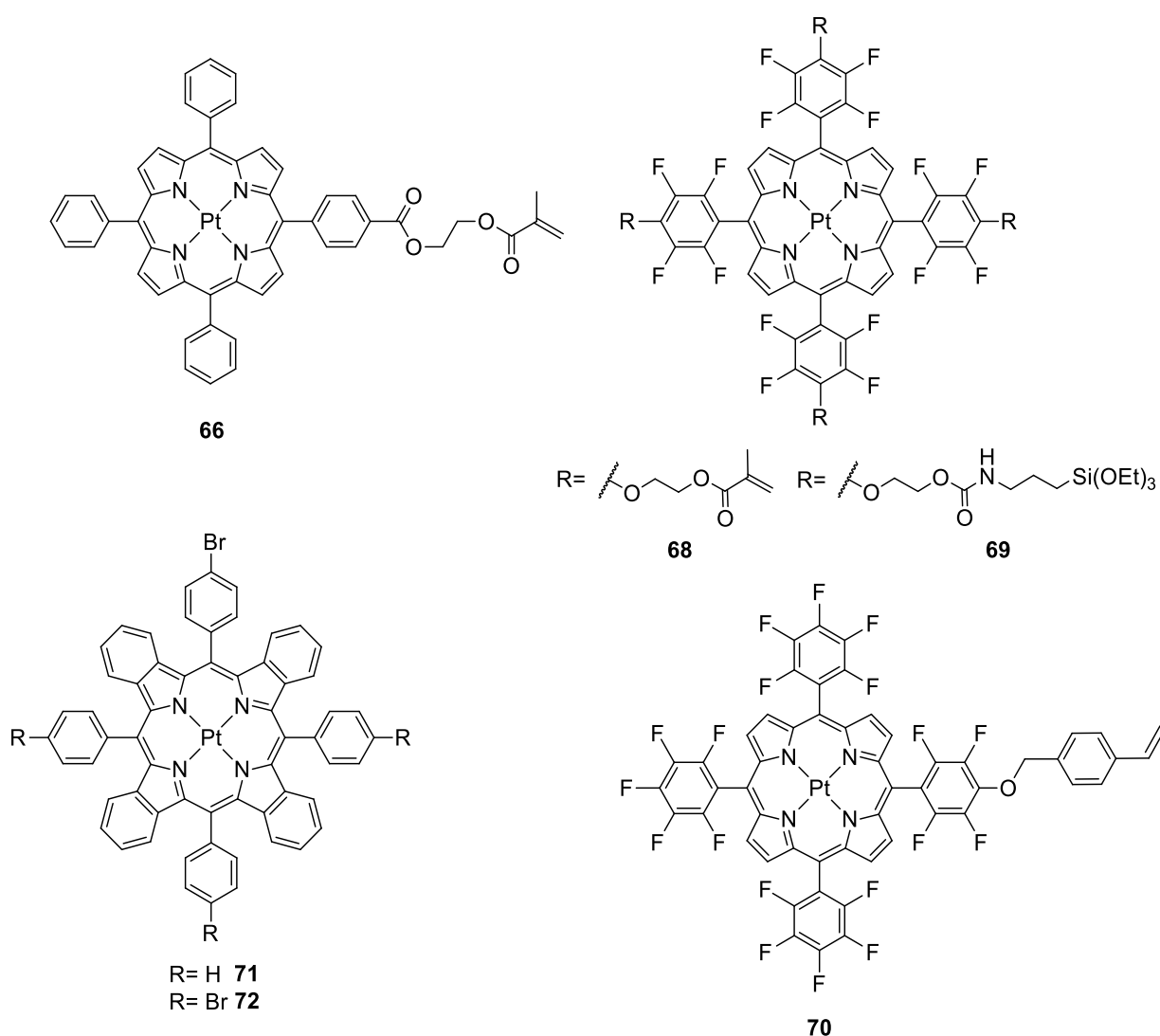
Figure 17: structures of polymerisable porphyrins

These sensing materials were obtained through the tetra-functionalisation of **79c** but there are examples of mono-functionalisation of **79c**, which allows the co-polymerisation but not the cross-linking of the porphyrin with the matrix. This approach was pursued by inserting a suitable function in

the matrix to attach the porphyrin to the pre-formed polymer or by introducing a single reactive group on the porphyrin.

In an example of the latter approach, platinum and palladium complexes of **79c** were covalently linked to amino modified silica-gel particles exploiting the reactivity of the *para* fluorine atoms on the aryl rings.[68] The terminal amines of the silica particles reacted with one of the *para* fluorine on the aryl rings of **79c**, forming a covalent bond and, therefore, anchoring the dye on the particle. Subsequently, the particles were dispersed in silicon rubber to give the sensor. Linear Stern-Volmer plot, high photostability and fast response time were detected for both the complexes, and as expected, a higher sensitivity to oxygen was detected for the palladium complex.[68] In a similar approach, styrene–pentafluorostyrene-copolymer was grafted with 1,3-propanedithiol by displacement of the *para* fluorine of pentafluorostyrene with a thiol group, following the first approach mentioned above. The dye was subsequently anchored to the substrate by nucleophilic substitution of the *para* fluorine atom on the porphyrin with the free thiol group on the propanedithiol chain, affording a material in which 1,3-propanedithiol acts as a spacer between the porphyrin and the polymer, as confirmed by ^{19}F-NMR spectroscopy.[142] When the three components (dye, polymer and thiol spacer) were added simultaneously, heavy cross-linking was detected, where the propanedithiol randomly bridged the porphyrin and pentafluorostyrene.[142]

79c was monofunctionalised with divinylbenzene moiety to give compound **70** (Figure 17) which was used to obtain oxygen sensing core-shell nanoparticles with a hydrophilic shell and a hydrophobic core.[143] The new sensor displayed favourable photophysical properties and no leakage of the dye. Thanks to its biocompatibility, it was employed for intracellular oxygen detection.[143]

Conjugatable derivatives of tetrabenzoporphyrin were also synthesised and employed as oxygen sensors (Figure 17)*.* Hutter *et al.* synthesized both the mono- (**71**) and the tetra-brominated (**72**) tetrabenzoporphyrin for covalent grafting on a polymeric matrix through C-C bond *via* Suzuki coupling.[144] The bromine atom was either replaced with a vinyl group used to co-polymerise the dye with vinyl monomers, or alternatively the Suzuki coupling was performed between the brominated dye and double-bond-functionalised polymer. The resulting sensor showed favourable photophysical properties, displaying high brightness, typical NIR emitting properties and no leakage of the dye from the polymer.[144]

Conjugatable and water-soluble porphyrins

The last sub-group of porphyrins discussed here is the most pertinent to the project. It comprises species that display both solubility in aqueous media and conjugatable group: these species were

developed to link covalently and selectively (*i.e.*, with no possibility of cross-linking the matrix) the sensing moiety to a matrix in aqueous medium.

Examples of such species are shown in *Figure 18*: these are A₃B type porphyrins with either positively charged or negatively charged groups.[145] The species were obtained *via* a mixed aldehyde condensation approach, with one of the aldehydes bearing a carboxylic group as the conjugatable moiety. Water solubility was attained by functionalising the three equivalent aryl rings to insert a net charge, positive (N-methyl-4-pyridinium) in the case of **73**, **74** and **75** and negative (4-sulphonatophenyl) in the case of **76**, **77** and **78**, respectively free base, platinum and palladium complexes. These dyes were anchored to amino-functionalised polyacrylamide nanoparticles (PAANPs) *via* N-hydroxysuccinimide/ethyldimethylaminocarbodimide (NHS/EDC) chemistry. Thanks to the water solubility of the porphyrins, the conjugation could be carried out in water and under mild reaction conditions.[146] Metal insertion was achieved employing microwave irradiation that reduced notably the reaction time and increased the yield. The photophysical properties of the stand-alone dyes and of the nanoconjugates were measured, showing a red shift in the emission wavelength and a broadening of the Soret band relative to the nano-conjugates.

M= 2H **73**, Pt **74**, Pd **75**

R=

M= 2H **76**, Pt **77**, Pd **78**
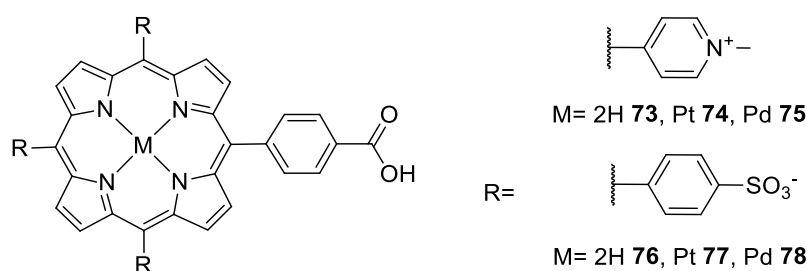
*Figure 18: structure of free base platinum (II) and palladium (II) 5-(4-carboxyphenyl)-10,15,20-(N-methyl-4-pyridyl)porphyrin (**73,74,75**) and 5-(4-carboxyphenyl)-10,15,20-(4-sulphonatophenyl)porphyrin (**76,77,78**)*

Giuntini *et al.* showed that the association of the porphyrin with the support caused a decrease in the quenching rate constant by one order of magnitude. All the dyes showed linear Stern-Volmer plots both in steady state and time-resolved measurements, and the linearity was maintained when the nano-probes were embedded in compressed collagen sheets.[146]

The same authors developed also a dual oxygen and pH ratiometric sensor exploiting compound **74** as oxygen probe, 6-carboxyfluorescein and Oregon green® as pH probes and carboxytetramethylrhodamine as a reference dye.[147] The new nanosensors responded to variations of oxygen over a 0-100% range and pH values in the fully biological range between 3.5 and 7.5.[147]

1.4 A closer look at porphyrins

Porphyrins are aromatic macrocycles made of four pyrrole rings connected by four methine bridges in a square planar conformation. Porphyrins have a 18-π electrons conjugated system, which is responsible for their very intense colour.[148] The name of these species is derived from the Greek word *porphyra*, meaning purple.[149] The macrocycle presents a tetra-dentate cavity suitable to coordinate different metal atoms, such as Zn (II), Fe(II) or Fe(III), Ni(II), Cu(II), Co(II), Pd(II), Pt(II).[150] The basic structure of a porphyrin is shown in Figure 19. Three different positions on the structure can be identified: *alpha, beta* and *meso* positions. When the *meso* position is substituted with aryl groups, the species are called *meso*-tetra-arylporphyrins.
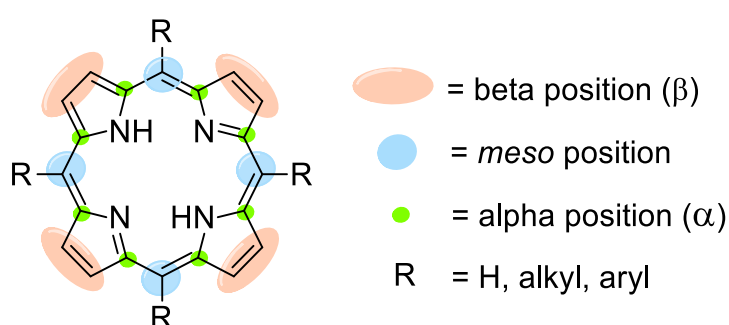
Figure 19: porphyrin structure

Due to their extended conjugated system, porphyrins present a very characteristic visible absorption spectrum (*Figure 20*). The most intense band appears around 400 nm and it is known as Soret band. This band is generated by the π → π* transition. In free porphyrins, four lower-intensity bands are visible between 450 nm and 650 nm, which are called Q-bands and are responsible for the vivid red colour that these compounds show. Modification on the aryl groups on the *meso* positions does not have a major influence on the intensity and wavelengths of the absorption spectrum, but the insertion of a metal atom causes a marked change in the absorption. Besides a more or less pronounced shift of the Soret bands, which depends on the nature of the metal ion, two of the four Q-bands disappear.[151] The latter feature is particularly useful when monitoring the metal insertion reactions.
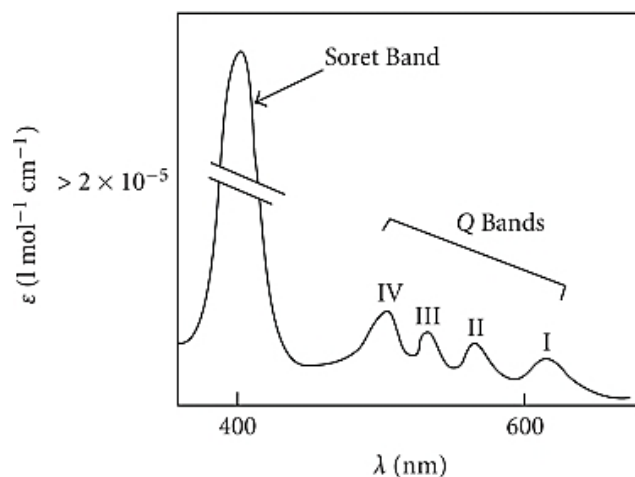
Figure 20: typical absorption spectrum of porphyrin

Some porphyrins and related tetrapyrroles are natural products and, due to their unique physico-chemical properties, they play major roles on the very process of life. The two most prominent examples are haem and chlorophylls, the pigments present in the red blood cells and in green plants and algae, respectively.

Haem (*Figure 21*) is the iron complex of protoporphyrin IX, and it is the prosthetic group of haemoglobin, the protein responsible for carrying oxygen from the airways to the cells and carbon dioxide from the cells to the airways. Molecular oxygen coordinates to the iron metal in the porphyrin core and it is transported in the blood stream to the districts of the body. Once it reaches a cell, the oxygen is released from the coordination complex, haem coordinates carbon dioxide and carries it to the heart and then the lungs. In other words, haemoglobin is a crucial element for the very existence of life.[152]
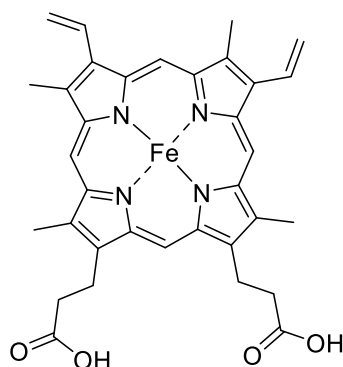
Figure 21: structure of haem group

The second naturally occurring porphyrins are found in plants (mainly in their leaves) and in green algae. In this case, a magnesium complex of a chlorin, a porphyrin in which one of the four pyrrole rings partially reduced, is involved. As haem is important for the life of multicellular animals,

chlorophyll is pivotal for plants life because it is part of the complex machinery deputed to photosynthesis, the process *via* which plants harvest light and convert it into energy. Many different types of chlorophyll are present in a plant leaf, as shown in

Figure 22, with different specific functions.

R= Me, R'= CH=CH$_2$, R''= X, R'''= CH$_2$CH$_3$ Chlorophyll **a**

R= CHO, R'= CH=CH$_2$, R''= X, R'''= CH$_2$CH$_3$ Chlorophyll **b**

R= Me, R'= CHO, R''= X, R'''= CH$_2$CH$_3$ Chlorophyll **d**

R= Me, R'= CH=CH$_2$, R''= Y, R'''= CH$_2$CH$_3$ Chlorophyll **c$_1$**

R= Me, R'= CH=CH$_2$, R''= Y, R'''= CH=CH$_2$ Chlorophyll **c$_2$**
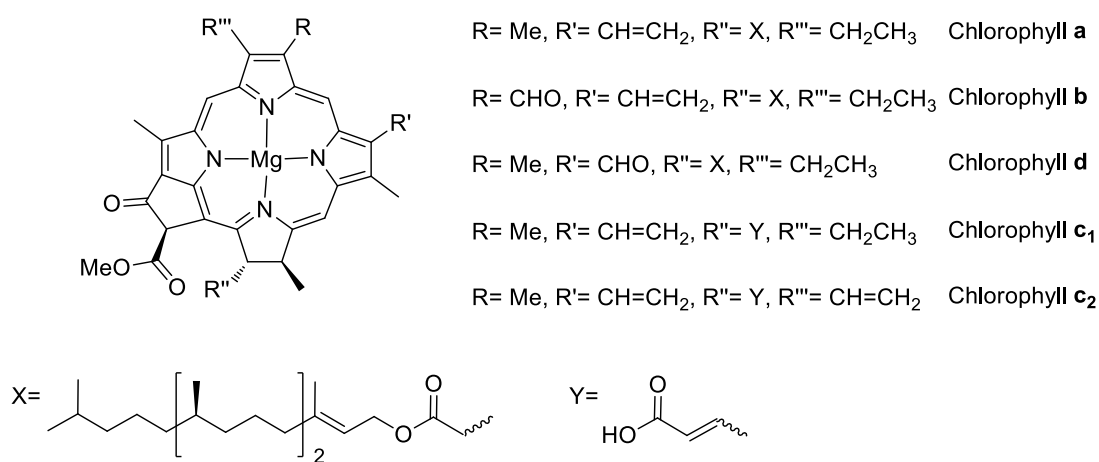
Figure 22: structure of different chlorophylls

Synthetic porphyrins

Porphyrins can be also artificially synthesised starting from simple building blocks. Different synthetic strategies follow the same development based onto the formation of a porphyrin core (*via* electrophilic substitutions on positions 2 and 5 of the pyrrole ring) followed by the oxidation of the latter. These protocols have been developed to achieve the synthesis of a wide variety of *meso-* and/or *beta*-substituted porphyrins. Synthetic approaches to porphyrins fall into three main strategies. The oldest and most employed strategy is based on the condensation of four pyrrole units to form the porphyrin core (*Scheme 1*).
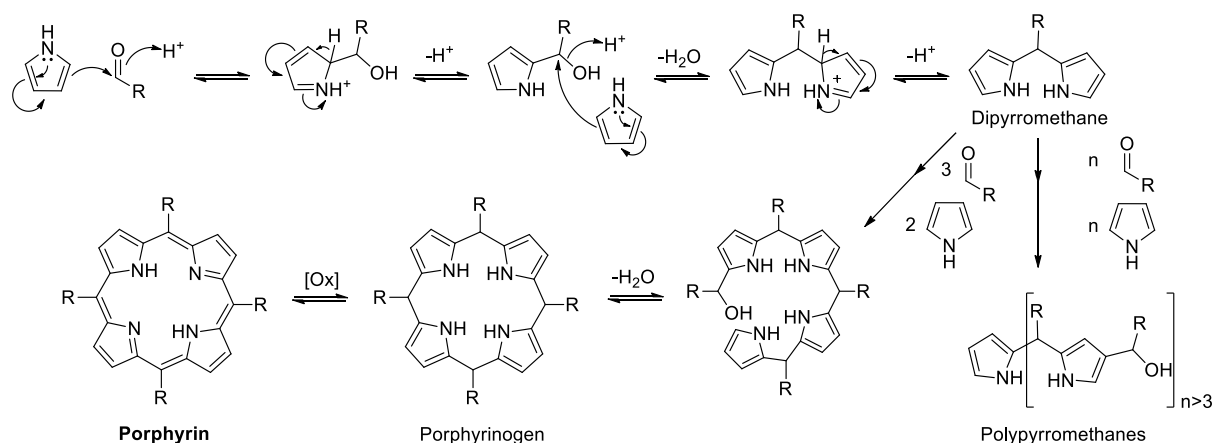
Scheme 1: aldehyde and pyrrole condensation mechanism

This approach does not give any control on the stereochemistry of the final product. To solve the problem, two strategies have been developed, both by reacting two dipyrromethane units previously synthesised, and by including a pyrrolic unit to a tripyrrane precursor.

In this paragraph, only the aldehyde and pyrrole condensation will be discussed in detail.

- Rothemund synthesis

The first porphyrin synthesis was performed in 1935 by Rothemund:[153] the scientist showed that heating acetaldehyde or formaldehyde with pyrrole in a sealed tube led to the formation of porphyrin. Few years later, in 1941, Rothemund described the first synthesis of *meso*-tetraphenylporphyrin,[154] performed in a sealed vessel in pyridine for 8 hours. These first synthetic approaches were extremely low yielding, so an intensive work of optimisation took place.

- Adler-Longo synthesis

The synthetic procedure mostly used nowadays to obtain porphyrins was developed in 1966 from the Rothemund procedure and it bears the name of the two authors: Adler-Longo.[155] This synthesis is performed in refluxing propionic or acetic acid, increasing notably the yield up to 20 %. In some cases, when propionic acid was employed, the product would precipitate in the reaction mixture upon cooling and could be obtained directly by filtration from the reaction mixture.[155] Together with the role of temperature, the amount of oxygen, and the reagents concentration, the authors have highlighted the influence of the reaction medium acidity. Thus, the protocol established follows the following recommendations: the condensation of pyrroles and aldehydes needs to be performed starting from an equimolar mixture dissolved in refluxing propionic acid (141 °C), under air and for at least 30 minutes. As for the previous Rothemund synthesis, this approach requires the use of aldehydes which can withstand the high temperatures but, despite the higher yield, most of the products formed are impurities. Over the years, the method was improved, and yields were moderately increased.

- Little synthesis, known as "mixed aldehydes"

Based on the work of Adler and Longo, Little proposed, in 1975, the synthesis of porphyrins bearing different substituents on *meso* positions to obtain asymmetric porphyrins (*Scheme 2*). Using the previous protocol, a mixture of two different aldehydes can condense with pyrrole to form asymmetric porphyrins.[156] Unlike the synthesis of a symmetric porphyrin, the procedure according to Little does not allow the synthesis of just one porphyrin.
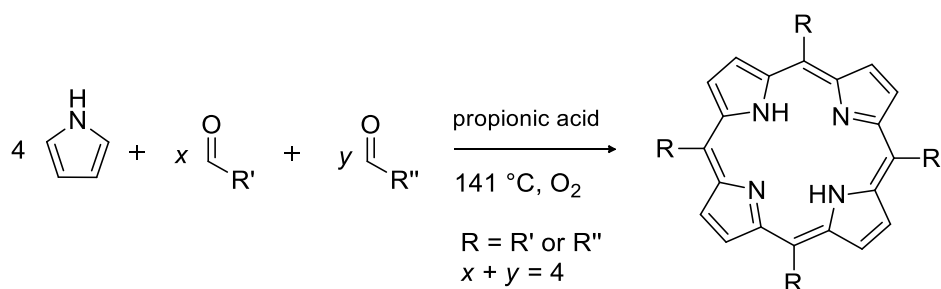
Scheme 2: Little's synthetic scheme for mixed aldehydes

In fact, using a mixture of two aldehydes leads to the formation of six different porphyrins (*Scheme 3*). When using this protocol, a "code" has been created to distinguish the different products. Starting from two different aldehydes A and B, the obtained porphyrins are labelled as follows:

A_4 for porphyrins with substituents just from reagent A

A_3B for porphyrins with 3 substituents from reagent A and 1 substituent from reagent B

A_2B_2 for porphyrins with 2 substituents from reagent A and 2 substituents from reagent B (2 isomers)

AB_3 for porphyrins with 1 substituents from reagent A and 3 substituents from reagent B

B_4 for porphyrins with substituents just due from reagent B

To obtain A_3B porphyrins, it is suggested to use 3 equivalents of aldehyde A, 1 equivalent of aldehyde B and 4 equivalents of pyrrole.[156] The synthesis of an A_3B porphyrin widely depends on the aldehydes used and the yield can vary from 5 to 25 %. Moreover, the purification requires the use of chromatographic techniques to separate the various porphyrins obtained. Nevertheless, the protocol remains the most utilised to obtain asymmetric porphyrins.
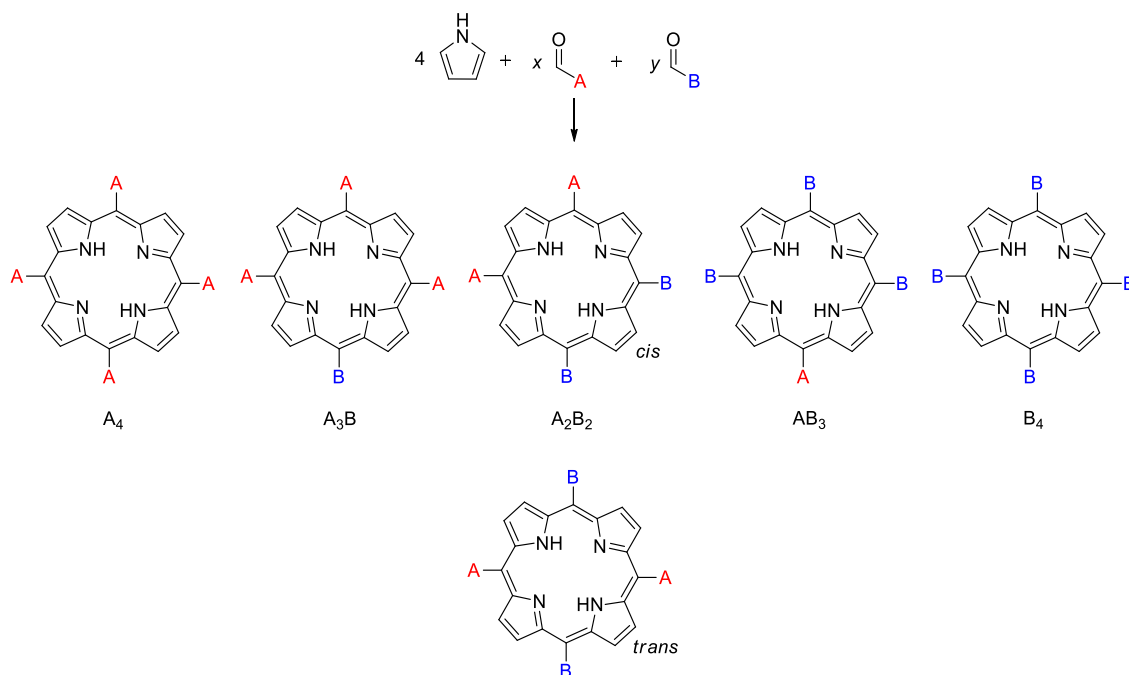
Scheme 3: different porphyrins produced during Little synthesis

- Lindsey synthesis

Another synthetic method to obtain *meso*-tetraphenylporphyrin was developed by Lindsey in 1986, and it involves the use of a Lewis acid as catalyst to form the porphyrinogen, later oxidised by the addition of an oxidant.[157] In this synthetic route, aldehyde and pyrrole are dissolved in a dry organic solvent like dichloromethane (DCM) or chloroform. Due to its sensitivity to the presence of oxygen, the reaction needs to be carried out under inert atmosphere.[158] The solution is then treated with Lewis acid catalyst: either trifluoroacetic acid (TFA) or BF_3-Et_2O complex in a ratio that varies between 10 % and 30 %, depending on the nature of the catalyst and of the reagents.[159] The addition of the catalyst leads to the formation of the porphyrinogen, which must be then oxidised by the addition of an oxidant such as chloranil or 2,3-Dichloro-5,6-dicyano-1,4-benzoquinone (DDQ) to obtain the desired porphyrin. The reaction temperature can vary depending on the aldehyde employed, however, it is generally lower compared to Adler–Longo synthetic method. This method is not applicable if aldehydes bearing Lewis basic groups are used, as these groups would react with the catalyst, preventing the formation of the porphyrinogen.

RESULTS AND DISCUSSION

2 *Beta*-functionalisation of A₄ porphyrins

2.1 Aim of the work

The aim of the work was to build a library of conjugatable and water-soluble oxygen-sensing porphyrins to obtain oxygen-sensing biomaterials for application in the biomedical field.

In this section of the work, the synthesis of symmetrical porphyrins A₄ and their subsequent functionalisation with a carboxymethyl group on the *beta* position of the structure will be described, as shown in *Scheme 4*. The side chain was strategically placed on the *beta* position, to leave the four aryl rings on the *meso* positions available for further functionalisation in order to impart water-solubility to the whole structure. The *beta* carboxylic acid, once activated, would be exploited as anchoring moiety to covalently link the dye to a solid support, made of biocompatible polymers. As mentioned previously, the presence of a conjugatable group was deemed necessary to prevent the leaching of the dye from its support.
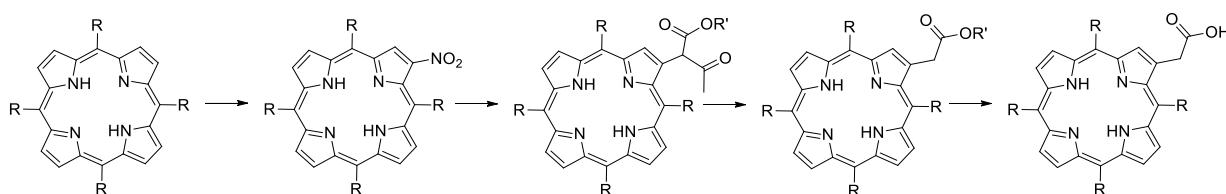
Scheme 4: general strategy for beta-functionalisation

2.2 Synthesis of A₄ porphyrins

The first approach employed to obtain a library of *meso*-substituted porphyrins was the Adler-Longo synthesis. According to this approach, pyrrole was added dropwise to refluxing solutions of aromatic aldehydes in propionic acid.[155] The method does not require any specific precautions and once the porphyrinogen is formed, it is oxidised by atmospheric oxygen to give the desired porphyrin. The simplest way to isolate the crude porphyrin was to filter it from the cooled reaction mixture and washing the solid with water and warm MeOH.[155] Despite the straightforward character of this method, in our hands it afforded little or no product due to partial and poorly reproducible solubility of the porphyrin in the solvent. The problem was circumvented by evaporation of the propionic acid under reduced pressure, and a filtration on silica pad and further crystallisation from DCM/MeOH to obtain the desired compound.

A general porphyrin structure **79** with different *meso*-substituents (**a**-**f**) is shown in *Figure 23.* The choice of different aldehydes was dictated by the interest in obtaining porphyrin with different

electronic features for the subsequent synthetic steps. Thus, the library included porphyrin with both electron withdrawing groups (EWG) such as fluorine (**c**), trifluoromethyl (**b**) and pyridyl (**f**), and electron donating groups (EDG), like methoxy (**d**,**e**) and the unsubstituted phenyl ring (**a**). A relatively wide range of aldehydes would provide a better platform to assess the applicability of the synthetic method, explained in detail later.

79
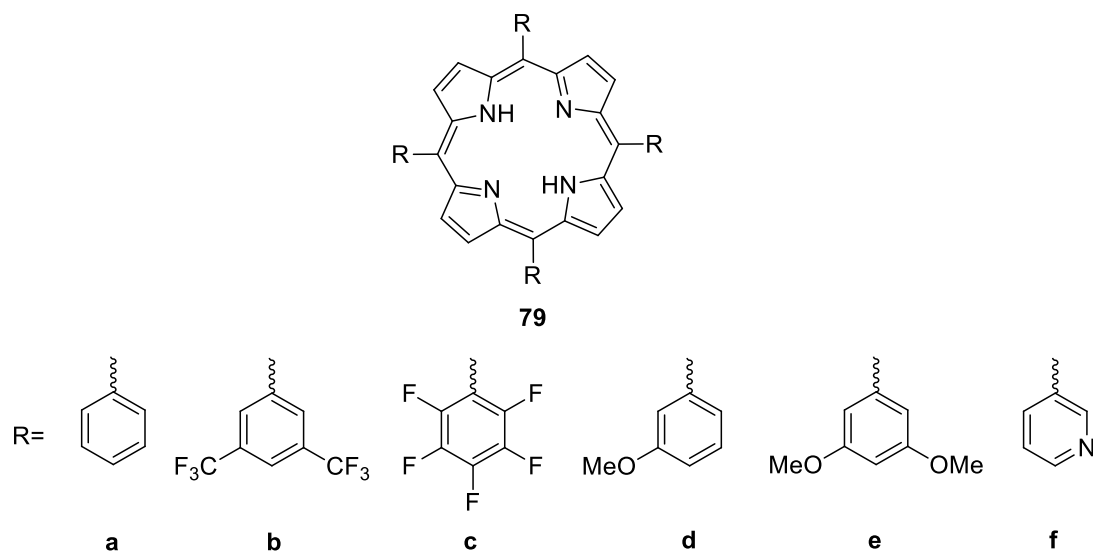
Figure 23: porphyrin general structures

Attempts to improve the yields by varying the reagents concentration, did not lead to significant variation on the yields, as shown in *Table 1*. Only compound **79c** displays a different result, a roughly five times lower yield than other porphyrins. As the pentafluorobenzaldehyde is the most expensive and most unstable aldehyde in the series, a different synthetic method was required.

Porphyrin	Propionic acid (mL)	Pyrrole (mL)	Yield (%)
79a	220	10	15
79b	120	2	14
79c	500	5	3.6
79d	500	5	14
79e	500	5	15
79f	220	10	12

Table 1: porphyrins synthesis conditions and yields

In the attempt to improve the yields of the starting porphyrins the focus was turned to the synthetic approach developed by Lindsey.[157] Thus, **79c** was successfully synthesised employing a modified

Lindsey approach, increasing the yield from 3.6 % to 38 % (*Table 2*).[160] According to this method, the reaction is carried out at a 10-fold higher reagent concentration compared to the conditions described by Lindsey. Under these conditions, dry solvent and inert atmosphere become pivotal as the yield is more sensitive to the presence of water and air. However, the method offers the advantages of reducing the dilution, hence improving the scalability and increasing the yield of a reaction whose starting material is rather expensive (pentafluorobenzaldehyde).

3,5-(bis-trifluoromethyl)phenyl porphyrin (**79b**) was also synthesised employing similar conditions, with higher reagent concentration compared to the original Lindsey method.[160] *Table 2* shows the differences in yield and reaction conditions for these two porphyrins.

Porphyrin	Rothemund			Lindsey		
	Propionic acid (mL)	Pyrrole (mL)	Yield (%)	DCM (mL)	Pyrrole (mL)	Yield (%)
79b	120	2	14	300	0.5	34
79c	500	5	3.6	600	1	38

Table 2: comparison between Rothemund and Lindsey reaction conditions and yields

^{1}H-NMR analysis of the porphyrin shows in all cases a peak at *ca.* 8.90 ppm with an integral value of 8H, generated by *beta*-hydrogens. Another peak common to all the spectra, at *ca.* −2.80 ppm, is generated by the internal hydrogens. Due to the high symmetry of the molecules, all the *beta*-hydrogens resonate at the same frequency, resulting in a singlet. NMR and UV-vis data are summarised in *Table 3*. The Soret band of all derivatives has its maximum between 410 nm and 422 nm, in line with the behaviour of porphyrins.[161]

Porphyrin	β-H	H_{int}	Soret (nm)	Logε
79a	8.90	−2.69	417	5.91
79b	8.80	−2.86	417	5.71
79c	8.91	−2.91	410	5.40
79d	8.90	−2.77	422	5.59
79e	8.94	−2.82	421	5.61
79f	8.91	−2.75	418	6.93

Table 3: chemical shifts of beta and internal hydrogens, plus Soret band and Logε values

2.3 Nitration of A₄ porphyrins

Porphyrin **79f** (*Figure 23*) is discussed separately from the other substrates, due to the different method required for the insertion of the nitro group on the *beta* position.
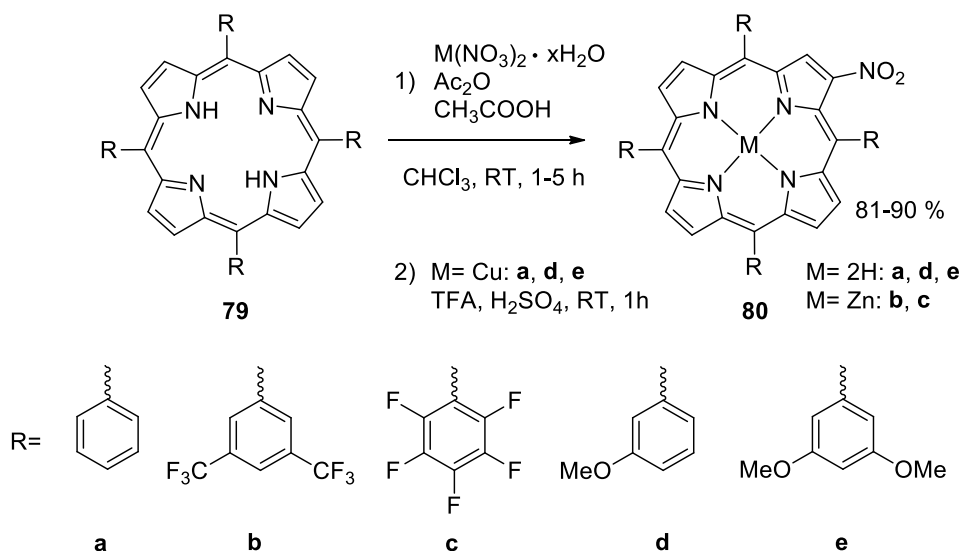
Scheme 5: nitration reaction

In order to insert a conjugatable moiety, later exploited to covalently link the porphyrin to a support or scaffold, a synthetic approach involving the insertion of a nitro group on the *beta* position of the porphyrin was chosen as the first step.[162] In this reaction the nitro group replaces a *beta*-hydrogen on the macrocycle, as shown in *Scheme 5*.[163] The reaction is performed employing a nitrate salt, usually copper or zinc.[164,165] Firstly the metal coordinates the macrocycle, and then the nitro group replaces a *beta*-hydrogen, as illustrated in *Scheme 6*.
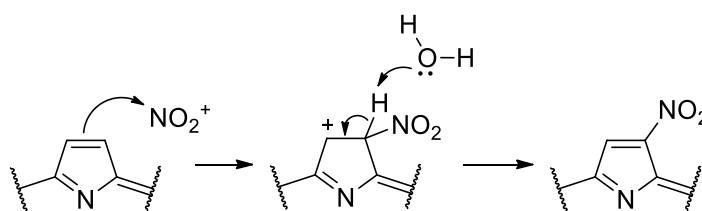
Scheme 6: nitration mechanism

Zinc offers the advantage of being easily removed from most porphyrins in the presence of acids, thus allowing metal exchange at a later stage. In addition, the nitration with zinc nitrate yields a diamagnetic species, which can be analysed by NMR spectroscopy. Copper, on the other hand, requires stronger acidic medium to be expelled from the porphyrin, and copper porphyrin complexes are paramagnetic, preventing NMR analysis. Despite many advantages of the zinc salt, copper nitrate

was chosen as metal salt for most of the porphyrins, because the nitration reaction progress is sluggish with zinc nitrate. It is worth noting that other metal nitrates can be used for the nitration reaction, but they can lead to species that cannot be easily demetallated or are more expensive for the purpose.[166]

Temperature control is an extremely important parameter for the outcome of the reaction. If not monitored, the reaction can progress to give doubly-nitrated species.[164] The second nitro group can insert in several positions of the porphyrin, leading to the formation of different porphyrins and giving an isomeric mixture very difficult to separate by column chromatography. Therefore, it is more convenient to stop the reaction as soon as traces of doubly-nitrated products are detected, even if the starting material is still present in the reaction mixture. The metal porphyrin not yet nitrated can be recycled and reused for another nitration. *Table 4* shows the nitration conditions for all the different substrates synthesised, except for tetra(3-pyridil) porphyrin (**79f**), which needed different reaction conditions, and it will be discussed separately.

Porphyrin	Yield (%)	Solvent	Metal salt	Time (h)	T (°C)
80a	89	chloroform	$Cu(NO_3)_2$	5	RT
80b	86	chloroform	$Zn(NO_3)_2$	1.5	RT
80c	83	chloroform	$Zn(NO_3)_2$	2	RT
80d	81	chloroform	$Cu(NO_3)_2$	1	RT
80e	90	chloroform	$Cu(NO_3)_2$	5	RT

Table 4: nitration reaction conditions and yields

The yields of the reaction are excellent and comparable among the different porphyrins, between 81 % and 90 %, and the values are in line with the literature data.[167] The solvent employed for all the substrates was chloroform and the reaction was performed at room temperature in all cases. In the case of porphyrins **79b** and **79c** it was found that zinc nitrate gave better yield, whereas copper nitrate was used for the remaining substrates as no nitration occurred employing the zinc salt with compounds **79a**, **79d** and **79e**.

The ^{1}H-NMR spectra of nitro-porphyrins shows that the presence of the nitro group has a large impact on the multiplicity of the signals. The singlet at *ca.* 8.90 ppm, assigned to *beta*-hydrogens, splits into several signals as a consequence of the asymmetry introduced in the structure by the nitro group. *Figure 24* shows the multiplicity of *beta*-hydrogens for porphyrin **80c**. The multiplicity changes from a singlet to a multiplet plus a singlet with integral values of 6H and 1H, respectively. The chemical shift of the multiplet is roughly the same as before, while the singlet appears almost 0.40 ppm downfield.
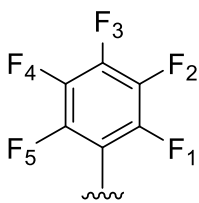
This effect is present not only in the ^{1}H-NMR spectra, but also in the ^{19}F-NMR, for porphyrins **80b** and **80c**. Porphyrin **80c** presents three main peaks, relative to *ortho*, *para* and *meta* fluorine, respectively, with increased multiplicity compared to the starting porphyrin, indicating a loss of symmetry. *Figure 25* shows the fluorine signal splitting before and after the nitration reaction. Before the introduction of the nitro group in the molecule, the multiplicity of the peaks arises from the fluorine-fluorine coupling.[168–170] The *ortho* fluorine (F_1) appears as a doublet of doublets, due to an *ortho*-coupling with the *meta* fluorine (F_2) and a *para*-coupling with the *meta* fluorine (F_4). *Para* fluorine (F_3), instead, appears as triplet due to the *ortho*-coupling with the magnetically equivalent *meta* fluorines (F_2, F_4). The last peak is generated by *meta* fluorine (F_2), and it appears as a triplet of doublets due to the *ortho*-coupling with two magnetically equivalent fluorines (F_1, F_3), and a para-coupling with the other *ortho* fluorine (F_5). The splitting pattern is similar to the one produced by the hydrogens of a phenyl ring.
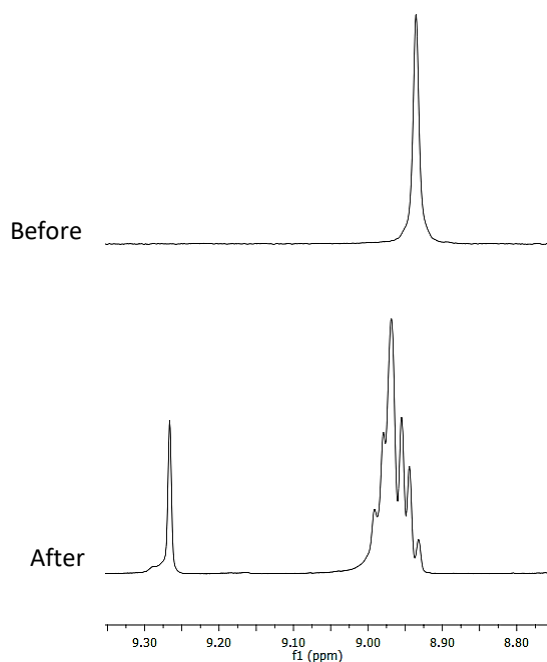
*Figure 24: ^{1}H-NMR spectrum comparison of pyrrolic hydrogens before and after nitration reaction for **80c** in CDCl$_3$ at 298 K and 300 MHz*

After nitration, and consequent introduction of asymmetry in the molecule structure, the ^{19}F-NMR appears markedly different. O*rtho*-fluorine appear as three peaks, each of them doublet of doublets. *Para*-fluorine splits into three triplets, and *meta*-fluorine into three triplets of doublets. Integration of the signals shows that each peak of the starting compound has split into three peaks with a 2:1:1 ratio.
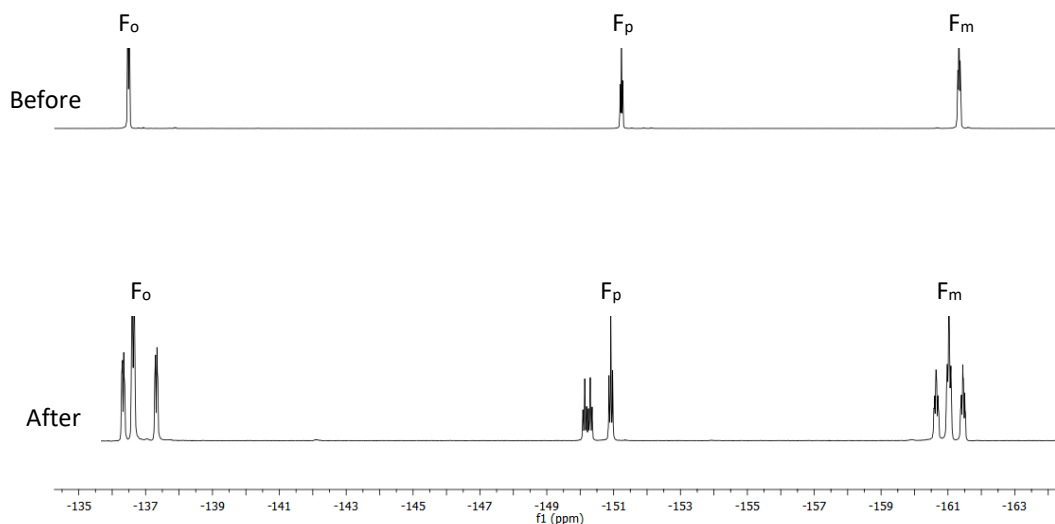
*Figure 25: $^{19}F\{^1H\}$-NMR spectrum comparison before and after nitration reaction for porphyrin **80c** in CDCl$_3$ at 298 K and 282 MHz*

These data indicate that the pentafluorophenyl rings of the porphyrin are located in three different environments, one of which contains two rings and gives signals that integrate for twice as many fluorines. The macrocycle can then be divided in four parts: one bearing the nitro group, two equivalent ones *cis*, and the last one *trans* to the part bearing the nitro group, as shown in *Figure 26*.
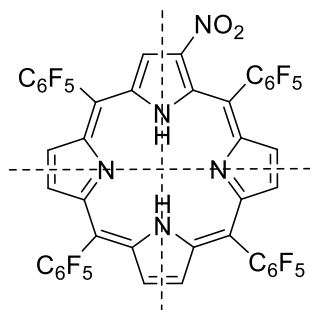
*Figure 26: possible asymmetry pattern in **80c***

The effect mentioned above is more pronounced for porphyrin **80c** than for porphyrin **80b**, for which very small changes in chemical shifts and multiplicity are observed.

| | Before nitration | | | |
Porphyrin	β-H	H_{int}	Soret (nm)	Logε
79a	8.90	−2.69	417	5.91
79b	8.80	−2.86	417	5.71
79c	8.91	−2.91	410	5.40
79d	8.90	−2.77	422	5.59
79e	8.94	−2.82	421	5.61

	After nitration			
80a	8.76-8.90	−2.56	427	5.80
80b	8.83-9.11	-	430	5.11
80c	8.93-9.27	-	422	5.60
80d	8.78-9.13	−2.62	430	5.56
80e	8.93-9.19	−2.62	434	5.38

Table 5: NMR and UV-Vis data before and after nitration

As shown in *Table 5*, in all cases the splitting in the *beta* hydrogens is observed after insertion of the nitro group. A general downfield shift for both internal and *beta* hydrogens is also observed. Some peaks, resulting from the splitting induced by the asymmetry, shifted downfield by 0.2-0.3 ppm. This effect is due to the electron withdrawing nature of the nitro group that subtracts electron density from the macrocycle leaving the system more electron poor. The introduction of the nitro group causes a red shift in the Soret band on the UV-vis absorption spectrum for all the substrates. This type of shift have been ascribed to the extension of the conjugation in the system by the nitro group, and a decrease in the HOMO-LUMO energy gap.[164,171,172]

2.4 Michael-like addition/elimination on nitroporphyrins
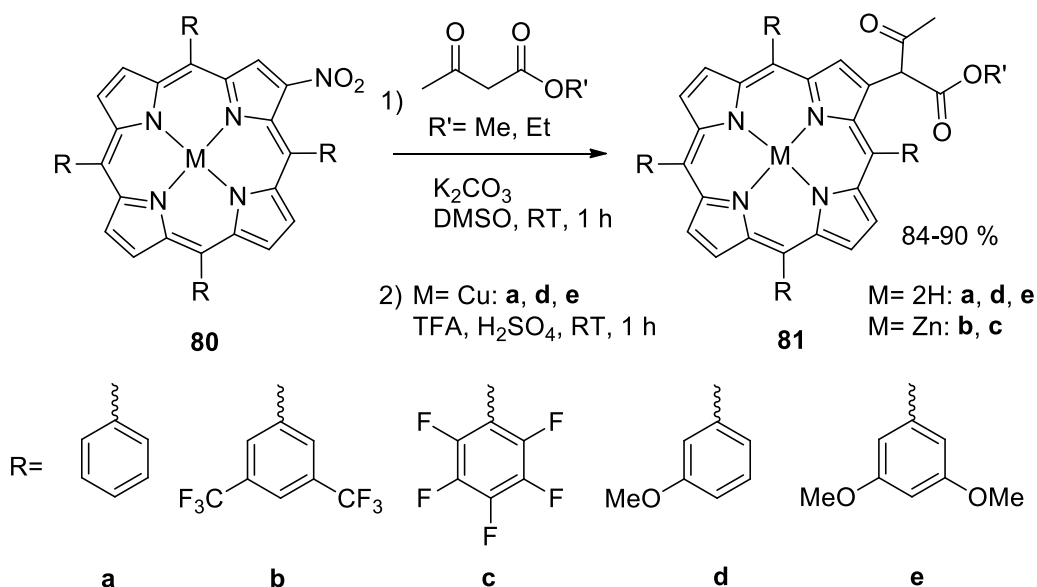
Scheme 7: Michael-like addition/elimination reaction scheme

Nitro group on the *beta*-position of the porphyrin can be successfully replaced by a nucleophile to build the conjugatable moiety for conjugation to protein scaffolds.[162] Different types of nucleophile can be employed for the addition/elimination reaction, and in general "S and O nucleophiles" like thiolates are thought to perform an *ipso*-attack[166,173,174] on the same position of the nitro group. On the other hand, "C nucleophiles" such as 3-ketoesters[175] preferentially react on the *beta*-position next to the nitro group in the same addition-elimination process, as shown in *Scheme 8*.[176–178]

The nucleophiles chosen for this work were ethyl and methylacetoacetate,[175] whose structure is shown in *Scheme 7*. The nucleophile is dissolved in dimethyl sulfoxide (DMSO) with a non-nucleophilic base (in this case K$_2$CO$_3$), which is necessary to deprotonate the *alpha*-carbon and form the reactive anion. Despite K$_2$CO$_3$ being not completely soluble in DMSO the deprotonation was still effective. Once the nucleophile was activated, the porphyrin was added to the mixture. Porphyrin **80c** was the first substrate on which this reaction was attempted. Carrying out the reaction in DMSO led to the formation of a mixture of products. It can be reasoned that under the reaction conditions (alkaline environment) DMSO could lead to the decomposition of the porphyrin. Thus, the reaction was performed in different solvents to avoid side product formation. Ethyl acetate resulted to be the most suitable solvent, and after one hour of reflux the reaction reached completion. Similarly, short reaction time was required for porphyrin **80b**. On the other hand, porphyrin **80a** required up to 72 hours to reach completion. However, degradation of the substrate was observed after prolonged heating times. Changing back the solvent to DMSO drastically increased the reaction rates to 1 hour for both

porphyrins, at room temperature. Not only did DMSO make the reaction quicker, but it also increased the yield by 15 %. DMSO was also successfully employed for compounds **80d** and **80e**, affording good yields and no side products. In addition, the purification resulted easier and quicker with DMSO than with ethyl acetate: the desired product was isolated by filtration from the reaction mixture following addition of brine. Given the advantages of using DMSO as solvent for this reaction, the same procedure was extended also to porphyrin **80c**.
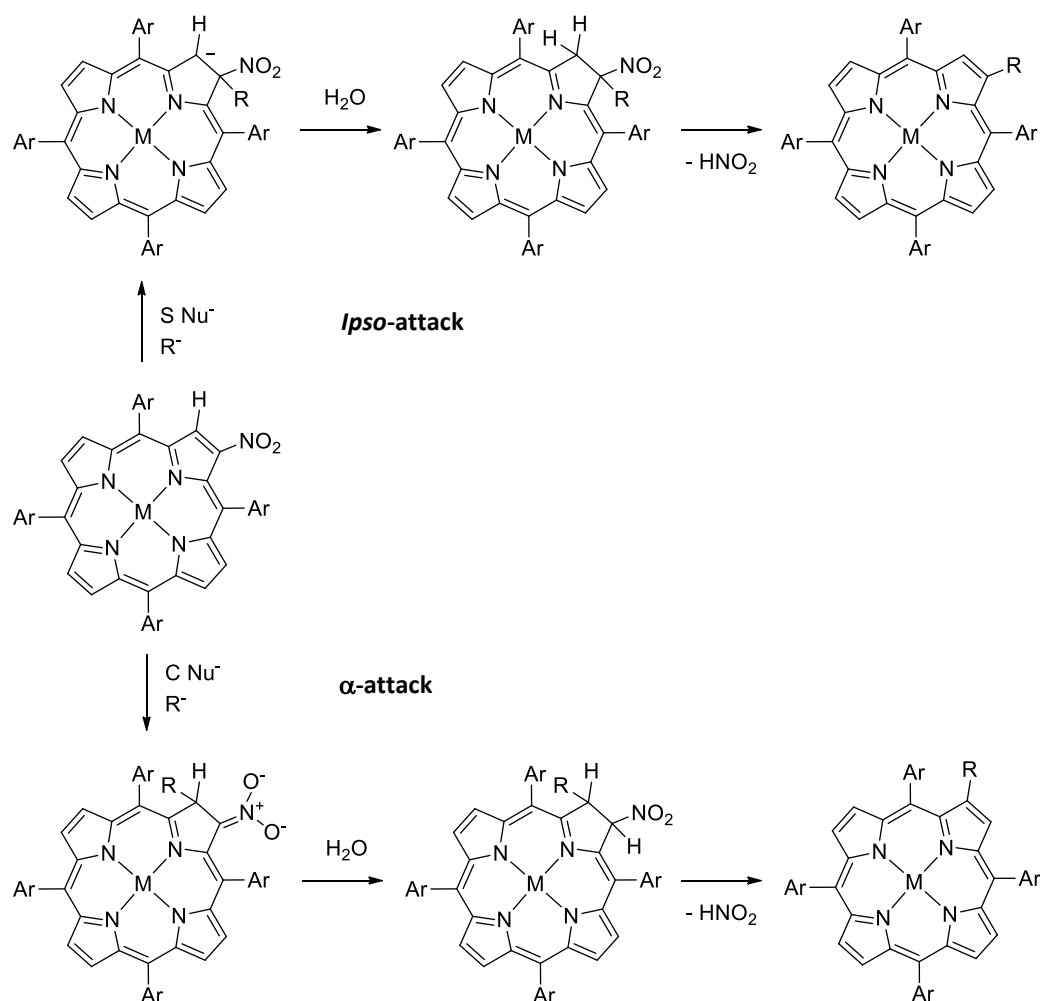
Scheme 8: nucleophile ipso- and α-attack on nitroporphyrins. Adopted from Serra et al. [162]

To stop or at least inhibit the formation of the side products, the reaction was performed in an ice bath. The nucleophile and the base were dissolved and sonicated in DMSO and cooled while vigorously stirring. The nitro porphyrin was then added to the mixture while still in the ice bath and the reaction was stopped few minutes later. As soon as the colour of the mixture changed from blue/purple to red, an indication of the reaction occurring, the mixture was poured in brine to stop the reaction. Any residual starting porphyrin was easily separated by column chromatography and used again. The lack of reaction completion was probably caused by the fact that DMSO solidifies at the reaction

temperature despite the vigorous stirring. *Table 6* shows the different reaction conditions for all the substrates.

Yields are comparable among the different porphyrins and vary between 84 % and 90 %. The yield of porphyrin **81c** increased notably after optimisation of the method. When performed in ethyl acetate, the reaction yielded just over 70 % of the product.

Porphyrin	Yield (%)	Time (h)	T (°C)
81a	88	1	RT
81b	85	1	RT
81c	90	5 min	ice-bath
81d	86	1	RT
81e	84	1	RT

Table 6: reaction conditions for Michael addition/elimination

All the Michael adducts synthesised bear a 1,3-ketoester moiety, and can exist in ketone or enol form: the peak at *ca.* 13 ppm, with integral value of 1H, is present in the spectra of all Michael adducts (see *Figure 27* for porphyrin **81c**) and it is generated by the OH proton of the enolic form, which for most of the Michael adduct seems to be the favoured one.[175]
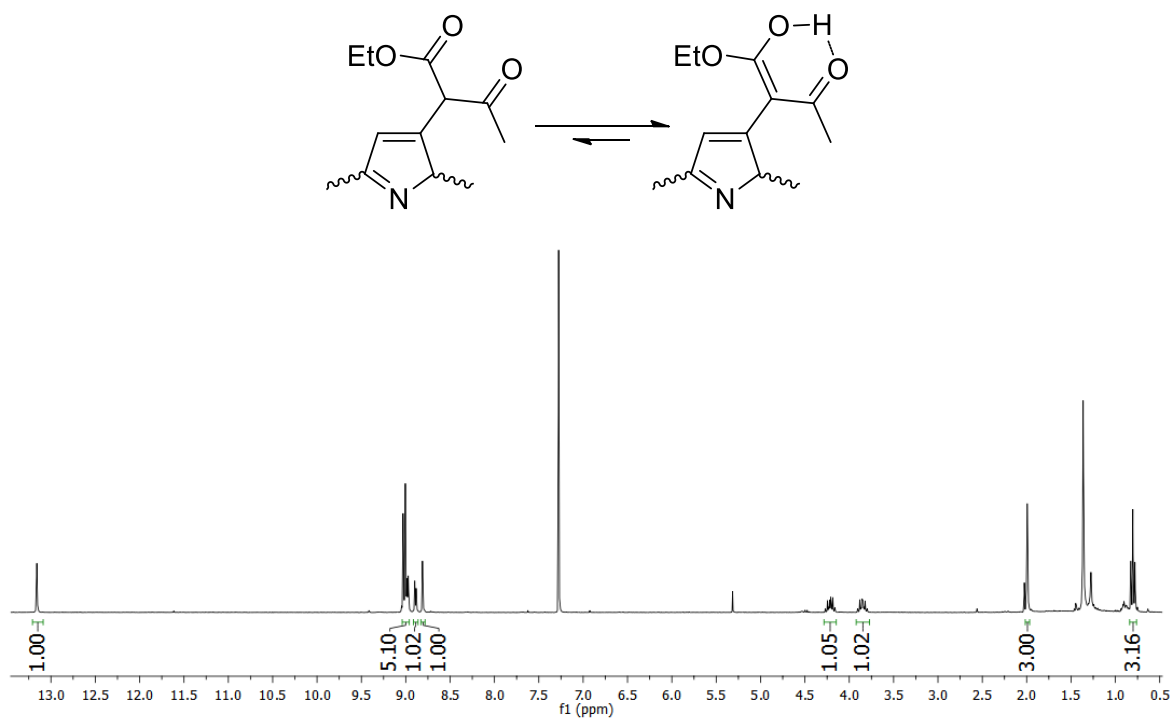
*Figure 27: ^{1}H-NMR spectrum of **81c**, plus keto-enolic equilibrium of Michael adduct in CDCl$_3$ at 298 K and 300 MHz*

The splitting of the *beta*-hydrogens remains the same, due to the asymmetry of the molecules. The aliphatic region presents two multiplets at *ca.* 4.0 ppm, each of which with integral value of 1H. These multiplets are generated by the two protons on the CH_2 in the ethoxy group, which due to the presence of a stereogenic centre, are diastereotopic, and as non-chemically equivalent hydrogens, they resonate at different frequency. Further upfield in the spectrum, a singlet and a triplet can be seen, which can be assigned to the methyl of the acetyl and ethoxy group, respectively, on the basis of their chemical shift and characteristic multiplicity.

Table 7 reports the nucleophiles employed and the chemical shifts of the Michael adducts, alongside with the position of the Soret band in the UV-visible spectrum and the corresponding Logε. The enolic proton resonates at *ca.* 12.8 ppm for all the porphyrins, except in the case of porphyrin **81c**, for which it is shifted downfield to 13.14 ppm. No internal hydrogens value (NH_{int}) appears for porphyrins **81b** and **81c** because these derivatives are zinc complexes.

In the case of porphyrin **81d**, obtained with ethyl acetoacetate, literature data suggest that the keto-enol equilibrium is shifted towards the ketone form, in a ratio 75:25.[175] However, the data collected suggest that the equilibrium in this case is shifted completely to the enolic form. Similarly, when methyl acetoacetate is employed, the equilibrium is shifted, as for other porphyrins, towards the enolic form.

Porphyrin	R of Nu⁻	OH (ppm)	β-H (ppm)	NH_{int} (ppm)	Soret (nm)	Logε
81a	ethyl	12.85	8.64-8.87	−2.68	419	5.62
81b	methyl	12.83	8.87-8.96	-	430	5.11
81c	ethyl	13.14	8.79-9.01	-	422	5.65
81d	methyl	12.87	8.74-8.92	−2.72	423	5.59
81e	methyl	12.91	8.72-8.92	−2.79	424	5.50

Table 7: NMR and UV-Vis data of porphyrins after Michael addition/elimination

2.5 Retro-Claisen cleavage of the moiety
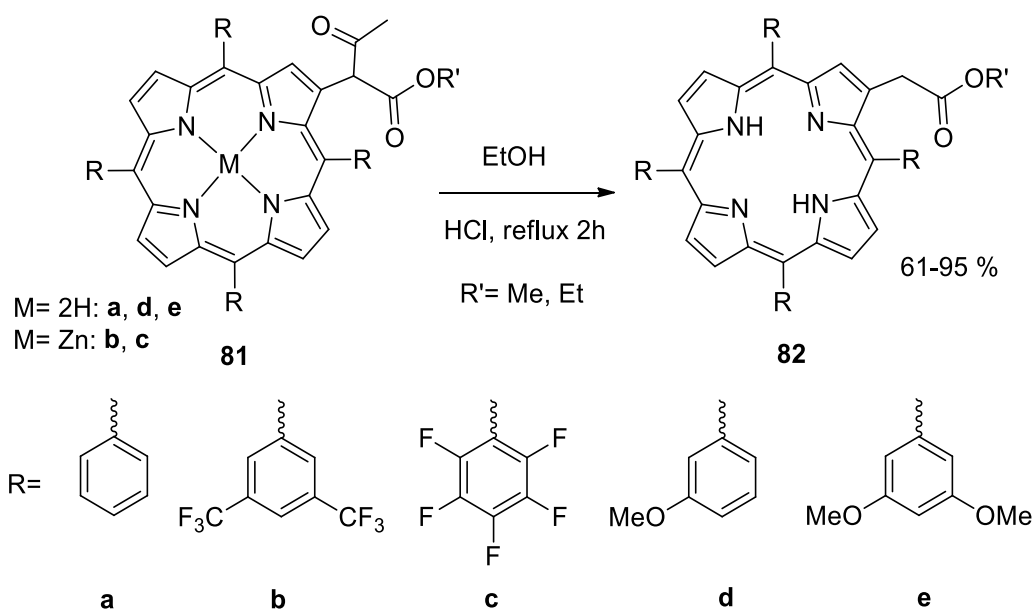
Scheme 9: retro-Claisen cleavage reaction scheme

Following Michael addition, the 1,3-ketoester moiety was transformed to obtain the final conjugatable group: a carboxylic acid. To unmask the carboxylic group, the Michael adduct needs first to lose the acetyl group, as shown in *Scheme 9*. The cleavage was achieved by refluxing the porphyrin in ethanol with 20 % aqueous HCl for two hours.[175] The concentration of the porphyrin in ethanol was a very important parameter for the reaction, because concentrated solutions caused the porphyrin to precipitate and prevented the reaction from reaching completion. In the case of compounds **81b** and **81c** the zinc complex was employed. As mentioned before, zinc (II) needs very mild reaction conditions to be removed from the macrocycle and 20 % HCl in ethanol is sufficient to promote demetallation. Porphyrins complexed with copper, on the other hand, need harsher reaction conditions to form the free base, and the reaction conditions for the Claisen cleavage are not sufficient for copper removal.[179,180] Crucially, when the copper complex was used as substrate of the Claisen cleavage, no desired product was detected. This led us to speculate that in this tandem reaction, demetallation occurs before the Claisen cleavage. In the case of porphyrins **82b** and **82d**, a transesterification took place during the reaction, and the Michael adducts obtained with methyl acetoacetate were transformed in the corresponding ethyl ester due to the use of ethanol as the reaction solvent. Using methanol as the solvent led to incomplete reaction even after prolonged reaction times, which can be ascribed to its lower boiling point. Interestingly, no transesterification was observed for **82e**, bearing the methyl ester group as well. *Table 8* shows the yield of the reaction, and the chemical shift of the *beta*, internal and the CH_2 group hydrogens, alongside with UV-vis data.

Porphyrin	Yield (%)	CH$_2$ (ppm)	β-H (ppm)	NH$_{int}$ (ppm)	Soret (nm)	Logε
82a	69	3.99	8.64-8.88	−2.69	418	5.98
82b	75	3.97	8.52-8.84	−2.81	421	5.68
82c	95	4.32	8.72-8.94	−2.85	415	5.59
82d	61	3.98	8.73-8.94	−2.71	421	5.64
82e	62	4.15	8.74-8.94	−2.82	423	5.58

Table 8: yield of the retro-Claisen cleavage and some NMR and UV-vis data

2.6 Hydrolysis of ester moiety
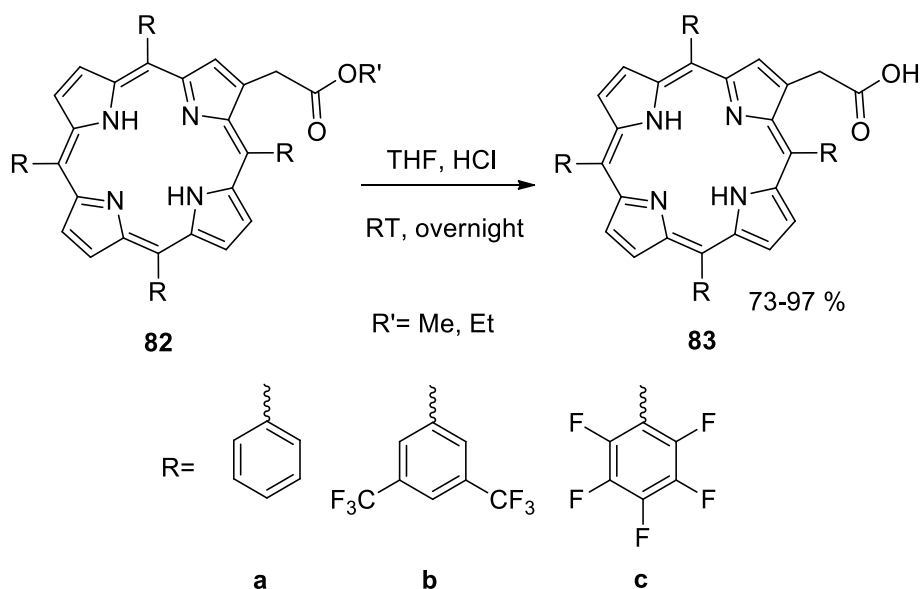
Scheme 10: Hydrolysis reaction scheme

The following step in the synthesis of the target conjugatable derivatives is the hydrolysis of the ester moiety, as shown in *Scheme 10*.[181] The reaction can take place in both acidic and basic conditions. We previously verified that **79c** undergoes degradation in basic media, so the reaction was carried out in concentrated aqueous HCl. In these conditions, the reaction time was very long (from 48 hours to two weeks) and complete conversion was never achieved. The poor solubility of porphyrins in water contributed to the inefficiency of this transformation, and indeed we verified that the addition of a co-solvent helped solubilisation, markedly shortening the reaction time and increasing the yield of the product. Thus, **82c** was dissolved in tetrahydrofuran (THF) and the resulting solution was treated with concentrated aqueous HCl. Complete conversion was achieved after overnight stirring at room temperature. Unlike what we observed in alkaline conditions, the acidic environment did not cause

alteration or degradation of the porphyrin. The same procedure was applied for all other substrates. *Table 9* shows selected spectroscopic data. It is worth noting that no COOH peak was detected on the ^{1}H-NMR spectra of the substrates, probably due to deuterium exchange with CDCl$_3$.

Porphyrin	Yield (%)	^{1}H-NMR			^{13}C-NMR		UV-Vis	
		CH$_2$ (ppm)	β-H (ppm)	NH$_{int}$ (ppm)	CH$_2$ (ppm)	COOH (ppm)	Soret (nm)	Logε
83a	97	4.00	8.63-8.87	−2.72	35.8	177.0	419	5.62
83b	73	4.01	8.50-8.82	−2.83	35.9	176.3	430	5.11
83c	78	4.36	8.72-8.95	−2.86	35.7	175.8	422	5.65

Table 9: Yield of hydrolysis and some ^{1}H-NMR,^{13}C-NMR and UV-Vis data

In the case of compounds **82d** and **82e** a one-pot deprotection of the ester and the methoxy groups on the aryl rings was attempted, to simultaneously unmasking the conjugatable group and impart water solubility to the porphyrin. Treatment of porphyrins **82d** and **82e** with BBr$_3$, the most common cleaving agent for aromatic methoxy groups, led to the formation of a mixture of products, presumably due to partial deprotection of the aromatic methoxy groups and partial cleavage of the carboxymethyl chain on the *beta* position. Column chromatography did not resolve the mixture due to the small difference in R$_f$ of the various products formed. Any attempt to force the reaction to completion (*i.e.*, complete cleavage of methoxy groups and of ester function) resulted in the degradation of the starting material and no evidence of formation of the desired product. For this reason, we decided to not proceed further to investigate the *beta* functionalisation of porphyrin **82d** and **82e**.

2.7 Water solubilisation of porphyrins

With the carboxylic group in place, the attention was focused on providing the porphyrins with water solubility. The different porphyrin structures required different synthetic approaches to reach this goal, however a general strategy for porphyrins **83a** and **83c** is illustrated in *Figure 28*.
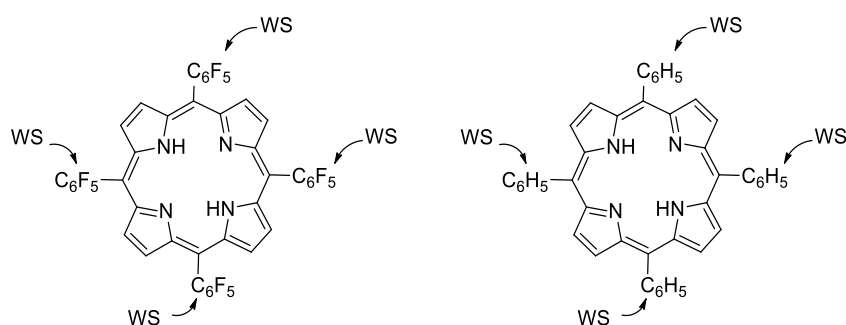
Figure 28: general water solubilisation reaction

Very few methods already exist to make **79c** water-soluble. All of them exploit the ability of the porphyrin to behave as an electrophile in aromatic nucleophilic substitution. Different nucleophiles have been employed for the purpose, such as sugars,[182] PEG chains[183] and cyclodextrins,[184] and many examples can be found where the *para* fluorine on the aryl rings is replaced by nucleophiles appended to hydrophobic groups.[185] In the majority of the examples, the nucleophilic displacing groups are thiols, amines and alcohols. Amines have been frequently used to functionalise pentafluorophenyl porphyrin. A base must be used to neutralise the hydrofluoric acid produced by the substitution, allowing the reaction to reach completion. The base must be non-nucleophilic to avoid possible competition with the desired nucleophile. *Table 10* shows the amines used in this work and the reaction conditions adopted. The conditions for the substitution reaction were optimised on **79c** before proceeding to functionalise **83c**.

Thanks to the presence of the strongly acidic sulphate group, taurine (**84** in *Table 10*) greatly enhances the aqueous solubility of the porphyrin independently of the pH. *Beta*-alanine (**85**), which bears a carboxylic group, can impart solubility at neutral and basic pH. Propargylamine (**86**) is not an intrinsically water-solubilising group but it can serve as substrate for further transformation *via* "click-chemistry".[186] A variety of solvents, either alone or mixed with a co-solvent, were employed for the substitution reaction. Co-solvents were employed to guarantee the solubility of the starting materials, mostly the amines. The reactions were performed in the presence or absence of a base, using either conventional or microwave-assisted heating approaches. Identification of reaction conditions that would lead to the formation of the desired tetra-substituted compound was not possible. In all cases,

mass spectrometry analysis of the reaction mixture revealed the presence of a mixture of compounds with different degrees of substitution (mono- to tetra-substitution).

Nucleophile	Solvent	Base	T (°C)	Time	MW
84 $H_2N\diagdown SO_3^- \ Li^+$	CHCl$_3$:MeOH, 5:1	-	140	10 min	√
	DMSO	-	140	5 min	√
	MeOH	K$_2$CO$_3$	reflux	1 h	-
	THF:H$_2$O, 3:1	K$_2$CO$_3$	120	30 min	√
	DMF	K$_2$CO$_3$	reflux	1 h	-
	NMP	-	200	15 min	√
	NMP	K$_2$CO$_3$	200	overnight	-
85 $H_2N\diagup\diagdown COOH$	acetone:H$_2$O, 3:1	K$_2$CO$_3$	130	5 h	√
	NMP	K$_2$CO$_3$	200	2 h	√
	DMF	KOH	130	3 h	-
	DMSO	K$_2$CO$_3$	200	1 h	√
	benzonitrile	K$_2$CO$_3$	220	1 h	√
	MeCN:H$_2$O, 2:1	K$_2$CO$_3$	150	2 h	√
	Ph$_2$O	K$_2$CO$_3$	200	2 h	√
86 $H_2N\diagdown$	Acetone:H$_2$O, 3:1	K$_2$CO$_3$	120	1 h	√
	NMP	-	190	45 min	√
	NMP	K$_2$CO$_3$	200	15 min	√
	DMF	-	80	overnight	-
87 HS	NMP	-	180	15 min	√
88 HS OH	DMF	-	80	overnight	-
89 NH$_2$	NMP	-	180	10 min	√
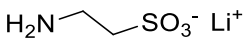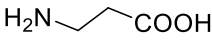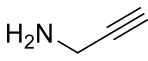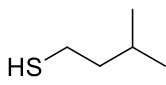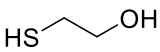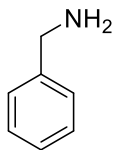
Table 10: different WS moieties and reaction conditions for nucleophilic substitution

Prolonged heating times, especially under microwave irradiation, resulted in degradation of the reagents. Due to the high polarity of the substitution products with compounds **84** and **85**, column chromatography was not viable for the isolation of the species obtained. Preparative-HPLC and -TLC were not considered viable options to purify the compounds due to the reduced amount of material they allow to process. Three other nucleophiles were employed in the optimization process of the reaction: two thiols (**87** and **88**) and one amine (**89**), all soluble in organic solvents. *Table 10* shows their structures and the reaction conditions. In the case of compounds **87** and **88** incomplete functionalisation was obtained, while the product of tetra-substitution was detected in the case of the benzylamine (**89**). Although thiols are reported to have a higher reactivity in aromatic nucleophilic displacement on porphyrins with respect to amines,[185] in our hands the reaction of **79c** with thiols **87** and **88** brought to the formation of a mixture of species with different degrees of substitution. This behaviour was attributed to the low solubility of the products derived from partial substitution in the reaction solvent. Further attempt to reach a full functionalisation was pursued through the employment of a phase transfer catalyst (PTC). Tetrabutylammonium chloride was chosen as PTC, **84** as nucleophile and a mixture of chloroform and water as solvent. These conditions did not lead to the formation of the desired products, neither at room temperature nor at high temperature.

Encouraging results were obtained when the reaction was carried out on the zinc complex of **79c** (**90** in *Scheme 11*). The reaction was performed with 20 equivalents of taurine (**84** in *Table 10*) per equivalent of porphyrin, which corresponds to a 5:1 ratio of nucleophile per leaving group. Lithium taurine **84** was obtained by treating taurine with lithium hydroxide: this is necessary to ensure the nucleophilicity of the amino group.[187,188] Overnight reflux in N-methyl-2-pyrrolidone (NMP) in the presence of K_2CO_3 led to the formation of the desired tetra-substituted product (**91**), even though neither **84** nor the base appeared to be completely soluble in the reaction medium (*Scheme 11*). A shorter reaction time or a lower reaction temperature yielded not only the tetra-substituted product, but also traces of the tri-functionalised one. Once the reaction conditions were optimised, the nucleophilic substitution was carried out on **83c**.

The reaction led to the formation of the desired product, but unfortunately, a side product was also generated: the substituent on the *beta* position underwent decarboxylation leaving the porphyrin with a *beta* methyl group. It was speculated that this was caused by the high reaction temperature. Attempts to reach fully substitution at a lower reaction temperature resulted in partially functionalised products, even with reaction times of up to two weeks. The use of other transition metals, such as copper or palladium did not improve the reactivity of the porphyrin towards the substitution, resulting in every case in incomplete functionalisation and/or the loss of the inserted carboxylic group.
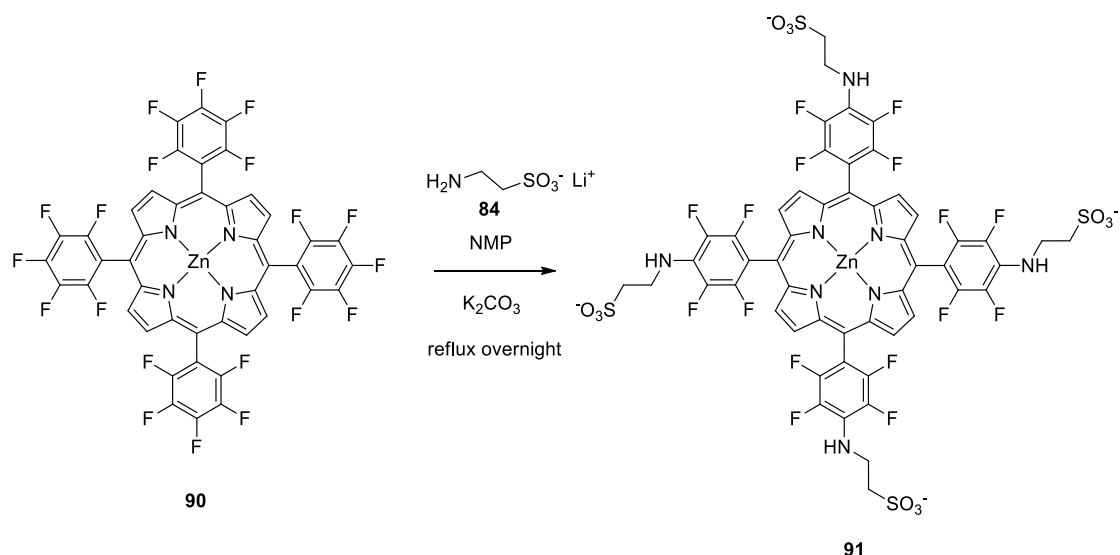
*Scheme 11: reaction between the zinc complex of **79c** and lithium taurine **84***

Once the reaction conditions were optimised, the challenge was the purification of a water-soluble nucleophile (taurine) from a water-soluble porphyrin functionalised with the same moiety. No method was available for such separation apart from preparative-HPLC. The crude product was isolated by pouring the reaction mixture in diethyl ether and filtering off the solid. As expected, ^{1}H-NMR analysis showed unreacted taurine. If the solid was dissolved in methanol or ethanol, and the solution left in the fridge for few hours, a white precipitate started to form, which proved to be unreacted taurine. After several steps of fractioned precipitation at low temperature, traces of unreacted taurine were still observable during the spectroscopic measurements.

The results show that the *beta* insertion of the carboxylic acid on **79c** was successful and gave good yields. The synthetic steps do not require harsh reaction conditions and can be performed with commercially available reagents. The overall synthesis can be easily scaled up to gram-scale maintaining the same reaction conditions. Unfortunately, though, the insertion of water-soluble moieties was unsuccessful. Complete functionalisation was achieved at the expense of the loss of the conjugatable functionality. Due to the reasons mentioned above, this approach was not considered viable for the preparation of the target water-soluble, conjugatable oxygen sensing species.

To prove that the high reaction temperature was the cause of the decarboxylation (*Scheme 12*), a test was performed on the *beta*-functionalised substrate **83c**. The porphyrin was dissolved in NMP and heated to 200° C for five minutes in a microwave reactor, in conditions similar to the reflux in NMP. Microwave heating was adopted to reach the desired temperature faster. The reaction gave a mixture of two porphyrins: the starting material and the decarboxylated derivative.
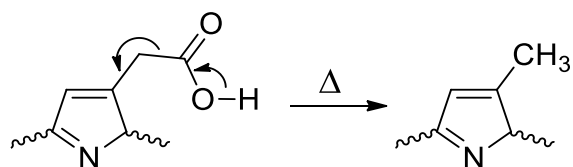
Scheme 12: decarboxylation reaction scheme

^{1}H-NMR of the mixture is shown in *Figure 29*. The characteristic porphyrin signals of *beta* hydrogens (8.70-8.95 ppm) and internal hydrogens at −2.87 ppm are present. The singlet at 4.36 ppm is the CH_2 group of the carboxylic group (see also *Table 9*), and the peak at 2.92 ppm was assigned to the methyl group formed (CH_3). Mass spectrometry also confirmed the presence of two compound: one matching the expected mass of **83c**, while the other one resulted in a loss of 44 units, weight of the CO_2 lost during the reaction.
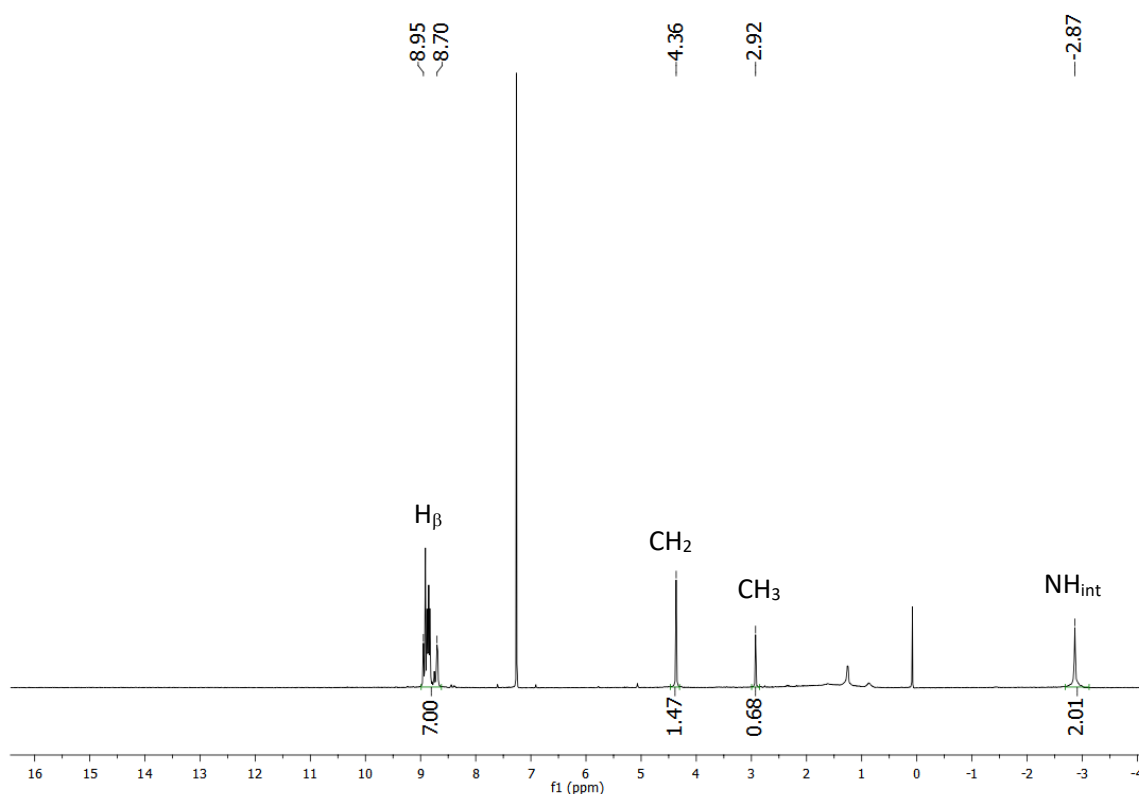
Figure 29: ^{1}H-NMR spectrum of **83c** after partial decarboxylation reaction in CDCl₃ at 298 K and 300 MHz

To prove that the decarboxylation reaction is not specific to **83c** but occurs also on other porphyrins, a test was performed on **83a**. As before, the porphyrin was dissolved in NMP and heated to 200 °C for five minutes in a microwave vial. The reaction yielded a mixture of compounds from which the product of the decarboxylation was isolated by column chromatography. The ^{1}H-NMR is shown in *Figure 30*. Seven *beta* hydrogens (8.63-8.87 ppm), 20 phenyl hydrogens (7.76-8.22 ppm) and the two internal

hydrogens with negative chemical shift are characteristic of **83a**. In the aliphatic region, a peak appears at 2.59 ppm, whose integration value is 3H. As in the case of **83c**, the peak generated by the methylene group at 4.00 ppm (*Table 9*) is no longer visible. Mass spectrometry also confirmed the molecular structure, highlighting a loss of 44 units, as seen before for **83c**.
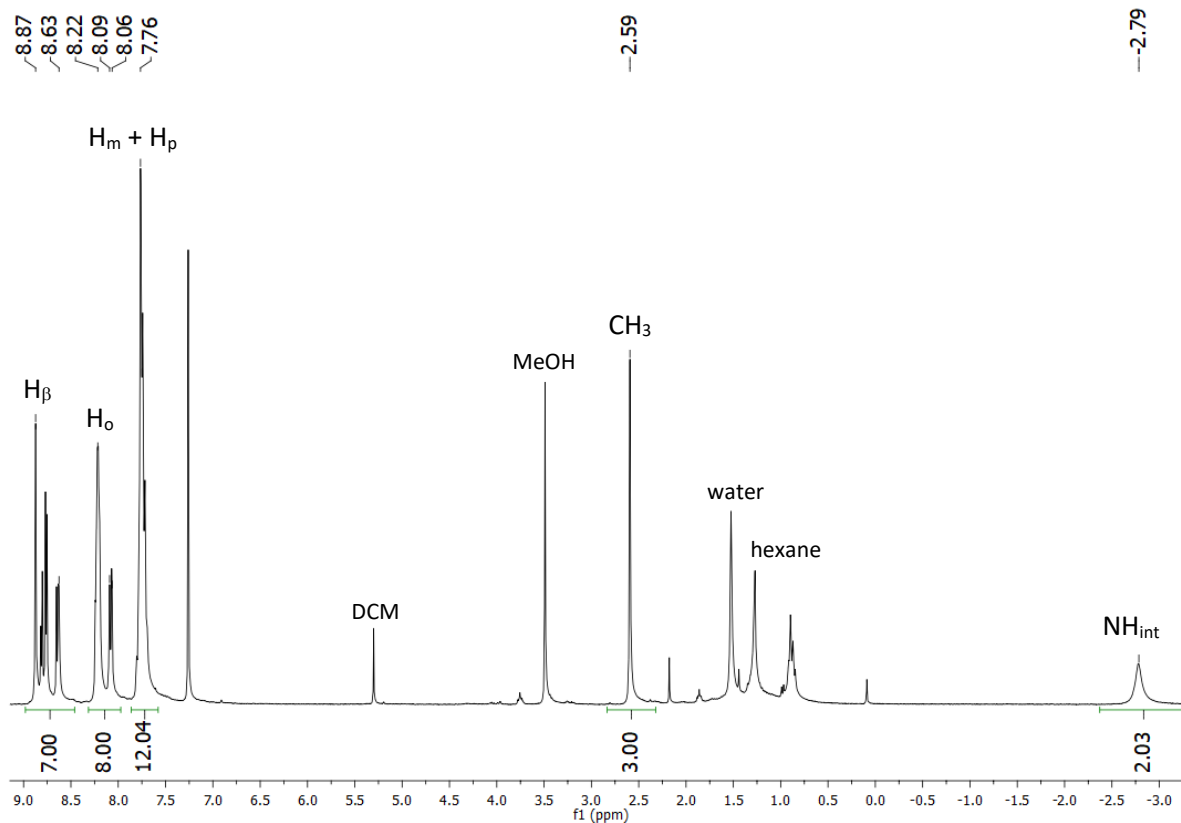

*Figure 30: ^{1}H-NMR spectrum of **83a** after decarboxylation reaction in CDCl$_3$ at 298 K and 300 MHz*
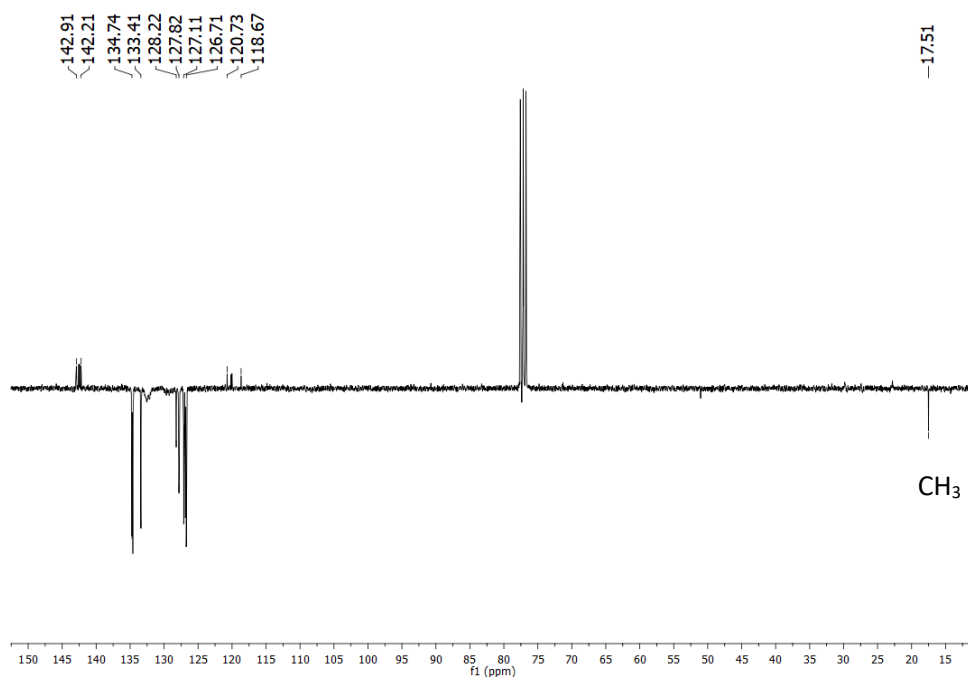
*Figure 31: ^{13}C{^{1}H}-NMR (DEPTQ) of **83a** after decarboxylation reaction in CDCl$_3$ at 298 K and 75 MHz*

^{13}C-NMR (DEPTQ) spectrum confirms the proposed structure. As shown in *Figure 31*, both the peak at 177.0 ppm and 35.8 ppm, due to the carboxylic acid and the CH_2 group, respectively, disappeared (*Table 9*). In addition, a peak in the aliphatic region appeared at 17.51 ppm (CH_3 *Figure 31*), further confirming that the decarboxylation took place. These findings suggest that despite the successful functionalisation on the *beta* position of different porphyrins via the Michael-Claisen approach, the species obtained are not stable at high temperatures, as they are prone to decarboxylation. This behaviour suggests that these *beta*-functionalised species are not ideal for insertion of platinum and palladium, as metal insertion, especially for platinum, requires high temperatures.

Tetraphenylporphyrin (**79a**) does not present any functionality that can be converted in a water-soluble group. An efficient method to make **79a** water-soluble is through the insertion of sulphate groups on the *para* position of the phenyl rings. This reaction can be performed either by treating the porphyrin with sulfuric acid,[189] or by using chlorosulphonic acid followed by a hydrolysis in water.[190–192] Each method presents advantages and disadvantages. The use of sulfuric acid allows the insertion of the desired function in a single step, but it makes the isolation and the purification of the water-soluble product more challenging, whereas the use of chlorosulphonic acid requires an additional step but the purification of the product is more straightforward. In the latter case, the chlorosulphonyl group is inserted by treatment with an excess of chlorosulphonic acid at room temperature, and the resulting porphyrin is refluxed in water overnight to hydrolyse the chlorosulphonic groups to sulphonates. Crucially, if the chlorosulphonation reaction reaches completion the subsequent hydrolysis step can be carried out on the crude material without further purification. In our hands, the reaction proceeded smoothly on **79a** as substrate, but when performed on the *beta* functionalised substrate **83a**, MS analysis showed that the porphyrin lost the entire carboxymethyl chain from the *beta* position. Complete loss of the chain on the *beta* position was also obtained when performing the reaction on **81a** or **82a**, highlighting the unstable nature of the side chain under the reaction conditions. We speculate that chlorosulphonic acid attacks the methylene adjacent to the carbonyl group, cleaving the chain on the *beta* position.[193] Reducing the equivalents of chlorosulphonic acid (4 equivalents) and/or reducing the reaction temperature (−10 °C) did not prevent the detachment of the side chain. Similarly to what was observed for **83c**, the desired *beta* functionalisation of **83c** was successfully achieved, but the reaction conditions to introduce the water-solubilising group were not compatible with the integrity of the carboxymethyl group. The behaviour observed for **83c** was the same as the one shown by porphyrins **82d** and **82e**, and in both cases, it led to a loss of the side chain from the *beta* position, caused by BBr_3 in the case of **82d** and **82e** and by HSO_3Cl in the case of **83a**.

2.8 β-functionalisation of 5,10,15,20-tetra(3-pyridyl) porphyrin

The starting porphyrin was obtained *via* the Rothemund synthesis, because the Lindsey approach cannot be used due to the basic nature of 3-pyridinecarboxaldehyde, which inactivates the Lewis acid catalyst and prevents the formation of the porphyrinogen. The yield of the reaction is shown in *Table 1* and it is in line with the previously reported data.[155]

Nitration

M= 2H **79f**, Cu **92**   M= Cu **93a**, 2H **93b**
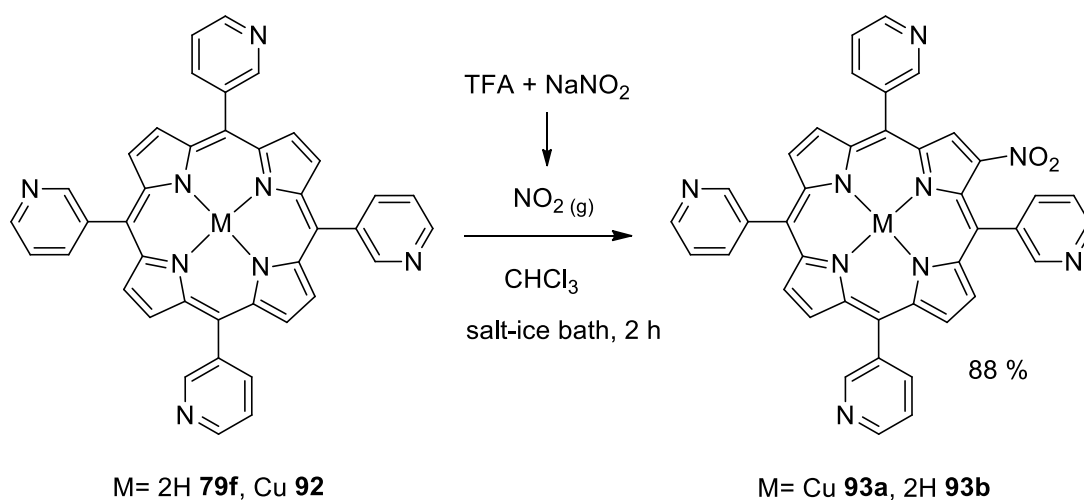
*Scheme 13: nitration reaction condition for copper complex of **79f***

Direct nitration of porphyrin **79f** in the presence of copper or zinc failed due to the formation of insoluble intermolecular complexes caused by the interactions of the pyridyl nitrogens with the metal ions.[194] To circumvent the problem, a different approach was adopted (*Scheme 13*): first the copper complex **92** was obtained by stirring a solution of porphyrin in acetic acid with an excess of copper sulphate,[195] then the nitration was carried out. Nitration of pyridyl-porphyrins can be performed by bubbling nitrogen dioxide in a chloroform solution of porphyrin.[196,197] A similar procedure was adopted with the difference that the nitrating species was generated *in situ* in a custom-made apparatus (*Figure 32*) rather than using a gas cylinder. In the apparatus, a dropping funnel (**A**) containing TFA was connected to a 2 necks flask (**B**) containing sodium nitrite and a magnetic stirrer. Flask **B** was connected via a cannula adapter (**C**) to a flask (**D**) containing the porphyrin dissolved in chloroform and kept in a salt-ice bath. The system was sealed to prevent contact with air. The reaction of TFA with sodium nitrite generates gaseous NO_2 (orange gas, *Figure 32*), which diffuses in the flask containing the porphyrin. When the reaction is carried out at room temperature, it leads to the formation of di-nitrated species, as detected by mass spectrometry, and to a poor yield of the desired product. Performing the reaction in a salt-ice bath (see right bottom corner of *Figure 32*) at −10 °C/−15 °C remarkably reduced the formation of side-products, thus increasing the yield. The lower temperature

also allowed the porphyrin to precipitate once functionalised, facilitating the purification. Optimised conditions gave a yield of 88 %, a value in line with the ones obtained in the nitration with the nitrate salt and acetic anhydride (see *Table 4* for comparison) and with the literature.[196] The nitro-porphyrin was analysed by NMR spectroscopy after copper removal (**93b**). As for other substrates, the ^{1}H-NMR showed increased multiplicity in the signals of the *beta* hydrogens, due to the introduction of asymmetry in the structure. The singlet present in the spectrum of the parent compound splits into a multiplet integrating 5H and a singlet integrating 2H, as shown in *Table 11*.

	β-H	H_{int}
before	8.91	-2.75
after	8.73-9.00	-2.68

*Table 11: NMR and UV-Vis data before and after nitration for **79f***
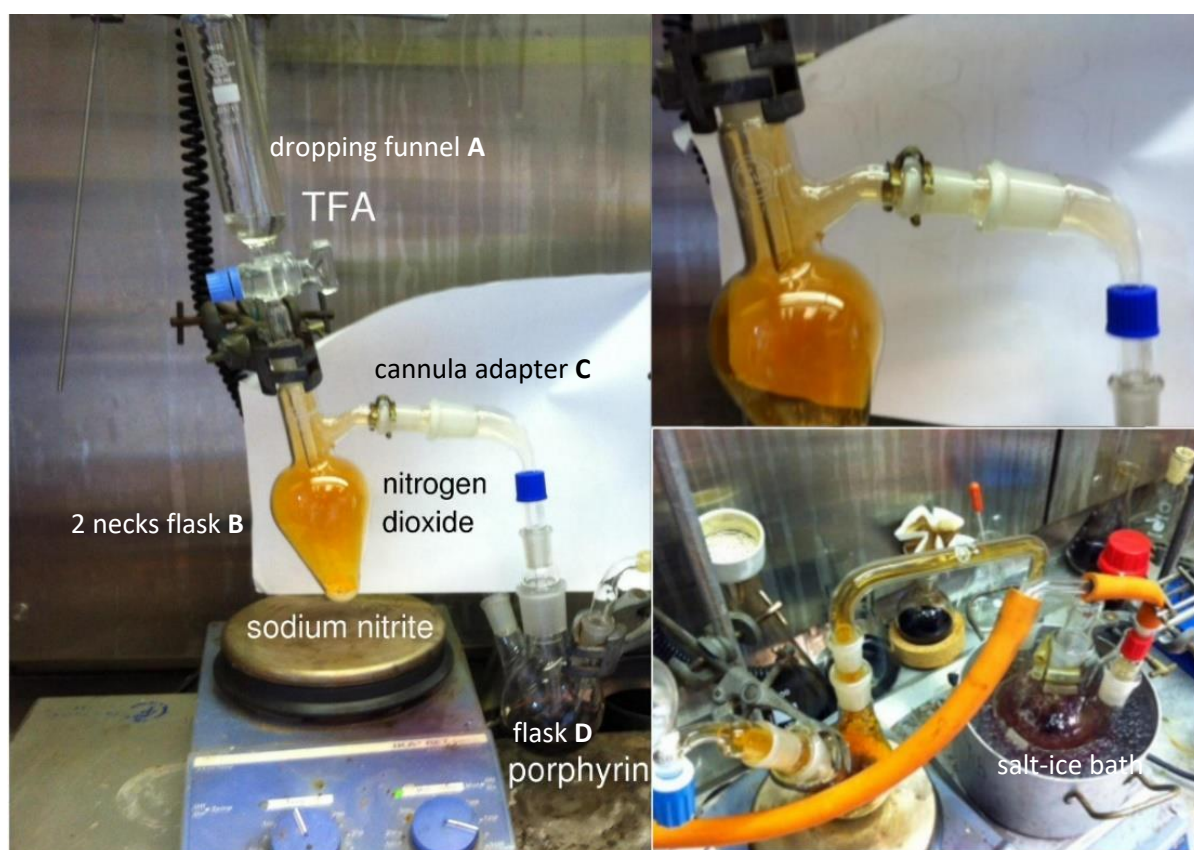
*Figure 32: apparatus setting for nitration reaction of **92***

Michael-like addition/elimination
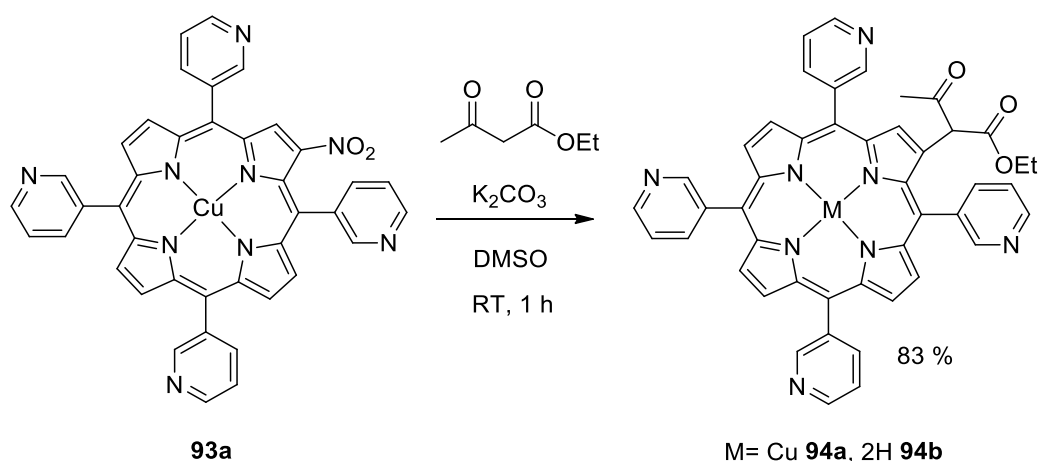
Scheme 14: Michael-like addition/elimination reaction scheme for **93a**

As for the other derivatives, Michael addition was carried out to replace the nitro group with ethyl acetoacetate (*Scheme 14*). The reaction was performed in DMSO with K_2CO_3 as a base, and it reached completion after 1 hour at room temperature. Removal of copper to obtain **94b** was performed with 20 % H_2SO_4 in TFA.[179,180] The harsh reaction conditions required for metal removal resulted in a mixture of products, and the Michael adduct was isolated by column chromatography. *Figure 33* shows the ^{1}H-NMR of compound **94b**.

Similarly to what observed for the other Michael adducts, a peak with integral value of 1H is present at 13.16 ppm, indicating that **94b** exists predominantly as the enolic tautomer. The *beta* hydrogens appear between 8.73 and 8.93 ppm and, as in the case of the porphyrin **93b**, the beta hydrogens in **94b** appear as multiplets (with integral value of 7H). At higher fields, the characteristic system already seen for the other substrates appears at *ca.* 4 ppm (*Figure 27*): two multiplets with integral value of 1H each are assigned to the CH_2 in the ethoxy group, indicating that the two protons are diastereotopic.
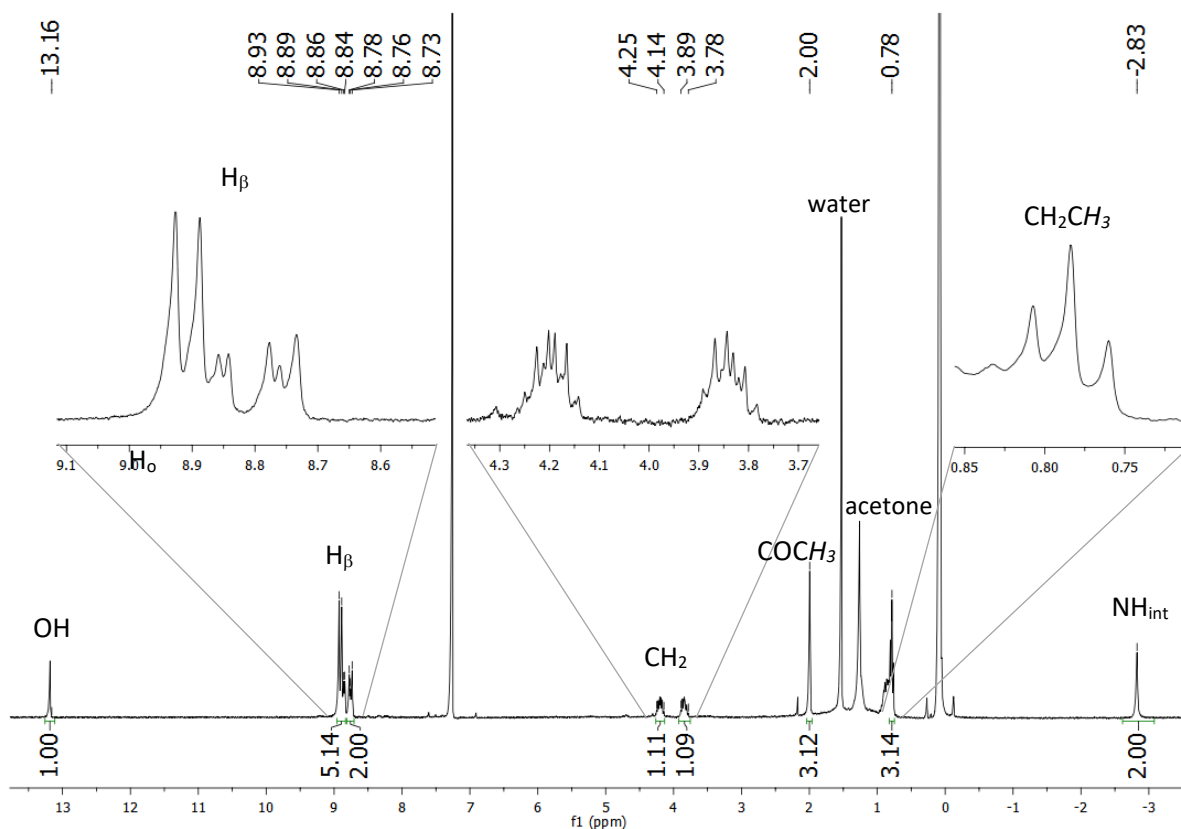
*Figure 33: ^{1}H-NMR spectrum of **94b** with expansions in CDCl$_3$ at 298 K and 300 MHz*

Astonishingly, the signals of the pyridyl hydrogens were not observed, but to our relief, mass spectrometry confirmed the formation of the expected molecule. In the aliphatic region, the singlet at 2.00 ppm and the triplet at 0.78 ppm (both with integral value of 3H) are assigned to the methyl in the acetyl group and in the ethoxy group, respectively.

Claisen cleavage and hydrolysis
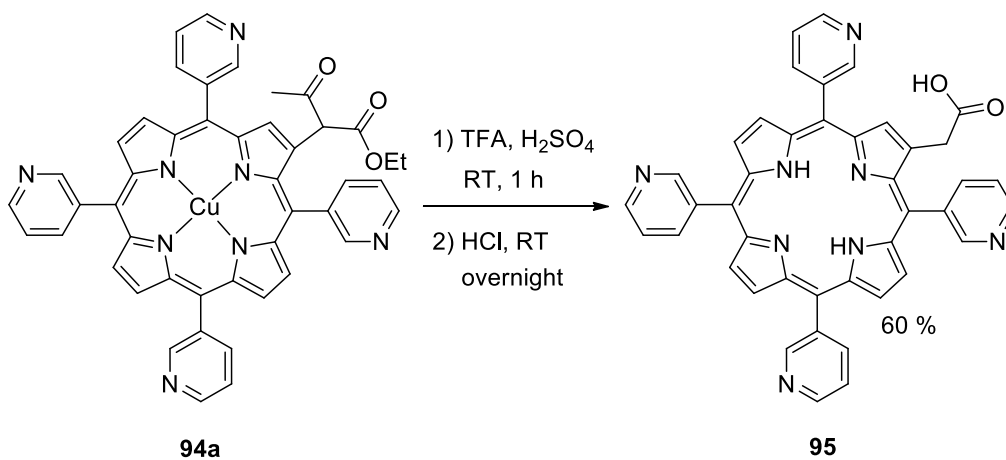
*Scheme 15: Claisen cleavage and hydrolysis for **94b***

We found that the Claisen cleavage and the hydrolysis reaction had to be performed together to obtain the desired product in high yields, as shown in *Scheme 15*: indeed, attempting either the Claisen cleavage step or the hydrolysis separately led to the formation of multiple reaction products, as verified by thin layer chromatography (TLC). Therefore, carrying out the two steps in tandem was the best option. Conveniently, the protonation of the nitrogen atoms on the pyridyl rings promoted the solubilisation of the porphyrin in the acidic aqueous reaction medium with no need for a co-solvent. TLC showed the formation of a mixture of products, one of which was highly polar and easily separable from the others. This product resulted to be the desired carboxylic-acid-functionalised porphyrin **95**. Compound **95** was analysed by NMR. ^{1}H-NMR and ^{13}C-NMR spectra are shown in *Figure 34* e *Figure 35*, respectively.

On the ^{1}H-NMR spectrum (*Figure 34*), a sharp peak is present at 15.28 ppm, which is assigned to the carboxylic group. Intriguingly, the integration of this peak shows a value of 3H, while at the same time no peak attributable to the internal hydrogens is seen at negative chemical shifts. We speculate that the peak at 15.28 ppm is caused by both the carboxylic acid and the internal hydrogens. This can be due to an instrumental artefact (folding), in which the processing shifted the internal hydrogens peak from one extreme to the other of the spectrum, causing the two signals to overlap. At higher fields two very broad peaks can be observed, one with integral value of 2H and the other with integral value of 5H, both assigned to the *beta* hydrogens (H_β). The pyridyl hydrogens signals are visible between 6.69 and 7.36 ppm as two doublets, a singlet and a doublet of doublets collapsed into a triplet, as summarised in *Table 12*. No CH_2 signal is detected from the ^{1}H-NMR spectrum, indicating that the signal may fall under the water peak at *ca.* 3.4 ppm.

Multiplicity	Chemical shift (ppm)	H	^{3}J (Hz)	
d	7.32-7.36	H_4	$^3J_{H4-H5}$ = 11.25 Hz	
d	7.05-7.08	H_6	$^3J_{H6-H5}$ = 9.6 Hz	
s	6.89	H_2	-	
dd	6.69-6.76	H_5	$^3J_{H5-H4}$ = 11.25 Hz $^3J_{H5-H6}$ = 9.6 Hz	
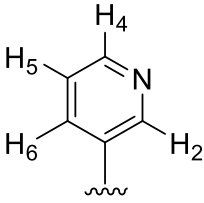
*Table 12: Pyridyl hydrogens ^{1}H-NMR data for **95***
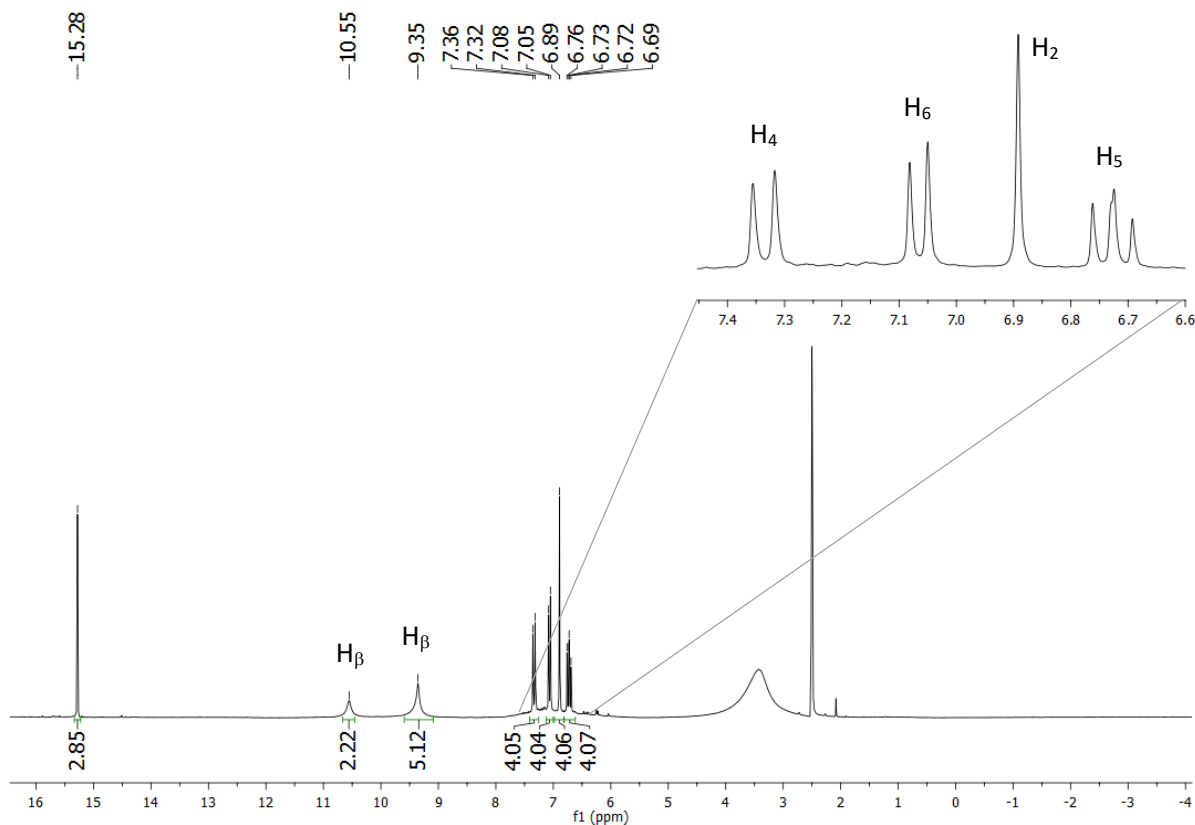
*Figure 34: ^{1}H-NMR spectrum of compound **95** in DMSO-d_6 at 298 K and 300 MHz*

The carbon (DEPTQ) spectrum is shown in *Figure 35*. The peak at 182.4 ppm is assigned to the carboxylic group (COOH *Figure 35*), although it appears at lower field compared to the other porphyrins (see *Table 9* for comparison), indicating a stronger electron withdrawing effect of the macrocycle on the carboxylic carbon. In the ^{13}C-NMR the signal relative to CH$_2$ group falls under the residual solvent peak at *ca.* 40 ppm. UV-vis and mass spectrometry analysis also confirmed the molecule was the expected product. The absorbance spectrum presented the characteristic Soret band at 419 nm, followed by four Q bands. Mass spectrometry confirmed the mass of the desired compound.
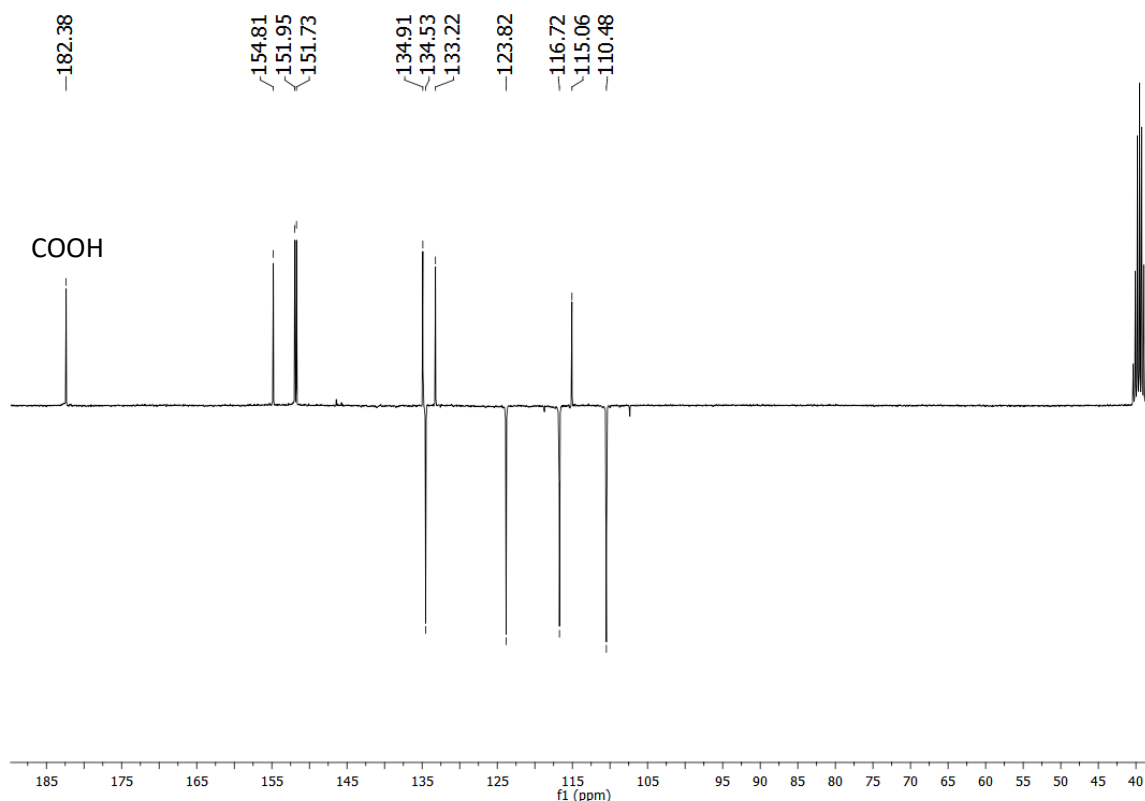
*Figure 35: $^{13}\{^1H\}C$-NMR (DEPTQ) spectrum of compound **95** in DMSO-d_6 at 298 K and 75 MHz*

Water solubilisation
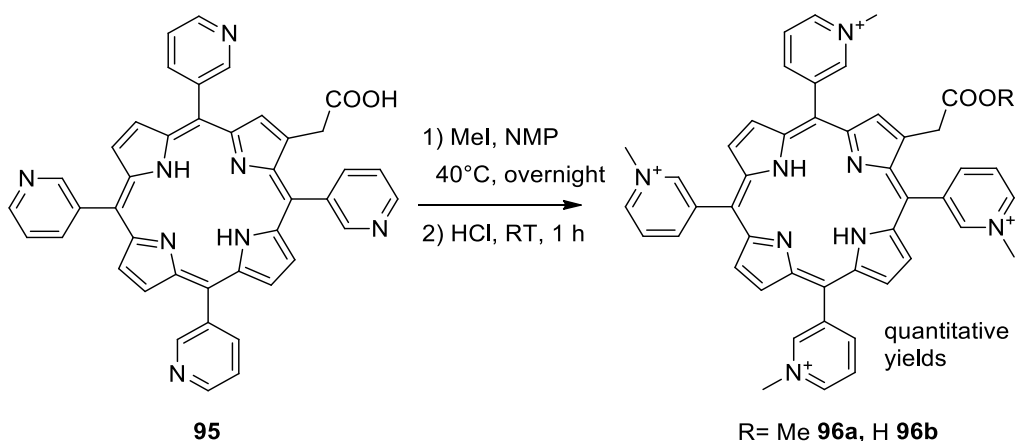
*Scheme 16: water solubilisation reaction scheme of **95***

Water solubility was introduced in the molecule as shown in *Scheme 16*. The porphyrin is generally treated with an excess of a methylating agent, either methyl *p*-toluenesulphonate[198,199] or methyl iodide.[200] Methylation of porphyrins is normally carried out in dimethylformamide (DMF), but NMP can also be used.[201] These polar aprotic solvents prevent the precipitation of partially methylated products in the reaction medium, allowing the reaction to reach completion. The purification of the

desired product was carried out *via* a double counterion exchange, and the method was optimised for the purification of A₃B porphyrins and will be discussed extensively in chapter 3. Inconveniently, the methylation occurred not only on the pyridyl nitrogens but also on the carboxylic acid on the *beta* position. Unfortunately, ¹H-NMR spectrum of compound **96a** does not give any structural information (*Figure 36*).
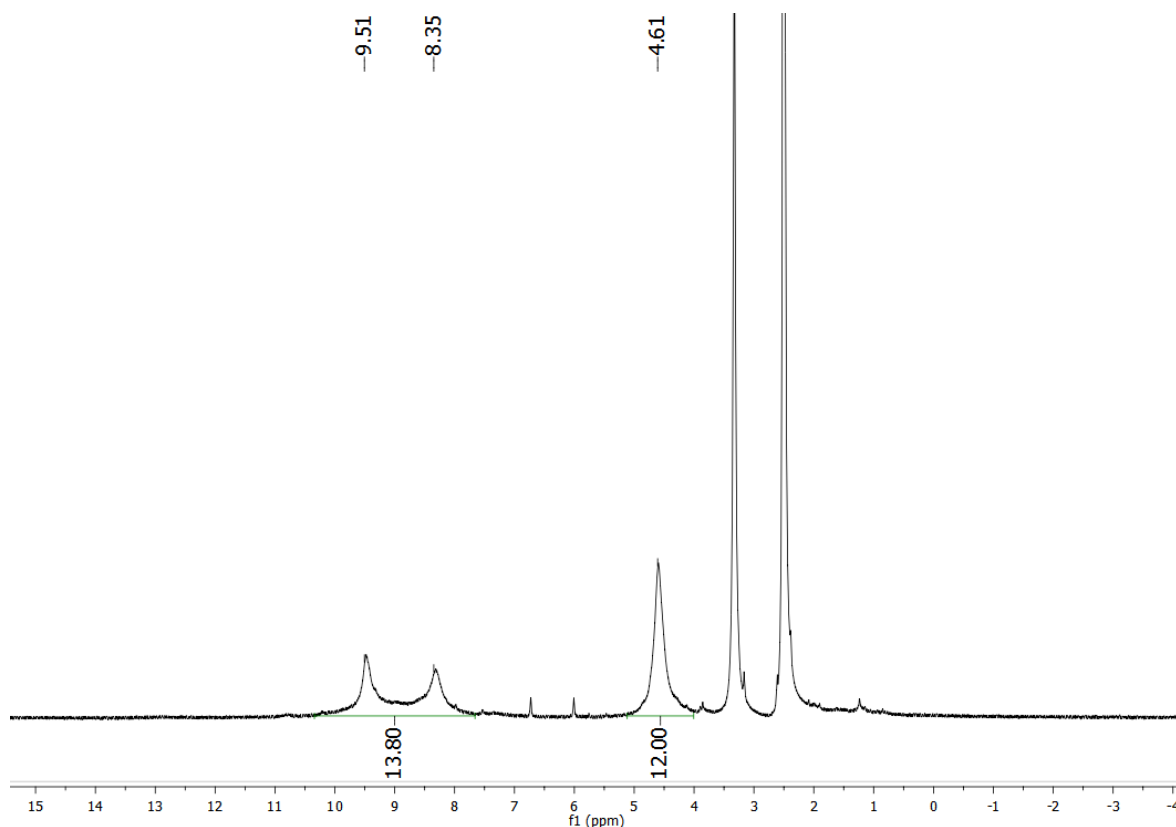
Figure 36: *¹H-NMR spectrum of **96a** in DMSO-d₆ at 298 K and 300 MHz*

From the position of the unresolved signals, the peak at 4.61 ppm can be tentatively attributed to the methyl-pyridyl group. The other two peaks at 9.51 ppm and 8.35 ppm could be the pyridyl or the *beta* hydrogens, or a combination of both. The NMR data collected is not enough to confirm the structure of the molecule, but mass spectrometry confirmed that the molecule is the desired product, and UV-vis spectrophotometry proved the presence of a porphyrin. The undesired methylation of the carboxylic group required us to proceed with a second hydrolysis to reveal the carboxylic acid (**96b**). To this end, the porphyrin was dissolved in concentrated aqueous HCl and left stirring overnight. The ¹H-NMR spectrum of compound **96b** is similar to the one obtained for the parent ester **96a** (*Figure 36*), and gives little information on the structure of the molecule. Mass spectrometry and UV-vis analysis, however, confirmed the expected mass and the absorbance of a porphyrin molecule, respectively.

2.9 *Beta*-functionalisation conclusions

Despite a few problems being encountered during the synthetic procedure, the *beta* functionalisation of different porphyrins was overall successful. A carboxylic acid functionality was successfully inserted on the *beta* position of macrocycles bearing different *meso*-aryl groups. The starting porphyrins were synthesised employing Rothemund or Lindsey synthetic method, the latter of which afforded higher yields.

The insertion of the nitro group on the *beta* position required different conditions for different porphyrins. **79b** and **79c**, the most electron withdrawing ones, were functionalised employing zinc nitrate, while for other substrates copper nitrate was the salt of choice. The nitration of **79f** was performed with nitrogen dioxide generated *in situ* on the copper complex of the porphyrin. The second step of the functionalisation was the substitution of the nitro group by a 1,3-ketoester, in this case methyl or ethyl acetoacetate. DMSO was the most suitable solvent for this transformation, despite the degradation observed for **79c**. For this derivative, the problem was circumvented performing the reaction in ice, with a constant monitoring. The reaction presented good yields on all the substrates, requires mild reaction conditions, has gram-scale applicability and employs commercially available starting materials.

The third step of the synthetic procedure was a Claisen cleavage of the acetyl group. As for the previous step, the reaction affords the desired products in good yields under relatively mild conditions. As highlighted in the previous sections, the substrate must undergo metal extrusion before the cleavage can take place.

The last step of the *beta* functionalisation was the hydrolysis of the ester to obtain the deprotected carboxylic acid. The reaction was performed in acidic aqueous conditions, with the use of a co-solvent to better dissolve the substrates, except for compound **94b**, in which the pyridyl nitrogens are protonated and enhance the solubility of the porphyrin in water. Good yields were obtained for this transformation under relatively mild reaction conditions. The carboxylic acid functionality was successfully introduced on the *beta* position of the different macrocycles.

Water solubilisation was the next step in the building of the oxygen sensor. Different approaches were necessary to reach this goal on the different porphyrins, according to the reactivity of the molecule. Unfortunately, most of the methods required reaction conditions that were not tolerated by the chain in the *beta* position. The carboxylic acid was unstable at high temperatures, undergoing a decarboxylation reaction or cleavage by both BBr_3 and chlorosulphonic acid. Only in the case of **95** the moiety remained in place after the quaternisation of the pyridyl nitrogens, despite the undesired esterification which required a further hydrolysis to obtain the carboxylic acid.

3   Synthetic approach for porphyrins A₃B

Based on the evidences discussed in the previous session, it was verified that the chain on the *beta* position was too labile to withstand insertion of platinum and palladium and further manipulation. A different approach was required to obtain conjugatable water-soluble oxygen-sensing porphyrin complexes. Therefore, we decided to focus the attention on the direct synthesis of porphyrins bearing a carboxylic group on their structures.

The chosen approach to reach the goal involved the synthesis of asymmetrically *meso*-substituted porphyrins, in which one aryl group bears a carboxylic function (*Scheme 17*). The synthesis is referred to condensation A₃B,[145] in which two different aldehydes are reacted together in a 3:1 ratio.[202] Three porphyrins were prepared employing this method (*Scheme 17*). The synthesis and the reactivity are specific for each porphyrin, and they will be evaluated one by one.
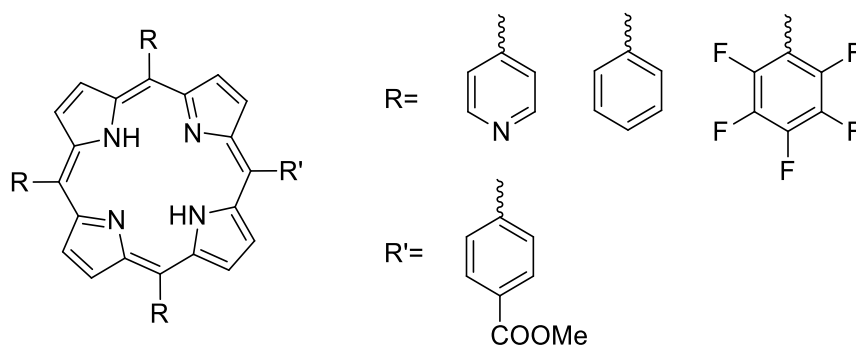
Scheme 17: A₃B porphyrins structures

3.1 A₃B porphyrins synthesis

A₃B porphyrins bearing pyridyl rings on the *meso* position are widely used for biological applications due to the possibility of straightforward transformation of the molecules in water-soluble species.[200,203,204] We chose to use 5-(4-carboxymethylphenyl)-10,15,20-tris(4-pyridyl)porphyrin **97**, whose synthesis is shown in *Scheme 18*.

Three equivalents of 4-pyridinecarboxaldehyde were reacted with one equivalent of methyl-4-formylbenzoate and four equivalents of pyrrole, in refluxing propionic acid following the Adler-Longo synthetic method.[155] As discussed earlier, the Lindsey approach cannot be used in the synthesis of this porphyrin because of the presence of the pyridyl nitrogen, which would inactivate the catalyst preventing the cyclisation.[158] The formation of the porphyrinogen is a reversible reaction: in time, it reaches the equilibrium forming all the combinations between the aldehydes, as shown in *Scheme 19*.
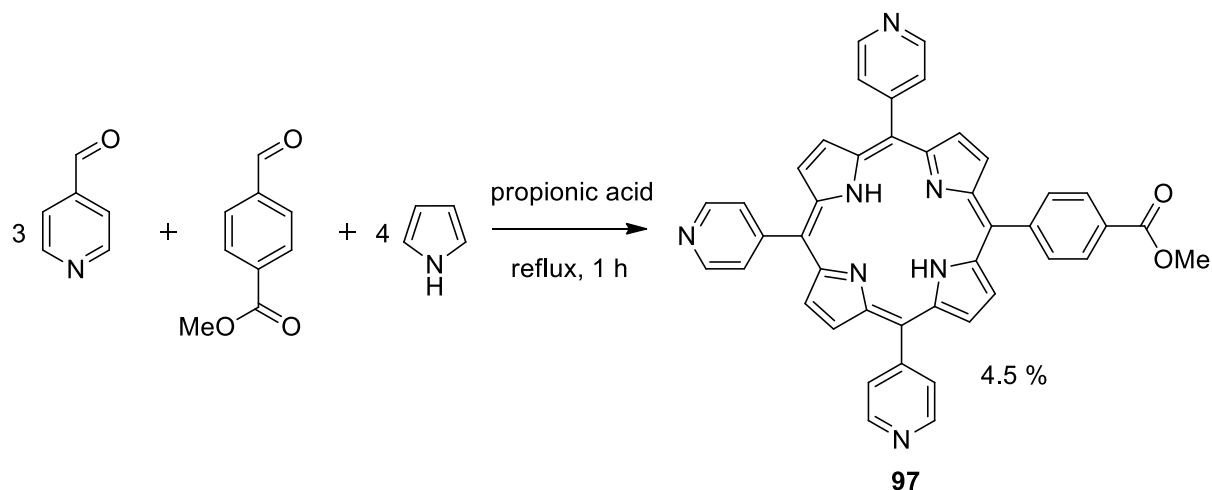
*Scheme 18: synthesis of pyridyl porphyrin **97***

The porphyrins **97a-e** are shown in order of increasing polarity, starting from the least polar 4-tetracarboxymethylphenyl porphyrin (**97a**), to finish with the most polar 4-tetrapyridyl porphyrin (**97e**). After filtration on a silica pad to remove the tar formed in the reaction, the desired A$_3$B derivative was isolated by column chromatography on silica gel. The strong polarity and the presence of basic groups make this process extremely challenging.
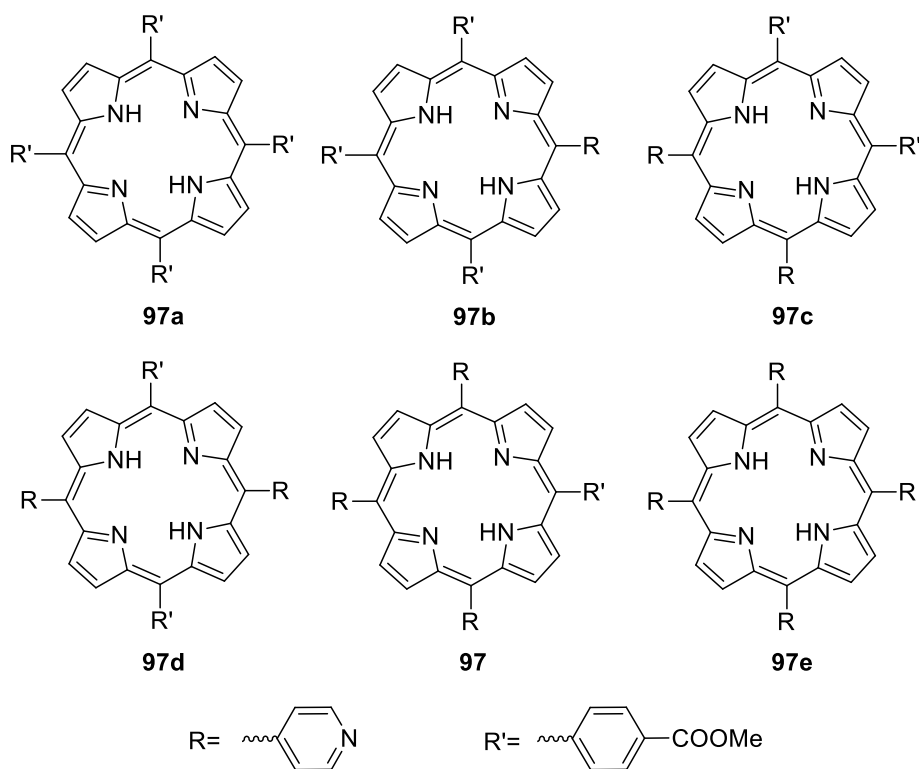
Scheme 19: different porphyrin isomers produced by the synthesis

The interactions of the pyridyl nitrogens with the silica reduce the retardation factor of the species and decrease the resolution power. The A_3B porphyrin **97** is the fifth in order of elution. We verified that remaining traces of propionic acid seriously hamper the purification process as they further reduce the resolution of the mixture. The yield of porphyrin **97** was very low (4.5 %), but in line with the results reported in the literature for similar species.[205,206] This approach allowed us to obtain in a single synthetic step a porphyrin bearing a protected anchoring moiety (the ester group) and groups that can be used to introduce water solubility (pyridyl nitrogens). With the approach discussed in the previous sections, four steps were required to obtain the same functionalisation of the molecule. Despite the very low yield of the A_3B derivatives, the gain in time and materials is advantageous compared to the *beta* functionalisation.

The ^{1}H-NMR spectrum of compound **97** (*Figure 37*) displays the characteristic signal at negative chemical shift for the two internal hydrogens (NH_{int}). The very sharp singlet at 4.13 ppm is assigned to the ester methoxy group (OCH_3) based on its characteristic chemical shift and integration value. In the aromatic region, the broad peak at 9.07 ppm is assigned to the hydrogens in *ortho* to the pyridyl nitrogen (H_{Py-o}). At higher field the eight *beta* hydrogens give a signal at *ca.* 8.86 ppm (H_β), which is composed of two overlapped signals. This effect is caused by the presence of one different *meso* substituent, which introduce a differentiation of the pyrrolic hydrogens. The integration value of the peaks is 6H and 2H, suggesting that the closest *beta* hydrogens to the carboxymethylphenyl ring are chemically different from the others. The two doublets integrating 2H each in the inset of *Figure 37* correspond to the *ortho* (H_{Ar-o}) and *meta* (H_{Ar-m}) hydrogens to the ester group in the phenyl ring, respectively. The signal at highest field in this region is assigned to the six hydrogens *meta* to the nitrogen in the pyridyl rings (H_{Py-m}). The spectrum is consistent with the data reported in the literature.[205,206] ^{13}C-NMR spectrum of **97**, not shown here, highlights the presence of a carbonyl species at 167.3 ppm.
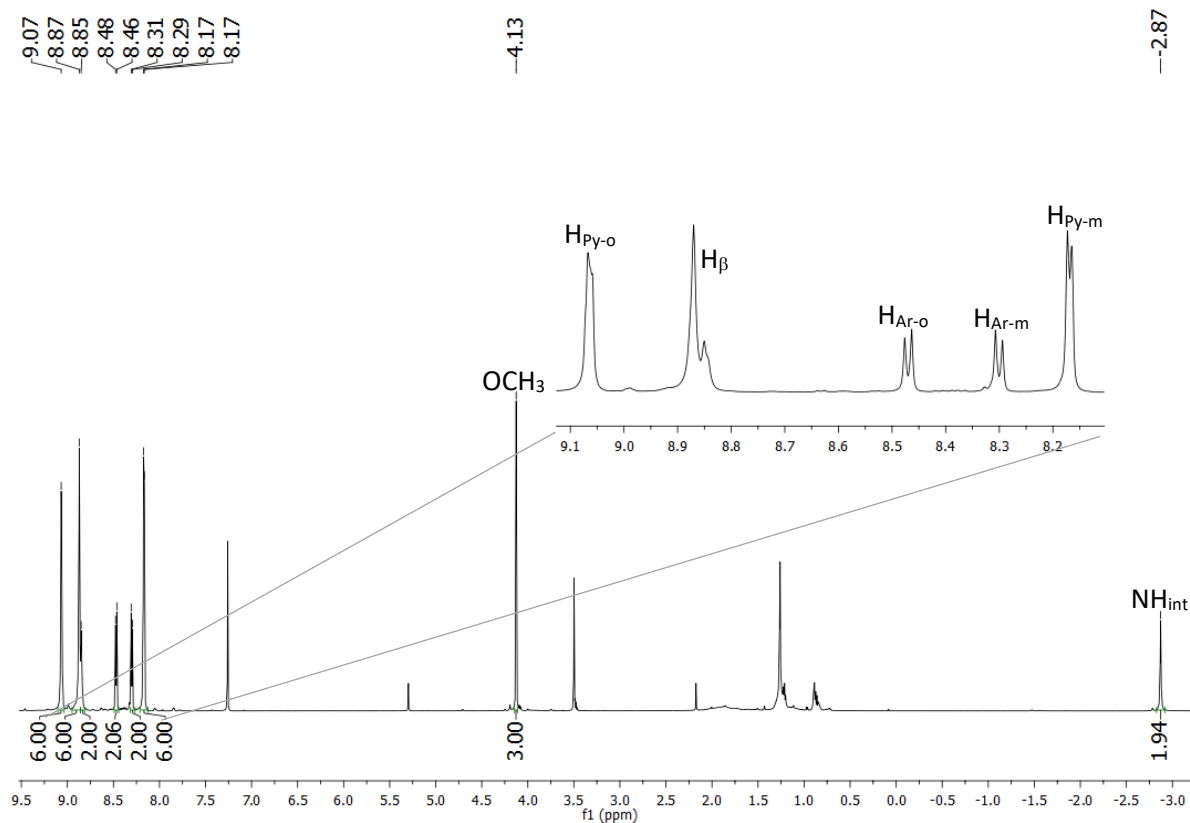
*Figure 37: ^{1}H-NMR spectrum with expansion of **97** in CDCl$_3$ at 298 K and 600 MHz*

The second porphyrin synthesised was 5-(4-carboxyphenyl)-10,15,20-triphenylporphyrin (**98**) shown in *Scheme 20*. Benzaldehyde was reacted with 4-formylbenzoic acid and pyrrole in a 3:1:4 ratio. Rothemund procedure was chosen because it allowed to obtain a porphyrin with a free carboxylic group instead of its methyl ester, which in this case facilitates the purification process by enhancing the R$_f$ difference between the products on silica. The disadvantage of this approach is that it precludes the use of Lindsey method, due to the presence of the free carboxylic acid, which would lead to the inactivation of the catalyst.[207] The two major product of the reaction were porphyrins A$_4$ **79a** and A$_3$B **98**, while other products derived from the possible combinations of the two aldehydes were present only in traces. Despite the low yield (4.6 %), the purification of the desired compounds was simpler and quicker. The spectrum is consistent with the data reported in the literature.[208]
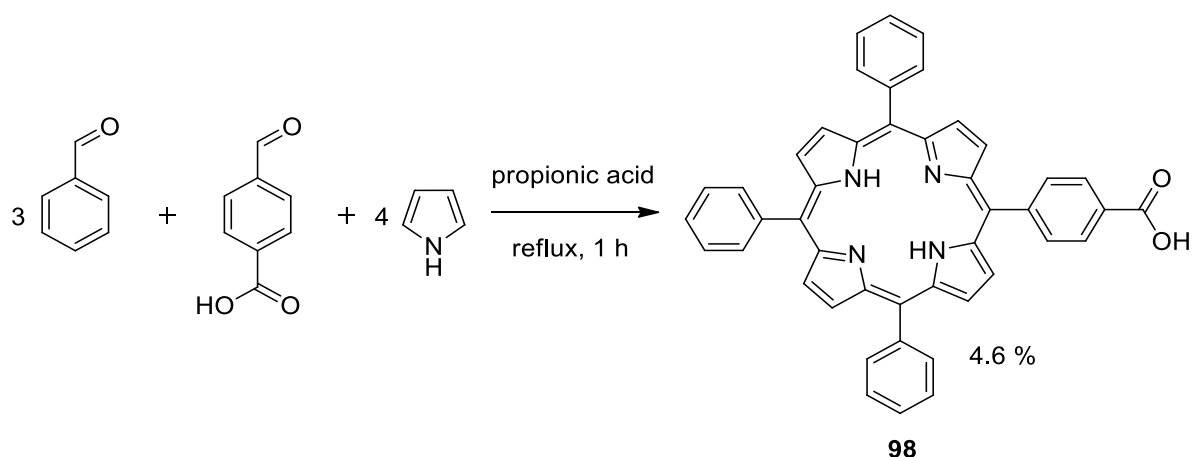
Scheme 20: 5-(4-carboxyphenyl)-10,15,20-triphenylporphyrin synthesis reaction scheme

A further A$_3$B derivative obtained was the 5-(4-carboxymethylphenyl)-10,15,20-*tris*(pentafluorophenyl) porphyrin **99** (*Scheme 21*). In this case, the higher-yielding Lindsey synthesis was employed[209–213] due relatively high price of 2,3,4,5,6-pentafluorobenzaldehyde and its poor stability under Adler-Longo conditions. As a consequence, the methyl ester of 4-formylbenzoic acid was used.[207] A 3:1 stoichiometric mixture of the two aldehydes was treated with BF$_3$·Et$_2$O in dry DCM under reflux conditions for 4 hours. An excess of chloranil was subsequently added to oxidise the porphyrinogen to the corresponding porphyrin. As in the case of **98**, the main products of the reaction were the A$_4$ porphyrin **79c** and A$_3$B **99**.
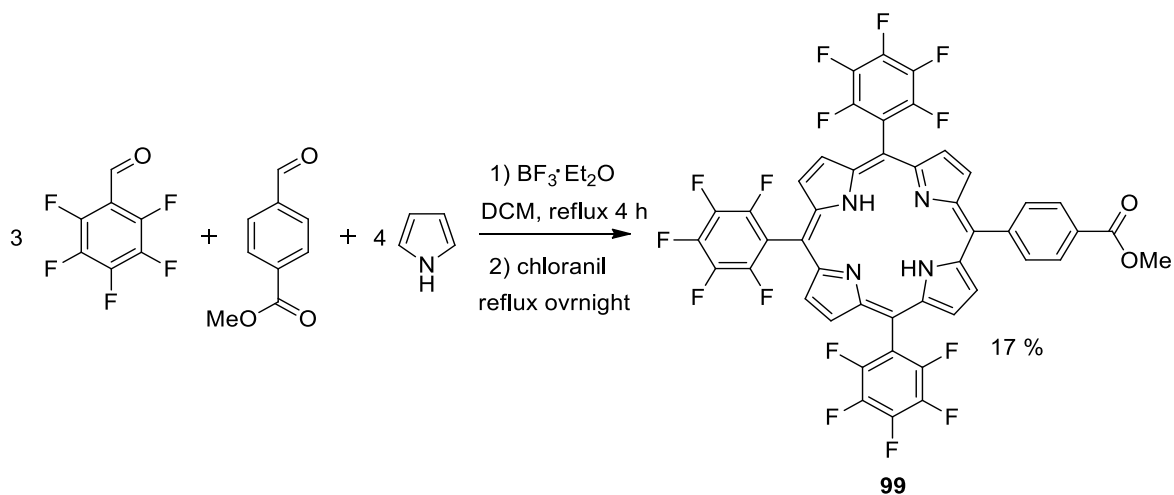
*Scheme 21: 5-(4-carboxymethylphenyl)-10,15,20-tris(pentafluorophenyl)porphyrin **99** reaction scheme*

Purification by chromatographic column gave **99** in 17 % yield, a considerable improvement over the yields of the derivatives previously described. A further advantage of this method consists in the possibility of scaling-up the reaction to obtain grams of porphyrins. Crucially, refluxing the reaction

mixture is desirable but not essential for porphyrinogen formation, as its effect is a faster starting material consumption: indeed, reactions performed at room temperature lead to consumption of the starting material over a period of two days, without significantly decrease of the yield. It is worth noting that **79c**, a side product of the reaction in this context, is actually a precious and expensive porphyrin that can be collected in high purity during the purification step, without further effort.

^{1}H-NMR of compound **99** is shown in *Figure 38*. At low fields, eight *beta* hydrogens (H_β) appear as two broad peaks instead of a sharp singlet, since the porphyrin bears a different substituent in one of the *meso* positions. Two doublets are present in the aromatic region, which are generated by the hydrogens in the *ortho* and *meta* positions relative to the methyl ester group (H_o and H_m). The two internal hydrogens appear at negative chemical shift (NH_{int}) and the methoxy group as singlet at 4.14 ppm (OCH_3). ^{19}F-NMR spectrum (*Figure 39*) shows three main peaks, generated by *ortho, para* and *meta* fluorines, respectively. Expansion of the spectrum highlights the coupling between the fluorines and the differentiation of the chemical shifts by the lower degree of symmetry of the molecule compared to **79c**. All the assignment are in agreement with those reported previously.[210,211]
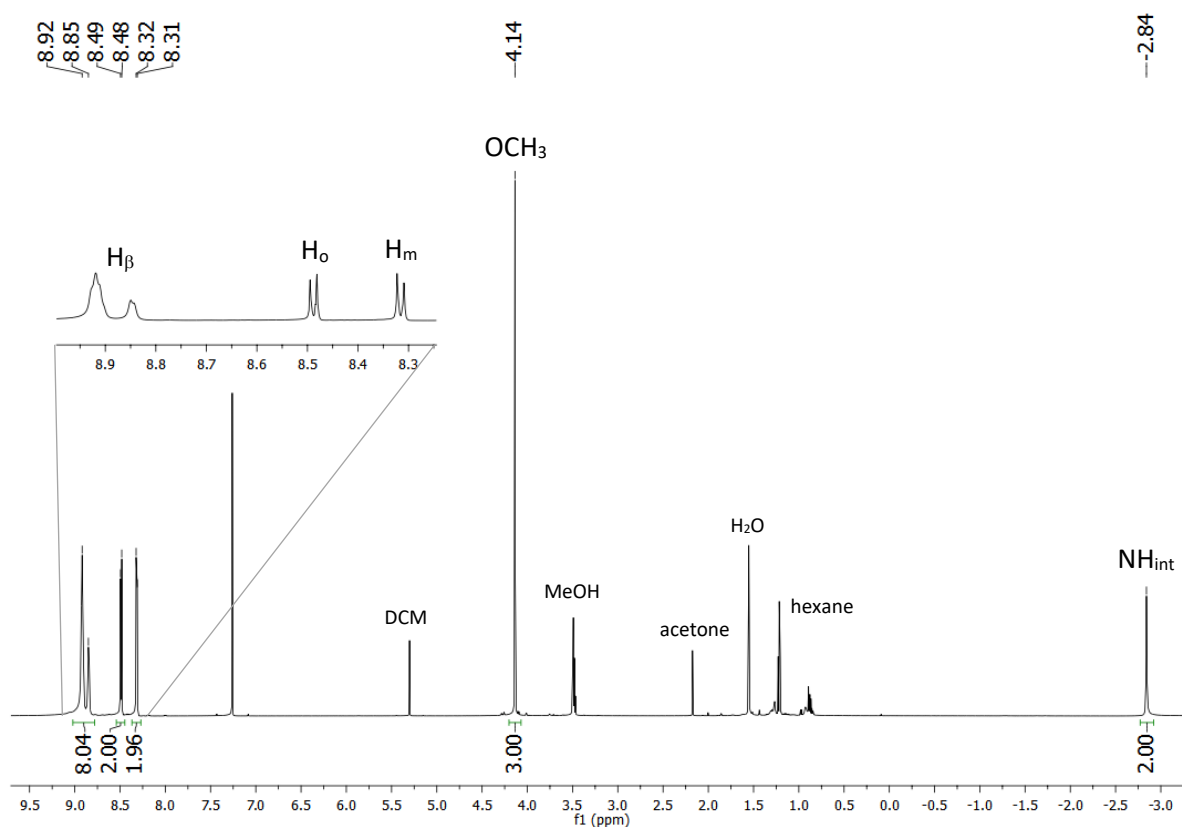
*Figure 38: ^{1}H-NMR spectrum with expansion of **99** in CDCl₃ at 298 K and 600 MHz*
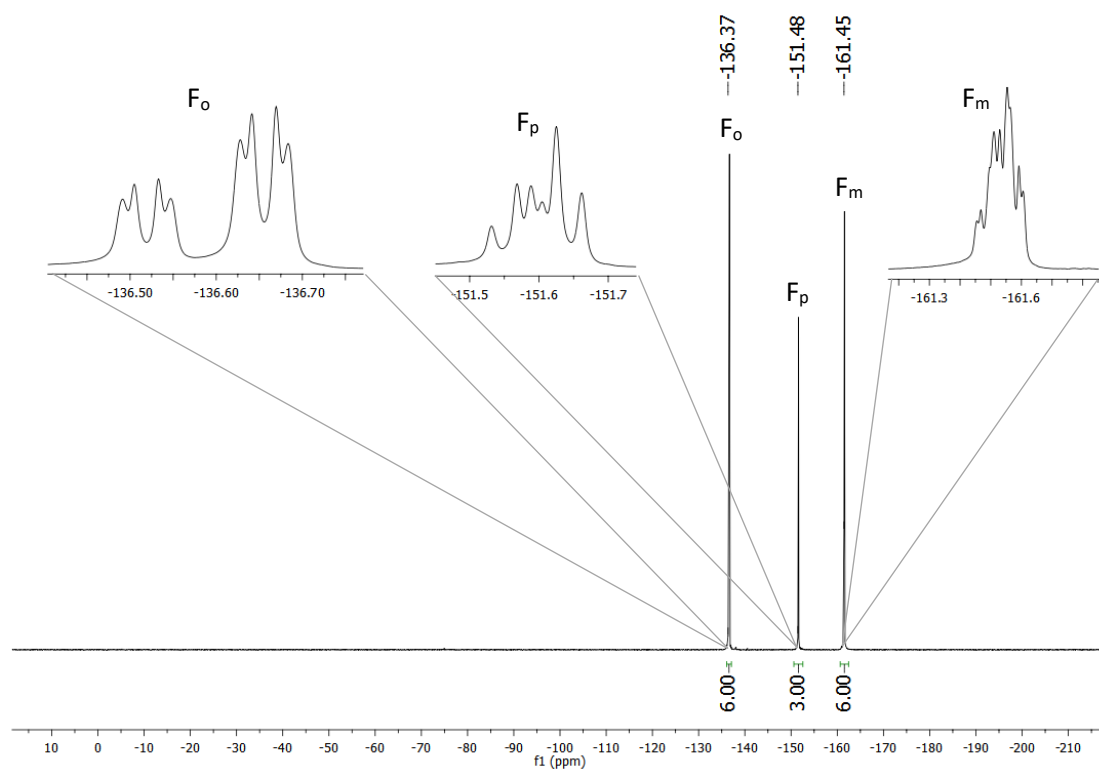
*Figure 39: $^{19}F\{^1H\}$-NMR spectrum with expansions of **99** in CDCl$_3$ at 298 K and 565 MHz*

3.2 Water solubilisation of A$_3$B porphyrins

Employing the same approach shown in *Figure 28* for the *beta*-functionalisation, the reaction to enable water solubilisation was carried out at the *meso*-substituted aryl rings. With the starting porphyrin **97** in hand, attention focused on the transformation needed to make the compound soluble in aqueous media (*Scheme 22*).
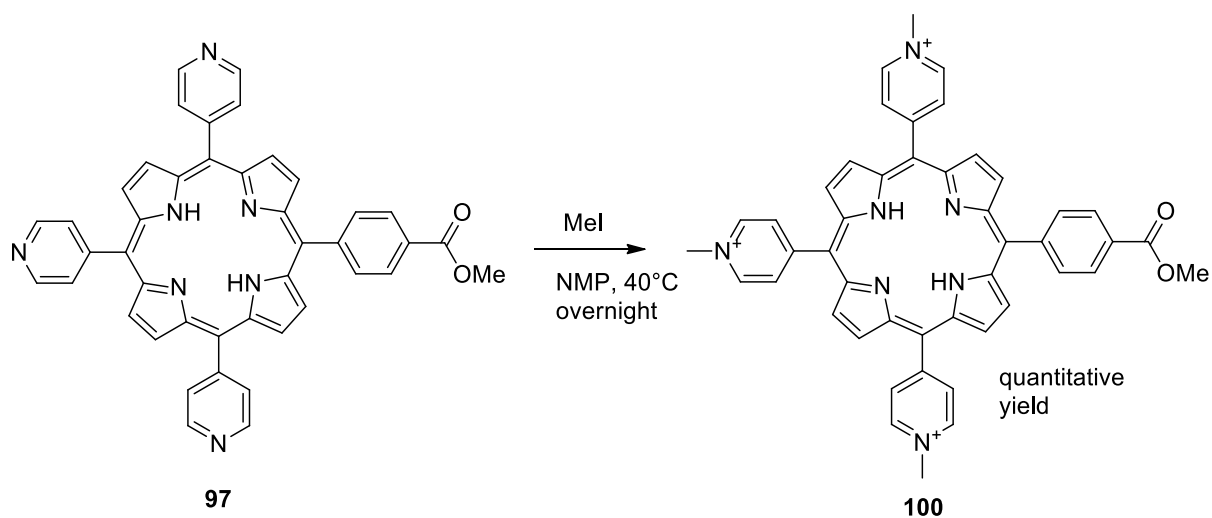
*Scheme 22: water solubilization reaction scheme for **97***

As discussed earlier, pyridyl-porphyrins can be made to be water-soluble by straightforward alkylation of the pyridyl nitrogens by treating with an excess of methyl iodide in NMP.[201] Since it was verified that the carboxylic group reacted with methyl iodide to form the corresponding methyl ester, even if not quantitatively, it was decided to carry out the methylation prior to the hydrolysis of the ester. This reaction afforded the desired species (**100**) in quantitative yield.

<u>Ion exchange purification method for positively charged porphyrins</u>[146,214,215]

Although cationic water-soluble porphyrins can be purified by reverse-phase liquid chromatography, the tendency of the macrocycles to strongly adhere to the silica, together with the cost of the columns and the time required to obtain sufficient quantity of product, made this purification method not ideal for the purposes of this work.

A method based on ion-exchange would allow the straightforward purification of the product from both water-soluble and non-water-soluble impurities, suitable for scale-up and not requiring expensive instrumentation.

The optimised purification method consisted of adding potassium hexafluorophosphate to an aqueous solution of the porphyrin triiodide obtained from the methylation reaction. This caused the water-insoluble hexafluorophosphate salt to precipitate from solution. The precipitate was dissolved in acetone and precipitated as the corresponding chloride salt after addition of tetrabutylammonium chloride (TBAC). Further crystallisation of the solid from MeOH/Et$_2$O afforded the desired species in high purity. This purification approach is based on drastic change of solubility of the salt driven by exchange of the counter-anion.[214] The porphyrin originally is soluble in polar solvents, like water and methanol, but not soluble in organic solvents such as acetone, chloroform and acetonitrile. The hexafluorophosphate salt, on the other hand, shows opposite solubility, so it precipitates from water and is soluble in acetone. Water-solubility is recovered in the last step by the addition of TBAC to the acetone solution, which leads to hexafluorophosphate/chloride exchange and causes the water-soluble chloride to precipitate from acetone.[146] The final crystallisation from MeOH/Et$_2$O is essential to eliminate remaining traces of TBAC. Cooling the suspension prior the filtration helped recovering the product by slowing down the evaporation of the solvent. A further advantage of this purification method is the increased water-solubility of the chloride salt of the porphyrin compared to the corresponding iodide salt. While optimising the purification method, different hexafluorophosphate salts were screened and it was found that ammonium, sodium and potassium hexafluorophosphate salts are equally efficient as precipitating agent. The choice of KPF$_6$ was based on its lowest price.

Crucially, the whole process can be carried out in a single centrifugation tube, thus limiting the loss of material that could arise from multiple filtration steps.

^{1}H-NMR spectrum of compound **100**, shown in *Figure 40*, contains one additional signal when compared to that of the starting material (**97**). The singlet at 4.74 ppm is assigned to the methyl groups introduced on the pyridyl nitrogens (N[+]CH$_3$). In fact, the integration value of this signal is 9H. Moreover, a general downfield shift of the signals can be noted, especially for the hydrogens *meta* to the pyridyl nitrogen (H$_{Py-m}$). All the signals are consistent with the previously reported data.[205,206]
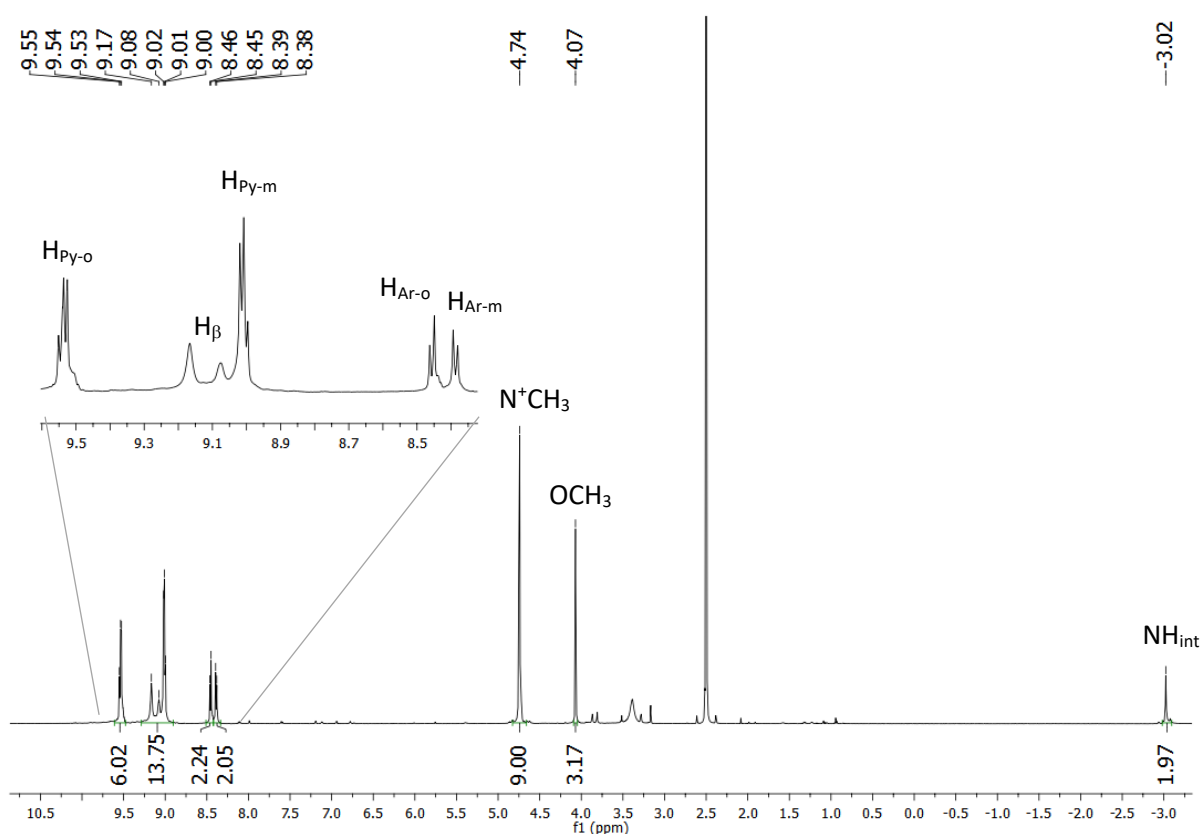
*Figure 40: ^{1}H-NMR spectrum with expansion of **100** in DMSO-d$_6$ at 298 K and 600 MHz*

The hydrolysis of the methyl ester was carried out in water in the presence of an excess of lithium hydroxide at room temperature (*Scheme 23*). TLC and MS analysis showed that completion was reached in one hour, and that prolonged reaction times resulted in porphyrin degradation, seemingly indicating the instability of the species in alkaline environments. The ion exchange approach described above was used to purify the desired product. Crucially, neutralisation of the base is necessary prior to the ion exchange purification, as no precipitation occurred when the hexafluorophosphate salt was added directly to the reaction environment. This behaviour can only be ascribed to the presence of

the hydroxide anions, which seems to prevent the interaction of the hexafluorophosphate ion with the porphyrin and the subsequent precipitation of the compound.
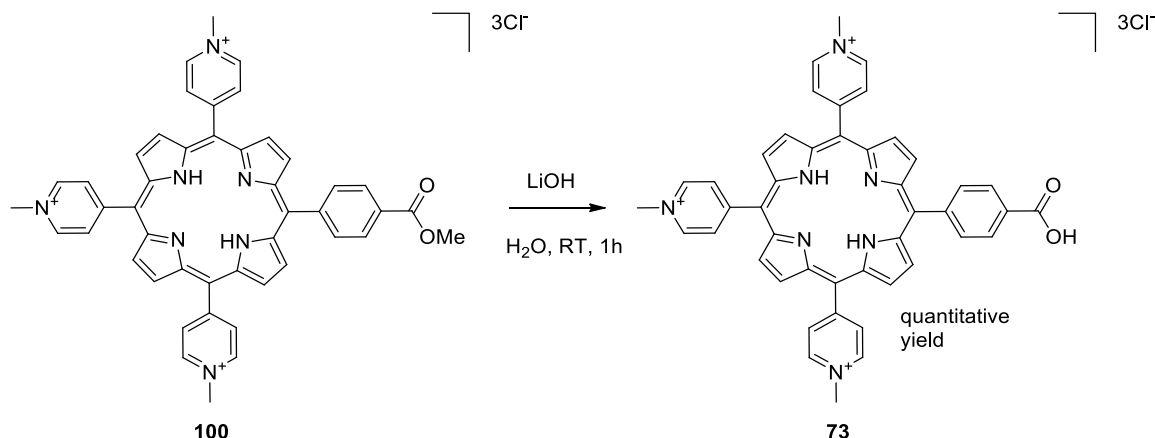
*Scheme 23: hydrolysis reaction scheme of **100***

The structure of the compound was confirmed by NMR spectroscopy. ^{1}H-NMR spectrum (*Figure 41*) indicates the loss of the methoxy group by the disappearance of the peak at 4.07 ppm, and the very broad signal that appears at down fields, at 13.24 ppm indicates the presence of carboxylic acid group (COOH). The signals in the aromatic region appear broader, which can be due to the aggregation of the porphyrin and subsequent precipitation in the NMR tube.
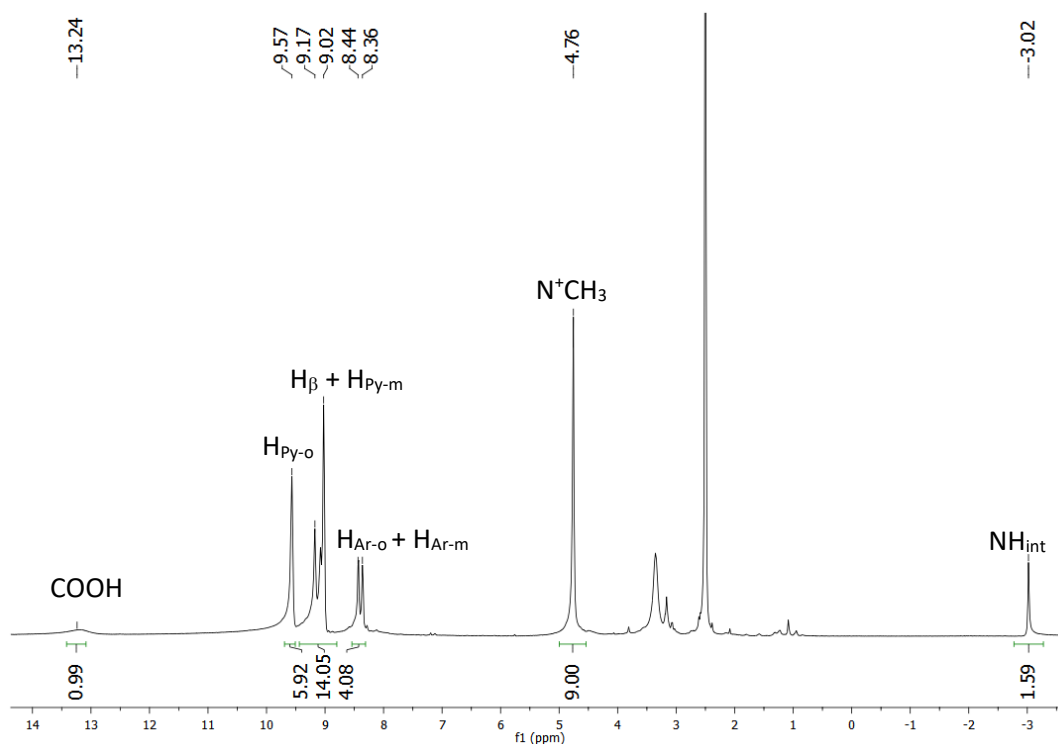
*Figure 41: ^{1}H-NMR spectrum of **73** in DMSO-d$_6$ at 298 K and 600 MHz*

The introduction of water-solubility on porphyrin **98** was achieved by treatment with chlorosulphonic acid and subsequent hydrolysis to insert sulphonate groups on the *meso*-phenyl groups (*Scheme 24*).[190,192] The reaction was performed in chloroform with an excess of chlorosulphonic acid. After one hour at room temperature, the reaction mixture was cooled in an ice bath and slowly neutralized with bicarbonate. The porphyrin, bearing chlorosulphonyl groups on the phenyl rings, is not water soluble and can be filtered from the aqueous mixture. The neutralisation step must be performed with care, because if the addition of the base is too fast, the temperature of the mixture increases, and partial hydrolysis of the chloride group takes place, leading to a mixture of partially water-soluble derivatives that hampers the purification step. The chlorosulphonyl porphyrin was then suspended in water and heated to reflux overnight, allowing the hydrolysis reaction to reach completion.
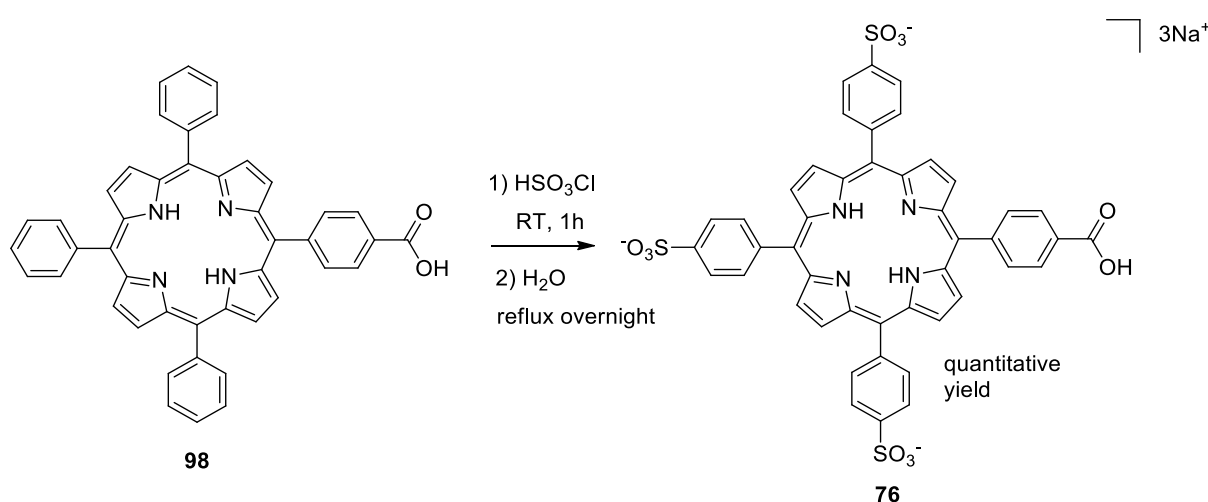
*Scheme 24: water solubilization reaction for **98***

The ^{1}H-NMR spectrum of compound **76** is shown in *Figure 42*. The signal generated by the internal hydrogens appears at negative chemical shift (NH_{int}), and the *beta* hydrogens appear at 8.86 ppm (H_β). Four further signals, all of them doublets, are present in the aromatic region. Two of them present an integral value of 2H and are assigned to the hydrogens *ortho* and *meta* to the carboxylic acid (5-Ar-H_o and 5-Ar-H_m). The remaining two signals present an integral value of 6H each and can be assigned to the hydrogens in *ortho* and *meta* positions relative to the sulphonate group (10,15,20-Ar-H_o and 10,15,20-Ar-H_m). The *para* hydrogens of the phenyl rings were replaced by the sulphonate groups, and therefore are not present in the spectrum. No signal was detected relative to the COOH group at down fields, due to probably exchange with the solvent. The spectrum agrees with the data reported in the literature.[146]
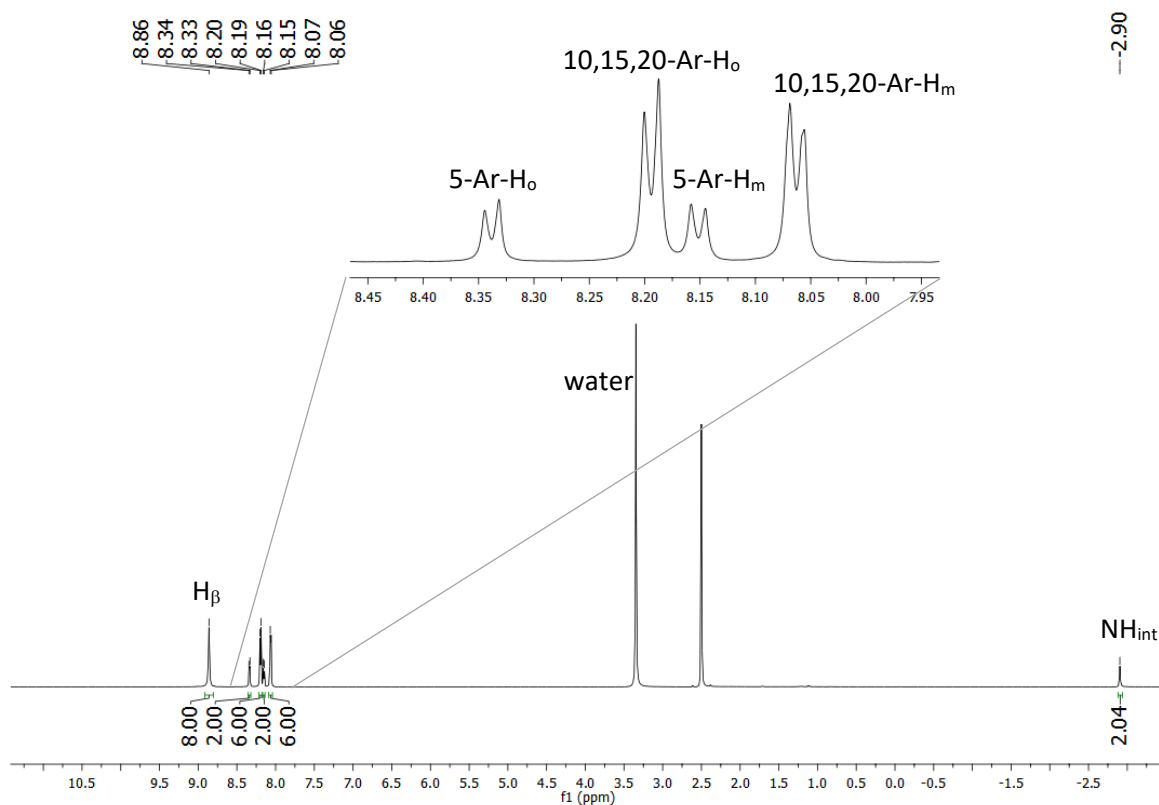
*Figure 42: ¹H-NMR spectrum with expansion of **76** in DMSO-d₆ at 298 K and 600 MHz*

Purification of **76** was achieved through an ion-exchange method that was developed as part of this work. The method was initially developed to purify **91** from the water-soluble nucleophiles employed for the aromatic nucleophilic displacement of the fluorines, and its details will be discussed later.

The approach to obtain water-soluble porphyrins based on derivative **99** was based on the aromatic nucleophilic substitution on the *para* fluorines, as discussed in section 2.7 for **79c**.[185] Functionalisation of **99** according to this strategy led to two conjugatable water-soluble porphyrins, one negatively and one positively charged.

Anionic water-soluble derivative of porphyrin **99**

Displacement of *para*-fluorine with taurine was carried out using the conditions adopted to obtain **91**. The reaction was performed on the zinc complex of **99** (**101,** *Scheme 25*), obtained by treatment of **99** with an excess of zinc acetate. NMR and UV-visible spectroscopy confirmed the formation of the complex, by disappearance of the internal hydrogens peak and of two Q bands, respectively. Complex **101** was treated with lithium taurine (**84**) in NMP overnight at 200 °C (*Scheme 25*). Complete functionalisation was achieved and in this case, unlike what was observed for the *beta*-functionalised derivative, the carboxylic group was unaffected by the reaction conditions.
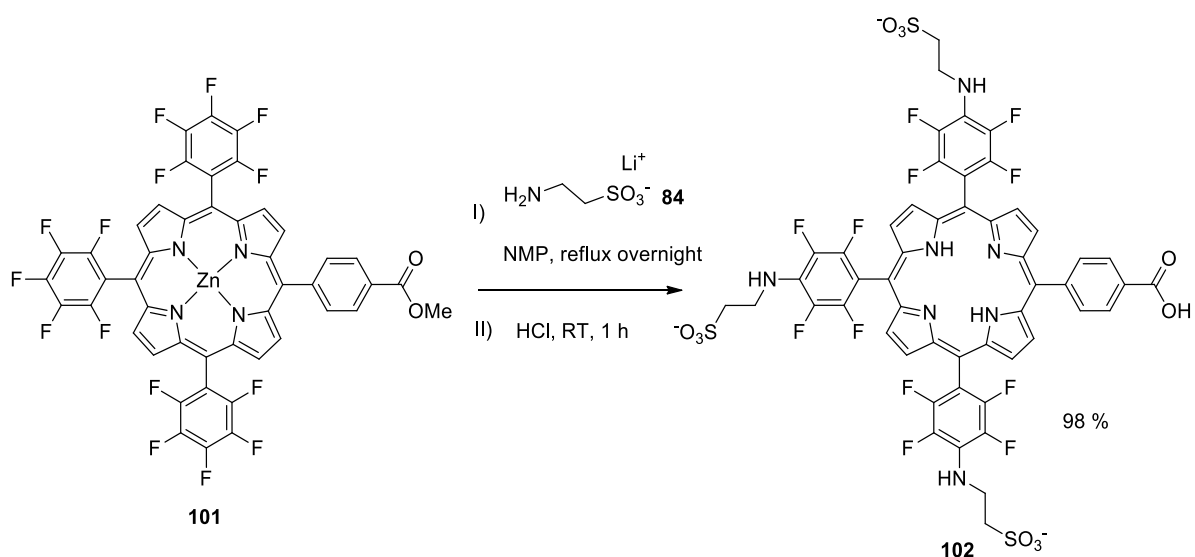
*Scheme 25: water solubilisation reaction for zinc complex of **99***

Following displacement of fluoride ions, addition of concentrated aqueous HCl to the reaction medium led to simultaneous demetallation of the porphyrin and hydrolysis of the methyl ester, affording the target water-soluble conjugatable species.

^{1}H-NMR analysis confirmed the structure of the porphyrin (*Figure 43*). In addition to the eight *beta* (H_β), four aryl (H_o and H_m) and two internal hydrogens (NH_{int}), new peaks are visible in the spectrum that confirm the presence of the taurine moiety. The singlet at 6.66 ppm was assigned to the amine hydrogens (NH_m), while the two broad singlets between 2.96 and 3.91 ppm are attributed to the CH_2 groups of the taurine moiety: the signal with higher chemical shift is assigned to the groups bearing the electron-withdrawing sulphonate (H_2), while the peak at 2.96 ppm to the methylenes attached to the amine groups (H_1). *Table 13* shows the structure of the molecule and the hydrogen assignments. The spectrum was recorded without spinning of the sample (256 transitions) to achieve a better

resolution, and the four carboxyphenyl hydrogens appear as two doublets with integral value of 2H each.

Multiplicity	^{1}H δ (ppm)	Integration value	Assignment
br m	9.22	6	H_β
br m	8.91	2	H_β
d	8.28	2	H_o
d	8.14	2	H_m
s	6.66	3	NH_m
t into br s	3.91	6	H_2
t into br s	2.96	6	H_1
Singlet	−3.03	2	NH_{int}
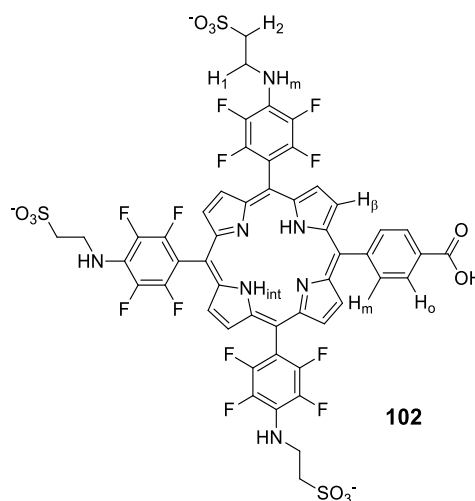
Table 13: peak assignment and structure of **102**
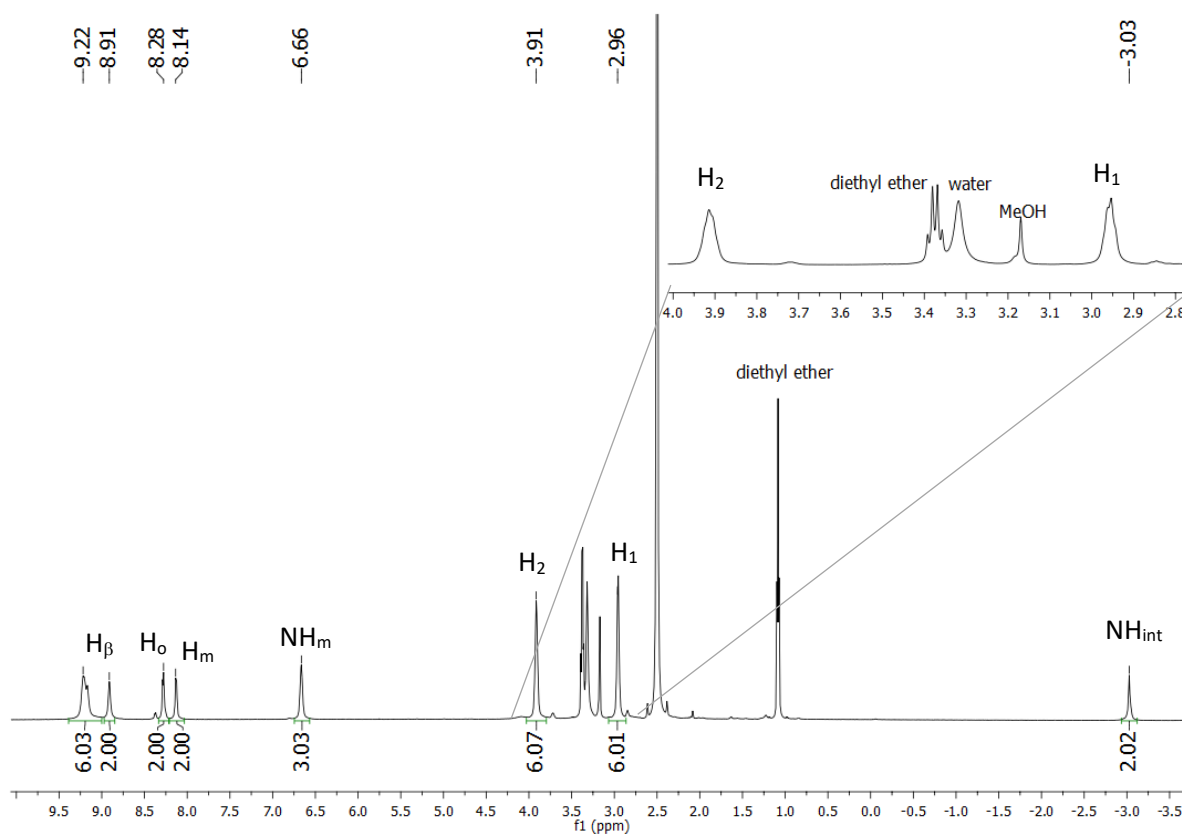
Figure 43: ^{1}H-NMR spectrum with expansion of **102** in DMSO-d_6 at 298 K and 600 MHz

^{19}F-NMR spectroscopy was very useful for the characterization of **102** (*Figure 44*). The peak at –
151.5 ppm generated by the *para* fluorines visible on the spectrum of **99** disappeared (*Figure 39*),
indicating that a complete functionalisation took place. The signals at –143.7 ppm and –162.6 ppm
are attributed to the *ortho* and *meta* fluorines, respectively.

All the ^{1}H-^{13}C assignments are summarised in *Table 14* below.

^{13}C δ (ppm)	Assignment	^{1}H δ (ppm)	Assignment
167.7	COOH	-	-
134.5	C_o	8.41	H_o
127.9	C_m	8.41	H_m
42.0	C_2	3.91	H_2
50.8	C_1	2.96	H_1
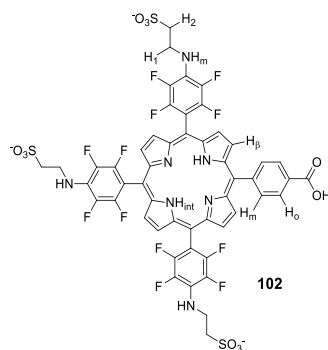
Table 14: hydrogen-carbon assignments and structure of **102**
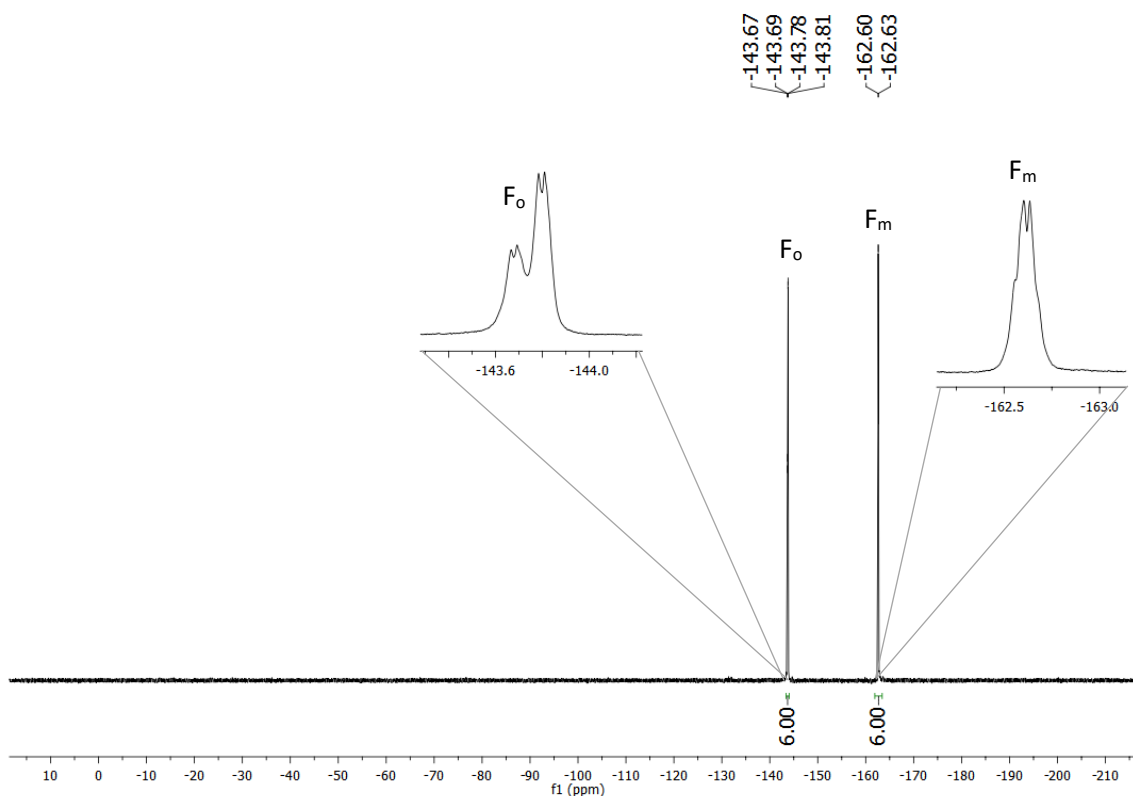
Figure 44: ^{19}F{^{1}H}-NMR spectrum with expansion of **102** *in DMSO-d$_6$ at 298 K 565 MHz*

Figure 45 and *Figure 46* show the hydrogen-carbon 2D-NMR correlation. DEPT-edited $^{1}H,^{13}C$-HSQC (*Figure* 45) helped to assign the hydrogens present in the taurine chains to the carbon atoms they are linked to, as highlighted in the expansion of the green circle in *Figure 45*. The hydrogen signals at 2.96 ppm (H_1) and 3.91 ppm (H_2) indicate a correlation with the carbons at 50.8 ppm and 42.0 ppm, respectively. The confirmation that the hydrogen signal at higher ppm corresponds to the CH_2 group directly attached to the sulphonate group, as suggested before, was achieved upon inspection of the $^{1}H,^{13}C$-HMBC spectrum shown in *Figure 46*. The blue circle of *Figure 46* highlights the ^{2}J correlation between the hydrogens in the amine groups with the closest carbon of the moiety, at 50.8 ppm. This carbon correlates with the hydrogen signal at 2.96 ppm (H_1), confirming the proposal. The dots indicated with an orange X in *Figure 46* represents the cross correlations between H_1 with C_2 and H_2 with C_1.
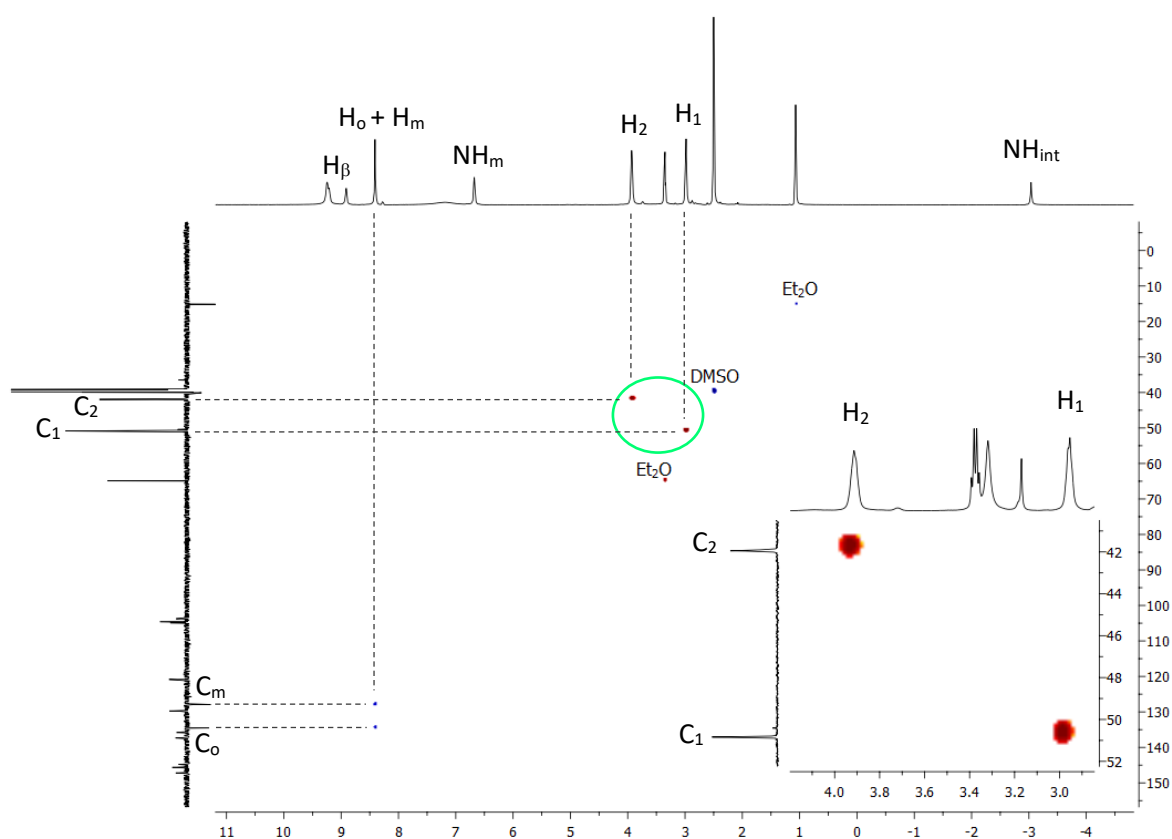
*Figure 45: DEPT-edited (135°) $^{1}H,^{13}C$-HSQC spectrum of **102** with expansion, red dots CH_2 up, blue dots CH/CH_3 down, in DMSO-d_6 at 298 K and 600 MHz and 150 MHz*
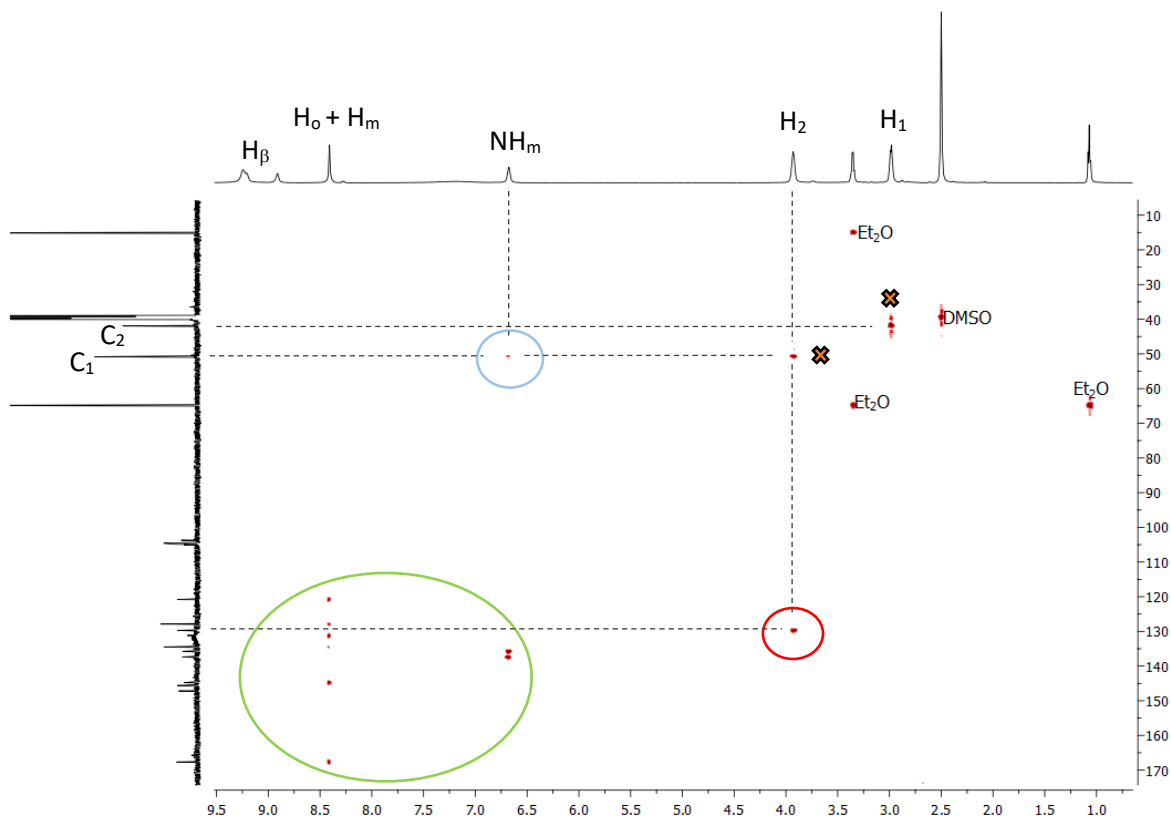
Figure 46: *$^1H,^{13}C$-HMBC spectrum of **102** in DMSO-d_6 at 298 K* and 600 MHz and 150 MHz

It is interesting to note that the hydrogen at 3.91 ppm (H$_2$) presents a correlation (red circle in *Figure 46*) with a carbon at 129.7 ppm. This hydrogen-carbon correlation is displayed on the 2D spectrum probably due to its high ^4J value. Inconveniently, the carboxyphenyl hydrogens appear as a singlet, preventing from a secure assignment to the relative carbons. However, it can be assumed that the signal at higher chemical shifts (134.5 ppm) is generated by the carbons in *ortho* to the carboxy group. Automatically, the signal at 127.9 ppm is assignable to the carbon in *meta* position of the carboxyphenyl ring, as summarized in *Table 14*.

The area in the green circle in *Figure 46* is expanded in *Figure 47*. The dots indicated with a purple X represents the cross correlations between the *ortho* hydrogens of the carboxyphenyl ring (H$_o$) with the *meta* carbons (C$_m$) and *vice versa*. The last correlation (red circle in *Figure 47*) is relative to the *ortho* hydrogens (H$_o$) with the carbonyl carbon at 167.7 ppm. Therefore, the remaining three correlations must be between the aryl hydrogens with the two quaternary carbons of the ring, and with the closest *meso* carbon, the one bearing the carboxyphenyl ring. No unequivocal assignment is possible with the data available, but the chemical shifts of the carbons are 120.8 ppm, 131.2 ppm and 144.8 ppm. Moreover, it can be noted in *Figure 47* (blue circle) that the amine hydrogens signal at 6.66 ppm presents two correlations with two different carbons, at 135.8 ppm and 137.4 ppm. These

two signals could be assigned to the two *para* carbons attached to the amines of the moieties on the two magnetically different aryl rings.
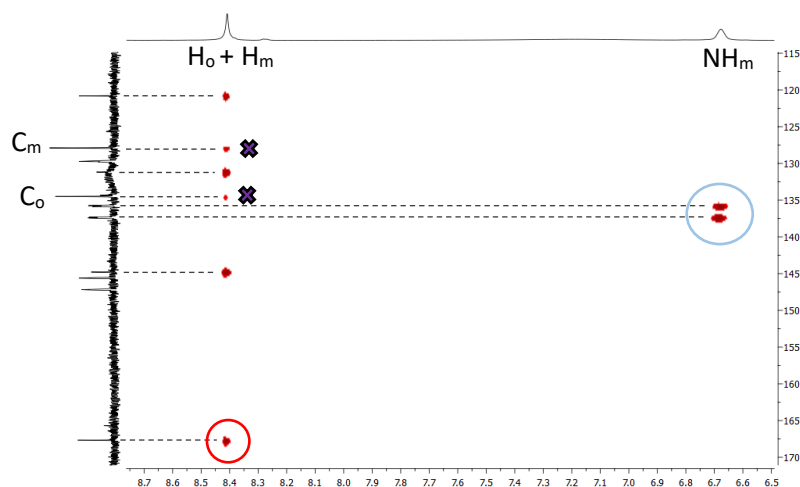
*Figure 47: expanded area of $^1H,^{13}C$-HMBC spectrum for **102** (green circle in Figure 46)*

Ion exchange purification method for negatively charged porphyrins

Purification methods for anionic water-soluble porphyrin are occasionally reported in the literature but they are extremely cumbersome. Separation of sulphonated porphyrins from inorganic salts mixtures has been carried out by continuous or fractioned extraction with methanol or ethanol until no inorganic salts were present,[216] or by treatment with methanolic ammonia followed by repeated precipitation of the inorganic impurities with addition of acetone.[217,218] Following sulphonation with sulphuric acid, the addition of calcium oxide can help removing the sulphate in excess by repeated precipitation in H_2O/acetone.[219] Several precipitations in acetone/MeOH with later dissolution in water and purification through a Sephadex column (G25) can also be carried out to purify the compound.[220] Despite these tedious and scarcely reproducible methods require relatively large volume of solvents, and the use of expensive solid supports leads to the loss of material with subsequent low yields, they are somewhat effective to obtain moderate amounts of sulphonated porphyrins.[217,218] In our hands, when applied to the purification of **102**, none of these approaches was successful. Separating lithium taurine from water-soluble **102** bearing three moieties essentially identical to taurine proved extremely challenging. Crystallisation of the unreacted taurine in cold methanol and subsequent filtration led to enrichment of the mixture but not to pure **102**, as highlighted by spectroscopic analysis.

Based on the success of the ion-exchange method to purify cationic species, the attention was focused on the development of a similar method for negatively charged derivatives. In order to carry out ion

exchange, a water-soluble salt whose cation would cause the precipitation of the negatively charged porphyrin in water was required. This non-water-soluble salt would need to be soluble in organic solvent, so that treatment with a sodium salt of similar solubility would cause the precipitation of the sodium salt of the porphyrin. The development of the method started from the few examples of purification of organic sulphonates using tertiary amines reported in the literature.[221,222]

In our hands, neither hydrochlorides of tertiary aliphatic amines nor tetra-alkyl ammonium salts were effective in inducing the precipitation of the sulphonate salt. Bulky hydrocarbon moieties could decrease the water solubility of the ion pair, so we turned our attention to aniline derivatives. The hydrochloride salt of dibutylaniline (**103** in *Figure 48*) proved suitable for the purpose, as the precipitation of **102** was induced by the addition of dibutylaniline followed by aqueous HCl to the porphyrin solution.

103
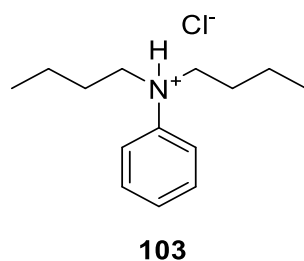
*Figure 48: structure of dibutylanilium chloride **103***

We found that the use of pre-formed **103** as a solid was more convenient. The salt was obtained by dissolving dibutylaniline in methanol, followed by methanolic HCl and precipitating **103** by addition of diethyl ether after 1 hour at room temperature. The salt, collected by filtration was sufficiently pure for the purpose.

Dibutylaniline (**104** in *Scheme 26*) is relatively expensive compared to dimethyl and diethyl aniline, so it seemed reasonable to try to obtain non-water-soluble porphyrin salts with cheaper starting materials. Both anilines were converted into the corresponding hydrochlorides, but interestingly, neither of the two behaved as expected. In both cases, the supernatant of the aqueous porphyrin solution retained partial colour after the addition of the hydrochloride salt, indicating incomplete precipitation. We speculate that the more efficient precipitation of the dibutylanilinium salt of the porphyrin is due to the contribution of the larger hydrophobic butyl groups, instead of two methyl or two ethyl groups. The precipitate, collected by centrifugation, was dissolved in acetone and the water-soluble sodium salt of the porphyrin was precipitated following addition of $NaPF_6$. This purification method not only allows to remove unreacted taurine, but also to purify **102** from any other contaminant present in the reaction mixture, either soluble in water or in organic solvents. The

purification method also worked flawlessly to purify compounds **57** and **76** from the aqueous mixture. No interactions were observed between the salt and the carboxylic acid function. As described, though, the purification method presented a non-negligible drawback: it cannot be used to isolate the porphyrin from alkaline reaction mixtures, since the hydrochloride salt would be converted to the corresponding base, preventing its association with the anionic porphyrin and, therefore, the precipitation.
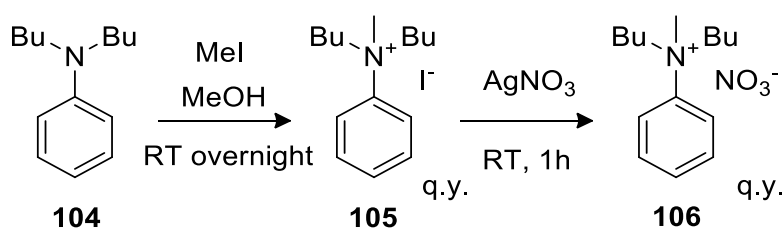
Scheme 26: methyl-dibutylanilinium chloride reaction scheme

It seemed necessary to further optimise the method to eliminate this shortcoming and expand its applicability, so **105** was prepared by methylation of dibutylaniline (*Scheme 26*).[223,224] Unexpectedly, the iodide salt obtained from the methylation reaction was ineffective as precipitating agent. Treatment of an aqueous solution of **105** with one equivalent of silver nitrate led to the precipitation of silver iodide (removed by precipitation) to obtain **106**. This species was as efficient as **103** to induce precipitation of porphyrins from aqueous solutions. The two-step process to synthesise **106** is undoubtedly less convenient compared to the preparation of **103**, but the resulting species can be used in aqueous environment at different pH values. In this work compound **103** was most frequently used, while compound **106** was employed only when the situation was requiring it. The applicability of the method was not limited to the specific case of **102**, but it could be extended also to other porphyrins bearing sulphonate groups, such as **57** and **76**. Future development of this method should include its application to a further class of anionic water-soluble porphyrins: those bearing phosphonate groups. Based on the observation, there is no reason to anticipate that this method would fail for phosphonate-bearing porphyrins: we feel confident in affirming that a new, cheap and expeditious purification method, easy to scale up and applicable to different classes of anionic water-soluble porphyrins has been created.

Cationic water-soluble derivative of compound **99**

To obtain the target library of conjugatable water-soluble porphyrins, one more compound was required: a water-soluble porphyrin based on the structure of **99** bearing positively charged groups.
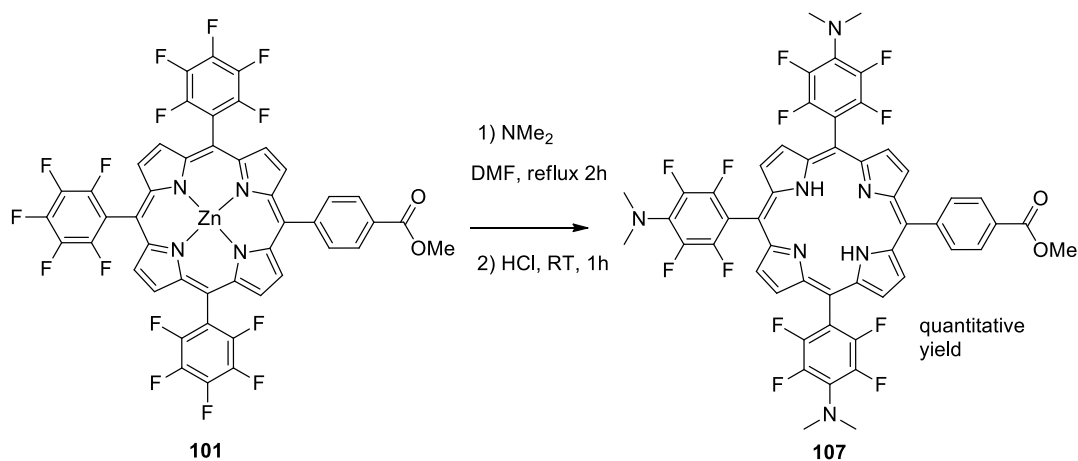
*Scheme 27: synthesis of **107***

Firstly, nucleophilic substitution of the *para*-fluorines of **101** was attempted with dimethyl amine.[225] The reaction is reported to occur in DMF, which undergoes degradation at high temperatures to produce the dimethyl amine nucleophile *in situ*. In our hands, the reaction failed to reach completion in the conditions described. The desired compound was obtained by treating **101** with a solution of dimethylamine in DMF at reflux in a sealed system, to prevent dimethylamine from escaping (*Scheme 27*). ^{1}H-NMR spectrum of compound **107** is shown in *Figure 49*. The sharp singlet at 3.29 ppm with an integration value of 18H is generated by the six methyl groups introduced in the molecule (($NCH_3)_2$). The other signals are similar to those observed in the spectrum of **99**: eight *beta* hydrogens, four hydrogens of the phenyl ring, three hydrogens relative to the methyl group and the internal ones. ^{19}F-NMR spectroscopy revealed a complete functionalisation, due to disappearance of the peak of the *para* fluorines.

To make this species water-soluble, methylation of the newly-introduced dimethylamino groups was necessary.[226] In our hands, the conditions described by Richards *et al.* did not lead to the formation of the desired tricationic derivative, neither when the free porphyrin nor the zinc complex was used as the starting material, so the attention was directed to the synthesis of a different species.
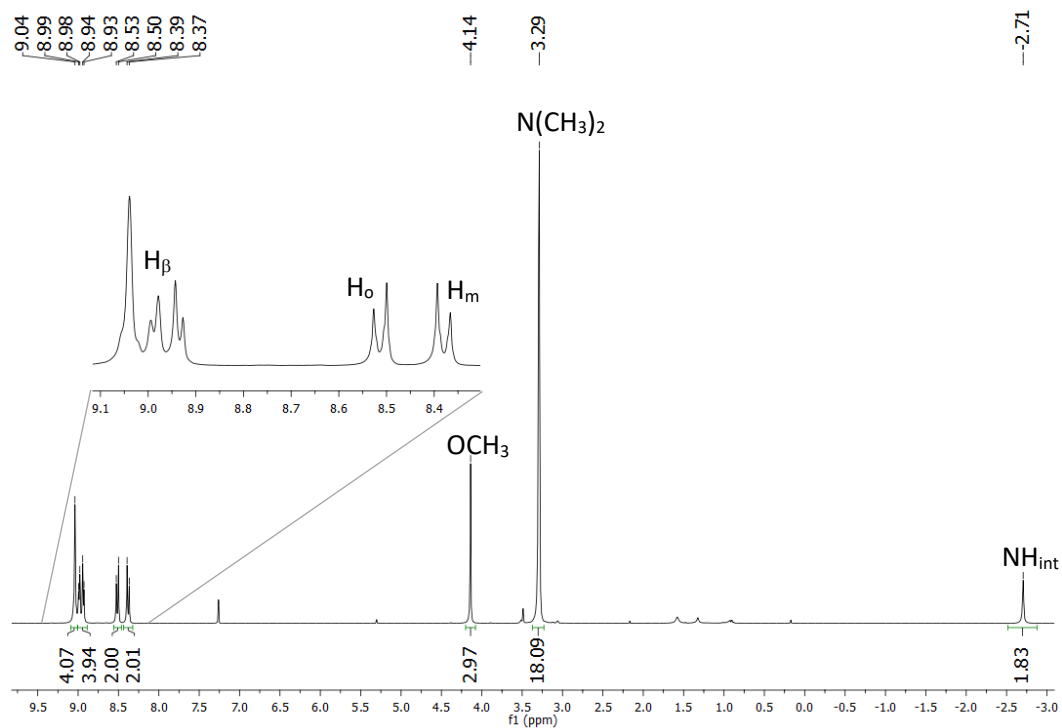
*Figure 49: ^{1}H-NMR spectrum with expansion of **107** in CDCl$_3$ at 298 K and 600 MHz*

Following the successful synthesis of porphyrin **102**, the aim was to synthesise a molecule with an identical skeleton but bearing trimethylammonium groups (-NMe$_3^+$) instead of the sulphonate groups (*Figure 50*). The target species **108** can be achieved either by replacing the *para*-fluorines with a cationic nucleophile, or by using a non-cationic nucleophile and inserting the cationic group at a later stage. Both approaches were attempted.

108
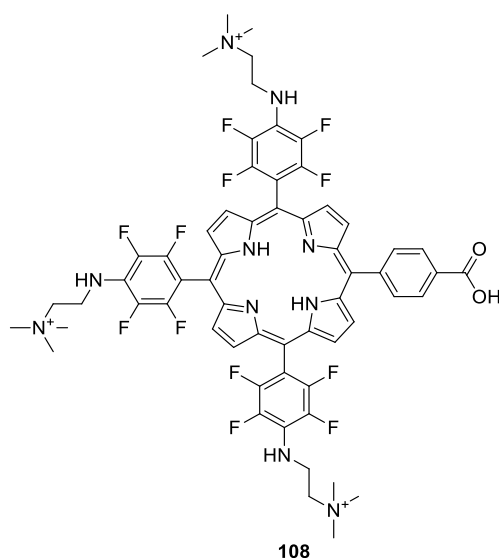
*Figure 50: target molecule (**108**) for cationic water-soluble **99***

In the first instance, a cationic water-soluble species with an amino group was obtained to carry out the nucleophilic displacement, starting from N-Boc-ethylenediamine (**109**) as shown in *Scheme 28*.[227–229]
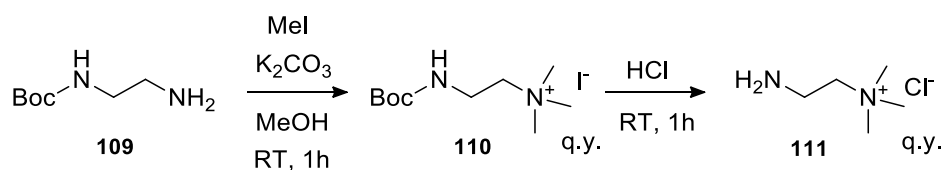
Scheme 28: synthesis of water-soluble positively charged moiety **111**

109 was treated with an excess of methyl iodide in methanol in the presence of K_2CO_3.[227,229] Following isolation of the cationic species **110**, the protecting group was removed in HCl, yielding the target compound **111**.[228] ^{1}H-NMR spectra of compounds **110** and **111** are shown in *Figure 51* and *Figure 52*, respectively. Compound **110** shows a peak at 3.48 ppm attributable to the three methyl groups attached to the amine (N$^+$(CH$_3$)$_3$, *Figure 51*). Deprotection of **110** led to the disappearance of the peak at 1.42 ppm (*t*-butyl group), while a broad peak at 8.66 ppm appeared (NH$_3$$^+$) indicating the formation of the target compound **111**.
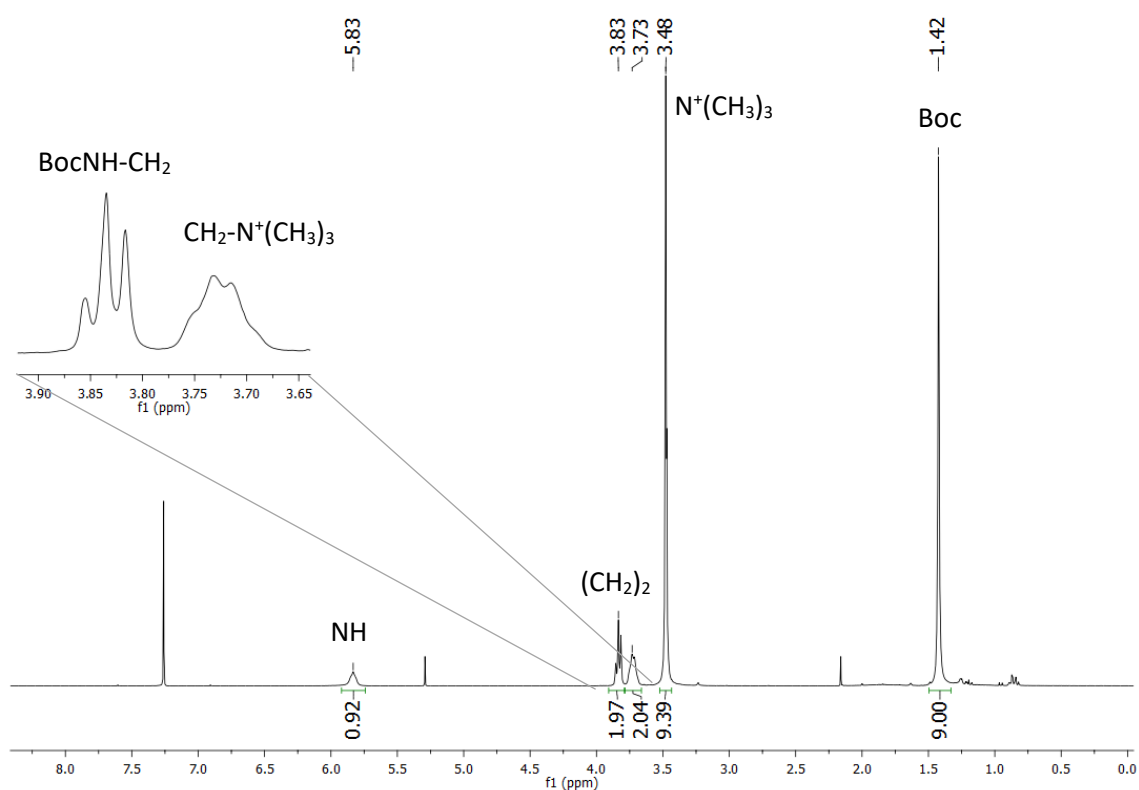
Figure 51: ^{1}H-NMR spectrum with expansion of **110** in CDCl$_3$ at 298 K and 600 MHz
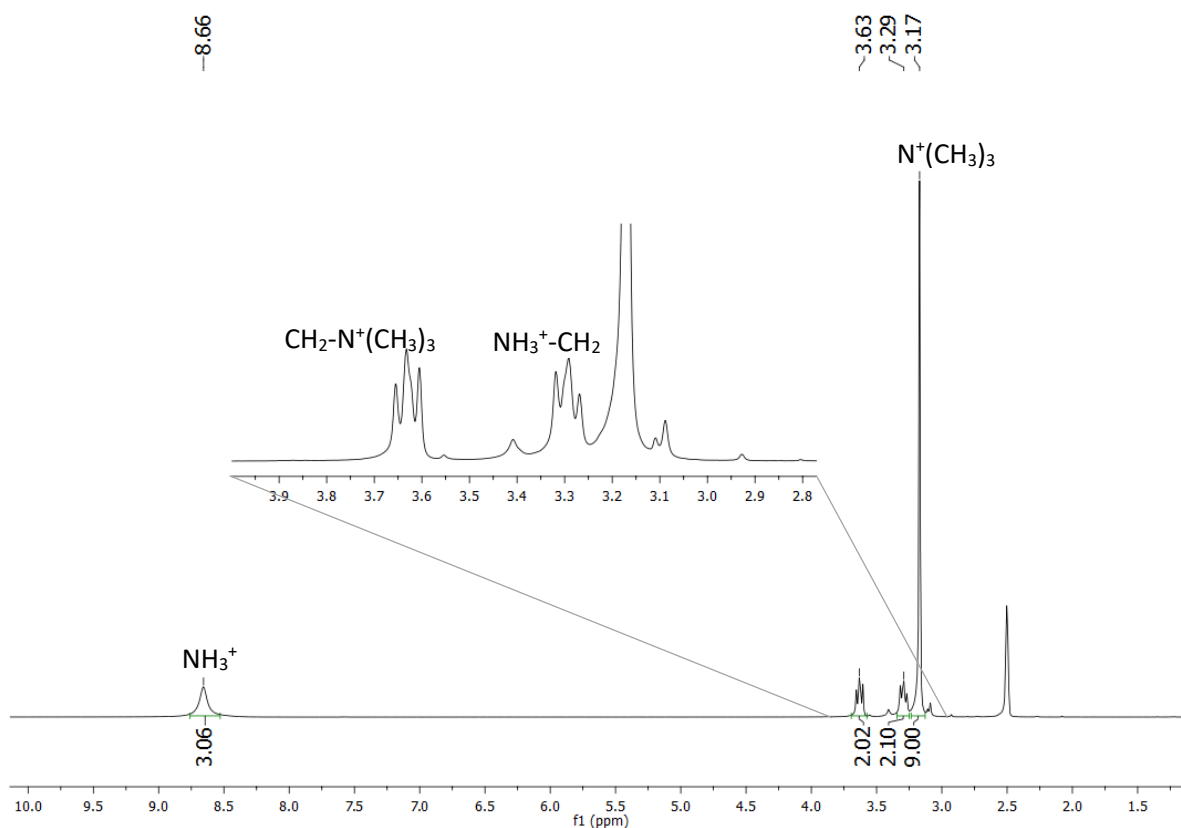
*Figure 52: ^{1}H-NMR spectrum with expansion of **111** in DMSO-d$_6$ at 298 K and 600 MHz*

Unfortunately, the nucleophilic aromatic displacement was unsuccessful. This prompted us to explore different reaction conditions, varying the base, the solvent, the reaction temperature and the nucleophile (*Table 15*). The substitution between **109** (*Table 15*) and **101** was attempted. After three weeks at reflux in 1,4-dioxane, MS analysis of the reaction mixture showed the presence of a mixture of products at different degrees of substitution. Performing the reaction under microwave heating (170 °C for 8 hours) did not improve the outcome of the reaction. After that time, traces of unreacted porphyrin were still present, meaning an even slower reaction rate compared to the three-carbon moiety employed in the literature.[230] The reaction between **109** and **79c** is reported in the literature,[183] but in our hands similar reaction conditions failed to give complete functionalisation of **99**. The literature procedure is described on a 5-mg scale: it is possible that the scale-up of the synthesis was either not attempted or it is not reported because of the poor performance of the reaction. When the reaction was attempted on 100 mg of starting porphyrin **99**, incomplete functionalisation and partial degradation of the substrate were observed. The displacement of the *para* fluorines by the cationic derivative **111** (*Table 15* and *Scheme 28*) or compound **112** (*Table 15*) gave equally disappointed results. No functionalisation at all was detected and degradation of both the porphyrin and the nucleophile were observed.

Side chain	Solvent	Base	T (°C)	Zn	MW	Time (h)	Substitution
111 H_2N–N$^+$	NMP	K_2CO_3	200	√	√	1	-
	NMP	K_2CO_3	200	-	√	1	-
	1,4-dioxane	K_2CO_3	100	-	-	2	-
112 H_2N–N	NMP	K_2CO_3	200	√	√	1	-
	NMP	K_2CO_3	200	-	√	1	-
	NMP	LiOH	200	√	√	1	-
	DMF	-	170	√	-	24	-
	DMSO	LiOH	100	√	-	8	-
	DMSO	LiOH	100	√	-	8	-
109 Boc–N(H)–NH_2	NMP	K_2CO_3	200	√	√	2	Incomplete
	NMP	K_2CO_3	200	-	√	2	Incomplete
	1,4-dioxane	K_2CO_3	170	√	√	8	Incomplete
	1,4-dioxane	K_2CO_3	170	√	-	500	Incomplete
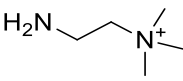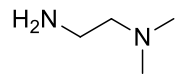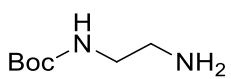
*Table 15: reaction conditions for nucleophilic substitution on **99** or **101***

Aromatic nucleophilic displacement of the *para* fluorines can be performed with nucleophiles such as thiols, amines and alcohols.[185] Among these species, thiols display the highest reactivity and can be used to functionalise perfluorinated porphyrins in mild reaction conditions. Amines require higher temperatures and longer reaction times to achieve a complete substitution. Alcohols are the least reactive nucleophiles and strong bases are often needed to deprotonate the hydroxy group and enhance the nucleophilicity.[231] We decided not to employ thiols because sulphur is known to act as a scavengers of reactive oxygen species (ROS),[193] which could interfere with the further optical oxygen measurements and also result in the cleavage of the relatively weak carbon-sulphur bond.[232] Having observed the lack of reactivity of amines, the attention was redirected to alcohols.

An in-depth study of the reactivity of oxygen nucleophiles towards **79c** and its Zinc (II) complex under different conditions is reported.[233] In this work, the reactivity of phenols and alcohols was described in the presence of a variety of bases (KOH, NEt₃, K_2CO_3, DBU and KOtBu) and solvents. Various alcohols were employed as nucleophiles, ranging from methanol to β-cholestanol, and the target tetra-substituted derivatives were obtained in good yield under mild reaction conditions. The reactions were performed at room temperature for 24-48 hours or shorter times at higher temperature. Optimum reaction conditions were found to be 24 hours at room temperature in dry THF with KOH as

base. Among the various alcohols, the authors used the Boc-protected ethanolamine **113**, under the previously described conditions, which afforded the tetra-substituted porphyrin **114** in 88% (*Scheme 29*).[233] Crucially, when **79c** was treated with non-protected ethanolamine, the amine group behaved as nucleophile rather than the alcohol.[231] The authors also showed that prolonged reaction times led to the substitution of the *para* fluorines with hydroxyl groups, a behaviour that was ascribed to the presence of high concentration of a nucleophilic base as KOH.
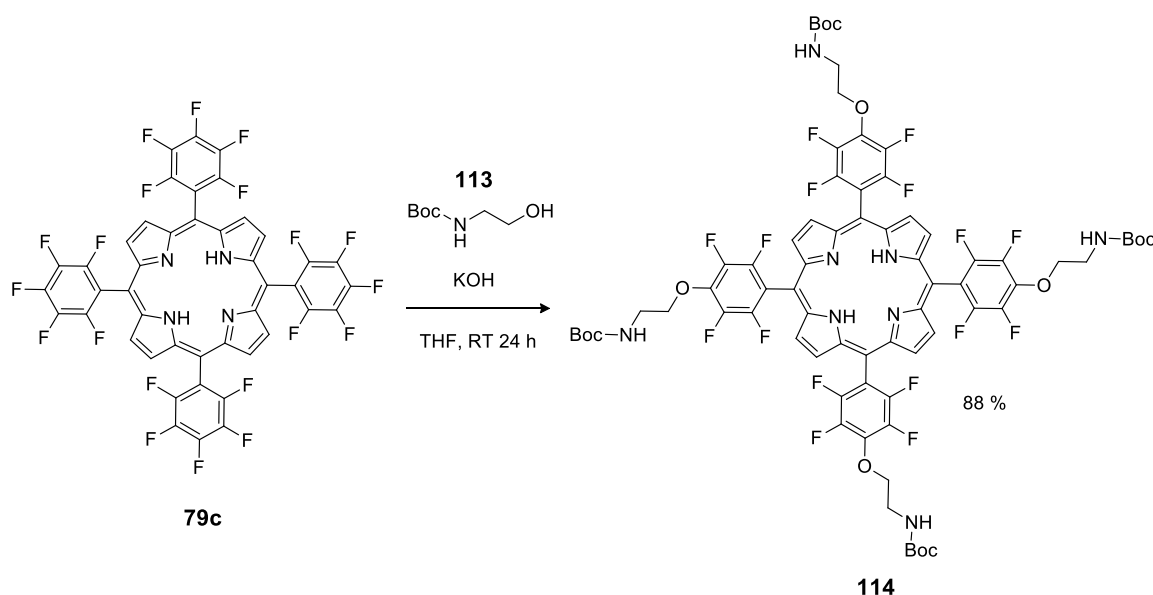
*Scheme 29: nucleophilic substitution on **79c** with Boc-ethanolamine*

The reaction using the cationic species **115** as the nucleophile, obtained by treatment of ethanolamine with methyl iodide (*Scheme 30*) was attempted first. The reaction conditions used were the ones described by Golf *et al.*, with DMSO as a solvent and LiOH as the base, stirring the mixture under argon at room temperature.[233] MS analysis showed that the reaction led to fluorine displacement by hydroxyl groups, and ^{19}F-NMR confirmed the complete substitution by disappearance of the relevant peak. The *m/z* of 922 detected matches the molecular weight of the trihydroxy-substituted product bearing the carboxylic acid, hydrolysed during the reaction. Both the free base and the zinc complex of **99** were tested, without success. Furthermore, the reaction conditions caused the hydrolysis of the ester to the corresponding carboxylic acid. The synthetic strategy was then reviewed, and the approach shown in *Scheme 31* was adopted.
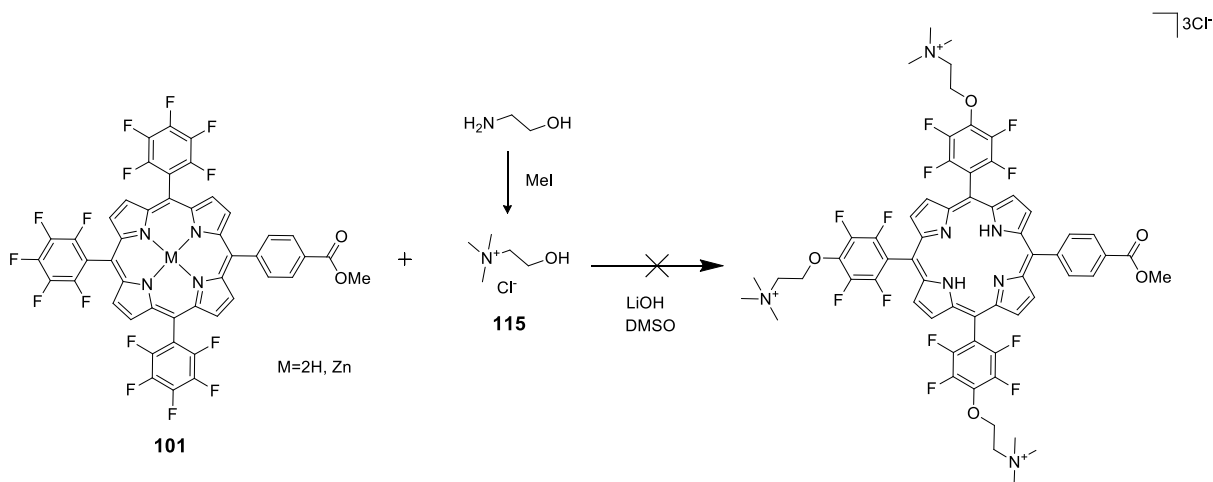
Scheme 30: attempted synthetic strategy

The reaction was performed with Boc-protected ethanolamine **113**, obtained by protection of ethanolamine with *tert*-butyldicarbonate, in dry DMSO with LiOH in equimolar ratio to **113** and in a large excess to the porphyrin to favour complete substitution. These conditions gave the desired trisubstituted product **116** in 73% yield up to multigram-scale. A further advantage of using **113** is that the reaction product can be purified by column chromatography. The reaction temperature appeared to be a crucial parameter for the success of the reaction. Performing the reaction at room temperature gave the desired product in good yield, but incomplete substitution was observed at temperatures below 33 °C even after two weeks. Maintaining the reaction mixture at 33-35 °C yielded **116** overnight, but temperatures equal or above 40 °C led to fluorine substitution with hydroxide ions within 5 minutes.
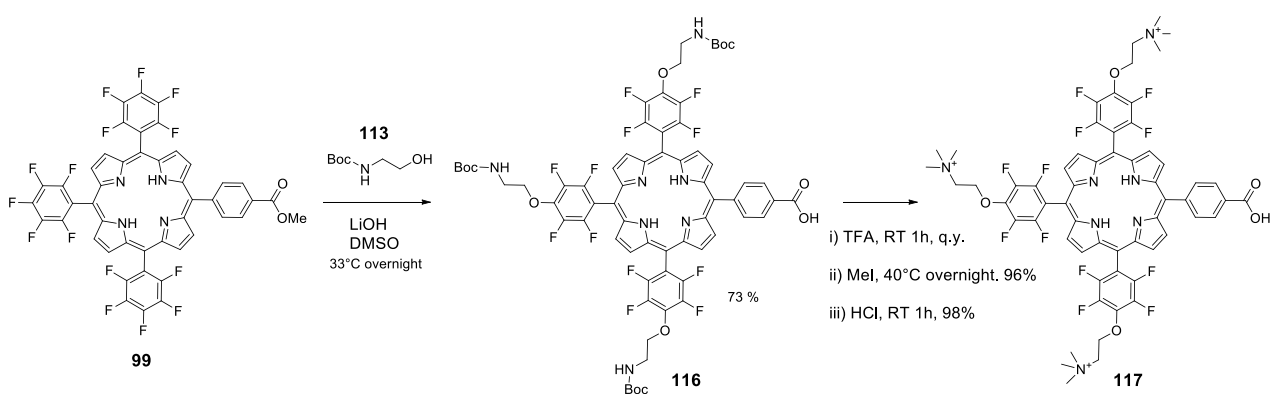
Scheme 31: successful synthetic strategy

As mentioned above, the reaction conditions caused the hydrolysis of the methyl ester yielding the tri-substituted carboxylic acid **116**: this proved helpful in the purification process, as the polarity of

the carboxylic acid decreased the retardation factor of the product, allowing for an easier purification by column chromatography on silica gel.

^{1}H-NMR spectrum of compound **116** is shown in *Figure 53*. Characteristic peaks corresponding to the ones of **99** are evident. The *beta* hydrogens appear at 8.93 ppm (H_β), the aryl hydrogens resonate as two doublets between 8.36 and 8.59 ppm (H_o and H_m), and the internal hydrogens are detected at high fields (NH_{int}). New peaks emerge between 1.0 and 6.0 ppm. The signals at 3.77 ppm and 4.67 ppm correspond to the CH_2 groups of the ethanolamine moieties, while the signal at 5.25 ppm can be assigned to the protected amine hydrogens (NH_m). The very sharp signal in the aliphatic region is produced by nine methyl groups (27H in total) present in the Boc moieties. All the peaks are summarized in *Table 16*.
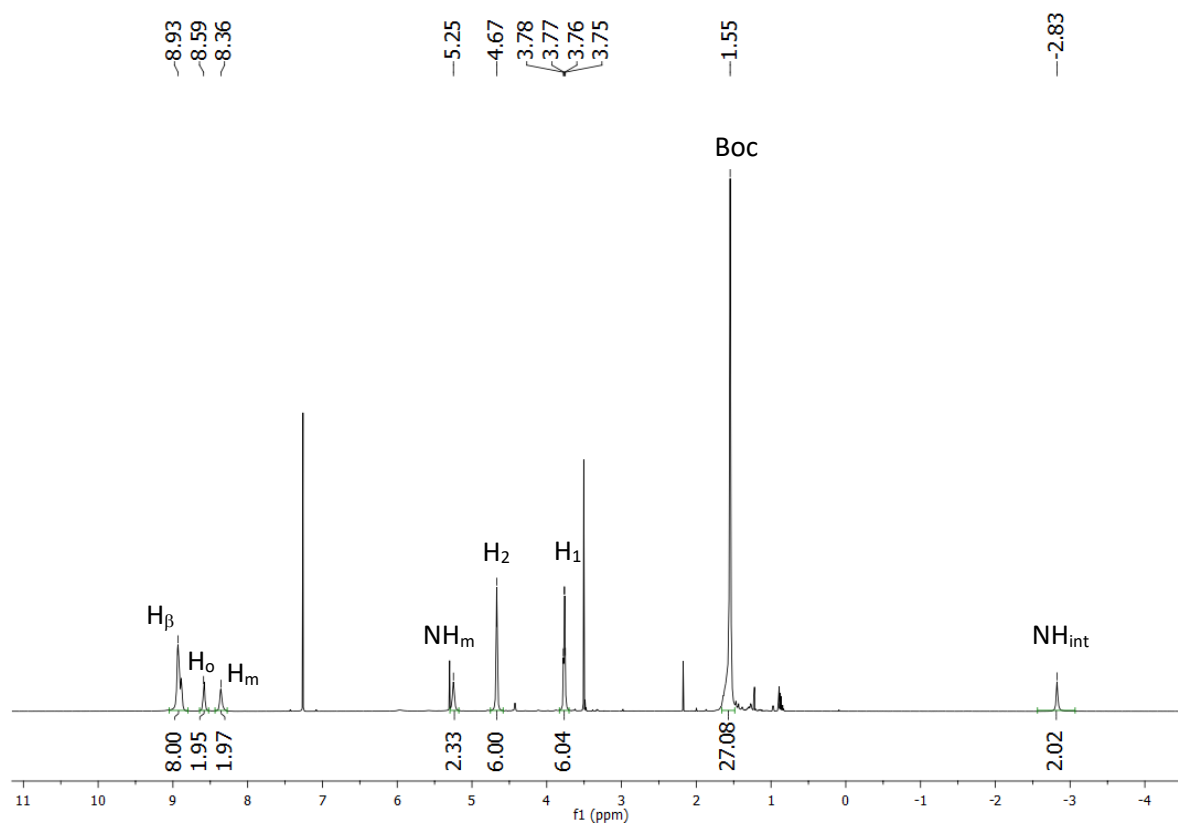
*Figure 53: ^{1}H-NMR spectrum of **116** in CDCl₃ at 298 K and 600 MHz*

^{19}F-NMR analysis of **116** is shown in *Figure 54*. The disappearance of the *para* fluorine signal at −151.5 ppm (see *Figure 39*) highlights a complete functionalisation of the molecule. The two doublets at *ca.* −138.4 ppm are assigned to the *ortho* fluorines on the three non-equivalent aromatic rings. The signal with an integration value of 4F is attributed to the *ortho* fluorines on the aryls opposite to each other on the porphyrin, while the doublet with integral value of 2F corresponds to the *ortho* fluorines on

the aryl ring opposite to the carboxy-substituted aryl ring. The signal at −157.2 ppm belongs to the *meta* fluorines.

Multiplicity	δ (ppm)	Integration value	Assignment
br m	8.93	8	H_β
br m	8.59	2	H_o
d	8.36	2	H_m
s	5.25	3	NH_m
t into br s	4.67	6	H_2
t into br s	3.77	6	H_1
s	1.54	27	Boc
s	−3.03	2	NH_{int}
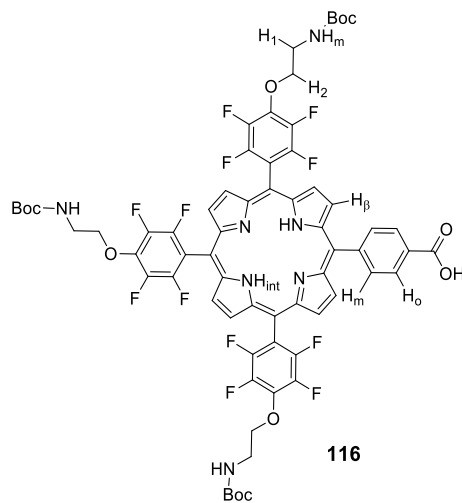
*Table 16: hydrogen signals assignment and structure of **116***
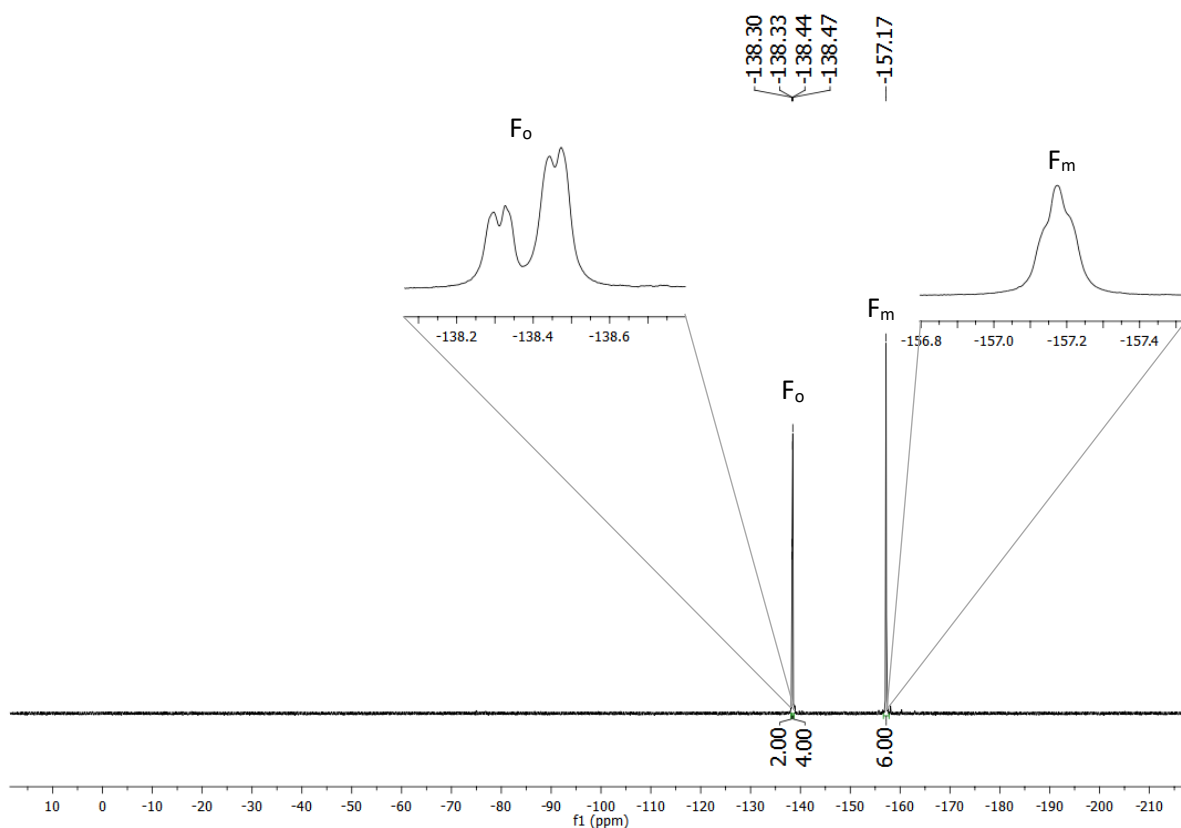
*Figure 54: $^{19}F\{^1H\}$-NMR spectrum of **116** in CDCl$_3$ at 298 K and 565 MHz*

The ^1J DEPT-edited $^1H,^{13}C$-HSQC shown in *Figure 55* allows attribution of several signals of carbon/hydrogen pairs. For instance, the methyl carbon in the Boc groups resonates at 28.6 ppm, while the carbon signals of the ethanolamine moieties appear at 74.8 and 41.0 ppm. The hydrogens in *ortho* and *meta* positions to the carboxylic group, with 8.59 and 8.36 ^1H chemical shifts, respectively, correlate with the carbon signals at 128.8 ppm and 134.8 ppm, respectively. All the hydrogen-carbon assignments are summarized in *Table 17*.

^{13}C δ (ppm)	Assignment	^1H δ (ppm)	Assignment
134.8	C_m	8.36	H_m
128.8	C_o	8.59	H_o
74.8	C_2	4.67	H_2
41.0	C_1	3.77	H_1
28.6	Boc	1.54	Boc
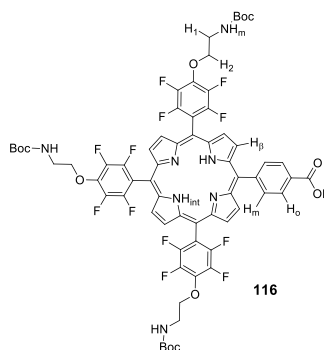
*Table 17: hydrogen-carbon signals assignment and structure of **116***
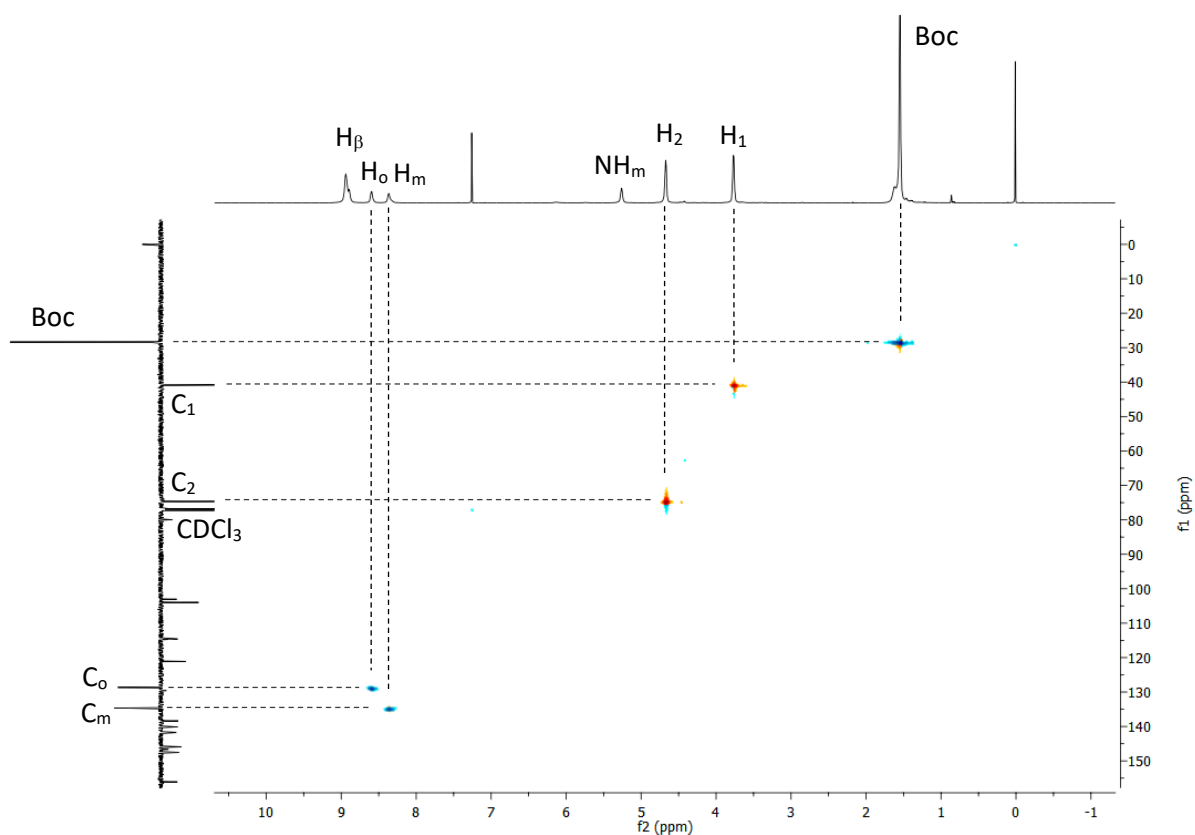
*Figure 55: DEPT-edited (135°) $^1H,^{13}C$-HSQC spectrum of **116**, blue dots CH/CH₃ up, orange dots CH₂ down, in CDCl₃ at 298 K and 600MHz and 150 MHz*
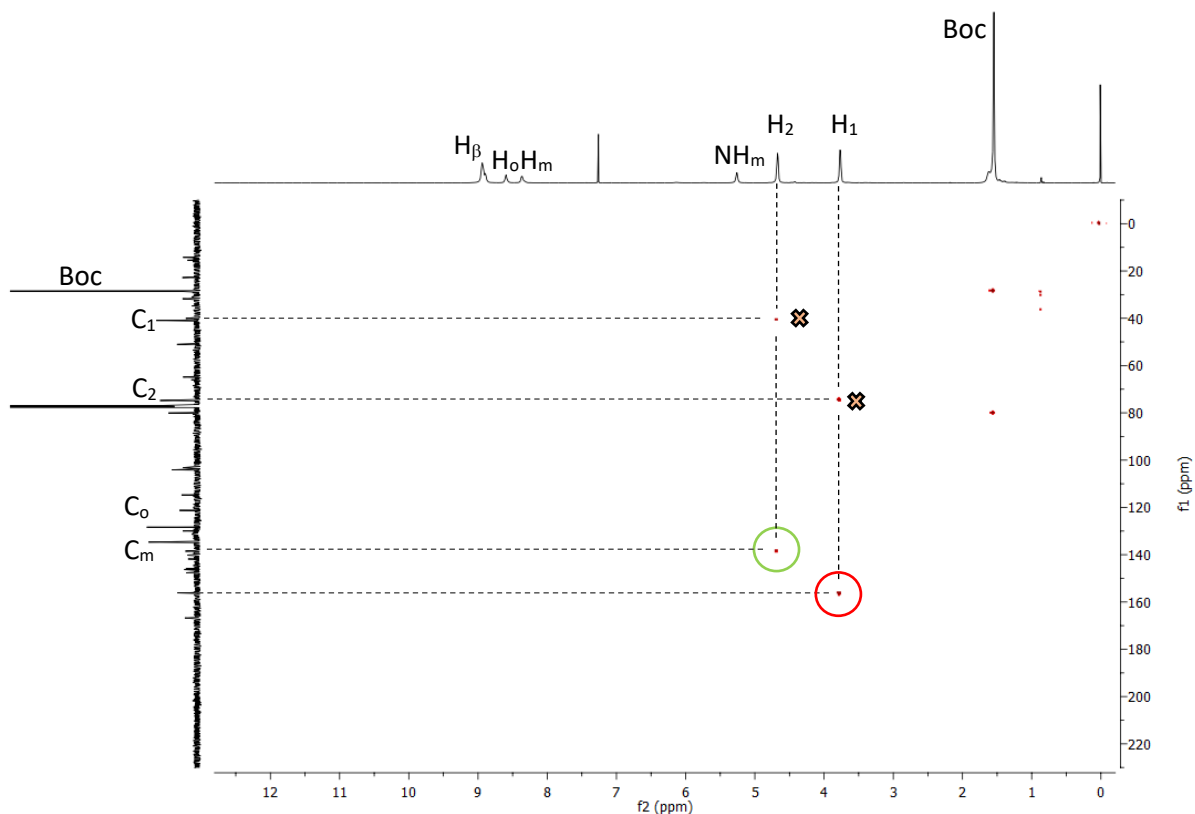
*Figure 56: $^1H,^{13}C$-HMBC spectrum of **116** in CDCl$_3$ at 298 K and 600MHz and 150 MHz*

Figure 56 displays the $^1H,^{13}C$-HMBC correlation spectrum. The dots indicated with an orange X are the cross correlations between H$_1$ with C$_2$ and H$_2$ with C$_1$. The dots highlighted by the red circle represent the correlation between the hydrogens at 3.77 ppm with a weak carbon signal at 156.2 ppm. This quaternary carbon presents a chemical shift typical of the carbonyl carbon in Boc protecting groups. The correlation is important because it allows to distinguish H$_1$ and H$_2$, as summarized in *Table 17*. On the other hand, the correlation highlighted by the green circle in *Figure 56* is between H$_2$, the CH$_2$ group of the moiety closest to the porphyrin, and the quaternary carbon directly attached to the oxygen, at 137.7 ppm.

The next step in the synthesis entailed the deprotection of the amino group (*Scheme 32*). The desired product **118** is not suitable to purification by chromatography on silica gel, therefore, it was important to rely on a deprotection reactions that would proceed to completion and afford the target species in sufficient degree of purity. A considerable advantage of Boc removal is that it leads to the formation of volatile side products (CO$_2$ and isobutene) which are easily removed during the isolation of the deprotected species. Thus, treatment of a solution of **116** in chloroform with an excess of TFA for 1 hour at room temperature and subsequent evaporation of the solvent under reduced pressure afforded **118** as the trifluoroacetate salt in quantitative yield.

^{1}H- and ^{19}F-NMR spectra shown in *Figure 57* and *Figure 58*, respectively, confirmed a high purity of the product, which was used in the following step without further manipulation. The yield of the reaction was quantitative.
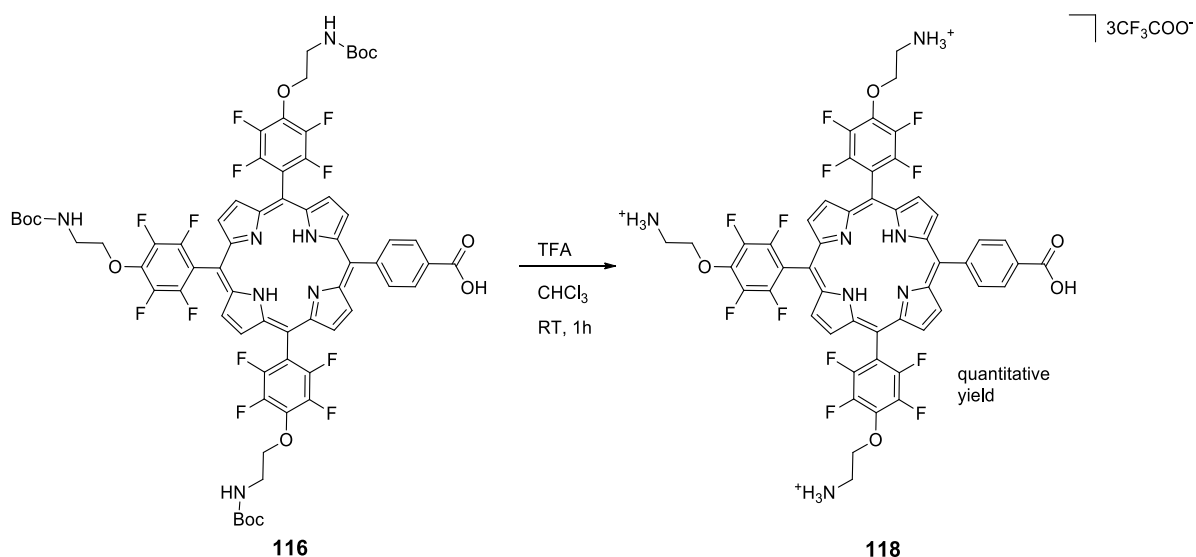
*Scheme 32: Boc deprotection of **116***

Four hydrogens on the carboxyphenyl ring appear now as a sharp singlet at 8.43 ppm (H_{Ar}) and the new peak at 8.34 ppm is assigned to nine terminal ammonium hydrogens (NH_3^+). The disappearance of the peak related to the *tert*-butyl methyl groups in the aliphatic region further confirm successful deprotection. A very broad peak appears at a lower field at *ca.* 13.5 ppm, which is assigned to the carboxylic group, visible due to absence of exchange with DMSO-d_6. In the ^{19}F-NMR spectrum the *ortho* and *meta* fluorine of the porphyrin appear at −140.8 ppm and −156.8 ppm, respectively, and the peak at −74.5 ppm is attributed to the trifluoroacetate groups. *Table 18* shows the assignment of the hydrogen signals.
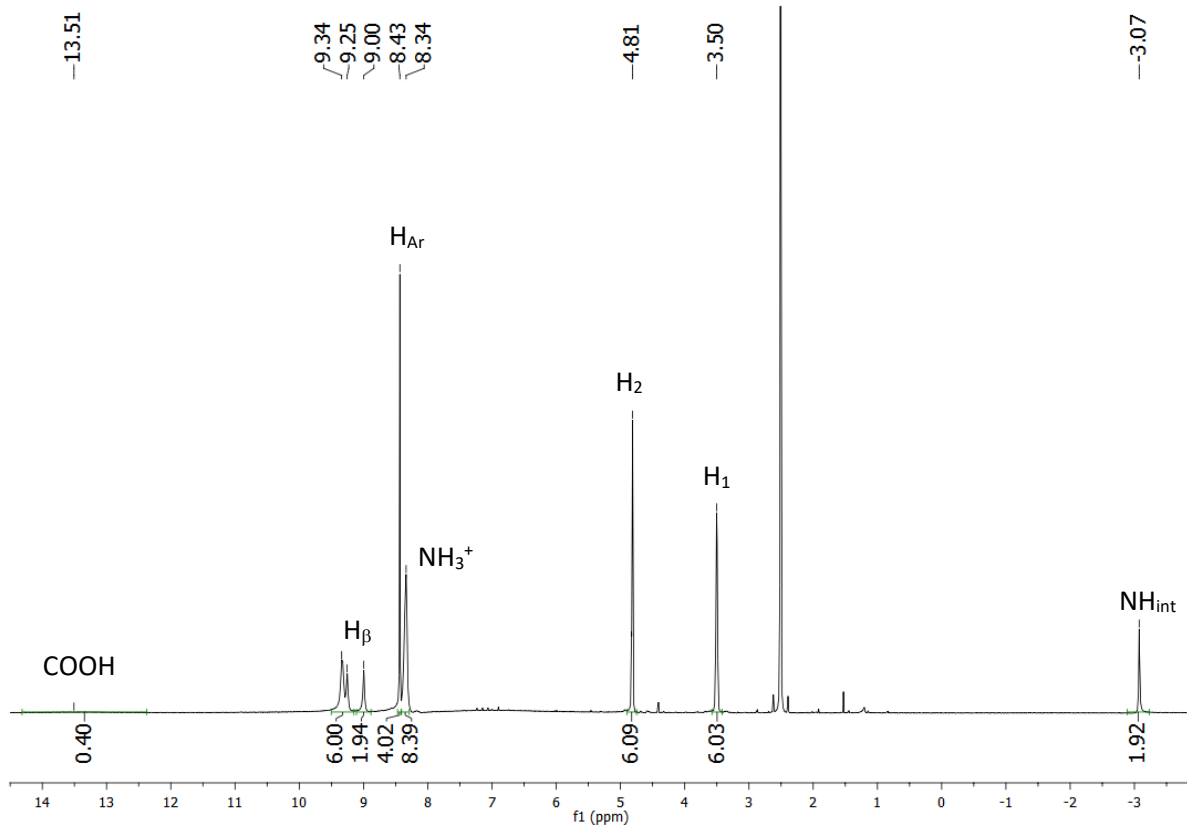
Figure 57: ^1H-NMR spectrum of **118** in DMSO-d_6 at 298 K and 600 MHz
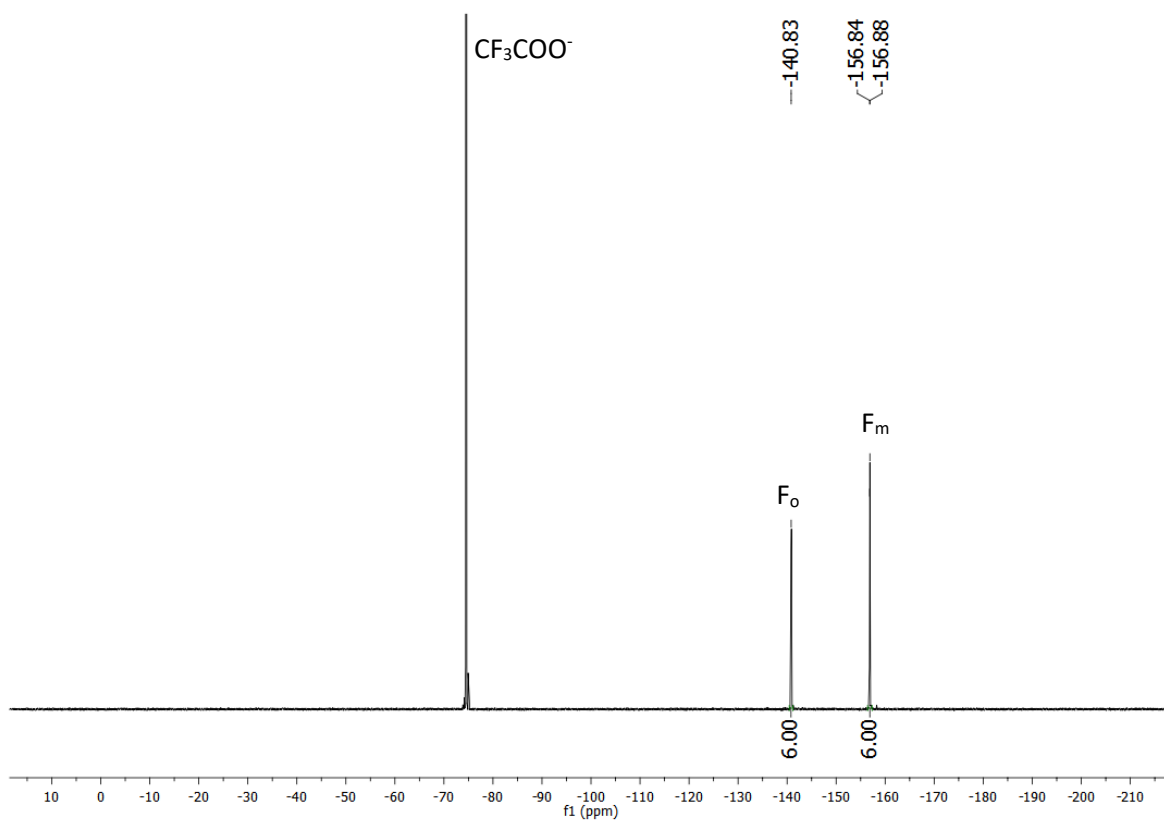
Figure 58: $^{19}F\{^1H\}$-NMR spectrum of **118** in DMSO-d_6 at 298 K and 565 MHz

Multiplicity	δ (ppm)	Integration value	Assignment
br s	13.51	1	COOH
m	9.25-9.34	6	H_β
m	9.00	2	H_β
2d into s	8.43	4	H_{Ar}
s	8.34	9	NH_3^+
t into m	4.81	6	H_2
t into m	3.50	6	H_1
s	−3.07	2	NH_{int}
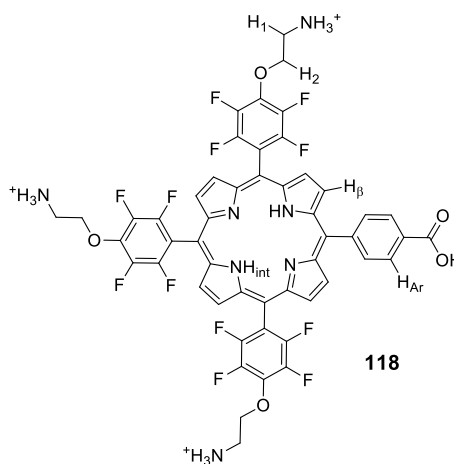
Table 18: hydrogen signals assignment and structure of 118

DEPT-edited $^1H,^{13}C$-HSQC, shown in *Figure 59*, allows to assign carbons/hydrogen pairs (*Table 19*). It is worth noting that one of the carbon signal of the ethanolamine moieties (C_1) is absent in the spectrum: the hydrogen-carbon correlation (red circle, *Figure 59*) allows assignment of the signal under the residual solvent peak, at *ca.* 39.5 ppm. Although the hydrogens on the carboxyphenyl ring appear as a singlet, two different carbons signals, at 134.6 ppm and 128.0 ppm, correlate with them. These peaks can be assigned to *meta* and *ortho* carbons, respectively, as in the case of compound 116 (see *Figure 55* and *Table 17*).

$^1H,^{13}C$-HMBC is shown in *Figure 60*. The signal generated by the four phenyl hydrogens shows correlations with multiple carbons in the aromatic region. The CH_2 signal at 4.67 ppm shows a correlation to a carbon (137.7 ppm) in the aromatic region (green circle, *Figure 60*), indicating that the signal is generated by the CH_2 group adjacent to the oxygen, as in the case of the previous compound (green circle, *Figure 56*). The dots indicated with an orange X are the cross correlations between H_1 with C_2 and H_2 with C_1.

| ^{13}C δ (ppm)	Assignment	^1H δ (ppm)	Assignment
167.4	COOH	13.51	COOH
134.6	C_m	8.43	H_{Ar}
128.0	C_o	8.43	H_{Ar}
74.8	C_2	4.67	H_2
39.5	C_1	3.77	H_1
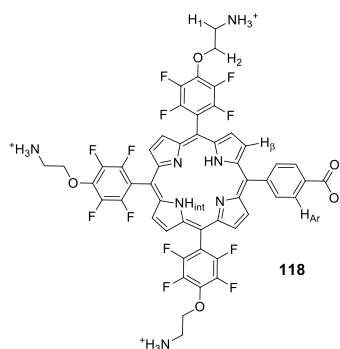
Table 19: hydrogen-carbon signals assignment and structure of 118
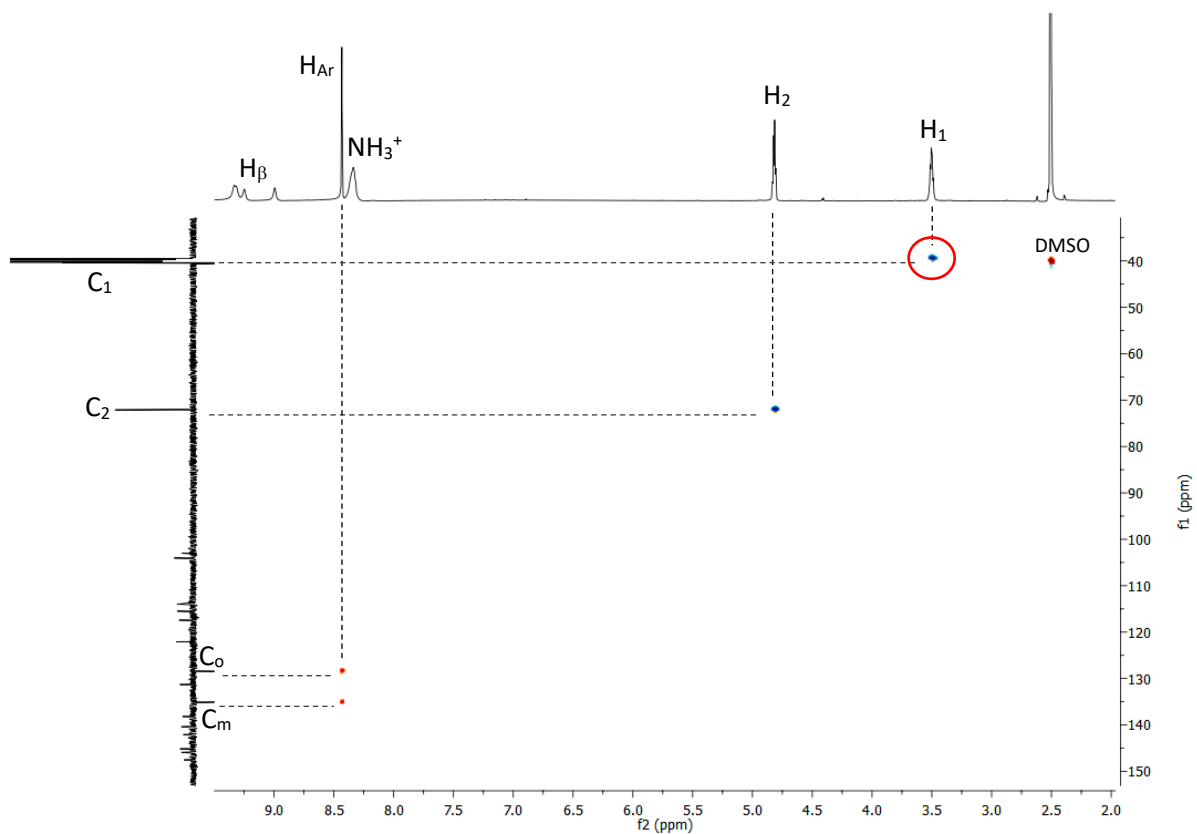
Figure 59: DEPT-edited *(135°)* ^{1}H,^{13}C-HSQC spectrum of **118**, red dots CH/CH$_3$ down, blue dots CH$_2$ up in DMSO-d$_6$ at 298 K and 600 MHz and 150 Mhz
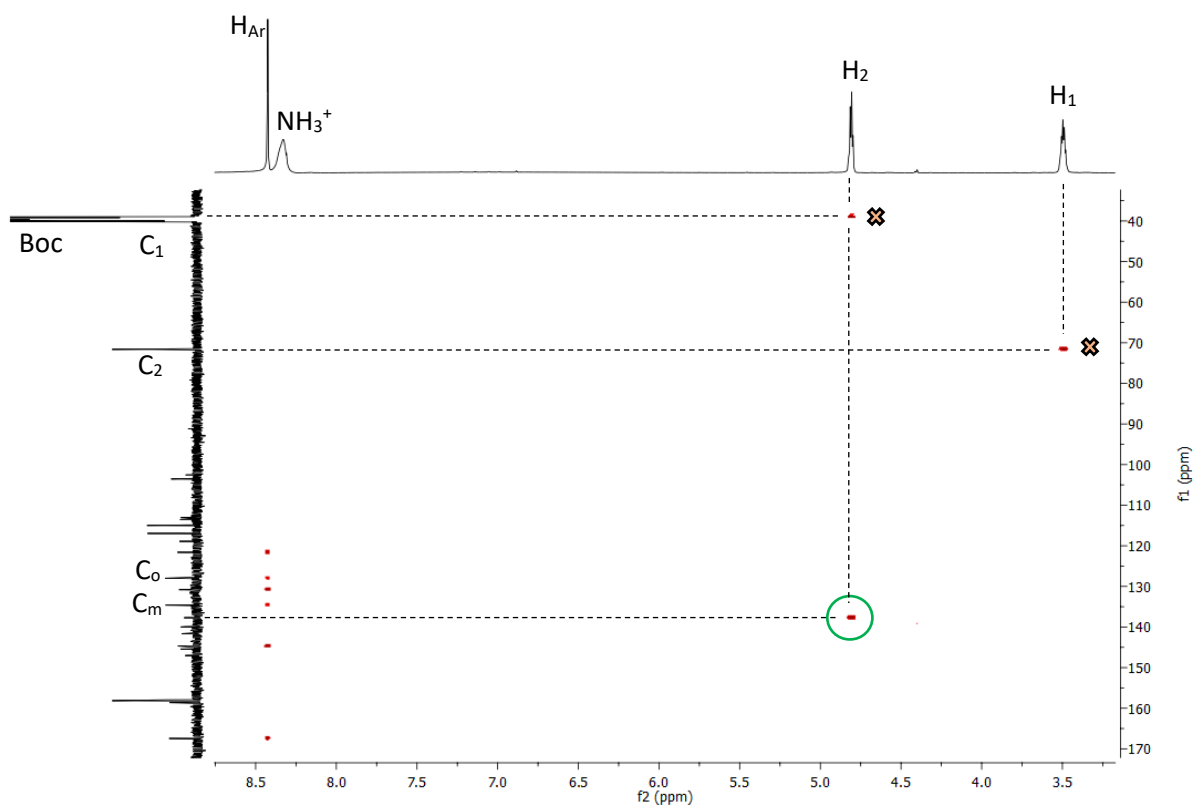
It is worth to pointing out that **118** displays water-solubility in acidic and neutral solutions, where the amine groups are protonated. Mildly basic environments, though, reveal the free amines causing a loss of the water-solubility. We reasoned that methylation of the amines to obtain the corresponding trimethylammonium derivatives would allow the use of **118** in aqueous solution irrespectively of the environment pH.

Target species **119** was obtained by treatment of **118** with methyl iodide in NMP (*Scheme 33*). Interestingly, porphyrin **118** appears as a green solid after solvent removal, the typical colour of porphyrins dissolved in acidic media where protonation of one or more internal nitrogens occurs.[234,235] Once dissolved in NMP, the colour of the solution immediately changed to vivid red, indicating a removal of the extra protons from the porphyrin core.
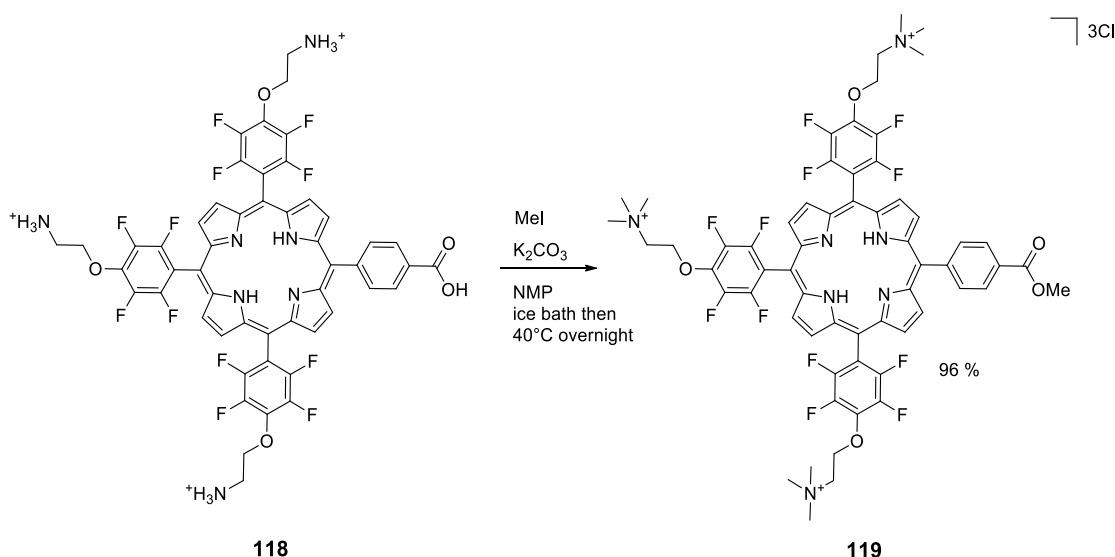
*Scheme 33: methylation of **118***

The substrate **118** was dissolved in NMP and K$_2$CO$_3$ was added to neutralise the protons liberated during the methylation steps. The mixture was stirred for 15 minutes under an argon flow, then a large excess of methyl iodide was added, and the reaction was left overnight at 40 °C. On a small scale, the reaction yielded the expected compound **119**, but when scaled up to 100 mg a mixture of products was detected. Mass spectrometry showed the presence of different products derived from the substitution of *para*-fluorine by hydroxyl groups. ^{19}F-NMR highlighted the presence of impurities, as the signal generated by the *meta* fluorines (−156.6 ppm) no longer appears as a singlet (*Figure 61*): partial substitution with hydroxyl groups caused a differentiation of the *meta* fluorine atoms. As mentioned earlier, column chromatography on silica was not a viable purification method due to high

polarity of the compounds formed. We reasoned that the formation of the undesired hydroxy-substituted products was likely to be promoted by the fast addition of MeI, causing a localized increasing of temperature and favouring the hydroxyl insertion.
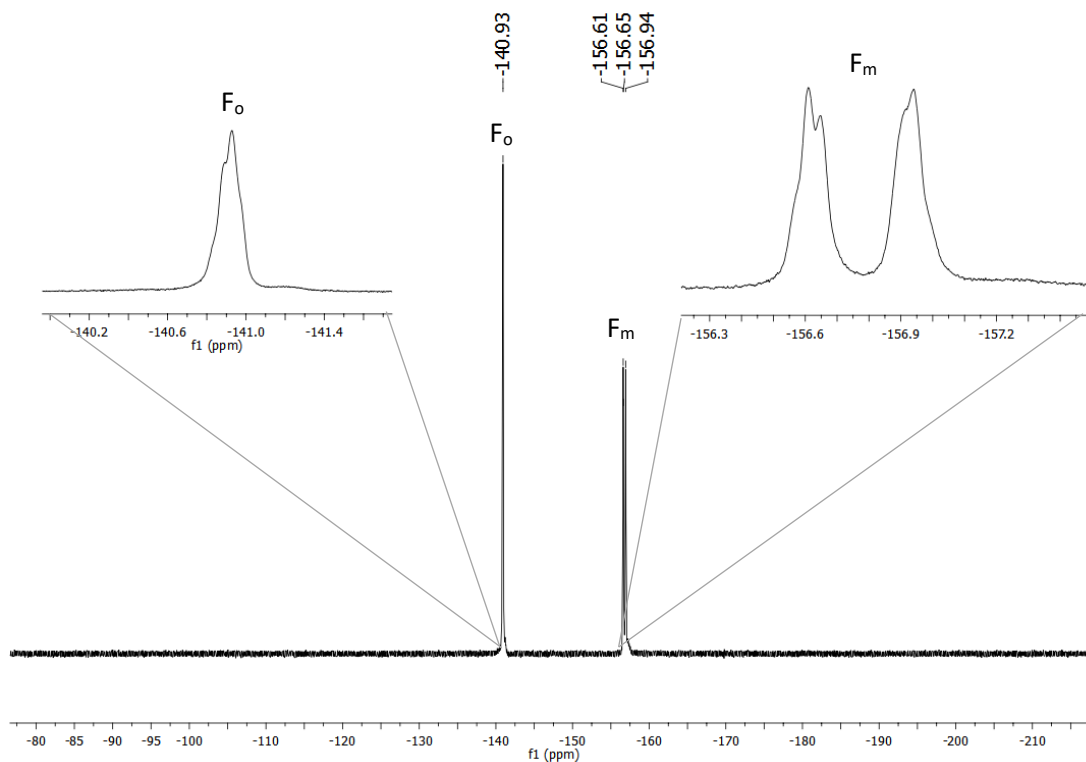
*Figure 61: $^{19}F\{^1H\}$-NMR spectrum of hydroxyl-substituted mix of **119** in DMSO-d_6 at 298 K and 565 MHz*

The quaternization of the terminal amines was successful when the reaction was carried out in an ice bath. It was also found that dropwise addition of methyl iodide as a solution in NMP was advantageous for the outcome of the reaction. This optimised method is applicable on a half-gram scale. Isolation of the reaction product was achieved by pouring the reaction mixture in brine, which promoted the precipitation of the porphyrin.

The iodide salt was insoluble in water but very soluble in acetone, which allowed us to obtain the porphyrin as the chloride salt by addition of TBAC. After centrifugation and supernatant removal, the compound was obtained pure following the ion exchange purification method developed for the cationic water-soluble porphyrin. The reaction yield was 96 %.

Inspection of the ^1H-NMR spectrum confirmed the expected structure of the molecule, as can be seen from *Figure 62*. The eight *beta* hydrogens and the four aryl hydrogens appear at low field in the aromatic region, and the internal hydrogens at higher field with the characteristic negative chemical shifts (NH$_{int}$). The CH$_2$ groups appear as two broad singlets at 5.19 ppm and 4.16 ppm. Two peaks

resulted from the methylation: a methoxy group and the methyl groups on the terminal amines. The peak at 4.05 ppm with integration value of 3H corresponds to the methoxy group (OCH$_3$), while the strong singlet at 3.43 ppm is attributed to the methyl groups, with integral value of 27H (N$^+$CH$_3$). *Table 20* summarises all the hydrogen assignments for compound **119**.
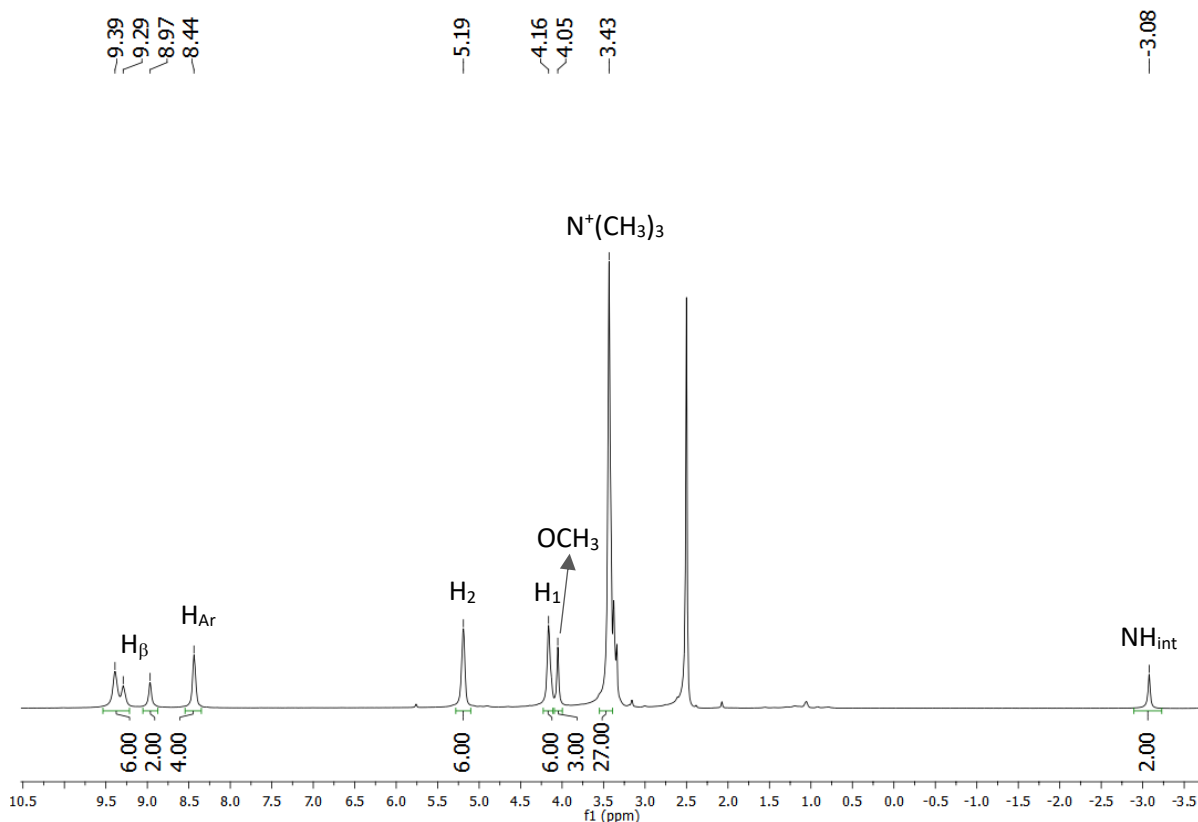
*Figure 62: ^{1}H-NMR spectrum of **119** in DMSO-d$_6$ at 298 K and 600 MHz*

Multiplicity	δ (ppm)	Integration value	Assignment
m	9.29-9.39	6	H$_\beta$
m	8.97	2	H$_\beta$
2d into s	8.44	4	H$_{Ar}$
t into s	5.19	6	H$_2$
t into s	4.16	6	H$_1$
s	4.05	3	OCH$_3$
s	3.43	27	N$^+$CH$_3$
s	−3.08	2	NH$_{int}$
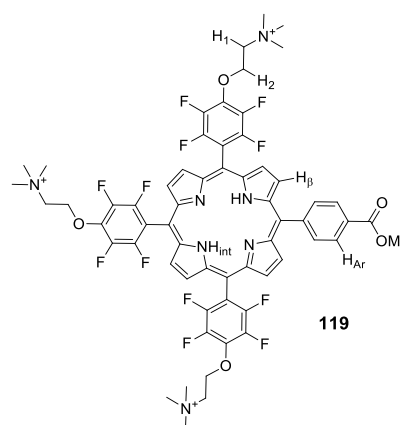
*Table 20: hydrogen signals assignment and structure of **119***

^{19}F-NMR spectrum, shown in *Figure 63*, displays only two signals relative to *ortho* and *meta* fluorines, respectively, meaning no hydroxyl groups is inserted in the molecule.
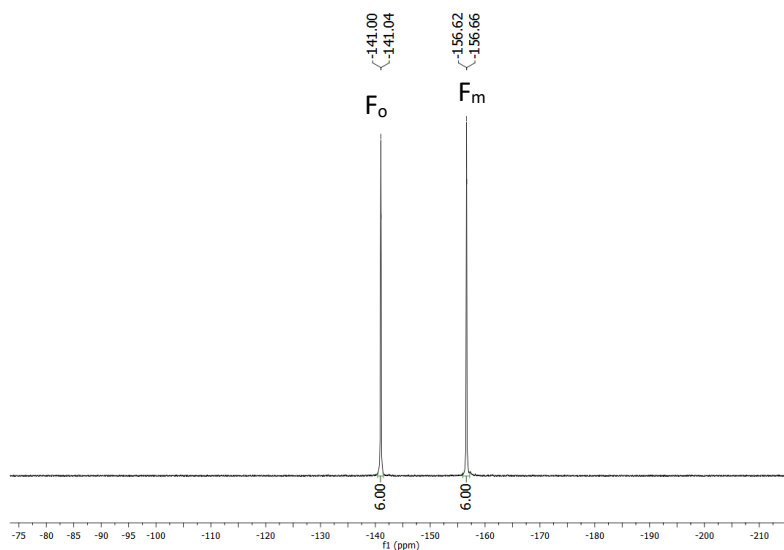
Figure 63: ^{19}F{^{1}H}-NMR spectrum of **119** *in DMSO-d$_6$ at 298 K and 565 Mhz*

The drawback of this reaction is that methylation also occurs on the carboxyl group, re-installing the ester functionality: this compels us to carry out an extra step to obtain the target molecule. To avoid the accidental substitution of the chain on the aromatic ring by hydroxyl groups, the hydrolysis of the methyl ester was carried out in concentrated aqueous HCl. The reaction mixture was maintained at 60 °C overnight, until mass spectroscopy revealed completed consumption of the starting material. The solvent was evaporated under reduced pressure, and the compound was purified by ion exchange. The yield of the reaction was 98 %. (*Scheme 34*).
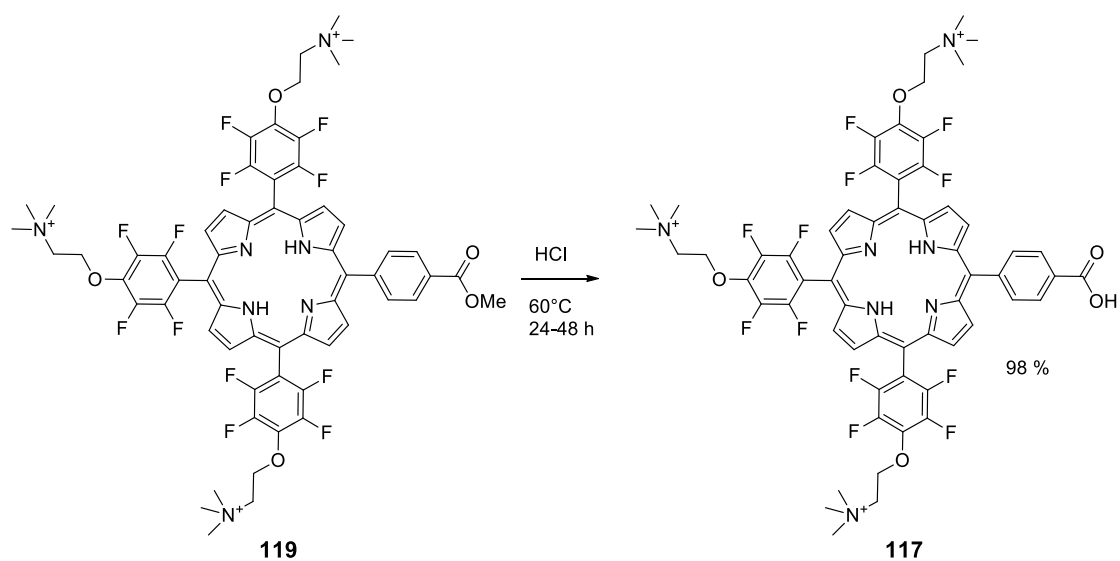
Scheme 34: hydrolysis of **119**

Despite several failed attempts to functionalise compound **99** with different nucleophiles, including water-soluble species **111** and **115**, it was finally devised a successful synthetic strategy to obtain a cationic water-soluble porphyrin. Initial findings showed that amines are poor nucleophiles in the system under study, as they required long reaction times and high temperatures to afford incomplete conversion. Although they are described as weaker nucleophiles, in our hands alcohols showed a more favourable behaviour and higher reactivity compared to amines.

Despite the higher number of steps required to obtain **117** compared to the anionic derivative **102**, the optimised synthetic approach based on Boc-protected ethanolamine **113** affords the desired final product in excellent overall yield (> 70%). The method uses reaction conditions compatible with the functional groups on the molecule and is applicable to gram-scale without any significant loss of yield. The purification method based on the ion exchange method for cationic water-soluble porphyrin worked flawless on all the various intermediates of the synthesis.

^{1}H-NMR spectrum of the target molecule **117** is shown in *Figure 64*. A broad peak is visible at 13.35 ppm and it is generated by the carboxylic hydrogen (shown as the expansion on the left of *Figure 64*). As expected, the signal of the methoxy group disappears from the spectrum indicating successful ester hydrolysis. *Table 21* summarises the assignment of the various hydrogens.
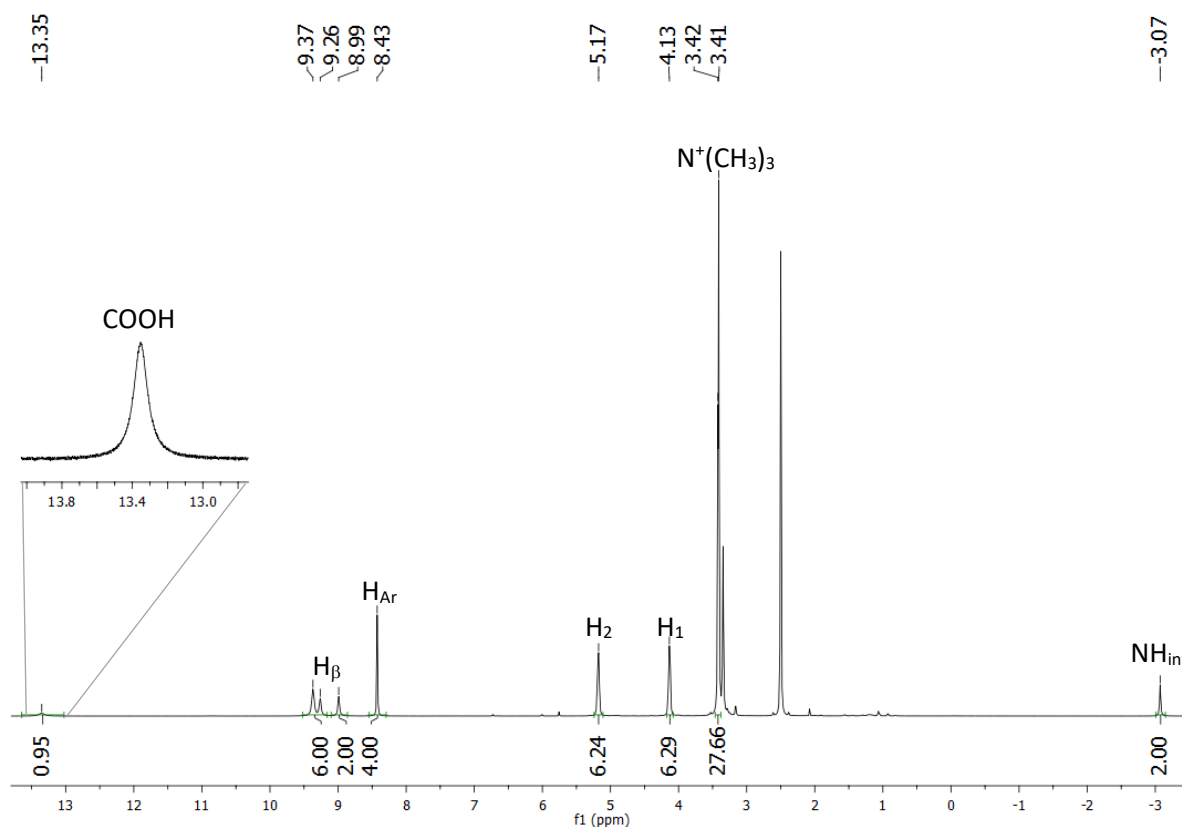
*Figure 64: ^{1}H-NMR spectrum with expansion of **117** in DMSO-d_6 at 298 K and 600 MHz*

Multiplicity	δ (ppm)	Integration value	Assignment
br s	13.53	1	COOH
m	9.26-9.37	6	H_β
m	8.99	2	H_β
2d into s	8.43	4	H_{Ar}
t into s	5.17	6	H_2
t into s	4.13	6	H_1
d	3.42	27	$N^+(CH_3)_3$
s	−3.07	2	NH_{int}
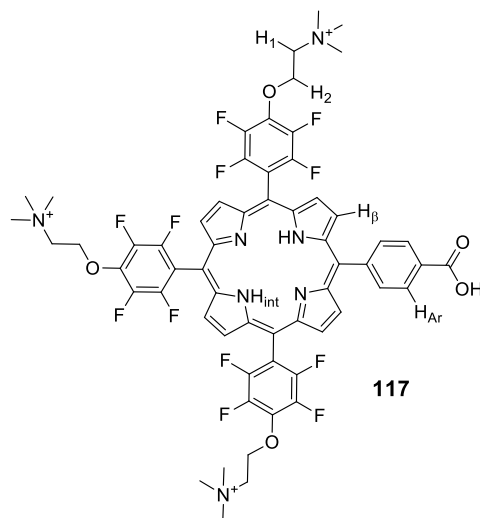
Table 21: hydrogen signals assignment and structure of **117**

Figure 65 shows the ^{19}F-NMR spectrum for compound **117**, with expansions for clarity. No hydroxyl substitution was detected from the analysis, as confirmed by the presence of just one peak related to *meta* fluorine.
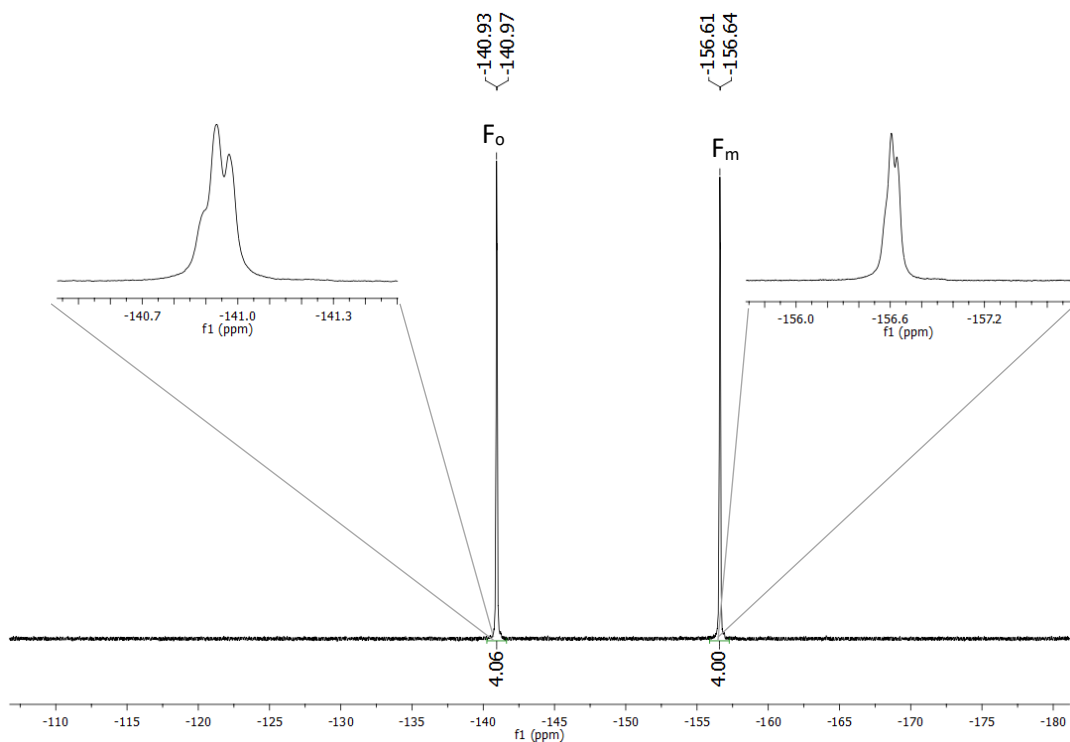
Figure 65: ^{19}F{^{1}H}-NMR spectrum with expansions of **117** *in DMSO-d$_6$ at 298 K and 565 MHz*

Carbon-hydrogen correlations, shown in *Figure 66* and *Figure 67*, allowed partial assignment of carbons to the relative hydrogens, as shown in the *Table 22*. The two peaks generated by H_1 and H_2 can be distinguished thanks to the $^1H,^{13}C$-HMBC in *Figure 67*. The correlation between the methyl groups and H_1 (red circle, *Figure 67*) indicates that the signal at 4.13 ppm is due to H_1. On the other hand, the signal at 5.17 ppm (H_2) presents a correlation with a quaternary carbon attached to the oxygen (green circle, *Figure 67*), as it was already seen for the previous intermediates **116** and **118**. The dots indicated with an orange X are the cross correlations between H_1 with C_2 and H_2 with C_1.

$^{13}C\ \delta$ (ppm)	Assignment	$^1H\ \delta$ (ppm)	Assignment
167.4	COOH	13.4	COOH
134.6	C_m	8.43	H_{Ar}
128.0	C_o	8.43	H_{Ar}
68.6	C_2	5.17	H_2
64.8	C_1	4.13	H_1
53.2	Me	3.42	CH_3
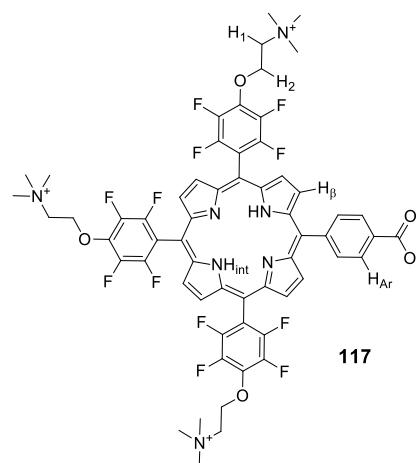
*Table 22: hydrogen-carbon signals assignment and structure of compound **117***
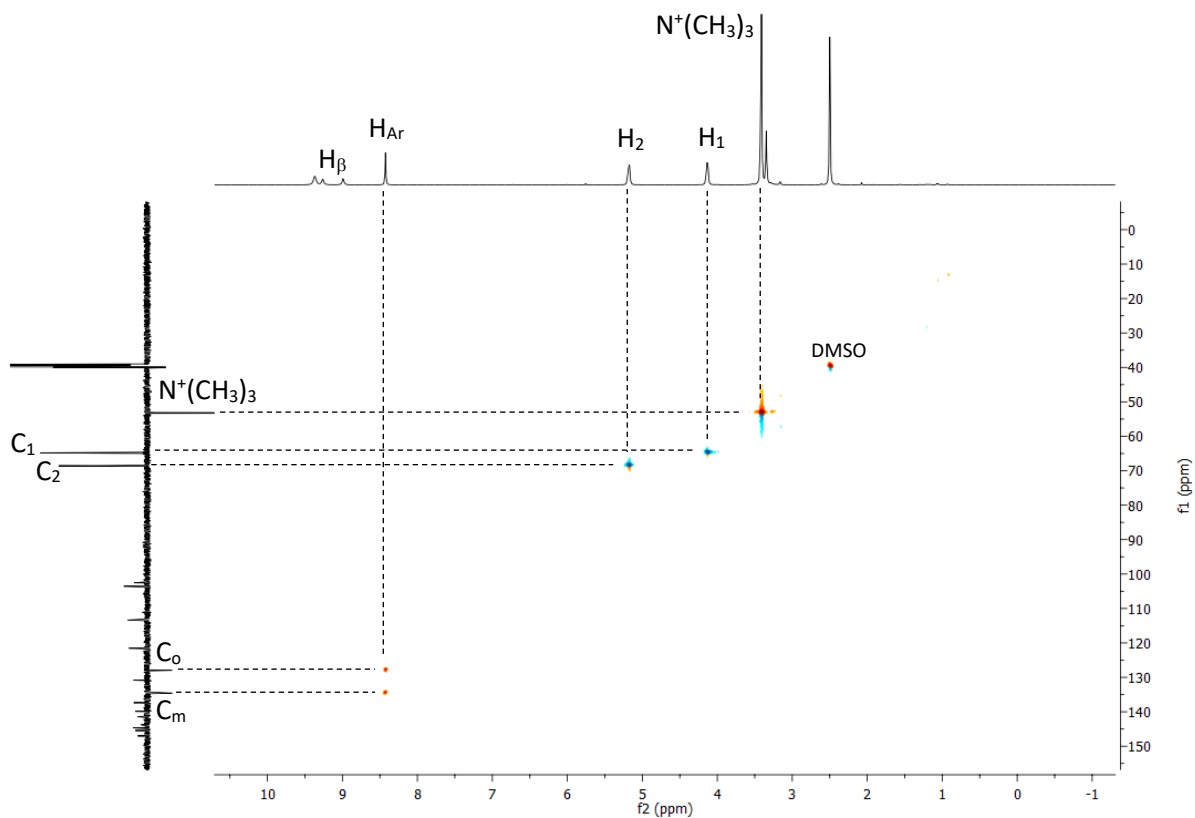
*Figure 66: DEPT-edited(135°)^{1}H,^{13}C-HSQC spectrum of **117**, blue dots CH$_2$ up, orange dots CH/CH$_3$ down in DMSO-d$_6$ at 298K*
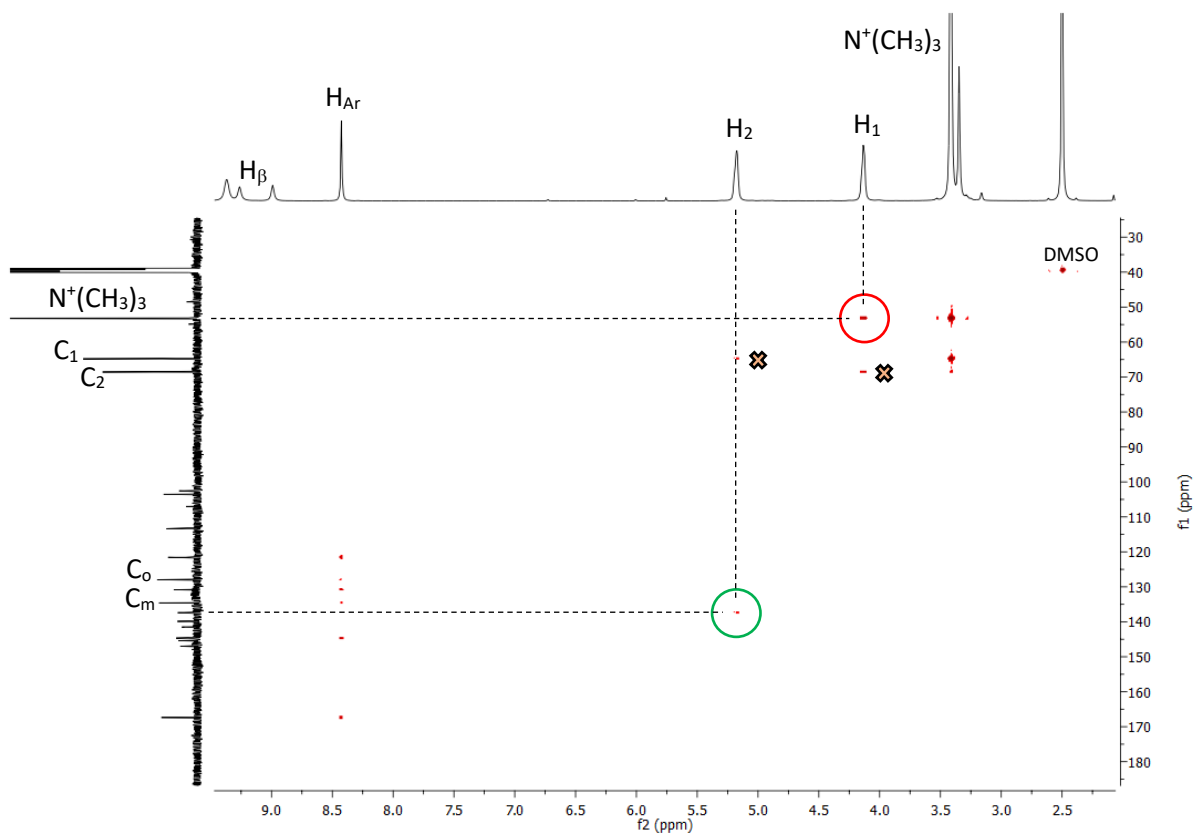
*Figure 67: ^{1}H,^{13}C-HMBC spectrum of **117** in DMSO-d$_6$ at 298 K and 600MHz and 150 MHz*

3.3 Metal insertion of A$_3$B porphyrins

The final step for the synthesis of the target oxygen-sensing species was the metal insertion. As stated before, the two metals that impart the most favourable oxygen-sensing properties to porphyrins are platinum and palladium.[146] These two metals are known to display an oxygen response, measured by the decrease of the luminescence intensity,[236–239] however platinum results more employed to build optical oxygen sensors,[129,240–243] due to its more favourable photophysical properties.

<u>Microwave-assisted metal insertion</u>

Microwave (MW) heating has been extensively used in organic chemistry in the last decades[244–247] and it has been applied to porphyrin synthesis with reasonable success.[248–251] MW heating allows to perform reactions at temperatures higher than the boiling point of the solvent used and to considerably reduce reaction times. According to the Arrhenius rule, the reaction time is halved for every 10 °C of temperature increase: this means that a reaction left 12 hours refluxing overnight in chloroform (bp 61 °C) can performed in a microwave tube in slightly over 10 minutes at 120 °C. In addition, less degradation of starting materials is detected employing MW irradiation, which has been ascribed to the fact that prolonged heating is more likely to cause the degradation of the compounds, compared to shorter reaction times at a higher temperature.[247] The choice of solvent employed for a reaction under microwave heating is pivotal for the success of the reaction. Polar solvents are the optimal choice, as they are easily heated under MW irradiation. Water, NMP, DMF, acetonitrile, acetone, ethanol and methanol are the most employed, while non-polar solvents such as hexane, chloroform, DCM and toluene are "transparent" to MW heating and unsuitable unless mixed with a polar co-solvent or employed with "heating stones", which dissipate the heat to the nearby solvent molecules. Solvents such as DMSO and DMF are not suitable for a high-temperatures pressurized reaction, because they undergo decomposition at high temperatures. DMSO, for example, decomposes above 200 °C producing volatile species, which cause a rapid pressure build-up in the sealed tube, with consequent explosion hazard. A drawback associated to the use of laboratory-scale microwave reactors arises from the fact that reactions must be performed in 10 mL or 30 mL tubes. These tubes can be filled only to half of their capacity to avoid over-pressurization, which indirectly limits the scalability of the reaction. Larger reaction vessels are available, but they are inherently more dangerous to use, as they need to tolerate higher pressures. The scale limitation can be circumvented by repeating smaller-scale reactions, especially if the reactor is connected to an auto-sampler.

Several papers report the MW-assisted porphyrin complexation, with reaction conditions that vary, depending on the metal and on the porphyrin. Both porphyrins soluble in organic solvents[150,249,252,253] and water-soluble[146] have been successfully metallated with different metals under MW irradiation.

The first example of MW-assisted metallation of porphyrin was published in 2007.[249] The authors employed a domestic microwave oven placing the vessel in the centre of the rotating plate after sealing it with cotton wool. The metal insertions were performed on tetraphenylporphyrin **79a** and two derivates (*para*-chlorine and *meta*-methoxy) employing DMF as solvent and the acetate salt of the relative metal, on a 100-mg scale. Five different metals were chosen: zinc (II), copper (II), nickel (II), cobalt (II) and manganese (III).[249] The yields resulted to be very high (from 73% to 95%) after only three minutes of heating at 480 W. The products were collected by filtration from the crude mixtures cooled at room temperature.[249] Despite the poor reproducibility due to the use of a domestic MW oven, the method proved very useful to obtain porphyrin complexes, markedly shortening the reaction times and increasing the yields compared to conventional heating. In another work, metal insertion was performed in a purpose-built microwave reactor (CEM Discover®) employing a sealed vessel.[150] Nickel (II), palladium (II) and platinum (II) were successfully inserted in tetraphenyl-porphyrin, -porpholactone, and -2,3-dihydroxychlorin derivatives.[150] The reactions were performed on a 10-20 mg scale employing a 10 mL microwave vessel filled with 3 mL of solvent. For the insertion of nickel and palladium, pyridine was employed as solvent; heating to 180 °C for 15 minutes gave quantitative yields of the desired complexes. Benzonitrile was employed as solvent for platinum insertion, allowing to reach higher temperatures (250 °C)[150]. At that temperature, pyridine caused pressure to exceed the limit tolerated by the instrument (300 psi). In the case of platinum and palladium the acetoacetate salt was employed as metal source, while in the case of nickel the acetate salt. In a more recent approach metal insertion was performed using ionic liquid 1-butyl-3-methylimidazolium bromide as the solvent.[253] Platinum (II) and palladium (II) complexes were successfully synthesised on compounds **51** and **79a** and their octa-brominated derivates. The reaction times for **51** and **79a** ranged between 15 and 30 minutes, respectively, yielding quantitative metal complexes. On the other hand, the *beta*-substituted compounds required 6 minutes of irradiation to afford the complex in slightly lower yields.[253] In all the examples mentioned, a three-fold molar excess of metal source was required to drive the reaction to completion.

In the case of water-soluble porphyrins, especially the anionic derivatives, MW irradiation is fundamental for the insertion of platinum (II), because it allows to reach 200 °C while still using aqueous solutions.[146] Due to the porphyrin solubility profile, water is the only solvent employable for the metal insertion: while palladium insertion can occur at lower temperatures, complexation with platinum requires temperatures higher than the boiling point of water. Microwave technology allows to combine the use of water with the high temperatures required for the reaction, resulting in a successful insertion in quantitative yields.[146]

<u>Palladium (II) insertion</u>

Palladium (II) can be inserted in porphyrins under milder conditions compared to platinum. For non-water-soluble substrates, the reaction proceeds in organic solvents such as chloroform, with the palladium salt dissolved in methanol added to the solution. Overnight reflux lead to complete metal insertion. The most common sources of palladium (II) for these reactions are $Pd(OAc)_2$ and $PdCl_2$.[232]

Palladium (II) was successfully inserted in cationic porphyrins **73** and **117** with no need for MW heating (*Scheme 35*).
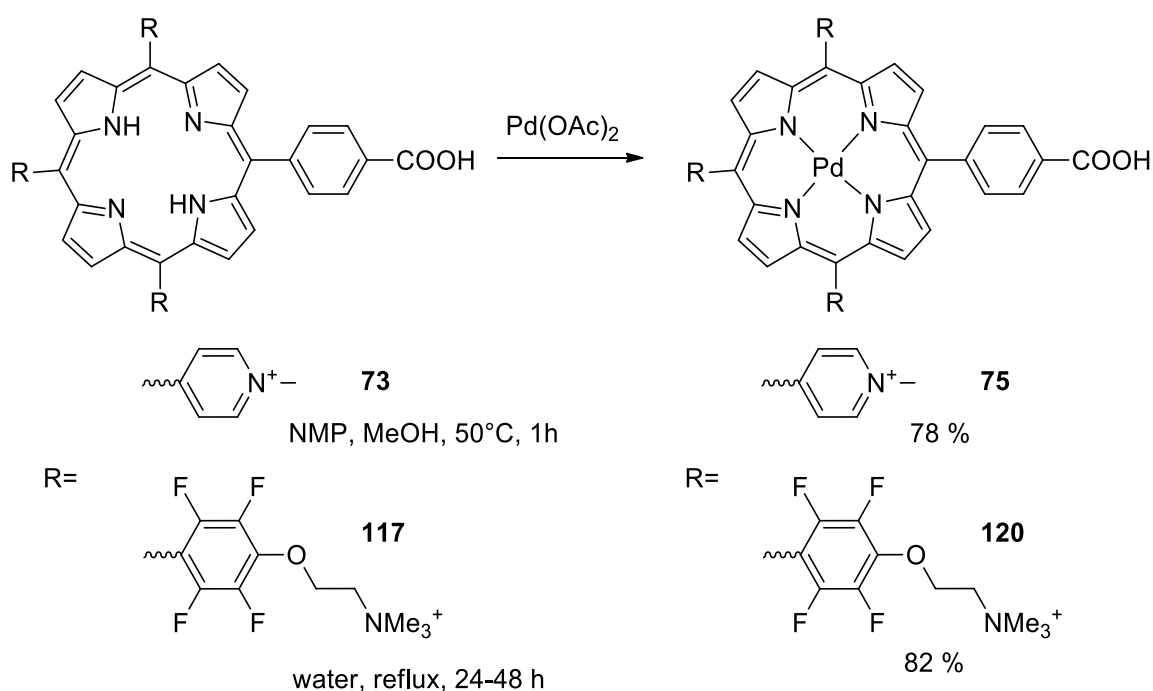
*Scheme 35: palladium (II) insertion of **73** and **117***

Compound **73** was dissolved in NMP and the palladium (II) salt (either chloride or acetate) was added as a methanolic solution. The reaction mixture was flushed with argon and allowed to proceed at 50 °C for 1 hour. Filtration through celite and addition of diethyl ether to the filtrate led to the precipitation of the desired complex **75**. The product was purified by ion-exchange method. The yield of the reaction was 78 %. Notably, a black layer of metallic palladium is deposited over the walls of the flask during the reaction.

The disappearance of the internal hydrogen peak with negative chemical shift on the ^{1}H-NMR spectrum of compound **73** (*Figure 68*) highlights complete metal insertion. The signals on the spectrum appear broader compared to the ones in the free base spectrum, indicating decreased solubility in DMSO-d_6 for the palladium (II) complex and a stronger tendency to aggregation. The

assignment of the signals can be found in *Table 23*, and it is in agreement with the previously reported data.[146]
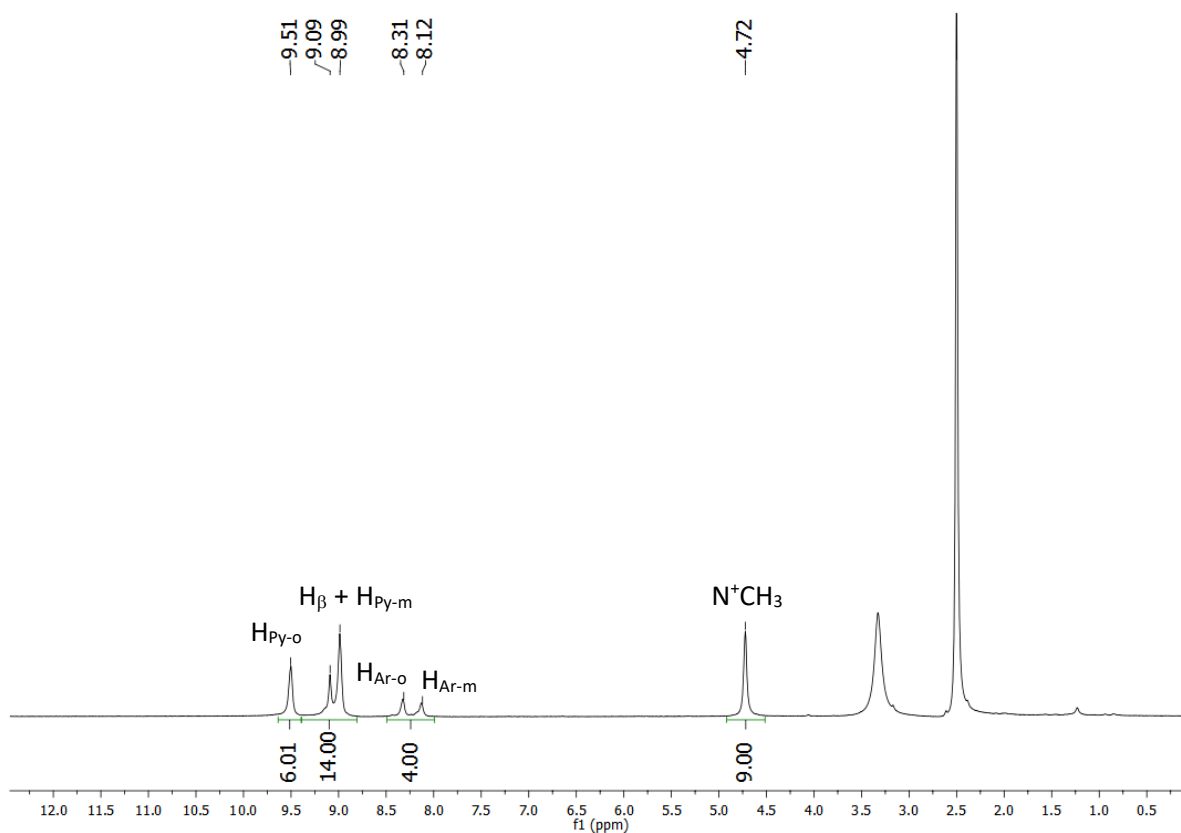
*Figure 68: ¹H-NMR spectrum of **75** in DMSO-d₆ at 298 K and 600 MHz*

Multiplicity	δ (ppm)	Integration value	Assignment
d into br s	9.51	6	$H_{Py\text{-}m}$
m into br s	9.09	6	H_{β}
d into br s	8.99	8	$H_{Py\text{-}o}$
d into br s	8.31	2	$H_{Ar\text{-}o}$
d into br s	8.12	2	$H_{Ar\text{-}m}$
br s	4.72	9	N^+CH_3
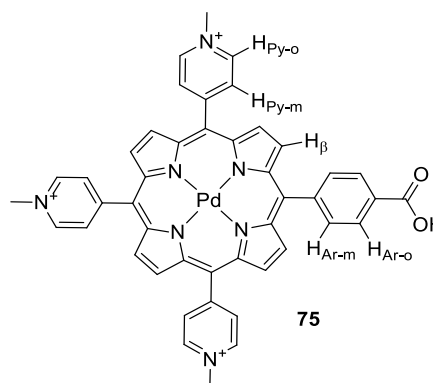
*Table 23: hydrogen signals assignment and structure of **75***

Complexation of compound **117** required harsher reaction conditions. When the reaction was performed in NMP incomplete metal insertion was obtained, probably due to poor solubility and/or aggregation of the substrate. Water better solubilized both the compound and the metal source,

facilitating the insertion, but the best results were obtained using porphyrin concentrations lower than 8×10^{-4} M: this instance prevented to perform the reaction under of MW irradiation in a satisfactory scale, due to the small volume of solution contained in microwave vessels. Any attempt to dissolve more than 10 mg of porphyrin in a MW tube, either in water or in NMP, resulted in the aggregation of the macrocycle, further exacerbated by the addition of the metal salt. Complexation of **117** had to be performed in a round-bottomed flask under conventional heating. A very large excess of metal source (up to 10 equivalents) was required to drive the reaction to completion; the reaction was allowed to proceed until no starting porphyrin was detected by mass spectrometry. After evaporation of the solvent, the crude was dissolved in methanol, filtered through celite to eliminate metallic palladium, the solvent was evaporated and the compound re-dissolved in water. The metal complex was then purified employing the ion-exchange method for cationic water-soluble porphyrins. The yield of the reaction was excellent (82 %).

^{1}H-NMR and ^{19}F-NMR spectra of palladium (II) complex **120** are shown in *Figure 69* and *Figure 70*, respectively. The peaks appear sharper compared to the spectrum of the free base (*Figure 64*), probably due to better solubility in DMSO-d_6. A full assignment of the signal is reported in *Table 24*. The broad peak at lower field (see expansion on *Figure 69*) corresponds to the carboxylic acid. The *beta* hydrogens appear as three peaks with integration values of 4H, 2H and 2H, respectively. The first peak on the left (H$_{\beta 3}$) is attributed to the four hydrogens far from the carboxylic acid functionality; the most shielded peak at 8.95 ppm is due to the two *beta* hydrogens closest to the carboxylic group (H$_{\beta 1}$), and the central doublet (H$_{\beta 2}$) can be then assigned to the two hydrogens *ortho* to the previous ones. The two signals generated by the hydrogens *ortho* and *meta* to the carboxylic group appear as two doublets. In the aliphatic region the signals relative to the nine methyl groups and to the two different CH_2 groups of the moieties are visible.

Figure 70 shows the signals of the *ortho* and *meta* fluorines: the presence of a single signal relative to the *meta* fluorine confirms that no hydroxyl group insertion took place.

Figure 71 shows the DEPT-edited ^{1}H,^{13}C-HSQC spectrum. Several carbon/hydrogen pairs can be assigned, as summarized in *Table 25*. Due to the high resolution of the hydrogen spectrum, the *beta* hydrogens can be assigned to the relative carbon signals. The expansion refers to the area delimited by the green rectangle of *Figure 71*.

Multiplicity	δ (ppm)	J (Hz)	Integration value	Assignment
br s	13.68	-	1	COOH
dd	9.33	4.2/9.6	4	$H_{\beta3}$
d	9.21	4.8	2	$H_{\beta2}$
d	8.95	4.8	2	$H_{\beta1}$
d	8.40	7.8	2	H_o
d	8.34	7.8	2	H_m
t into br s	5.16	-	6	H_2
t into br s	4.12	-	6	H_1
s	3.40	-	27	$N^+(CH_3)_3$
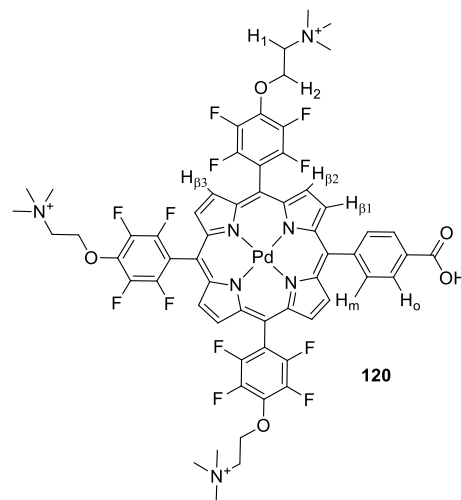
Table 24: hydrogen signals assignment and structure of **120**
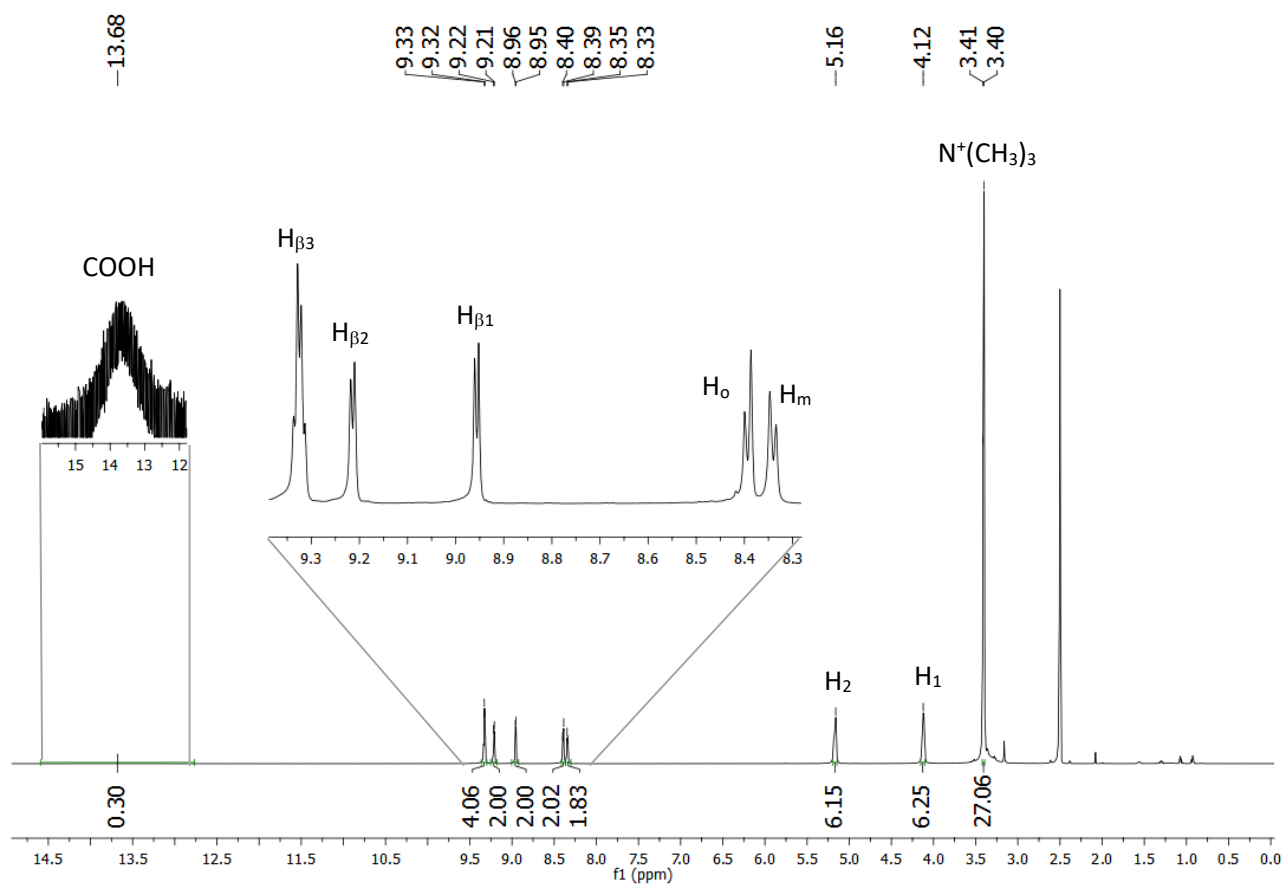
Figure 69: ^{1}H-NMR spectrum with expansions of **120** in DMSO-d_6 at 298 K and 600 MHz
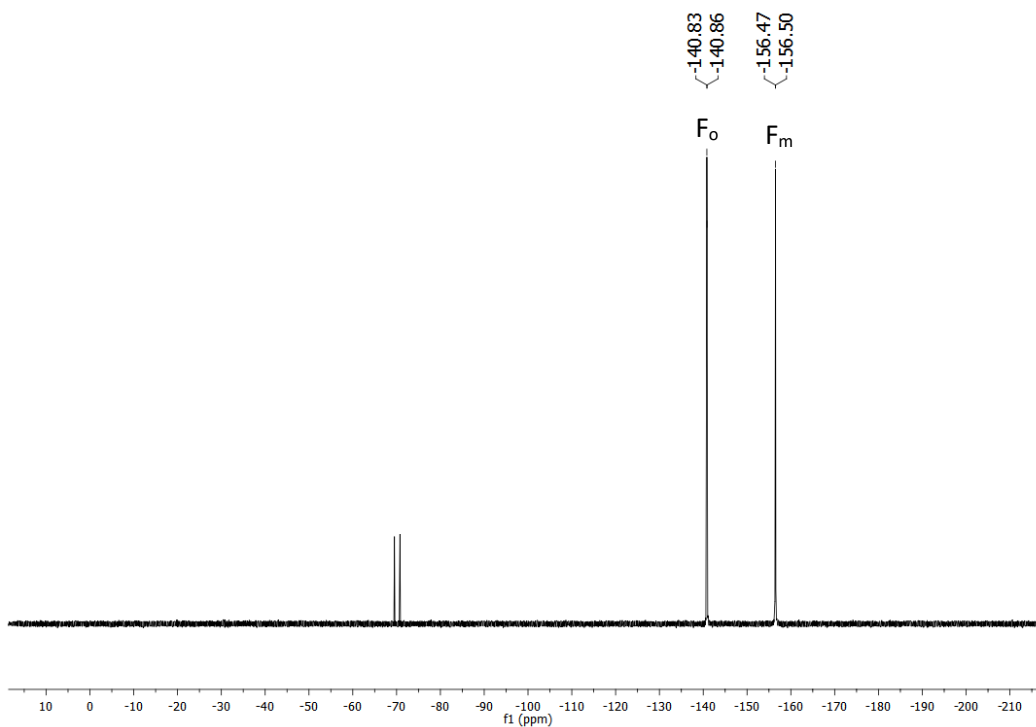
Figure 70: $^{19}F\{^1H\}$-NMR spectrum of **120** in DMSO-d_6 at 298 K and 565 MHz
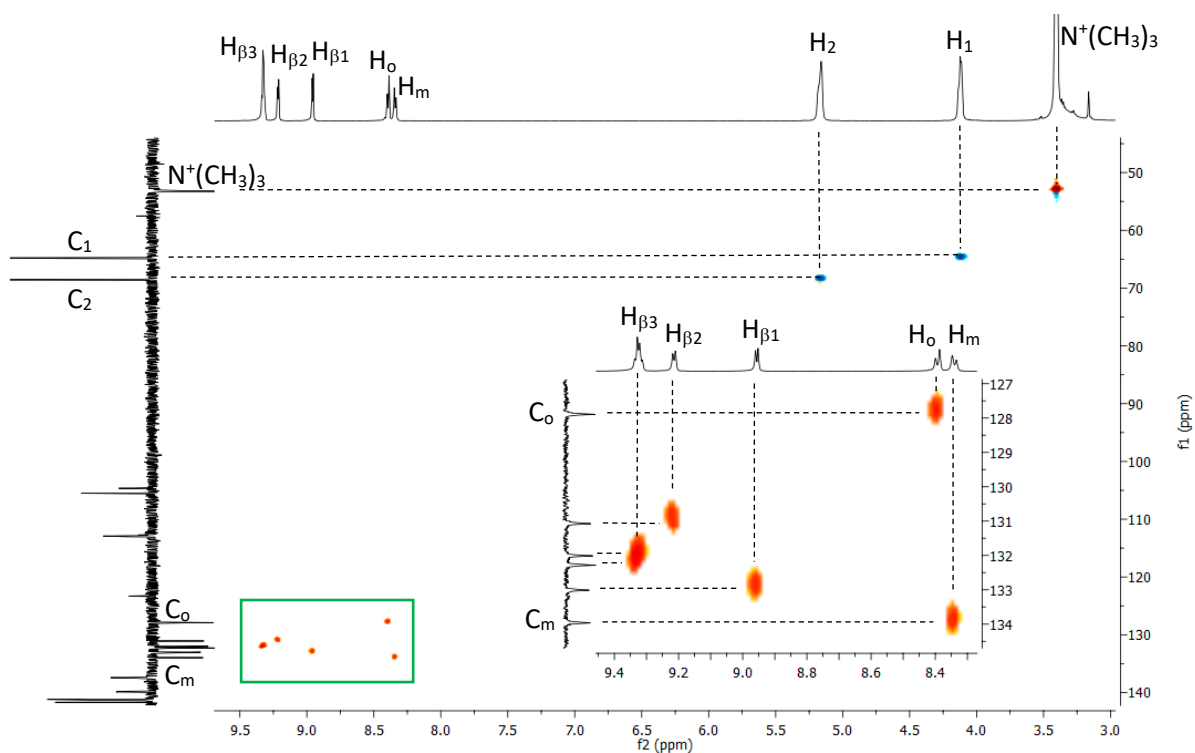
Figure 71: DEPT-edited (135°) ^1H,^{13}C-HSQC spectrum of **120** with expansion, orange dots CH/CH$_3$ down, blue dots CH$_2$ up, in DMSO-d_6 at 298 K and 600Mhz and 150 MHz

^{1}H,^{13}C-HMBC spectrum, shown in *Figure 72*, confirms the assignments hydrogen-carbon detected and allows the discrimination of the two CH_2 groups. The carbon signal of the nine methyl groups shows a correlation peak with one of the hydrogen signals of the chain (green circle, *Figure 72*): this signal is due to H_1, which is closest to the methyl groups. The dots indicated with an orange X are the cross correlations between H_1 with C_2 and H_2 with C_1. The correlation indicated with a red circle is presumably between H_2 and the quaternary carbons attached to the oxygens, as already seen for the previous derivatives.

^{13}C δ (ppm)	Assignment	^{1}H δ (ppm)	Assignment
132.0/132.3	$C_{\beta 3}$	9.33	$H_{\beta 3}$
131.1	$C_{\beta 2}$	9.21	$H_{\beta 2}$
133.0	$C_{\beta 1}$	8.95	$H_{\beta 1}$
127.9	C_o	8.40	H_o
134.0	C_m	8.34	H_m
68.6	C_2	5.16	H_2
64.8	C_1	4.12	H_1
53.2	Me	3.40	$N^+(CH_3)_3$
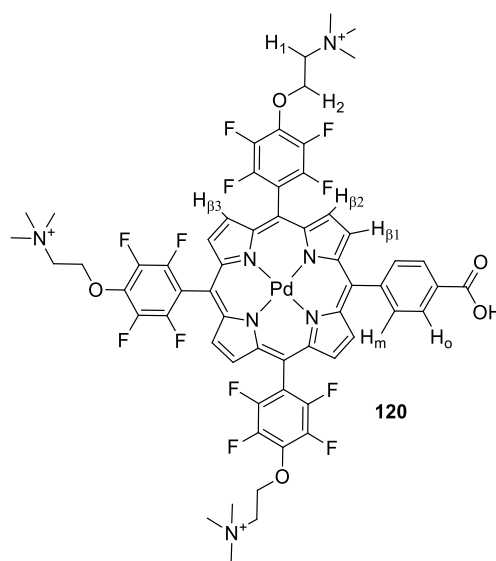
*Table 25: hydrogen-carbon signals assignment and structure of **120***
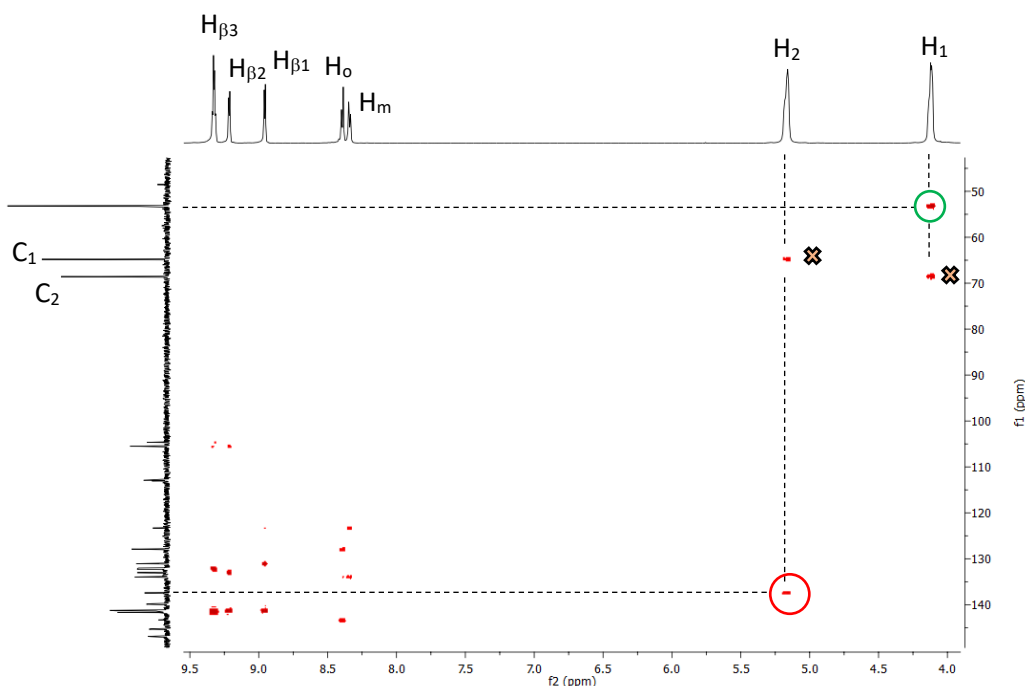
*Figure 72: ^{1}H,^{13}C-HMBC spectrum expanded in the interested region of **120** in DMSO-d$_6$ at 298 K and 600Mhz and 150 MHz*

Anionic water-soluble porphyrins required harsher reaction condition for palladium (II) insertion. In this case MW irradiation was necessary to achieve complete metal insertion on both **76** and **102** (*Scheme 36*). The metal insertion did occur under standard heating (reflux), but it did not reach completion, yielding an inseparable mixture of free porphyrin and palladium (II) complex.
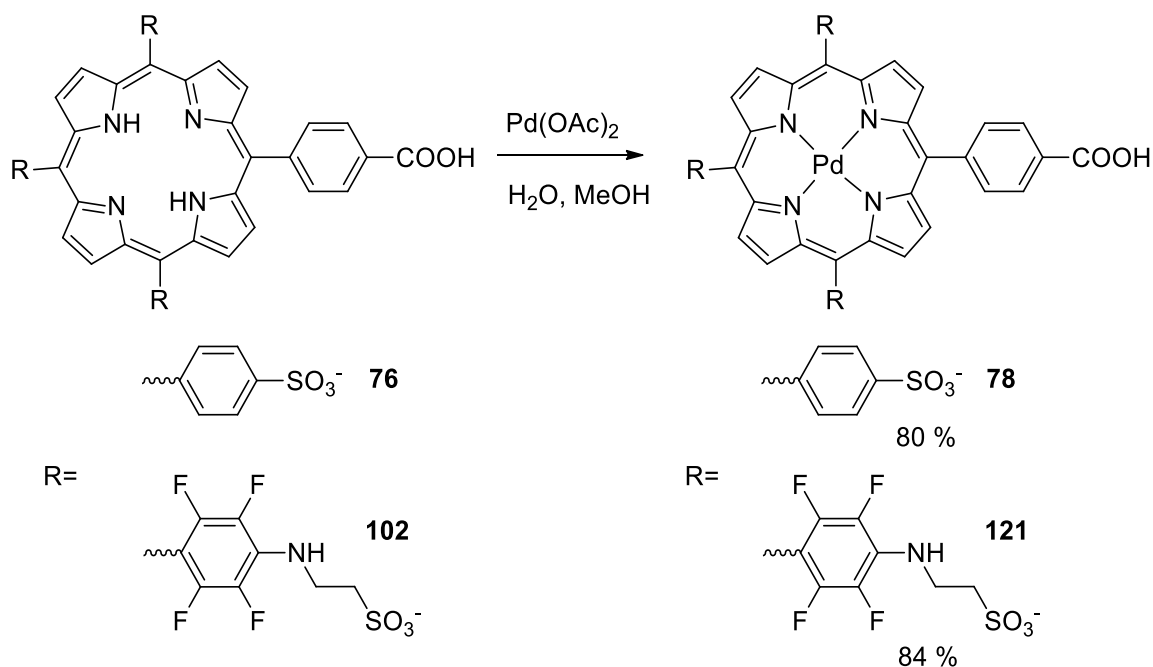
*Scheme 36: palladium (II) insertion for **76** and **102***

Table 26 shows the reaction conditions and the yields for both the anionic substrates. NMP could not be used in this transformation due to the low solubility and strong aggregation of the substrates in this solvent, but the reaction successfully took place in water. A methanolic solution of the palladium (II) salt was added to the porphyrin dissolved in water. The reaction mixture was flushed with argon for 10 minutes and it was heated in a microwave tube to the temperature specified in *Table 26*. It is worth noting that much lower yield was detected for porphyrin **121** when the reaction was performed at 150 °C, due to the degradation of the substrate. Carrying out the reaction at 110 °C, on the other hand, resulted in complete metal insertion and isolation of the complex in excellent yield. Complexation of **78** required higher temperature to reach completion. The yields of complexes **121** and **78** were comparable.

Porphyrin	Yield (%)	Time (min)	T (°C)
121	84	15	110
78	80	10	150

*Table 26: palladium (II) insertion conditions, yield and MW settings for **78** and **121***

Isolation of the desired products was carried out in the same way as outlined above for cationic derivates and purified using the ion-exchange method for anionic porphyrins.

^{1}H-NMR spectrum of compound **78** is showed in *Figure 73*. Complete metal insertion is confirmed by the disappearance of the internal hydrogens peaks. The very broad signal at down fields is assigned to the carboxylic group, while the multiplet in the aromatic region, at 8.43 ppm, is assigned to the eight *beta* hydrogens. The hydrogens in *ortho* and *meta* to the carboxylic group appear as a doublet of doublets, due to "roof effect" typical of second-order interactions.[254] These signals are two distinct doublets, of which the one at lowest field is attributed to the hydrogens in *ortho* position to the COOH group. The hydrogens *ortho* and *meta* to the sulphonate group, in the three phenyl rings, appear as two doublets at 8.15 and 8.03 ppm, respectively, also displaying second order interactions. All the assignments are summarized in *Table 27* and they agree with the previously reported data.[146]

Multiplicity	δ (ppm)	J (Hz)	Integration value	Assignment
br s	13.29	-	1	COOH
m	8.83	-	8	H_β
d	8.38	8.2	2	H_o
d	8.33	8.2	2	H_m
d into br s	8.15	8.1	6	H_1
d into br s	8.03	8.1	6	H_2
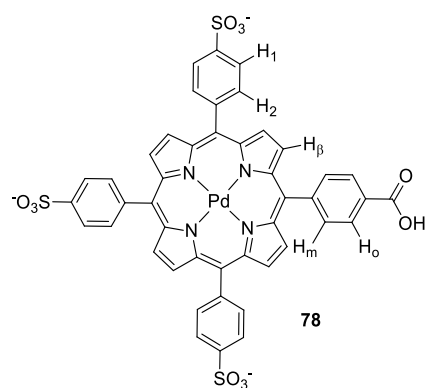
*Table 27: hydrogen signals assignment and structure of **78***
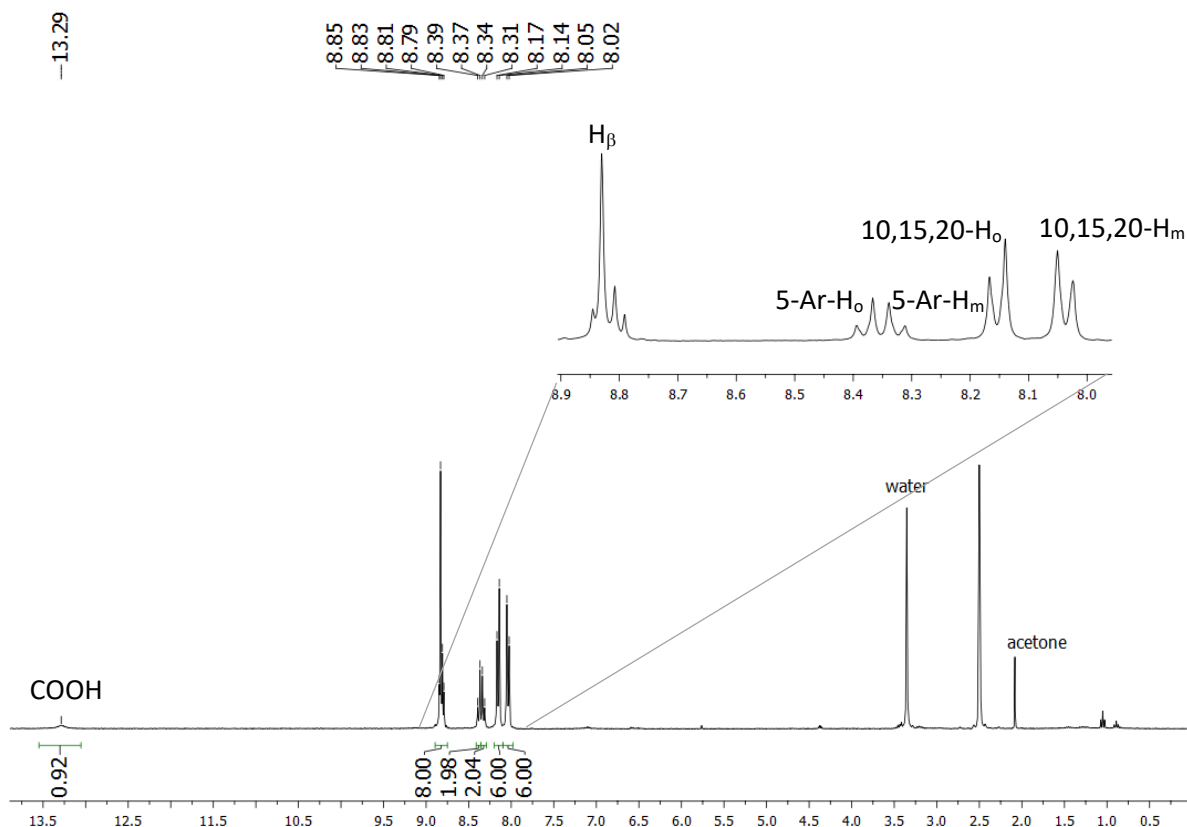
*Figure 73: ^{1}H-NMR spectrum with expansion of **78** in DMSO-d$_6$ at 298 K and 600 MHz*

Figure 74 shows the ^{1}H-NMR spectrum of **121**, once again the lack of peak at negative chemical shift confirms complete metal insertion. The broad peak at lower field, which did not appear in spectrum of **102** (*Figure 43*), is assigned to the carboxylic acid. In the aromatic region, the eight *beta* hydrogens and the four hydrogens on the carboxyphenyl ring can be seen at 9.22 and 8.39 ppm, respectively. The amine hydrogens attached to the aromatic rings appear as a singlet at 6.68 ppm, while the CH$_2$ groups appear as two singlets at 3.93 ppm and 2.98 ppm, as summarized in *Table 28*.

A broad peak at 3.35 ppm is evident in the aliphatic region in *Figure 74*: this peak is a result of the overlap between the signals produced by traces of water with traces of diethyl ether. Despite the meticulous drying process, which consisted in maintaining the compound in vacuum at 60 °C for prolonged times, traces of diethyl ether employed for the crystallisation step were always detected in the spectra. *Figure 75* shows the long-range hydrogen-carbon correlation for the compound. No additional structural information compared to the free base compound can be deducted from the analysis.

120
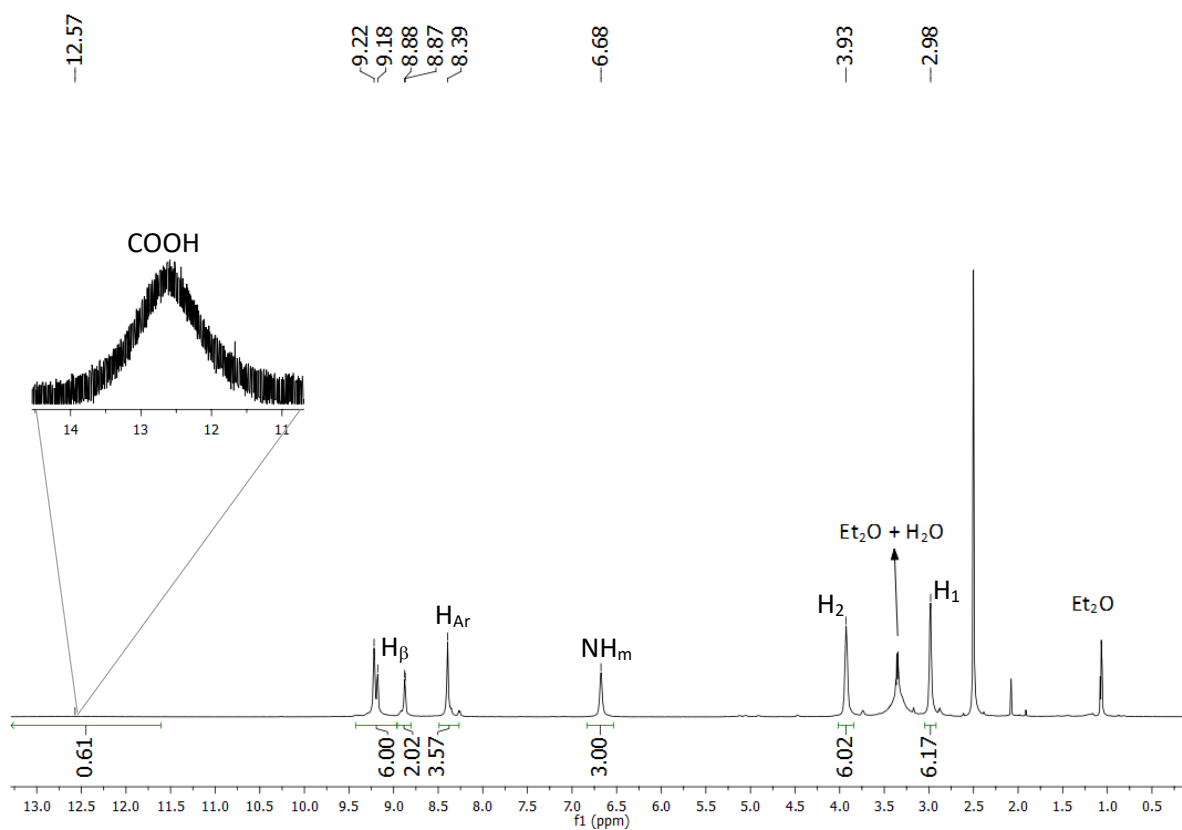
*Figure 74: ^{1}H-NMR spectrum of **121** in DMSO-d$_6$ at 298 K and 600 Mhz*

Multiplicity	δ (ppm)	Integration value	Assignment
br s	12.64	1	COOH
m	9.18-9.22	6	H$_\beta$
m	8.87	2	H$_\beta$
2d into s	8.38	4	H$_{Ar}$
s	6.68	3	NH$_m$
t into s	3.93	6	H$_2$
t into s	2.98	6	H$_1$

*Table 28: hydrogen signals assignment and structure of **121***

121

Figure 75: $^1H,^{13}C$-HMBC expanded interested region for 121 in DMSO-d_6 at 298 K and 600Mhz and 150 MHz

<u>Platinum (II) insertion</u>

Due to its larger size, platinum (II) insertion in porphyrin macrocycles is considerably more challenging than palladium. High temperatures and very prolonged reaction times are usually required for complexation, and a typical procedure consists of refluxing the free base in benzonitrile with $PtCl_2$ for several hours.[255] A more recent approach described the use of lower-boiling chlorobenzene instead of benzonitrile, in the presence of a base such as sodium acetate to neutralise the HCl generated during the reaction.[256] This procedure afforded the desired complexes in quantitative yields and faster reaction compared to $PtCl_2$/benzonitrile method. These synthetic procedures are suitable for porphyrins soluble in organic solvents, with or without the help of microwave irradiation.

Water-soluble porphyrins are usually not soluble in benzonitrile or chlorobenzene, hence a different procedure is necessary. Pasternack *et al.* showed that reactions carried out in water with platinum (II) chloride or K_2PtCl_4 as metal sources were unsuccessful,[214] but when complex $[Pt(H_2O)_2(DMSO)_2]^{2+}$ **125** (*Scheme 37*) was used, complexation of **51** occurred. **125** is not a stable species and it needs to be generated *in situ*:[257,258] first $PtCl_2$ (**122**) is dissolved in benzonitrile and stirred at 100 °C for 4 hours to generate the tetracoordinated $PtCl_2(PhCN)_2$ **123** (*Scheme 37*), which is precipitated with hexane and collected by filtration. Compound **123** is air- and moisture-stable and has a long shelf life. To form **125**, complex **123** is stirred in DMSO until completely dissolved: in this step, two DMSO molecules replace the benzonitrile ligands to give **124**. $PtCl_2(DMSO)_2$ is finally converted in the corresponding diaqua-ion by treatment with an equimolar amount of silver nitrate as an aqueous solution. The addition of silver nitrate leads to the precipitation of silver chloride, which is filtered off to give the aqueous solution of **125** employed in the complexation reaction.

$$PtCl_2 \xrightarrow[100°C,\ 4h]{PhCN} Pt(PhCN)_2Cl_2 \xrightarrow[3h]{DMSO} Pt(DMSO)_2Cl_2 \xrightarrow[AgNO_3]{H_2O} Pt(DMSO)_2(H_2O)_2$$

122   **123**   **124**   **125**

*Scheme 37: synthetic procedure of **125***

It is worth noting that the solution containing the active source of platinum (II) can contain DMSO from the synthesis of **124**. If the metal insertion is achieved employing MW irradiation, care must be taken to reduce the DMSO to a minimum, in order to reduce the risk of explosion. Due to limited volume of the MW tubes, the volume of the solution must also be contained. Lastly, the amount of silver nitrate must be carefully controlled, because any remaining silver ions will lead to the formation of the silver complex of the porphyrins and prevent platinum insertion. Refluxing **125** with the free porphyrin in water for 15 hours led to complete insertion.[214] A more recent approach described a

modification of this procedure involving MW irradiation to obtain platinum in water-soluble porphyrins,[146] which markedly decrease the reaction rate.

This procedure was applied to obtain platinum (II) complexes of cationic water-soluble porphyrins. Overnight reflux of porphyrin **73** with complex **125** in water (Scheme 38) led to the formation of the target species **74**. We found that the addition of a small amount of ethanol to the reaction mixture resulted in a smoother boiling. Isolation of **74** was performed in the same way as described for the palladium (II) complexes.
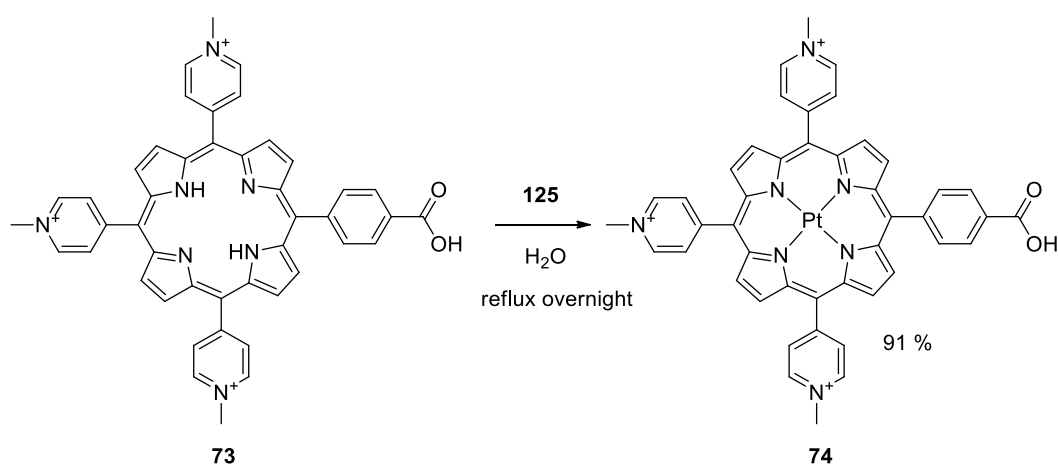
*Scheme 38: platinum insertion reaction scheme for **73***

^{1}H-NMR spectrum is shown in *Figure 76*. The signals generated by the six hydrogens in *meta* to the pyridyl nitrogen, a multiplet composed of the six hydrogens *ortho* in the pyridyl rings, together with the eight *beta* hydrogens, and the four hydrogens *ortho* and *meta* to the carboxylic group are found in the aromatic region of the spectrum. The peak at 4.73 ppm is generated by the methyl groups on the pyridyl rings. All the assignments are summarized in *Table 29* and they are in agreement with the previously reported data.[146]
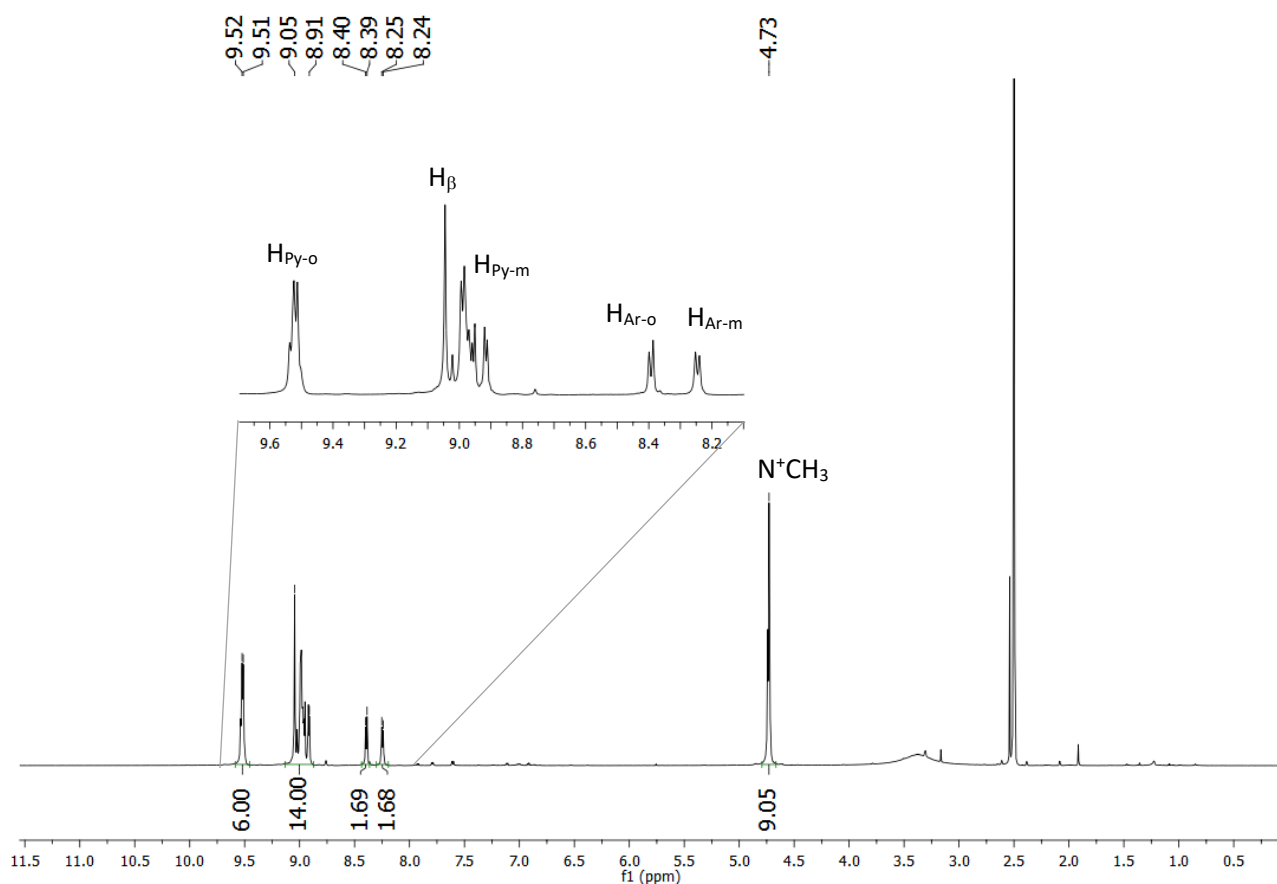
Figure 76: ^1H-NMR spectrum with expansion of **74** in DMSO-d_6 at 298 K and 600 MHz

Multiplicity	δ (ppm)	J (Hz)	Integration value	Assignment
m	9.52	-	6	H_{Py-m}
m	9.00	-	14	H_{Py-o} + H_β
d	8.40	7.8	4	H_{Ar-o}
d	8.25	7.8	4	H_{Ar-m}
s	3.93		6	CH_3
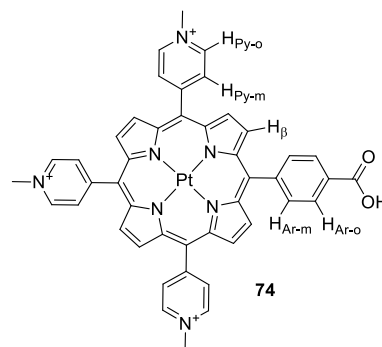
Table 29: hydrogen signals assignment and structure of **74**

Compound **117** was unstable under the reaction conditions required for platinum (II) insertion, hence the corresponding complex could not be obtained.

Platinum (II) insertion on **117** was attempted in different solvents, under conventional heating or MW irradiation, but all reactions led to a mixture of compounds (*Scheme 39*). The target platinum complex

was obtained, but alongside with it, the product of partial substitution of the alkoxy chain by hydroxide was detected by both NMR spectroscopy (*Figure 77*) and mass spectrometry (*Figure 78*).
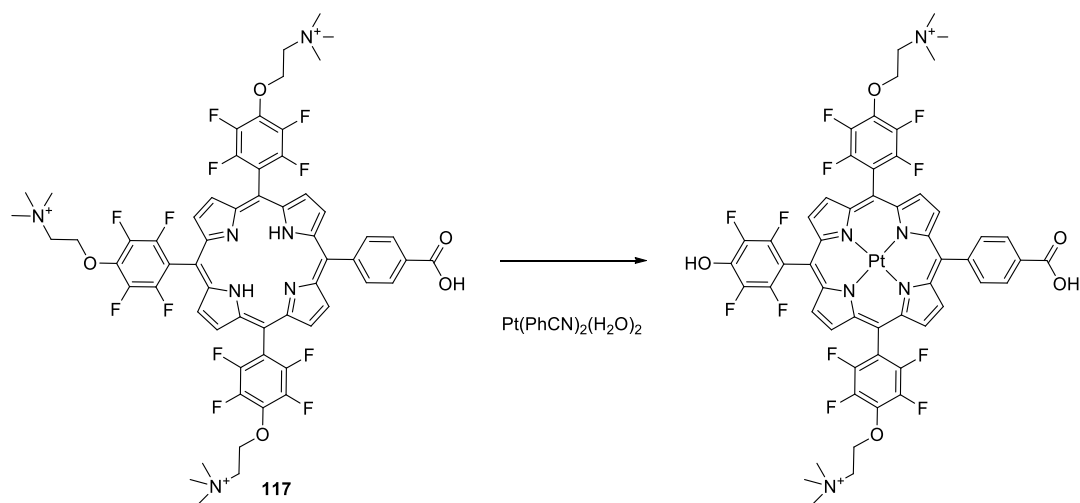
*Scheme 39: observed platinum insertion on **117***

^{1}H-NMR spectrum (*Figure 77*) showed an unexpectedly high number of signals, indicating the presence of more than one species. Mass spectrometry analysis (*Figure 78*) confirmed the OH replacement, although it was not possible to establish which of the three alkoxy-groups was replaced. *Figure 78* is an expansion of the area of interest, and it can be seen the peak relative to triple-charge free base at 393.12, and the triply-charge platinum complex at 458.21. The peak relative to triple-charge platinum complex bearing one hydroxyl group is present at 428.86. This evidence shows that alkoxy chain replacement can occur either previous to or following metal insertion. Crucially, the mass value of the platinum complex bearing one hydroxyl group coincides with that of the silver complex of **117**. With the aim to elucidate the identity of the side product, the reaction was performed in the presence of a large excess of **125**, prepared with less equivalents of silver nitrate in order to ensure the absence of silver ions. The outcome of the reaction was unchanged, confirming that the silver did not play a role in the formation of the side product.

Decreasing the reaction temperature to avoid hydroxyl replacement resulted in incomplete metal insertion. Unfortunately, the separation of **117** from its platinum complex was not achievable, so the synthesis of platinum complex of compound **117** was abandoned.
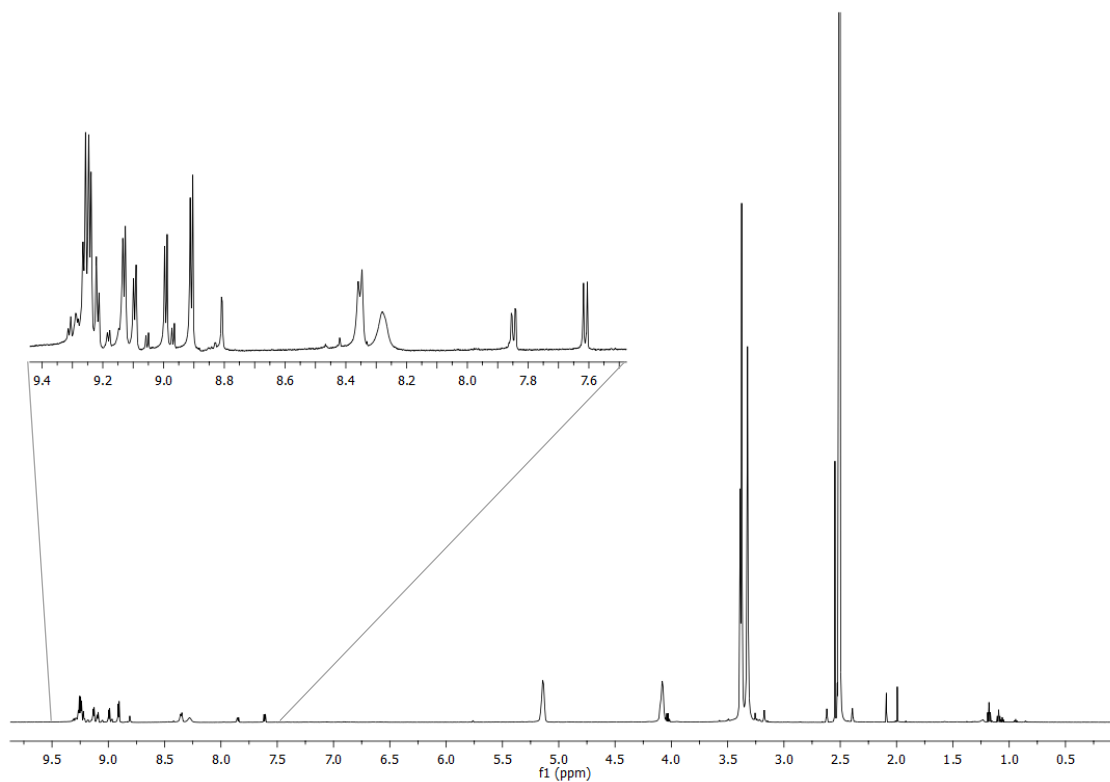
*Figure 77: ^{1}H-NMR spectrum with expansion of platinum complex of **117** in DMSO-d$_6$ at 298 K and 600 MHz*
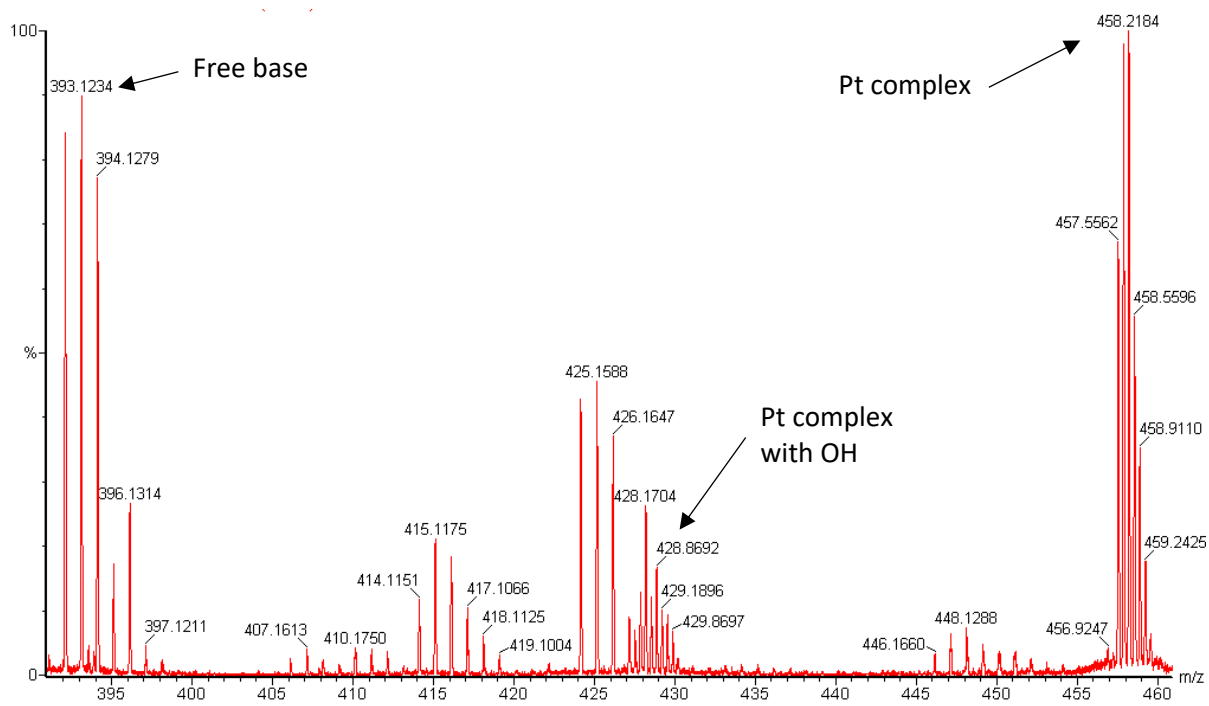
*Figure 78: ESI mass picture of platinum complex of **117** in MeOH at 298 K*

Microwave irradiation was necessary for a complete metal insertion in both **76** and **102**, as shown in *Scheme 40*. Attempts to achieve metal insertion employing conventional heating were unsuccessful. Complexation of the porphyrins prior insertion of the water-solubilising groups was not viable because the platinum (II) complexes do not withstand strongly acidic conditions.[146]
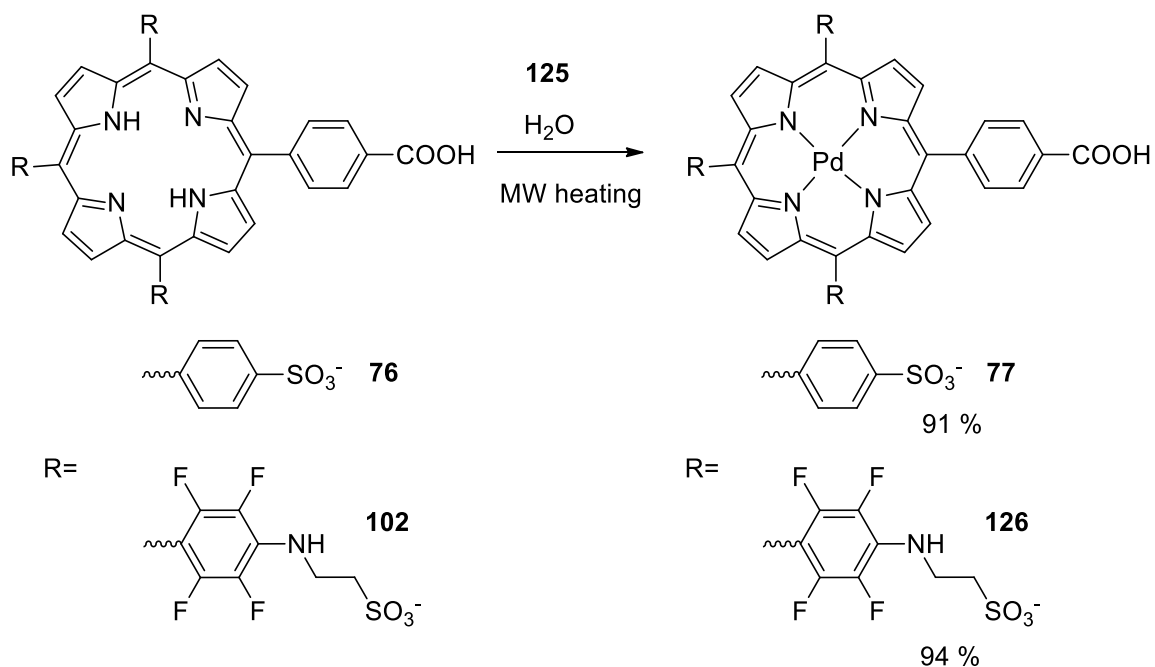
Scheme 40: platinum insertion of **76** and **102**

Table 30 shows the reaction conditions and the yields for both anionic substrates. In both cases, the porphyrins were dissolved in water with the active platinum source and the reaction performed. Nearly quantitative yields were obtained for both reactions. Compound **76** required a slightly longer reaction time to reach complete metal insertion.

Porphyrin	Yield (%)	Time (min)	T (°C)
77	91	20	200
126	94	15	200

Table 30: platinum insertion conditions, yield and MW settings

Figure 79: precipitation of 77

As in the previous cases, the products were isolated by filtration of the reaction mixture through celite to remove metallic platinum residues, and they were purified employing the ion exchange method for anionic porphyrins. *Figure 79* illustrates porphyrin **77** precipitated from water following treatment with compound **103**.

The ^{1}H-NMR spectrum of compound **77**, not shown here, confirmed a complete metal insertion by disappearance of the internal hydrogens peaks. Mass spectrometry also confirmed complete insertion. The ^{1}H-NMR spectrum shows a broad signal at low field generated by the carboxylic group, a multiplet from the eight *beta* hydrogens, signals from the hydrogens in *ortho* and *meta* to the carboxylic group appearing as a doublet of doublets, and two signals generated by the hydrogens on the phenyl rings. All the assignments are summarized in *Table 31* and they are in agreement with the previously reported data.[146]

Multiplicity	δ (ppm)	J (Hz)	Integration value	Assignment
br s	11.08	-	1	COOH
m into s	8.77	-	8	H_β
d	8.37	8.2	2	H_o
d	8.31	8.2	2	H_m
d	8.15	8.1	6	H_1
d	8.05	8.1	6	H_2
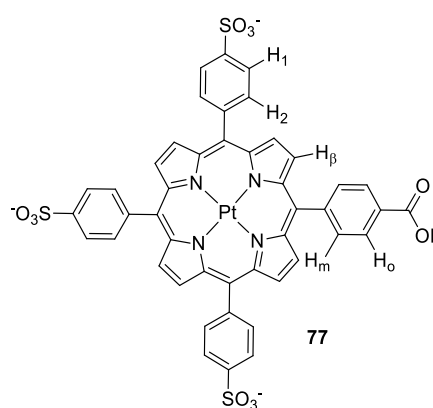
Table 31: hydrogen signals assignment and structure of 77

^{1}H-NMR spectrum for compound **126** (*Figure 80*) shows the expected disappearance of the internal hydrogens. In the aliphatic region, residual diethyl ether from the crystallisation displays two signals, as indicated in *Figure 80*.
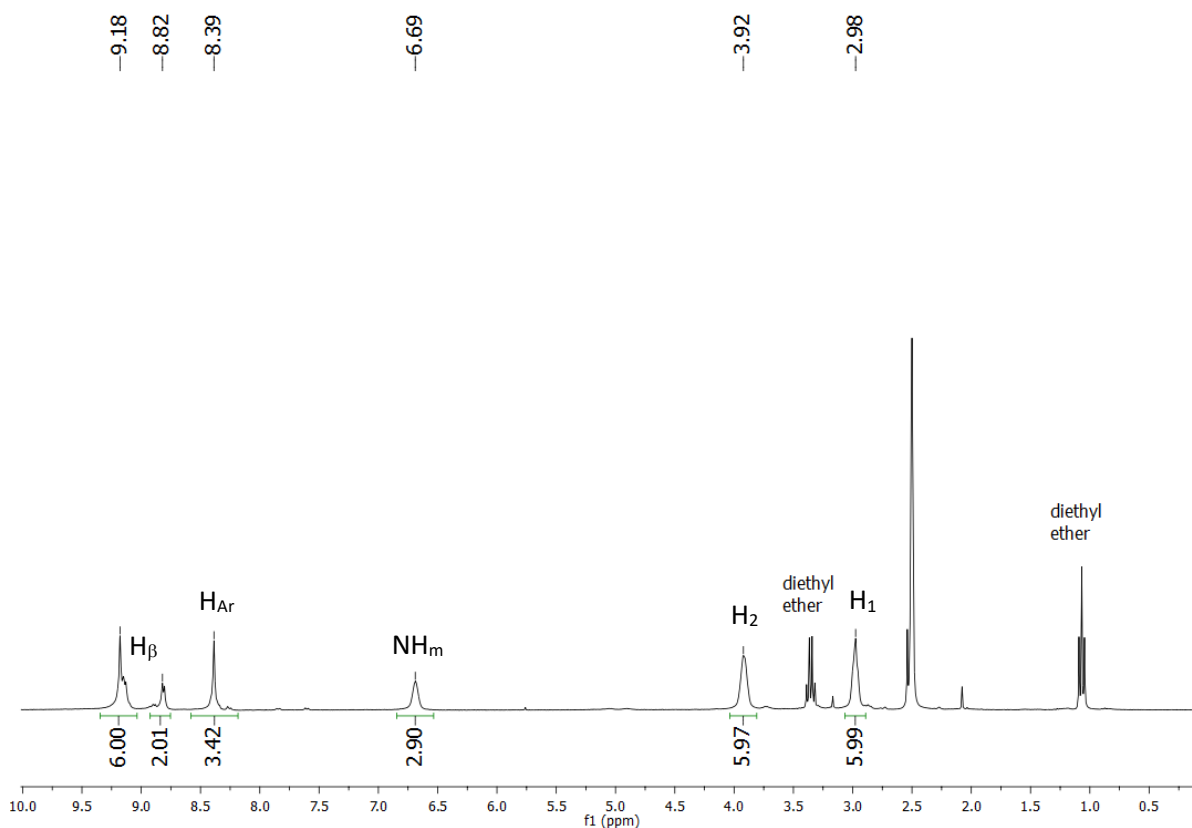
*Figure 80: ¹H-NMR spectrum of **126** in DMSO-d₆ at 298 K and 600 MHz*

The interpretation of the spectrum was similar to compound **121**, as shown in *Table 32*. The peak relative to the carboxylic group at lower field is not visible in the analysis, probably due to exchange with the deuterated solvent. At higher fields, signals from the eight *beta* and the four aryl hydrogens, are visible followed by the signals of the aromatic amine hydrogens and the two CH_2 groups.

Hydrogen-carbon correlations, DEPT-edited $^1H,^{13}C$-HSQC and $^1H,^{13}C$-HMBC are shown in *Figure 81* and in *Figure 82*, respectively. The correlations show the same structural features already identified for the free base **102**.

Multiplicity	δ (ppm)	Integration value	Assignment
m	9.18	6	$H_β$
m	8.82	2	$H_β$
2d into s	8.39	4	H_{Ar}
s	6.69	3	NH_m
t into s	3.92	6	H_2
t into s	2.98	6	H_1
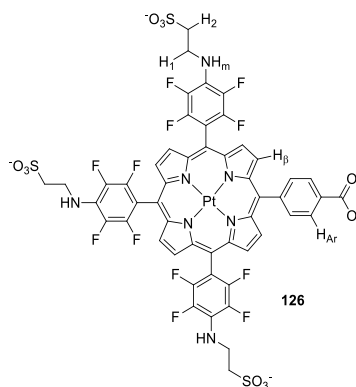
*Table 32: hydrogen signals assignment and structure of **126***
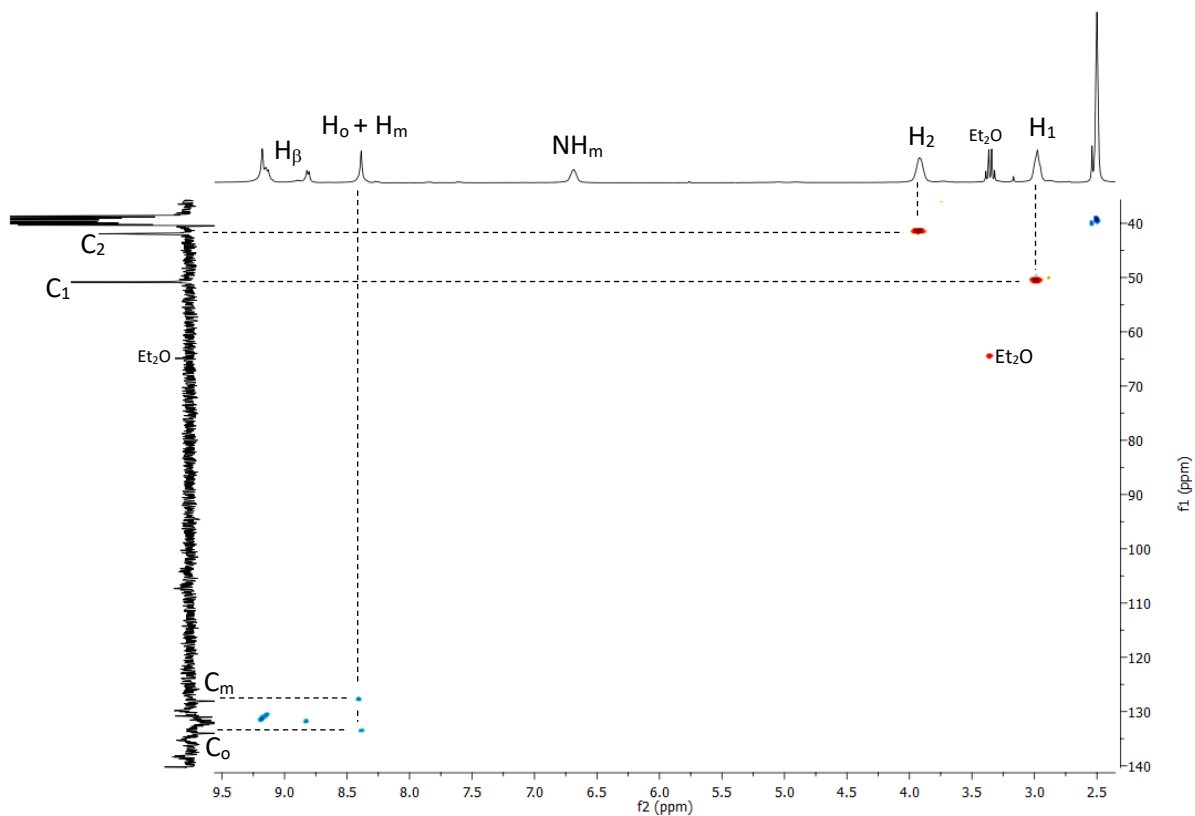
*Figure 81: DEPT-edited(135°)^{1}H,^{13}C-HSQC spectrum of **126** orange dots CH$_2$ up, blue dots CH/CH$_3$ down, in DMSO-d$_6$ at 298K*
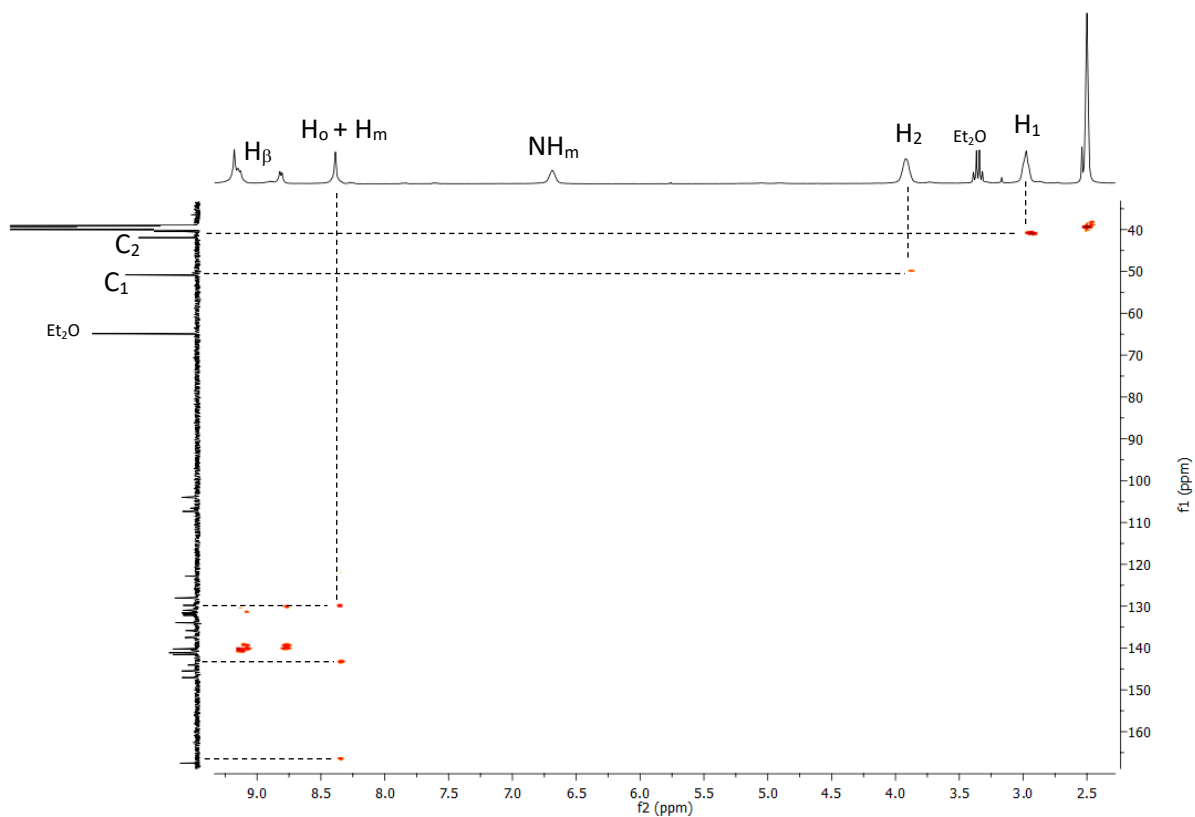
*Figure 82: ^{1}H,^{13}C-HMBC expanded interested region of **126** in DMSO-d$_6$ at 298 K and 600 MHz and 150 Mhz*

Metallation of water-soluble species: expanding the applicability of the synthesis and purification

Based on the success of the MW-assisted metal insertion in water-soluble porphyrins and of the ion-exchange procedure, it seemed reasonable to verify that their applicability can be expanded beyond the production of palladium (II) and platinum (II) complexes.

Among the transition metals, iridium (III) showed interesting luminescence properties following interaction with the oxygen.[259–261] It has been reported that iridium porphyrins behave like platinum and palladium, showing an increase of luminescence proportional to the decrease of oxygen. Therefore, water-soluble and conjugatable iridium porphyrins could be used to obtain an oxygen sensing material.

Examples of iridium complexes of porphyrin are reported in the literature,[133,262–264] mostly for catalytic applications, but only one example of water-soluble iridium porphyrin is described,[265] whose synthesis is shown in *Scheme 41*. The reaction occurs on porphyrin **57** in ethylene glycol at 140 °C for 5 hours.
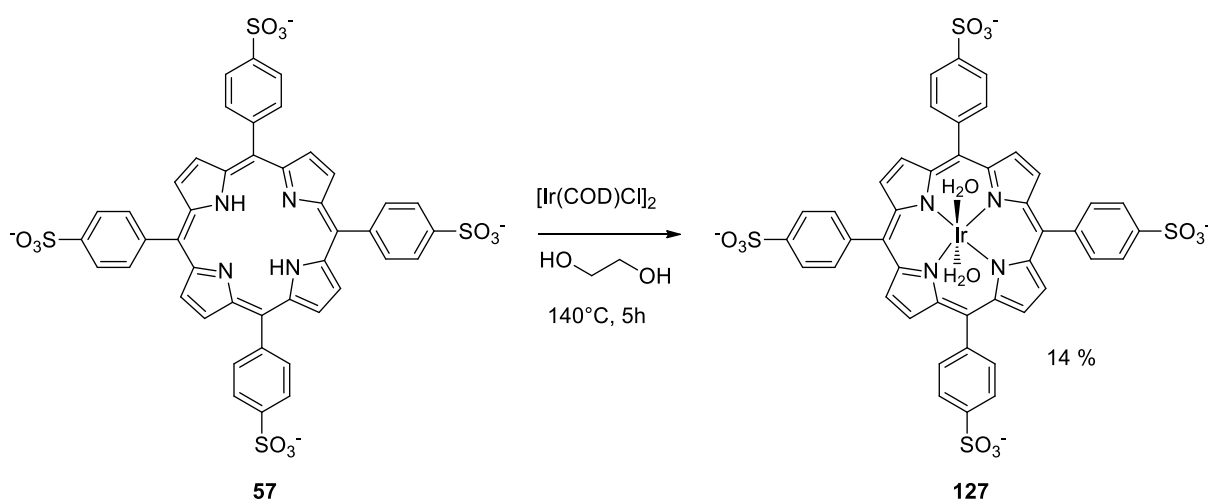
*Scheme 41: iridium insertion inside porphyrin **57** [265]*

The purification process consisted of solvent evaporation, and subsequent dissolution of the crude reaction crude in water. The authors then added an acetone solution of benzo-18-crown-6-ether to the crude solution, causing precipitation of **127** which was collected by filtration (*Figure 83*).[265] The precipitation was caused by the coordination of benzo-18-crown-6-ether to the sodium ions. The yield was low (14%) but the process produced a single crystal suitable for X-ray analysis.

Attempts to replicate the results on compound **76** failed, therefore, a different solvent was employed. NMP was unsuitable, because although it is a good solvent for the iridium source, it does not solubilise **76**. Complete metal insertion was achieved in water, dissolving the iridium source in THF and heating

the reaction mixture at 200 °C under MW irradiation (Scheme 42). The metal insertion was also carried out on porphyrins **73** and **102** (*Table 33*): confirming that cationic porphyrins did not require microwave irradiation to achieve complete metal insertion.
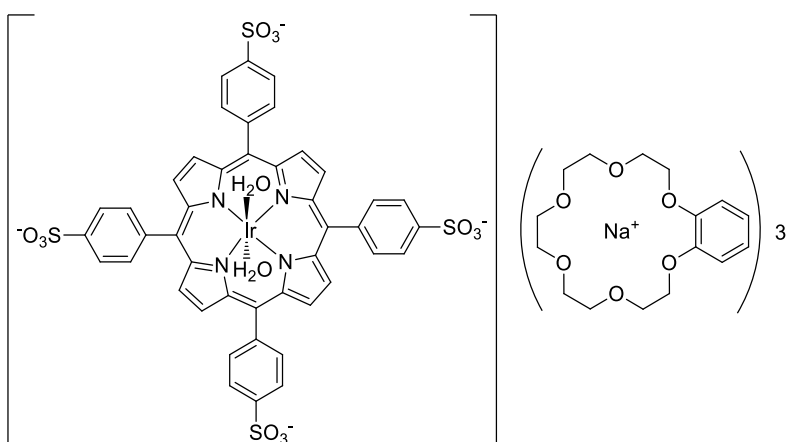
*Figure 83: complex **127** complexed with benzo-18-crown-6-ether* [265]

Reaction progress was monitored by mass spectrometry, following the disappearance of the peak of the free base. However, several peaks were detected for the iridium complex due to the exchange of the axial ligands coordinated to the metal. Other than the species without axial ligands, chlorine and hydroxyl as ligands were detected.
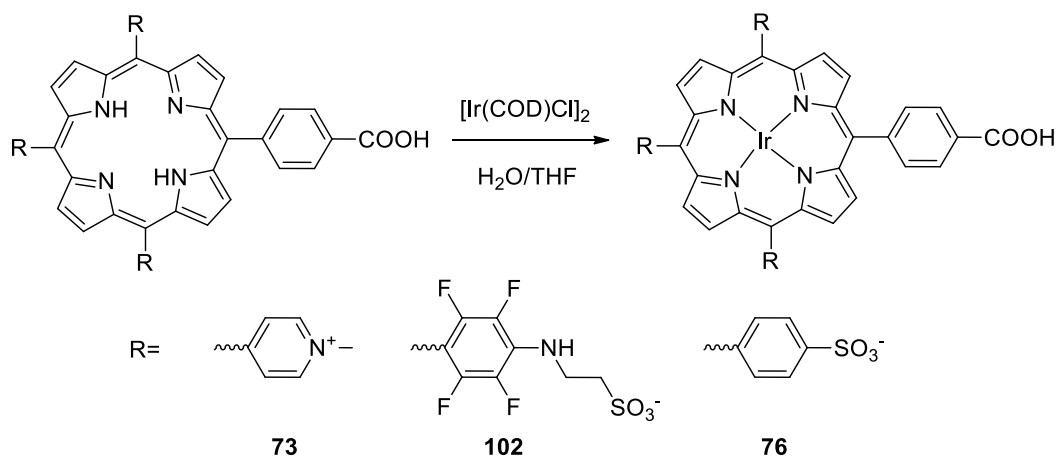
Scheme 42: iridium insertion scheme

Porphyrin	Yield (%)	Time	T (°C)	MW
73	80	overnight	100	-
76	76	20 min	200	√
102	63	20 min	150	√

Table 33: yields and reaction conditions for iridium insertion

NMR spectroscopy was not very conclusive, as shown for **73** in *Figure 84*. The spectrum shows a peak pattern typical of structures such as **73**, with signals attributable to methyl groups at 4.70 ppm and aromatic signals between 8.11 and 9.49 ppm. The aromatic region between 8.11 and 9.49 ppm shows overlapping signals, due to the presence of species with different axial ligands coordinated to the metal, this prevented further unequivocal peak assignments to be made.

The mass-spectrum (*Figure 85*) shows the iridium complex of porphyrin **102**, and the peak with *m/z* relative to triple-charge complex bearing no axial ligands can be seen at 477.23. Two smaller peaks with the m/z of 482.92 and 488.90 correspond to the triple-charge signals relative, respectively, to the complex bearing a hydroxy group (Ir-OH) and to the complex bearing a chloride (Ir-Cl).
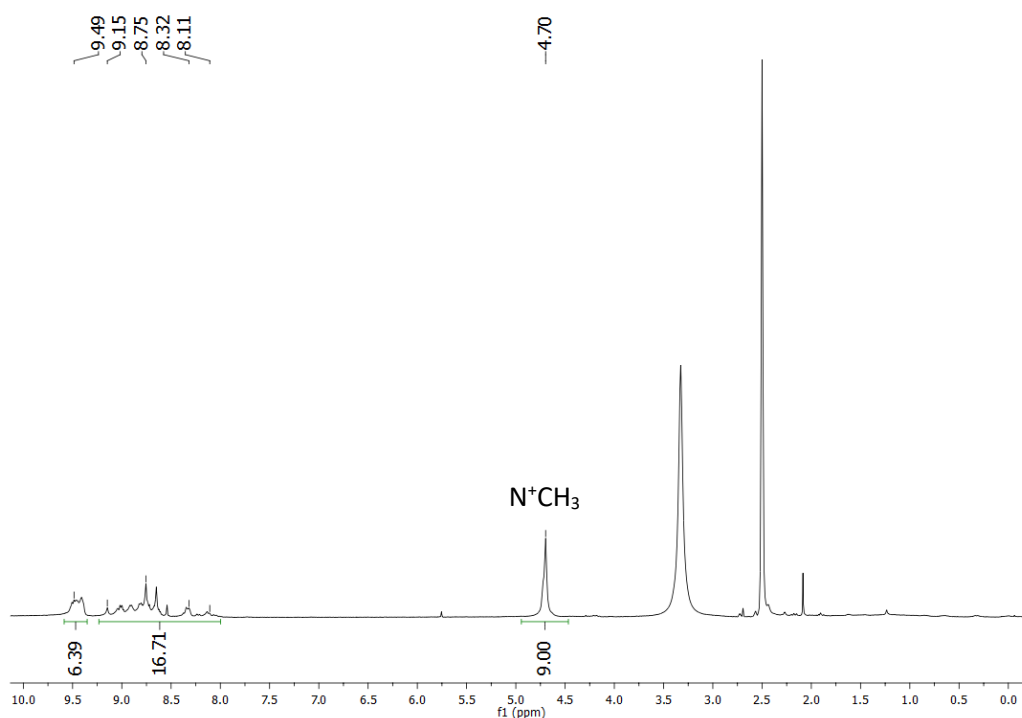
*Figure 84: ^{1}H-NMR spectrum of iridium complex of **73** in DMSO-d$_6$ at 298 K and 600 MHz*
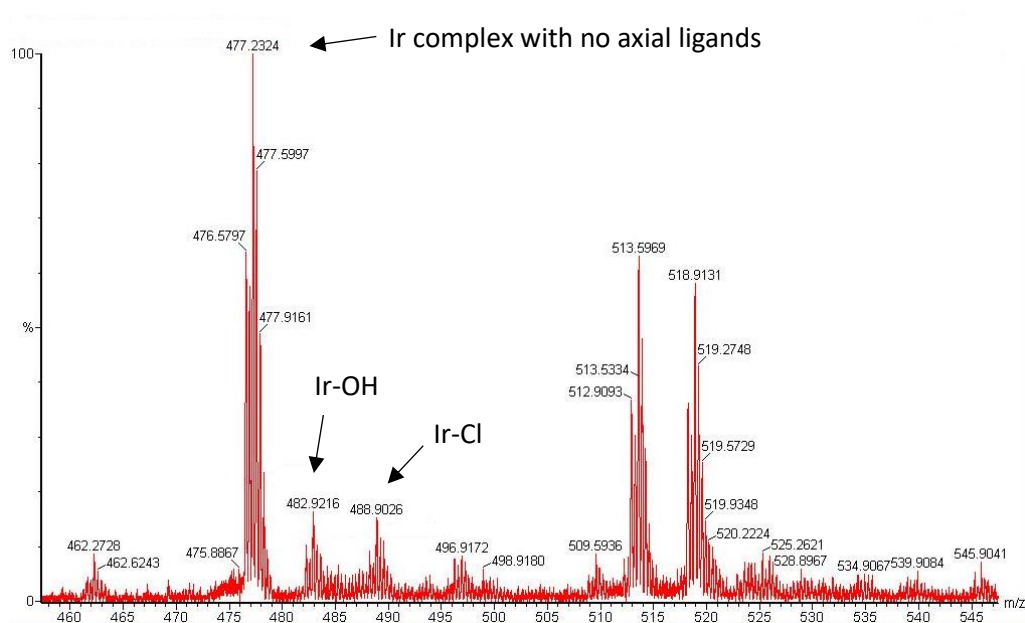
*Figure 85: ESI mass picture of iridium complex of **102** bearing different axial ligands in MeOH*

Indium (III) complexes of both water-soluble[266–268] and non-water-soluble[165,269–273] porphyrin are reported in the literature. Functionalised analogues of the water-soluble **51** have been successfully employed as labelling agents after insertion of radioactive ^{111}In.[268] Singlet oxygen production for photodynamic therapy (PDT) applications has been investigated on a water-soluble glucopyranoside-conjugated porphyrin.[267] Moreover, indium complexes of both porphyrins **73** and **76** have been synthesised to study their anion catalysed acid solvolysis.[266]

Scheme 43 shows the metal insertions performed on substrates **73**, **76** and **102**. As observed for platinum and palladium complexation, cationic **72** did not require microwave irradiation for metal insertion. The reaction proceeded to completion in refluxing water overnight in the presence of an excess of indium trichloride as shown in *Table 34*.

MW irradiation was necessary to achieve metal insertion in derivatives **76** and **102**. The reactions were performed in water at 120 °C and were complete in 15 minutes.

Porphyrin	Yield (%)	Time	T (°C)	MW
127	98	overnight	100	-
128	83	15 min	120	√
129	84	15 min	120	√

Table 34: yields and reaction conditions for iridium insertion
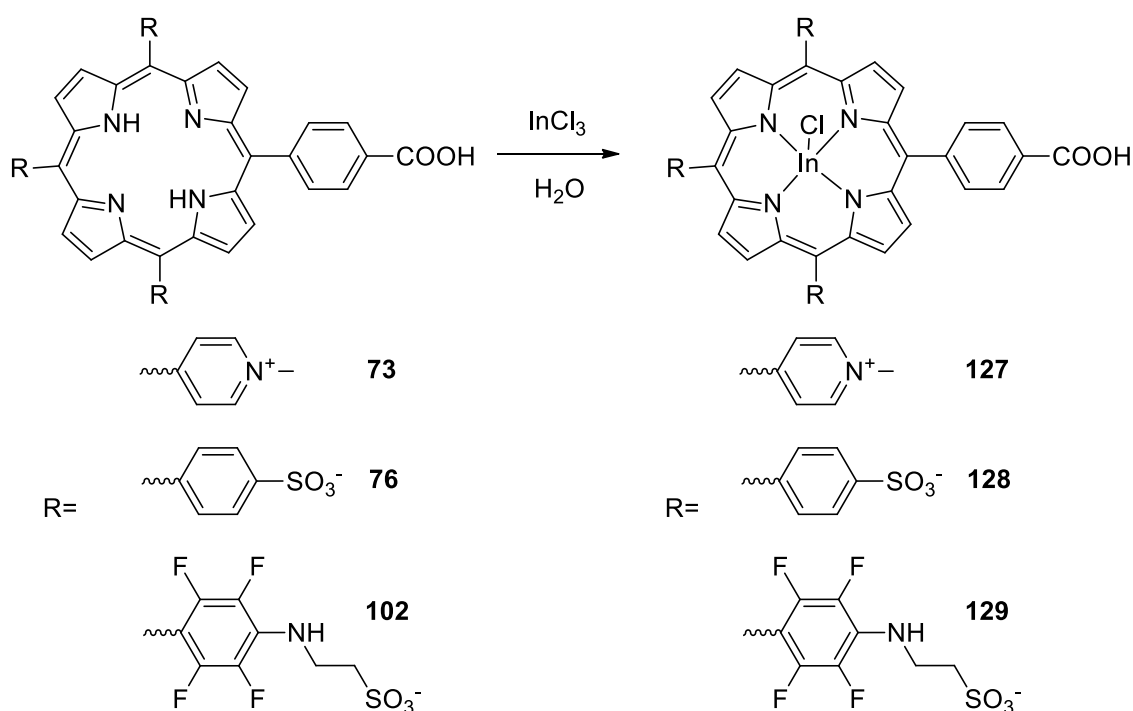
Scheme 43: indium insertion scheme

^{1}H-NMR spectrum of compound **127** is shown in *Figure 86*. A very broad peak appears down-fields, highlighting the presence of a carboxylic acid group and the internal hydrogen signal at negative ppm disappeared, once again indicating complete metal insertion. Although the integration values match with the hydrogen count in the structure, the aromatic region appears poorly resolved. Mass spectrometry confirmed the formation of the expected complex **127** with no side products. Six pyridyl hydrogens are visible, followed by a multiplet produced by the eight *beta* and the other six pyridyl hydrogens; the four phenyl hydrogens appear as broad multiplets. The nine hydrogens relative to the methyl groups appear as signal at 4.74 ppm. Unequivocal signal assignment was not possible due to the broadening of the signals.
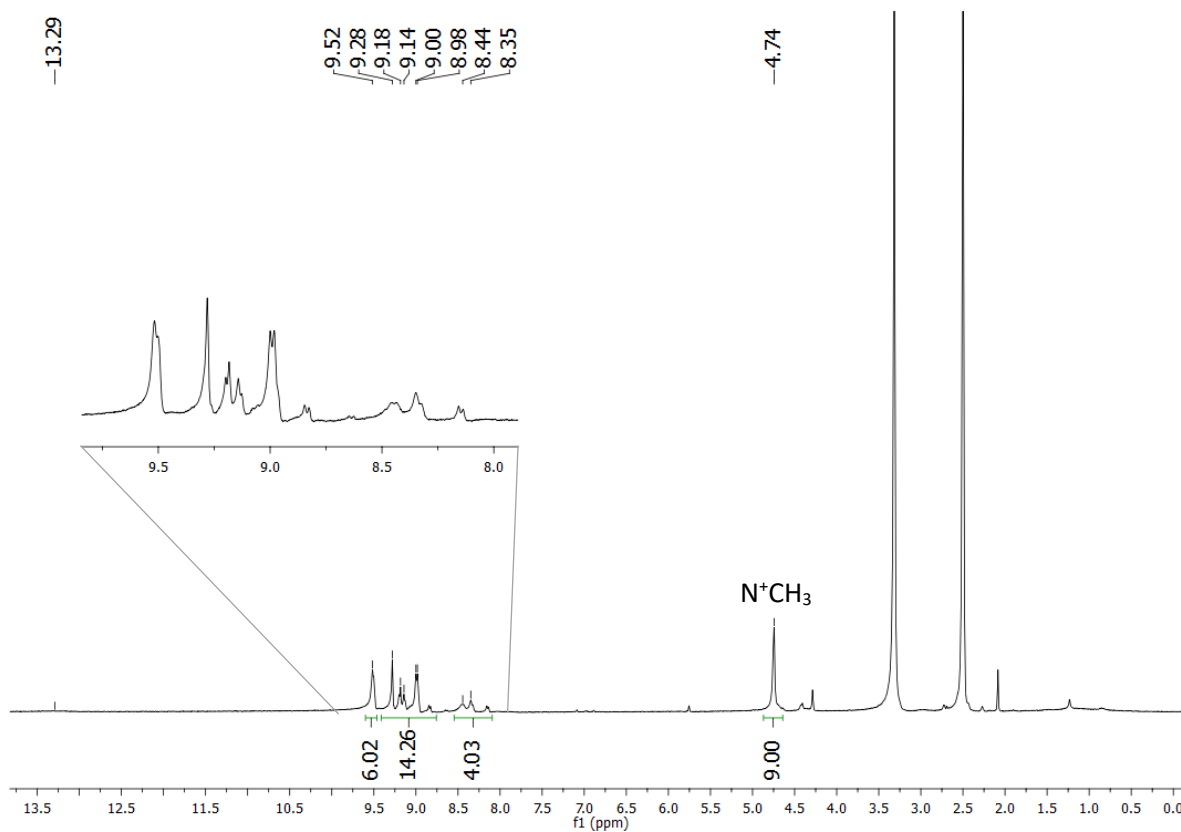
*Figure 86: ^{1}H-NMR spectrum with expansion of **127** in DMSO-d$_6$ at 298 K and 600 MHz*

^{1}H-NMR spectrum of compound **128** is shown in *Figure 87*. Complete metal insertion was detected by disappearance of the internal hydrogens. The broad signal from the COOH group appears at 13.22 ppm, and the eight *beta* hydrogens in the aromatic region appear as a sharp multiplets. The remaining signals are assigned to the phenyl and the carboxyphenyl rings, as shown in *Table 35*. The aliphatic region presents some signals relative to residual solvent from the purification process, such as diethyl ether water and acetone, which prolonged permanence in vacuum could not remove.

137
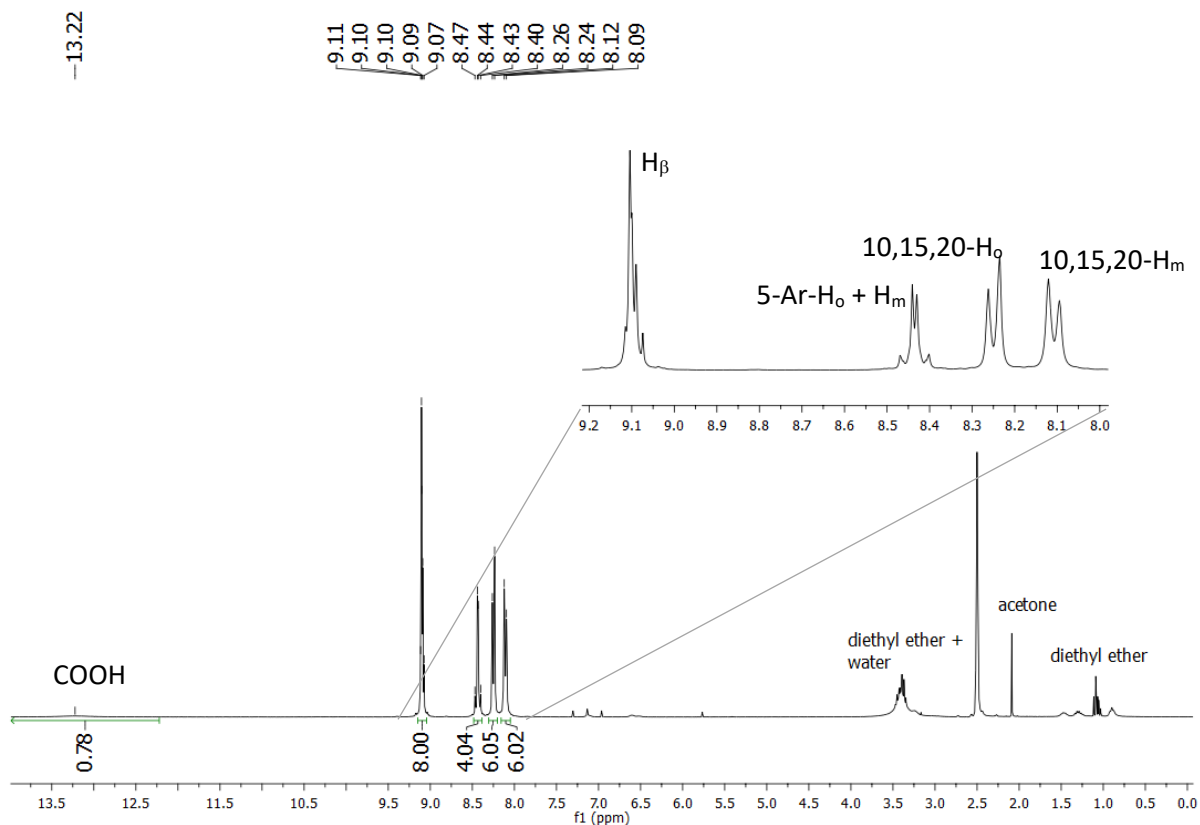
*Figure 87: ^{1}H-NMR spectrum with expansion of **128** in DMSO-d_6 at 298 K and 600 MHz*

Multiplicity	δ (ppm)	J (Hz)	Integration value	Assignment
br s	13.22	-	1	COOH
m	9.07-9.11	-	8	H_β
2d into dd	8.43	8.2/11.4	4	H_{Ar}
d	8.25	8.1	6	H_1
d	8.11	7.8	6	H_2
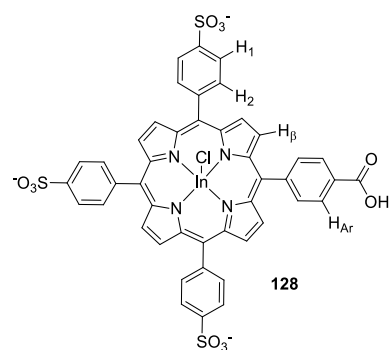
*Table 35: hydrogen signals assignment and structure of **128***

^{1}H-NMR spectrum of complex **129**, not shown here, was not conclusive, displaying very broad signals and overcrowded aromatic region, but both UV-vis and mass spectrometry confirmed the formation of the expected compound.

Metal insertion in porphyrins is a widely employed approach to create complexes useful in many applications, ranging from catalysis to chemical sensing. Sonodynamic therapy (SDT) is gaining increasing interest, due to the possible applications in medicine as a complementary approach to photodynamic therapy (PDT) in the cure of cancer and inactivation of microbial cells.[274] In PDT, singlet oxygen and other cytotoxic reactive oxygen species responsible for cell death are generated following the interaction of a photosensitiser and visible light in the presence of oxygen. A considerable limitation of this approach is determined by the poor penetration of light in tissues (few millimetres). In sonodynamic therapy, reactive oxygen species are generated following the interaction of a sensitiser (in this case sonosensitiser) with ultrasound waves. Transparency of tissues to ultrasound allow the delivery of SDT treatment to deeply-seated lesions.[274] The efficacy of SDT has been demonstrated both *in vitro* and *in vivo* animal models,[275–278] but additional studies need to be carried out to fully understand the mechanism underpinning sonosensitisation of cells. It has been shown that cells death happens due to phenomena like sonoporation,[279] cell membrane breakage,[280] acoustic cavitation,[281] heat[282] and free radicals generation,[283] or a combination of any of these events. Numerous studies attribute SDT effect to acoustic cavitation, defined as nucleation and growth of gas bubbles in an ultrasound field, which collapse violently releasing a sufficient amount of energy to cause irreversible cell damage.[284,285] It has been demonstrated that bubble implosion can result in light emission (sonoluminescence).[286,287] Based on the observation that most known sonosensitisers are also photosensitisers in PDT, it has been speculated that sonoluminescence could be involved in the generation of reactive oxygen species in SDT via a mechanism similar to that PDT.[288] In order to shed light in this emerging fields, and to better comprehend the differences and the correlations between photo- and sonodynamic therapy, a series of experiments have been carried out in collaboration with researchers at the University of Turin, comparing the effect of different porphyrins on cells following exposure to light and ultrasounds.

As part of a collaboration with this group, different metal complexes of porphyrin **51** were prepared, that reinforced the wide applicability of the method developed for the purification of cationic water-soluble species.

Three metal complexes of compound **51** were synthesised, to compare with the free base porphyrin. Zinc (II), iron (III) and palladium (II) were chosen as metals, as they give the macrocycle different photophysical behaviour and different efficiency to generate reactive oxygen species. The synthesis of these complexes was described by Pasternack *et al*., but the purification method, also based on ion-exchange, was different from the one developed during this work.[289] The reactions were performed in water under reflux conditions overnight, employing the relative metal salt shown in *Table 36*.

A 1:5 ratio between the porphyrin and the metal salt was employed to ensure complete metal insertion (*Scheme 44*).

Metal	Yield	Metal salt
Zn	84%	$Zn(OAc)_2$
Pd	78%	$Pd(OAc)_2$
Fe	78%	$FeCl_2$

Table 36: yields and reaction conditions for metal insertion

R= 51   M= Zn **130**, Pd **53**, Fe(Cl) **131**
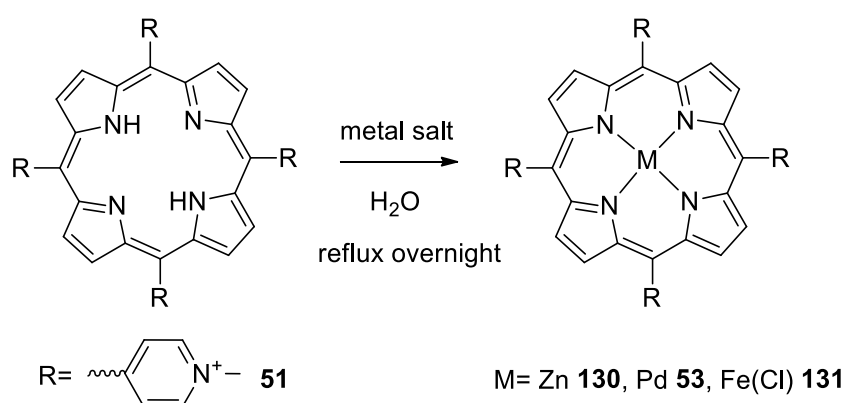
Scheme 44: metal insertion scheme for 51

The metal complexes were purified employing the ion-exchange method for cationic water-soluble porphyrins. Gratifyingly, the ion-exchange worked flawlessly on **130**, **53** and **131** yielding high purity complexes, and further confirming the wider applicability of the method. ^{1}H-NMR spectra of the free base **51** (*Figure 88*), the zinc complex **130** (*Figure 89*) and the palladium **53** (*Figure 90*) complexes are presented below. *Table 37* summarises the hydrogen assignments, the chemical shifts and integral values of these compounds.

Assignment	51	53	130	Integration value
	2H	Pd	Zn	
H_o	9.54	9.51	9.47	8
H_β	9.19	9.13	9.01	8
H_m	9.01	8.97	8.89	8
CH_3	4.75	4.73	4.73	12
M	−3.10	-	-	2
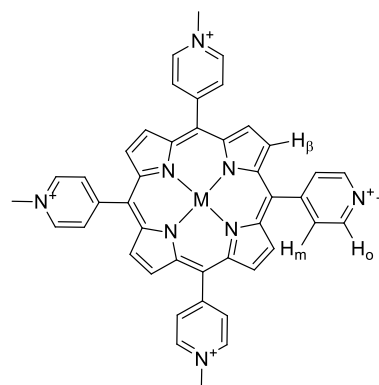
Table 37: hydrogen signals assignment for 51 and its palladium and zinc complexes with general structure

The signals in the spectra are broad and poorly resolved, due to the strong aggregation tendency of porphyrins in DMSO-d_6. The structure of the free base and the metal complexes formation was confirmed also by mass spectrometry and UV-vis spectroscopy.
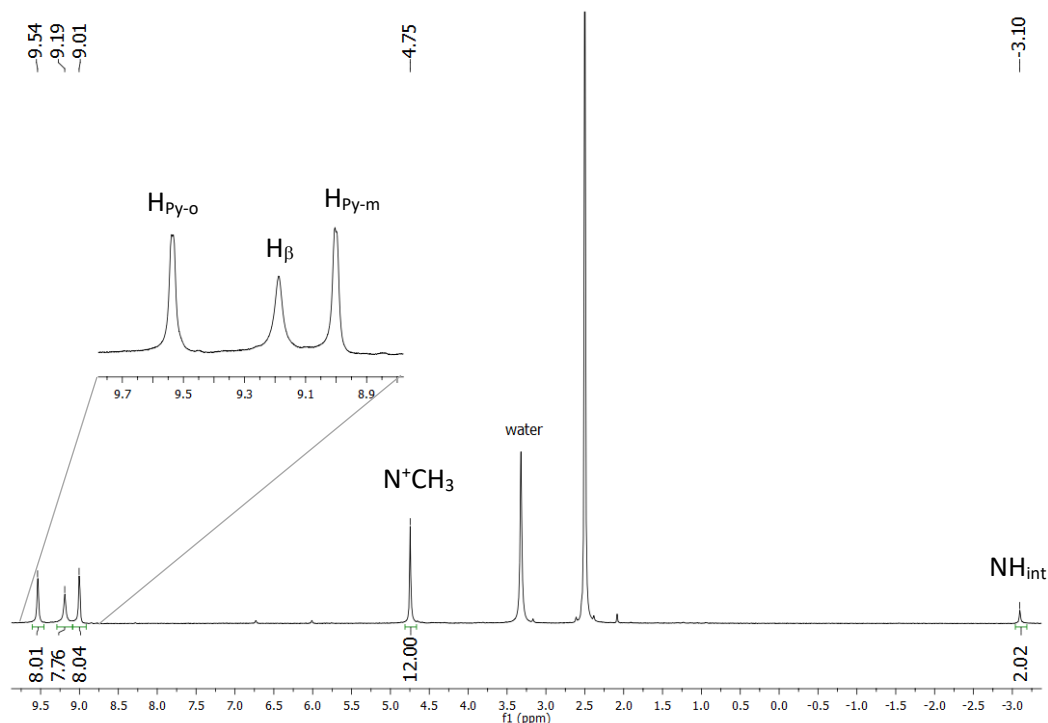
Figure 88: ^{1}H-NMR spectrum with expansion of **51** in DMSO-d_6 at 298 K and 600 MHz

The zinc complex gave a spectrum with sharper and better-resolved peaks (*Figure 89*), showing the hydrogens on the pyridyl rings as doublets, with a coupling constant of 6.6 Hz.

This part of the work allowed to confirm that the ion exchange purification method can be extended to species bearing different metal complexes, from palladium and platinum to zinc and iron. Cationic species **73** and **117** and a variety of their complexes can be purified employing this method, which is faster than chromatography and better suited to scale-up.
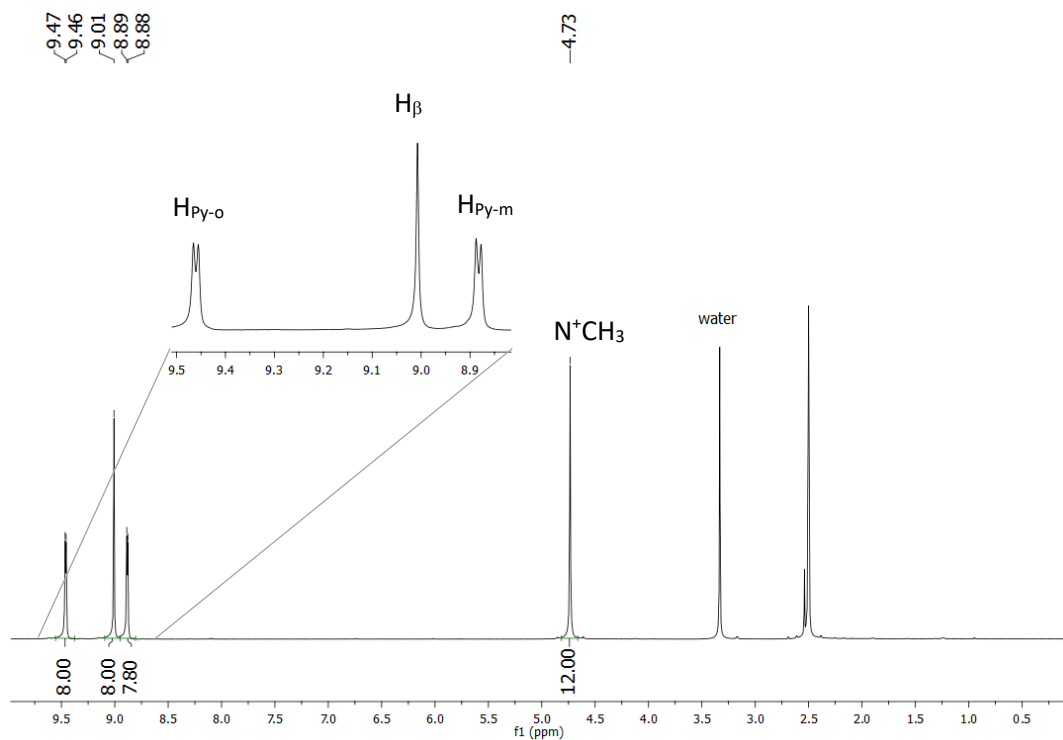
*Figure 89: ^{1}H-NMR spectrum with expansion of **130** in DMSO-d$_6$ at 298 K and 600 MHz*
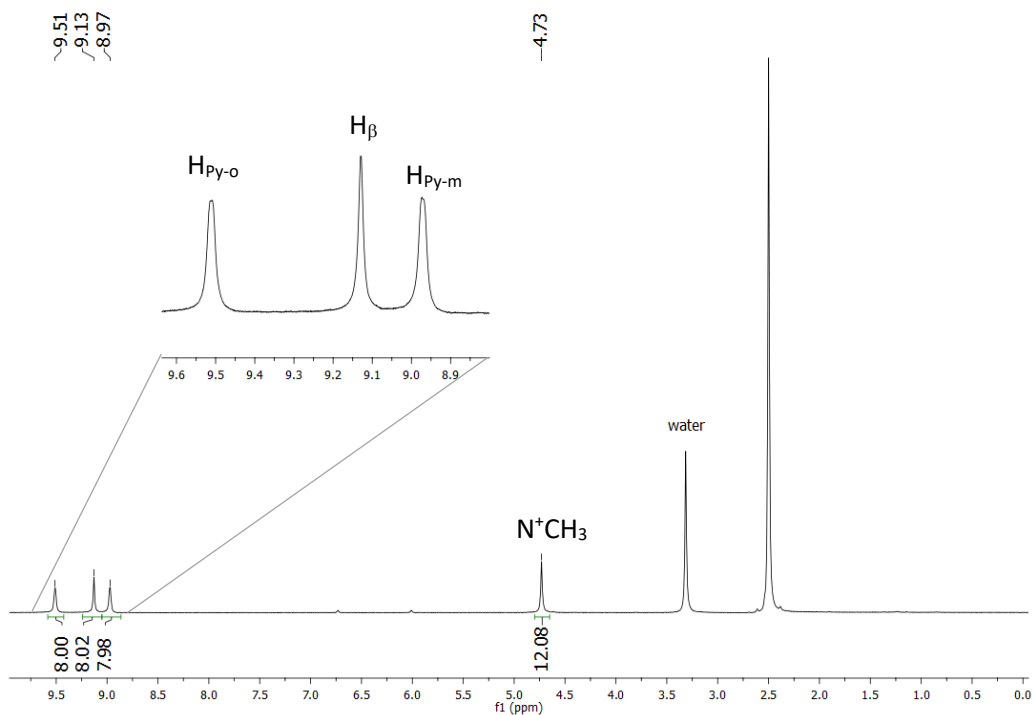
*Figure 90: ^{1}H-NMR spectrum with expansion of **53** in DMSO-d$_6$ at 298 K and 600 MHz*

3.4 Activation of carboxylic acid for conjugation reactions

The next step of the work involved the preparation of species suitable for conjugation to biomacromolecules. Many approaches have been used to conjugate porphyrins to proteins and peptides, including bio-orthogonal strategies (*e.g.*, copper catalysed cycloaddition between an azide and a propargyl group,[290] metathesis reactions between two double bonds,[291] etc.), strategies targeting less-abundant residues (e.g., thiol-maleimide ligation)[292] and non-bio-orthogonal strategies based on the formation of an amide bond between the porphyrin and the substrate. A common approach to form amide bonds involve the transformation of the carboxylic group (generally located on the porphyrin) into the corresponding *N*-hydroxysuccinimide ester (NHS ester), using N-hydroxysuccinimide and a carbodiimide activator.[146] The latter approach was the one employed for this project. Activation of complexes **74**, **75**, **77**, **78**, **117**, **121** and **126** was undertaken *via* the formation of the corresponding hydroxysuccinimide-esters. The isolation of the active ester was not a necessary step, as the activation can be performed *in situ* with the scaffold already present in the reaction environment. However, *in situ* activation can lead to unwanted cross-linking between groups on the protein. In addition, NHS esters can be stored and can be used as stand-alone reagents for conjugation.

A general reaction scheme is presented in *Scheme 45*. The reactions were performed with a large excess of NHS and EDC hydrochloride (up to 10 equivalents) in DMSO for 12-48 hours at 40 °C, as shown in *Table 38*.
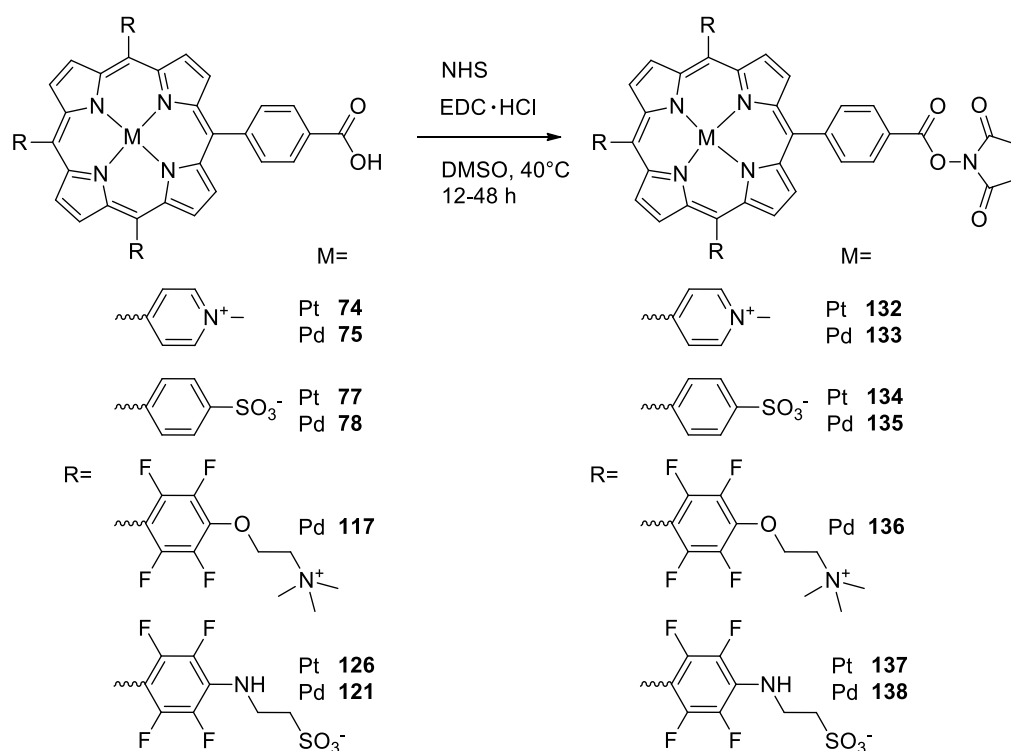
Scheme 45: ester activation reaction scheme

Product formation was monitored by mass spectrometry and the reaction was stopped when no starting material was detected. It is worth noting that the reaction did not reach completion if the substrate was not completely dissolved, and in some cases, addition of DMSO was necessary after 24 hours if the reaction was not complete: this was the case of the complexes **74** and **75**, as shown in *Table 38*. Interestingly, when the free base of EDC was used only traces of active ester were detected in the reaction mixture, probably due to degradation of the coupling reagent. The products were purified with the ion-exchange methods, which, gratifyingly, did not cause degradation of the activated ester group. When the ion-exchange method was not applied, the reaction product resulted contaminated with residues of EDC and NHS.

Complex	^{1}H δ (ppm)	^{1}H Figure	Scale (mg)	Yield (%)	Time (h)
132	3.01	Figure 92	99	86	48h
133	3.02	Figure 91	10	78	48h
134	3.00	Figure 95	110	72	24h
135	3.00	Figure 94	100	71	24h
136	3.02	Figure 93	78	87	12h
137	3.01	Figure 97	145	91	24h
138	3.01	Figure 96	100	73	24h

Table 38: ester activation reaction conditions and chemical shift of succinimide CH$_2$ for all substrates

Activated species **138** was obtained in 91 % yield on a 150-mg scale reaction: this was the highest yielding activation reaction, presumably due to the excellent solubility of the substrate in DMSO. Complex **117** reacted faster than the other substrates, reaching completion in just 12 hours, confirming the importance of the solubility of the starting material in the reaction mixture.

^{1}H-NMR spectra of the different active esters are shown below. The appearance of a peak at *ca.* 3.00 ppm due to the succinimide CH$_2$ hydrogens is apparent in all spectra. The general poor solubility of the substrates made the integration of the peaks on ^{1}H-NMR spectra inaccurate, although the chemical shifts were in line with what was expected. Aggregation and precipitation in the NMR tube, even at low concentrations, was evident, which decreased the resolution of the spectra. On the other hand, too diluted sample gave non-legible spectra, therefore a compromise had to be found between resolution and sensitivity. The presence of the succinimide group was also confirmed by the presence of a peak in the aliphatic region of the ^{13}C-NMR spectra of all synthesised species (*ca.* 25 ppm). Mass spectrometry also confirmed the structure of the target compounds.

Seven different metalloporphyrins bearing an active ester for conjugation have been synthesised and characterized.
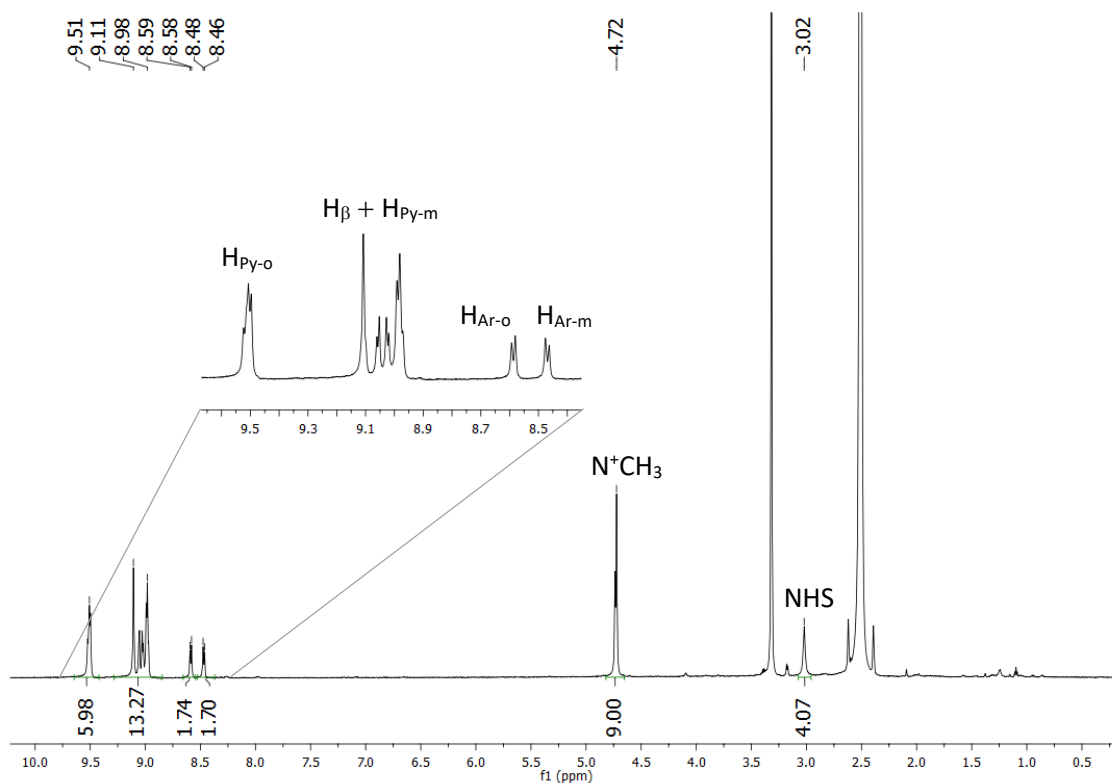
Figure 91: ^{1}H-NMR spectrum with expansion of **133** in DMSO-d$_6$ at 298 K and 600 MHz
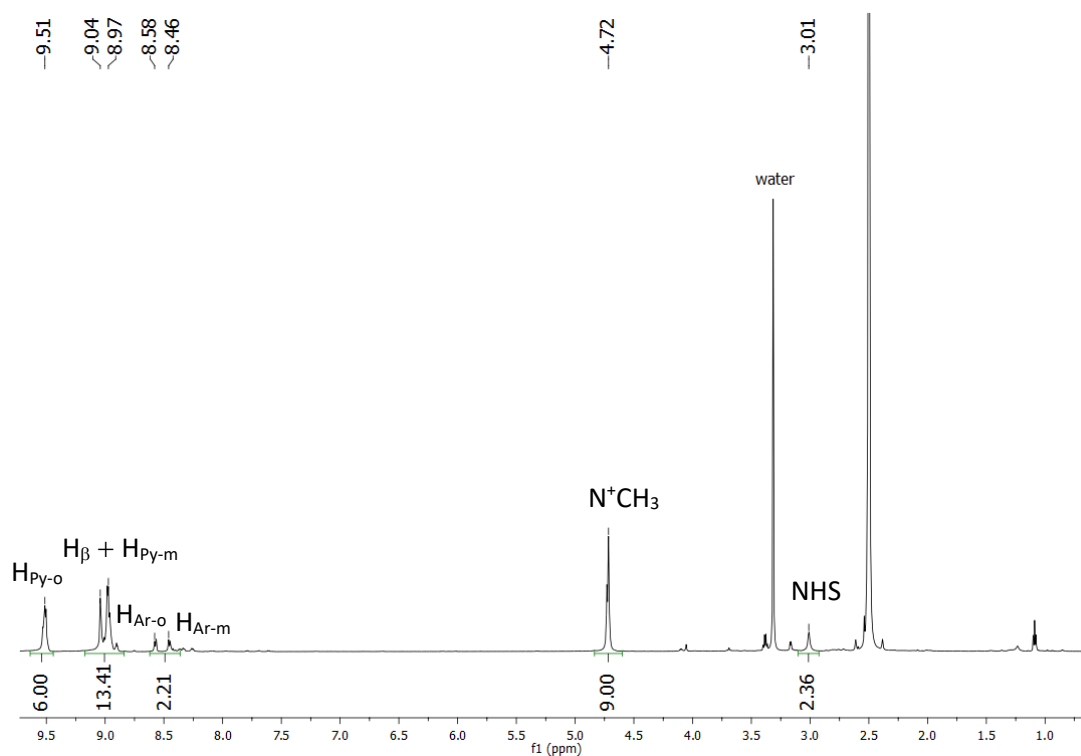
Figure 92: ^{1}H-NMR spectrum of **132** in DMSO-d$_6$ at 298 K and 600 MHz
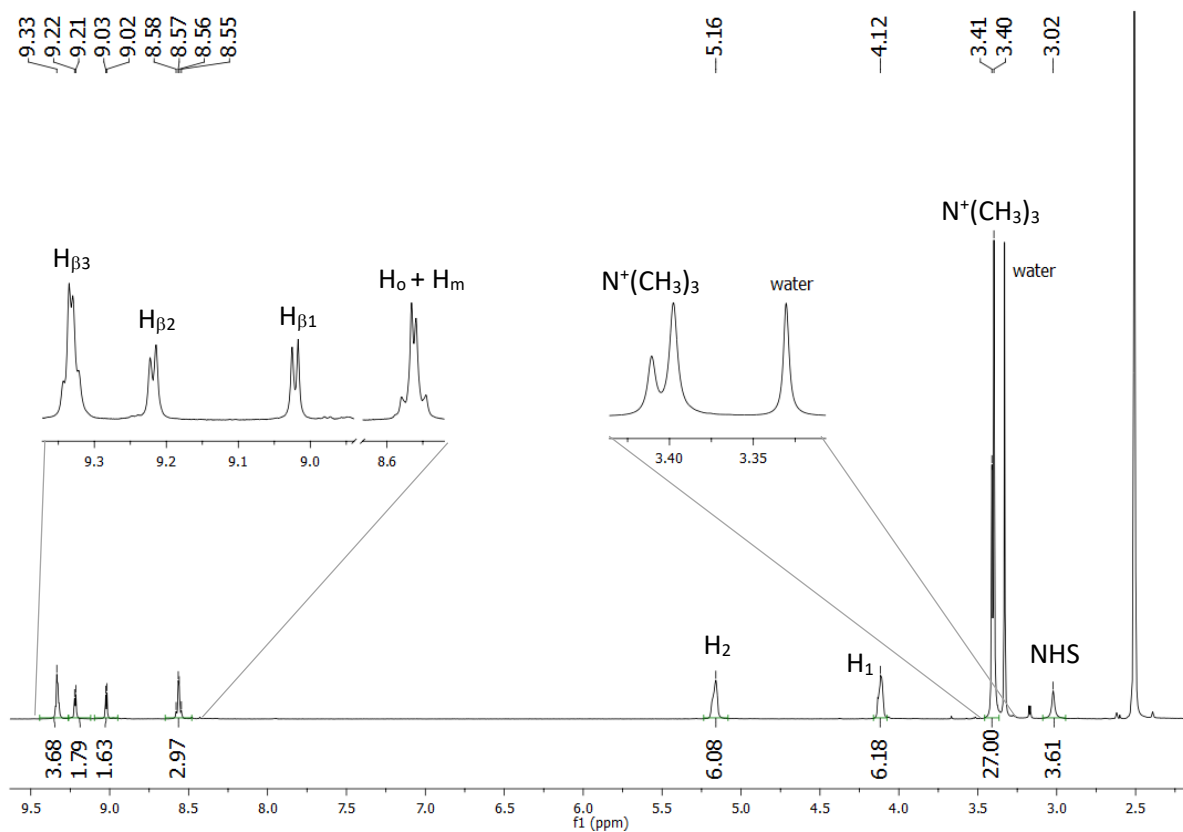
*Figure 93: ¹H-NMR spectrum with expansion of **136** in DMSO-d₆ at 298 K and 600 MHz*
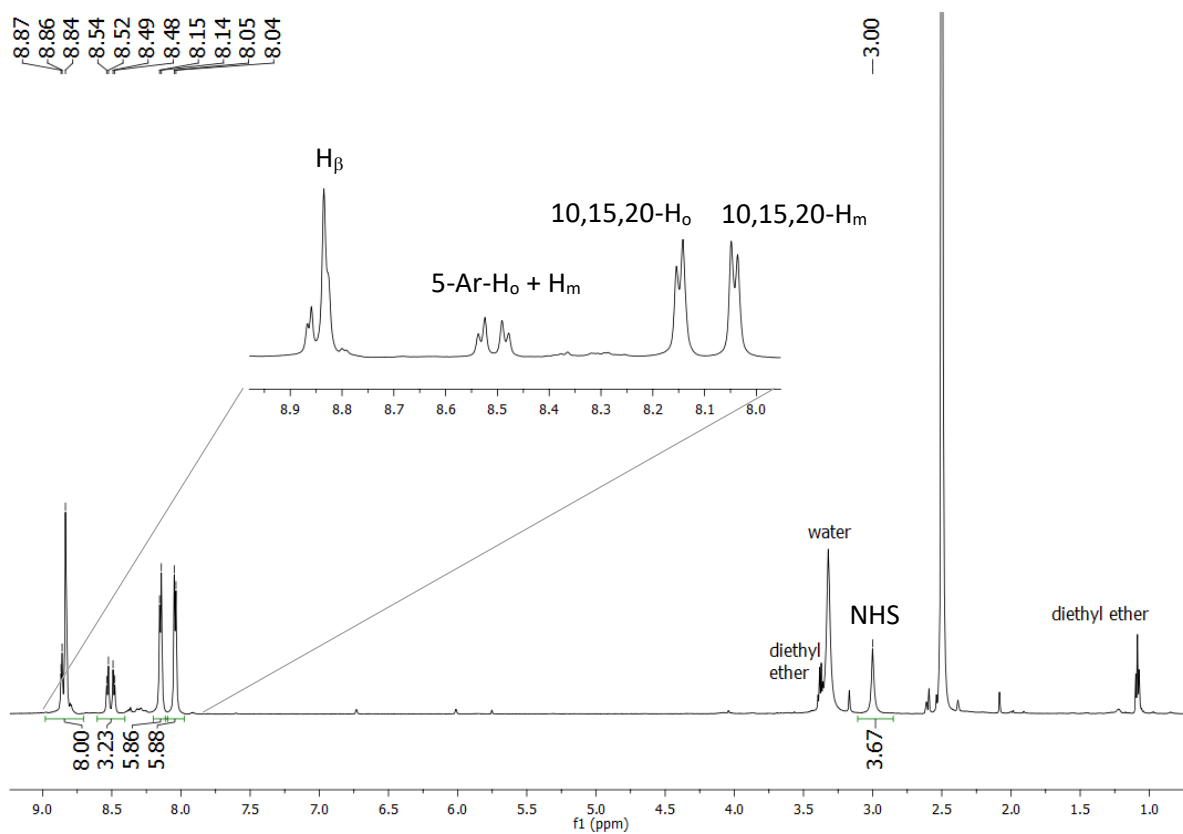
*Figure 94: ¹H-NMR spectrum with expansion of **135** in DMSO-d₆ at 298 K and 600 MHz*

146
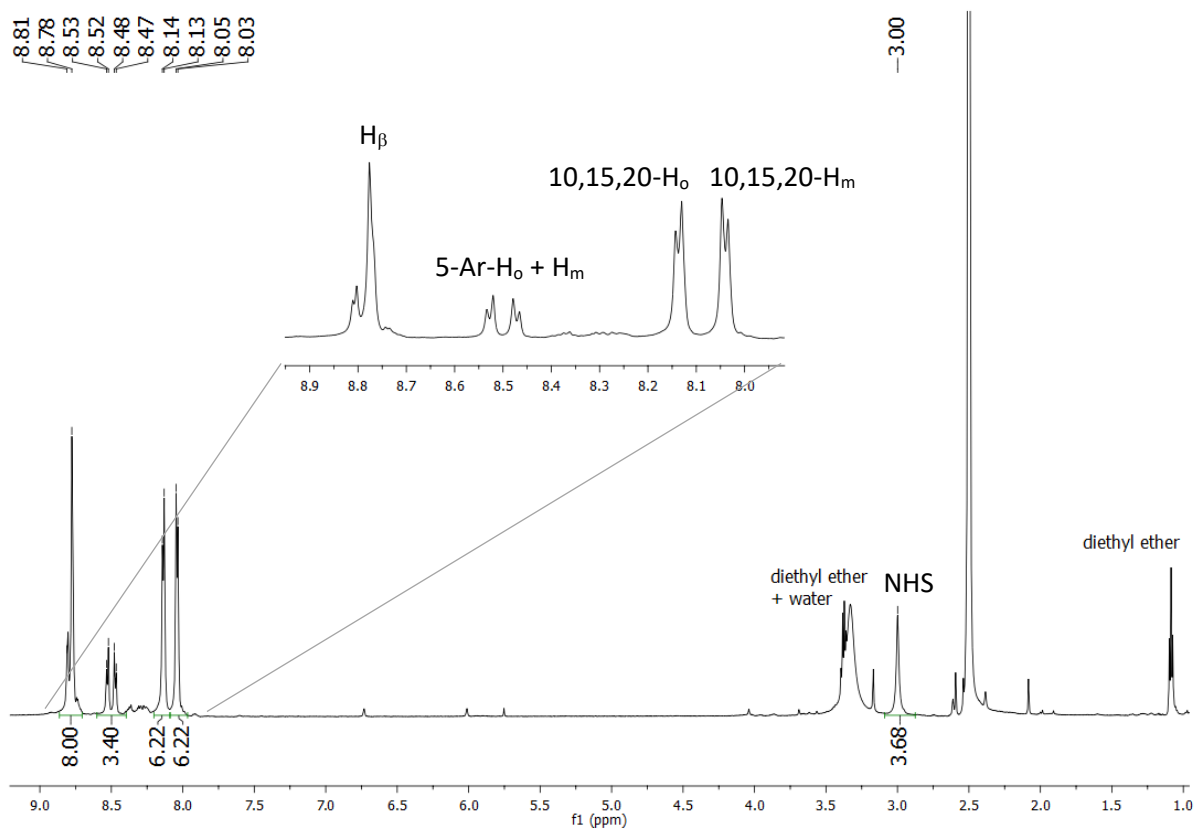
*Figure 95: ^1H-NMR spectrum with expansion of **134** in DMSO-d$_6$ at 298 K and 600 MHz*
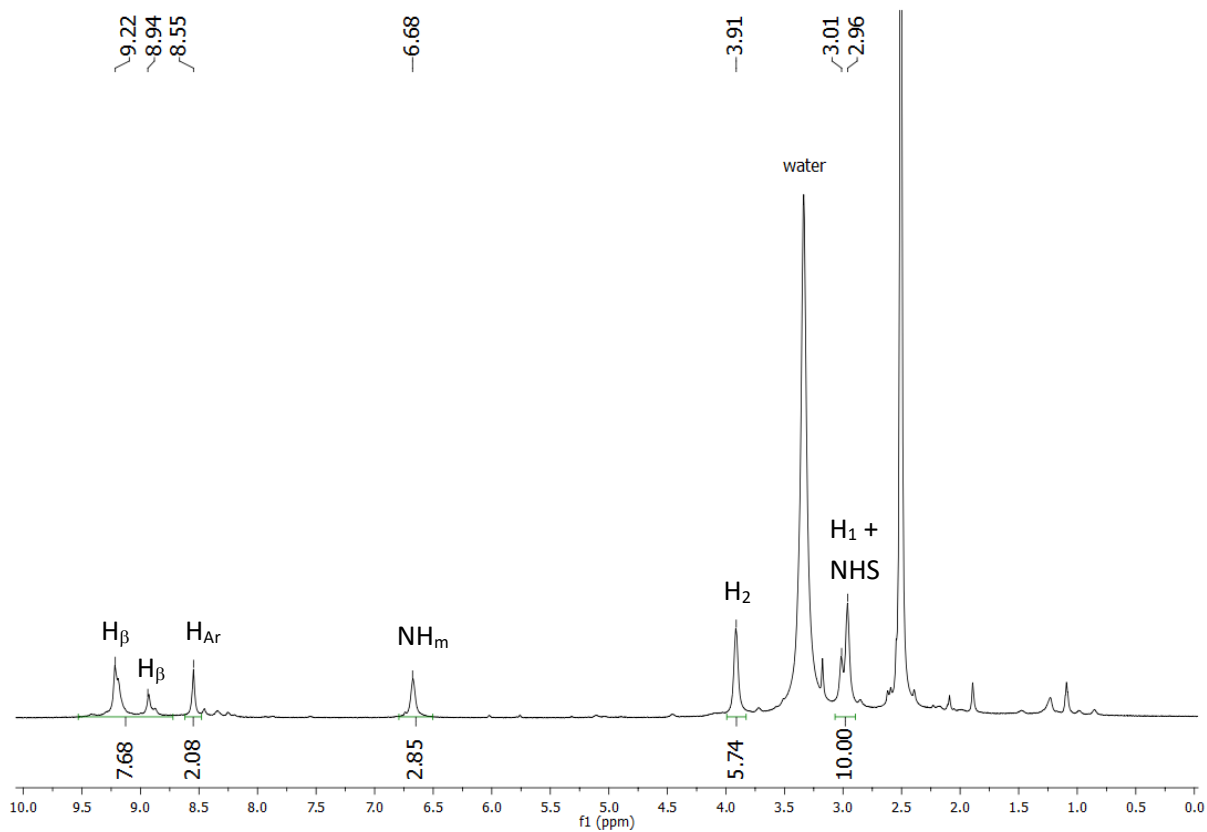
*Figure 96: ^1H-NMR spectrum of **138** in DMSO-d$_6$ at 298 K and 600 MHz*
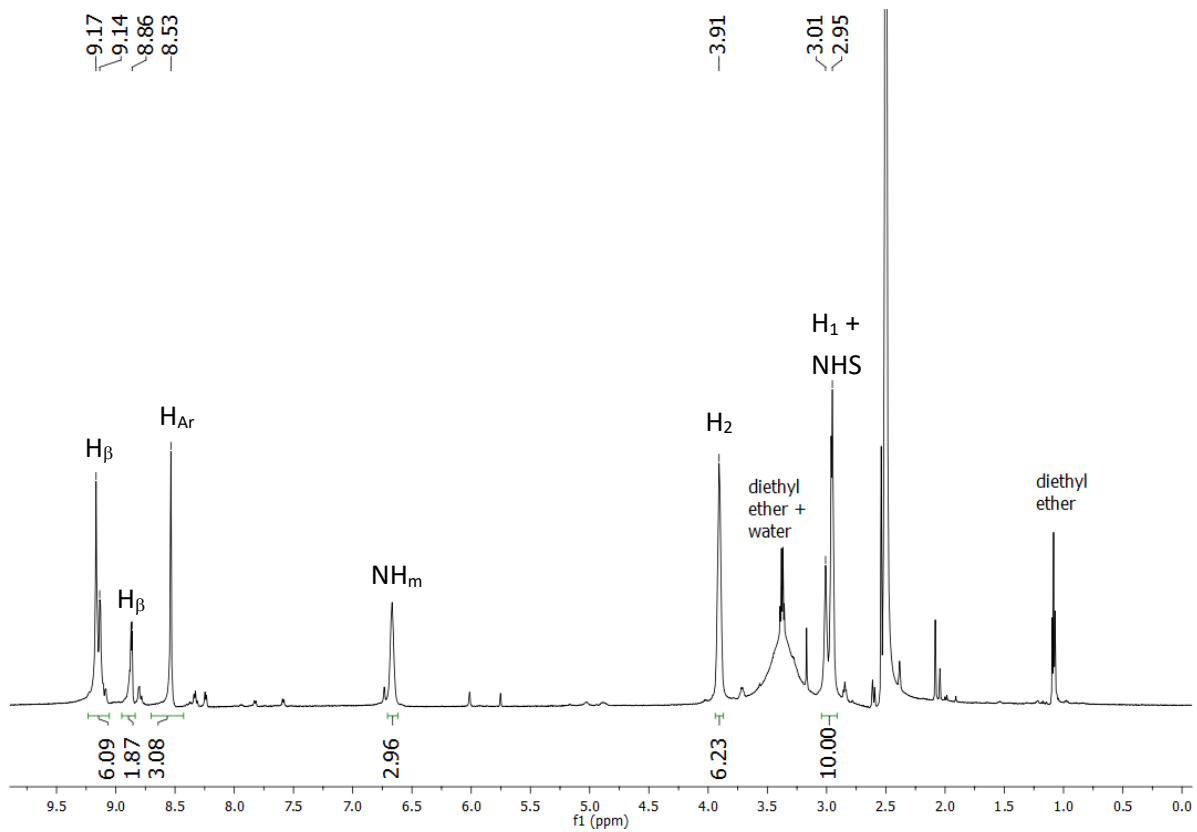
*Figure 97: ^{1}H-NMR spectrum of **137** in DMSO-d$_6$ at 298 K and 600 MHz*

3.5 Synthetic approach for porphyrins A$_3$B conclusions

During this work, the attention was focused on the synthesis, characterisation and metal insertion of two novel water-soluble and conjugatable porphyrins. In addition, two known water-soluble and conjugatable porphyrins were synthesised, characterised and metallated as comparison with the new species. The porphyrins were of the type A$_3$B, with one of the *meso*-substituents bearing a carboxylic function, later exploited as anchoring moiety to build macromolecule-supported oxygen sensors. The novel water-soluble porphyrins are based on the same perfluorinated precursor **99**, differently functionalised on the three equivalent *meso*-positions, to obtain both positively and negatively charged molecules.

In both cases, a nucleophilic substitution on the *para*-fluorines of the aryl rings was performed to render the macrocycle soluble in water. More specifically, the anionic derivative was obtained using taurine, an intrinsically water-soluble moiety. In the case of the cationic derivative, on the other hand, water solubility was introduced by modification of the chain after attachment to the porphyrin. The overall syntheses showed extraordinarily high yields, gram-scale applicability and occurred in relatively mild reaction conditions employing commercially available reagents. Moreover, the synthetic approach and the purification of the two known porphyrins, one positively and one negatively charged as well, were optimised and improved to suite gram-scale applicability.

Metal insertion of palladium (II) and platinum (II) was performed on all the porphyrins synthesised to obtain suitable species for optical oxygen detection. In addition, several different metals were inserted in the macrocycles with good yields, with or without the employment of microwave irradiation, proving the wider applicability of the method. Lastly, the carboxylic acid was activated *via* NHS-mediated chemistry in order to obtain conjugatable water-soluble porphyrins suitable for anchoring on solid supports.

Crucially, during this work new purification methods for cationic and anionic water-soluble porphyrins were developed and optimised. The methods are based on a double ion-exchange on the charged molecule, inducing a precipitation from water solutions first, and from organic solvents later. The purification of cationic derivatives was optimised and improved for gram-scale applicability, while the method suitable for anionic derivatives was designed and developed here, and it constitutes, to the best of our knowledge, the first cheap and scalable purification method applicable to sulphonated porphyrins.

4 Oxygen-sensing protein hydrogels

The final objective of this work was to verify the response of the new platinum (II) and palladium (II) porphyrins to changing oxygen levels in aqueous environment, both as stand-alone sensors and supported on protein-based hydrogels.

To this end, the conjugation of the porphyrins to proteins able to form hydrogels known to support cell growth was undertaken. The two proteins chosen were silk fibroin and type I collagen.

Fibroin is a naturally occurring protein produced by insects such as spiders (*Nephila clavipes*), silkworms (*Bombix mori*) and moths (mostly belonging to the family of *Saturniidae*). Fibroin is one of the two main constituents of raw silk, and its properties makes it suitable for the fabrication of bio-materials.[293–295] Fibroin is normally extracted from *Bombyx mori* cocoons, where it is found in association with sericin, a water-soluble glycoprotein that covers the surface of fibroin fibres.[293] Fibroin structure consists of antiparallel β-sheets layers, with a primary sequence of recurring amino acids: glycine-serine-glycine-alanine-glycine-alanine (Gly-Ser-Gly-Ala-Gly-Ala), as shown in *Figure 98*.
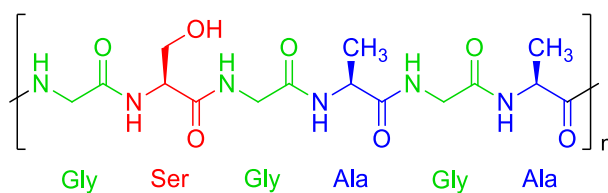
Figure 98: fibroin primary sequence of amino acids

The high content of glycine is responsible for the tight packing of the sheets, ultimately conferring great mechanical strength to the material.[296] Fibroin fibres are harder than Kevlar® fibres,[297] and show higher mechanical strength than other biocompatible materials like collagen and poly-L-lactic acid (PLA).[298] Beyond showing these remarkable mechanical properties, silk fibroin is fully biocompatible after sericin removal,[297] slowly biodegradable,[299] and it offers the possibility to be chemically modified[300] and manufactured to obtain a variety of bio-material.[296]

Silk has been used for centuries as suture thread to close wounds[293] and recently, due to the possibility of fabricating material with different mechanical properties, its applications have been extended to tissue engineering.[296] Silk fibroin-based scaffolds are suitable for cells attachment and proliferation, both for primary human meniscal cells[294] and for human osteoblast MG63 cells.[295] Fibroin can be processed into films or sponges to obtain wound dressing,[301] or scaffolds in which both hepatic[302] and bone cells can grow and proliferate.[303] Hydrogels made of fibroin find applications in bone tissues[304]

and cartilage tissue engineering,[305] while fibroin fibres are excellent material for ligament[306] and tendon tissues.[307] Non-woven mats of fibroin are suitable to mimic connective tissues,[308] endothelial and blood vessels.[309] In addition, micro- and nanospheres of silk fibroin can be employed as drug delivery system.[310,311]

Collagen is the most abundant and most important structural protein in animals. Collagen is the main component of the extracellular matrix in connective tissues and the main constituent of tendons, ligaments and skin. Collagen has been a popular source of bio-materials in the last decades.[312] It is biodegradable, biocompatible, it presents low toxicity, high versatility and weak antigenicity.[313] Different types of collagen exist, which are more or less abundant in different kind of tissues: all collagen types display a characteristic triple-helix structure, although only few types are capable of forming fibres.[313] Collagen molecules are composed of three α-helices coiled together, and each α-helix is formed by more than a thousand amino acids with recurring sequence glycine-proline-hydroxyproline (Gly-Pro-Hyp) as showed in *Figure 99*.
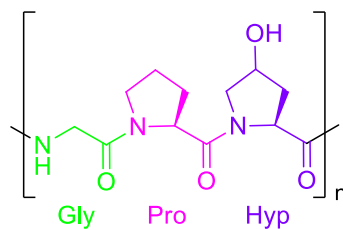
Figure 99: collagen typical amino acids sequence

The presence of glycine every three amino acids is essential for the tight packaging of the α-helices to form collagen fibrils, which in turn form collagen fibres as showed in *Figure 100*.[314]
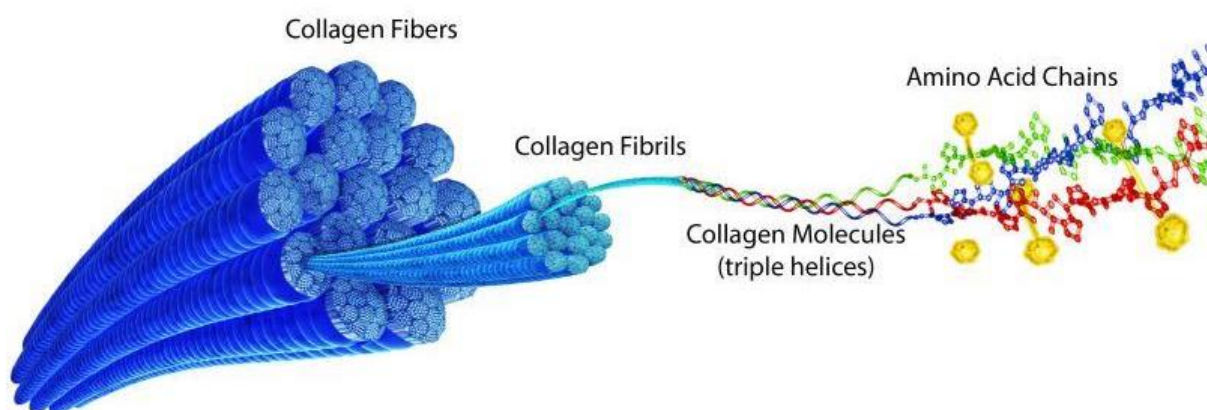
Figure 100: collagen structure [314]

151

Based on the conformation and composition of the α-helices, 29 different types of collagen are known, but only a few can be employed for biomedical applications.[313] Its suitability for biological applications arise from the fact that it provides an environment for cell growth that closely mimics physiological conditions. Collagen has been used in electrophysiological studies[315] and as a matrix for nervous system models.[316] Collagen gives useful information on the behaviour of cells growing in 3D scaffolds,[313] and because of this it has been used to elucidate mechanisms of tissue invasion by cancer cells,[317,318] and to evaluate the efficiency of anticancer agents on 3D cell cultures.[319] Furthermore, collagen-based hydrogels can be employed as anchoring biomaterial to cultivate organs *ex vivo*.[320] Following mineralization with calcium phosphate, collagen can be used as biomaterial for bone tissue engineering.[321] Collagen-based flexible biomaterials were used to promote cartilage regeneration[322] and to replace heart valves and vascular conduits.[323] Wound dressings made of collagen are employed to treat skin burns and ulcers[324] and as drug delivery systems.[325,326] Collagen-based biomaterials also find applications in plastic surgery, where they can be employed as dermal fillers.[327] Type I collagen is the most employed type of collagen for biomedical applications,[328] and it is normally extracted from bovine tendons and skin, rat tails and pig skin.[313]

In this work, a commercially available solution of type I collagen in 0.1 M acetic acid (protein content: 2 mg/mL) was used. Gelation was carried out according to a procedure reported in the literature with minor variations.[329] Briefly, the pH of the solution was adjusted to a value around 7.0 with a 1 M aqueous solution of NaOH. The use of a concentrated solution of NaOH was preferred to avoid increasing the volume of the collagen solution, which would cause the protein content to decrease and subsequently the gelation process to fail. Optimal gelation condition entailed the neutralisation of the collagen solution with 1 M aqueous NaOH (10 % v/v respect to the protein solution) and incubation at 37 °C for 30 minutes.

4.1 Conjugation to support

For the conjugations, a calculated amount of the porphyrins was dissolved in 10 mL of deionized water to reach a concentration of 5×10^{-4} M (*Table 39*). The stock solutions were stored in the fridge to prevent decomposition of the activated ester.

Porphyrin	MW	mg	[M]
132	1101.17	5.5	$5 \cdot 10^{-4}$ M
133	1012.11	5.1	$5 \cdot 10^{-4}$ M
134	1254.02	6.3	$5 \cdot 10^{-4}$ M
135	1164.96	5.8	$5 \cdot 10^{-4}$ M
136	1486.21	7.4	$5 \cdot 10^{-4}$ M
137	1599.03	8.0	$5 \cdot 10^{-4}$ M
138	1509.97	7.5	$5 \cdot 10^{-4}$ M

Table 39: Amounts of porphyrins in stock solutions

<u>Fibroin</u>

Procedures for extracting fibroin from *Bombyx mori* cocoons are well characterised in the literature.[293] Cocoons cut in small pieces must be first treated with a 0.02 M aqueous solution of Na_2CO_3 for 30 minutes to eliminate sericin from the fibres (degumming process). The raw fibres are then rinsed in water, dried and treated with a 9.3 M aqueous solution of LiBr at 40 °C for 4 hours or until completely dissolved. The fibroin solution is dialyzed against water for 48 hours, centrifuged to eliminate any insoluble materials and stored at 4 °C. The fibroin thus obtained is suitable to manufacture hydrogels, nanoparticles and fibres. Hydrogels are obtained triggering low degrees of crystallinity by addition of alcohol or water annealing.[293]

In this work the method for fibroin extraction described above was adopted.[293] In our hands, fibroin did not dissolve completely after stirring overnight at 40 °C, and following centrifugation, the remaining agglomerates of fibres were treated again with a 9.3 M aqueous solution of LiBr for 4 hours at 60 °C. Both batches were dialysed to give optically transparent fibroin solutions.

To estimate the protein content of the solutions, 1 mL of each solution was transferred in a previously weighted flask and dried under reduced pressure. Weighting the residues revealed that the first solution had a fibroin concentration of 62 mg/mL, while the second one 23 mg/mL.

Figure 101: fibroin inversion test

Next, gelation conditions were optimised to obtain an optically transparent gel that would lend itself to be used in fluorescence measurement, but stiff enough to withstand the inversion test (*i.e.*, not flowing, following inversion of the vial). The gels were obtained by alcohol addition. Preliminary experiments showed that the solution containing 62 mg/mL of fibroin was too concentrated to produce a gel with suitable optical properties: the gel, although very stable and firm in the inversion test, was too opalescent due to the high protein content. Gels prepared with the less concentrated fibroin solution (23 mg/mL) displayed favourable transparency, as showed in *Figure 99.* Optimal gelation conditions entailed the use of two parts of protein solution and one part of ethanol by volume. Protein solution and ethanol were slowly mixed and allowed to stand at room temperature for 30 minutes. Gel samples were produced employing 200 μL of protein solution 23 mg/mL and 100 μL of ethanol.

To conjugate complexes to fibroin, 2 mL of the porphyrin stock solutions were added to 10 mL of protein solution and the resulting mixture was allowed to stand for 4 hours at room temperature. The volume of the stock solutions used was calculated to obtain 1×10^{-3} mmol of porphyrin per 230 mg of protein. Preliminary attempts to perform the conjugation on the 62 mg/mL fibroin solution resulted in the gelation of the mixture during conjugation, which prevented the uniform distribution of the porphyrin in the reaction medium. When the less concentrated fibroin solution was employed (23 mg/mL), gelation did not occur until ethanol was added. The reaction mixtures were poured in dialysis tubes and dialyzed overnight against deionised water to remove any unreacted porphyrin and the side-products from the conjugation reaction. The functionalised fibroin solutions were transferred into vials and stored in the fridge to prevent unwanted gelation. It is worth to note that no porphyrin was released in the dialysate (verified by UV-vis spectroscopy), indicating that all the porphyrin added was conjugated to the protein. In light of this, no further test was performed to quantify the amount of dye attached to the protein, as it was assumed the final load to be 4.35×10^{-6} mmol of porphyrin per mg of protein.

In the condition adopted, we assumed that the conjugation undoubtedly involved N-terminus Lys-NH$_2$, but we cannot exclude reactions with thiols present in the protein as well as the alcohol groups present in serine and hydroxyproline residues (Ser-OH and Hyp-OH).

<u>Collagen</u>

Collagen is sold as a 0.1 M acetic acid solution to prevent gelation, a process that occurs in neutral or basic conditions. In order to perform the conjugation, however, sodium acetate was added to the collagen solution to buffer it at pH 4.7, a value compatible with the solubility of the fibres and suitable for the conjugation of the activated ester.[330] Gelation of collagen at pH 4.7 is very slow, allowing the conjugation to be carried out in solution. The porphyrin/protein ratio was adjusted to maintain the same porphyrin-to-protein ratio adopted for the fibroin conjugation. Therefore, 200 μL of the porphyrin stock solutions were added to 10 mL of collagen solution, resulting in 5.0×10^{-6} mmol of porphyrin per mg of protein. Unexpectedly, addition of the porphyrin solution caused the formation of non-evenly distributed agglomerates in the collagen solution. The agglomerates appeared coloured, suggesting that the aggregation was triggered by the addition of the porphyrin. It was noticed that this behaviour was more pronounced with porphyrins **134**, **135**, **137** and **138**, which are negatively charged. We therefore speculated that the aggregation was triggered by the local increase of ionic strength of the medium and the formation of insoluble ionic pairs between the protein and the porphyrins. The problem of the aggregation was circumvented by employing ethanol as a co-solvent, which efficiently prevented the unfavourable interaction of collagen with the porphyrin, while still being compatible with the solubility of the protein. Visual examination of the conjugation solution led to consider that too little porphyrin was present in the sample, which would potentially lead to challenges in the detection of the porphyrin luminescence in the presence of oxygen. The conjugations were then performed with a larger amount of dye. 300 μL of porphyrin stock solution and 500 μL of ethanol were added to 10 mL of collagen solution; the solution was shaken on a vortex to allow uniform distribution of the dye and slow stirring was continued for 4 hours at room temperature to allow complete conjugation. After this time, the solutions were poured in dialysis tubes and dialyzed against a 0.1 M solution of acetic acid overnight. No porphyrin was detected in the dialysate or coloured dialysis tube were observed, suggesting once again that the dye employed was completely conjugated to the support. The functionalised collagen solutions were poured in a vial and stored in the fridge to prevent unwanted gelation. The final porphyrin load was 7.5×10^{-6} mmol of dye per mg of protein.

It is worth noting that for both protein conjugates no differences in the gelation behaviour was observed compared to the protein alone. Therefore, it was reasonable to assume that proteins and conjugates will afford gels with similar properties with respect to oxygen diffusion.

4.2 Oxygen response

The oxygen sensing behaviour of the porphyrins **136**, **137** and **138** was characterised in aqueous solution and supported on protein hydrogels. The responsiveness to oxygen of protein hydrogels containing porphyrins **132**, **133**, **134** and **135** was also studied.

The experiments consisted in varying the oxygen tension in the medium (aqueous solution or hydrogel) and recording the intensity of luminescence of the porphyrins using the wavelength of the Soret band for excitation. The oxygen tension was varied by saturating the medium with oxygen (to attain 100 % oxygen tension) or argon (to attain 0 % oxygen tension) and allowing the system to equilibrate with air (giving an oxygen tension of *ca.* 21 %). The oxygen tension was measured with an optical oxygen probe (Ocean Optics NeoFox NFB0181) immersed in the medium, previously calibrated at 0 % and 100 % oxygen tension points by flushing pure argon and oxygen, respectively. All measurements were carried out at 298 K and in deionised water.

4.2.1   Stand-alone porphyrins

In order to compare the response of the different metalloporphyrins, stock solutions of the different dyes and of the conjugates were prepared. A known volume of the porphyrin stock solutions was diluted in deionised water to obtain a final concentration of 5×10^{-3} mg/mL (*Table 40*). To facilitate the comparison of the behaviour of the porphyrins, the concentrations were adjusted to bring the intensity of the Soret band to a value of 0.1 A.

Porphyrin	μL	Final Volume	Concentration
136	6.7	10 mL	$5 \cdot 10^{-3}$ mg/mL
137	6.3	10 mL	$5 \cdot 10^{-3}$ mg/mL
138	6.6	10 mL	$5 \cdot 10^{-3}$ mg/mL

Table 40: stock solution volumes and concentrations of novel porphyrins

In each experiment, 10 mL of the prepared solutions was placed into a 20-mL vial equipped with a magnetic stirrer. The oxygen probe was immersed in the solution and held in place with a clamp while the solution was stirred. A needle connected to an argon balloon was then placed in the solution, allowing the gas to diffuse and saturate the environment replacing the air dissolved. Once the probe registered 0 % oxygen tension, a 1 mL sample was transferred in a fluorescence cuvette by means of a micropipette and the fluorescence intensity was measured. The content of the cuvette was returned to the vial, stirring was continued for few seconds and a new fluorescence measurement was carried out in correspondence of a different level of oxygen tension. The readings of fluorescence were

156

repeated until a value of oxygen tension of *ca.* 21 % was reached, indicating that equilibrium with air had been attained. The procedure was repeated using an oxygen-filled balloon to carry out measurements at oxygen levels above atmospheric. In order to minimise variations of oxygen tension in solution between the sampling and the fluorescence analysis, the experiment was carried out in proximity of the fluorimeter. It is worth noting that while it was possible to reach values of oxygen tension close to 0 %, the maximum oxygen percentage achieved was *ca.* 80 %. Despite the incomplete range of oxygen percentage, the biological range of interest was fully covered. The fluorescence data were combined in a chart showing the decrease of fluorescence intensity for increasing oxygen tension.

The experiment detailed above was performed on solutions of porphyrins **136**, **137** and **138**. For the remaining known porphyrins the oxygen response was measured only on support, due to time restrictions and due to the data are already present in the literature.[146,147]

Chart 1 shows the variation of fluorescence emission of complex **137** for increasing concentrations of oxygen. As expected, the intensity of emission decreases for increasing oxygen tension. Larger changes in emission intensity were observed for oxygen fluctuations below atmospheric level.
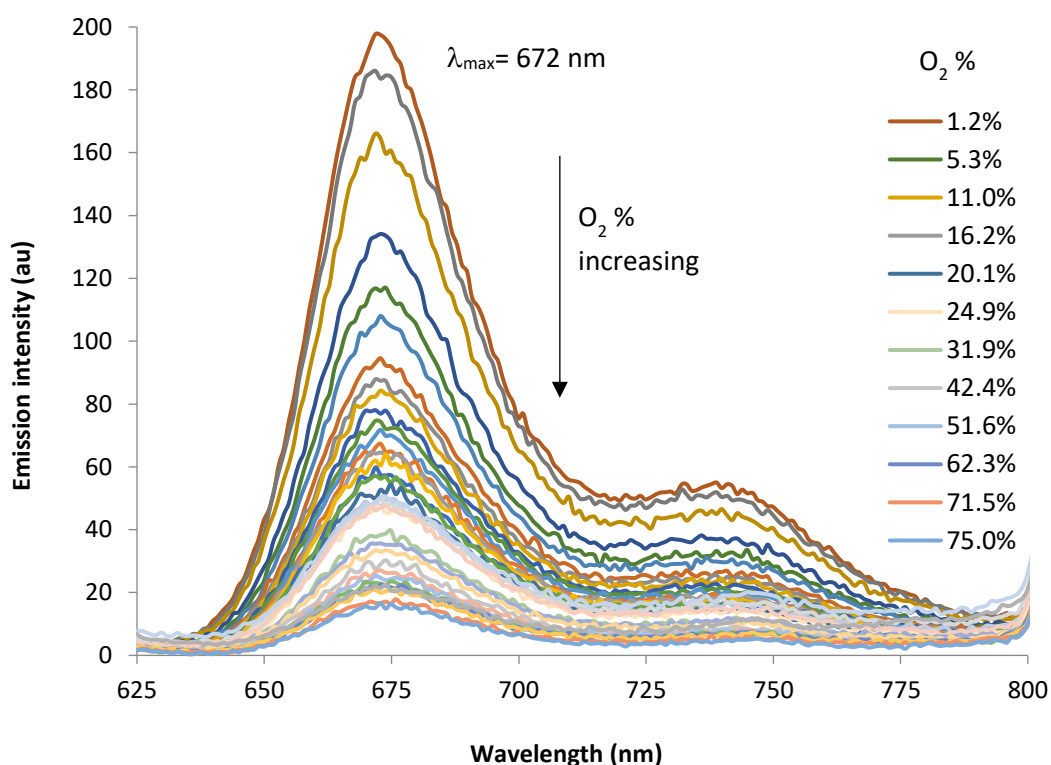
*Chart 1: emission intensity vs wavelength for complex **137** in solution (deionised water at 298 K)*

157

Chart 2 shows the normalised intensity in correspondence of the emission maximum (λ_{max} = 672 nm) versus the dissolved oxygen percentage (0 % to 80 %). The trend line highlights that the behaviour fits the expected exponential decay typical of these systems.[146]
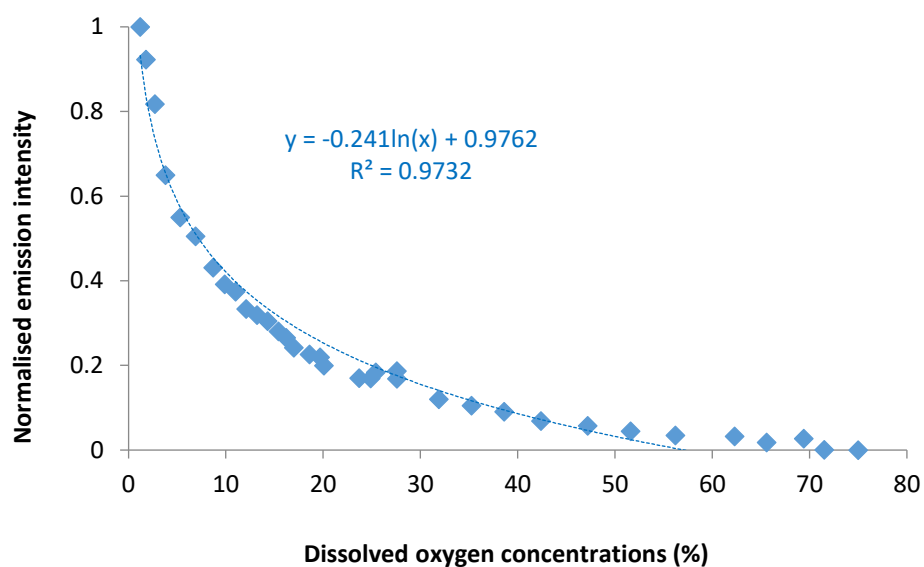
*Chart 2: normalized emission intensity at 672 nm vs dissolved oxygen concentrations for complex **137** in solution (deionised water at 298 K)*

The data points can be elaborated to obtain the corresponding Stern-Volmer plot (see *Equation 1*). *Chart 3* shows an excellent linear correlation of the reciprocal of fluorescence intensity (1/I) with oxygen concentration, particularly considering the wide interval of oxygen tensions examined (R^2 = 0.985).
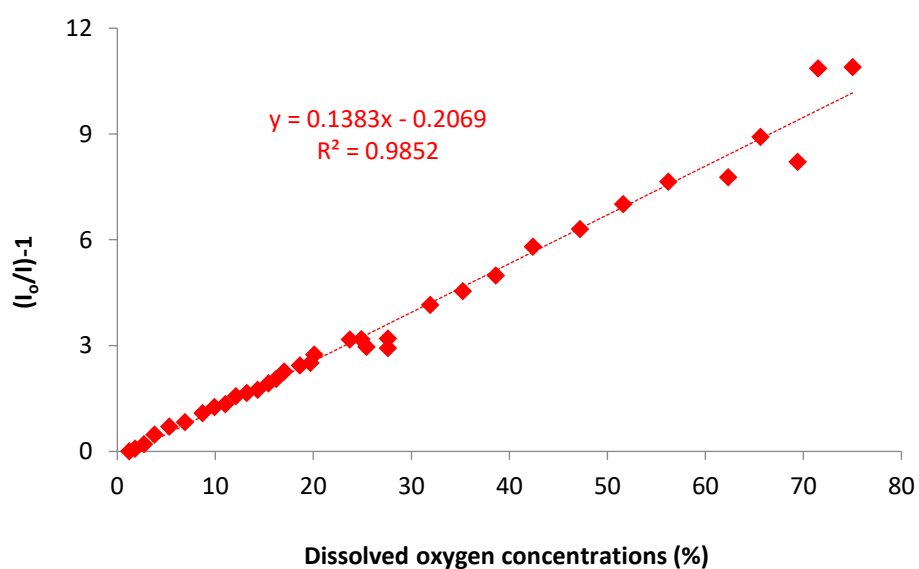
*Chart 3: Stern-Volmer transformation for complex **137** in solution (deionised water at 298 K)*

Linearity of response is higher at concentrations of oxygen below atmospheric value (0 % to 20 %), which is advantageous for biological applications, and the relative Stern-Volmer plot shows a correlation factor of 0.995 (*Chart 4*).

$$y = 0.1374x - 0.127$$
$$R^2 = 0.9954$$
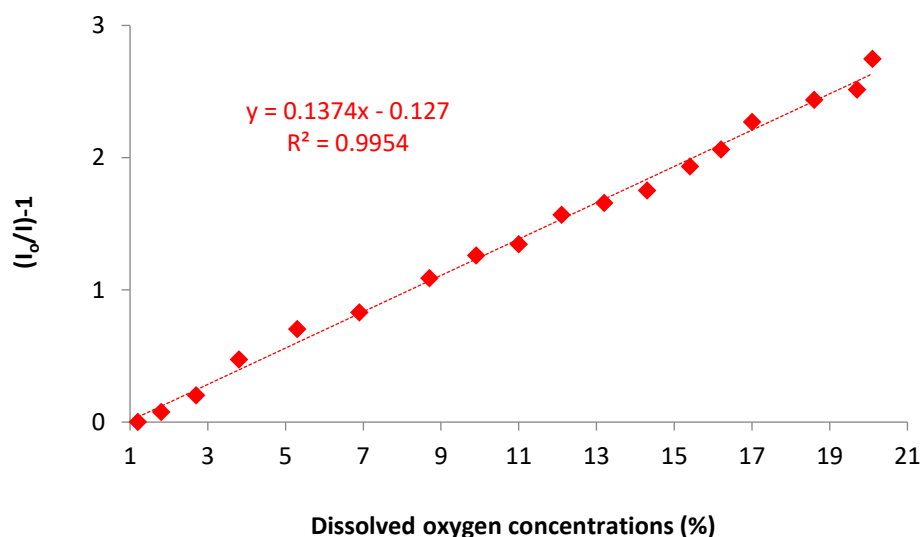
Chart 4: Stern-Volmer transformation for complex 137 in solution from 0 % to atmospheric O_2 % (deionised water at 298 K)

The slope of the plots above gives the value of the Stern-Volmer constant (K_{SV}) expressed in $\%^{-1}\,s^{-1}$, which can be converted to oxygen partial pressure (pO_2) expressed in mmHg as shown in *Equation 2*.

$$pO_2 = (x/100) \cdot 742.23 \text{ mmHg }^{[147]}$$

Equation 2: conversion of O_2 % in partial pressure

In turn, the partial pressure can be converted in molarity as shown in *Equation 3*.

$$[O_2] \text{ (M)} = (pO_2 \text{ mmHg}) / (760 \text{ mmHg atm}^{-1}) \cdot (757 \text{ atm M}^{-1})^{[146,147]}$$

Equation 3: conversion of pO2 in molarity

Table 41 shows the parameters of the Stern-Volmer plot (K_{SV}) for **137** in aqueous solutions in 0-75 % and 0-20 % oxygen concentration.

$[O_2]$ (%)	$[O_2]$ (M)	K_{sw} $(M^{-1}\,s^{-1})$	$(\pm\sigma)$	R^2	I_0/I_{min}
0 - 20.1	$0 - 2.6 \cdot 10^{-4}$	$1.06 \cdot 10^4$	$0.02 \cdot 10^4$	0.995	3.75
0 - 75.0	$0 - 1.0 \cdot 10^{-3}$	$1.07 \cdot 10^4$	$0.02 \cdot 10^4$	0.985	11.90

Table 41: K_{sw}, R^2, I_0/I_{min} for complex 137 in solution at 672 nm

Palladium complex **138** displayed very low fluorescence intensity emission compared to the platinum complex of the same porphyrin, which makes the readings of the emission intensity at λ_{max} unsuitable to obtain a Stern-Volmer plot (*Chart 5*).

Similarly, compound **136** displays negligible fluorescence emission in aqueous solutions. Steady-state measurements do not allow elucidation of this behaviour, which could be due either to a poor quantum yield of the excited state or to its very efficient quenching by molecular oxygen. To gain insight in the properties of the molecule excited state, time-resolved studies should be carried out.
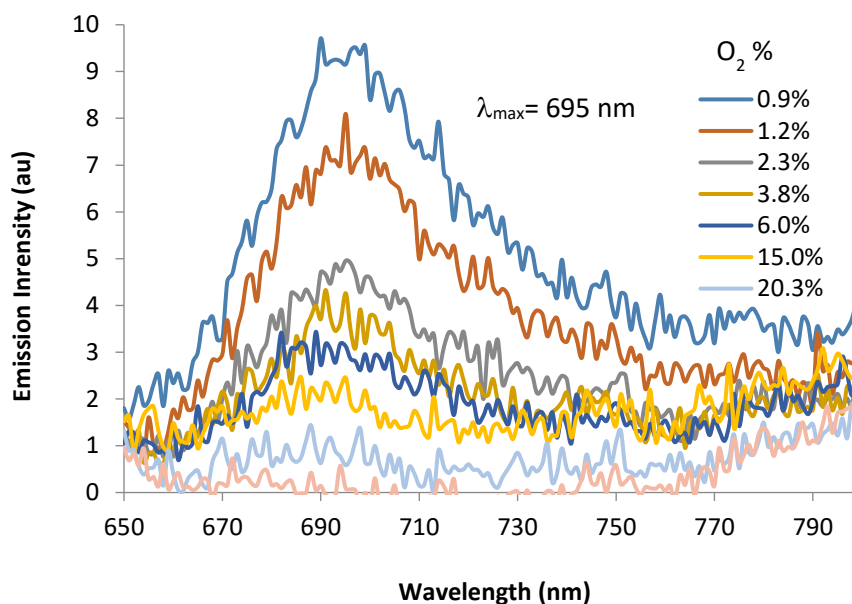
*Chart 5: emission intensity vs wavelength for complex **138** in solution (deionised water at 298 K)*

Chart 6 shows a comparison of the fluorescence emission obtained by equimolar solutions of **137** and **138** ($5 \cdot 10^{-3}$ mg/mL) at 1.2 % of oxygen. **137** shows a fluorescence emission 25 times more intense that the corresponding palladium derivative.
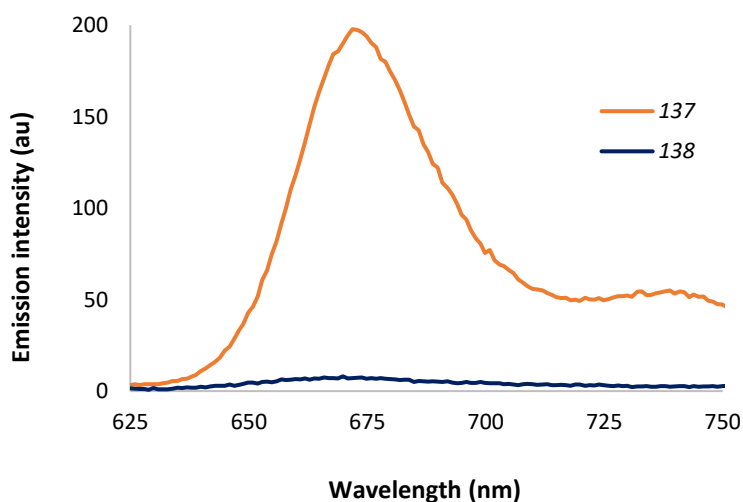
*Chart 6: comparison of emission intensity vs wavelength between complexes **137** and **138** in solution at 1.2 % O_2 (deionised water at 298 K)*

4.2.2 Porphyrins in protein hydrogels

Measuring the oxygen responsiveness of the porphyrin in semisolid hydrogels presented few logistic challenges. Firstly, since the gels could not be transferred in a cuvette to carry out the readings, an experimental setting needed to be designed that would allow fluorescence analysis to be carried out in the same container where the gelation takes place. To overcome this issue 96-well plates were employed: the protein solution was transferred in the wells where the gelation was triggered, and the plate was then used to carry out fluorescence measurement in a plate reader. We decided to employ 96-well plates, because the small volume of the wells (300 μL) allowed to prepare a relatively high number of samples and replicates, while limiting the amount of solution employed. Filling the wells to the top with *ca.* 300 μL of solution allowed enough sample volume for the oxygen probe tip to be inserted in the gel, in order to detect the amount of oxygen dissolved.

To promote the gelation of collagen, it was necessary to incubate the plates with the collagen solutions at pH 4.7 at 37 °C for 30 minutes. Fortunately, fibroin gelation was not affected by this additional step and the same plate could be used for both conjugates. *Table 42* shows the volumes employed for both fibroin and collagen in the preparation of the gels.

Protein	μL solution	μL EtOH	μL 1M NaOH	Tot. volume
Fibroin	200	100	-	300 μL
Collagen	250	-	25	275 μL

Table 42: volumes employed to prepare the gels

Next, the attention was focused on designing the experimental conditions to obtain efficient gas diffusion and attain the minimum and maximum values of oxygen tension. Once the gel was formed, the plate was placed in a desiccator, which was connected to the vacuum for a few seconds and then filled with argon. Three cycles of vacuum-argon were performed before leaving the desiccator sealed overnight. The same process was applied for oxygen equilibration.

To measure the percentage of oxygen, the probe was inserted in the gel before the fluorescence reading. Unfortunately, once the gel was broken by the probe, it could neither be employed for the reading of the fluorescence intensity nor for further oxygen measurement with the probe. Because of this, several blank gels of fibroin and collagen were prepared to serve as reference wells for the probe. With this setting, the porphyrin-containing gels were employed for the fluorescence readings.
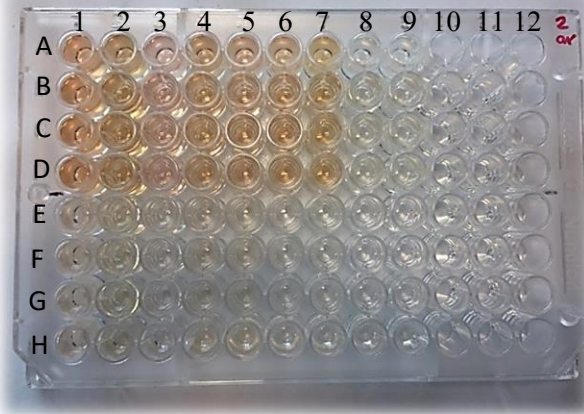
Figure 102: 96 well-plates example for oxygen response on support

In a typical plate, the wells in the top half of the plate (rows A-D) were filled with functionalised fibroin, while the bottom half (rows E-H) with functionalised collagen (Figure 102). Columns 1-7 contained functionalised material (as evidenced by the colour), while columns 8-12 were used as reference wells, as detailed above. Successful gel formation was verified by the inversion test, and the plates that presented leaks or incompletely set gels were discarded. The plate was then placed in a desiccator and exposed to either argon or oxygen as detailed above, and left standing overnight. Oxygen tension was then measured, and the fluorescence readings were performed. The plate was then left to equilibrate with air and further fluorescence readings were taken, until atmospheric oxygen percentage was attained. It is interesting to note that the gas diffusion in hydrogels was considerably slower than in aqueous solution. Significant differences in oxygen levels in the gels were attained in minutes, rather than in seconds, as was the case for the porphyrin solutions. This behaviour was ascribed to two factors: the inherently slower diffusion of small molecules in hydrogels compared to liquids,[331] and the fact that the gel was in contact with the atmosphere only through its upper surface, which, unlike in the case of the solutions, was not renewed by stirring. The latter instance is likely to determine the formation of a gradient of oxygen concentration which slows down the equilibration process. Equilibration of the sample with air was attained between 6 and 8 hours.

<u>Oxygen response in fibroin hydrogels</u>

The fluorescence measurements of protein-supported dyes were carried out with excitation wavelength set at 400 nm and recording the emission between 600 nm and 800 nm. As for the experiments in solution, the data were combined into charts showing the change of fluorescence intensity at different oxygen tensions. As discussed above, the reduced diffusion of oxygen in the gel allowed to measure the fluorescence for oxygen tensions between 9 % and 40 %. Despite the narrower range achieved, the new sensing material were oxygen permeable and responsive over a biologically relevant range of oxygen tension, hence they are suitable for biological applications.

Chart 7 shows the emission intensity of **137** supported on fibroin, showing a decrease of fluorescence intensity for increasing oxygen tension.
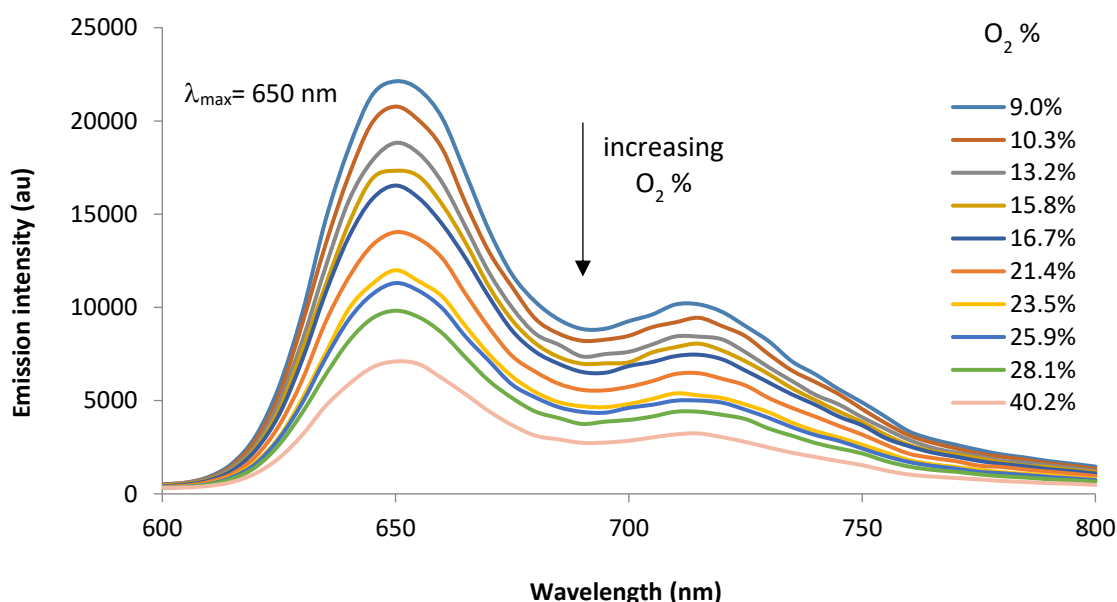
*Chart 7: emission intensity vs wavelength for complex **137** supported on fibroin at 298 K*

Interestingly, the maximum of emission appeared at 650 nm, showing a marked blue shift compared to the porphyrin in solution (λ_{max} = 672 nm). The shift in fluorescence emission are known to be determined by interaction of the fluorophore with macromolecular supports, resulting in the formation of aggregates.[332] Lawless *et al.* detected a marked red shift of the fluorescence emission of different coumarin dyes in doped sol-gel silica, and attributed the effect to the microenvironment entrapping the fluorophores. Similar phenomena can account for the blue shift (22 nm) detected for **137** attached to fibroin.

Chart 8 and *Chart 9* show the emission spectra recorded at different oxygen tensions for platinum porphyrins **134** and **132** in fibroin hydrogel, respectively. For these species the emissions maxima (λ_{max}

= 670 nm) are closer to the values observed in the literature (667 nm for **132**, and 663 nm for **134**).[146] This evidence suggests a less pronounced interaction of the matrix with **132** and **134** compared to **137**.
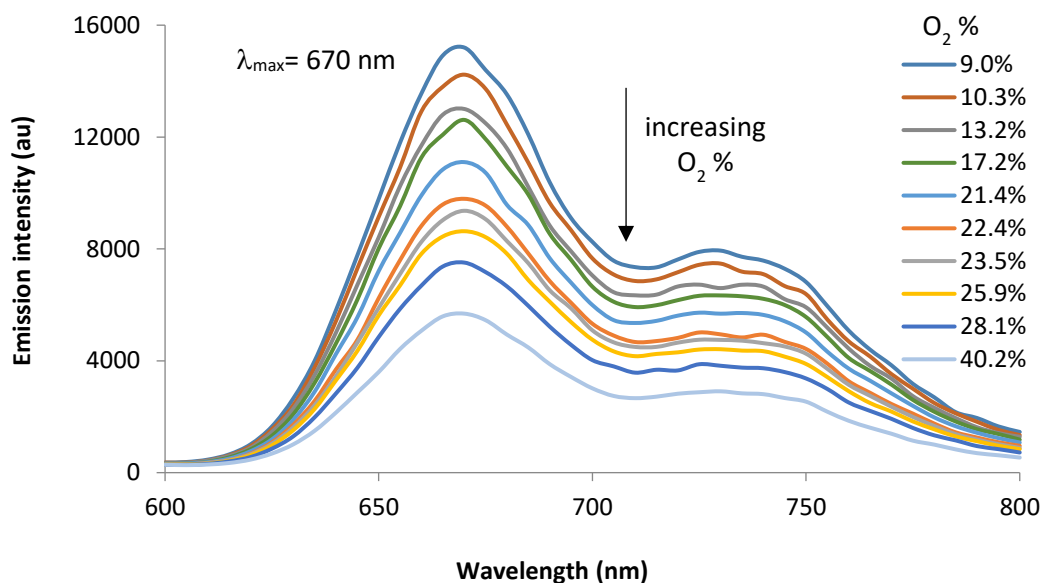
*Chart 8: emission intensity vs wavelength for complex **134** supported on fibroin at 298 K*
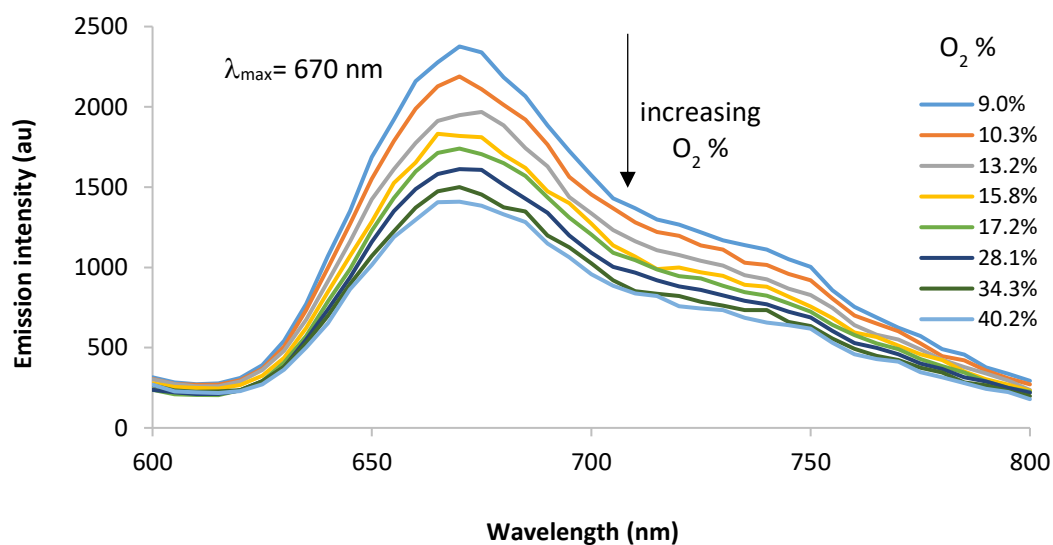
*Chart 9: emission intensity vs wavelength for complex **132** supported on fibroin at 298 K*

Chart 10, *Chart 11*, *Chart 12* and *Chart 13* show the emission spectra at varying concentrations of oxygen for fibroin hydrogels containing complexes **136**, **135**, **138** and **133**, respectively. Complexes **136**, **135** and **138** show the expected decrease in fluorescence emission for increasing oxygen tension, while the weak fluorescence of **133** (*Chart 13*) did not allow to differentiate reliably the intensity of the different emission curves. Interestingly, the fluorescence emission of complex **136** in fibroin

hydrogel showed oxygen-dependence (*Chart 10*), a behaviour not observed for the same complex in solution, where hardly any fluorescence was detected. In the light of this evidence, it can be inferred that the fluorescence quenching of **136** by molecular oxygen is highly efficient in water where oxygen diffuses rapidly. On the contrary, the reduced oxygen diffusivity in fibroin hydrogel limits the quenching efficiency allowing luminescence detection.
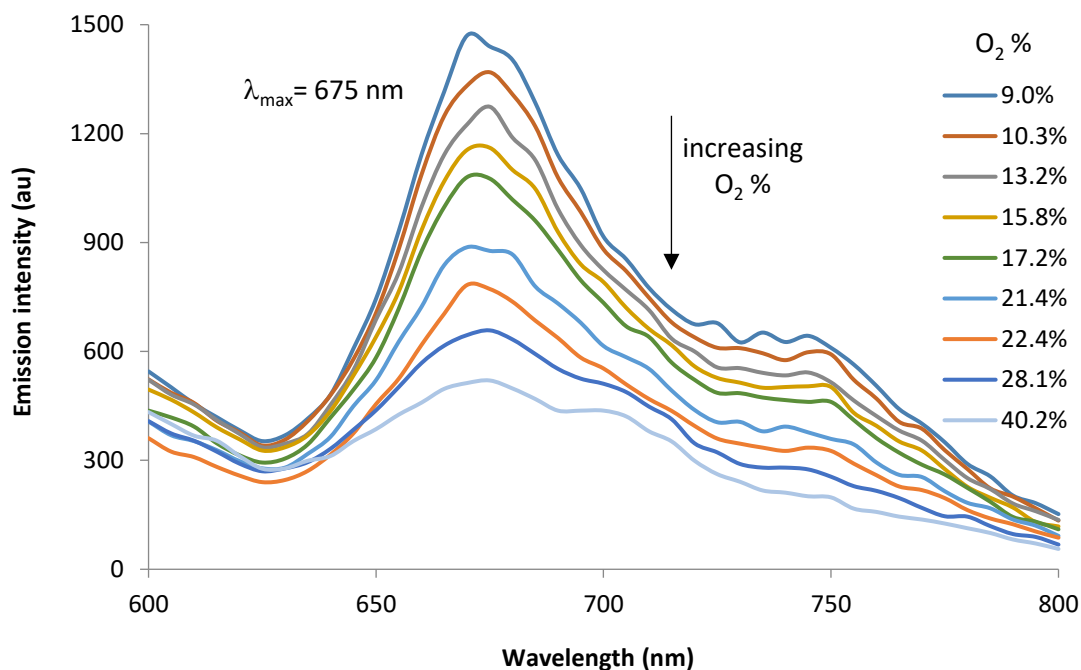
*Chart 10: emission intensity vs wavelength for complex **136** supported on fibroin at 298 K*
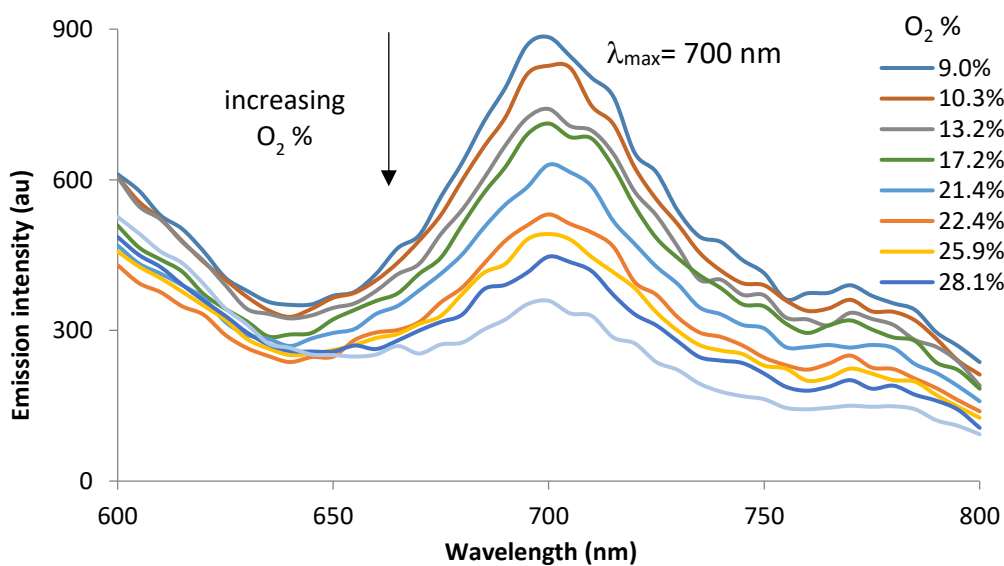
*Chart 11: emission intensity vs wavelength for complex **135** supported on fibroin at 298 K*
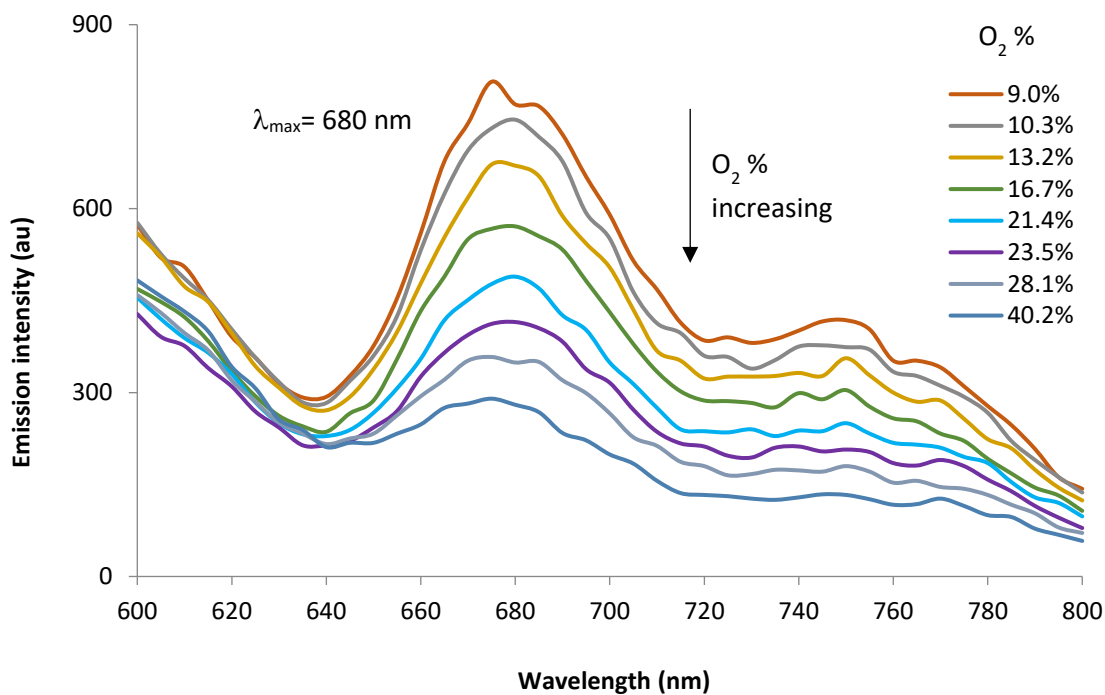
*Chart 12: emission intensity vs wavelength for complex **138** supported on fibroin at 298 K*
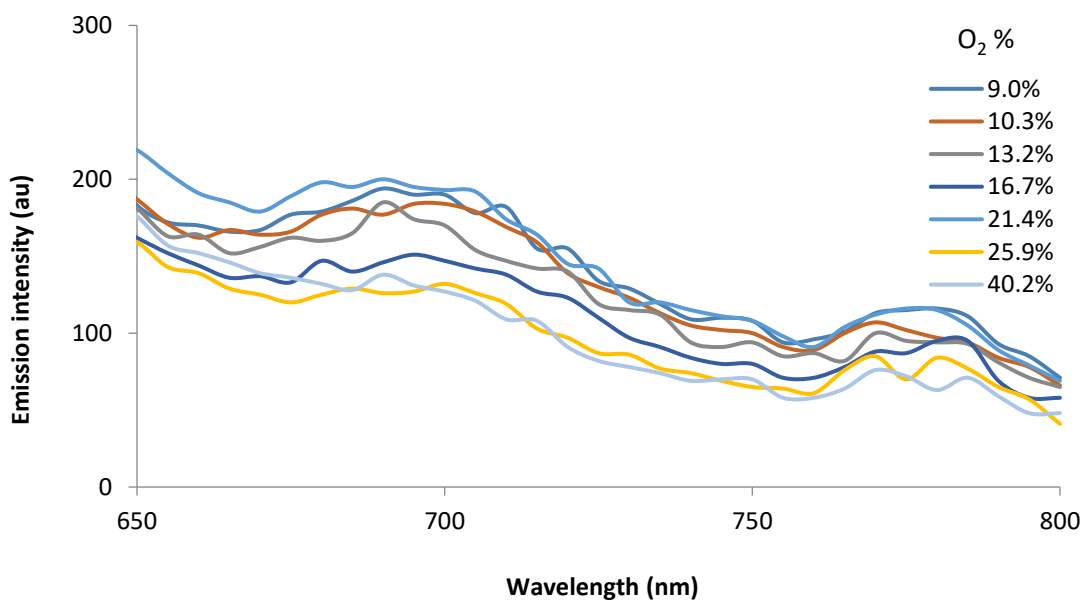
*Chart 13: emission intensity vs wavelength for complex **133** supported on fibroin at 298 K*

Chart 14 shows the fluorescence emission curves for the three platinum complexes supported in fibroin hydrogel at 9.0 % of oxygen. Complexes **137** (orange curve) and **134** (blue curve) displayed a very strong fluorescence intensity at low concentrations of oxygen, while complex **132** (green curve) showed a 10 times lower emission in comparison.
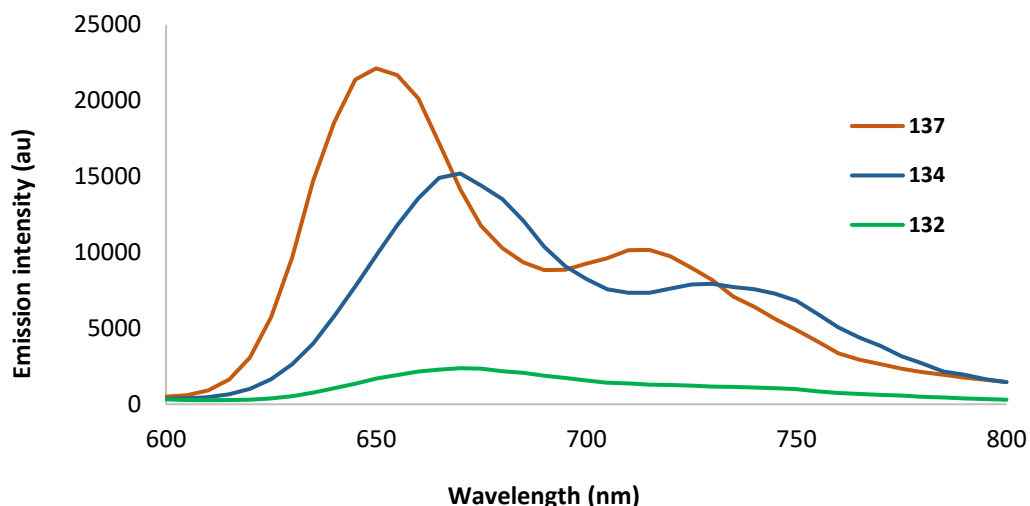
Chart 14: emission intensity curves of the platinum complexes supported on fibroin at 9.0% O_2 at 298 K

The emission of the four palladium complexes recorded in the same conditions is shown in *Chart 15*. Complex **136** (purple line) showed the most intense fluorescence emission, followed by complex **135** (red line) and **136** (green line), while complex **133** (black line) displayed a very poor fluorescence emission. A comparison among the fluorescence emission by the different dyes was possible because the samples contained the same concentration of porphyrin, and the readings were performed at the same oxygen concentration.
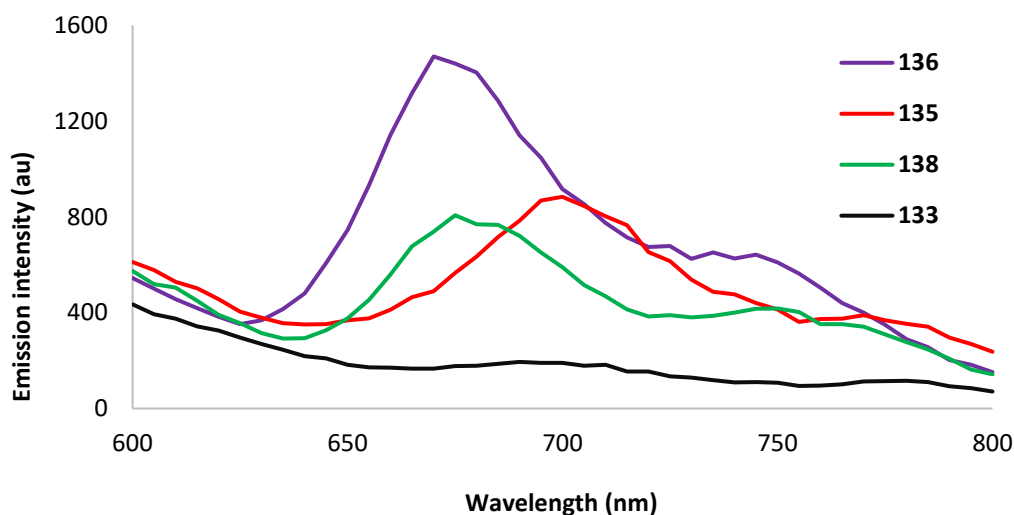
Chart 15: emission intensity curves of the palladium complexes supported on fibroin at 9.0% O_2 at 298 K

These data highlight that platinum complexes fluoresce more intensely than the corresponding palladium derivatives and that, within series of porphyrins with the same metal, the anionic derivatives show higher fluorescence emission than the cationic ones, with the exception of palladium cationic complex **136**. This behaviour is in line with previous findings for platinum and palladium porphyrins.[146,147]

<u>Oxygen response in collagen hydrogels</u>

As in the case of fibroin, the measurements in collagen hydrogel were carried out in a plate reader, with excitation wavelength set at 400 nm and emission recorded between 600 nm and 800 nm. The data were then combined in charts showing the fluorescence emission intensity at different oxygen tension values.

Chart 16 shows the emission curves for collagen hydrogel containing complex **134** at different oxygen concentrations.
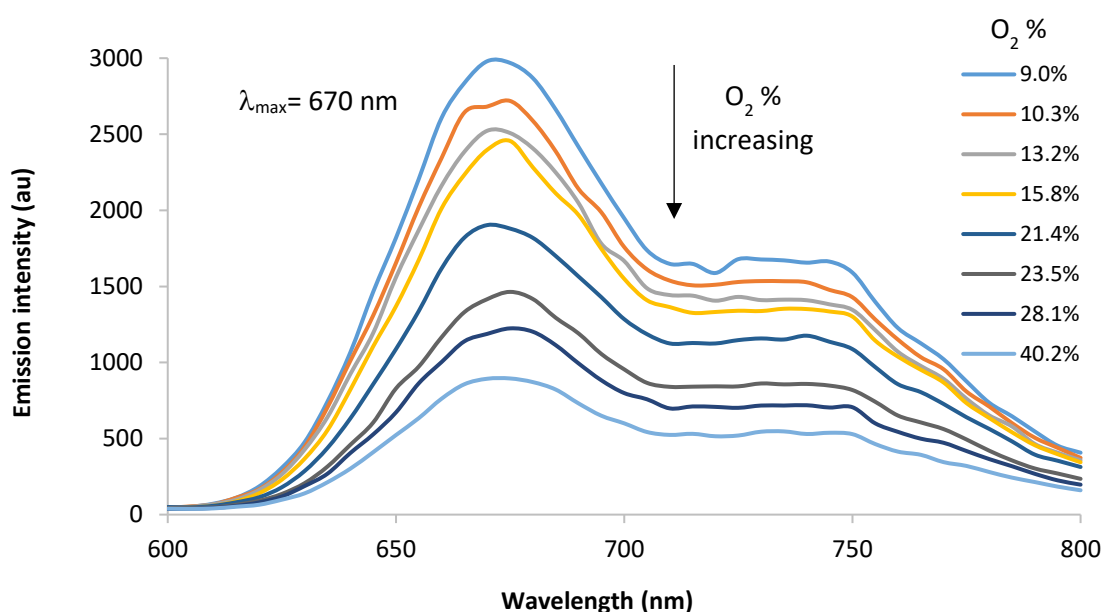
*Chart 16: emission intensity vs wavelength for complex **134** supported on collagen at 298 K*

The fluorescence is oxygen-dependent and its intensity decreases for increasing oxygen concentrations. The anionic complex **134** showed good oxygen response despite the intrinsically lower fluorescence emission compared to the one observed in fibroin hydrogel (Chart 8).

Chart 17*,* Chart 18 and *Chart 19* show the emission curves for the palladium complexes **136**, **135** and **138** in collagen hydrogel, respectively. Species **136** and **135** show a decrease in fluorescence emission with increasing oxygen concentration. Complex **138** displays a similar behaviour but the intensity of emission is very low, intrinsically limiting the applicability of this complex. The emission of collagen hydrogels containing complex **132** and **137** varied erratically with the oxygen concentration showing no evidence of oxygen dependence. As observed in the case of fibroin hydrogel, collagen hydrogel containing complex **133** showed extremely poor fluorescence emission, and the difference between the curves obtained at different oxygen concentrations were hardly detectable. Complexes **132** and **133** showed low fluorescence emission already at low oxygen concentrations, which hampers the

reliability of the sensor response and causes fluorescence emission curves to overlap. As observed for the complexes in fibroin hydrogel, palladium complexes are intrinsically less fluorescent than platinum ones.
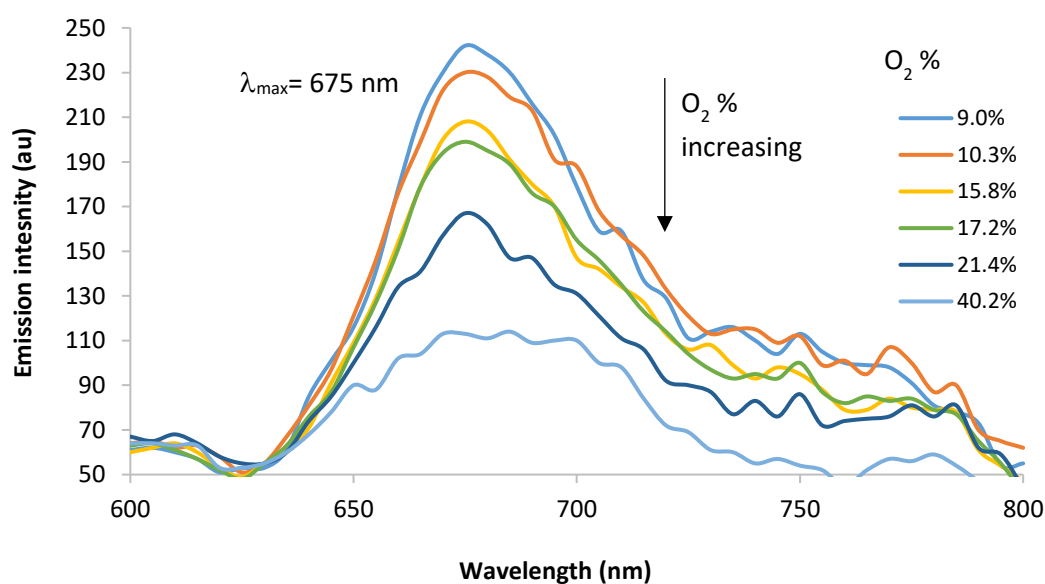
*Chart 17: emission intensity vs wavelength for complex **136** supported on collagen at 298 K*

Overall, these data showed that the oxygen responsiveness of porphyrins in collagen hydrogel is less favourable compared to the one observed in fibroin. The fluorescence emission in collagen was generally weaker, which may arise from non-specific quenching of the excited states following from interaction of the porphyrin with the hydrogel matrix. In addition, it is worth pointing out that collagen hydrogels contained lower amounts of protein (in mg/mL) compared to the fibroin ones: this inherently makes the porphyrin concentration in fibroin hydrogel roughly 10 times higher than in collagen.

Lastly, bearing in mind that the first attempts of porphyrins conjugation to collagen fibres resulted in the macroscopic formation of aggregates, even though the problem was apparently circumvented by the use of ethanol as co-solvent, formation of smaller aggregates invisible to the naked eye cannot be excluded. The presence of such species could have contributed to the uneven distribution of the fluorophore in the hydrogel, which could have caused the less favourable fluorescent behaviour and worse oxygen response compared to fibroin.
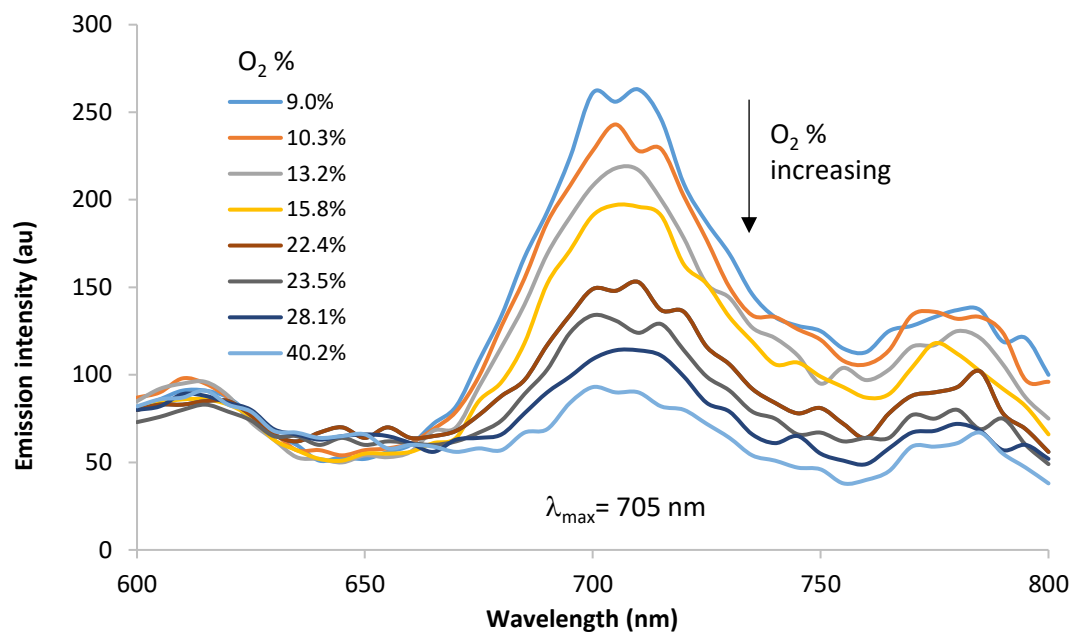
*Chart 18: emission intensity vs wavelength for complex **135** supported on collagen at 298 K*
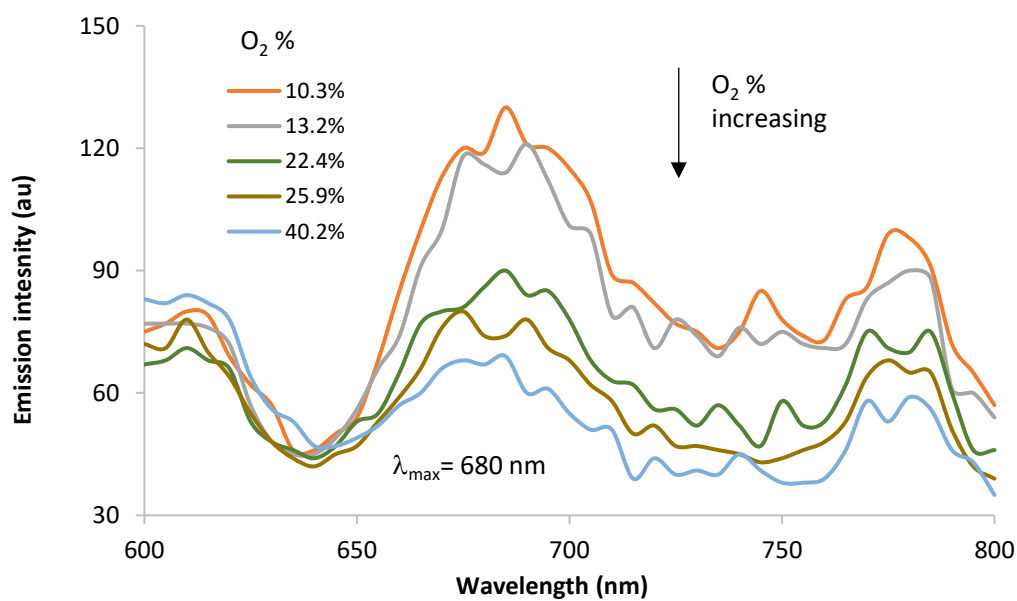
*Chart 19: emission intensity vs wavelength for complex **138** supported on collagen at 298 K*

Oxygen-sensing in protein hydrogels: quantitative considerations

From the data shown above it emerges that, with few exceptions, the porphyrins under study display oxygen-dependent fluorescence in hydrogels. The use of this information for quantitative purposes [147] (*i.e.*, to correlate the emission intensity with the oxygen concentration in the environment) requires the evaluation of the linearity of the response. This entails the treatment of the data to obtain the Stern-Volmer plots, as illustrated above for porphyrin **137** in aqueous solution (Chart 2 and *Chart 3*).

For each porphyrin, the average values of fluorescence intensity at the maximum of emission obtained from three experiments were plotted versus the oxygen concentrations, as exemplified for compound **137** in fibroin hydrogel (blue circles, *Chart 20*). The data points correlate well with an exponential decay ($R_2 = 0.975$).
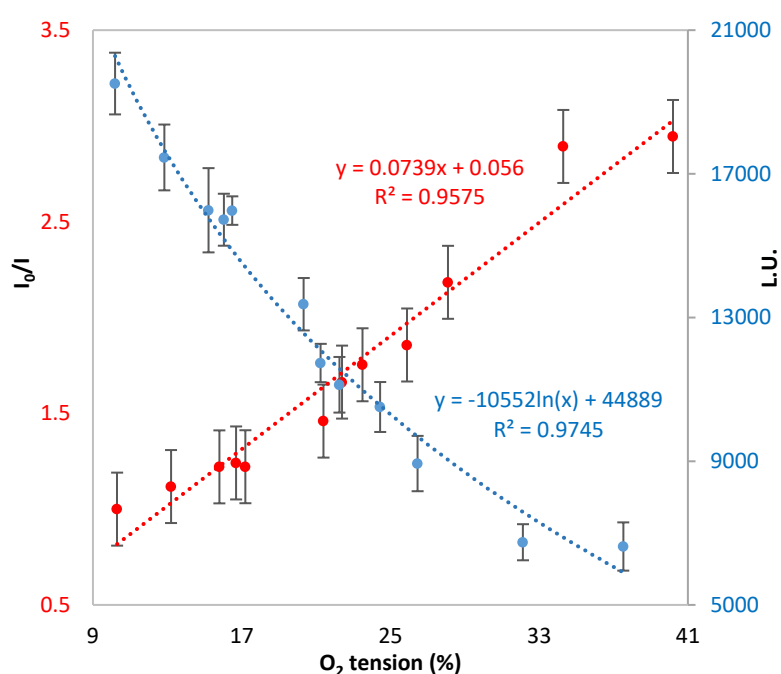
*Chart 20: exponential decay of fluorescence intensity (blue circles, right axis) and I_0/I values (red circles, left axis) versus oxygen concentration for compound **137** in fibroin hydrogel at 298 K*

The data points are transformed to give the Stern-Volmer plot (red circles in *Chart 20*), which show a good linearity between the values of I_0/I and oxygen concentration ($R^2 = 0.9575$). Observing this degree of linearity in a heterogeneous system like a hydrogel is remarkable. The interactions of the porphyrin with the protein fibres enhance non-specific quenching of the excited state, inherently lowering the efficiency of quenching by molecular oxygen: verifying good linearity of the Stern-Volmer plot in these conditions is a demonstration of the potential of porphyrin **137** as an optical oxygen sensor. For all the porphyrin-hydrogel combinations showing oxygen-dependent fluorescence, the

data obtained from the fluorescent measurements at varying oxygen concentration were treated as detailed above. In fibroin, species **134** and **136** displayed an equally promising behaviour (Chart 21, panels **A** and **B**), although the correlation factors are slightly lower. Despite their oxygen-dependent fluorescence, derivatives **132**, **135** and **138** show rather poor correlation for both their fluorescence decay and Stern-Volmer equation (Chart 21, panels **C**, **D** and **E** respectively). These species also display a smaller K_{SV} value compared to **137**, **134** and **136** (*Table 43*), indication of lower responsiveness to oxygen variations.
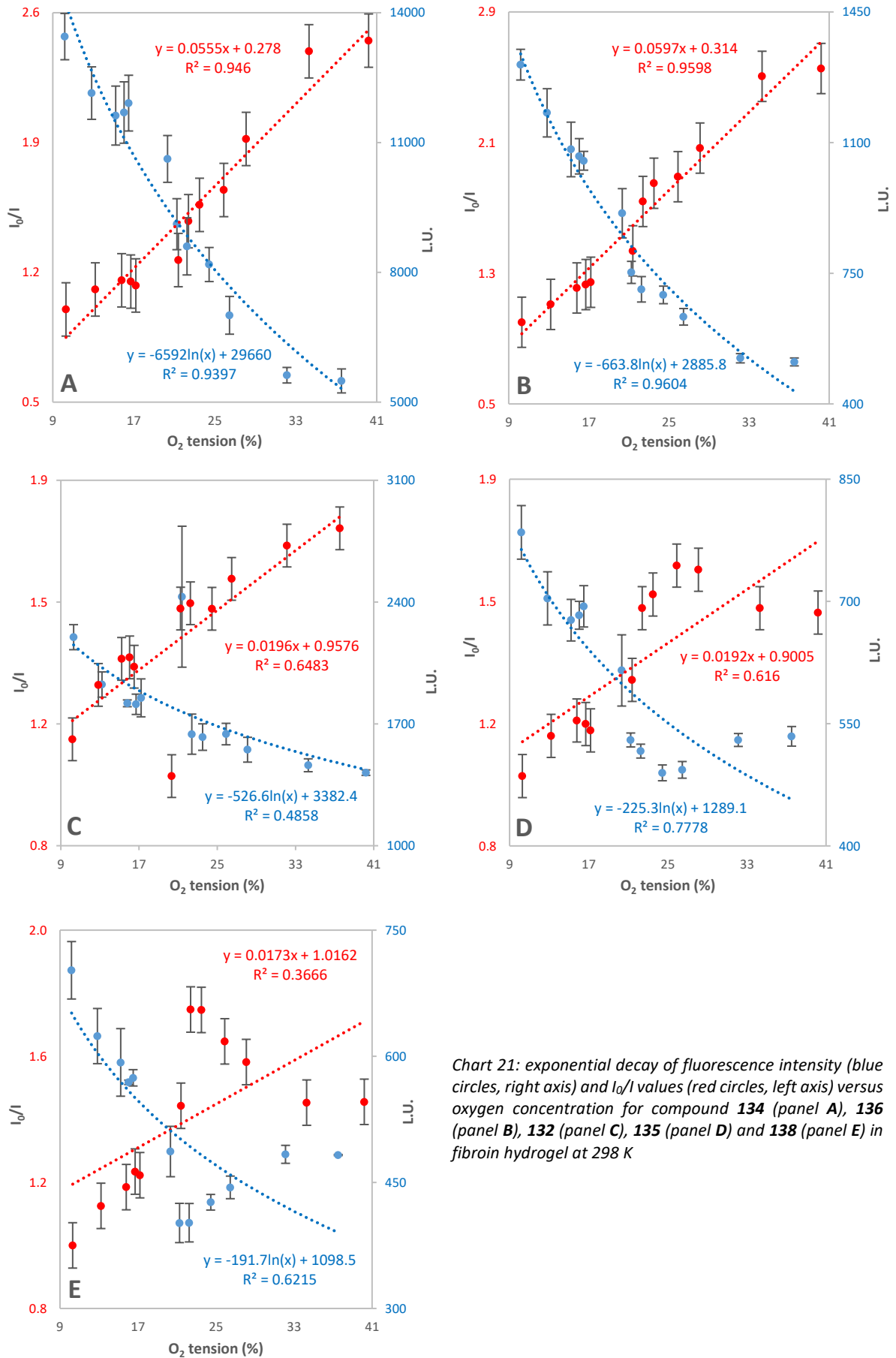
Chart 21: exponential decay of fluorescence intensity (blue circles, right axis) and I_0/I values (red circles, left axis) versus oxygen concentration for compound **134** (panel **A**), **136** (panel **B**), **132** (panel **C**), **135** (panel **D**) and **138** (panel **E**) in fibroin hydrogel at 298 K

In collagen hydrogel except for anionic derivatives **134** and **135** the linearity of response is lost (*Chart 22* panels **A** and **B**). These two species show an exponential fluorescence decay and a linear Stern-Volmer plot with relatively high K_{SV} values (*Table 44*), indicating a rather good responsiveness to oxygen concentration changes. Derivative **136** maintains some linearity of response, but species **138** and **137** show poor correlation (*Chart 22*, panels **C**, **D** and **E** respectively). The small standard deviation associated to most of the experiments indicate a reliable experimental setting.

Table 43 reports the K_{SV} values for the porphyrins complexes in fibroin hydrogels, expressed in $M^{-1} s^{-1}$ (see Equation 2 and Equation 3). Complex **137** shows the greatest K_{SV} value and, therefore, the highest sensitivity among the oxygen sensors studied here. Its intense fluorescence emission makes it suitable for applications in which only limited amount of complex can be used.

Complex	Charge	λ_{max} (nm)	K_{SV} ($M^{-1} s^{-1}$)	($\pm\sigma$)	R^2	I_0/I_{min}
Platinum complexes						
137	-	650	$5.73 \cdot 10^5$	$0.38 \cdot 10^5$	0.9575	3.37
134	-	670	$4.30 \cdot 10^5$	$0.33 \cdot 10^5$	0.9460	2.68
132	+	670	$1.52 \cdot 10^5$	$0.35 \cdot 10^5$	0.6483	1.79
Palladium complexes						
135	-	700	$1.49 \cdot 10^5$	$0.37 \cdot 10^5$	0.6160	1.57
138	-	680	$1.34 \cdot 10^5$	$0.56 \cdot 10^5$	0.3666	1.54
136	+	675	$4.63 \cdot 10^5$	$0.30 \cdot 10^5$	0.9598	2.71

Table 43: λ_{max}, K_{SV}, R^2, I_0/I_{min} for fibroin-supported dyes

Table 44 shows the K_{SV} values for oxygen concentrations expressed in molarity. Platinum and palladium complexes of porphyrin **73** (complexes **132** and **133**) showed non-linear Stern-Volmer plots, therefore the corresponding values of K_{SV} are not given in *Table 44*. Complex **137** showed the lowest K_{SV} value, while the highest K_{SV} value was shown by anionic platinum complex **134**.

Complex	Charge	λ_{max} (nm)	K_{SV} (M^{-1} s^{-1})	($\pm\sigma$)	R^2	I_0/I_{min}
Pt complexes						
137	-	650	$1.61 \cdot 10^5$	$0.46 \cdot 10^5$	0.5546	1.79
134	-	670	$6.63 \cdot 10^5$	$0.58 \cdot 10^5$	0.9298	3.42
Pd complexes						
135	-	705	$5.28 \cdot 10^5$	$0.42 \cdot 10^5$	0.9341	2.97
138	-	680	$2.19 \cdot 10^5$	$0.49 \cdot 10^5$	0.6634	1.71
136	+	675	$3.56 \cdot 10^5$	$0.48 \cdot 10^5$	0.8439	2.28

Table 44: λ_{max}, K_{sw}, R^2, I_0/I_{min} for collagen-supported dyes
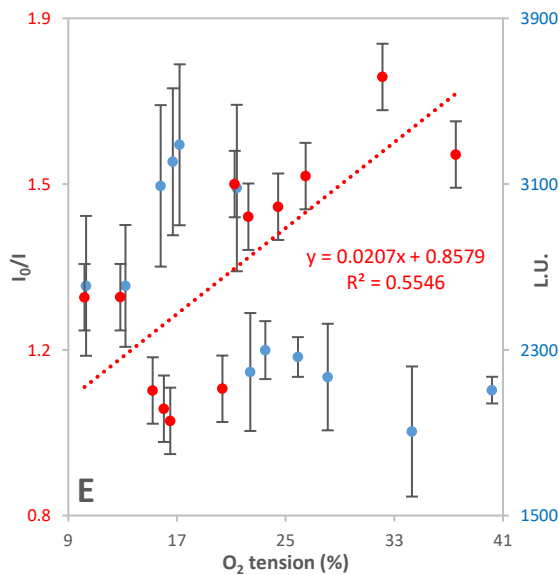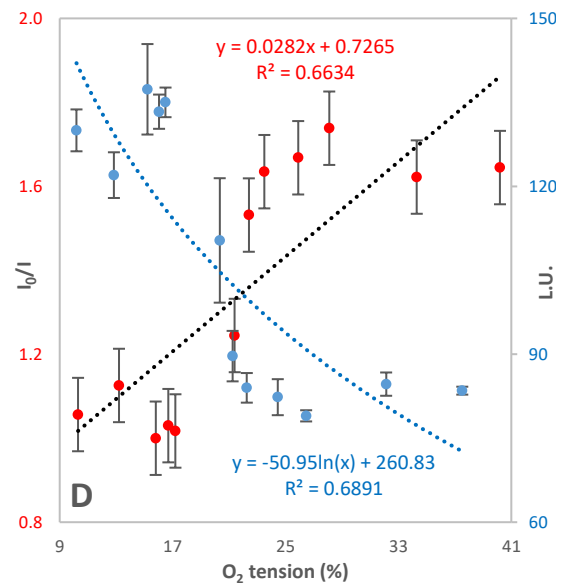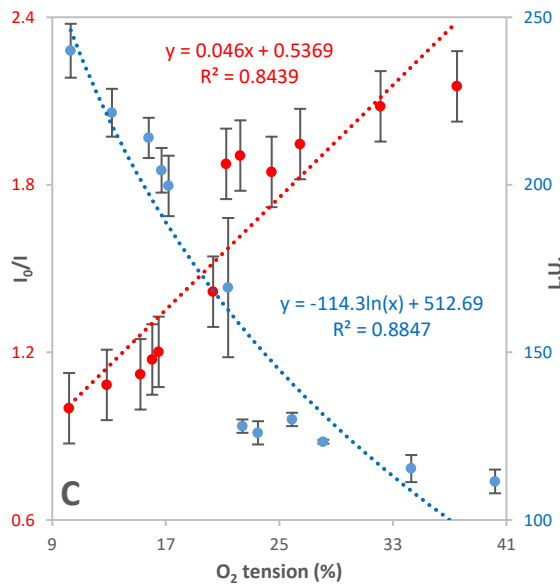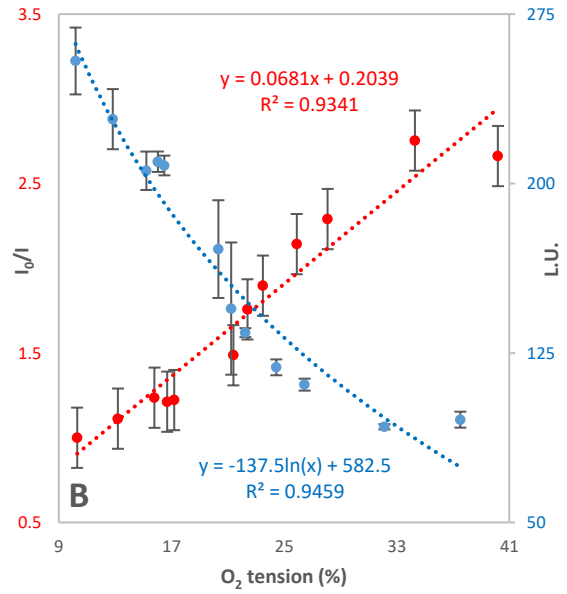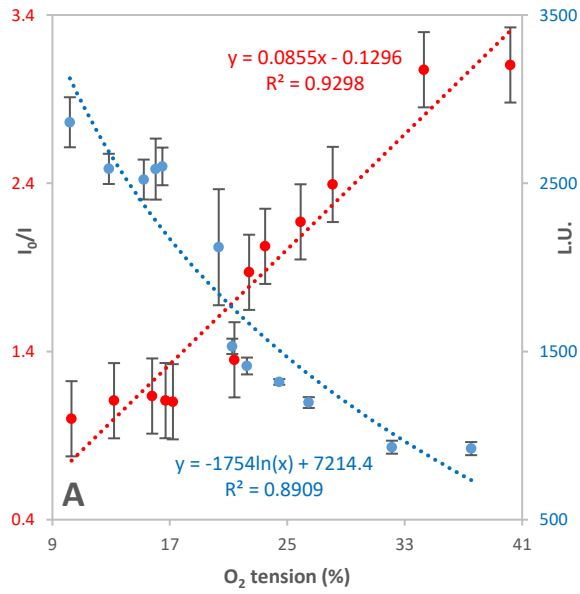
Chart 22: exponential decay of fluorescence intensity (blue circles, right axis) and I_0/I values (red circles, left axis) versus oxygen concentration for compound **134** (panel **A**), **135** (panel **B**), **136** (panel **C**), **138** (panel **D**) and **137** (panel **E**) in collagen hydrogel at 298 K

4.3 Oxygen-sensing protein hydrogels conclusions

The water-soluble porphyrins synthesised were tested for the oxygen response in aqueous solution and in hydrogels made of fibroin and collagen. Platinum complex **137** showed 25 times stronger fluorescence emission compared to its palladium analogue, and a linear Stern-Volmer plot in aqueous solution. To obtain hydrogels containing porphyrins, conjugations were carried out with the N-hydroxysuccinimide esters of the porphyrin derivatives on the proteins in solution. Moreover, to measure the oxygen response of the species supported on hydrogels, a new experimental set-up was developed.

Most of the porphyrins showed an oxygen-dependent fluorescence in hydrogels. In fibroin hydrogel, this was the case for all the dyes except complex **133**, for which the curves at different oxygen concentrations overlapped. The oxygen responsiveness of porphyrins in collagen was less evident than in fibroin, making the species less suitable for oxygen sensing in this system. Cationic platinum and palladium complexes **132** and **133** and anionic complex **137**, in particular, showed no oxygen-dependent fluorescence. This unexpected behaviour can be ascribed to three factors: the lower concentration of porphyrin in collagen hydrogel, the possible stronger interactions of the dyes with the collagen fibres, and the hypothetical presence of aggregates in the gel. The small standard deviations associated with most of the measurements are an indication of the reliability of the new experimental set-up developed to measure the oxygen-dependence in hydrogels.

Overall, the platinum complexes showed a stronger fluorescence emission than the corresponding palladium analogues both in hydrogels and in solution, and this behaviour was more pronounced at low oxygen concentrations. Palladium complexes showed oxygen-dependent fluorescence, but the emission was generally low, hampering quantitative measurements. In addition, anionic complexes generally showed stronger fluorescence emission compared to the cationic derivatives.

A number of derivatives showed exponential decay of fluorescence with increasing concentration of oxygen and a linear Stern-Volmer plot. These species would be amenable to use for quantitative determination of oxygen concentration in systems based on hydrogels (e.g., 3D cell cultures).

The novel anionic water-soluble platinum complex **137** showed favourable oxygen sensing behaviour both in aqueous solution and conjugated in fibroin hydrogel. The presence of the sulphonate groups ensure the water solubility of this species, and its synthesis is applicable to gram scale. Its strong fluorescence emission, on the other hand, potentially allows oxygen sensing to be performed using relatively low concentration of the fluorophore.

5 General conclusions

Oxygen is an important and vital molecule for life as we know it, therefore, its accurate measurement is pivotal to better understand the mechanisms behind cell behaviour.

The aim of the project was to build a library of porphyrins for optical oxygen sensing applications in the biomedical field. For these applications, the porphyrins must be (1) platinum or palladium complex to display oxygen responsiveness, (2) water-soluble and (3) provided with a functional group to allow conjugation to biomacromolecules. We first focused our attention on the synthesis of tetra *meso*-substituted porphyrins bearing the conjugatable moiety on one of the *beta*-positions of the macrocycle. The synthesis entailed the nitration of the porphyrin and subsequent Michael addition with alkyl-acetoacetate, followed by retro-Claisen degradation and hydrolysis. This synthetic approach was overall successful and led to the formation of the desired derivatives, but the conjugatable side-chain was too labile to withstand the conditions required to introduce the metal in the macrocycles. For some porphyrins a decarboxylation reaction occurred, while in other cases a complete cleavage of the side-chain was observed.

The focus was then redirected to the synthesis of porphyrin A_3B, bearing the conjugable moiety on one of the *meso*-substituted aryl ring. These species are synthesised in generally lower yields, but they allow to obtain a porphyrin with a conjugatable function in one step. Porphyrin **99** served as starting material to obtain two novel water-soluble derivatives, one positively and one negatively charged. The new species were obtained in overall good yields employing relatively mild reaction conditions, and could be synthesised on gram-scale. In addition, the synthetic approach to obtain two known water-soluble and conjugatable species, one cationic and one anionic, was repeated and improved. This process led to develop a highly valuable purification approach for water-soluble species based on ion-exchange: this method was effective in the purification of different species, thus proving a wide applicability. Formation of platinum (II) and palladium (II) complexes was performed to impart the oxygen-sensing properties to the porphyrins. MW irradiation guaranteed good yield and fast reaction times for the synthesis of several complexes. The conjugation of the porphyrins to the proteins chosen as matrices for hydrogels (silk fibroin and collagen) was performed *via* NHS-mediated chemistry.

Oxygen response of the new complexes was tested both in aqueous solution and in hydrogels of fibroin and collagen. The majority of the porphyrins maintained oxygen-dependent fluorescence in the hydrogels, and that in several cases translated in a linear Stern-Volmer plot, indicating the suitability of the new species to monitor the oxygen tension in a heterogeneous system such as a hydrogel. To the best of our knowledge, this work represents the first example of optical oxygen measurements in silk fibroin hydrogels.

6 Expanding the conjugations: different applications for porphyrins

<u>Duramycin</u>

Duramycin, a 19 amino acids tetracyclic peptide[333,334] produced by the bacterium *Streptoverticillium cinnamoneus*,[335] is a selective molecular probe for cancer cells targeting and imaging[336] thanks to its selective binding with membrane phospholipid phosphatidylethanolamine [337] overexpressed in cancer cells. If duramycin is conjugated with a photosensitizer it can increase the selectivity of photodynamic agents for the target cancer cells.[338]

The conjugate was obtained by reaction of **139** and duramycin in DMSO, as shown in *Scheme 46*. The active ester on the porphyrin reacted with a terminal primary amine present on duramycin B (red circle in *Scheme 46*) forming the desired conjugate. The conjugation of the porphyrin to the terminal amine does not prevent the binding of duramycin B with the membrane phospholipid phosphatidylethanolamine present on the cancer cell surface.
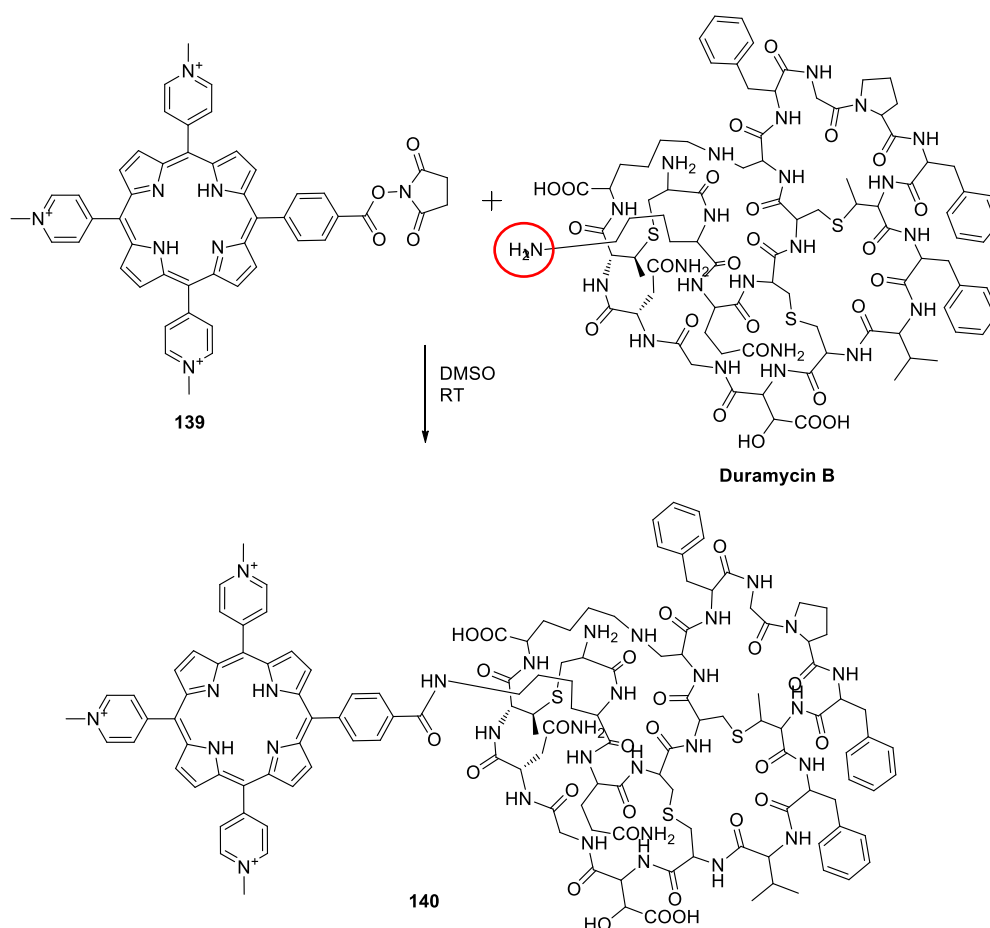
*Scheme 46: conjugation reaction between duramycin B and **4PyNHS***

The reaction was monitored by HPLC-MS (*Figure 103*, upper part) and the desired conjugate **140** was isolated by semi-preparative HPLC. The retention time of conjugate **140** was detected at 5.70 minutes

(blue circle, upper part of *Figure 103*), while the retention time of duramycin B was detected at 6.39 minutes (green circle, upper part of *Figure 103*). The peak at 5.18 minutes (purple circle, upper part of *Figure 103*) is relative to porphyrin **140**.
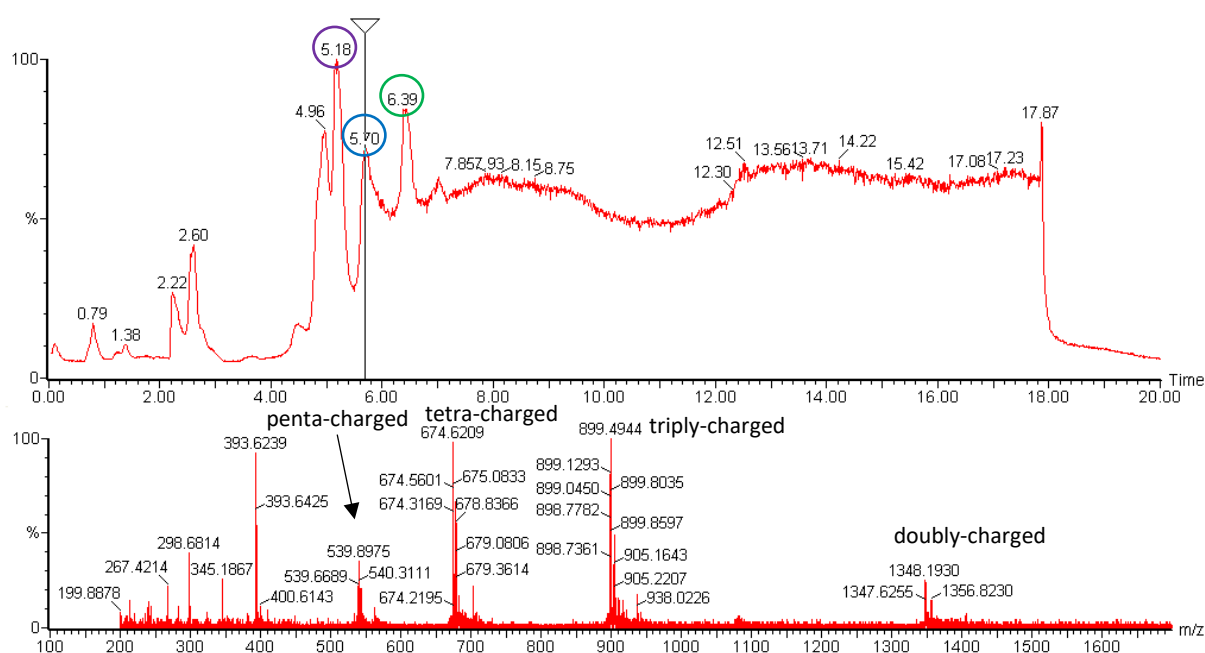
Figure 103: LC-MS trace (above) and ESI mass spectrum at 5.70 minutes (below) of conjugate 140

Table 45 shows the *m/z* for the molecular ions calculated and found for the conjugate. Four peaks were identified in the MS spectrum, all of which were assigned to multiple-charged ions (*Figure 103, lower part*). The single-charge species was not visible in the spectrum, but the double-charge molecular ion was detected at 1348.19, the triple- and the quadruple-charge ions at 899.49 and 674.62 respectively, and a five-charge molecular ion peak at 539.90, as summarized in *Table 45*.

Mass Conjugate 139	Calculated	Found
M	2700.13	-
$[M - H - 3Cl]^{2+}/2$	1349.57	1348.19
$[M - 3Cl]^{3+}/3$	900.04	899.49
$[M + H - 3Cl]^{4+}/4$	675.28	674.62
$[M + 2H - 3Cl]^{5+}/5$	540.43	539.90

Table 45: m/z for the molecular ions calculated and detected for conjugate 140

The conjugate porphyrin-duramycin was then purified through a semi-preparative HPLC, and the fractions collected have been sent to Hull University to perform the biological tests. It was shown that

the duramycin-porphyrin conjugate preserved the binding affinity for its target and, after irradiation, inhibited cell proliferation of pancreatic and ovarian cancer cell lines.[338]

Deferoxamine

Deferoxamine B is a naturally occurring tris-hydroxamic acid obtained by a metabolite of Actinomycetes (*Streptomyces pilosus*)[339] and employed as iron complexing agent.[340] Deferoxamine B is particularly useful in medicine to treat iron poisoning, facilitating its elimination through the urine. Deferoxamine B, after deprotonation of the three hydroxamic groups, chelates a ferric ion as showed in *Scheme 47*, forming a complex called Ferrioxamine B.[341]
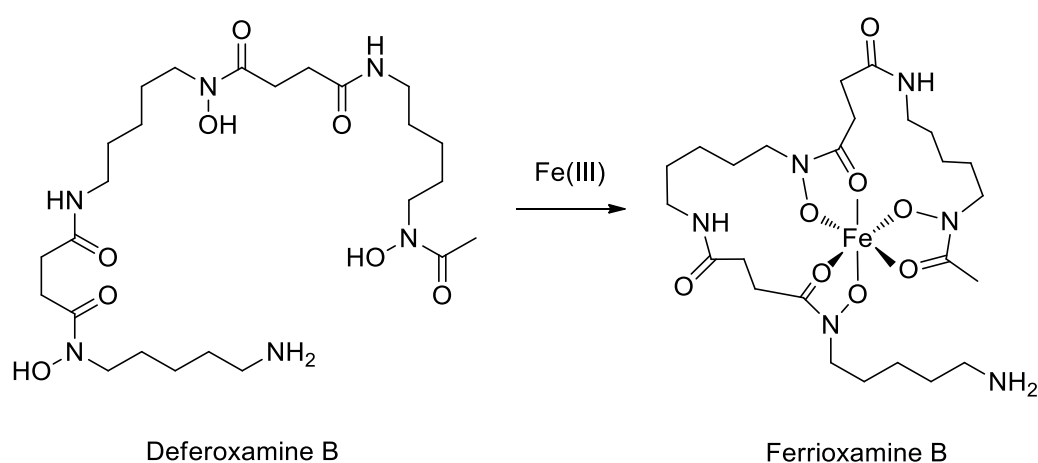
Scheme 47: complexation of deferoxamine with Iron (III) ion

Iron (III) complexes, due to their paramagnetic properties, are able to quench the singlet excited state of a porphyrin nearby in solution.[342] The intensity of the fluorescence emission of the porphyrin decreases on increasing the amount of iron(III) complex. The iron complex acts as a quencher (like the oxygen) of the porphyrin excited state, resulting in a decrease of the fluorescence intensity.

The idea was to build an iron (III) sensor combining the chelation properties of deferoxamine B with the photophysical properties of a metal porphyrin. The two molecules were covalently linked without employing a spacer to insure a short distance suitable for the quenching. The sensor would be able to determine the quantity of iron (III) in the environment through spectroscopic measurements. The complexation of a ferric ion by deferoxamine B results in a paramagnetic species capable of quenching the fluorescence emission of the metal porphyrin, after irradiation of the latter at the wavelength of the Soret band.

The iron(III) sensor was built conjugating deferoxamine with porphyrin **127**, previously synthesised, as shown in *Scheme 48*. It was decided to employ the indium (III) complex because it showed intense

fluorescence emission compared to the other metal complexes of porphyrin **73**, hence it could serve as an ideal platform for a highly sensitive iron sensor. The conjugate was obtained *via* NHS-mediated chemistry. The NHS activated ester was generated *in situ* by treating the porphyrin with NHS and EDC hydrochloride in water at 40 °C prior to exposure to deferoxamine. The desired conjugate was isolated by precipitation from water as the hexafluorophosphate salt, and subsequent ion-exchange with TBAC to afford the corresponding chloride.
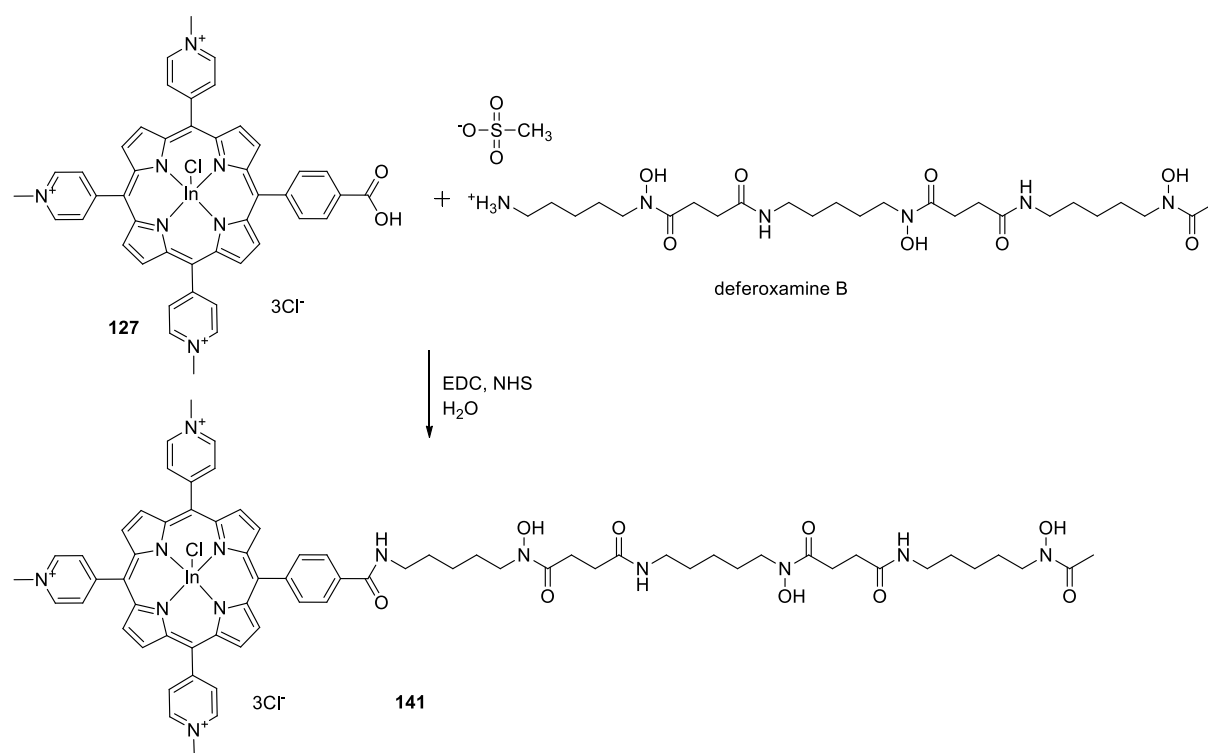
*Scheme 48: conjugation between complex **127** and deferoxamine B*

NMR spectra are shown below. *Figure 104* contains ^{1}H-NMR spectrum of the mesylate salt of deferoxamine acquired in D_2O. Due to fast exchange of hydrogens from the amine and hydroxyl functionalities with the deuterated solvent, those do not appear in the spectrum. The hydrogen count, not considering the exchangeable protons, is 44H, matching well with the integral value on *Figure 104*, and with the literature data.[340]
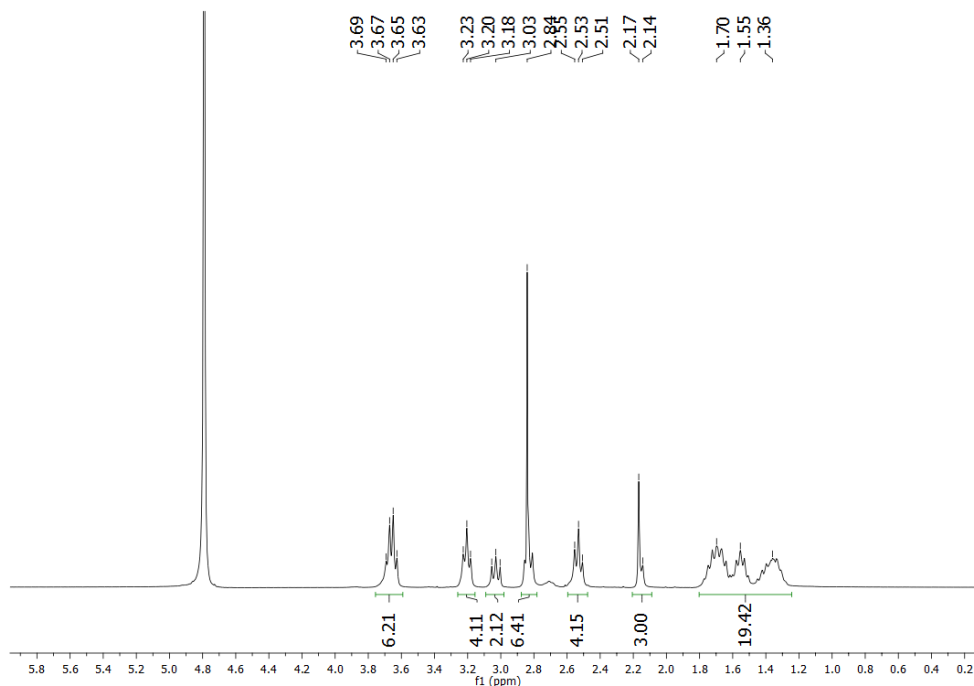
Figure 104: ¹H-NMR spectrum of deferoxamine B mesylate salt in D₂O at 298 K

Figure 105 shows the ¹H-NMR spectrum of the conjugate **141** in DMSO-d₆. Signals from the *beta* and pyridyl hydrogens are present as multiplets in the range between 8.99 and 9.54 ppm, while the signals detected in the aliphatic region are relative to the deferoxamine part of the conjugate. The hydrogens in *ortho* to the pyridyl nitrogens (H$_{Py-o}$) appear as a singlet at 9.54 ppm, while multiplets in the 8.99-9.28 ppm range are due to remaining hydrogens in the pyridyl rings (H$_{Py-m}$) and the *beta* hydrogens (H$_\beta$). The singlet at 4.72 ppm, whit the integration value of 9H, can be assigned to the three methyl groups (N⁺CH₃). In this case, the four hydrogens of the phenyl ring appear as a multiplet in the 7.81-8.59 ppm range (H$_{Ar-o}$ + H$_{Ar-m}$), with an integration value of 6H. It is unclear whether two hydrogens from the deferoxamine moiety are downfield-shifted or the integral value is altered by the presence of impurities. The count of the hydrogens in the aliphatic part, where the signals are generated by the deferoxamine portion of the conjugate, is 40H, matching well with the proposed structure in *Scheme 48*.
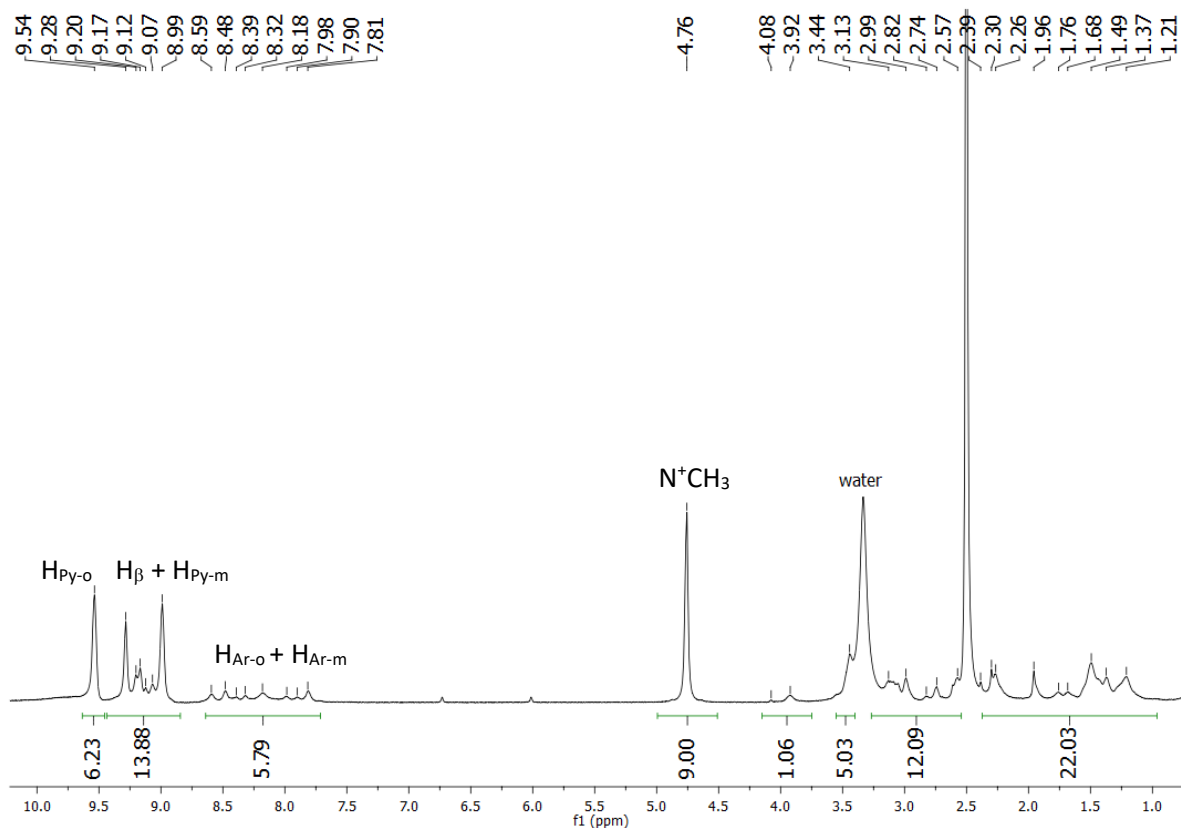
*Figure 105: ^{1}H-NMR spectrum of conjugate **141** in DMSO-d_6 at 298 K*

Hydrogen-carbon 2D NMR correlations, showed in *Figure 106*, *Figure 107* and *Figure 108* allow us to assign few carbon signals to the relative hydrogens. DEPT-edited ^{1}H,^{13}C-HSQC spectrum, showed in *Figure 106,* highlights the presence of several CH$_2$ groups (blue dots) in the aliphatic region that can be assigned to the CH$_2$ groups present in the carbon chains of deferoxamine. ^{1}H (1.96 ppm) and ^{13}C (20.37 ppm) signals of the terminal methyl group of the deferoxamine chain are shown as a red dot (green circle top right *Figure 106*). The carbon relative to the methyl groups (N$^+$CH$_3$) resonates at 47.78 ppm (red circle of *Figure 106*). In the aromatic region, a very intense correlation is evident between the pyridyl and the *beta* hydrogens of the porphyrin and respective carbon signals. *Figure 108* contains the previous DEPT-edited ^{1}H,^{13}C-HSQC correlation where decoupled ^{13}C spectrum is used as an external projection.
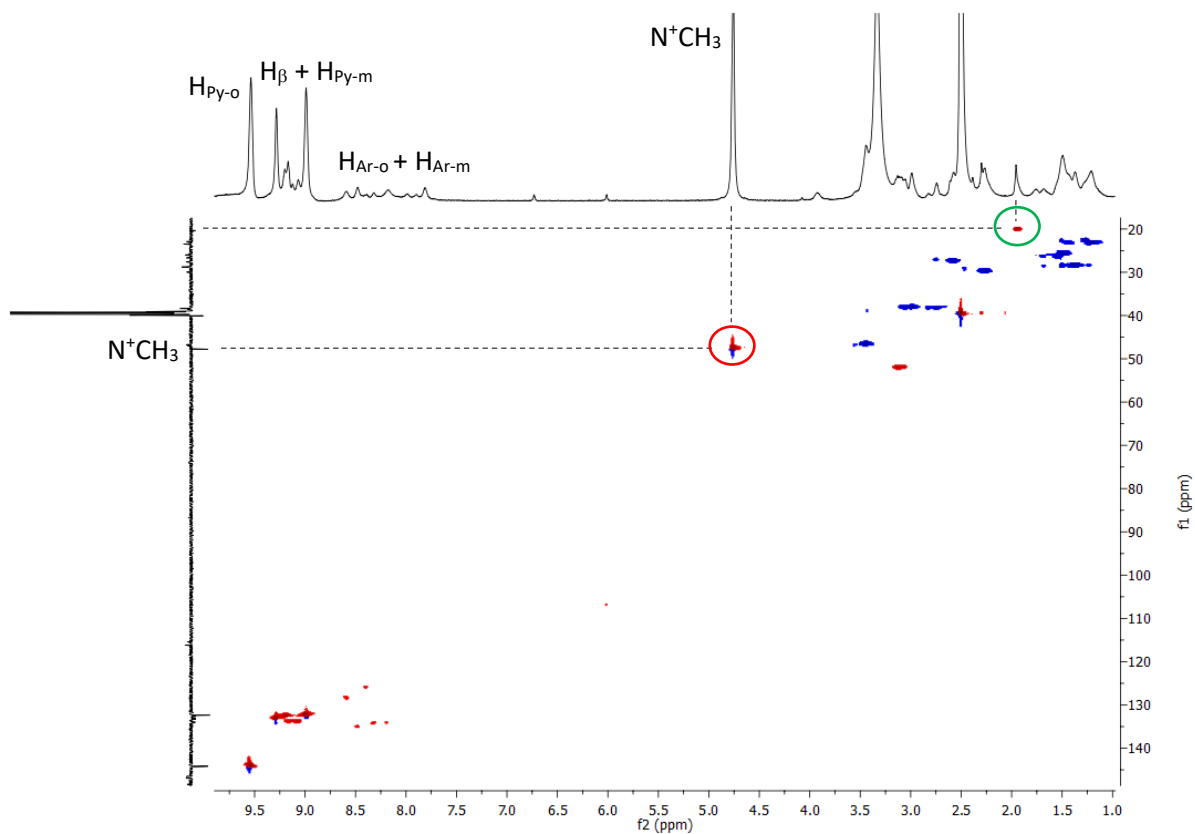
*Figure 106: DEPT-edited (135°) $^1H,^{13}C$-HSQC of conjugate **141** in DMSO-d_6 at 298 K, blue dots CH_2 up, red dots CH/CH_3 down*

$^1H,^{13}C$-HMBC correlation, showed in *Figure 107*, revealed four correlations between the low-field carbon signals of carbonyl groups with three aliphatic hydrogens assignable to deferoxamine (red oval of *Figure 107*) and one signal at 7.81 ppm, relative to the phenyl hydrogens (H_{Ar-o} + H_{Ar-m}) (blue circle of *Figure 107*). This is a further evidence which confirms that the multiplet between 7.81 ppm and 8.59 ppm is assignable to the four hydrogens of the phenyl ring, from which deferoxamine is connected.

185
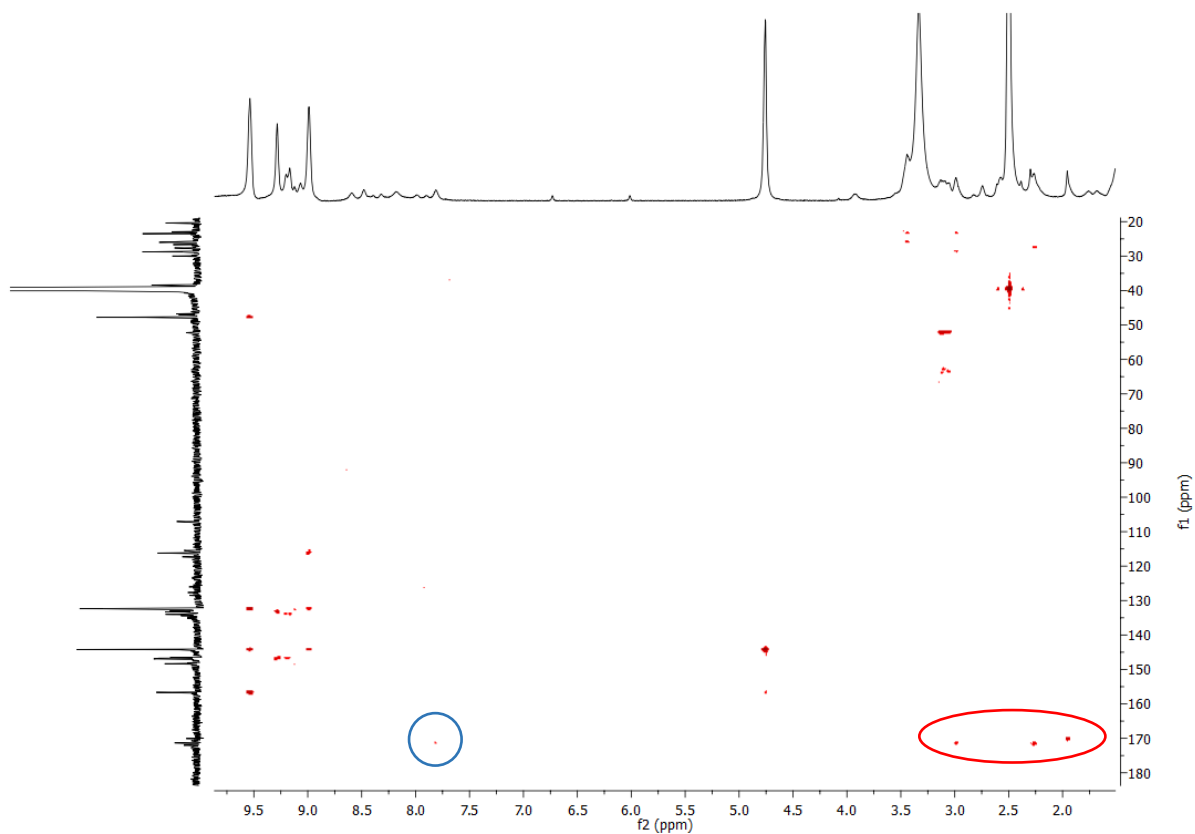
*Figure 107: $^1H,^{13}C$-HMBC of conjugate **141** in DMSO-d$_6$ at 298 K*
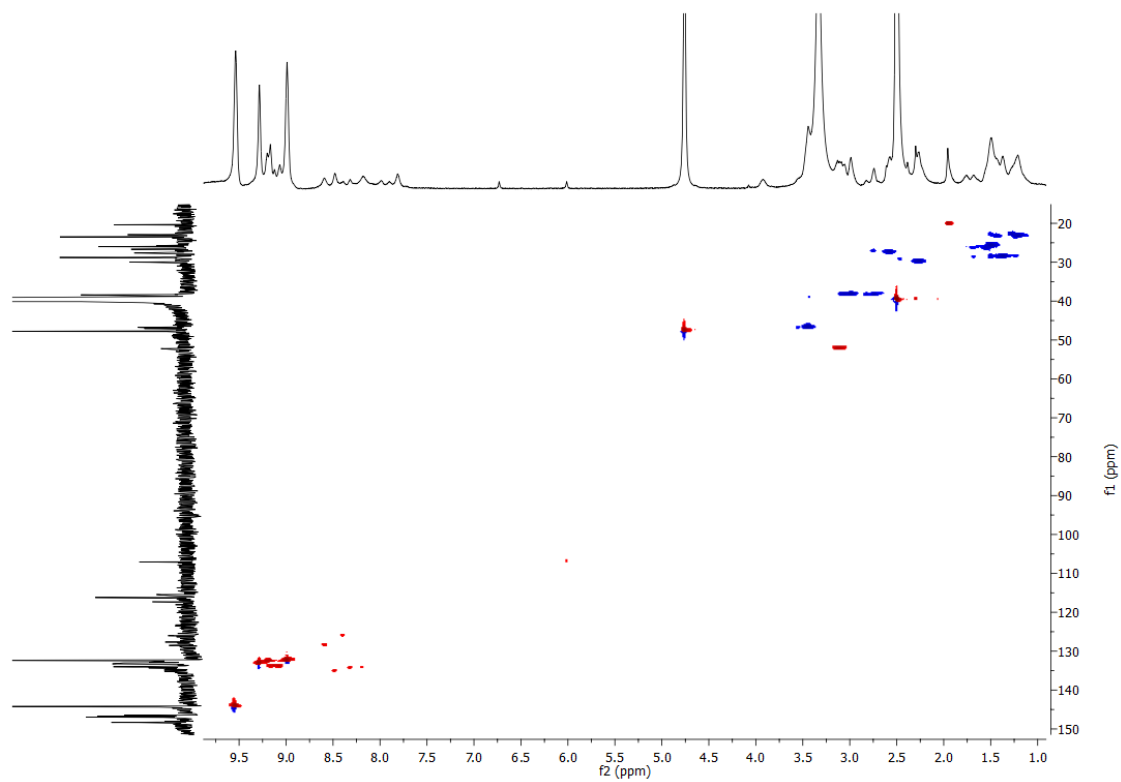
*Figure 108: DEPT-edited (135°) $^1H,^{13}C$-HSQC using $^{13}C\{^1H\}$ as external projection for conjugate **141** in DMSO-d$_6$ at 298 K, blue dots CH$_2$, red dots CH/CH$_3$*

EXPERIMENTAL

Reagents were purchased from Fluorochem, Sigma Aldrich, Fischer Scientific or Tokyo Chemical Industries, and were used as received unless otherwise specified. All solvents, either analytical or HPLC grade, were purchased from Fisher Scientific and used as received, unless otherwise specified. TLC analysis was performed using Fluorochem Silica Gel 60 Å, 20 X 20 cm, F254 plates. Silica gel chromatography was performed employing silica gel 60 Å purchased from Fluorochem. Melting points were recorded on a Stuart SMP10. UV-Vis analyses were performed on a Thermo Nicolet Evolution 300. Mass spectrometer analyses were performed on a Waters Micromass LCT equipped with an electrospray ionization (ESI) source and time of flight (ToF) detector. HPLC analyses were performed on a Waters separations module 2695. The separations were performed on a Gemini C18, 5 μm, 150 x 4.6 mm, 110 Å (Phenomenex, UK) at a flow rate of 0.8 mL·min^{-1}. Two methods were employed depending on the nature of the compound. Method A: the mobile phase consisted of 0.1% FA in water (solvent A) and 0.1% FA in acetonitrile (solvent B). Gradient: 0.0-10.0 min, 0-95% B; 10.0-15.0 min, 95% B; 15.0-16.0 min, 95-5% B; 16.0-18.0 min, 5% B. Method B: the mobile phase consisted of 0.1M ammonium acetate (NH_4OAc) in water (solvent A), and 0.1M ammonium acetate (NH_4OAc) in 1:1 acetonitrile-water (solvent B). Gradient: 0.0-10.0 min, 0-95% B; 10.0-15.0 min, 95% B; 15.0-16.0 min, 95-5% B; 16.0-18.0 min, 5% B. NMR analyses were performed employing either a Bruker 300 MHz (operating at 300.18 MHz for ^{1}H and 75.48 MHz for ^{13}C) or a Bruker 600 MHz (operating at 600.31 MHz for ^{1}H, 150.95 MHz for ^{13}C and 564.86 MHz for ^{19}F) NMR spectrometers. $CDCl_3$, DMSO-d$_6$, CD_3OD and D_2O were purchased either from Sigma-Aldrich or Fluorochem. $CDCl_3$, CD_3OD and D_2O were employed as received, DMSO-d$_6$ was dried over 3 Å molecular sieves and stored under argon. Chemical shifts are reported in ppm, referenced to either $CHCl_3$ (^{1}H, 7.26 ppm; ^{13}C, 77.16 ppm), DMSO (^{1}H, 2.50 ppm; ^{13}C, 39.52 ppm), MeOH (^{1}H, 3.31 ppm; ^{13}C 49.00 ppm) or D_2O (^{1}H, 4.79 ppm). Coupling constants (J) are reported in Hertz (Hz) and significant multiplicities are described by singlet (s), doublet (d), triplet (t), quartet (q), doublet of doublets (dd), doublet of triplets (dt), triplet of boublets (td), multiplet (m) or broad (br). Metal insertion, where specified, were performed employing microwave heating on a CEM microwave oven Discover SP®. Dialysis tubing was purchased from Sigma Aldrich, and it was made of cellulose with MWCO= 14'000 (14 kD). Fluorescence analyses in solution were performed employing a Varian Cary Eclipse Fluorescence Spectrometer. Fluorescence analyses on solid support were performed employing a Tecan Spark 10M microplates reader.

Synthesis of [5,10,15,20-*tetrakis*(4-methyl-pyridinium)porphyrin] tetrachloride (**51**)
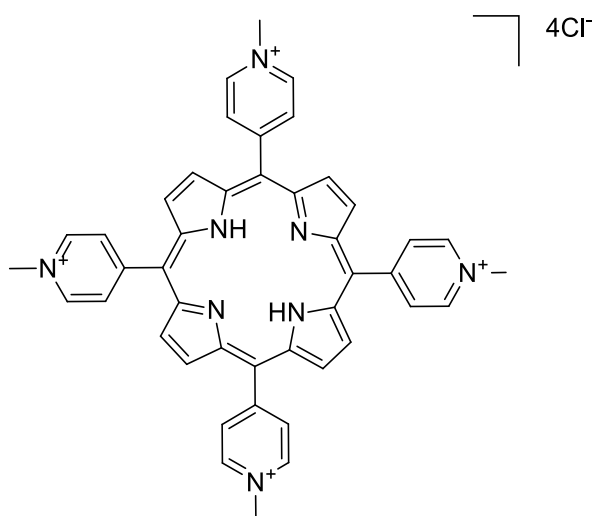
Tetra-(4-pyridine)porphyrin (500 mg, 0.61 mmol) was dissolved in water (80 mL) in a 250-mL round bottom flask sealed with a rubber septum. Methyl iodide (3.4 mL, 61 mmol) was added to the solution while stirring. The resulting mixture was heated to 40 °C and left under stirring overnight. Once the solution was cooled down to room temperature, it was diluted with water (120 mL) and treated with sodium hexafluorophosphate, to induce precipitation of the title compound. The resulting suspension was centrifuged and the precipitate was re-dissolved in acetone (160 mL). The resulting mixture was treated with 10 % TBAC in acetone, leading to flocculation of the title compound, successively centrifuged and collected after further crystallisation from methanol–diethyl ether. (**51**) (438 mg, 0.54 mmol, 89 %)

^{1}H-NMR (600 MHz, DMSO-d_6, 298 K) δ, ppm: 9.54 (br s, 6H, Py-H_m), 9.19 (br s, 8H, + β-H), 9.01 (br s, 8H, Py-H_o), 4.75 (s, 12H, NCH_3), -3.10 (s, 2H, NH$_{int}$)

^{13}C-NMR (150 MHz, DMSO-d_6, 298 K) δ, ppm: 156.2, 144.3, 132.1, 117.3, 115.8, 107.0, 47.8

m.p. (°C): > 300

UV-Vis (H$_2$O, nm) λ_{max}: Soret, 424; Q bands, 521, 558, 590, 645; Log ε_{424}: 5.38

ESI-MS (+ve) (m/z): 169.25 [M − 4Cl]$^{4+}$/4; 338.50 [M − 2H − 4Cl]$^{2+}$/2; 676.99 [M − 3H − 4Cl]$^+$

HPLC (method A), t_R: 1.24 min

Synthesis of 5,10,15,20-*tetrakis*(4-pyridyl)porphyrin (**51'**)

4-pyridinecarboxaldehyde (13 mL, 138 mmol) was dissolved in propionic acid (220 mL) in a 500-mL 3 necks round bottom flask. The resulting mixture was heated to 70 °C under stirring. Pyrrole (10 mL, 144 mmol) was dissolved in 30 mL of propionic acid and added drop-wise to the solution in a 30 minutes time. The resulting mixture was heated to reflux for 1 hour protected from light. Once the solution was cooled down to room temperature, the solvent was removed under reduced pressure and the crude mixture was dissolved in CH_2Cl_2 and filtrated on silica gel. The solvent was then evaporated under reduced pressure and the crude product was isolated by re-crystallisation from CH_2Cl_2/methanol, yielding a purple crystalline solid (2.78 g, 4.50 mmol, 13 %).

^{1}H-NMR (600 MHz, CDCl$_3$, 298 K) δ, ppm: 8.92 (d, 8H, J=4.8 Hz, Py-H$_{3,5}$), 8.79 (br s, 8H, β-H), 8.13 (d, 8H, Py-H$_{2,6}$), -3.02 (br s, 2H, NH$_{int}$)

^{13}C-NMR (150 MHz, CDCl$_3$, 298 K) δ, ppm: 142.4, 134.7, 131.4, 127.9, 126.8, 120.3

m.p. (°C): > 300

UV-Vis (CH$_2$Cl$_2$, nm) λ_{max}: Soret, 418; Q bands, 515, 548, 592, 645; Log ε_{418}: 5.26

ESI-MS (+ve) (m/z): 619.57 [M+H]$^+$

Synthesis of [5,10,15,20-*tetrakis*(4-methyl-pyridinium)porphyrin] palladium (II) tetrachloride (**53**)
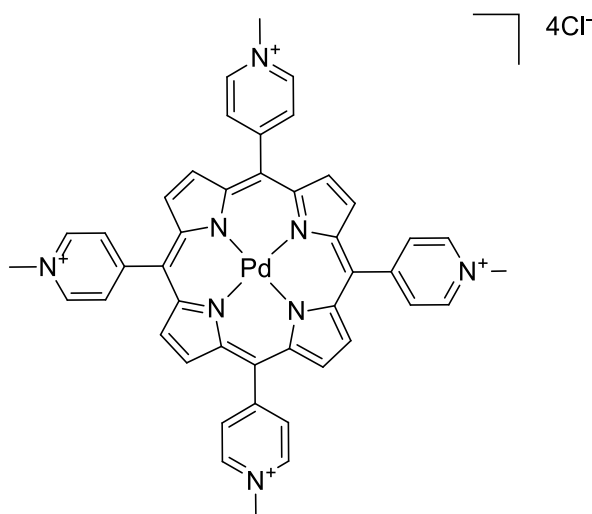
Compound **51** (139 mg, 0.17 mmol) was dissolved in water (40 mL) in a 100-mL round bottom flask. Palladium acetate (190 mg, 0.85 mmol) was added to the solution while stirring. The resulting mixture was heated to reflux overnight. Once the solution was cooled down to room temperature, it was diluted with water (120 mL) and treated with sodium hexafluorophosphate, to induce precipitation of the title compound. The resulting suspension was centrifuged and the precipitate was re-dissolved in acetone (40 mL). The resulting mixture was treated with 10 % TBAC in acetone, leading to flocculation of the title compound, successively centrifuged and collected after further crystallisation from methanol–diethyl ether. (**53**) (144 mg, 0.16 mmol, 95 %)

^{1}H-NMR (600 MHz, DMSO-d_6, 298 K) δ, ppm: 9.51 (br s, 6H, J=6.6Hz, Py-H$_m$), 9.13 (br s, 8H, β-H), 8.97 (br s, 8H, J= 6.6Hz, Py-H$_o$), 4.73 (s, 12H, NCH_3)

^{13}C-NMR (150 MHz, DMSO-d_6, 298 K) δ, ppm: 155.7, 144.4, 140.1, 132.5, 131.8, 117.5, 107.0, 47.7

UV-Vis (H$_2$O, nm) λ_{max}: Soret, 419; Q bands, 528, 563: Log ε_{419}: 5.22

ESI-MS (+ve) (m/z): 195.50 [M − 4Cl]$^{4+}$/4; 260.34 [M − H − 4Cl]$^{3+}$/3; 390.01 [M − 2H − 4Cl]$^{2+}$/2; 781.02 [M − 3H − 4Cl]$^+$

HPLC (method A), t$_R$: 1.21 min

Synthesis of [5-(4-carboxyphenyl)-10,15,20-*tris*(4-methyl-pyridinium)porphyrin] trichloride (**73**)
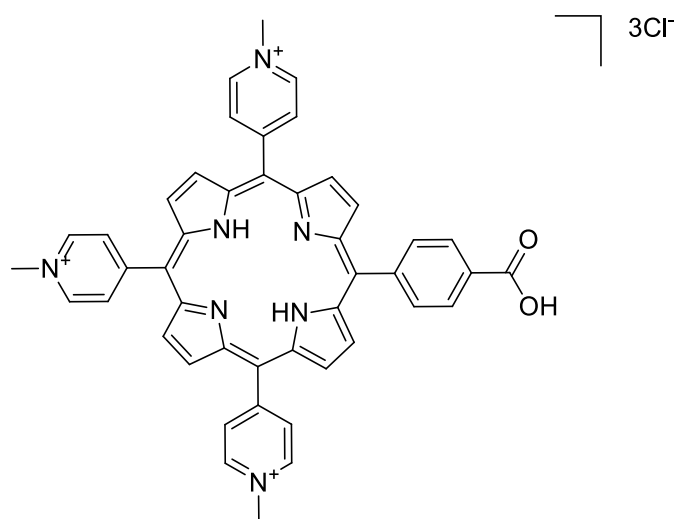
Compound **100** (500 mg, 0.61 mmol) was dissolved in water (80 mL) in a 250-mL round bottom flask. Lithium hydroxide (256 mg, 6.1 mmol) was added to the solution while stirring. The resulting mixture was heated to 40 °C and left under stirring for 1 hour. Once the solution was cooled down to room temperature, it was diluted with water (120 mL) and treated with sodium hexafluorophosphate, to induce precipitation of the title compound. The resulting suspension was centrifuged and the precipitate was re-dissolved in acetone (40 mL). The resulting mixture was treated with 10 % TBAC in acetone, leading to flocculation of the title compound, successively centrifuged and collected after further crystallisation from methanol–diethyl ether. (**73**) (438 mg, 0.54 mmol, 89 %)

^{1}H-NMR (600 MHz, CDCl$_3$, 298 K) δ, ppm: 13.24 (br s, 1H, OH), 9.57 (br s, 6H, Py-H$_m$), 9.02-9.17 (m, 14H, Py-H$_o$ + β-H), 8.36-8.44 (d, 4H, Ar-H$_o$ + Ar-H$_m$), 4.76 (s, 9H, NC*H$_3$*), -3.02 (s, 2H, NH$_{int}$)

^{13}C-NMR (75 MHz, DMSO-d$_6$, DEPTQ, 298 K) δ, ppm: 167.6, 156.5, 144.2, 134.3, 132.1, 128.0, 126.0, 115.4, 47.8

m.p. (°C): > 300

UV-Vis (H$_2$O, nm) λ_{max}: Soret, 422; Q bands, 520, 558, 584, 640; Log ϵ_{422}: 5.35

ESI-MS (+ve) (m/z): 235.56 [M − 3Cl]$^{3+}$/3; 352.85 [M − H − 3Cl]$^{2+}$/2

HPLC (method A), t$_R$: 5.32 min

Synthesis of [5-(4-carboxyphenyl)-10,15,20-*tris*(4-methyl-pyridinium)porphyrinato]platinum (II) trichloride (**74**)
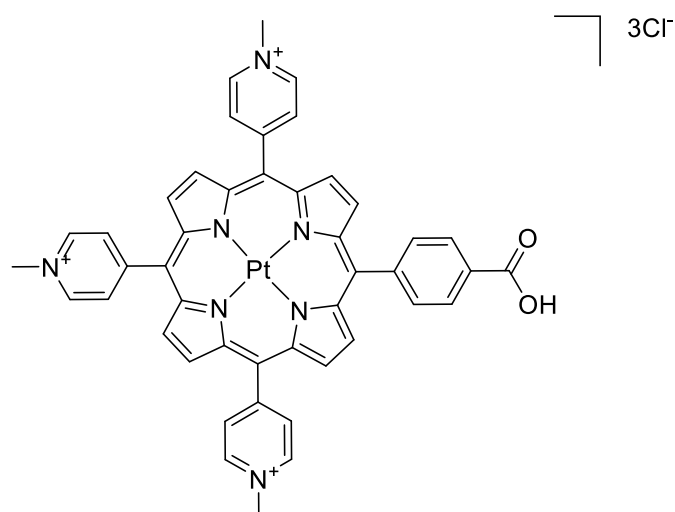
Compound **125** (356 mg, 0.75 mmol) was dissolved in DMSO (3 mL) and stirred at room temperature for 3 hours. Compound **73** (200 mg, 0.25 mmol), silver nitrate (382 mg, 2.25 mmol, 9 equivalents) and water (10 mL) were added to mixture, that was protected from light with tin foil and stirred at room temperature for 3 hours. The mixture was subsequently centrifuged and then filtered to remove all silver chloride formed. The precipitate was diluted with water (50 mL) and heated to reflux overnight. Once the solution was cooled down to room temperature, it was filtered through celite. The filtrate was treated with sodium hexafluorophosphate, to induce precipitation of the title compound. The resulting suspension was centrifuged and the precipitate was re-dissolved in acetone (40 mL). The resulting mixture was treated with 10 % TBAC in acetone, leading to flocculation of the title compound, successively centrifuged and collected after further crystallisation from methanol–diethyl ether. (**74**) (234 mg, 0.26 mmol, 93 %)

^{1}H-NMR (600 MHz, DMSO-d$_6$, 298 K) δ, ppm: 9.52 (m, 6H, Py-H$_m$), 8.91-9.05 (m, 14H, Py-H$_o$ + β-H), 8.40 (d, 2H, J=7.8 Hz, Ar-H$_o$), 8.25 (d, 2H, J=7.2 Hz, Ar-H$_m$), 4.73 (s, 9H, NCH_3)

^{13}C-NMR (150 MHz, DMSO-d$_6$, 298 K) δ, ppm: 167.6, 155.7, 155.5, 155.5, 144.5, 140.8, 139.2, 139.2, 138.9, 133.7, 132.6, 132.0, 131.7, 131.7, 131.4, 128.1, 123.6, 117.8, 117.3, 47.9

m.p. (°C): > 300

UV-Vis (H$_2$O, nm) λ_{max}: Soret, 419; Q bands, 529, 565; Log ε_{419}: 5.29

ESI-MS (+ve) (m/z): 299.70 [M − 3Cl]$^{3+}$/3; 449.24 [M − H − 3Cl]$^{2+}$/2; 899.33 [M − 3Cl]$^+$

HPLC (method A), t$_R$: 4.91 min

Synthesis of [5-(4-carboxyphenyl)-10,15,20-*tris*(4-methyl-pyridinium)porphyrinato]palladium (II) trichloride (**75**)
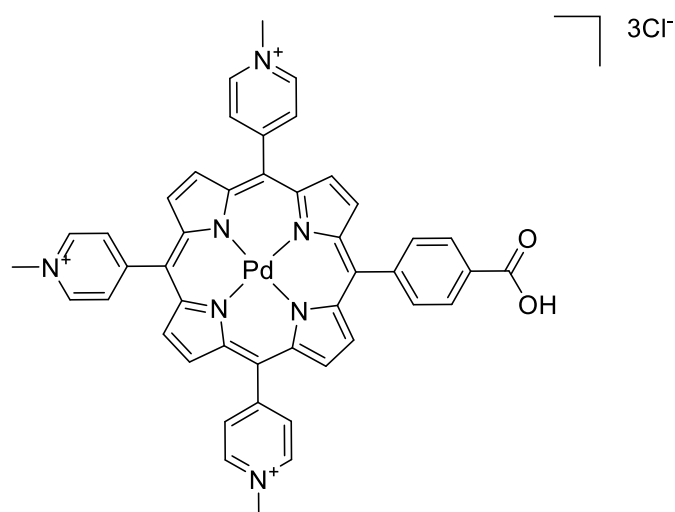
Compound **73** (200 mg, 0.25 mmol) was dissolved in NMP (10 mL) in a 100-mL round bottom flask. Palladium acetate (160 mg, 0.71 mmol) was dissolved in methanol (5 mL) and added to the solution while stirring. The resulting mixture was heated to 50 °C and left under stirring for 1 hour. Once the solution was cooled down to room temperature, it was filtered through celite. Diethyl ether (50 mL) was added to the filtrate to induce precipitation of the porphyrin, collected by filtration on paper. The precipitate was dissolved in water (80 mL) and treated with sodium hexafluorophosphate, to induce precipitation of the title compound. The resulting suspension was centrifuged and the precipitate was re-dissolved in acetone (40 mL). The resulting mixture was treated with 10 % TBAC in acetone, leading to flocculation of the title compound, successively centrifuged and collected after further crystallisation from methanol–diethyl ether. (**75**) (178 mg, 0.22 mmol, 78 %)

^{1}H-NMR (600 MHz, DMSO-d$_6$, 298 K) δ, ppm: 9.51 (br s, 6H, Py-H$_m$), 8.99-9.09 (d, 14H, Py-H$_o$ + β-H), 8.31 (br s, 2H, Ar-H$_o$), 8.12 (br s, 2H, Ar-H$_m$), 4.72 (s, 9H, NC*H$_3$*)

^{13}C-NMR (150 MHz, DMSO-d$_6$, 298 K) δ, ppm: 167.7, 156.0, 144.3, 141.7, 139.9, 139.8, 139.5, 133.3, 133.0, 132.1, 131.9, 131.8, 131.5, 127.8, 117.1, 116.5, 47.8

m.p. (°C): > 300

UV-Vis (H$_2$O, nm) λ_{max}: Soret, 419; Q bands, 529, 565; Log ε_{419}: 5.29

ESI-MS (+ve) (m/z): 270.14 [M − 3Cl]$^{3+}$/3; 404.68 [M − H − 3Cl]$^{2+}$/2; 810.41 [M − 3Cl]$^+$

HPLC (method A), t$_R$: 5.14 min

Synthesis of [5-(4-carboxyphenyl)-10,15,20-*tris*(4-sulphonatophenyl)porphyrinato] trisodium (**76**)
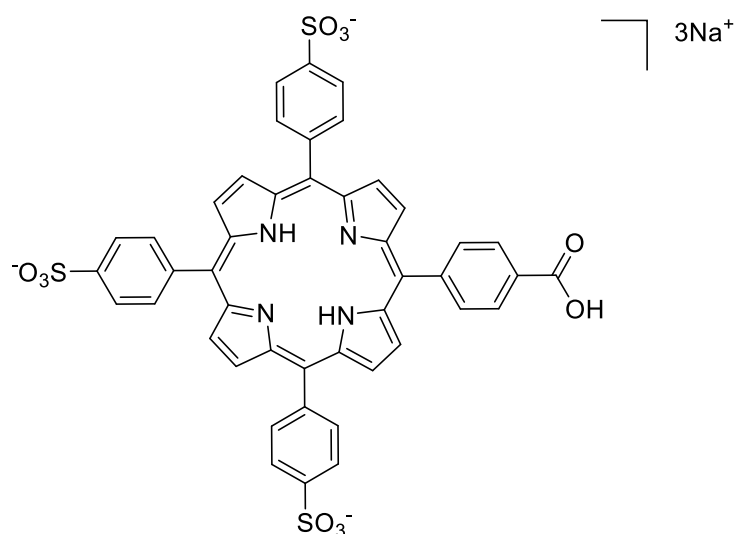
Compound **98** (500 mg, 0.76 mmol) was dissolved in chloroform (50 mL) in a 100-mL round bottom flask equipped with a rubber septum. Chlorosulphonic acid (12 mL, 130 mmol) was slowly added to the solution while stirring with a syringe. The resulting mixture was stirred at room temperature for 1 hour. Then the solution was cooled down with an ice bath, and a saturated solution of $NaHCO_3$ (150 mL) was slowly added to the mixture, causing the product to precipitate. After filtration on paper, the purple solid was suspended in water (150 mL) in a 250-mL round bottom flask. The solution was heated to reflux under stirring overnight. Once the solution was cooled down to room temperature, it was treated with compound **103**, to induce precipitation of the title compound. The resulting suspension was centrifuged and the precipitate was re-dissolved in acetone (120 mL). The resulting mixture was treated with sodium hexafluorophosphate, leading to flocculation of the title compound, successively centrifuged and collected after further crystallisation from methanol–diethyl ether (**76**). (0.65 g, 0.73 mmol, 96 %)

^{1}H-NMR (600 MHz, DMSO-d_6, 298 K) δ, ppm: 8.84-8.87 (m, 8H, β-H), 8.34 (d, 2H, J=7.2 Hz, 5-Ar-$H_{3,5}$), 8.19 (d, 6H, J=7.8 Hz, 10,15,20-Ar-$H_{3,5}$), 8.15 (d, 2H, J=7.8 Hz, 5-Ar-$H_{2,6}$), 8.07 (d, 6H, J=7.8 Hz, 10,15,20-Ar-$H_{2,6}$), -2.90 (br s, 2H, NH_{int})

^{13}C-NMR (150 MHz, DMSO-d_6, 298 K) δ, ppm: 169.9, 147.9, 141.5, 141.3, 139.8, 133.7, 133.5, 127.5, 124.2, 120.6, 119.7, 119.6

m.p. (°C): > 300

UV-Vis (H_2O, nm) λ_{max}: Soret, 416 (shoulder 433); Q bands, 519, 556, 586, 645; Log ϵ_{416}: 5.55

ESI-MS (-ve) (m/z): 298.35 [M − 3Na]$^{3-}$/3; 447.99 [M + H − 3Na]$^{2+}$/2; 897.00 [M + 2H − 3Na]$^-$

HPLC (method B), t_R: 8.43 min

<u>Synthesis of [5-(4-carboxyphenyl)-10,15,20-*tris*(4-sulphonatophenyl)porphyrinato]platinum (II) trisodium (**77**)</u>
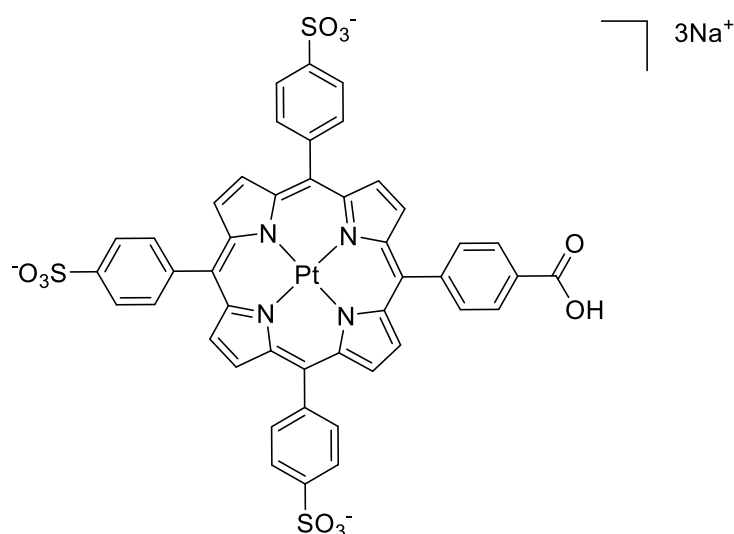
Compound **125** (100 mg, 0.21 mmol) was dissolved in DMSO (2 mL) and stirred at room temperature for 3 hours. Silver nitrate (72 mg, 0.42 mmol) and water (10 mL) were added to mixture, protected from light with tin foil, and stirred at room temperature for 3 hours. The mixture was subsequently centrifuged and then filtered to remove all silver chloride formed. The solution was transferred in a 35-mL microwave vial and compound **76** (100 mg, 0.10 mmol) was then added while stirring. The resulting mixture was flushed with argon for 10 minutes and exposed to microwave heating (200 °C, 300 W, 20 minutes). Once the solution was cooled down to room temperature, it was diluted with water (30 mL) and filtered through celite. The filtrate was treated with compound **103**, to induce precipitation of the title compound. The resulting suspension was centrifuged and the precipitate was re-dissolved in acetone (40 mL). The resulting mixture was treated with sodium hexafluorophosphate, leading to flocculation of the title compound, successively centrifuged and collected after further crystallisation from methanol–diethyl ether (**77**). (109 mg, 0.9 mmol, 91 %)

^{1}H-NMR (300 MHz, DMSO-d$_6$, 298 K) δ, ppm: 11.08 (br s, 1H, COO*H*), 8.75-8.78 (m, 8H, β-H), 8.37 (d, 2H, J=7.8 Hz, 5-Ar-H$_{2,6}$), 8.31 (d, 2H, J=7.5 Hz, 5-Ar-H$_{3,5}$), 8.15 (d, 6H, J= 7.2 Hz, 10,15,20-Ar-H$_{3,5}$), 8.05 (d, 6H, J= 7.2 Hz, 10,15,20-Ar-H$_{2,6}$)

^{13}C-NMR (75 MHz, DMSO-d$_6$, DEPTQ, 298 K) δ, ppm: 167.6, 147.8, 144.9, 140.7, 140.3, 140.3, 139.9, 134.0, 133.3, 131.3, 130.8, 130.0, 128.3, 124.5, 122.2, 121.5

m.p. (°C): > 300

UV-Vis (H$_2$O, nm) λ_{max}: Soret, 399; Q bands, 512, 542; Log ε_{399}: 5.17

ESI-MS (-ve) (m/z): 362.13 [M − 3Na]$^{3-}$/3; 544.37 [M + H − 3Na]$^{2-}$/2; 1090.99 [M + 2H − 3Na]$^-$

HPLC (method B), t$_R$: 8.26 min

<u>Synthesis of [5-(4-carboxyphenyl)-10,15,20-*tris*(4-sulphonatophenyl)porphyrinato]palladium (II) trisodium (**78**)</u>
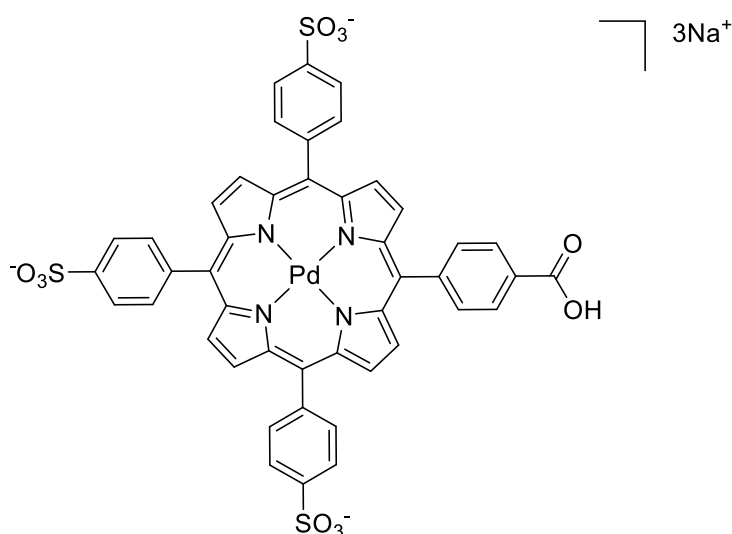
Compound **76** (100 mg, 0.10 mmol) was dissolved in water (10 mL) in a 35-mL microwave vial. Palladium acetate (69 mg, 0.31 mmol) was dissolved in methanol (3 mL) and added to the solution while stirring. The resulting mixture was flushed with argon for 10 minutes and exposed to microwave heating (150 °C, 250 W, 15 minutes). Once the solution was cooled down to room temperature, it was diluted with water (30 mL) and filtered through celite. The filtrate was treated with compound **103**, to induce precipitation of the title compound. The resulting suspension was centrifuged and the precipitate was re-dissolved in acetone (40 mL). The resulting mixture was treated with sodium hexafluorophosphate, leading to flocculation of the title compound, successively centrifuged and collected after further crystallisation from methanol–diethyl ether (**78**). (85 mg, 0.080 mmol, 80 %)

^{1}H-NMR (300 MHz, DMSO-d$_6$, 298 K) δ, ppm: 13.29 (br s, 1H, COO*H*), 8.79-8.85 (m, 8H, β-H), 8.38 (d, 2H, J=8.2 Hz, 5-Ar-H$_{2,6}$), 8.33 (d, 2H, J=8.2 Hz, 5-Ar-H$_{3,5}$), 8.15 (d, 6H, J=8.1 Hz, 10,15,20-Ar-H$_{3,5}$), 8.03 (d, 6H, J=8.1 Hz, 10,15,20-Ar-H$_{2,6}$)

^{13}C-NMR (75 MHz, DMSO-d$_6$, DEPTQ, 298 K) δ, ppm: 167.4, 148.0, 145.2, 140.9, 140.9, 140.8, 140.7, 140.4, 134.1, 133.3, 131.5, 131.2, 130.6, 128.0, 124.3, 121.7, 121.6, 120.7

m.p. (°C): > 300

UV-Vis (H$_2$O, nm) λ_{max}: Soret, 412; Q bands, 526; Log ε_{412}: 5.30

ESI-MS (-ve) (m/z): 332.60 [M − 3Na]$^{3-}$/3; 499.39 [M + H − 3Na]$^{2-}$/2

HPLC (method B), t$_R$: 8.33 min

Synthesis of 5,10,15,20-*tetrakis*-phenylporphyrin (**79a**)
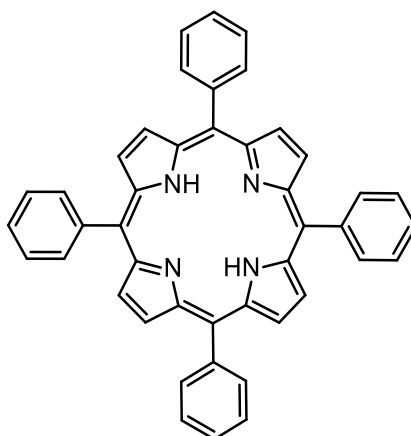
Benzaldehyde (15 mL, 147 mmol) was dissolved in propionic acid (220 mL) in a 500-mL 3 necks round bottom flask. The resulting mixture was heated to 70 °C under stirring. Pyrrole (10 mL, 144 mmol) was dissolved in 30 mL of propionic acid and added drop-wise to the solution over a 30 minutes time. The resulting mixture was heated to reflux for 1 hour protected from light. Once the solution was cooled down to room temperature, the solvent was removed under reduced pressure and the crude mixture was dissolved in CH_2Cl_2 and filtered on silica gel. The solvent was then evaporated under reduced pressure and the crude product was isolated by re-crystallisation from CH_2Cl_2/methanol, yielding **79a** as purple crystalline solid (3.15 g, 5.1 mmol, 15 %).

^{1}H-NMR (300 MHz, $CDCl_3$, 298 K) δ, ppm: 8.88 (s, 8H, β-H), 8.24-8.27 (m, 8H, Ar-H_o), 7.76-7.79 (m, 12H, Ar-H_m + Ar-H_p), -2.71 (s, 2H, NH_{int})

^{13}C-NMR (75 MHz, $CDCl_3$, 298 K) δ, ppm: 148.1, 147.9, 145.8, 142.2, 134.7, 128.6, 128.0, 126.9, 120.6, 118.5

m.p. (°C): > 300

UV-Vis (CH_2Cl_2, nm) λ_{max}: Soret, 417; Q bands, 515, 550, 590, 647; Log ε_{417}: 5.91

ESI-MS (+ve) (*m/z*): 615.65 [M+H]$^+$

Adler-Longo synthesis of 5,10,15,20-*tetrakis*[3,5-bis(trifluoromethyl)phenyl]porphyrin (**79b**)
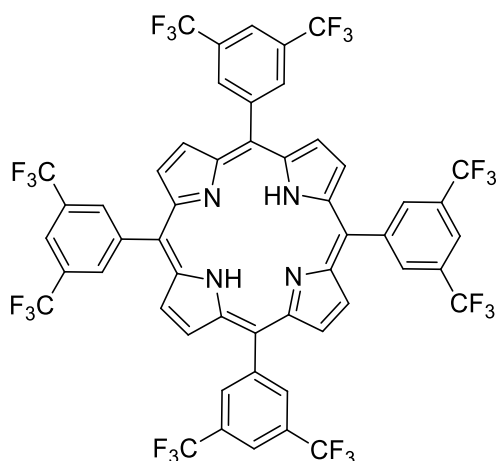
3,5-Bis(trifluoromethyl)benzaldehyde (4 mL, 29 mmol) was dissolved in propionic acid (120 mL) in a 250-mL 3 necks round bottom flask. The resulting mixture was heated to 50 °C under stirring. Pyrrole (2 mL, 29 mmol) was dissolved in 10 mL of propionic acid and added drop-wise to the solution in a 30 minutes time. The resulting mixture was heated to reflux for 1 hour protected from light. Once the solution was cooled down to room temperature, the solvent was removed under reduced pressure and the crude mixture was dissolved in CH_2Cl_2 and filtrated on silica gel. The solvent was then evaporated under reduced pressure and the crude product was isolated by re-crystallisation from CH_2Cl_2/methanol, yielding **79b** as brown solid (1.27 g, 1.1 mmol, 15 %).

^{1}H-NMR (300 MHz, CDCl$_3$, 298 K) δ, ppm: 8.80 (s, 8H, β-H), 8.69 (br s, 8H, Ar-H$_o$), 8.39 (br s, 4H, Ar-H$_p$), -2.86 (s, 2H, NH$_{int}$)

^{13}C-NMR (75 MHz, CDCl$_3$, 298 K) δ, ppm: 144.2, 134.4, 131.5, 131.2, 125.2, 123.6, 123.1, 118.3

^{19}F-NMR (564 MHz, CDCl$_3$, 298 K) δ, ppm: -62.4 (s, 24F)

m.p. (°C): > 300

UV-Vis (CH$_2$Cl$_2$, nm) λ_{max}: Soret, 417; Q bands, 512, 545, 587; 642 Log ε_{417}: 5.71

ESI-MS (+ve) (m/z): 1158.63 [M]$^+$, 580.01 [M + 2H]$^{2+}$/2

Lindsey Synthesis of 5,10,15,20-*tetrakis*[3,5-bis(trifluoromethyl)phenyl]porphyrin (**79b**)
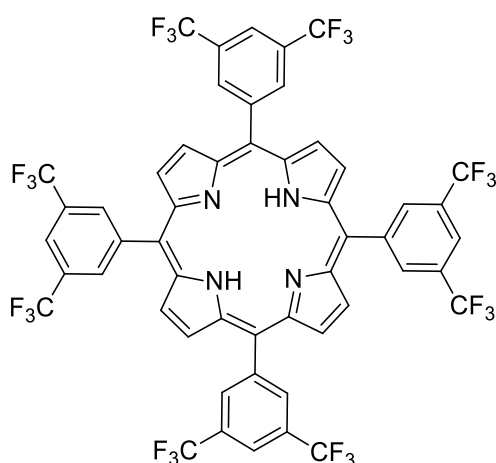
3,5-Bis(trifluoromethyl)benzaldehyde (1 mL, 6.4 mmol), pyrrole (0.5 mL, 7.2 mmol) were dissolved in CH_2Cl_2 (300 mL) in a 500 mL 3 necks round bottom flask. The resulting mixture was stirred for 30 minutes under a nitrogen atmosphere. $BF_3 \cdot Et_2O$ (0.3 mL, 2.4 mmol, 30% to aldehyde) was added. The resulting mixture was heated to 40 °C for 4 hours protected from light. After this time, chloranil (1.7 g, 7 mmol) was added to the mixture and the reaction was heated to reflux overnight (15 hours). The mixture was allowed to cool down to room temperature, washed with a saturated solution of $NaHCO_3$ (300 mL) and dried over anhydrous Na_2SO_4. The organic phase was separated and filtrated on silica gel. The solvent was then evaporated under reduced pressure and the crude product was isolated by re-crystallisation from CH_2Cl_2/methanol, yielding **79b** as brown solid (0.63 g, 0.55 mmol, 34 %).

^{1}H-NMR (300 MHz, $CDCl_3$, 298 K) δ, ppm: 8.80 (s, 8H, β-H), 8.69 (br s, 8H, Ar-H_o), 8.39 (br s, 4H, Ar-H_p), -2.86 (s, 2H, NH_{int})

^{13}C-NMR (75 MHz, $CDCl_3$, 298 K) δ, ppm: 144.2, 134.4, 131.5, 131.2, 125.2, 123.6, 123.1, 118.3

^{19}F-NMR (564 MHz, $CDCl_3$, 298 K) δ, ppm: -62.4 (s, 24F)

m.p. (°C): > 300

UV-Vis (CH_2Cl_2, nm) λ_{max}: Soret, 417; Q bands, 512, 545, 587; 642 Log ε_{417}: 5.71

ESI-MS (+ve) (m/z): 1158.63 $[M]^+$, 580.01 $[M + 2H]^{2+}/2$

Adler-Longo synthesis of 5,10,15,20-*tetrakis*(pentafluorophenyl)porphyrin (**79c**)
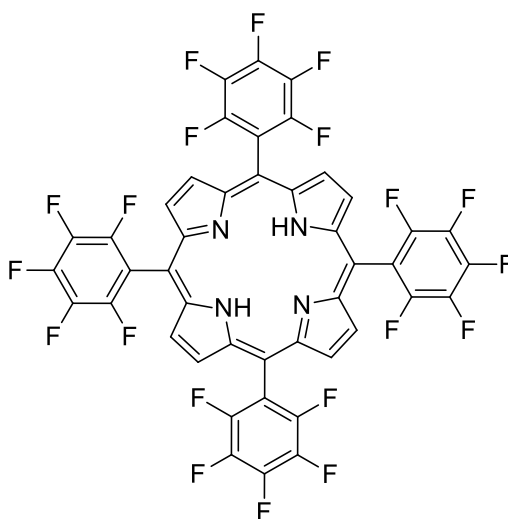
2,3,4,5,6-pentafluorobenzaldehyde (14 g, 72 mmol) was dissolved in propionic acid (500 mL) in a 1 L 3 necks round bottom flask. The resulting mixture was heated to reflux under stirring. Pyrrole (5 mL, 72 mmol) was dissolved in 10 mL of propionic acid and added drop-wise to the solution in a 30 minutes time. The resulting mixture was heated to reflux for 1 hour protected from light. Once the solution was cooled down to room temperature, the solvent was removed under reduced pressure and the crude mixture was dissolved in CH_2Cl_2 and filtrated on silica gel. The solvent was then evaporated under reduced pressure and the crude product was isolated by re-crystallisation from CH_2Cl_2/methanol, yielding **79c** as purple crystalline solid (0.63 g, 0.65 mmol, 3.6 %).

^{1}H-NMR (300 MHz, $CDCl_3$, 298 K) δ, ppm: 8.91 (s, 8H, β-H), -2.91 (s, 2H, NH_{int})

^{13}C-NMR (150 MHz, $CDCl_3$, 298 K) δ, ppm: 147.6, 145.9, 143.4, 141.6, 138.6, 136.9, 131.4, 115.8, 115.7, 115.6, 103.8

^{19}F-NMR (564 MHz, $CDCl_3$, 298 K) δ, ppm: -136.5 (dd, J_o=7.8 Hz, J_p=24.6 Hz, F_o) -151.2 (t, 4F, J_o=22.2 Hz, F_p), -161.3 (dt, 8F, J_p=7.8Hz, J_o=24 Hz, F_m)

m.p. (°C): > 300

UV-Vis (CH_2Cl_2, nm) λ_{max}: Soret, 410; Q bands, 504, 539, 582; 638 Log ε_{410}: 5.40

ESI-MS (+ve) (m/z): 974.07 [M]$^+$

Lindsey synthesis of 5,10,15,20-*tetrakis*(pentafluorophenyl)porphyrin (**79c**)
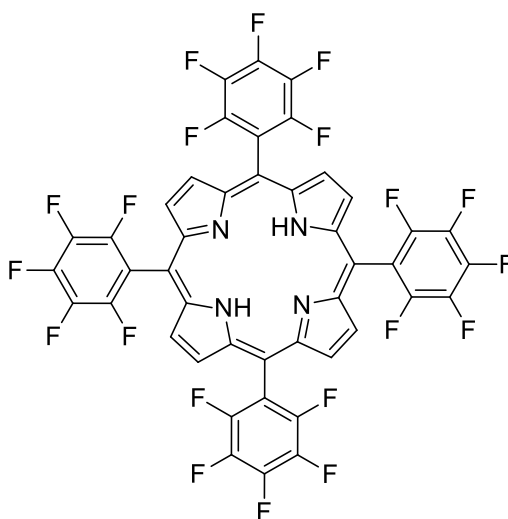
2,3,4,5,6-pentafluorobenzaldehyde (2.5 g, 12.7 mmol) and pyrrole (1.0 mL, 14.4 mmol) were dissolved in CH_2Cl_2 (600 mL) in a 1 L 3 necks round bottom flask. The resulting mixture was stirred for 30 minutes under a nitrogen atmosphere. $BF_3·Et_2O$ (0.5 mL, 4 mmol, 30 % to aldehyde) was added. The resulting mixture was heated to 40 °C for 4 hours protected from light. After this time, chloranil (3.5 g, 14 mmol) was added to the mixture and the reaction was heated to reflux overnight (15 hours). The mixture was allowed to cool down to room temperature, washed with a saturated solution of $NaHCO_3$ (500 mL) and dried over anhydrous Na_2SO_4. The organic phase was separated and filtrated on silica gel. The solvent was then evaporated under reduced pressure and the crude product was isolated by re-crystallisation from CH_2Cl_2/methanol, yielding **79c** as purple crystalline solid (1.17 g, 1.2 mmol, 38 %).

^{1}H-NMR (300 MHz, $CDCl_3$, 298 K) δ, ppm: 8.91 (s, 8H, β-H), -2.91 (s, 2H, NH_{int})

^{13}C-NMR (150 MHz, $CDCl_3$, 298 K) δ, ppm: 147.6, 145.9, 143.4, 141.6, 138.6, 136.9, 131.4, 115.8, 115.7, 115.6, 103.8

^{19}F-NMR (564 MHz, $CDCl_3$, 298 K) δ, ppm: -136.5 (dd, J_o=7.8 Hz, J_p=24.6 Hz, F_o) -151.2 (t, 4F, J_o=22.2 Hz, F_p), -161.3 (dt, 8F, J_p=7.8Hz, J_o=24 Hz, F_m)

m.p. (°C): > 300

UV-Vis (CH_2Cl_2, nm) λ_{max}: Soret, 410; Q bands, 504, 539, 582; 638 Log ε_{410}: 5.40

ESI-MS (+ve) (m/z): 974.07 $[M]^+$

Synthesis of 5,10,15,20-*tetrakis*(3-methoxyphenyl)porphyrin (**79d**)
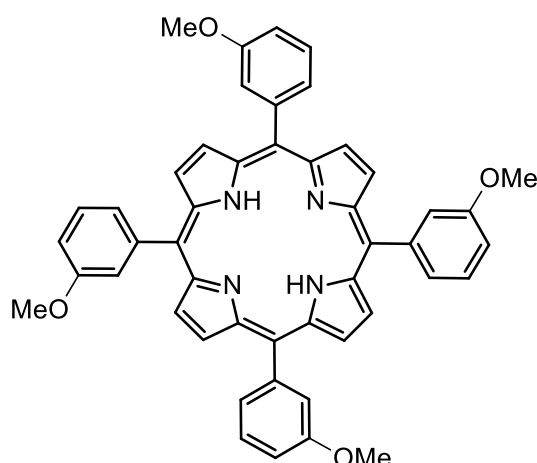
3-methoxybenzaldehyde (8.8 mL, 72 mmol) was dissolved in propionic acid (500 mL) in a 1 L 3 necks round bottom flask. The resulting mixture was heated to reflux under stirring. Pyrrole (5 mL, 72 mmol) was dissolved in 10 mL of propionic acid and added drop-wise to the solution in a 30 minutes time. The resulting mixture was heated to reflux for 1 hour protected from light. Once the solution was cooled down to room temperature, the solvent was removed under reduced pressure and the crude mixture was dissolved in CH_2Cl_2 and filtrated on silica gel. The solvent was then evaporated under reduced pressure and the crude product was isolated by re-crystallisation from CH_2Cl_2/methanol, yielding **79d** as purple crystalline solid (1.85 g, 2.5 mmol, 14 %).

^{1}H-NMR (300 MHz, CDCl$_3$, 298 K) δ, ppm: 8.90 (s, 8H, β-H), 7.80-7.84 (br m, 8H, Ar-H$_o$), 7.65 (t, 4H, J=9.0 Hz, Ar-H$_p$), 7.32-7.36 (dd, 4H, Ar-H$_m$), 3.99 (s, 12H, OCH$_3$), -2.77 (s, 2H, NH$_{int}$)

^{13}C-NMR (150 MHz, CDCl$_3$, 298 K) δ, ppm: 158.1, 143.6, 131.1, 127.8, 127.6, 120.6, 120.0, 113.7, 55.7

m.p. (°C): > 300

UV-Vis (CH$_2$Cl$_2$, nm) λ_{max}: Soret, 422; Q bands, 515, 549, 591, 647; Log ε_{422}: 5.59

ESI-MS (+ve) (m/z): 735.29 [M+H]$^{+}$

Synthesis of 5,10,15,20-*tetrakis*(3,5-dimethoxyphenyl)porphyrin (**79e**)
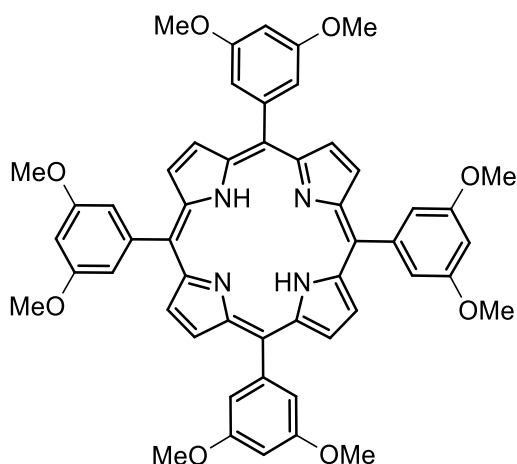
3,5-dimethoxybenzaldehyde (12 g, 72 mmol) was dissolved in propionic acid (500 mL) in a 1 L 3 necks round bottom flask. The resulting mixture was heated to reflux under stirring. Pyrrole (5 mL, 72 mmol) was dissolved in 10 mL of propionic acid and added drop-wise to the solution in a 30 minutes time. The resulting mixture was heated to reflux for 1 hour protected from light. Once the solution was cooled down to room temperature, the solvent was removed under reduced pressure and the crude mixture was dissolved in CH_2Cl_2 and filtrated on silica gel. The solvent was then evaporated under reduced pressure and the crude product was isolated by re-crystallisation from CH_2Cl_2/methanol, yielding **79e** as purple crystalline solid (2.08 g, 2.4 mmol, 14 %).

^{1}H-NMR (300 MHz, CDCl$_3$, 298 K) δ, ppm: 8.94 (s, 8H, β-H), 7.40-7.41 (d, 8H, ^{4}J=2.4 Hz, Ar-H$_o$), 6.90 (t, 4H, ^{4}J=2.4 Hz, Ar-H$_p$), 3.96 (s, 24H, OCH$_3$), -2.82 (s, 2H, NH$_{int}$),

^{13}C-NMR (150 MHz, CDCl$_3$, 298 K) δ, ppm: 159.0 144.2, 131.1, 120.0, 114.0, 100.3, 55.8

m.p. (°C): > 300

UV-Vis (CH$_2$Cl$_2$, nm) λ_{max}: Soret, 421; Q bands, 514, 549, 589, 645; Log ε_{421}: 5.61

ESI-MS (+ve) (m/z): 855.32 [M+H]$^+$

Synthesis of 5,10,15,20-*tetrakis*(3-pyridyl)porphyrin (**79f**)

3-pyridinecarboxaldehyde (13 mL, 138 mmol) was dissolved in propionic acid (220 mL) in a 500-mL 3 necks round bottom flask. The resulting mixture was heated to 70 °C under stirring. Pyrrole (10 mL, 144 mmol) was dissolved in 30 mL of propionic acid and added drop-wise to the solution in a 30 minutes time. The resulting mixture was heated to reflux for 1 hour protected from light. Once the solution was cooled down to room temperature, the solvent was removed under reduced pressure and the crude mixture was dissolved in CH_2Cl_2 and filtrated on silica gel. The solvent was then evaporated under reduced pressure and the crude product was isolated by re-crystallisation from CH_2Cl_2/methanol, yielding **79f** as purple crystalline solid (2.61 g, 4.22 mmol, 12 %).

^{1}H-NMR (300 MHz, $CDCl_3$, 298 K) δ, ppm: 9.50-9.51 (br d, 4H, $^4J_{2\text{-}6}$=1.5 Hz, Py-H$_2$), 9.07-9.09 (dd, 4H, $^3J_{5\text{-}6}$=5.1 Hz, $^4J_{2\text{-}6}$=1.5 Hz, Py-H$_6$), 8.91 (s, 8H, β-H), 8.55-8.58 (d, 4H, $^3J_{4\text{-}5}$=7.8 Hz, Py-H$_4$), 7.76-7.80 (dd, 4H, $^3J_{4\text{-}5}$=7.8 Hz, $^3J_{5\text{-}6}$=5.1 Hz, Py-H$_5$), -2.75 (s, 2H, NH$_{int}$)

^{13}C-NMR (150 MHz, $CDCl_3$, 298 K) δ, ppm: 153.7, 149.5, 141.1, 137.8, 131.5, 122.2, 116.9

m.p. (°C): > 300

UV-Vis (CH_2Cl_2, nm) λ_{max}: Soret, 418; Q bands, 515, 550, 590, 647; Log ε_{418}: 6.93

ESI-MS (+ve) (m/z): 619.57 [M+H]$^+$

Synthesis of [2-nitro-5,10,15,20-*tetrakis*-phenylporphyrinato]copper (II) (**80a**)
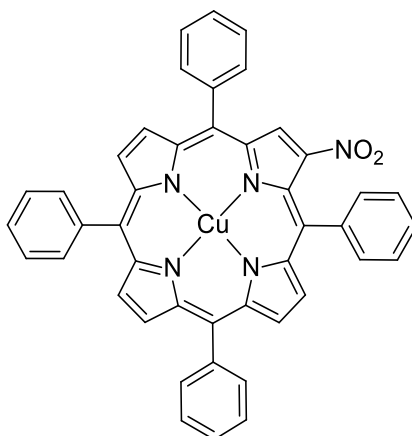
Compound **79a** (500 mg, 0.81 mmol) was dissolved in $CHCl_3$ (500 mL) in a 1 L round bottom flask. $Cu(NO_3)_2 \cdot 3H_2O$ (500 mg, 2.07 mmol) was dissolved in acetic anhydride (20 mL) and added to the mixture, together with acetic acid (2 mL, 0.035 mmol). The solution was then stirred at room temperature, and the reaction was monitored with TLC. The reaction was stopped as soon as traces of di-nitrated product were detected, after 5 hours of stirring. A saturated solution of $NaHCO_3$ (500 mL) was then added to the mixture. The organic phase was separated, washed with water, and dried over anhydrous Na_2SO_4. The solvent was then removed under reduced pressure and the desired product was isolated by flash chromatography (silica, eluent: CH_2Cl_2-hexane 4:6). The solid was then re-crystallised form CH_2Cl_2/hexane as a crystalline dark purplish solid (**80a**) (0.52 g, 0.72 mmol, 89 %).

m.p. (°C): > 300

UV-Vis (CH_2Cl_2, nm) λ_{max}: Soret, 420; Q bands, 545, 590; Log ε_{420}: 5.25

ESI-MS (+ve) (*m/z*): 721.26 [M+H]$^+$

Synthesis of 2-nitro-5,10,15,20-*tetrakis*-phenylporphyrin (**80a'**)
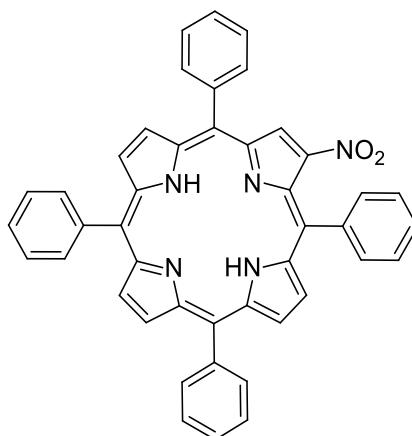
Compound **80a** (100 mg, 0.14 mmol) was dissolved in TFA (5 mL) in a 50-mL round bottom flask, and then H_2SO_4 (500 µl) was added. The solution was stirred for 1hour at room temperature. Then the solution was cooled down with an ice bath, and a saturated solution of $NaHCO_3$ (150 mL) was slowly added to the mixture, causing the product to precipitate. After filtration on paper, the purple solid was re-dissolved in CH_2Cl_2, washed with water and dried over anhydrous Na_2SO_4. The solvent was then removed under reduced pressure and the crude product was isolated by re-crystallisation from CH_2Cl_2/methanol, yielding a black crystalline solid (86 mg, 0.13 mmol, 93 %).

^{1}H-NMR (300 MHz, $CDCl_3$, 298 K) δ, ppm: 8.93-9.10 (m, 5H, β-H), 8.76 (s, 2H, β-H), 8.24-8.31 (m, 8H, Ar-H_o), 7.72-7.84 (m, 12H, Ar-H_m + Ar-H_p) -2.56 (s, 2H, NH_{int})

^{13}C-NMR (75 MHz, $CDCl_3$, 298 K, DEPTQ) δ, ppm: 156.7, 156.5, 153.3, 146.2, 142.6, 120.3, 141.8, 141.5, 141.3, 140.5, 140.4, 139.6, 138.2, 135.6, 135.2 134.9, 134.7, 132.0, 130.1, 129.6, 129.1, 128.7, 128.6, 128.4, 128.2, 127.2, 127.1, 127.1, 127.0, 123.2, 121.0, 120.8, 120.3

m.p. (°C): > 300

UV-Vis (CH_2Cl_2, nm) λ_{max}: Soret, 427; Q bands: 526, 564, 605, 665; Log ε_{427}: 5.80

ESI-MS (+ve) (*m/z*): 660.83 [M+H]$^+$

Synthesis of {2-nitro-5,10,15,20-*tetrakis*[3,5-bis(trifluoromethyl)phenyl]porphyrinato}zinc (II) (**80b**)
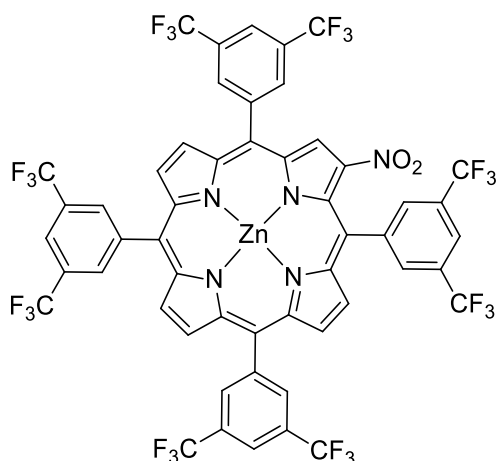
Compound **79b** (500 mg, 0.43 mmol) was dissolved in CHCl$_3$ (500 mL) in a 1 L round bottom flask. Zn(NO$_3$)$_2$·6H$_2$O (500 mg, 1.68 mmol) was dissolved in acetic anhydride (20 mL) under sonication and added to the mixture, together with acetic acid (2 mL, 0.035 mmol). The solution was then stirred at room temperature, and the reaction was monitored with TLC (CH$_2$Cl$_2$:hexane 1:1). The reaction was stopped as soon as traces of di-nitrated product were detected, after 1 hour and 15 minutes of stirring. A saturated solution of NaHCO$_3$ (350 mL) was then added to the mixture. The organic phase was separated, washed with water, and dried over anhydrous Na$_2$SO$_4$. The solvent was then removed under reduced pressure and the desired product was isolated by flash chromatography (silica, eluent: CH$_2$Cl$_2$-hexane 4:6, then 1:1, then pure CH$_2$Cl$_2$). The solid was then re-crystallised form CH$_2$Cl$_2$/hexane as a crystalline green solid (**80b**) (0.47 g, 0.37 mmol, 86 %).

^{1}H-NMR (300 MHz, CDCl$_3$, 298 K) δ, ppm: 9.11 (s, 1H, β-H), 8.83-8.90 (m, 6H, β-H), 8.66 (br s, 6H, Ar-H$_o$), 8.63 (br s, 2H, Ar-H$_o$), 8.41 (br s, 1H, Ar-H$_p$), 8.39 (br s, 2H, Ar-H$_p$), 8.32 (br s, 1H, Ar-H$_p$)
^{13}C-NMR (75 MHz, CDCl$_3$, 298 K) δ, ppm: 134.3, 133.7, 133.6, 133.5, 133.4, 133.2, 133.1, 133.0, 128.3, 122.8, 122.6, 122.4
^{19}F-NMR (564 MHz, CDCl$_3$, 298 K) δ, ppm: -62.2 (s, 6F), -62.3 (br s, 12F), -62.5 (s, 6F)
m.p. (°C): > 300
UV-Vis (CH$_2$Cl$_2$, nm) λ$_{max}$: Soret, 430; Q bands, 559, 605 Log ε$_{430}$: 5.11
ESI-MS (+ve) (m/z): 1265.54 [M]$^+$
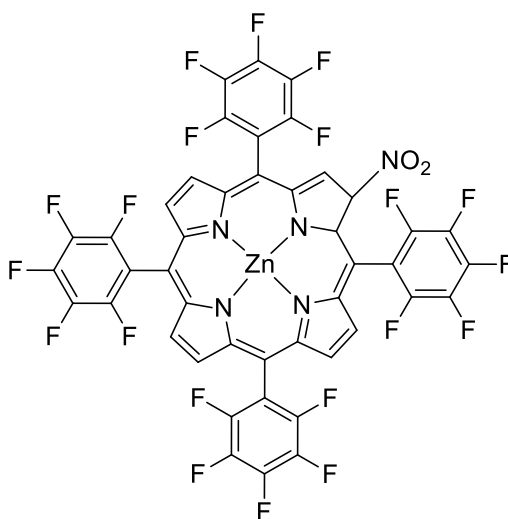
Compound **79c** (500 mg, 0.51 mmol) was dissolved in $CHCl_3$ (500 mL) in a 1 L round bottom flask. $Zn(NO_3)_2 \cdot 6H_2O$ (500 mg, 1.68 mmol) was dissolved in acetic anhydride (20 mL) under sonication and added to the mixture, together with acetic acid (2 mL, 0.035 mmol). The solution was then stirred at room temperature, and the reaction was monitored with TLC. The reaction was stopped as soon as traces of di-nitrated product were detected, after 2 hours stirring. A saturated solution of $NaHCO_3$ (500 mL) was then added to the mixture. The organic phase was separated, washed with water, and dried over anhydrous Na_2SO_4. The solvent was then removed under reduced pressure and the desired product was isolated by flash chromatography (silica, eluent: CH_2Cl_2-hexane 1:1, then 7:3). The solid was then re-crystallised form CH_2Cl_2/hexane as a crystalline green/purplish solid (**80c**) (0.47 g, 0.43 mmol, 83 %).

^{1}H-NMR (300 MHz, $CDCl_3$, 298 K) δ, ppm: 9.27 (s, 1H, β-H), 8.93-8.99 (m, 6H, β-H)
^{13}C-NMR (75 MHz, $CDCl_3$, 298 K) δ, ppm: 134.0, 133.3, 133.2, 133.1, 132.5, 127.9
^{19}F-NMR (564 MHz, $CDCl_3$, 298 K) δ, ppm: -136.3 (dd, 2F, F_o), -136.6 (dd, 4F, F_o), -137.3 (dd, 2F, F_o), -150.1 (t, 1F, F_p), -150.3 (t, 1F, F_p), -150.9 (t, 2F, F_p), -160.6 (dt, 2F, F_m), -161.0 (dt, 4F, F_m), -161.4 (dt, 2F, F_m)
m.p. (°C): > 300
UV-Vis (CH_2Cl_2, nm) λ_{max}: Soret, 422; Q bands, 547, 577; Log ε_{422}: 5.60
ESI-MS (+ve) (m/z): 1081.16 $[M+H]^+$

Synthesis of [2-nitro-5,10,15,20-*tetrakis*(3-methoxyphenyl)porphyrinato]copper (II) (**80d**)
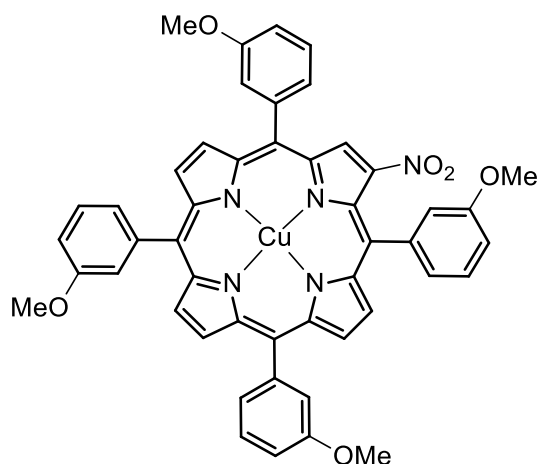
Compound **79d** (500 mg, 0.68 mmol) was dissolved in CHCl$_3$ (500 mL) in a 1 L round bottom flask. Cu(NO$_3$)$_2$·3H$_2$O (500 mg, 2.07 mmol) was dissolved in acetic anhydride (20 mL) and added to the mixture, together with acetic acid (2 mL, 0.035 mmol). The solution was then stirred at room temperature, and the reaction was monitored with TLC. The reaction was stopped as soon as traces of di-nitrated product were detected, after 1 hour stirring. A saturated solution of NaHCO$_3$ (500 mL) was then added to the mixture. The organic phase was separated, washed with water, and dried over anhydrous Na$_2$SO$_4$. The solvent was then removed under reduced pressure and the desired product was isolated by flash chromatography (silica, eluent: CH$_2$Cl$_2$-hexane 1:1 with 2 % Et$_2$O). The solid was then re-crystallised form CH$_2$Cl$_2$/methanol as a crystalline purple solid (**80d**) (0.46 g, 0.55 mmol, 81 %).

m.p. (°C): 198-200

UV-Vis (CH$_2$Cl$_2$, nm) λ_{max}: Soret, 427; Q bands, 551, 597; Log ε_{427}: 5.23

ESI-MS (+ve) (*m/z*): 841.20 [M+H]$^+$

Synthesis of 2-nitro-5,10,15,20-*tetrakis*(3-methoxyphenyl)porphyrin (**80d'**)
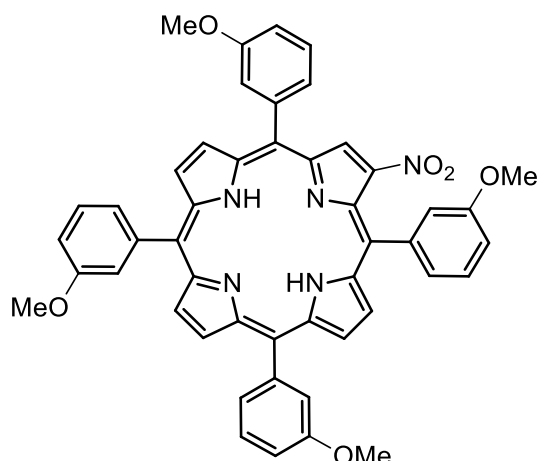
Compound **80d** (100 mg, 0.12 mmol) was dissolved in TFA (5 mL) in a 50-mL round bottom flask, and then H_2SO_4 (500 µl) was added. The solution was stirred for 1 hour at room temperature. Then the solution was cooled down with an ice bath, and a saturated solution of $NaHCO_3$ (150 mL) was slowly added to the mixture, causing the product to precipitate. After filtration on paper, the purple solid was re-dissolved in CH_2Cl_2, washed with water and dried over anhydrous Na_2SO_4. The solvent was then removed under reduced pressure and the crude product was isolated by re-crystallisation from CH_2Cl_2/methanol, yielding a black crystalline solid (82 mg, 0.11 mmol, 88 %).

^{1}H-NMR (300 MHz, CDCl$_3$, 298 K) δ, ppm: 9.10-9.13 (m, 2H, β-H), 9.00-9.02 (m, 1H, β-H), 8.96-8.97 (m, 2H, β-H), 8.78-8.79 (m, 2H, β-H), 7.78-7.89 (m, 8H, Ar-H$_o$), 7.61-7.69 (m, 4H, Ar-H$_p$), 7.32-7.37 (m, 4H, Ar-H$_m$), 4.01-4.02 (dd, 12H, OCH$_3$), -2.62 (s, 2H, NH$_{int}$)
^{13}C-NMR (75 MHz, CDCl$_3$, 298 K, DEPTQ) δ, ppm: 156.7, 156.7, 153.5, 151.6, 151.1, 150.6, 150.4, 149.9, 149.7, 149.4, 149.4, 149.3, 143.1, 142.5, 142.4, 142.2, 136.1, 135.6, 135.4, 51.3
m.p. (°C): 291-293
UV-Vis (CH$_2$Cl$_2$, nm) λ_{max}: Soret, 430; Q bands: 526, 602, 662; Log ϵ_{430}: 5.56
ESI-MS (+ve) (m/z): 780.26 [M+H]$^+$

Synthesis of [2-nitro-5,10,15,20-*tetrakis*(3,5-dimethoxyphenyl)porphyrinato]copper (II) (**80e**)
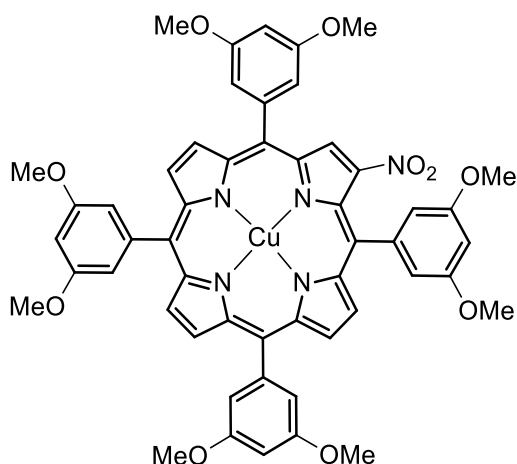
Compound **79c** (500 mg, 0.59 mmol) was dissolved in $CHCl_3$ (500 mL) in a 1 L round bottom flask. $Cu(NO_3)_2 \cdot 3H_2O$ (500 mg, 2.07 mmol) was dissolved in acetic anhydride (20 mL) and added to the mixture, together with acetic acid (2 mL, 0.035 mmol). The solution was then stirred at room temperature, and the reaction was monitored with TLC. The reaction was stopped as soon as traces of di-nitrated product were detected, after 5 hours stirring. A saturated solution of $NaHCO_3$ (500 mL) was then added to the mixture. The organic phase was separated, washed with water, and dried over anhydrous Na_2SO_4. The solvent was then removed under reduced pressure and the desired product was isolated by flash chromatography (silica, eluent: CH_2Cl_2-hexane 7:3). The solid was then re-crystallised form CH_2Cl_2/hexane as a crystalline dark purple solid (**80e**) (0.51 g, 0.53 mmol, 90 %).

m.p. (°C): > 300

UV-Vis (CH_2Cl_2, nm) λ_{max}: Soret, 427; Q bands, 551, 596; Log ε_{427}: 5.15

ESI-MS (+ve) (m/z): 961.22 [M+H]$^+$

Synthesis of 2-nitro-5,10,15,20-*tetrakis*(3,5-dimethoxyphenyl)porphyrin (**80e'**)
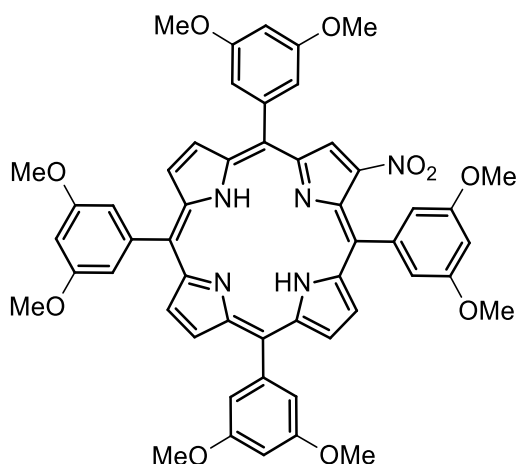
Compound **80e** (100 mg, 0.10 mmol) was dissolved in TFA (5 mL) in a 50-mL round bottom flask, and then H_2SO_4 (500 μl) was added. The solution was stirred for 1hour at room temperature. Then the solution was cooled down with an ice bath, and a saturated solution of $NaHCO_3$ (150 mL) was slowly added to the mixture, causing the product to precipitate. After filtration on paper, the purple solid was re-dissolved in CH_2Cl_2, washed with water and dried over anhydrous Na_2SO_4. The solvent was then removed under reduced pressure and the crude product was isolated by re-crystallisation from CH_2Cl_2/methanol, yielding a black crystalline solid (79 mg, 0.09 mmol, 87 %).

^{1}H-NMR (300 MHz, CDCl$_3$, 298 K) δ, ppm: 9.17-9.19 (m, 2H, β-H), 9.04-9.05 (d, 1H, J=3.9 Hz, β-H), 9.00-9.01 (d, 2H, J=4.2 Hz, β-H), 8.93 (t, 2H, J=3.6 Hz, β-H), 7.46 (d, 2H, J=1.8 Hz, Ar-H$_o$), 7.39 (dd, 6H, J=1.8 Hz, J=3.6 Hz, Ar-H$_o$), 6.92 (m, 3H, Ar-H$_p$), 6.89 (t, 1H, J=1.8 Hz, Ar-H$_p$), 3.99 (dd, 24H, J=2.1 Hz, J=3 Hz OCH$_3$), -2.62 (s, 2H, NH$_{int}$)

^{13}C-NMR (75 MHz, CDCl$_3$, 298 K) δ, ppm: 156.5, 156.5, 153.32, 151.4, 151.0, 150.3, 149.7, 136.7, 135.6, 135.6, 135.4, 122.5, 121.9, 121.7

m.p. (°C): 291-293

UV-Vis (CH$_2$Cl$_2$, nm) λ$_{max}$: Soret, 434; Q bands: 530, 606, 665; Log ε$_{434}$: 5.38

ESI-MS (+ve) (m/z): 900.31 [M+H]$^+$

Synthesis of [2-(1-acetyl-1-ethoxycarbonylmethyl)-5,10,15,20-*tetrakis*-phenylporphyrinato]copper II (**81a'**)
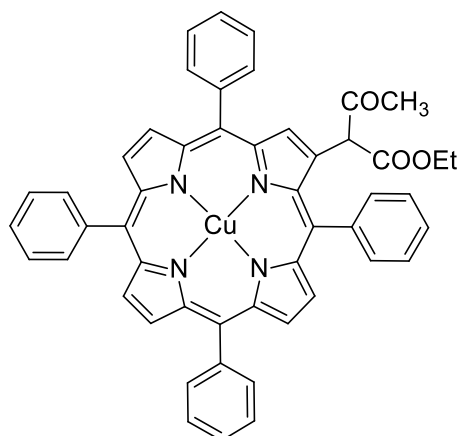
Ethyl acetoacetate (0.88 mL, 6.93 mmol) and K_2CO_3 (958 mg, 6.93 mmol) were dissolved in a 50-mL round bottom flask with DMSO (15 mL), and sonicated for 15 minutes. Compound **80a** (500 mg, 0.69 mmol) was added to the mixture and stirred for 1 hour at room temperature. The mixture was then poured in 250 mL of brine solution, causing the product to precipitate. After filtration on paper, the purple solid was re-dissolved in CH_2Cl_2, washed with water and dried over anhydrous Na_2SO_4. The solvent was then removed under reduced and the desired product was isolated by flash chromatography (silica, eluent: CH_2Cl_2-hexane 4:6). The solid was then re-crystallised form CH_2Cl_2/methanol as a crystalline dark red solid (0.49 g, 0.61 mmol, 88 %).

m.p. (°C): 255-258

UV-Vis (CH_2Cl_2, nm) λ_{max}: Soret, 416; Q bands, 539; Log ε_{416}: 5.45

ESI-MS (+ve) (m/z): 803.81 $[M]^+$

Synthesis of 2-(1-acetyl-1-ethoxycarbonylmethyl)-5,10,15,20-*tetrakis*-phenylporphyrin (**81a**)
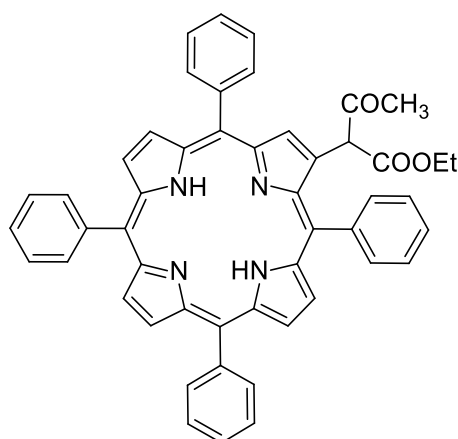
Compound **Cu81a** (100 mg, 0.125 mmol) was dissolved in TFA (5 mL) in a 50-mL round bottom flask, and then H_2SO_4 (500 μl) was added. The solution was stirred for 10 minutes at room temperature. Then the solution was cooled down with an ice bath, and a saturated solution of $NaHCO_3$ (150 mL) was slowly added to the mixture, causing the product to precipitate. After filtration on paper, the purple solid was re-dissolved in CH_2Cl_2, washed with water and dried over anhydrous Na_2SO_4. The solvent was then removed under reduced pressure and the crude product was isolated by re-crystallisation from CH_2Cl_2/methanol, yielding a dark purple crystalline solid (**81a**) (87 mg, 0.117 mmol, 94 %).

^{1}H-NMR (300 MHz, $CDCl_3$, 298 K) δ, ppm: 12.85 (s, 1H, OH), 8.80-8.87 (m, 4H, β-H), 8.76 (d, 1H, β-H), 8.62-8.65 (m, 2H, β-H), 8.22 (br s, 6H, Ar-H$_o$), 8.01 (d, 1H, Ar-H$_o$), 7.91 (d, 1H, Ar-H$_o$), 7.56-7.77 (m, 12H, Ar-H$_m$ + Ar-H$_p$), 3.92-4.13 (m, 2H, OCH_2CH$_3$), 1.80 (s, 3H, CH$_3$), 0.85-0.89 (m, 3H, OCH$_2$CH_3), -2.68 (s, 2H, NH$_{int}$)

^{13}C-NMR (150 MHz, $CDCl_3$, 298 K) δ, ppm: 173.5, 172.2, 142.7, 142.1, 134.8, 134.8, 132.9, 132.8, 128.1, 127.9, 127.9, 126.9, 126.8, 126.8, 126.6, 126.5, 120.5, 119.8, 100.8, 60.5, 20.7, 14.1

m.p. (°C): > 300

UV-Vis (CH_2Cl_2, nm) λ_{max}: Soret, 419; Q bands: 517, 559, 591, 646; Log ε_{419}: 5.62

ESI-MS (+ve) (m/z): 742.90 [M]$^+$

Synthesis of {2-(1-acetyl-1-ethoxycarbonylmethyl)-5,10,15,20-*tetrakis* [3,5-bis(trifluoromethyl)phenyl]porphyrinato} zinc (II) (**81b**)
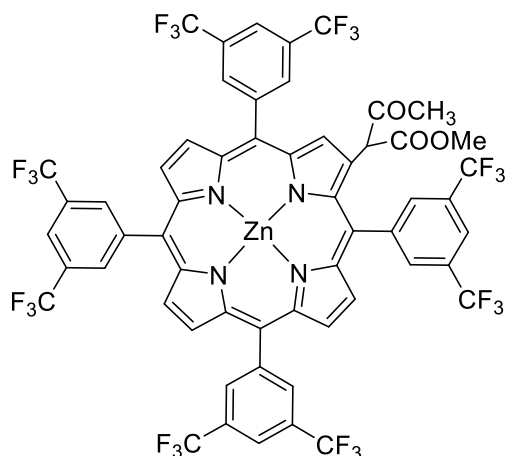
Methyl acetoacetate (0.45 mL, 4.0 mmol) and K_2CO_3 (553 mg, 4.0 mmol) were dissolved in a 50-mL round bottom flask with DMSO (15 mL), and sonicated for 15 minutes. Compound **80b** (500 mg, 0.40 mmol) was added to the mixture and stirred for 1 hour at room temperature. The mixture was then poured in 500 mL of brine solution, causing the product to precipitate. After filtration on paper, the purple solid was re-dissolved in CH_2Cl_2, washed with water and dried over anhydrous Na_2SO_4. The solvent was then removed under reduced pressure and the desired product was isolated by flash chromatography (silica, eluent: CH_2Cl_2-hexane 1:1). The solid was then re-crystallised form CH_2Cl_2/methanol as a crystalline bright pink solid (**81b**) (0.46 g, 0.34 mmol, 85 %).

^{1}H-NMR (600 MHz, CDCl$_3$, 298 K) δ, ppm: 12.83 (s, 1H, OH), 8.95-8.98 (q, 2H, J=13.2 Hz, β-H), 8.93 (s, 2H, β-H), 8.87 (d, 1H, J=4.2 Hz, β-H), 8.76 (br s, 1H, Ar-H$_o$), 8.72 (br d, 2H, Ar-H$_o$), 8.69 (m, 2H, Ar-H$_o$), 8.66 (s, 1H, Ar-H$_o$), 8.49 (br s, 1H, β-H), 8.42 (m, 4H, Ar-H$_p$), 8.27 (br s, 1H, β-H), 4.25 (m, 1H, OCH_2CH$_3$), 3.85 (m, 1H, OCH_2CH$_3$), 1.87 (s, 3H, COCH_3), 0.87 (t, 3H, OCH$_2$CH_3)

^{13}C-NMR (150 MHz, CDCl$_3$, 298 K) δ, ppm: 174.1, 171.6, 151.2, 150.5, 150.3, 150.3, 150.2, 150.1, 148.8, 148.0, 144.5, 144.3, 143.9, 140.6, 136.6, 134.0, 133.7, 133.1, 133.0, 132.8, 132.8, 132.8, 132.7, 132.4, 130.8, 126.4, 124.6, 122.8, 122.8, 122.6, 122.3, 121.0, 119.0, 118.8, 118.7, 118.1, 100.6, 60.8, 20.6, 14.0

^{19}F-NMR (564 MHz, CDCl$_3$, 298 K) δ, ppm: -62.1 (br s, 3F), -62.4 (m, 18F), -62.4 (br s, 3F)

m.p. (°C): > 300

UV-Vis (CH$_2$Cl$_2$, nm) λ_{max}: Soret, 424; Q bands, 514, 548, 590; 643 Log ε_{424}: 5.84

ESI-MS (+ve) (m/z): 1335.62 [M + H]$^+$

Synthesis of [2-(1-acetyl-1-ethoxycarbonylmethyl)-5,10,15,20-*tetrakis* (pentafluorophenyl)porphyrinato]zinc (II) (**81c**)
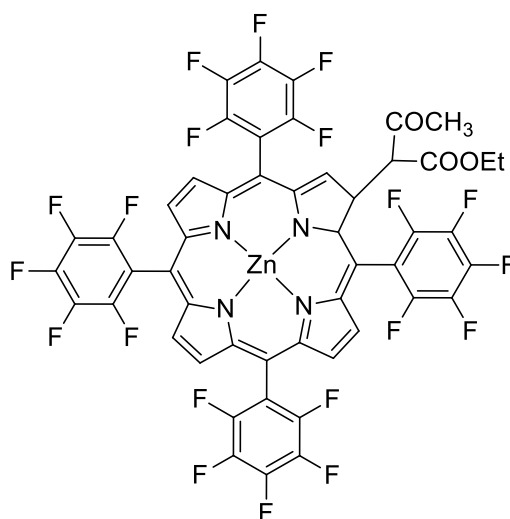
Ethyl acetoacetate (0.59 mL, 4.6 mmol) and K_2CO_3 (636 mg, 4.6 mmol) were dissolved in a 50-mL round bottom flask with DMSO (15 mL), sonicated for 15 minutes and poured in an ice bath while stirring. Compound **80c** (500 mg, 0.46 mmol) was then added to the mixture and stirred for 5 minutes, until the colour changes from greenish to red. The mixture was then poured in 500 mL of brine solution, causing the product to precipitate. After filtration on paper, the bright purple solid was re-dissolved in CH_2Cl_2, washed with water and dried over anhydrous Na_2SO_4. The solvent was then removed under reduced pressure and the desired product was isolated by flash chromatography (silica, eluent: CH_2Cl_2-hexane 7:3). The solid was then re-crystallised form CH_2Cl_2/methanol as a crystalline bright pink solid (**81c**) (0.48 g, 0.41 mmol, 90 %).

^{1}H-NMR (600 MHz, CDCl$_3$, 298 K) δ, ppm: 13.14 (s, 1H, OH), 8.95-9.01 (m, 5H, β-H), 8.88 (d, 1H, β-H), 8.79 (s, 1H, β-H), 4.15-4.25 (m, 1H, OC*H$_2$*CH$_3$), 3.78-3.89 (m, 1H, OC*H$_2$*CH$_3$), 1.98 (s, 3H, CH$_3$), 0.79 (t, 3H, OCH$_2$C*H$_3$*)

^{13}C-NMR (150 MHz, CDCl$_3$, 298 K) δ, ppm: 174.9, 172.3, 150.5, 150.4, 150.3, 150.3, 148.5, 140.8, 135.6, 132.4, 132.3, 132.2, 132.1, 131.9, 116.5, 104.7, 104.3, 104.2, 103.6, 99.1, 64.1, 61.3, 20.4, 20.4, 13.9, 13.6

^{19}F-NMR (564 MHz, CDCl$_3$, 298 K) δ, ppm: -134.5 (d, 1F, F$_o$), -136.3 (dd, 1F, F$_o$), -136.7 (m, 5F, F$_o$), -137.3 (d, 1F, F$_o$), -151.4 (t, 1F, F$_p$), -151.7 (t, 3F, F$_p$), -161.5 (m, 6F, F$_m$), -162.3 (dt, 1F, F$_m$), -163.2 (dt, 1F, F$_m$)

m.p. (°C): > 300

UV-Vis (CH$_2$Cl$_2$, nm) λ_{max}: Soret, 422; Q bands, 541; Log ε_{422}: 5.65

ESI-MS (+ve) (m/z): 1164.94 [M+H]$^+$

Synthesis of [2-(1-acetyl-1-ethoxycarbonylmethyl)-5,10,15,20-*tetrakis*(3-methoxyphenyl)porphyrinato]copper (II) (**81d'**)
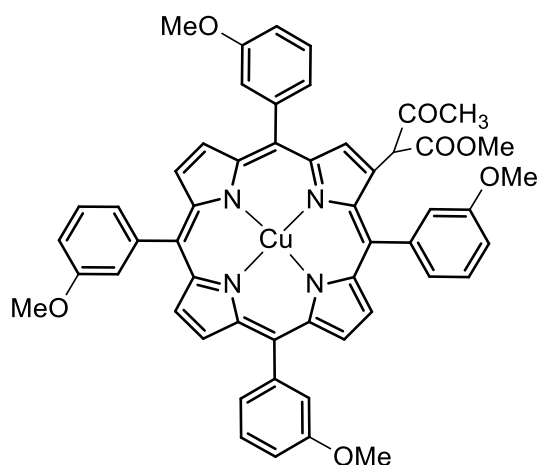

Methyl acetoacetate (0.65 mL, 6.0 mmol) and K_2CO_3 (829 mg, 6.0 mmol) were dissolved in a 50-mL round bottom flask with DMSO (15 mL), and sonicated for 15 minutes. Compound **80d** (500 mg, 0.60 mmol) was added to the mixture and stirred for 1 hour at room temperature. The mixture was then poured in 250 mL of brine solution, causing the product to precipitate. After filtration on paper, the purple solid was re-dissolved in CH_2Cl_2, washed with water and dried over anhydrous Na_2SO_4. The solvent was then removed under reduced and the desired product was isolated by flash chromatography (silica, eluent: CH_2Cl_2-hexane 1:1 with 2 % Et_2O). The solid was then re-crystallised form CH_2Cl_2/methanol as a crystalline red solid (0.47 g, 0.52 mmol, 86 %).

m.p. (°C): 248-251

UV-Vis (CH_2Cl_2, nm) λ_{max}: Soret, 418; Q bands, 541; Log ε_{418}: 4.69

ESI-MS (+ve) (m/z): 910.21 [M+H]$^+$

<u>Synthesis of 2-(1-acetyl-1-methoxycarbonylmethyl)-5,10,15,20-*tetrakis*(3-methoxyphenyl)porphyrin</u>
<u>(**81d**)</u>
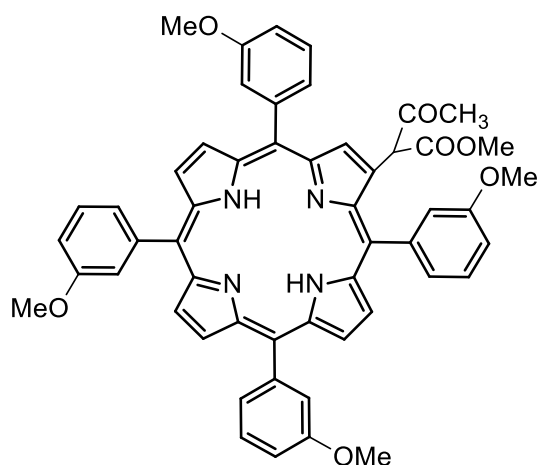
Compound **Cu81d** (100 mg, 0.11 mmol) was dissolved in TFA (5 mL) in a 50-mL round bottom flask, and then H_2SO_4 (500 µl) was added. The solution was stirred for 10 minutes at room temperature. Then the solution was cooled down with an ice bath, and a saturated solution of $NaHCO_3$ (150 mL) was slowly added to the mixture, causing the product to precipitate. After filtration on paper, the purple solid was re-dissolved in CH_2Cl_2, washed with water and dried over anhydrous Na_2SO_4. The solvent was then removed under reduced pressure and the crude product was isolated by re-crystallisation from CH_2Cl_2/methanol, yielding a dark purple crystalline solid (**81d**) (89 mg, 0.10 mmol, 95 %).

^{1}H-NMR (300 MHz, $CDCl_3$, 298 K) δ, ppm: 12.87 (d, 1H, OH), 8.87-8.92 (m, 4H, β-H), 8.83-8.84 (d, 1H, β-H), 8.74 (t, 1H, β-H), 8.69 (s, 1H, β-H), 7.81-7.91 (br s, 6H, Ar-H$_o$), 7.66-7.68 (m, 6H, Ar-H$_o$ + Ar-H$_p$), 7.35 (m, 4H, Ar-H$_m$), 3.54 (d, 3H, COOCH_3), 1.86 (dd, 3H, CH_3), 3.98-4.01 (m, 12H, OCH_3), -2.72 (s, 2H, NH$_{int}$)

^{13}C-NMR (150 MHz, $CDCl_3$, 298 K) δ, ppm: 179.7, 179.1, 149.4, 149.4, 149.3, 149.2, 149.1, 149.0, 148.9, 147.5, 142.1, 141.4, 135.2, 134.9, 134.8, 133.7, 121.5, 73.2, 73.0, 42.2, 42.1, 39.9

m.p. (°C): 248-251

UV-Vis (CH_2Cl_2, nm) λ_{max}: Soret, 423; Q bands: 528, 547, 590, 641; Log ε_{423}: 5.59

ESI-MS (+ve) (m/z): 849.33 [M+H]$^+$

Synthesis of [2-(1-acetyl-1-ethoxycarbonylmethyl)-5,10,15,20-*tetrakis*(3,5-dimethoxyphenyl)porphyrinato]copper (II) (**81e'**)
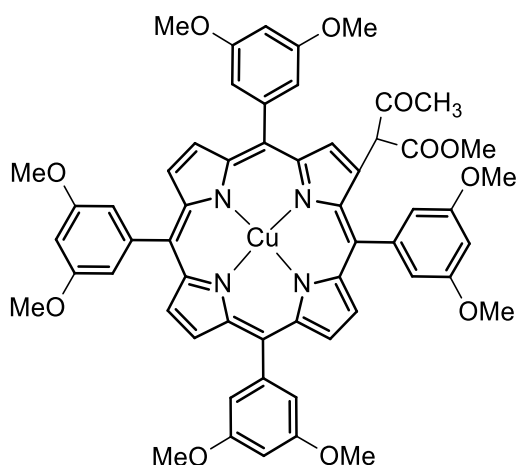
Methyl acetoacetate (0.56 mL, 5.2 mmol) and K_2CO_3 (720 mg, 5.2 mmol) were dissolved in a 50-mL round bottom flask with DMSO (15 mL), and sonicated for 15 minutes. Compound **80e** (500 mg, 0.52 mmol) was added to the mixture and stirred for 1 hour at room temperature. The mixture was then poured in 250 mL of brine solution, causing the product to precipitate. After filtration on paper, the purple solid was re-dissolved in CH_2Cl_2, washed with water and dried over anhydrous Na_2SO_4. The solvent was then removed under reduced and the desired product was isolated by flash chromatography (silica, eluent: CH_2Cl_2-hexane 7:3 with 2 % Et_2O). The solid was then re-crystallised form CH_2Cl_2/methanol as a crystalline red solid (0.45 g, 0.44 mmol, 84 %).

m.p. (°C): > 300

UV-Vis (CH_2Cl_2, nm) λ_{max}: Soret, 428; Q bands, 541; Log ε_{428}: 4.69

ESI-MS (+ve) (m/z): 1030.30 $[M+H]^+$

Synthesis of 2-(1-acetyl-1-ethoxycarbonylmethyl)-5,10,15,20-*tetrakis*(3,5-dimethoxyphenyl)porphyrin (**81e**)
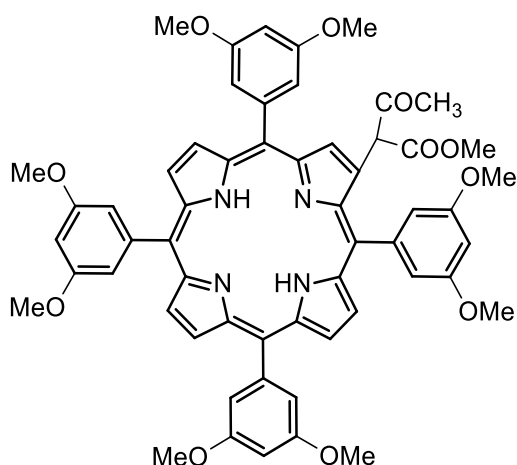
Compound **Cu81e** (100 mg, 0.10 mmol) was dissolved in TFA (5 mL) in a 50-mL round bottom flask, and then H_2SO_4 (500 µl) was added. The solution was stirred for 10 minutes at room temperature. Then the solution was cooled down with an ice bath, and a saturated solution of $NaHCO_3$ (150 mL) was slowly added to the mixture, causing the product to precipitate. After filtration on paper, the purple solid was re-dissolved in CH_2Cl_2, washed with water and dried over anhydrous Na_2SO_4. The solvent was then removed under reduced pressure and the crude product was isolated by re-crystallisation from CH_2Cl_2/methanol, yielding a dark purple crystalline solid (**81e**) (87 mg, 0.09 mmol, 90 %).

^{1}H-NMR (300 MHz, CDCl$_3$, 298 K) δ, ppm: 12.91 (d, 1H, OH), 8.92 (br d, 4H, J=6 Hz β-H), 8.86 (d, 1H, J=3.6 Hz, β-H), 8.79-8.80 (d, 1H, J=3.6 Hz, β-H), 8.72 (s, 1H, β-H), 7.46 (br s, 1H, Ar-H$_o$), 7.36-7.40 (m, 5H, Ar-H$_o$), 7.11-7.13 (m, 1H, Ar-H$_o$), 7.11 (m, 1H, Ar-H$_o$), 6.88-6.91 (m, 3H, Ar-H$_p$), 6.77 (t, 1H, J=1.5 Hz, Ar-H$_p$), 3.96 (dd, 12H, J=1.5 Hz, J=3.9 Hz, OCH$_3$), 3.55 (s, 3H, COOCH_3), 1.82 (s, 3H, CH$_3$), -2.79 (br s, 2H, NH$_{int}$)

^{13}C-NMR (150 MHz, CDCl$_3$, 298 K) δ, ppm: 173.5, 172.7, 166.9, 159.8, 159.3, 159.0, 159.0, 158.9, 158.8, 158.8, 150.7, 144.3, 144.1, 143.8, 143.1, 129.6, 126.8, 121.4, 120.0, 119.8, 119.6, 119.3, 116.9, 114.2, 114.2, 114.0, 114.0, 113.9, 113.9, 113.9, 112.3, 102.4, 101.0, 100.3, 100.2, 100.2, 99.9, 99.3, 55.7, 55.7, 55.6, 55.6, 51.5, 20.6

m.p. (°C): > 300

UV-Vis (CH$_2$Cl$_2$, nm) λ_{max}: Soret, 424; Q bands: 519, 547, 593, 649; Log ε_{424}: 5.50

ESI-MS (+ve) (m/z): 969.33 [M+H]$^+$

Synthesis of 2-(ethoxycarbonylmethyl)-5,10,15,20-*tetrakis*-phenylporphyrin (**82a**)
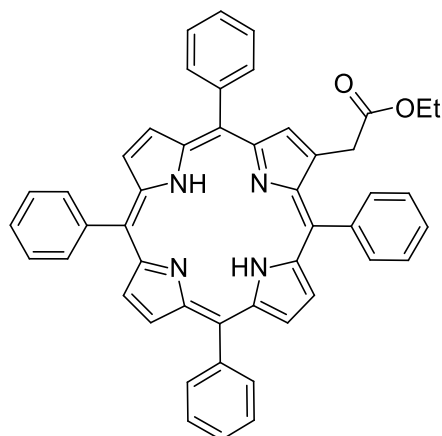
Compound **81a** (100 mg, 0.135 mmol) was dissolved in a 100-mL round bottom flask with ethanol (50 mL). HCl (10 mL, 20% to EtOH) was added to the mixture, and the solution was heated to reflux for 2 hours. Then the mixture was allowed to cool to room temperature, and CH_2Cl_2 (150 mL) was added. The resulting solution was washed with a saturated solution of $NaHCO_3$ (150 mL) and dried over anhydrous Na_2SO_4. The solvent was then removed under reduced pressure and the desired product was isolated by flash chromatography (silica, eluent: CH_2Cl_2-hexane 1:1). The solid was then isolated by re-crystallisation from CH_2Cl_2/methanol, yielding a brown solid (**82a**) (65 mg, 0.093 mmol, 69 %).

^{1}H-NMR (300 MHz, CDCl$_3$, 298 K) δ, ppm: 8.79-8.88 (m, 5H, β-H), 8.76 (br s, 1H, β-H), 8.64-8.65 (d, 1H, β-H), 8.24-8.26 (m, 6H, Ar-H$_o$), 8.11 (d, 2H, Ar-H$_o$), 7.70-7.84 (m, 12H, Ar-H$_m$ + Ar-H$_p$), 4.10-4.17 (q, 2H, O*CH$_2$*CH$_3$), 3.99 (s, 2H, CH$_2$), 1.22 (t, 3H, OCH$_2$C*H$_3$*), -2.69 (s, 2H, NH$_{int}$),

^{13}C-NMR (75 MHz, CDCl$_3$, 298 K, DEPTQ) δ, ppm: 171.9, 142.7, 142.5, 142.1, 141.9, 134.8, 134.7, 134.7, 133.6, 131.7, 130.8, 128.5, 127.9, 127.2, 126.9, 126.8, 126.7, 120.7, 120.3, 119.7, 119.6, 60.8, 36.5, 14.3

m.p. (°C): 264-265

UV-Vis (CH$_2$Cl$_2$, nm) λ_{max}: Soret, 418; Q bands: 516, 550, 591, 646; Log ε_{418}: 5.98

ESI-MS (+ve) (m/z): 700.93 [M]$^+$

<u>Synthesis of 2-(ethoxycarbonylmethyl)-5,10,15,20-*tetrakis*[3,5-bis(trifluoromethyl)phenyl]porphyrin</u>
(**82b**)
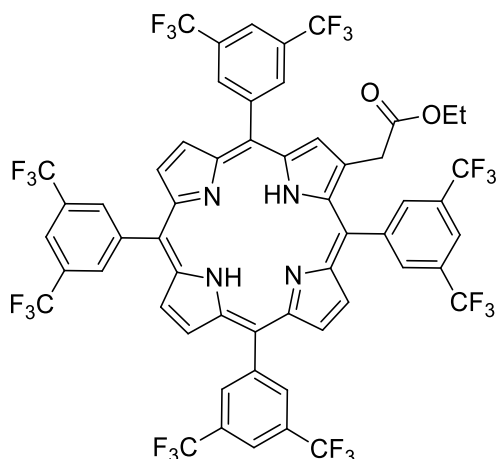
Compound **81b** (100 mg, 0.07 mmol) was dissolved in a 100-mL round bottom flask with ethanol (50 mL). HCl (10 mL, 20% to EtOH) was added to the mixture, and the solution was heated to reflux for 2 hours. Then the mixture was allowed to cool to room temperature, and CH_2Cl_2 (150 mL) was added. The resulting solution was washed with a saturated solution of $NaHCO_3$ (150 mL) and dried over anhydrous Na_2SO_4. The solvent was then removed under reduced pressure and the desired product was isolated by flash chromatography (silica, eluent: CH_2Cl_2-hexane 7:3). The solid was then re-crystallised form CH_2Cl_2/methanol as a brown solid (**82b**) (78 mg, 0.05 mmol, 75 %).

^{1}H-NMR (300 MHz, $CDCl_3$, 298 K) δ, ppm: 8.81-8.84 (q, 2H, J=3.6Hz, J=6.3 Hz, β-H), 8.79 (d, 1H, J=3.6 Hz, β-H), 8.70-8.74 (br m, 8H, Ar-H$_o$), 8.66 (br s, 1H, β-H), 8.62 (br s, 2H, β-H), 8.52-8.53 (d, 1H, J=3.6 Hz, β-H), 8.40-8.41 (br d, 4H, Ar-H$_p$), 4.08 (q, 2H, OCH_2CH$_3$), 3.97 (s, 2H, CH$_2$), 1.17 (t, 3H, OCH$_2$CH_3), -2.81 (s, 2H, NH$_{int}$)

^{13}C-NMR (150 MHz, $CDCl_3$, 298 K) δ, ppm: 170.7, 144.1, 143.9, 143.5, 143.3, 133.8, 133.8, 133.2, 131.3, 131.1, 131.0, 130.9, 130.9, 130.8, 130.8, 133.7, 130.6, 130.6, 126.3, 126.2, 124.5, 124.4, 123.0, 122.7, 122.6, 122.5, 122.5, 120.9, 120.8, 118.0, 117.8, 117.3, 117.1, 61.5, 36.5, 14.0

^{19}F-NMR (564 MHz, $CDCl_3$, 298 K) δ, ppm: -62.1 (br s, 6F), -62.2 (br m, 6F), -62.2 (br d, 12F)

m.p. (°C): > 300

UV-Vis (CH_2Cl_2, nm) λ_{max}: Soret, 421; Q bands, 515, 547, 589; 641 Log ϵ_{421}: 5.68

ESI-MS (+ve) (m/z): 1245.33 [M+H]$^+$

Synthesis of 2-(ethoxycarbonylmethyl)-5,10,15,20-*tetrakis*(pentafluorophenyl)porphyrin (**82c**)
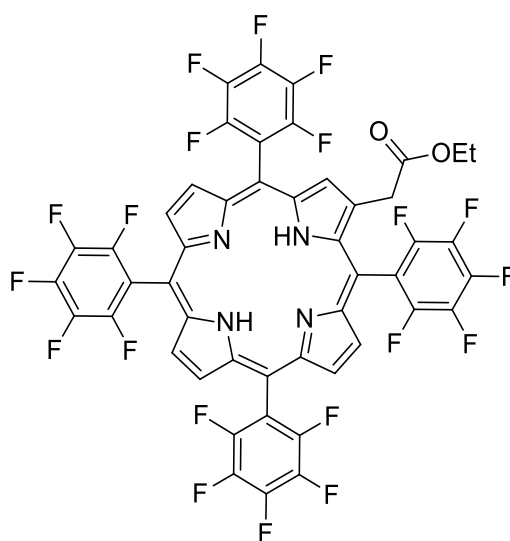
Compound **81c** (100 mg, 0.09 mmol) was dissolved in a 100-mL round bottom flask with ethanol (50 mL). HCl (10 mL, 20 % to EtOH) was added to the mixture, and the solution was heated to reflux for 2 hours. Then the mixture was allowed to cool to room temperature, and CH_2Cl_2 (150 mL) was added. The resulting solution was washed with a saturated solution of $NaHCO_3$ (150 mL) and dried over anhydrous Na_2SO_4. The solvent was then removed under reduced pressure and the desired product was isolated by flash chromatography (silica, eluent: CH_2Cl_2-hexane 1:1). The solid was then re-crystallised form CH_2Cl_2/methanol as a brown solid (**82c**) (91 mg, 0.08 mmol, 95 %).

^{1}H-NMR (600 MHz, $CDCl_3$, 298 K) δ, ppm: 8.94 (s, 2H, β-H), 8.85-8.89 (m, 4H, β-H), 8.72 (d, 1H, J=4.8 Hz, β-H), 4.32 (s, 2H, CH_2), 4.15-4.19 (q, 2H, J=5.0 Hz, CH_2), 1.19 (t, 3H, J=6.6 Hz, OCH_2CH_3), -2.85 (br s, 2H, NH_{int})

^{13}C-NMR (150 MHz, $CDCl_3$, 298 K) δ, ppm: 170.0, 147.5, 145.9, 141.6, 138.6, 137.0, 132.3, 115.4, 115.3, 104.2, 103.8, 103.1, 103.0, 61.9, 36.2, 29.9, 14.0

^{19}F-NMR (564 MHz, $CDCl_3$, 298 K) δ, ppm: -135.5 (dd, 2F, F_o), -136.1 (dd, 2F, F_o), -136.4 (d, 4F, F_o), -150.3 (t, 1F, F_p), -151.0 (m, 3F, F_p), -160.6 (dt, 2F, F_m), -161.1 (m, 6F, F_m)

m.p. (°C): > 300

UV-Vis (CH_2Cl_2, nm) λ_{max}: Soret, 415; Q bands, 506, 538, 580; 641 Log ε_{415}: 5.59

ESI-MS (+ve) (m/z): 1061.36 $[M+H]^+$

Synthesis of 2-(ethoxycarbonylmethyl)-5,10,15,20-*tetrakis*(3-methoxyphenyl)porphyrin (**82d**)
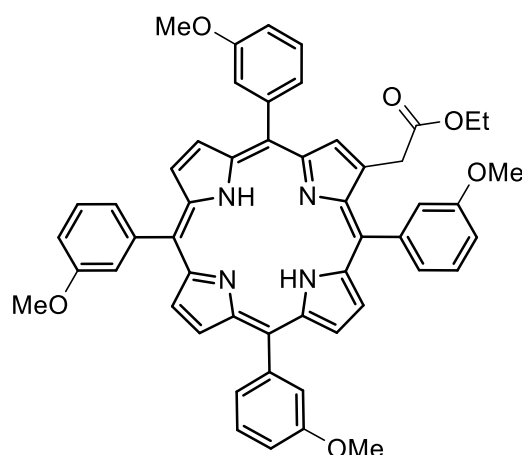
Compound **81d** (100 mg, 0.12 mmol) was dissolved in a 100-mL round bottom flask with ethanol (50 mL). HCl (10 mL, 20 % to EtOH) was added to the mixture, and the solution was heated to reflux for 2 hours. Then the mixture was allowed to cool to room temperature, and CH_2Cl_2 (150 mL) was added. The resulting solution was washed with a saturated solution of $NaHCO_3$ (150 mL) and dried over anhydrous Na_2SO_4. The solvent was then removed under reduced pressure and the desired product was isolated by flash chromatography (silica, eluent: CH_2Cl_2-hexane 8:2). The solid was then isolated by re-crystallisation from CH_2Cl_2/methanol, yielding a dark purple crystalline solid (**82d**) (59 mg, 0.07 mmol, 61 %).

^{1}H-NMR (600 MHz, CDCl$_3$, 298 K) δ, ppm: 8.94 (d, 2H, J=3 Hz, β-H), 8.91 (d, 1H, J=4.2 Hz, β-H), 8.88 (d, 1H, J=4.8 Hz, β-H), 8.86 (d, 1H, J=4.8 Hz, β-H), 8.82 (br s, 1H, β-H), 8.73 (d, 1H, J=4.2 Hz, β-H), 7.64-7.84 (br m, 12H, Ar-H$_o$ + Ar-H$_p$), 7.35-7.37 (m, 4H, Ar-H$_m$), 4.15 (m, 2H, CH_2CH$_3$), 4.05 (s, 10H, OCH_3), 3.98 (s, 2H, CH_2), 1.23 (t, 3H, CH$_2$CH_3), -2.78 (br s, 2H, NH$_{int}$)

^{13}C-NMR (150 MHz, CDCl$_3$, 298 K) δ, ppm: 172.0, 158.4, 158.2, 158.1, 158.0, 144.0, 143.7, 143.7, 143.4, 143.1, 128.1, 127.8, 127.8, 127.7, 127.6, 127.5, 126.5, 120.7, 120.6, 120.5, 120.3, 120.0, 119.6, 119.4, 119.3, 114.4, 113.7, 60.9, 55.6, 55.5, 36.3

m.p. (°C): > 300

UV-Vis (CH_2Cl_2, nm) λ_{max}: Soret, 421; Q bands: 518, 550, 593, 649; Log ε_{421}: 5.64

ESI-MS (+ve) (m/z): 821.35 [M+H]$^+$

Synthesis of 2-(1-ethoxycarbonylmethyl)-5,10,15,20-*tetrakis*(3,5-dimethoxyphenyl)porphyrin (**82e**)
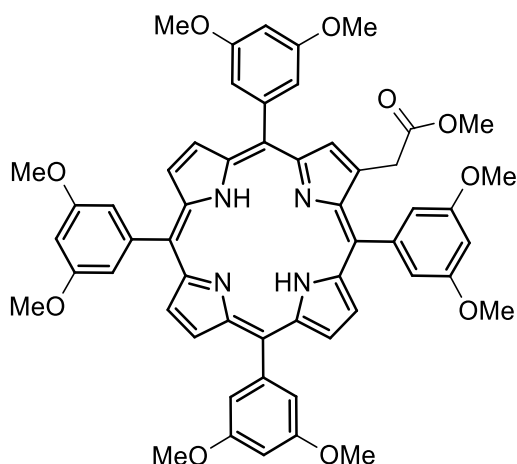
Compound **81e** (100 mg, 0.10 mmol) was dissolved in a 100-mL round bottom flask with ethanol (50 mL). HCl (10 mL, 20 % to EtOH) was added to the mixture, and the solution was heated to reflux for 2 hours. Then the mixture was allowed to cool to room temperature, and CH_2Cl_2 (150 mL) was added. The resulting solution was washed with a saturated solution of $NaHCO_3$ (150 mL) and dried over anhydrous Na_2SO_4. The solvent was then removed under reduced pressure and the desired product was isolated by flash chromatography (silica, eluent: CH_2Cl_2-hexane 7:3). The solid was then isolated by re-crystallisation from CH_2Cl_2/methanol, yielding a dark purple crystalline solid (58 mg, 0.06 mmol, 62 %).

^{1}H-NMR (300 MHz, $CDCl_3$, 298 K) δ, ppm: 8.94 (t, 2H, J=4.2 Hz, β-H), 8.89 (dd, 2H, J=3.6 Hz, J=8.4 Hz, β-H), 8.86 (d, 1H, J=3.6 Hz, β-H), 8.83 (br s, 1H, β-H), 8.74-8.75 (d, 1H, J=3.6 Hz, β-H), 7.39-7.40 (m, 6H, Ar-H$_o$), 7.24 (dd, 2H, Ar-H$_o$), 6.88-6.91 (m, 3H, Ar-H$_p$), 6.89-6.90 (m, 4H, Ar-H$_p$), 4.15 (s, 2H, CH_2), 3.96 (br dt, 18H, OCH_3), 3.93 (s, 6H, OCH_3), 3.69 (s, 3H, COOCH_3),-2.82 (br s, 2H, NH$_{int}$)

^{13}C-NMR (75 MHz, $CDCl_3$, 298 K) δ, ppm: 172.6, 159.5, 159.1, 159.0, 158.9, 144.5, 144.3, 143.9, 143.5, 120.2, 119.9, 119.3, 119.3, 114.1, 114.0, 113.9, 113.0, 100.7, 100.4, 100.4, 100.3, 55.8, 55.7, 51.9, 35.9

m.p. (°C): > 300

UV-Vis (CH_2Cl_2, nm) λ_{max}: Soret, 423; Q bands: 518, 549, 592, 648; Log ε_{423}: 5.58

ESI-MS (+ve) (m/z): 926.34 [M+H]$^+$

Synthesis of 2-(carboxymethyl)-5,10,15,20-*tetrakis*-phenylporphyrin (**83a**)
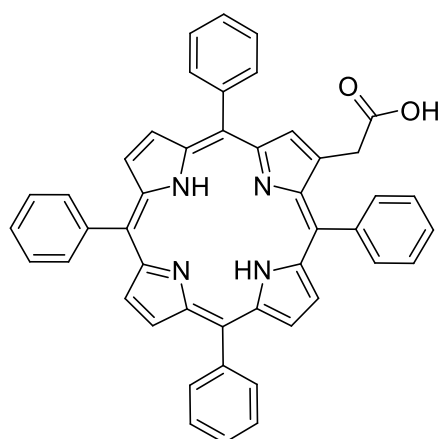
Compound **82a** (100 mg, 0.143 mmol) was dissolved in a 50-mL round bottom flask with THF (10 mL). HCl (20 mL) was added to the mixture, and the solution was stirred overnight (15 hours). The mixture was diluted with CH_2Cl_2 (150 mL) and the resulting solution was washed with a saturated solution of $NaHCO_3$ (150 mL) and dried over anhydrous Na_2SO_4. The solvent was then removed under reduced pressure and the crude product was isolated by re-crystallisation from CH_2Cl_2/methanol, yielding a brown/reddish solid (**83a**) (93 mg, 0.138 mmol, 97 %).

^{1}H-NMR (300 MHz, $CDCl_3$, 298 K) δ, ppm: 8.83-8.87 (m, 3H, β-H), 8.79 (t, 2H, β-H), 8.75 (s, 1H, β-H), 8.63 (d, 1H, β-H), 8.19-8.24 (m, 6H, Ar-H$_o$), 8.07-8.09 (d, 2H, Ar-H$_o$), 7.62-7.78 (m, 12H, Ar-H$_m$ + Ar-H$_p$), 4.00 (s, 2H, CH$_2$), -2.72 (br s, 2H, NH$_{int}$),

^{13}C-NMR (75 MHz, $CDCl_3$, DEPTQ, 298 K,) δ, ppm: 177.0, 142.6, 142.4, 142.0, 141.7, 134.8, 134.7, 134.6, 133.6, 131.3, 128.6, 127.9, 127.4, 126.9, 126.8, 126.7, 120.6, 120.3, 119.7, 119.6, 35.8

m.p. (°C): > 300

UV-Vis (CH_2Cl_2, nm) λ_{max}: Soret, 420; Q bands: 519, 552, 594, 647; Log ε_{420}: 5.49

ESI-MS (+ve) (m/z): 673.47 [M+H]$^+$

Synthesis of 2-methyl-5,10,15,20-*tetrakis*-phenylporphyrin (**83a'**)
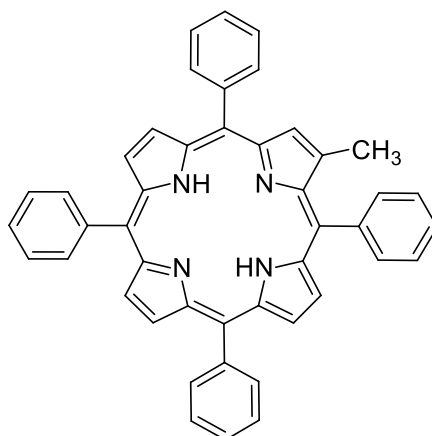
Compound **83a** (20 mg, 0.03 mmol) was dissolved in a 10-mL microwave vessel with NMP (3 mL). The mixture was heated to 200 °C for 5 minutes. After the mix cooled down, it was diluted with CH_2Cl_2 (50 mL), washed with water (150 mL) and dried over anhydrous Na_2SO_4. The solvent was removed under reduced pressure and the product was isolated by re-crystallisation from CH_2Cl_2/methanol, yielding a brown solid (18.7 mg, 0.03 mmol, 99 %).

^{1}H-NMR (300 MHz, $CDCl_3$, 298 K) δ, ppm: 8.63-8.87 (m, 7H, β-H), 8.07-8.24 (m, 8H, Ar-H$_o$), 7.70-7.81 (m, 12H, Ar-H$_m$ + Ar-H$_p$), 2.59 (s, 3H, CH_3), -2.78 (br s, 2H, NH$_{int}$),

^{13}C-NMR (75 MHz, $CDCl_3$, DEPTQ, 298 K) δ, ppm: 142.9, 142.6, 142.4, 142.2, 134.7, 134.6, 134.6, 133.4, 132.5, 128.2, 127.8, 127.8, 127.1, 126.9, 126.8, 126.7, 120.7, 120.1, 120.0, 118.7, 17.5

m.p. (°C): > 300

UV-Vis (CH_2Cl_2, nm) λ_{max}: Soret, 416; Q bands, 513, 549, 592, 648; Log ε_{417}: 5.87

ESI-MS (+ve) (m/z): 629.75 [M+H]$^+$

Synthesis of 2-(carboxymethyl)-5,10,15,20-*tetrakis*[3,5-bis(trifluoromethyl)phenyl]porphyrin (**83b**)
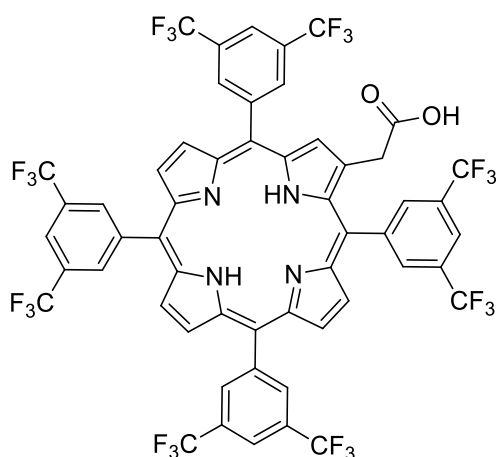
Compound **82b** (100 mg, 0.08 mmol) was dissolved in a 50-mL round bottom flask with THF (10 mL). HCl (20 mL) was added to the mixture, and the solution was stirred overnight (15 hours). The mixture was diluted with CH_2Cl_2 (150 mL) and the resulting solution was washed with a saturated solution of $NaHCO_3$ (150 mL) and dried over anhydrous Na_2SO_4. The solvent was then removed under reduced pressure and the desired product was isolated by flash chromatography (silica, eluent: CH_2Cl_2-hexane 7:3, then pure CH_2Cl_2). The solid was then re-crystallised form CH_2Cl_2/methanol as a brown solid (**83b**) (71 mg, 0.06 mmol, 73 %).

^{1}H-NMR (600 MHz, CDCl$_3$, 298 K) δ, ppm: 8.82 (br s, 1H, β-H), 8.80 (br d, 2H, J=2.4 Hz, β-H), 8.76 (br d, 1H, J=4.8 Hz, β-H), 8.70 (br s, 5H, Ar-H$_o$), 8.66 (br s, 3H, β-H), 8.56 (br s, 2H, β-H), 8.50 (d, 1H, J=4.8 Hz, β-H), 8.41 (br s, 2H, Ar-H$_p$), 8.40 (br s, 1H, Ar-H$_p$), 8.34 (br s, 1H, Ar-H$_p$), 4.01 (s, 2H, CH$_2$), -2.83 (s, 2H, NH$_{int}$)

^{13}C-NMR (150 MHz, CDCl$_3$, 298 K) δ, ppm: 176.3, 144.0, 143.8, 143.4, 143.1, 133.9, 133.8, 133.1, 131.1, 131.0, 130.9, 130.9, 130.8, 130.7, 130.6, 130.6, 126.3, 124.5, 124.3, 122.7, 120.9, 118.0, 117.8, 117.2, 117.1, 35.9

^{19}F-NMR (564 MHz, CDCl$_3$, 298 K) δ, ppm: -62.4 (m, 18F), -62.7 (s, 6F)

m.p. (°C): > 300

UV-Vis (CH$_2$Cl$_2$, nm) λ_{max}: Soret, 421; Q bands, 515, 549, 587; 640 Log ε_{421}: 5.58

ESI-MS (+ve) (m/z): 1217.61 [M+H]$^+$

Synthesis of 2-(carboxymethyl)-5,10,15,20-*tetrakis*(pentafluorophenyl)porphyrin (**83c**)
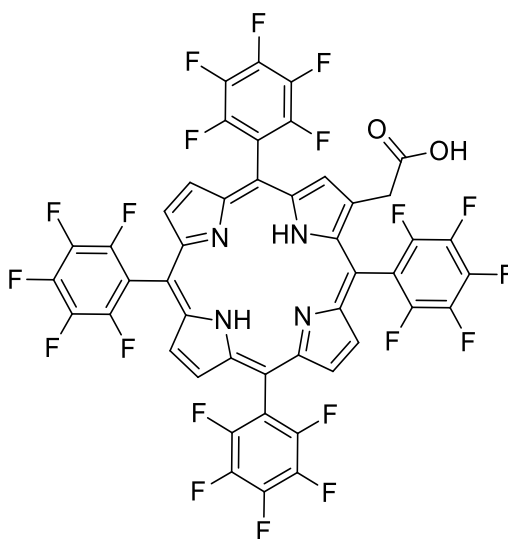
Compound **82c** (100 mg, 0.09 mmol) was dissolved in a 50-mL round bottom flask with THF (10 mL). HCl (20 mL) was added to the mixture, and the solution was stirred overnight (15 hours). The mixture was diluted with CH_2Cl_2 (150 mL) and the resulting solution was washed with a saturated solution of $NaHCO_3$ (150 mL) and dried over anhydrous Na_2SO_4. The solvent was then removed under reduced pressure and the desired product was isolated by flash chromatography (silica, eluent: CH_2Cl_2, then 0.1 % methanol). The solid was then re-crystallised form CH_2Cl_2/methanol as a brown solid (**83c**) (72 mg, 0.07 mmol, 78 %).

^{1}H-NMR (300 MHz, CDCl$_3$, 298 K) δ, ppm: 8.83-8.91 (m, 6H, β-H), 8.70 (d, 1H, J=4.8 Hz, β-H), 4.36 (s, 2H, CH$_2$), -2.86 (br s, 2H, NH$_{int}$)

^{13}C-NMR (150 MHz, CDCl$_3$, 298 K) δ, ppm: 175.8, 147.5, 145.9, 143.8, 143.4, 142.1, 141.7, 139.0, 138.6, 137.3, 136.9, 134.3, 132.0, 130.8, 116.2, 116.1, 116.0, 115.9, 115.7, 115.5, 115.4, 115.3, 115.1, 115.0, 104.2, 103.9, 103.2, 103.0, 35.7

^{19}F-NMR (564 MHz, CDCl$_3$, 298 K) δ, ppm: -135.5 (dd, 2F, F$_o$), -136.2 (dd, 2F, F$_o$), -136.4 (m, 4F, F$_o$), -150.0 (t, 1F, F$_p$), -151.0 (q, 2F, F$_p$), -151.2 (t, 1F, F$_p$), -160.6 (dt, 2F, F$_m$), -161.1 (m, 6F, F$_m$)

m.p. (°C): > 300

UV-Vis (CH_2Cl_2, nm) λ_{max}: Soret, 414; Q bands, 510, 587, 643; Log ε_{414}: 5.26

ESI-MS (+ve) (m/z): 1033.29 [M+H]$^+$

Synthesis of lithium 2-aminoethanesulphonate (**84**)

H_2N⌒⌒$SO_3^-Li^+$
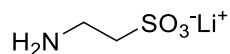
2-aminoethanesulphonic acid (10 g, 79.9 mmol) was dissolved in a 100-mL round bottom flask with water (40 mL). lithium hydroxide (3.352 g, 79.9 mmol) was added to the solution while stirring. The reaction was left stirring at room temperature for 24 hours. The solvent was then removed under reduced pressure, and acetone (100 mL) was added, causing the product to precipitate and to be collected by paper filtration. The desired product was collected as a white powder after further washing with acetone. (**6884**) (10.468 g, 79.9 mmol, quantitative yield)

^{1}H-NMR (600 MHz, D$_2$O, 298 K) δ, ppm: 3.12 (br s, 2H, NH_2), 2.81 (t, 2H, J=12.6 Hz, NHCH_2), 2.54 (t, 2H, J=13.2 Hz, CH_2SO$_3$)

^{13}C-NMR (150 MHz, CDCl$_3$, 298 K) δ, ppm: 53.5, 38.0

ESI-MS (+ve) (m/z): 132.00 [M+H]$^+$

Synthesis of [5,10,15,20--*tetrakis*(3-pyridyl)porphyrinato]copper (II) (**92**)
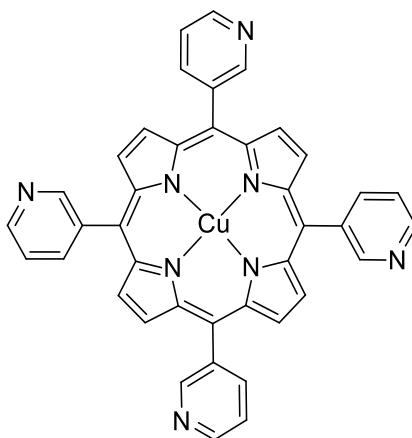
Compound **79f** (500 mg, 0.81 mmol) was dissolved in acetic acid (50 mL) in a 100-mL round bottom flask. $Cu(OAc)_2$ (735 mg, 4.05 mmol) was added to the mixture, stirred at room temperature for 1 hour. The solvent is removed under reduced pressure, and a saturated solution of $NaHCO_3$ (300 mL) was then added to the mixture, causing the product to precipitate. After filtration on paper, the crude compound is re-dissolved in CH_2Cl_2 and the organic phase was washed with water, and dried over anhydrous Na_2SO_4. The solvent was then removed under reduced pressure and the crude product was isolated by re-crystallisation form CH_2Cl_2/methanol as a crystalline dark purple solid (**31**) (0.53 g, 0.78 mmol, 96 %).

m.p. (°C): > 300

UV-Vis (CHCl$_3$, nm) λ_{max}: Soret, 416; Q bands, 539; Log ε_{416}: 5.71

ESI-MS (+ve) (m/z): 680.56 [M+H]$^+$

Synthesis of [2-nitro-5,10,15,20-*tetrakis*(3-pyridyl)porphyrinato]copper (II) (**93a**)
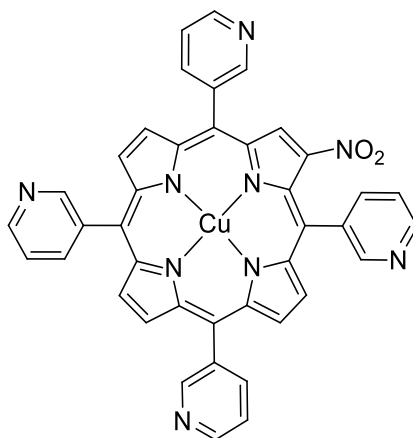
Compound **92** (500 mg, 0.69 mmol) was dissolved in $CHCl_3$ (350 mL) in a 500-mL 3 necks round bottom flask, and the solution was cooled down with an ice bath. $NaNO_2$ (950 mg, 13.77 mmol) was placed in a 100-mL 2 necks round bottom flask equipped with a dropping funnel, containing TFA (10 mL). The flasks were connected with a glass bridge (partially immersed in the flask containing $CHCl_3$), and TFA was added drop-wise to $NaNO_2$. Immediately an orange gas was realised (NO_2), bubbling into the mixture. The solution was then stirred, and the reaction was monitored with TLC (CH_2Cl_2 with 3 % MeOH). The reaction was stopped as soon as traces of di-nitrated product was detected, after 4.5 hours stirring. A saturated solution of $NaHCO_3$ (300 mL) was then added to the mixture. The organic phase was separated, washed with water, and dried over anhydrous Na_2SO_4. The solvent was then removed under reduced pressure and the desired product was isolated by flash chromatography (silica, eluent: CH_2Cl_2 with 3 % MeOH, then increased to 5 %). The solid was then re-crystallised form CH_2Cl_2/methanol as a crystalline dark solid (**93a**) (0.44 g, 0.60 mmol, 88 %).

m.p. (°C): > 300

UV-Vis ($CHCl_3$, nm) λ_{max}: Soret, 421; Q bands, 542; Log ε_{421}: 5.61

ESI-MS (+ve) (m/z): 680.56 [M+H]$^+$

Synthesis of 2-nitro-5,10,15,20--*tetrakis*(3-pyridyl)porphyrin (**93b**)
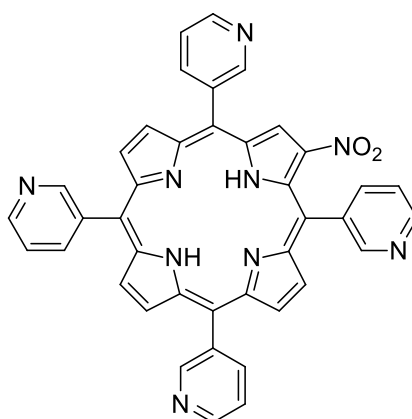
Compound **93a** (100 mg, 0.15 mmol) was dissolved in TFA (5 mL) in a 50-mL round bottom flask, and then H_2SO_4 (500 µl) was added. The solution was stirred for 1hour at room temperature. Then the solution was cooled down with an ice bath, and a saturated solution of $NaHCO_3$ (150 mL) was slowly added to the mixture, causing the product to precipitate. After filtration on paper, the purple solid was re-dissolved in CH_2Cl_2, washed with water and dried over anhydrous Na_2SO_4. The solvent was then removed under reduced pressure and the crude product was isolated by re-crystallisation from CH_2Cl_2/methanol, yielding a black crystalline solid (**93b**) (92 mg, 0.14 mmol, 93 %).

^{1}H-NMR (300 MHz, $CDCl_3$, 298 K) δ, ppm: 9.45 (br s, 4H, Py-H_2), 9.04 and 9.11 (br s, 4H, Py-H_6), 8.92-9.00 (m, 5H, β-H), 8.73 (t, 2H, J=5.1 Hz, β-H), 8.54 (br d, 4H, J=6.3 Hz, Py-H_4), 7.81-7.83 (m, 3H, Py-H_5), 7.69-7.73 (m, 1H, Py-H_5), -2.68 (s, 2H, NH_{int})

^{13}C-NMR (75 MHz, $CDCl_3$, 298 K) δ, ppm: 153.8, 148.5, 141.0, 139.4, 136.5, 130.0, 121.4, 118.0

m.p. (°C): > 300

UV-Vis (CH_2Cl_2, nm) λ_{max}: Soret, 428; Q bands: 539, 598; Log ε_{428}: 5.83

ESI-MS (+ve) (m/z): 664.78 [M+H]$^+$

Synthesis of [2-(1-acetyl-1-ethoxycarbonylmethyl)-5,10,15,20-*tetrakis*(3-pyridyl)porphyrinato]copper (II) (**94a**)
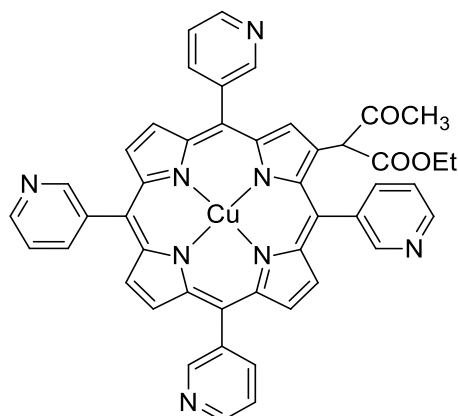
Ethyl acetoacetate (0.88 mL, 6.93 mmol) and K_2CO_3 (958 mg, 6.93 mmol) were dissolved in a 50-mL round bottom flask with DMSO (15 mL), and sonicated for 15 minutes. Compound **93a** (500 mg, 0.69 mmol) was added to the mixture and stirred for 1 hour at room temperature. The mixture was then poured in 250 mL of brine solution, causing the product to precipitate. After filtration on paper, the purple solid was re-dissolved in CH_2Cl_2, washed with water and dried over anhydrous Na_2SO_4. The solvent was then removed under reduced pressure and the desired product was isolated by flash chromatography (silica, eluent: CH_2Cl_2 with 2 % MeOH, then increased to 4 %). The solid was then re-crystallised form CH_2Cl_2/methanol as a crystalline dark solid (**94a**) (0.46 g, 0.57 mmol, 83 %).

m.p. (°C): > 300

UV-Vis (CH_2Cl_2, nm) λ_{max}: Soret, 426; Q bands, 537, 551; Log ε_{426}: 5.45

ESI-MS (+ve) (m/z): 808.71 [M]$^+$

Synthesis of 2-(1-acetyl-1-ethoxycarbonylmethyl)-5,10,15,20-*tetrakis*(3-pyridyl)porphyrin (**94b**)

Compound **94a** (100 mg, 0.12 mmol) was dissolved in TFA (5 mL) in a 50-mL round bottom flask, and then H_2SO_4 (500 μl) was added. The solution was stirred for 1 hour at room temperature. Then the solution was cooled down with an ice bath, and a saturated solution of $NaHCO_3$ (150 mL) was slowly added to the mixture, causing the product to precipitate. After filtration on paper, the purple solid was re-dissolved in CH_2Cl_2, washed with water and dried over anhydrous Na_2SO_4. The solvent was then removed under reduced pressure and the crude product was isolated by re-crystallisation from CH_2Cl_2/methanol, yielding a black crystalline solid (**94b**) (51 mg, 0.07 mmol, 57 %).

^{1}H-NMR (300 MHz, $CDCl_3$, 298 K) δ, ppm: 13.16 (s, 1H, OH), 8.73-8.93 (m, 7H, β-H), 4.14-4.25 (m, 1H, CH_2), 3.78-3.89 (m, 1H, CH_2CH$_3$), 2.00 (s, 3H, COCH_3), 0.78 (t, 3H, CH$_2$CH_3), -2.83 (s, 2H, NH$_{int}$)

^{13}C-NMR (75 MHz, $CDCl_3$, 298 K) δ, ppm: 153.7, 149.4, 148.7, 141.0, 140.0, 128.0, 122.2, 121.6, 61.2, 36.9, 29.8, 14.2

m.p. (°C): > 300

UV-Vis (CH_2Cl_2, nm) λ_{max}: Soret, 420; Q bands, 518, 549, 597; Log ε_{420}: 5.21

ESI-MS (+ve) (m/z): 747.53 [M+H]$^+$

Synthesis of 2-(carboxymethyl)-5,10,15,20--*tetrakis*(3-pyridyl)porphyrin (**95**)
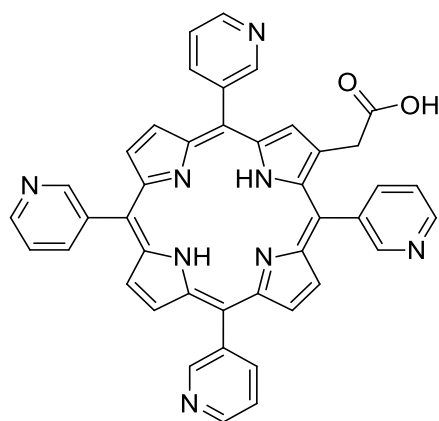
Compound **94a** (100 mg, 0.12 mmol) was dissolved in HCl (37 % v/v) (15 mL) in a 50-mL round bottom flask. The solution was stirred for 48 hours at room temperature. Then the solution was cooled down with an ice bath, and a saturated solution of NaHCO$_3$ (150 mL) was slowly added to the mixture, causing the product to precipitate. After filtration on paper, the purple solid was re-dissolved in CH$_2$Cl$_2$, washed with water and dried over anhydrous Na$_2$SO$_4$. The solvent was then removed under reduced pressure and the desired product was isolated by flash chromatography (silica, eluent: CH$_2$Cl$_2$ with 5 % MeOH, then increased to 10 %, 15 % and 20 %). The solid was then re-crystallised form CH$_2$Cl$_2$/methanol as a crystalline dark red solid. (**95**) (49 mg, 0.07 mmol, 60 %)

^{1}H-NMR (300 MHz, DMSO-d$_6$, 298 K) δ, ppm: 10.55 (br s, 2H, β-H), 9.35 (br s, 5H, β-H), 7.34 (d, 4H, $^3J_{4-5}$=11.4, Py-H$_4$), 7.07 (d, 4H, ^3J=9.3 Hz, Py-H$_6$), 6.89 (s, 4H, Py-H$_2$), 6.69-6.76 (dd def. to t, 4H, $^3J_{5-6}$=9.9 Hz $^3J_{5-4}$=11.1 Hz, Py-H$_5$)

^{13}C-NMR (75 MHz, CDCl$_3$, 298 K) δ, ppm: 182.4, 154.8, 151.9, 151.7, 134.9, 134.5, 133.2, 123.8, 116.7, 115.1, 110.5,

m.p. (°C): > 300

UV-Vis (CH$_2$Cl$_2$, nm) λ_{max}: Soret, 419; Q bands, 519, 548, 594, 648; Log ϵ_{419}: 4.93

ESI-MS (+ve) (m/z): 677.45 [M]$^+$

Synthesis of 5-(4-carboxymethylphenyl)-10,15,20-*tris*(4-pyridyl)porphyrin (**97**)
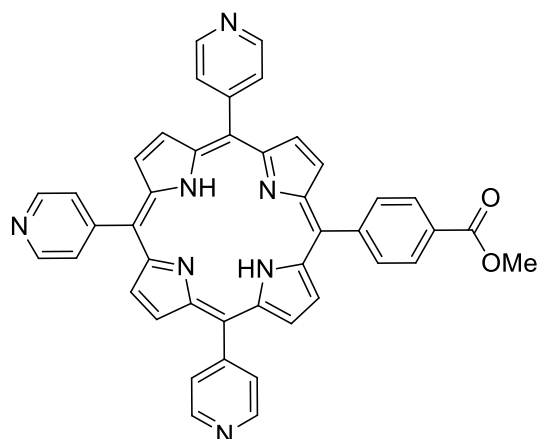
4-Pyridinecarboxaldehyde (5 mL, 53 mmol) and methyl-4-formylbenzoate (3.2 g, 20 mmol) were dissolved in propionic acid (500 mL) in a 1 L 3 necks round bottom flask. The resulting mixture was heated to reflux under stirring. Pyrrole (5 mL, 72 mmol) was added drop-wise to the solution in a 30 minutes time. The resulting mixture was heated to reflux for 1.5 hours protected from light. Once the solution was cooled down to room temperature, the solvent was removed under reduced pressure and the crude mixture was dissolved in CH_2Cl_2 with 7 % methanol and filtrated on silica gel. The solvent was then removed under reduced pressure and the desired product was isolated by flash chromatography (silica, eluent: CH_2Cl_2 with 5 % MeOH, then increased slowly to 5.5 %). The solid was then re-crystallised form CH_2Cl_2/methanol as a purple solid. (**97**) (0.55 g, 0.81 mmol, 4.5 %).

^{1}H-NMR (600 MHz, CDCl$_3$, 298 K) δ, ppm: 9.07 (d into s, 6H, Py-H$_o$), 8.85-8.87 (d, 8H, β-H), 8.47 (d, 2H, ^{3}J= 4.2 Hz, Ar-H$_o$), 8.30 (d, 2H, ^{3}J$_{4-5}$=3.9 Hz, Ar-H$_m$), 8.17 (d, 6H, ^{3}J=2.4 Hz, Py-H$_m$), 4.13 (s, 3H, OCH$_3$), -2.87 (s, 2H, NH$_{int}$)

^{13}C-NMR (150 MHz, CDCl$_3$, DEPTQ, 298 K) δ, ppm: 167.3, 150.1, 150.1, 148.5, 148.5, 146.4, 134.7, 130.2, 129.5, 128.2, 120.3, 117.8, 117.6, 52.7

m.p. (°C): > 300

UV-Vis (CH$_2$Cl$_2$, nm) λ_{max}: Soret, 419; Q bands, 516, 552, 591, 650; Log ϵ_{415}: 5.63

ESI-MS (+ve) (m/z): 676.21 [M + H]$^+$

Synthesis of 5-(4-carboxyphenyl)-10,15,20-*tris*phenylporphyrin (**98**)
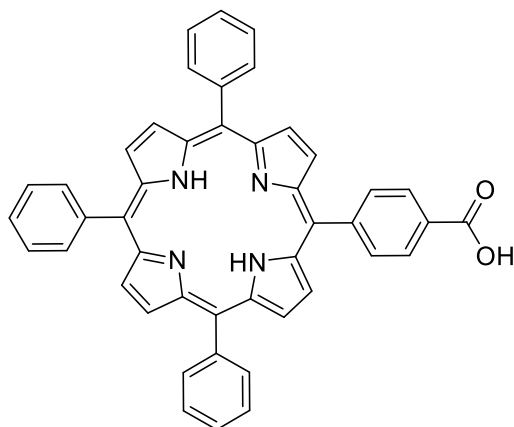
Benzaldehyde (5.5 mL, 54 mmol) and 4-formylbenzoic acid (3.6 g, 22 mmol) were dissolved in propionic acid (500 mL) in a 1 L 3 necks round bottom flask. The resulting mixture was heated to reflux under stirring. Pyrrole (5 mL, 72 mmol) was added drop-wise to the solution in a 30 minutes time. The resulting mixture was heated to reflux for 1.5 hours protected from light. Once the solution was cooled down to room temperature, the solvent was removed under reduced pressure and the crude mixture was dissolved in CH_2Cl_2 with 2 % methanol and filtrated on silica gel. The solvent was then removed under reduced pressure and the desired product was isolated by flash chromatography (silica, eluent: CH_2Cl_2/hexane 8:2, then increased to 9:1). The solid was then re-crystallised form CH_2Cl_2/methanol as a brown solid. (**98**) (0.55 g, 0.84 mmol, 4.6 %).

^{1}H-NMR (600 MHz, $CDCl_3$, 298 K) δ, ppm: 8.81-8.91 (m, 8H, β-H), 8.52 (d, 2H, J= 7.8 Hz, 5-Ar-$H_{3,5}$), 8.37 (d, 2H, J_{4-5}=7.8 Hz, 5-Ar-$H_{2,6}$), 8.22 (d, 6H, J=6.6 Hz, 10,15,20-Ar-$H_{2,6}$), 7.76-7.79 (br d, 9H, 10,15,20-Ar-$H_{2,4,6}$), -2.76 (s, 2H, NH_{int})

^{13}C-NMR (150 MHz, $CDCl_3$, 298 K) δ, ppm: 148.2, 141.6, 141.1, 137.7, 135.9, 133.4, 129.0, 122.9, 121.2

m.p. (°C): > 300

UV-Vis (CH_2Cl_2, nm) λ_{max}: Soret, 416; Q bands, 519, 557, 584, 637; Log ε_{416}: 5.56

ESI-MS (+ve) (m/z): 659.02 [M+H]$^+$

Synthesis of 5-(4-carboxymethylphenyl)-10,15,20-*tris*(pentafluorophenyl)porphyrin (**99**)
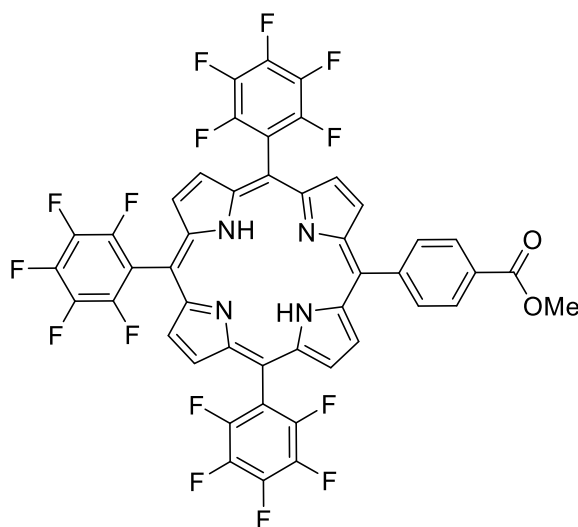
2,3,4,5,6-pentafluorobenzaldehyde (6.1 g, 31 mmol), methyl-4-formylbenzoate (1.3 g, 8 mmol) and pyrrole (3.0 mL, 43 mmol) were dissolved in CH_2Cl_2 (1600 mL) in a 2 L 3 necks round bottom flask. The resulting mixture was stirred for 30 minutes under a nitrogen atmosphere. $BF_3 \cdot Et_2O$ (0.6 mL, 2.4 mmol) was added. The resulting mixture was heated to reflux for 4 hours protected from light. After this time, chloranil (3.6 g, 15 mmol) was added to the mixture and the reaction was heated to reflux overnight (15 hours). The mixture was allowed to cool down to room temperature, washed with a saturated solution of $NaHCO_3$ (500 mL) and dried over anhydrous Na_2SO_4. The organic phase was separated and filtrated on silica gel. The solvent was then removed under reduced pressure and the desired product was isolated by flash chromatography (silica, eluent: CH_2Cl_2/hexane 2:3, then increased to 3:2). The solid was then re-crystallised form CH_2Cl_2/methanol as a brown solid. (**99**) (1.28 g, 1.35 mmol, 17 %).

^{1}H-NMR (600 MHz, $CDCl_3$, 298 K) δ, ppm: 8.85-8.92 (m, 8H, β-H), 8.48 (d, 2H, J=8.4 Hz, Ar-H$_o$), 8.31 (d, 2H, J=8.4 Hz, Ar-H$_m$), 4.14 (s, 3H, OCH_3), -2.84 (s, 2H, NH$_{int}$)

^{13}C-NMR (150 MHz, $CDCl_3$, 298 K) δ, ppm: 167.2, 147.5, 145.8, 143.2, 141.5, 138.6, 136.9, 134.7, 130.4, 128.3, 121.9, 116.2, 116.0, 115.9, 103.4, 102.4, 52.7

^{19}F-NMR (564 MHz, $CDCl_3$, 298 K) δ, ppm: -136.5 (dd, 2F, J= 8 Hz, J= 24 Hz, F$_o$), -136.7 (dd, 4F, J=8 Hz, J=24 Hz, F$_o$), -151.5 (m, 3F, F$_p$), -161.4 (m, 6F, F$_m$)

m.p. (°C): > 300

UV-Vis (CH_2Cl_2, nm) λ_{max}: Soret, 416; Q bands, 511, 539, 587, 641; Log ε_{416}: 5.38

ESI-MS (+ve) (m/z): 942.89 [M+H]$^+$

Synthesis of [5-(4-carboxymethylphenyl)-10,15,20-*tris*(4-methyl-pyridinium)porphyrin] trichloride (**100**)
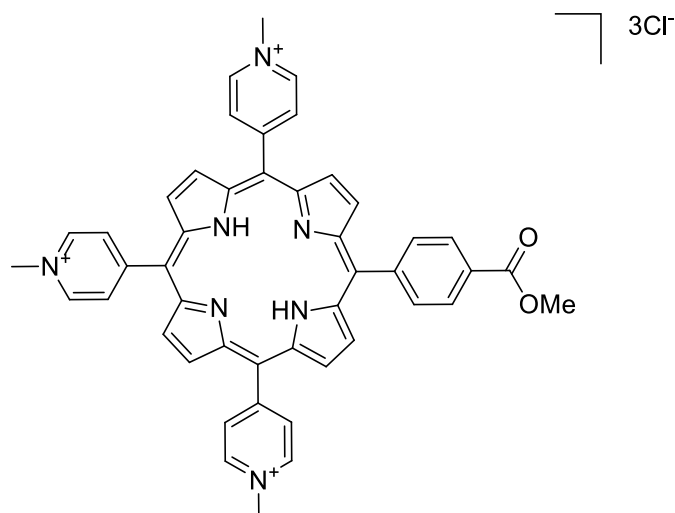
Compound **97** (500 mg, 0.74 mmol) was dissolved in NMP (30 mL) in a 100-mL round bottom flask equipped with a rubber septum. Methyl iodide (5 mL, 80 mmol) was slowly added to the solution while stirring with a syringe. The resulting mixture was heated to 40 °C and left under stirring overnight. Once the solution was cooled down to room temperature, diethyl ether (70 mL) was added to the mixture and the resulting suspension was filtrated through cotton. The filtrate was dissolved in water (200 mL) and treated with sodium hexafluorophosphate, to induce precipitation of the title compound. The resulting suspension was centrifuged, and the precipitate was re-dissolved in acetone (40 mL). The resulting mixture was treated with 10 % TBAC in acetone, leading to flocculation of the title compound, successively centrifuged and collected after further crystallisation from methanol–diethyl ether (**100**). (0.59 g, 0.73 mmol, 97 %).

^{1}H-NMR (600 MHz, DMSO-d$_6$, 298 K) δ, ppm: 9.53-9.55 (m, 6H, Py-H$_o$), 9.00-9.17 (m, 14H, β-H + Ar-H$_m$), 8.46 (d, 2H, J= 8.1 Hz, Ar-H$_o$), 8.39 (d, 2H, J$_{4-5}$=8.1 Hz, Ar-H$_m$), 4.74 (s, 9H, N$^+$CH_3), 4.07 (s, 3H, OCH_3), -3.02 (s, 2H, NH$_{int}$)

^{13}C-NMR (150 MHz, DMSO-d$_6$, 298 K) δ, ppm: 166.3, 156.4, 156.4, 145.1, 144.2, 134.6, 132.1, 129.7, 128.0, 121.3, 115.4, 114.8, 52.5, 47.8

m.p. (°C): > 300

UV-Vis (H$_2$O, nm) λ_{max}: Soret, 420; Q bands, 519, 554, 590, 647; Log ε_{420}: 5.53

ESI-MS (+ve) (m/z): 240.24 [M − 3Cl]$^{3+}$/3; 360.86 [M + H − 3Cl]$^{2+}$/2

HPLC (method A), t$_R$: 5.28 min

Synthesis of [5-(4-carboxymethylphenyl)-10,15,20-*tris*(pentafluorophenyl)porphyrinato] zinc (II) (**101**)
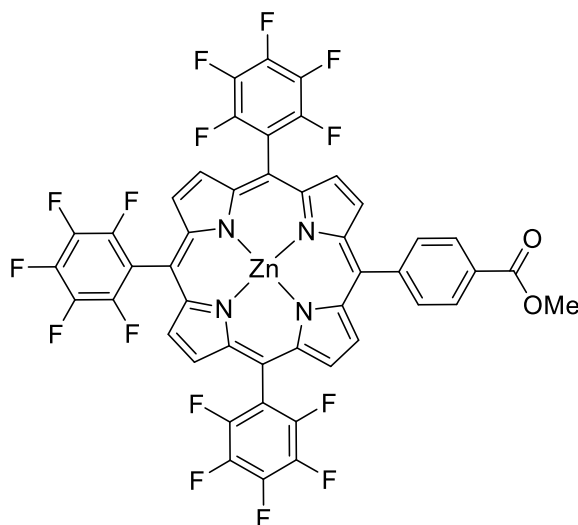
Compound **99** (500 mg, 0.53 mmol) was dissolved in chloroform (100 mL) in a 250-mL round bottom flask. Zinc acetate dihydrate (1.16 g, 5.3 mmol) was dissolved in methanol (25 mL) and added to the mixture. The reaction was heated to reflux overnight. The mixture was then allowed to cool down to room temperature, washed with water (500 mL) and dried over anhydrous Na_2SO_4. The desired product was first filtrated on silica gel, and then re-crystallised form CH_2Cl_2/methanol as a pink/purple shiny solid. (**101**) (0.52 g, 0.52 mmol, 98 %).

^{1}H-NMR (300 MHz, CDCl$_3$, 298 K) δ, ppm: 8.84-8.93 (m, 8H, β-H), 8.42 (d, 2H, J=8.4 Hz, Ar-H$_o$), 8.30 (d, 2H, J=8.4 Hz, Ar-H$_m$), 4.08 (s, 3H, OCH_3)

^{13}C-NMR (150 MHz, CDCl$_3$, 298 K) δ, ppm: 167.5, 150.4, 150.3, 150.0, 149.8, 148.3, 147.3, 145.0, 134.7, 133.6, 131.7, 131.4, 130.6, 129.7, 127.9, 122.2, 117.2, 103.3, 52.6

^{19}F-NMR (564 MHz, CDCl$_3$, 298 K) δ, ppm: -136.9 (d, 2F, J= 17.8 Hz, F$_o$), -137.0 (d, 4F, J=17.8 Hz, F$_o$), -152.3 (m, 3F, F$_p$), -161.9 (m, 6F, F$_m$)

m.p. (°C): > 300

UV-Vis (CH$_2$Cl$_2$, nm) λ_{max}: Soret, 417; Q bands, 548; Log ε_{417}: 5.59

ESI-MS (+ve) (m/z): 1005.42 [M+H]$^+$

Synthesis of {5-(4-carboxyphenyl)-10,15,20-*tris*[4-(2-sulphonatoethyl)amino-2,3,5,6-tetrafluorophenyl]porphyrinato} trisodium (**102**)
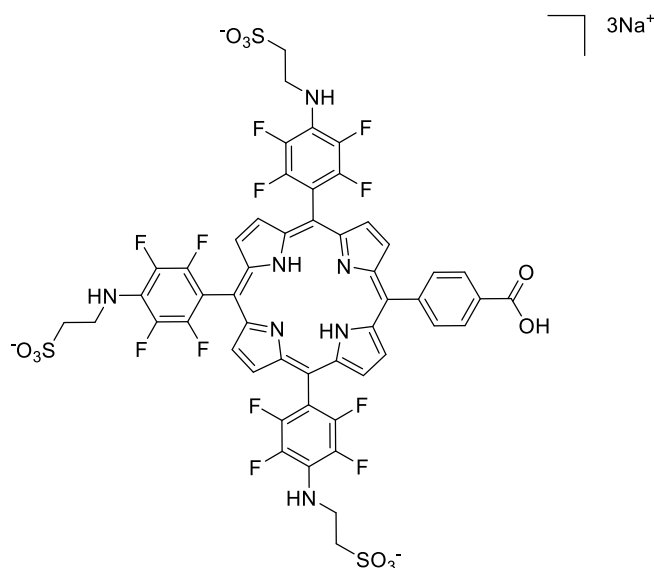
Compound **101** (500 mg, 0.50 mmol) was dissolved in NMP (50 mL) in a 100-mL round bottom flask. Compound **84** (1.31 g, 10 mmol, 20 equivalents) was added to the mixture. The reaction was heated to reflux overnight. Once the solution was cooled down to room temperature, it was filtered through celite. Diethyl ether (200 mL) was then added to the mixture to induce precipitation of the title compound. The filtrate was dissolved in water (40 mL) and HCl (10 mL) was slowly added to the stirring solution. The reaction was stirred for 2 hours at room temperature. Then the mixture was treated with compound **103**, to induce precipitation of the title compound. The resulting suspension was centrifuged and the precipitate was re-dissolved in acetone (40 mL). The resulting mixture was treated with sodium hexafluorophosphate, leading to flocculation of the title compound, successively centrifuged and collected after further crystallisation from methanol–diethyl ether (**102**). (0.64 g, 0.49 mmol, 98 %)

^{1}H-NMR (600 MHz, DMSO-d$_6$, 298 K) δ, ppm: 8.91-9.22 (m, 8H, β-H), 8.42 (d, 2H, J=6.9 Hz, Ar-H$_o$), 8.13 (d, 2H, J=6.9 Hz, Ar-H$_m$), 6.66 (s, 3H, Ar-N*H*), 3.91 (d into s, 6H, C*H$_2$*SO$_3$), 2.96 (d into s, 6H, NHC*H$_2$*), -3.03 (s, 2H, NH$_{int}$)

^{13}C-NMR (150 MHz, DMSO-d$_6$, 298 K) δ, ppm: 167.7, 147.2, 145.6, 144.8, 137.4, 135.8, 134.5, 131.2, 129.7, 127.9, 120.8, 105.0, 104.9, 104.8, 104.6, 103.7, 50.8, 41.9

^{19}F-NMR (564 MHz, DMSO-d$_6$, 298 K) δ, ppm: -143.7 (d, 6F, F$_o$), -162.6 (m, 6F, F$_m$)

m.p. (°C): > 300

UV-Vis (CH$_2$Cl$_2$, nm) λ_{max}: Soret, 417; Q bands, 517, 554, 581, 637; Log ε_{417}: 5.42

ESI-MS (-ve) (m/z): 413.46 [M – 3Na]$^{3-}$/3; 620.05 [M + H – 3Na]$^{2-}$/2; 1241.22 [M + 2H – 3Na]$^-$

HPLC (method B), t$_R$: 10.34 min

<u>Synthesis of N,N-dibutylanilinium chloride (**103**)</u>
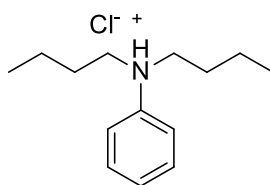
N,N-dibutylaniline (5 mL, 40 mmol) **104** was poured in a 25-mL round bottom flask equipped with a magnetic stirrer. HCl in 2-propanol (15 mL) was slowly added to the stirring solution. The reaction was left stirring at room temperature for 1 hour. The solvent was then removed under reduced pressure, and diethyl ether (50 mL) was added, causing the product to precipitate and to be collected by paper filtration. The desired product was collected as a white powder after further washing with diethyl ether. (**103**) (9.67 g, 40 mmol, quantitative yield)

^{1}H-NMR (300 MHz, D$_2$O, 298 K) δ, ppm: 7.59 (br m, 5H, Ar-H), 3.57 (t, 6H, Bu), 3.27 (s, 2H, Bu), 1.57 (br s, 2H, N$^+$H), 1.31 (br s, 6H, Bu). 0.85 (t, 6H, CH$_3$-Bu)

ESI-MS (+ve) (m/z): 207.20 [M+H]$^+$

<u>Synthesis of N,N,N-dibutylmethylanilinium nitrate (**106**)</u>
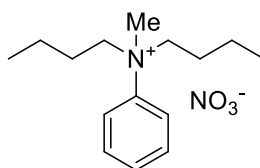
N,N-dibutylaniline (1 mL, 4.66 mmol) **104** was dissolved in acetone (5 mL) in a 10-mL round bottom flask equipped with a magnetic stirrer. Methyl iodide (2.5 mL, 40 mmol) was then added and the reaction left stirring at 50 °C overnight. The solvent was then removed under reduced pressure, and the solid was dissolved in DCM, precipitated after the addition of diethyl ether (5 mL) and collected by paper filtration. The product was dissolved in water (10 mL) and silver nitrate was added. After filtration of the yellow precipitate, the desired product was collected as a white powder after further washing with diethyl ether. (**106**) (9.67 g, 40 mmol, quantitative yield)

^{1}H-NMR (600 MHz, DMSO-d$_6$, 298 K) δ, ppm: 7.86 (d, 2H, Ar-H), 7.55-7.67 (m, 5H, Ar-H), 3.95-4.04 (m, 2H, Bu), 3.75-3.85 (m, 2H, Bu), 3.54 (s, 3H, Me), 1.52-1.66 (m, 2H, Bu), 1.13-1.31 (m, 4H, Bu), 0.93-1.08 (m, 2H, Bu), 0.80 (t, 6H, CH$_3$-Bu)

^{13}C-NMR (150 MHz, DMSO-d$_6$, 298 K) δ, ppm: 137.8, 130.3, 121.9, 58.3, 26.7, 19.1, 12.3

ESI-MS (+ve) (m/z): 220.19 [M]$^+$

Synthesis of *N*-(*tert*-butoxycarbonyl)ethanolamine (**113**)

HO⌒NHBoc
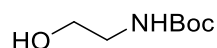
Ethanolamine (3 mL, 49.7 mmol) was dissolved in a 1 neck 100 mL round bottom flask in THF (30 mL). 25 mL of 2M solution of NaOH in water was added, and the mixture was cooled down in an ice bath for 30min while stirring. Then di-*tert*-butyl dicarbonate (14 mL, 61 mmol, 1.2 eq) was slowly added to the mixture that was left stirring at room temperature overnight. The mixture is filtrated on paper. The desired product was collected as a light brown oil after further crystallisation from methanol–diethyl ether. (8 g, 49 mmol, 100%)

^{1}H-NMR (300 MHz, CDCl$_3$, 298 K) δ, ppm: 5.07 (br s, 1H, N*H*Boc), 3.66 (t, 2H, J=5.4 Hz , C*H$_2$*OH), 3.25 (dd, 2H, J=5.4 Hz, J=10.5 Hz, C*H$_2$*NHBoc), 2.92 (br s, 1H, O*H*), 1.43 (s, 9H, NHBoc)

^{13}C-NMR (150 MHz, CDCl$_3$, DEPTQ, 298 K) δ, ppm: 156.3, 78.6, 61.0, 42.5, 27.9

ESI-MS (+ve) (m/z): 162.13 [M+H]$^+$
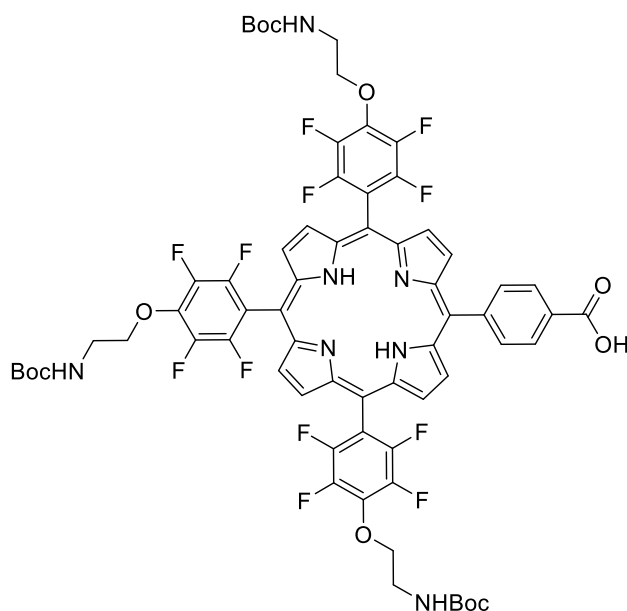
Compound **99** (780 mg, 0.83 mmol) was dissolved in dry-DMSO (20 mL) in a 50-mL round bottom flask while stirring. Compound **113** (2.5 mL, 15.9 mmol) was added to the mixture. Lithium hydroxyde (380 mg, 15.9 mmol, 30 equivalents) was triturated in a mortar and then added. The flask was sealed with a rubber septum and flushed with argon for 10 min. The solution was left stirring overnight at 33°C in a water bath. The mixture was poured in 300 mL of brine solution, causing the porphyrin to precipitate and to be collected by filtration on paper. The filtrate was dissolved in ethyl acetate, washed with water (500 mL) and dried over anhydrous Na_2SO_4. The organic phase was separated and the solvent was then removed under reduced pressure. The desired product was isolated by flash chromatography (silica, eluent: AcOEt/hexane 2:3, then increased to 3:2, then pure AcOEt). The solid was then re-crystallised form CH_2Cl_2/hexane as a brown solid. (**116**) (824 mg, 0.61 mmol, 73 %)

^{1}H-NMR (600 MHz, $CDCl_3$, 298 K) δ, ppm: 8.88-8.92 (br m, 8H, β-H), 8.59 (br s, 2H, Ar-H$_o$), 8.36 (br s, 2H, Ar-H$_m$), 5.24 (br s, 3H, N*H*Boc), 4.66 (br s, 6H, OC*H$_2$*), 3.75 (br s, 6H, C*H$_2$*NHBoc), 1.54 (s, 27H, tBu) -2.83 (br s, 2H, NH$_{int}$)

^{13}C-NMR (150 MHz, $CDCl_3$, 298 K) δ, ppm: 170.8, 156.2, 147.7, 146.8, 146.1, 141.9, 141.8, 140.3, 140.2, 138.5, 134.8, 129.6, 128.8, 121.2, 114.9, 114.7, 114.6, 104.1, 103.2, 80.1, 74.8, 40.96, 28.6

^{19}F-NMR (564 MHz, $CDCl_3$, 298 K) δ, ppm: -138.3 (d, 2F, J=16.8 Hz, F$_o$), -138.5 (d, 4F, J=16.8 Hz, F$_o$), -157.2 (br s, 6F, F$_m$)

m.p. (°C): > 300

UV-Vis (CH_2Cl_2, nm) λ_{max}: Soret, 417; Q bands, 512, 588, 646; Log ε_{417}: 5.56

ESI-MS (+ve) (m/z): 677.22 [M + 3H]$^{2+}$/2; 1353.34 [M + 2H]$^+$

Synthesis of {5-(4-carboxyphenyl)-10,15,20-*tris*[4-(2-(N,N,N-trimethylaminium)ethoxy-2,3,5,6-tetrafluorophenyl]porphyrinato} trichloride (**117**)
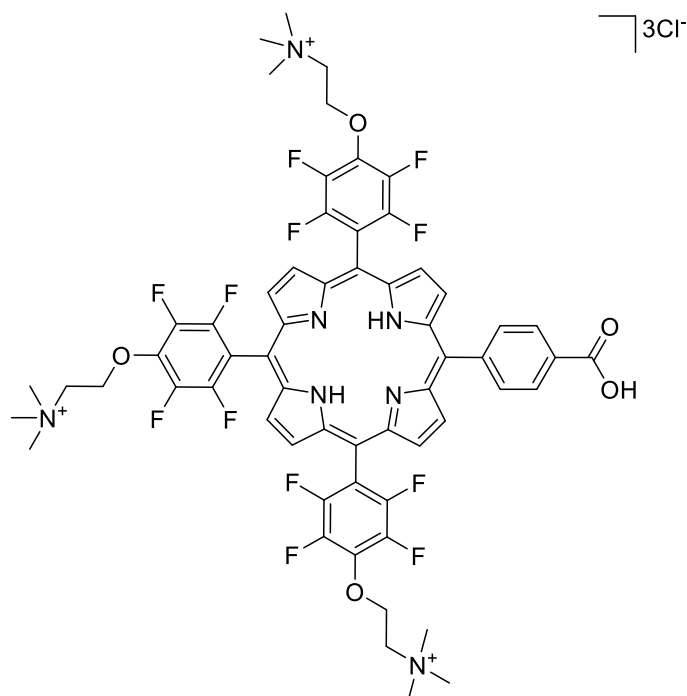
Compound **119** (500 mg, 0.38 mmol) was dissolved in water (80 mL) in a 250-mL round bottom flask. Concentrated HCl (20 mL) was added. The reaction was then heated to 60 °C overnight, and monitored with mass spectrometry. Once the solution was cooled down to room temperature, the solvent was removed under reduced pressure. The resulting solid was treated with sodium hexafluorophosphate, to induce precipitation of the title compound. The resulting suspension was centrifuged and the precipitate was re-dissolved in acetone (200 mL) and treated with 10 % TBAC in acetone, leading to flocculation of the title compound. The resulting suspension was centrifuged and the desired product was isolated after crystallisation from methanol–diethyl ether (**117**). (479 mg, 0.37 mmol, 98 %).

^{1}H-NMR (600 MHz, DMSO-d$_6$, 298 K) δ, ppm: 13.36 (br s, 1H, COO*H*), 9.37 (br s, 4H, β-H), 9.26 (br s, 2H, β-H), 8.99 (br s, 2H, β-H), 8.43 (s, 4H, Ar-H$_o$ + Ar-H$_m$), 5.17 (br s, 6H, OC*H$_2$*), 4.13 (br s, 6H, C*H$_2$*NMe$_3$), 3.41 (s, 27H, NC*H$_3$*) -3.07 (br s, 2H, NH$_{int}$)

^{13}C-NMR (150 MHz, CDCl$_3$, DEPTQ, 298 K) δ, ppm: 167.4, 147.0, 145.4, 144.7, 141.5, 139.9, 137.4, 134.6, 130.8, 128.0, 121.6, 113.5, 113.4, 113.2, 107.0, 103.5, 102.5, 68.6, 64.8, 53.2

^{19}F-NMR (564 MHz, CDCl$_3$, 298 K) δ, ppm: -141.0 (d, 6F, F$_o$), -156.6 (d, 6F, F$_m$)

m.p. (°C): > 300

UV-Vis (H$_2$O, nm) λ_{max}: Soret, 412; Q bands, 513, 581; Log ε_{412}: 5.41

ESI-MS (+ve) (m/z): 393.39 [M − 3Cl]$^{3+}$/3; 590.09 [M − H − 3Cl]$^{2+}$/2

HPLC (method A), t$_R$: 6.33

Synthesis of {5-(4-carboxyphenyl)-10,15,20-*tris*[4-(2-(tert-butoxycarbonyl)amino)ethoxy-2,3,5,6-tetrafluorophenyl]porphyrinato} tri(trifluoroacetate) (**118**)
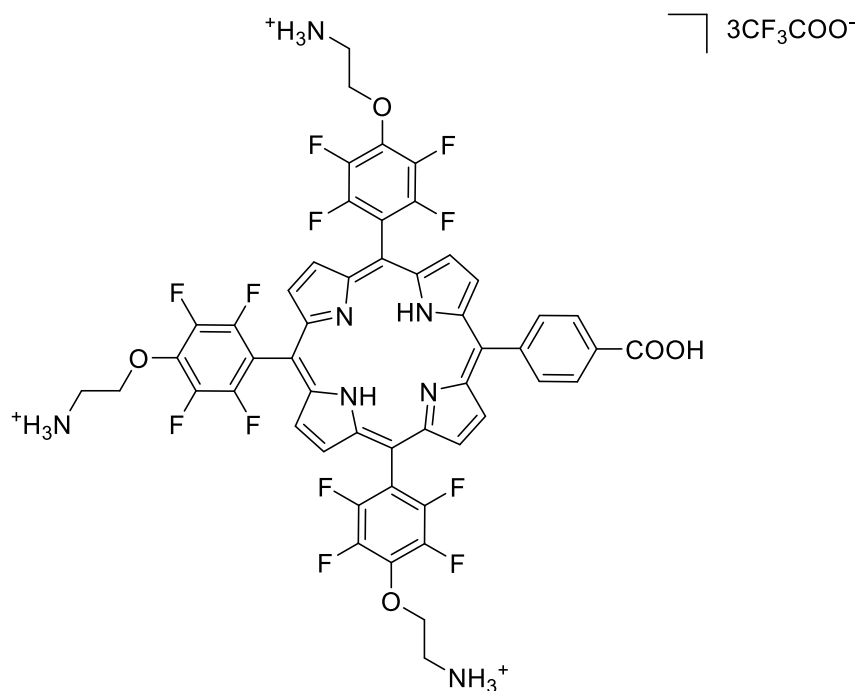
Compound **116** (500 mg, 0.37 mmol) was dissolved in chloroform (150 mL) in a 250-mL round bottom flask while stirring. The mixture was cooled down in an ice bath and TFA (5 mL, 65 mmol) was added. The solution was allowed to warm up to room temperature and stirred for 2 hours. The desired product was isolated by solvent removal under reduced pressure as a purple/bluish shiny crystal. (**118**) (390 mg, 0.37 mmol, quantitative yield)

^{1}H-NMR (600 MHz, CDCl$_3$, 298 K) δ, ppm: 13.51 (br s, 1H, COOH), 9.00-9.34 (m, 8H, β-H), 8.43 (s, 4H, Ar-H$_o$ + Ar-H$_m$), 8.34 (br s, 9H, NH_3), 4.81 (m, 6H, OCH_2), 3.50 (m, 6H, CH_2NH$_2$), -3.07 (br s, 2H, NH$_{int}$)

^{13}C-NMR (150 MHz, CDCl$_3$, 298 K) δ, ppm: 167.5, 158.6, 158.4, 158.2, 158.0, 147.1, 145.5, 144.7, 141.7, 140.0, 139.9, 137.7, 134.6, 130.8, 128.0, 121.6, 118.9, 117.0, 115.0, 113.6, 113.5, 113.4, 113.1, 103.6, 102.5, 71.6, 40.1

^{19}F-NMR (564 MHz, CDCl$_3$, 298 K) δ, ppm: -74.5 (s, CF$_3$COO$^-$), -140.8 (m, 6F, F$_o$), -156.8 (d, 6F, J=21.4 Hz, F$_m$)

m.p. (°C): > 300

UV-Vis (H$_2$O, nm) λ_{max}: Soret, 412; Q bands, 514, 580; Log ε_{412}: 5.30

ESI-MS (+ve) (m/z): 351.65 [M − 3CF$_3$COO]$^{3+}$/3; 526.55 [M − H − 3CF$_3$COO]$^{2+}$/2; 1051.01 [M − 2H − 3CF$_3$COO]$^+$

HPLC (method A), t$_R$: 6.12

<u>Synthesis of {5-(4-carboxymethylphenyl)-10,15,20-*tris*[4-(2-(N,N,N-trimethylaminium)ethoxy-2,3,5,6-tetrafluorophenyl]porphyrinato} trichloride (**119**)</u>
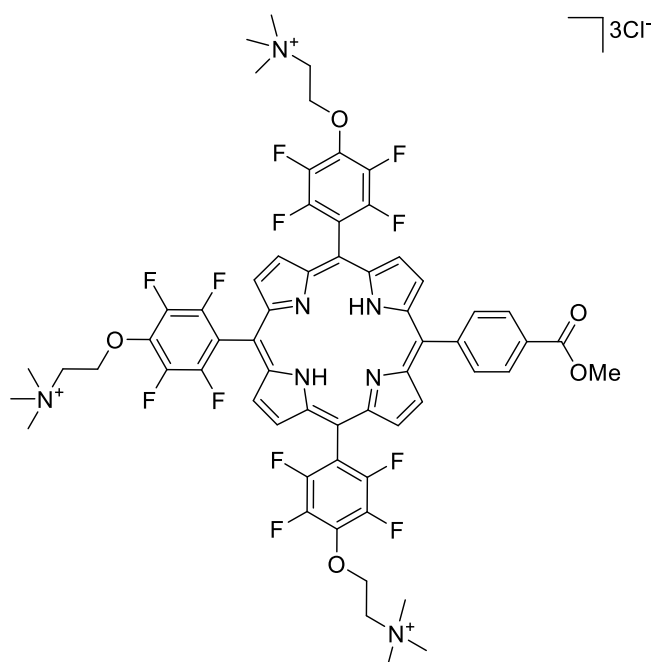
Compound **118** (500 mg, 0.39 mmol) was dissolved in NMP (20 mL) in a 50-mL round bottom flask, sealed with a rubber septum and flushed with argon for 10 minutes, while cooling down in an ice bath. Methyl iodide (2.3 mL, 37 mmol) was mixed with NMP (5mL) and slowly added with a syringe to the mixture while stirring. The reaction was then heated to 40 °C overnight. Once the solution was cooled down to room temperature, brine (200 mL) was added to the mixture and the resulting suspension was filtrated through paper. The filtrate was dissolved in acetone (200 mL) and treated with 10 % TBAC in acetone, to induce precipitation of the title compound. The resulting suspension was centrifuged and the desired product was isolated after further crystallisation from methanol–diethyl ether (**119**). (486 mg, 0.37 mmol, 96 %).

^{1}H-NMR (600 MHz, DMSO-d_6, 298 K) δ, ppm: 8.97-9.39 (m, 8H, β-H), 8.44 (br s, 4H, Ar-H$_o$ + Ar-H$_m$), 5.19 (br s, 6H, OCH_2), 4.16 (br s, 6H, CH_2NMe$_3$), 4.05 (br s, 3H, COOCH_3), 3.43 (s, 27H, NMe$_3$) -3.08 (br s, 2H, NH$_{int}$)

^{13}C-NMR (150 MHz, CDCl$_3$, 298 K) δ, ppm: 166.4, 147.0, 145.4, 145.1, 141.4, 139.9, 137.4, 134.7, 129.6, 127.8, 121.2, 113.5, 113.3, 113.2, 113.1, 113.0, 103.6, 102.6, 53.2, 52.5, 40.0

^{19}F-NMR (564 MHz, CDCl$_3$, 298 K) δ, ppm: -141.0 (d, 6F, F$_o$), -156.6 (d, 6F, F$_m$)

m.p. (°C): > 300

UV-Vis (H$_2$O, nm) λ_{max}: Soret, 412; Q bands, 514, 580; Log ε_{412}: 5.26

ESI-MS (+ve) (m/z): 398.29 [M − 3Cl]$^{3+}$/3

HPLC (method A), t$_R$: 6.57

Synthesis of {5-(4-carboxyphenyl)-10,15,20-*tris*[4-(2-(N,N,N-trimethylaminium)ethoxy-2,3,5,6-tetrafluorophenyl]porphyrinato} palladium (II) trichloride (**120**)
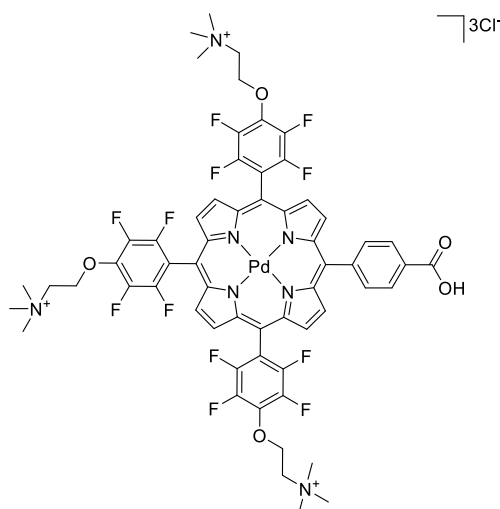
Compound **117** (100 mg, 0.078 mmol) was dissolved in water (50 mL) in a 100-mL round bottom flask, equipped with a condenser. Palladium acetate (175 mg, 0.78 mmol) was dissolved under sonication in methanol (5 mL) and then added to the mixture. The reaction was then heated to reflux and monitored with mass spectrometry. Once the solution was cooled down to room temperature, the solvent was removed under reduced pressure and the resulting solid was dissolved in methanol and filtrated through celite. Subsequently, the solvent was removed under reduced pressure and the crude re-dissolved in water. The resulting solution was treated with sodium hexafluorophosphate, to induce precipitation of the title compound. The resulting suspension was centrifuged and the precipitate was re-dissolved in acetone (200 mL) and treated with 10 % TBAC in acetone, leading to flocculation of the title compound. The resulting suspension was centrifuged and the desired product was isolated after further crystallisation from methanol–diethyl ether (**120**). (88 mg, 0.064 mmol, 82 %).

^{1}H-NMR (600 MHz, DMSO-d$_6$, 298 K) δ, ppm: 13.68 (br s, 1H, COO*H*), 9.33 (br dd, 4H, J=4.2 Hz, J=9.6 Hz, β-H), 9.21 (br d, 2H, J=4.8 Hz, β-H), 8.95 (br d, 2H, J=4.8 Hz, β-H), 8.40 (br d, 2H, J=7.8 Hz, Ar-H$_m$), 8.34 (br d, 2H, J=7.8 Hz, Ar-H$_o$), 5.16 (br s, 6H, OC*H$_2$*), 4.12 (br s, 6H, C*H$_2$*NMe$_3$), 3.40 (d, 27H, NC*H$_3$*)

^{13}C-NMR (150 MHz, CDCl$_3$, 298 K) δ, ppm: 167.7, 146.9, 145.3, 141.7, 141.5, 141.3, 141.2, 141.2, 139.9, 139.8, 137.4, 134.0, 133.0, 132.3, 132.0, 131.1, 127.9, 113.0, 112.9, 112.9, 105.5, 104.7, 68.6, 64.8, 53.2

^{19}F-NMR (564 MHz, CDCl$_3$, 298 K) δ, ppm: -140.8 (d, 6F, F$_o$), -156.5 (d, 6F, F$_m$)

m.p. (°C): > 300

UV-Vis (H$_2$O, nm) λ_{max}: Soret, 408; Q bands, 522, 556; Log ε_{408}: 5.21

ESI-MS (+ve) (m/z): 428.24 [M – 3Cl]$^{3+}$/3

HPLC (method A), t$_R$: 6.32

Synthesis of {5-(4-carboxyphenyl)-10,15,20-*tris*[4-(2-sulphonatoethyl)amino-2,3,5,6-tetrafluorophenyl]porphyrinato}palladium (II) trisodium (**121**)
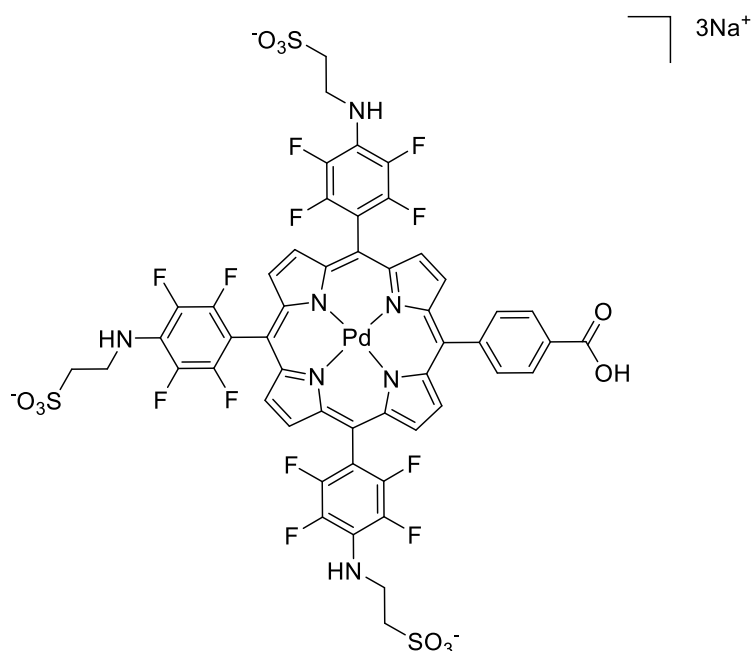
Compound **102** (100 mg, 0.076 mmol) was dissolved in water (10 mL) in a 35-mL microwave vial. Palladium acetate (171 mg, 0.23 mmol) was dissolved in methanol (3 mL) and added to the solution while stirring. The resulting mixture was flushed with argon for 10 minutes and exposed to microwave heating (110 °C, 250 W, 15 minutes). Once the solution was cooled down to room temperature, it was diluted with water (30 mL) and filtered through celite. The filtrate was treated with compound **103**, to induce precipitation of the title compound. The resulting suspension was centrifuged and the precipitate was re-dissolved in acetone (40 mL). The resulting mixture was treated with sodium hexafluorophosphate, leading to flocculation of the title compound, successively centrifuged and collected after further crystallisation from methanol–diethyl ether (**121**). (90 mg, 0.063 mmol, 84 %)

^{1}H-NMR (600 MHz, DMSO-d$_6$, 298 K) δ, ppm: 12.64 (br s, 1H, COO*H*), 8.87-9.20 (m, 8H, β-H), 8.39 (2d into br s, 4H, Ar-H$_o$ + Ar-H$_m$), 6.68 (br s, 3H, Ar-N*H*), 3.93 (d into s, 6H, C*H$_2$*SO$_3$), 2.98 (d into s, 6H, NHC*H$_2$*)

^{13}C-NMR (150 MHz, DMSO-d$_6$, 298 K) δ, ppm: 167.4, 147.1, 145.5, 144.6, 142.1, 141.7, 140.9, 137.3, 135.8, 134.2, 132.5, 132.1, 131.9, 131.3, 130.8, 129.8, 128.0, 122.2, 106.6, 105.9, 104.4, 50.8, 41.9

^{19}F-NMR (564 MHz, DMSO-d$_6$, 298 K) δ, ppm: -142.9 (br s, 6F, F$_o$), -160.7 (br s, 6F, F$_m$)

m.p. (°C): > 300

UV-Vis (CH$_2$Cl$_2$, nm) λ_{max}: Soret, 413; Q bands, 523, 555; Log ε_{413}: 5.29

ESI-MS (-ve) (m/z): 336.30 [M − H − 3Na]$^{4-}$/4; 448.04 [M − 3Na]$^{3-}$/3

HPLC (method B), t$_R$: 10.03

Synthesis of bis(benzonitrile)dichloroplatinum (II) (**123**)

$$Pt(PhCN)_2Cl_2$$

Platinum bis(benzonitrile)dichloride (1.6 g, 6 mmol) **122** was dissolved in benzonitrile (50 mL) a 25-mL round bottom flask equipped with a magnetic stirrer. The reaction was heated to 100 °C for 4 hours. The solution was then filtered and the filtrate was collected. Hexane (200 mL) was then added to the solution, causing the product to precipitate and to be collected by paper filtration. The desired product was collected as a yellow powder after further washing with hexane. (**123**) (2.52 g, 5.35 mmol, 89 %)

ESI-MS (+ve) (m/z): 472.02 $[M+H]^+$

Synthesis of platinum diaqua(DMSO) (**125**)

$$Pt(DMSO)_2(H_2O)_2$$
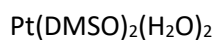
Platinum dichloride (400 mg, 0.85 mmol) **122** was dissolved in DMSO (30 mL) a 10-mL round bottom flask equipped with a magnetic stirrer and stirred for 3 hours. After this time silver nitrate (288 mg, 1.7 mmol) was dissolved in H_2O (7 mL) and added to the stirring solution. The mixture was stirred for further 4 hours protected from light, filtered and employed immediately for the metal insertion. (**125**) (2.52 g, 5.35 mmol, 89 %)

<u>Synthesis of {5-(4-carboxyphenyl)-10,15,20-*tris*[4-{2-sulphonatoethyl}amino-2,3,5,6-tetrafluorophenyl]porphyrinato}platinum (II) trisodium (**126**)</u>
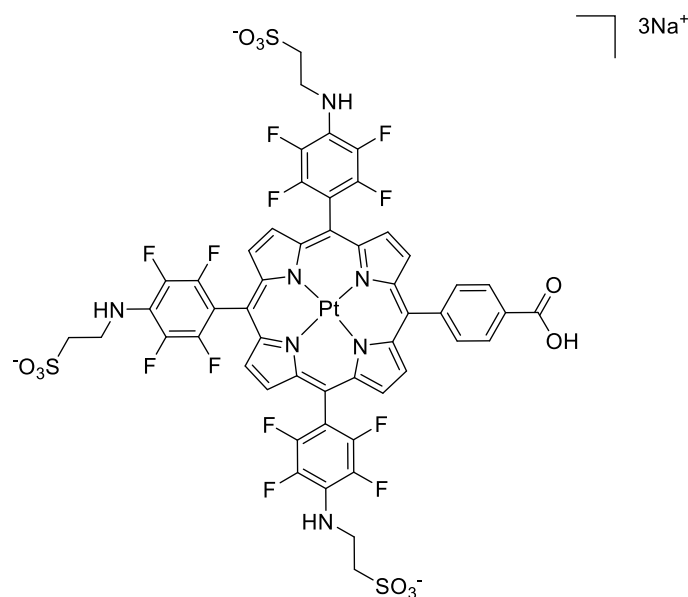
Compound **125** (217 mg, 0.46 mmol) was dissolved in DMSO (1.5 mL) and stirred at room temperature for 3 hours. Silver nitrate (156 mg, 0.92 mmol) and water (11.5 mL) were added to mixture, protected from light with tin foil, and stirred at room temperature for 3 hours. The mixture was subsequently centrifuged and then filtered to remove all silver chloride formed. The solution was transferred in a 35-mL microwave vial and compound **102** (200 mg, 0.15 mmol) was then added while stirring. The resulting mixture was flushed with argon for 10 minutes and exposed to microwave heating (200 °C, 300 W, 20 minutes). Once the solution was cooled down to room temperature, it was diluted with water (30 mL) and filtered through celite. The filtrate was treated with compound **103**, to induce precipitation of the title compound. The resulting suspension was centrifuged and the precipitate was re-dissolved in acetone (40 mL). The resulting mixture was treated with sodium hexafluorophosphate, leading to flocculation of the title compound, successively centrifuged and collected after further crystallisation from methanol–diethyl ether (**126**). (215 mg, 0.14 mmol, 94 %)

^{1}H-NMR (600 MHz, DMSO-d$_6$, 298 K) δ, ppm: 8.81-9.18 (br m, 8H, β-H), 8.39 (br s, 4H, Ar-H$_o$ + Ar-H$_m$), 6.69 (s, 3H, Ar-N*H*), 3.92 (br s, 6H, C*H$_2$*SO$_3$), 2.98 (br s, 6H, NHC*H$_2$*)

^{13}C-NMR (150 MHz, DMSO-d$_6$, 298 K) δ, ppm: 167.4, 147.1, 145.5, 144.6, 142.1, 141.7, 140.9, 137.3, 1353.8, 134.2, 132.5, 132.1, 131.9, 131.3, 130.8, 129.8, 127.9, 122.2, 106.6, 105.9, 104.4, 50.8, 41.9

^{19}F-NMR (564 MHz, DMSO-d$_6$, 298 K) δ, ppm: -142.9 (br s, 6F, F$_o$), -160.8 (br s, 6F, F$_m$)

m.p. (°C): > 300

UV-Vis (CH$_2$Cl$_2$, nm) λ_{max}: Soret, 399; Q bands, 511, 543; Log ε_{399}: 5.18

ESI-MS (-ve) (m/z): 477.56 [M – 3Na]$^{3-}$/3; 717.90 [M + H – 3Na]$^{2-}$/2;

HPLC (method B), t$_R$: 10.19 min

<u>Synthesis of [5-(4-carboxyphenyl)-10,15,20-*tris*(4-methyl-pyridinium)porphyrinato]indium chloride
(III) trichloride (**127**)</u>
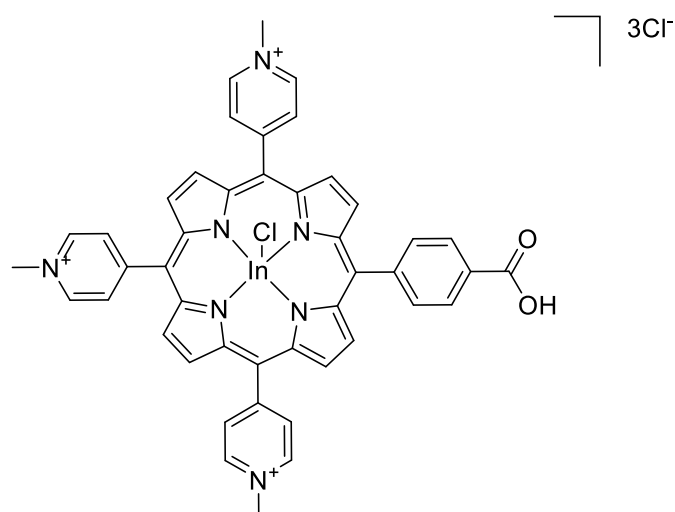
Compound **73** (200 mg, 0.25 mmol) was dissolved in water (40 mL) in a 100-mL round bottom flask. Indium chloride (166 mg, 0.75 mmol) was added, and the solution was heated to reflux overnight. Once the solution was cooled down to room temperature, it was filtered through celite. The filtrate was diluted with water (40 mL) and treated with sodium hexafluorophosphate, to induce precipitation of the title compound. The resulting suspension was centrifuged and the precipitate was re-dissolved in acetone (40 mL). The resulting mixture was treated with 10 % TBAC in acetone, leading to flocculation of the title compound, successively centrifuged and collected after further crystallisation from methanol–diethyl ether. (**127**) (235 mg, 0.24 mmol, 98 %)

^{1}H-NMR (600 MHz, CDCl$_3$, 298 K) δ, ppm: 13.29 (br s, 1H, OH), 9.52 (d into br s, 6H, Py-H$_m$), 8.98-9.28 (m, 14H, Py-H$_o$ + β-H), 8.35-8.44 (d, 4H, Ar-H$_o$ + Ar-H$_m$), 4.74 (s, 9H, NC*H$_3$*)

^{13}C-NMR (75 MHz, DMSO-d$_6$, DEPTQ, 298 K) δ, ppm: 167.5, 156.1, 143.7, 141.4, 140.0, 139.9, 139.7, 133.0, 132.9, 132.4, 131.7, 131.6, 131.5, 128.0, 117.1, 116.6, 47.7

m.p. (°C): > 300

UV-Vis (H$_2$O, nm) λ_{max}: Soret, 419; Q bands, 529, 565; Log ε_{419}: 5.29

ESI-MS (+ve) (m/z): 284.69 [M − 3Cl]$^{3+}$/3; 426.52 [M − H − 3Cl]$^{2+}$/2; 854.08 [M − 3Cl]$^+$

HPLC (method A), t$_R$: 1.39 min

Synthesis of [5-(4-carboxyphenyl)-10,15,20-*tris*(4-sulphonatophenyl)porphyrinato]indium (III) chloride trisodium (**128**)
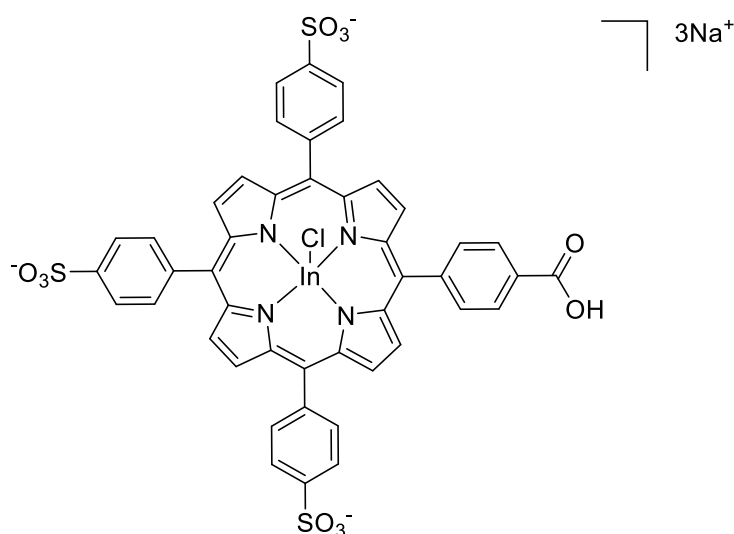
Compound **76** (100 mg, 0.10 mmol) was dissolved in water (10 mL) in a 35-mL microwave vial. Indium chloride (69 mg, 0.31 mmol) was added to the solution while stirring. The resulting mixture was flushed with argon for 10 minutes and exposed to microwave heating (120 °C, 250 W, 15 minutes). Once the solution was cooled down to room temperature, it was diluted with water (30 mL) and filtered through celite. The filtrate was treated with compound **103**, to induce precipitation of the title compound. The resulting suspension was centrifuged and the precipitate was re-dissolved in acetone (40 mL). The resulting mixture was treated with sodium hexafluorophosphate, leading to flocculation of the title compound, successively centrifuged and collected after further crystallisation from methanol–diethyl ether (**128**). (95 mg, 0.08 mmol, 83 %)

^{1}H-NMR (300 MHz, DMSO-d$_6$, 298 K) δ, ppm: 13.22 (br s, 1H, COO*H*), 9.07-9.11 (m, 8H, β-H), 8.43 (q, 4H, 5-Ar-H$_o$ + 5-Ar-H$_m$), 8.25 (d, 6H, J=8.1 Hz, 10,15,20-Ar-H$_{3,5}$), 8.11 (d, 6H, J=7.8 Hz, 10,15,20-Ar-H$_{2,6}$)

^{13}C-NMR (75 MHz, DMSO-d$_6$, DEPTQ, 298 K) δ, ppm: 167.5, 148.2, 148.1, 148.0, 147.6, 145.4, 141.0, 134.8, 134.1, 133.4, 133.1, 130.7, 128.0, 124.3, 121.8, 121.6, 120.6

m.p. (°C): > 300

UV-Vis (H$_2$O, nm) λ_{max}: Soret, 412; Q bands, 526; Log ε_{412}: 5.30

ESI-MS (-ve) (m/z): 347.73 [M – 3Na]$^{3-}$/3

HPLC (method B), t$_R$: 8.43 min

Synthesis of [5,10,15,20-*tetrakis*(4-methyl-pyridinium)porphyrin] zinc (II) tetrachloride (**130**)
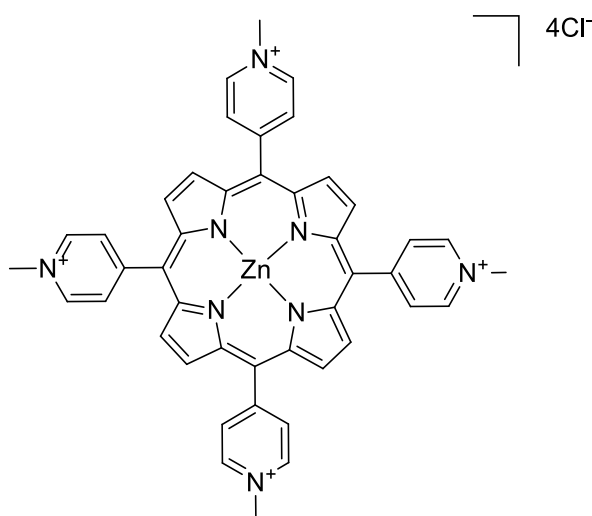
Compound **51** (208 mg, 0.25 mmol) was dissolved in water (40 mL) in a 100-mL round bottom flask. Zinc acetate (280 mg, 1.27 mmol) was added to the solution while stirring. The resulting mixture was heated to reflux overnight. Once the solution was cooled down to room temperature, it was diluted with water (120 mL) and treated with sodium hexafluorophosphate, to induce precipitation of the title compound. The resulting suspension was centrifuged and the precipitate was re-dissolved in acetone (40 mL). The resulting mixture was treated with 10 % TBAC in acetone, leading to flocculation of the title compound, successively centrifuged and collected after further crystallisation from methanol– diethyl ether. (**130**) (188 mg, 0.21 mmol, 84 %)

^{1}H-NMR (600 MHz, DMSO-d$_6$, 298 K) δ, ppm: 9.46 (d, 6H, J=6.6 Hz, Py-H$_m$), 9.01 (br s, 8H, β-H), 8.88 (d, 8H, J= 6.6 Hz, Py-H$_o$), 4.73 (s, 12H, NC*H$_3$*)

^{13}C-NMR (150 MHz, DMSO-d$_6$, 298 K) δ, ppm: 158.2, 148.4, 143.7, 132.4, 132.0, 115.9, 47.7

UV-Vis (H$_2$O, nm) λ_{max}: Soret, 439; Q bands, 567, 612; Log ε_{439}: 5.27

ESI-MS (+ve) (m/z): 185.01 [M − 4Cl]$^{4+}$/4; 246.34 [M − H − 4Cl]$^{3+}$/3; 370.05 [M −2H − 4Cl]$^{2+}$/2

HPLC (method A), t$_R$: 1.21 min

Synthesis of [5,10,15,20-*tetrakis*(4-methyl-pyridinium)porphyrin] iron (III) tetrachloride (**131**)
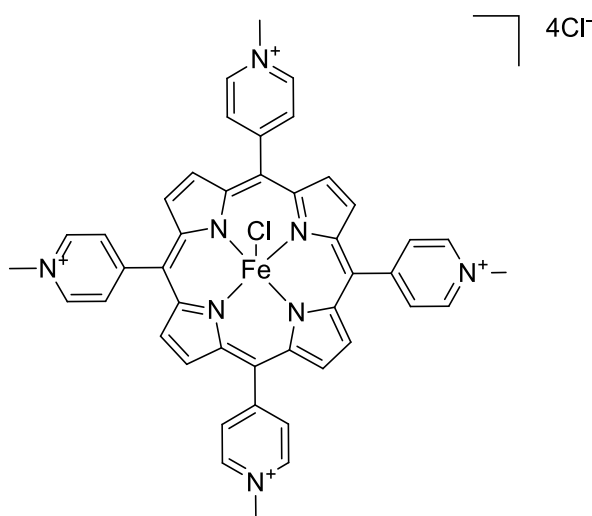
Compound **51** (140 mg, 0.17 mmol) was dissolved in water (40 mL) in a 100-mL round bottom flask. Iron dichloride tetrahydrate (170 mg, 0.85 mmol) was added to the solution while stirring. The resulting mixture was heated to reflux overnight. Once the solution was cooled down to room temperature, it was diluted with water (120 mL) and treated with sodium hexafluorophosphate NaPF$_6$, to induce precipitation of the title compound. The resulting suspension was centrifuged and the precipitate was re-dissolved in acetone (40 mL). The resulting mixture was treated with 10 % TBAC in acetone, leading to flocculation of the title compound, successively centrifuged and collected after further crystallisation from methanol–diethyl ether. (**131**) (122 mg, 0.13 mmol, 78 %)

UV-Vis (H$_2$O, nm) λ_{max}: Soret, 426; Q bands, 600, 641; Log ε_{426}: 4.77

ESI-MS (+ve) (m/z): 255.66 [M − H − 4Cl]$^{3+}$/3

HPLC (method A), t$_R$: 1.30 min

Synthesis of {5-[4-(N-succinimidyloxycarbonyl)phenyl]-10,15,20-*tris*(4-methyl-pyridinium)porphyrinato}platinum (II) trichloride (**132**)
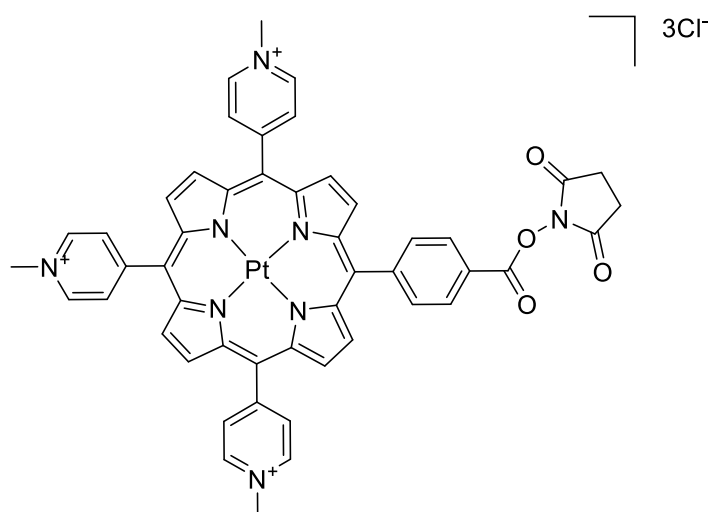
Compound **74** (99 mg, 0.09 mmol) and N-hydroxysuccinimide (115 mg, 1.0 mmol) were dissolved in DMSO (10 mL) in a 20-mL vial equipped with magnetic stir bar. 1-ethyl-3-(3-dimethylaminopropyl)carbodiimide hydrochloride (192 mg, 1.0 mmol) was then added to the mixture. The reaction was heated to 40 °C for 24 hours. Once the solution was cooled down to room temperature, the mixture was diluted with water (40 mL) and treated with sodium hexafluorophosphate, to induce precipitation of the title compound. The resulting suspension was centrifuged and the precipitate was re-dissolved in acetone (40 mL). The resulting mixture was treated with 10 % TBAC in acetone, leading to flocculation of the title compound, successively centrifuged and collected after further crystallisation from methanol–diethyl ether. (**132**) (85 mg, 0.077 mmol, 86 %)

^{1}H-NMR (600 MHz, CDCl$_3$, 298 K) δ, ppm: 9.51 (d into s, 6H, Py-H$_m$), 8.97-9.04 (m, 14H, Py-H$_o$ + β-H), 8.58 (d, 2H, Ar-H), 4.73 (s, 9H, NCH_3), 3.01 (s, 4H, NHS-CH$_2$)

^{13}C-NMR (150 MHz, DMSO-d$_6$, 298 K) δ, ppm: 170.4, 161.9, 160.4, 155.4, 144.5, 140.5, 139.2, 139.0, 134.5, 131.6, 129.0, 117.8, 47.8, 25.7

m.p. (°C): > 300

UV-Vis (H$_2$O, nm) λ_{max}: Soret, 404; Q bands, 515, 548; Log ε_{404}: 5.29

ESI-MS (+ve) (m/z): 332.27 [M − 3Cl]$^{3+}$/3; 497.90 [M − H − 3Cl]$^{2+}$/2,

HPLC (method A), t$_R$: 5.43 min

Synthesis of {5-[4-(N-succinimidyloxycarbonyl)phenyl]-10,15,20-*tris*(4-methyl-pyridinium)porphyrinato}palladium (II) trichloride (**133**)
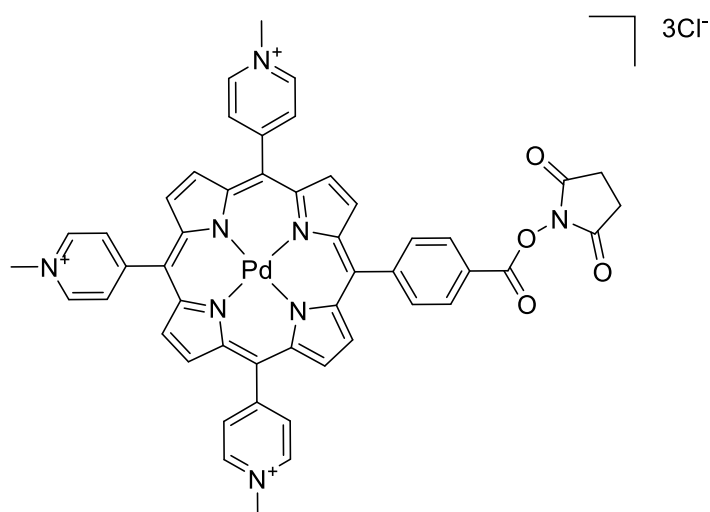
Compound **75** (10 mg, 0.011 mmol) and N-hydroxysuccinimide (25 mg, 0.22 mmol) were dissolved in DMSO (5 mL) in a 10-mL vial equipped with magnetic stir bar. 1-ethyl-3-(3-dimethylaminopropyl)carbodiimide hydrochloride (42 mg, 0.22 mmol) was then added to the mixture. The reaction was heated to 40 °C for 24 hours. Once the solution was cooled down to room temperature, the mixture was diluted with water (40 mL) and treated with sodium hexafluorophosphate, to induce precipitation of the title compound. The resulting suspension was centrifuged and the precipitate was re-dissolved in acetone (40 mL). The resulting mixture was treated with 10 % TBAC in acetone, leading to flocculation of the title compound, successively centrifuged and collected after further crystallisation from methanol–diethyl ether. (**133**) (8.6 mg, 0.0086 mmol, 78 %)

^{1}H-NMR (600 MHz, CDCl$_3$, 298 K) δ, ppm: 9.51 (d into s, 6H, Py-H$_m$), 8.98-9.11 (m, 14H, Py-H$_o$ + β-H), 8.58 (d, 2H, J=8.4 Hz, Ar-H$_o$), 8.46 (d, 2H, J=8.4 Hz, Ar-H$_m$), 4.73 (s, 9H, NCH_3), 3.02 (br s, 4H, NHS-CH$_2$)

^{13}C-NMR (150 MHz, DMSO-d$_6$, 298 K) δ, ppm: 170.5, 155.9, 144.3, 141.1, 139.9, 139.7, 134.7, 132.1, 128.9, 117.2, 47.8, 25.7

m.p. (°C): > 300

UV-Vis (H$_2$O, nm) λ_{max}: Soret, 419; Q bands, 528, 563; Log ε_{419}: 5.01

ESI-MS (+ve) (m/z): 302.56 [M − 3Cl]$^{3+}$/3; 453.36 [M − H − 3Cl]$^{2+}$/2

HPLC (method A), t$_R$: 5.45 min

Synthesis of {5-[4-(N-succinimidyloxycarbonyl)phenyl]-10,15,20-*tris*(4-sulphonatophenyl)porphyrinato}platinum (II) trichloride (**134**)
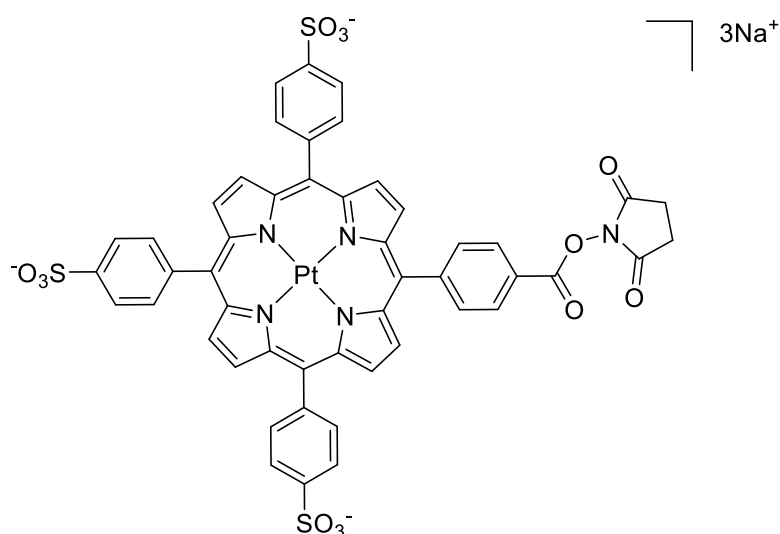
Compound **77** (110 mg, 0.095 mmol) and N-hydroxysuccinimide (115 mg, 1.0 mmol) were dissolved in DMSO (5 mL) in a 10-mL vial equipped with stir bar. 1-ethyl-3-(3-dimethylaminopropyl)carbodiimide hydrochloride (192 mg, 1.0 mmol) was then added to the mixture. The reaction was heated to 40 °C for 24 hours. Once the solution was cooled down to room temperature, it was diluted with water (40 mL) and filtered through celite. The filtrate was treated with compound **103**, to induce precipitation of the title compound. The resulting suspension was centrifuged and the precipitate was re-dissolved in acetone (40 mL). The resulting mixture was treated with sodium hexafluorophosphate, leading to flocculation of the title compound, successively centrifuged and collected after further crystallisation from methanol–diethyl ether. (**134**) (87 mg, 0.069 mmol, 72 %)

^{1}H-NMR (600 MHz, DMSO-d_6, 298 K) δ, ppm: 8.78-8.81 (m, 8H, β-H), 8.53 (d, 2H, J=7.8 Hz, 5-Ar-H_o), 8.48 (d, 2H, J=7.8 Hz, 5-Ar-H_m), 8.14 (d, 6H, J=7.2 Hz, 10,15,20-Ar-$H_{3,5}$), 8.05 (d, 6H, J=7.8 Hz, 10,15,20-Ar-$H_{2,6}$), 3.00 (br s, 4H, NHS-CH_2)

^{13}C-NMR (150 MHz, DMSO-d_6, 298 K) δ, ppm: 170.4, 162.0, 148.1, 140.2, 140.2, 140.1, 139.4, 134.6, 133.1, 131.3, 131.1, 130.9, 128.8, 124.3, 122.2, 25.7, 25.2

m.p. (°C): > 300

UV-Vis (H_2O, nm) λ_{max}: Soret, 399; Q bands, 511; Log ε_{419}: 5.26

ESI-MS (-ve) (m/z): 394.73 [M − 3Na]$^{3-}$/3; 592.60 [M + H − 3Na]$^{2-}$/2

HPLC (method B), t_R: 10.16

Synthesis of {5-[4-(N-succinimidyloxycarbonyl)phenyl]-10,15,20-*tris*(4-sulphonatophenyl)porphyrinato}palladium (II) trichloride (**135**)
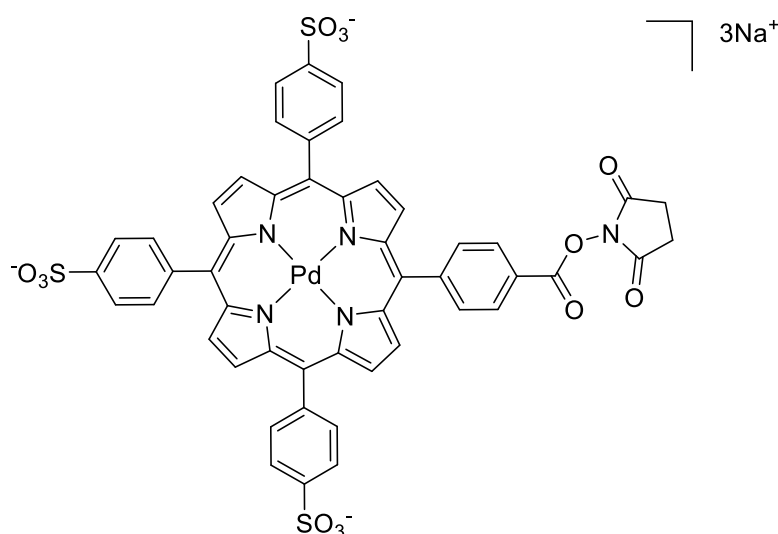
Compound 7**8** (100 mg, 0.094 mmol) and N-hydroxysuccinimide (216 mg, 1.88 mmol) were dissolved in DMSO (5 mL) in a 10-mL vial equipped with stir bar. 1-ethyl-3-(3-dimethylaminopropyl)carbodiimide hydrochloride (360 mg, 1.88 mmol) was then added to the mixture. The reaction was heated to 40 °C for 24 hours. Once the solution was cooled down to room temperature, it was diluted with water (40 mL) and treated with compound **103**, to induce precipitation of the title compound. The resulting suspension was centrifuged and the precipitate was re-dissolved in acetone (40 mL). The resulting mixture was treated with sodium hexafluorophosphate, leading to flocculation of the title compound, successively centrifuged and collected after further crystallisation from methanol–diethyl ether. (**135**) (78 mg, 0.067 mmol, 71 %)

^{1}H-NMR (600 MHz, DMSO-d$_6$, 298 K) δ, ppm: 8.78-8.87 (m, 8H, β-H), 8.53 (d, 2H, J=7.8 Hz, 5-Ar-H$_o$), 8.48 (d, 2H, J=7.8 Hz, 5-Ar-H$_m$), 8.15 (d, 6H, J=7.2 Hz, 10,15,20-Ar-H$_{3,5}$), 8.04 (d, 6H, J=7.8 Hz, 10,15,20-Ar-H$_{2,6}$), 3.00 (br s, 4H, NHS-CH$_2$)

^{13}C-NMR (150 MHz, DMSO-d$_6$, 298 K) δ, ppm: 170.4, 162.0, 148.1, 147.8, 141.0, 140.9, 140.8, 140.6, 140.2, 134.8, 133.3, 131.6, 131.5, 131.4, 131.1, 128.7, 124.2, 121.8, 121.6, 119.8, 25.6, 25.2

m.p. (°C): > 300

UV-Vis (H$_2$O, nm) λ_{max}: Soret, 412; Q bands, 527; Log ε_{419}: 5.07

ESI-MS (-ve) (m/z): 364.85 [M − 3Na]$^{3-}$/3; 548.76 [M + H − 3Na]$^{2-}$/2

HPLC (method B), t$_R$: 10.01 min

Synthesis of {5-[4-(N-succinimidyloxycarbonyl)phenyl]-10,15,20-*tris*[4-(2-(N,N,N-trimethylaminium)ethoxy-2,3,5,6-tetrafluorophenyl]porphyrinato} palladium (II) trichloride (**136**)
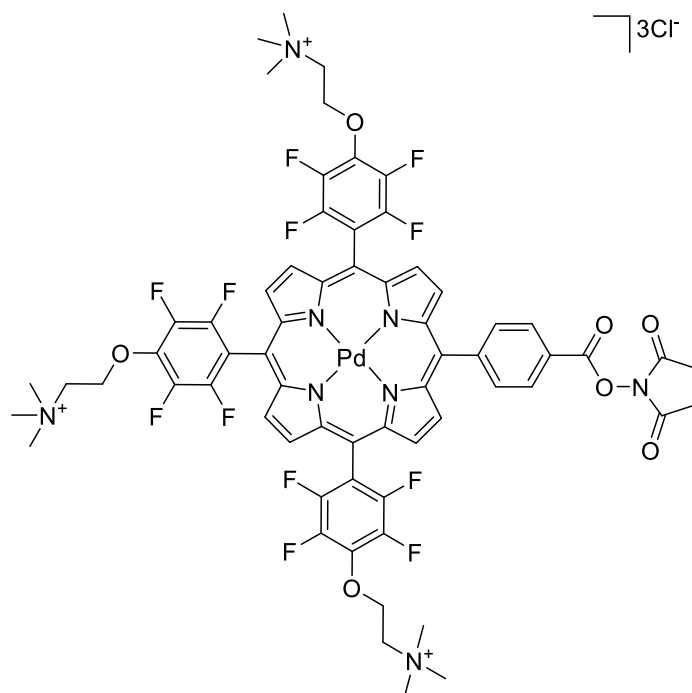
Compound **120** (78 mg, 0.052 mmol) and N-hydroxysuccinimide (120 mg, 1.05 mmol) were dissolved in DMSO (5 mL) in a 10-mL vial equipped with stir bar. 1-ethyl-3-(3-dimethylaminopropyl)carbodiimide hydrochloride (201 mg, 1.05 mmol) was then added to the mixture. The reaction was heated to 40 °C overnight. Once the solution was cooled down to room temperature, it was diluted with water (35 mL) and treated with sodium hexafluorophosphate, to induce precipitation of the title compound. The resulting suspension was centrifuged and the precipitate was re-dissolved in acetone (80 mL). The resulting mixture was treated with 10 % TBAC in acetone, leading to flocculation of the title compound, successively centrifuged and collected after further crystallisation from methanol–diethyl ether. (**136**) (67 mg, 0.045 mmol, 87 %)

^{1}H-NMR (600 MHz, DMSO-d$_6$, 298 K) δ, ppm: 9.33 (br dd, 4H, J=4.8 Hz, J=7.8 Hz, β-H), 9.21 (br d, 2H, J=4.8 Hz, β-H), 9.02 (br d, 2H, J=4.8 Hz, β-H), 8.55 (br dd, 2H, Ar-H$_m$ + Ar-H$_o$), 5.17 (br s, 6H, OCH_2), 4.11 (br s, 6H, CH_2NMe$_3$), 3.40 (d, 27H, NCH_3), 3.02 (br s, 4H, NHS-CH$_2$)

^{13}C-NMR (150 MHz, CDCl$_3$, 298 K) δ, ppm: 170.5, 162.0, 146.9, 145.3, 141.7, 141.3, 141.0, 139.9, 137.4, 134.9, 133.0, 132.3, 132.1, 131.3, 128.8, 124.6, 122.1, 105.6, 68.6, 64.8, 53.2, 25.7

^{19}F-NMR (564 MHz, CDCl$_3$, 298 K) δ, ppm: -140.9 (t, 6F, F$_o$), -156.5 (d, 6F, F$_m$)

m.p. (°C): > 300

UV-Vis (H$_2$O, nm) λ_{max}: Soret, 408; Q bands, 522, 556; Log ε_{408}: 4.77

ESI-MS (+ve) (m/z): 460.64 [M – 3Cl]$^{3+}$/3

HPLC (method A), t$_R$: 6.49
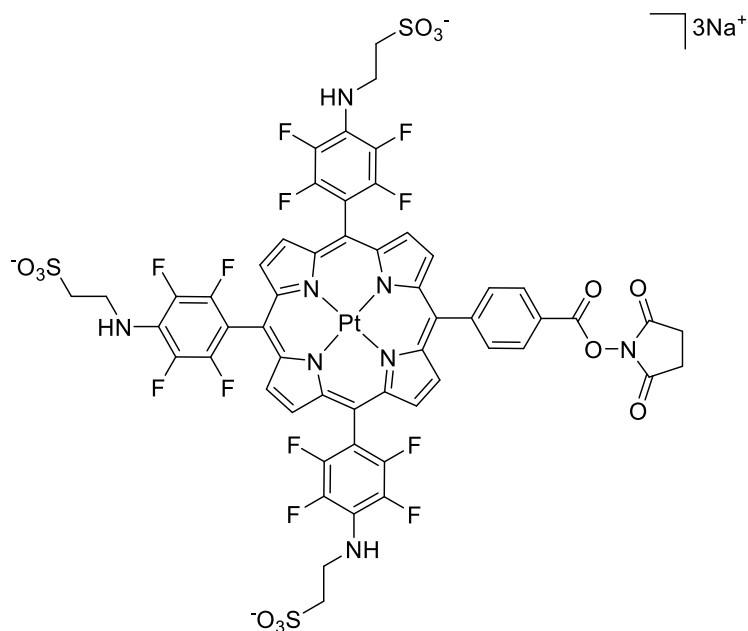
Compound **126** (150 mg, 0.1 mmol) and N-hydroxysuccinimide (23 mg, 2.0 mmol) were dissolved in DMSO (7 mL) in a 10-mL vial equipped with stir bar. 1-ethyl-3-(3-dimethylaminopropyl)carbodiimide hydrochloride (383 mg, 2.0 mmol) was then added to the mixture. The reaction was heated to 40 °C for 24 hours. Once the solution was cooled down to room temperature, it was diluted with water (40 mL) and filtered through celite. The filtrate was treated with compound **103**, to induce precipitation of the title compound. The resulting suspension was centrifuged and the precipitate was re-dissolved in acetone (40 mL). The resulting mixture was treated with sodium hexafluorophosphate, leading to flocculation of the title compound, successively centrifuged and collected after further crystallisation from methanol–diethyl ether. (**137**) (145 mg, 0.091 mmol, 91 %)

^{1}H-NMR (600 MHz, DMSO-d$_6$, 298 K) δ, ppm: 8.86-9.14 (m, 8H, β-H), 8.53 (s, 4H, Ar-H$_o$ + Ar-H$_m$), 6.67 (s, 3H, Ar-N*H*), 3.91 (s, 6H, C*H$_2$*SO$_3$), 3.00 (s, 4H, NHS-CH$_2$), 2.98 (br s, 6H, NHC*H$_2$*)

^{13}C-NMR (150 MHz, DMSO-d$_6$, 298 K) δ, ppm: 170.4, 162.0, 154.8, 154.6, 147.0, 145.5, 141.6, 141.2, 140.0, 137.4, 135.9, 134.7, 128.8, 107.4, 107.1, 103.9, 50.8, 41.9, 40.4, 25.7

^{19}F-NMR (564 MHz, DMSO-d$_6$, 298 K) δ, ppm: -143.0 (s, 6F, F$_o$), -160.7 (br s, 6F, F$_m$)

m.p. (°C): > 300

UV-Vis (H$_2$O, nm) λ_{max}: Soret, 400; Q bands, 512, 544; Log ε_{400}: 5.10

ESI-MS (+ve) (m/z): 384.49 [M − H − 3Na]$^{4-}$/4; 509.66 [M − 3Na]$^{3-}$/3; 765.00 [M + H − 3Na]$^{2-}$/2; 1531.08 [M + 2H − 3Na]$^-$

HPLC (method B), t$_R$: 10.68 min
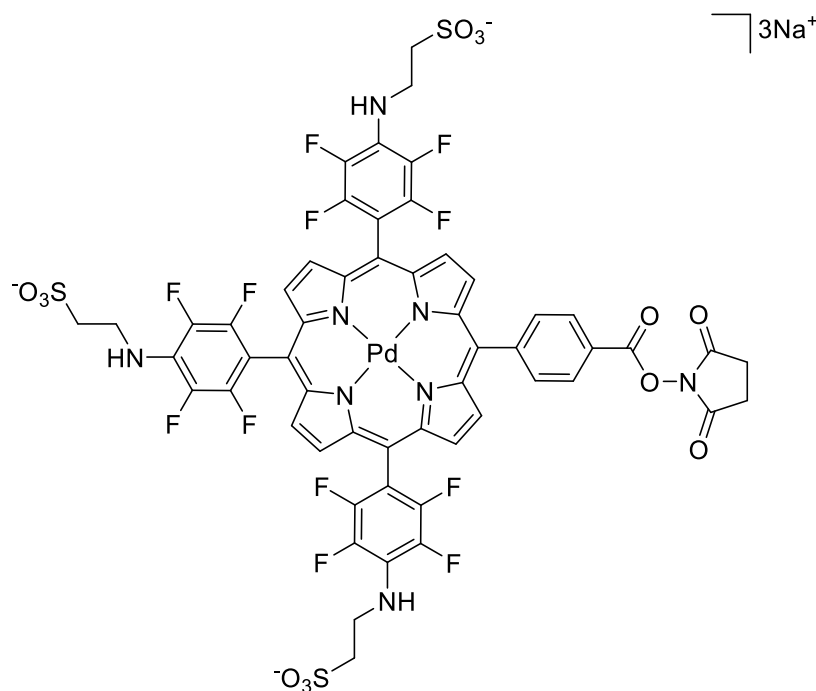
Compound **121** (128 mg, 0.091 mmol) and N-hydroxysuccinimide (207 mg, 1.8 mmol) were dissolved in DMSO (5 mL) in a 10-mL vial equipped with stir bar. 1-ethyl-3-(3-dimethylaminopropyl)carbodiimide hydrochloride (345 mg, 1.8 mmol) was then added to the mixture. The reaction was heated to 40 °C for 24 hours. Once the solution was cooled down to room temperature, it was diluted with water (40 mL) and filtered through celite. The filtrate was treated with compound **103**, to induce precipitation of the title compound. The resulting suspension was centrifuged and the precipitate was re-dissolved in acetone (40 mL). The resulting mixture was treated with sodium hexafluorophosphate, leading to flocculation of the title compound, successively centrifuged and collected after further crystallisation from methanol–diethyl ether. (**138**) (100 mg, 0.066 mmol, 73 %)

^{1}H-NMR (600 MHz, DMSO-d$_6$, 298 K) δ, ppm: 8.93-9.22 (br m, 8H, β-H), 8.54 (2d into br s, 4H, Ar-H$_o$ + Ar-H$_m$), 6.67 (s, 3H, Ar-N*H*), 3.91 (br s, 6H, C*H$_2$*SO$_3$), 3.01 (br s, 4H, NHS-CH$_2$), 2.95 (br s, 6H, NHC*H$_2$*)

^{13}C-NMR (150 MHz, DMSO-d$_6$, 298 K) δ, ppm: 170.4, 147.1, 145.6, 142.1, 141.7, 137.3, 135.8, 1343.9, 132.1, 131.8, 129.8, 104.4, 50.8, 42.0, 25.2

^{19}F-NMR (564 MHz, DMSO-d$_6$, 298 K) δ, ppm: -142.9 (s, 6F, F$_o$), -160.8 (br s, 6F, F$_m$)

m.p. (°C): > 300

UV-Vis (H$_2$O, nm) λ_{max}: Soret, 413; Q bands, 525, 557; Log ε_{413}: 5.11

ESI-MS (-ve) (m/z): 479.69 [M − 3Na]$^{3-}$/3; 720.04 [M + H − 3Na]$^{2-}$/2; 1441.16 [M + 2H − 3Na]$^-$

HPLC (method B), t$_R$: 9.84 min

Synthesis of conjugate Duramycin-[5-(4-carboxyphenyl)-10,15,20-*tris*(4-methyl-pyridinium)porphyrin] trichloride (**140**)
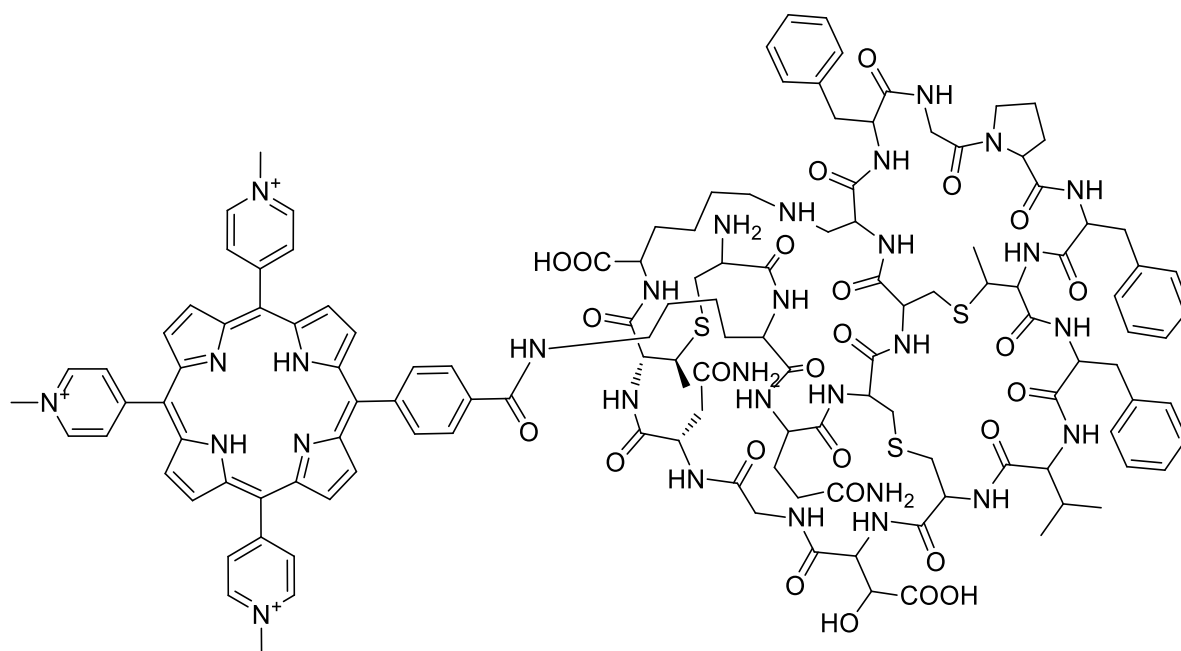
Duramycin B (10 mg, 4.97·10^{-3} mmol) was dissolved in 1 mL of DMSO directly in the bottle as received. **139** (14 mg, 1.5·10^{-2} mmol) was dissolved in 200 µl of DMSO in a vial, and the two solutions were mixed together in a vial and left on a rotating shaker for 48 hours at room temperature. The progression of the conjugation was monitored by LC-MS. After 48 hours, the reaction was transferred in an incubator at 37 °C for 2 hours and 30 minutes. After 72 hours the reaction was stopped adding DCM to the mix and filtrating on paper the resulting precipitate (**140**).

ESI-MS (+ve) (m/z): 539.90 [M + 2H − 3Cl]$^{5+}$/5; 674.62 [M + H − 3Cl]$^{4+}$/4; 899.49 [M − 3Cl]$^{3+}$/3; 1348.19 [M − H − 3Cl]$^{2+}$/2

HPLC (Method A), t$_R$: 5.70 min

Synthesis of conjugate deferoxamine-[5-(4-carboxyphenyl)-10,15,20-*tris*(4-methyl-pyridinium)porphyrinato] indium (III) trichloride (**141**)
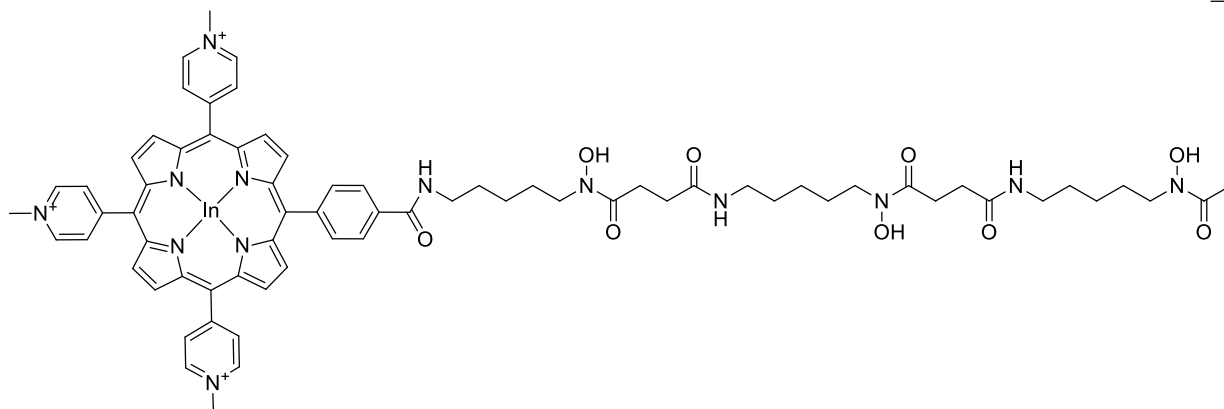
127 (143 mg, 0.15 mmol) was dissolved in water (15 mL), 1-ethyl-3-(3-dimethylaminopropyl)carbodiimide hydrochloride (287 mg, 1.5 mmol) and N-hydroxysuccinimide (173 mg, 1.5 mmol) were added to the mixture. The reaction was left stirring at 40 °C overnight. Once the mixture cooled down, deferoxamine B (276 mg, 0.42 mmol) was dissolved in water (5 mL) and added to the mixture. The reaction was left stirring at 40 °C overnight. Once the solution was cooled down to room temperature, it was diluted with water (80 mL) and treated with sodium hexafluorophosphate, to induce precipitation of the title compound. The resulting suspension was centrifuged and the precipitate was re-dissolved in acetone (40 mL). The resulting mixture was treated with 10 % TBAC in acetone, leading to flocculation of the title compound, successively centrifuged and collected after further crystallisation from methanol–diethyl ether. (**141**) (193 mg, 0.125 mmol, 83 %)

^{1}H-NMR (600 MHz, DMSO-d$_6$, 298 K) δ, ppm: 9.54 (br s, 6H, Py-H$_m$), 8.99-9.28 (m, 14H, β-H + Py-H$_o$), 7.81-8.59 (m, 4H, Ar-H), 4.76 (s, 9H, NC*H$_3$*), 1.21-4.08 (br m, 40H, deferoxamine part)

^{13}C-NMR (150 MHz, DMSO-d$_6$, 298 K) δ, ppm: 172.0, 171.3, 170.1, 156.6, 148.3, 148.0, 146.9, 146.7, 146.6, 146.5, 144.2, 135.2, 134.8, 134.4, 134.3, 134.0, 133.3, 133.0, 132.9, 132.6, 132.4, 128.5, 127.7, 126.0, 116.3, 116.2, 115.7, 115.4, 52.2, 47.8, 47.1, 46.8, 38.6, 38.5, 38.4, 30.0, 28.8, 27.6, 26.7, 26.0, 25.7, 23.5, 22.9, 20.4

UV-Vis (H$_2$O, nm) λ_{max}: Soret, 428; Q bands, 562, 609: Log ε_{428}: 5.43

ESI-MS (+ve) (m/z): 453.10 [M − 4Cl]$^{3+}$/3

HPLC (method A), t$_R$: 6.49

<u>Fibroin extraction from *Bombyx mori* cocoons</u>

20 g of *Bombyx mori* cocoon were cut in pieces and dissolved in 2 L of a 0.02 M solution of Na_2CO_3. The solution was left boiling for 30 minutes. The material was rinsed three times with deionized water. After drying, 16.0 g of raw fibres were dissolved in 80 mL of a 9.3 M solution of lithium bromide in water, in a 250-mL conical flask equipped with a magnetic stirrer. The reaction was left with a very slow stirring at 60 °C for 4 hours, time that resulted not enough to completely dissolve all the fibres. After the addition of 20 mL of a 9.3 M solution of lithium bromide, the reaction was left overnight at 40 °C with a very slow stirring. The following day almost complete dissolution was observed, and the mixture was first cooled down and then centrifuged, to remove all the solid impurities. The supernatant was carefully transferred in a dialysis tube and dialyzed against water for 48 hours, until no traces of lithium bromine could be detected. silver nitrate was employed as indicator of the bromines presence in the mix, by precipitation of silver bromide, salt insoluble in water. After completion of dialysis process, the solution was stored in 50-mL Falcon vials in the fridge to avoid unwanted gelation process to happen.

Abbreviations

Acac: acetylacetonate

Boc: tert-butyloxycarbonyl group

BPY: benzoperylene

$CDCl_3$: deuterated chloroform

DBU: 1,8-Diazabicyclo[5.4.0]undec-7-ene

DCY: decacyclene

DDQ: 2,3-Dichloro-5,6-dicyano-1,4-benzoquinone

DEPT-Q: Distortionless Enhancement by Polarization Transfer

DMF: Dimethylformamide

DMSO: dimethyl sulfoxide

DMSO-d_6: deuterated dimethyl sulfoxide

FA: formic acid

HMBC: Heteronuclear Multiple Quantum Coherence

HPTS: 8-Hydroxypyrene-1,3,6-trisulphonic acid trisodium salt

HSQC: Heteronuclear Single Quantum Correlation

LED: light emitting diode

LMOF: luminescent metal-organic framework

MLCT: metal-ligand charge transfer

NHS: N-hydroxysuccinimide

NIR: Near infrared

NMP: N-Methyl-2-pyrrolidone

OEP: Octaethylporphyrin

OEPK: octaethylporphyrinketone

OOS: Optical Oxygen Sensing

PAANPs: Polyacrylamide nanoparticles

PAHs: Polycyclic aromatic hydrocarbons

PAN: polyacrylonitrile

PDMS: Poly(dimethyl siloxane)

PDT: photodynamic therapy

PEG: polyethylene glycol

PEMA: poly(ethyl methacrylate)

PHEMA-co-PAM: poly(2-hydroxyethyl methacrylate)-co-poly(acrylamide)

PMMA: poly(methyl methacrylate)

PS: polystyrene

Pt(Thpy): Cis-bis[2-(2'-thienyl)pyridine]platinum(II)

PTC: Phase Transfer Catalyst

PVA: Polyvinyl alcohol

PVC: poly(vinyl chloride)

QD: quantum dots

q.y. : quantitative yield

SDT: sonodynamic therapy

TBAC: tetrabutylammonium chloride

TCPP: *Meso*-tetra(4-carboxyphenyl)porphyrin

TFA: trifluoroacetic acid

TFPP: meso-tetrakis(pentafluorophenyl)porphyrin

TFPPL: meso-tetrakis(pentafluorophenyl)porphyrin lactone

THF: tetrahydrofuran

TLC: Think Layer Chromatography

TPTBP: meso-tetraphenyltetrabenzoporphyrin

References

1. https://plus.google.com/+IrreverentMonk/posts/j2sm9K3a5xr.

2. Altemeier WA, Sinclair SE. Hyperoxia in the intensive care unit: why more is not always better. *Curr Opin Crit Care*. 2007;13(1):73-78. doi:10.1097/MCC.0b013e32801162cb.

3. Chawla A, Lavania AK. OXYGEN TOXICITY. *Med journal, Armed Forces India*. 2001;57(2):131-133. doi:10.1016/S0377-1237(01)80133-7.

4. Han J, Zhong J-J. Effects of oxygen partial pressure on cell growth and ginsenoside and polysaccharide production in high density cell cultures of Panax notoginseng. *Enzyme Microb Technol*. 2003;32(3-4):498-503. doi:10.1016/S0141-0229(02)00337-X.

5. Griffith LG, Swartz MA. Capturing complex 3D tissue physiology in vitro. *Nat Rev Mol Cell Biol*. 2006;7(3):211-224. doi:10.1038/nrm1858.

6. Skoog DA, West DM, Holler FJ. Fundamentals of Analytical Chemistry. *ed D A Skoog, Saunders Coll Publ New York, 5th edn*. 1988:344.

7. Chang SC, Stetter JR, Cha CS. Amperometric gas sensors. *Talanta*. 1993;40(4):461-477. doi:10.1016/0039-9140(93)80002-9.

8. Freeman TM, Seitz WR. Oxygen Probe Based on Tetrakis(Alkylamino)Ethylene Chemi-Luminescence. *Anal Chem*. 1981;53(1):98-102. doi:10.1021/ac00224a025.

9. Hendricks HD. Method of detecting Oxygen in gas. *US Pat*. 1973:3709663.

10. http://www.fondriest.com/environmental-measurements/equipment/measuring-water-quality/dissolved-oxygen-sensors-and-methods/.

11. https://en.wikipedia.org/wiki/Clark_electrode.

12. Amao Y. Probes and Polymers for Optical Sensing of Oxygen. *Microchim Acta*. 2003;143(1):1-12. doi:10.1007/s00604-003-0037-x.

13. Xu H, Aylott JW, Kopelman R, Miller TJ, Philbert MA. A real-time ratiometric method for the determination of molecular oxygen inside living cells using sol-gel-based spherical optical nanosensors with applications to rat C6 glioma. *Anal Chem*. 2001;73(17):4124-4133. doi:10.1021/ac0102718.

14. Koo Y-EL, Cao Y, Kopelman R, Koo SM, Brasuel M, Philbert M a. Real-time measurements of dissolved oxygen inside live cells by organically modified silicate fluorescent nanosensors. *Anal Chem*. 2004;76(9):2498-2505. doi:10.1021/ac035493f.

15. Vanderkooi J, Wilson D. A New Method for Measuring Oxygen Concentration in Biological Systems. Longmuir I, ed. *Oxyg Transp to Tissue VIII SE - 25*. 1986;200:189-193. doi:10.1007/978-1-4684-5188-7_25.

16. Atkins P, De Paula J. *Physical Chemistry*. 8Rev Ed. Oxford University Press; 2006. http://www.amazon.com/exec/obidos/redirect?tag=citeulike07-20&path=ASIN/0198700725.

17. Neil H, Garley S. Oxygen quenching of tris (2 , 2 ' -bipyridine) thin organic films complexes in. 1994;80:283-288.

18. Vaughan A a., Baron MG, Narayanaswamy R. Optical ammonia sensing films based on an immobilized metalloporphyrin. *Anal Commun*. 1996;33(11):393. doi:10.1039/ac9963300393.

19. Peterson JI, Fitzgerald R V, Buckhold DK. Fiber-optic probe for in vivo measurement of oxygen partial pressure. *Anal Chem*. 1984;56(18):62-67. doi:10.1021/ac00265a017.

20. Potzkei J, Kunze M, Drepper T, Gensch T, Jaeger K-E, Büchs J. Real-time determination of intracellular oxygen in bacteria using a genetically encoded FRET-based biosensor. *BMC Biol*. 2012;10:28. doi:10.1186/1741-7007-10-28.

21. Basu BJ, Anandan C, Rajam KS. Study of the mechanism of degradation of pyrene-based pressure sensitive paints. *Sensors Actuators, B Chem*. 2003;94(3):257-266. doi:10.1016/S0925-4005(03)00450-7.

22. Zilberstein J, Bromberg A, Berkovic G. Fluorescence study of pyrene chemically bound to controlled-pore glasses. *J Photochem Photobiol A Chem*. 1994;77(1):69-81. doi:10.1016/1010-6030(94)80010-3.

23. Longmuir IS, Knopp JA. Measurement of tissue oxygen with a fluorescent probe. *J Appl Physiol*. 1976;41(4):598-602.

24. Mitnick MH, Jöbsis FF. Pyrenebutyric acid as an optical oxygen probe in the intact cerebral cortex. *J Appl Physiol*. 1976;41(4):593-597. http://www.ncbi.nlm.nih.gov/pubmed/985407.

25. Xu W, Schmidt R, Whaley M, et al. Oxygen sensors based on luminescence quenching: interactions of pyrene with the polymer supports. *Anal Chem*. 1995;67(18):3172-3180. doi:10.1021/ac00114a012.

26. Okazaki T, Imasaka T, Ishibashi N. Optical-fiber sensor based on the second-harmonic emission of a near-infrared semiconductor laser as light source. *Anal Chim Acta*. 1988;209:327-331.

27. Wolfbels OS, Carlini FM. Long-wavelength fluorescent indicators for the determination of oxygen partial pressure. *Anal Chim Acta*. 1984;160:301-304.

28. Wolfbeis OS, Posch HE, Kroneis HW. Fiber optical fluorosensor for determination of halothane and or oxygen. *Anal Chem*. 1985;57(13):2556-2561. doi:10.1021/ac00290a028.

29. Trettnak W, Leiner M, Wolfbeis O. Optical sensors. Part 34. Fibre optic glucose biosensor with an oxygen optrode as the transducer. *Analyst*. 1988;113(October):1519-1523. doi:10.1039/AN9881301519.

30. Nagl S, Baleizão C, Borisov SM, Schäferling M, Berberan-Santos MN, Wolfbeis OS. Optical sensing and imaging of trace oxygen with record response. *Angew Chemie - Int Ed*. 2007;46(13):2317-2319. doi:10.1002/anie.200603754.

31. Baleiža C, Nagl S, Schäferling M, Berberan-Santos MN, Wolfbeis OS. Dual fluorescence sensor for trace oxygen and temperature with unmatched range and sensitivity. *Anal Chem*. 2008;80(16):6449-6457. doi:10.1021/ac801034p.

32. Amao Y, Asai K, Okura I. High Sensitive Oxygen Sensor Based on Quenching of Triplet-triplet Absorption of Fullerene C60-Polystyrene Film. *Bull Chem Soc Jpn*. 1999;72(10):2223.

33. Wang X, Wolfbeis OS. Optical methods for sensing and imaging oxygen: materials, spectroscopies and applications. *Chem Soc Rev*. 2014;43(10):3666-3761. doi:10.1039/c4cs00039k.

34. Klimant I, Wolfbeis OS. Oxygen-sensitive luminescent materials based on silicone-soluble ruthenium diimine complexes. *Anal Chem*. 1995;67(18):3160-3166. doi:10.1021/ac00114a010.

35. Wolfbeis OS, Leiner MJP, Posch HE. A new sensing material for optical oxygen measurement, with the indicator embedded in an aqueous phase. *Mikrochim Acta*. 1986;90(5-6):359-366. doi:10.1007/BF01199278.

36. Li L, Walt DR. Dual-analyte fiber-optic sensor for the simultaneous and continuous measurement of glucose and oxygen. *Anal Chem*. 1995;67(20):3746-3752.

37. Amao Y, Okura I. Optical oxygen sensing materials: Chemisorption film of ruthenium(II) polypyridyl complexes attached to anionic polymer. *Sensors Actuators, B Chem*. 2003;88(2):162-167. doi:10.1016/S0925-4005(02)00320-9.

38. Liebsch G, Klimant I, Wolfbeis OS. Luminescence Lifetime Temperature Sensing Based on Sol-Gels and Poly(acrylonitrile)s Dyed with Ruthenium Metal-Ligand Complexes. *Adv Mater*. 1999;11(15):1296-1299.

39. Bacon JR, Demas JN. Determination of Oxygen Concentrations by Luminescence Quenching of a Polymer-Immobilized Transition-Metal Complex. *Am Chem Soc*. 1987;59(23):2780-2785. doi:10.1021/ac00150a012.

40. Carraway ER, Demas JN, Degraff BA. Luminescence Quenching Mechanism for Microheterogeneous Systems. *Anal Chem*. 1991;63(7):332-336.

41. McNamara KP, Li X, Stull AD, Rosenzweig Z. Fiber-optic oxygen sensor based on the fluorescence quenching of tris (5-acrylamido, 1,10 phenanthroline) ruthenium chloride. *Anal Chim Acta*. 1998;361(1-2):73-83. doi:10.1016/S0003-2670(97)00703-4.

42. Holder E, Oelkrug D, Egelhaaf HJ, Mayer HA, Lindner E. Synthesis, Characterization, and Luminescence Spectroscopic Accessibility Studies of Tris (2,2′-Bipyridine)Ruthenium(II)-Labeled Inorganic-Organic Hybrid Polymers. *J Fluoresc*. 2002;12(3-4):383-395. doi:10.1023/A:1021309925702.

43. Malins C, Glever HG, MacCraith BD, Fanni S, Vos JG. The preparation of a sol–gel glass oxygen sensor incorporating a covalently bound fluorescent dye. *Anal Commun*. 1999;36(1):3-4. doi:10.1039/a808731h.

44. McGee KA, Veitkamp DJ, Marquardt BJ, Mann KR. Porous crystalline ruthenium complexes are oxygen sensors. *J Am Chem Soc*. 2007;129(49):15092-15093. doi:10.1021/ja0681772.

45. McGee KA, Marquardt BJ, Mann KR. Concurrent sensing of benzene and oxygen by a crystalline salt of tris(5,6-dimethyl-1,10-phenanthroline)ruthenium(II). *Inorg Chem*. 2008;47(20):9143-9145. doi:10.1021/ic801287p.

46. McGee KA, Mann KR. Inefficient crystal packing in chiral [Ru(phen)3](PF 6)2 enables oxygen molecule quenching of the solid-state MLCT emission. *J Am Chem Soc*. 2009;131(5):1896-1902. doi:10.1021/ja8075605.

47. Xu W, Kneas K a, Demas JN, Degraff B a. Oxygen sensors based on luminescence quenching of metal complexes: osmium complexes suitable for laser diode excitation. *Anal Chem*. 1996;68(15):2605-2609. doi:10.1021/ac960083v.

48. Kober EM, Marshall JL, Dressick WJ, Sullivan BP, Caspar J V, Meyer TJ. Synthetic control of excited states. Nonchromophoric ligand variations in polypyridyl complexes of osmium(II). *Inorg Chem* . 1985;24(18):2755-2763. papers3://publication/uuid/EF99074A-1A21-47D0-B953-35DF408578F8.

49. Kober EM, Caspar J V., Lumpkin RS, Meyer TJ. Application of the energy gap law to excited-state decay of osmium(II)-polypyridine complexes: calculation of relative nonradiative decay rates from emission spectral profiles. *J Phys Chem*. 1986;90(16):3722-3734. doi:10.1021/j100407a046.

50. Sacksteder L, Lee M. Long-lived, highly luminescent rhenium (I) complexes as molecular probes: intra-and intermolecular excited-state interactions. *J Am Chem Soc*. 1993;115(c):8230-8238. doi:10.1021/ja00071a036.

51. Kneas K a, Xu W, Demas JN, Degraff B a, Zipp AP. Luminescence-Based Oxygen Sensors : ReL(CO)3Cl and ReL(CO)3CN Complexes on Copolymer Supports. *J Fluoresc*. 1998;8(4):295-300.

52. Sacksteder LA, Demas JN, Degraff BA. Design of Oxygen Sensors Based on Quenching of Luminescent Metal-Complexes - Effect of Ligand Size on Heterogeneity. *Anal Chem*. 1993;65(23):3480-3483. doi:10.1021/ac00071a024.

53. Amao Y, Okura I, Miyashita T. Optical oxygen sensing based on the luminescence quenching of europium(III) complex immobilized in fluoropolymer film. *Bull Chem Soc Jpn*. 2000;73(12):2663-2668. doi:10.1246/bcsj.73.2663.

54. Amao Y, Okura I, Miyashita T. Photoluminescent Oxygen Sensing Using Tris (acethylacetonato) 1,10-Phenanthroline Terbium (III) Complex Doped on Alumina Film. 2000;(Iii):2-3.

55. Borisov SM, Klimant I. New luminescent oxygen-sensing and temperature-sensing materials based on gadolinium(III) and europium(III) complexes embedded in an acridone-polystyrene conjugate. *Anal Bioanal Chem*. 2012;404(10):2797-2806. doi:10.1007/s00216-012-6244-8.

56. Amao Y, Ishikawa Y, Okura I. Green luminescent iridium(III) complex immobilized in fluoropolymer film as optical oxygen-sensing material. *Anal Chim Acta*. 2001;445(2):177-182. doi:10.1016/S0003-2670(01)01254-5.

57. Huynh L, Wang Z, Yang J, et al. Evaluation of phosphorescent rhenium and iridium complexes in polythionylphosphazene films for oxygen sensor applications. *Chem Mater*. 2005;17(19):4765-4773. doi:10.1021/cm047794r.

58. Mak CSK, Penflehner D, Stich M, Wolfbeis OS, Chan WK, Yersin H. Exceptional oxygen sensing capabilities and triplet state properties of Ir(ppy-NPh2)3. *Chem Mater*. 2009;21(11):2173-2175. doi:10.1021/cm9003678.

59. Borisov SM, Klimant I. Ultrabright oxygen optodes based on cyclometalated iridium(III) coumarin complexes. *Anal Chem*. 2007;79(19):7501-7509. doi:10.1021/ac0710836.

60. DeRosa MC, Mosher PJ, Yap GP a, Focsaneanu K-S, Crutchley RJ, Evans CEB. Synthesis, characterization, and evaluation of [Ir(ppy)2(vpy)Cl] as a polymer-bound oxygen sensor. *Inorg Chem*. 2003;42(16):4864-4872. doi:10.1021/ic026230r.

61. DeRosa MC, Hodgson DJ, Enright GD, Dawson B, Evans CEB, Crutchley RJ. Iridium luminophore complexes for unimolecular oxygen sensors. *J Am Chem Soc*. 2004;126(24):7619-7626. doi:10.1021/ja049872h.

62. Donckt E Vander, Camerman B, Herne R, Vandeloise R. Fibre-optic oxygen sensor based on luminescence quenching of a Pt (II) complex embedded in polymer matrices. *Sensors Actuators B*. 1996;32:121-127.

63. Liu Y, Guo H, Zhao J. Ratiometric luminescent molecular oxygen sensors based on uni-luminophores of C∠N Pt(ii)(acac) complexes that show intense visible-light absorption and balanced fluorescence/phosphorescence dual emission. *Chem Commun*. 2011;47(41):11471. doi:10.1039/c1cc14582g.

64. Wu W, Wu W, Ji S, Guo H, Zhao J. Tuning the emission property of carbazole-caped cyclometalated platinum(II) complexes and its application for enhanced luminescent oxygen sensing. *J Organomet Chem*. 2011;696(11-12):2388-2398. doi:10.1016/j.jorganchem.2011.03.002.

65. Houten K a Van, Walters K a, Schanze KS, Pilato RS. Study of the Heterocyclic-Substituted Platinum-1,2-Enedithiolate 3ILCT Excited States by Transient Absorption Spectroscopy. *J Fluoresc*. 2000;10(1):35-40.

66. Eastwood D, Gouterman M. Porphyrins: Luminescence of (CO), (Ni), Pd, Pt complexes. *J Mol Spectrosc*. 1970;35(3):359-375. doi:10.1016/0022-2852(70)90179-7.

67. Lee S-K, Okura I. Photostable Optical Oxygen Sensing Material: Platinum Tetrakis(pentafluorophenyl)porphyrin Immobilized in Polystyrene. *Anal Commun*. 1997;34(June):185-188. doi:10.1039/a701130j.

68. Borisov SM, Lehner P, Klimant I. Novel optical trace oxygen sensors based on platinum(II) and palladium(II) complexes with 5,10,15,20-meso-tetrakis-(2,3,4,5,6-pentafluorphenyl)-porphyrin covalently immobilized on silica-gel particles. *Anal Chim Acta*. 2011;690(1):108-115. doi:10.1016/j.aca.2011.01.057.

69. Atwater BW. Substituent effects on the excited-state properties of platinum meso-tetraphenylporphyrins. *J Fluoresc*. 1992;2(4):237-246. doi:10.1007/BF00865282.

70. Lee S-K, Okura I. Photoluminescent determination of oxygen using metalloporphyrin-polymer sensing systems. *Spectrochim Acta, Part A Mol Biomol Spectrosc*. 1998;54A(1):91-100. doi:10.1016/S1386-1425(97)00206-0.

71. Papkovsky DB. New oxygen sensors and their application to biosensing. *Sensors Actuators B*. 1995;29:213-218.

72. Klimant I, Kühl M, Glud RN, Holst G. Optical measurement of oxygen and temperature in microscale: strategies and biological applications. *Sensors Actuators B Chem*. 1997;38(1-3):29-37. doi:10.1016/S0925-4005(97)80168-2.

73. Papkovsky DB, Olah J, Troyanovsky I V., et al. Phosphorescent polymer films for optical oxygen sensors. *Biosens Bioelectron*. 1991;7:199-206. doi:10.1016/0956-5663(92)87016-I.

74. Douglas P, Eaton K. Response characteristics of thin film oxygen sensors, Pt and Pd octaethylporphyrins in polymer films. *Sensors Actuators, B Chem*. 2002;82(2-3):200-208. doi:10.1016/S0925-4005(01)01006-1.

75. Lee S-K, Okura I. Optical Sensor for Oxygen Using a Porphyrin-doped Sol–Gel Glass. *Analyst*. 1997;122(1):81-84. doi:10.1039/a604885d.

76. Lee SK, Okura I. Porphyrin-doped sol-gel glass as a probe for oxygen sensing. *Anal Chim Acta*. 1997;342(2-3):181-188. doi:10.1016/S0003-2670(96)00562-4.

77. Amao Y, Asai K, Okura I, Shinohara H, Nishide H. Platinum porphyrin embedded in poly (1-trimethylsilyl-1-propyne) film as an optical sensor for trace analysis of oxygen. *Analyst*. 2000;125(11):1911-1914. doi:10.1039/b005838f.

78. Amao Y, Miyashita T, Okura I. Optical oxygen detection based on luminescence change of metalloporphyrins immobilized in poly(isobutylmethacrylate-co-trifluoroethylmethacrylate) film. *Anal Chim Acta*. 2000;421(2):167-174. doi:10.1016/S0003-2670(00)01048-5.

79. Amao Y, Tabuchi Y, Yamashita Y, Kimura K. Novel optical oxygen sensing material: Metalloporphyrin dispersed in fluorinated poly(aryl ether ketone) films. *Eur Polym J*. 2002;38(4):675-681. doi:10.1016/S0014-3057(01)00235-X.

80. Bansal AK, Holzer W, Penzkofer A, Tsuboi T. Absorption and emission spectroscopic characterization of platinum-octaethyl-porphyrin (PtOEP). *Chem Phys*. 2006;330(1-2):118-129. doi:10.1016/j.chemphys.2006.08.002.

81. Braga MS, Matos KRM, Borges VF, Gomes OF, Salcedo WJ. Photoluminescence-based oxygen sensor with platinum-octaethylporphyrin dye integrated into oxidized porous silicon layer. *Chip Curitiba 2013 - SBMicro 2013 28th Symp Microelectron Technol Devices*. 2013;0-4. doi:10.1109/SBMicro.2013.6676164.

82. Davenport JJ, Hickey M, Phillips JP, Kyriacou PA. Fiber-optic fluorescence-quenching oxygen partial pressure sensor using platinum octaethylporphyrin. *Appl Opt*. 2016;55(21):5603. doi:10.1364/AO.55.005603.

83. Jiang Z, Yu X, Hao Y. Design and fabrication of a ratiometric planar optode for simultaneous imaging of pH and oxygen. *Sensors (Switzerland)*. 2017;17(6). doi:10.3390/s17061316.

84. Davenport J, Hickey M, Phillips JP, Kyriacou P. Dual pO2 / pCO2 fibre optic sensing film. *Analyst*. 2017;161(21):160-1719. doi:10.1039/c7an00173h.

85. Fercher A, Borisov SM, Zhdanov A V, Klimant I, Papkovsky DB. Intracellular O2 Sensing Probe Based on Cell-Penetrating Phosphorescent Nanoparticles. *ACS Nano*. 2011;5(7):5499-5508. doi:10.1021/nn200807g.

86. Yeh TS, Chu CS, Lo YL. Highly sensitive optical fiber oxygen sensor using Pt(II) complex embedded in sol-gel matrices. *Sensors Actuators, B Chem*. 2006;119(2):701-707. doi:10.1016/j.snb.2006.01.051.

87. Fischer LH, Borisov SM, Schaeferling M, Klimant I, Wolfbeis OS. Dual sensing of pO(2) and temperature using a

water-based and sprayable fluorescent paint. *Analyst*. 2010;135(Dld):1224-1229. doi:10.1039/b927255k.

88. Lo KH, Kontis K. Static and wind-on performance of polymer-based pressure-sensitive paints using platinum and ruthenium as the luminophore. *Sensors (Switzerland)*. 2016;16(5). doi:10.3390/s16050595.

89. Coyle LM, Gouterman M. Correcting lifetime measurements for temperature. *Sensors Actuators, B Chem*. 1999;61(1):92-99. doi:10.1016/S0925-4005(99)00289-0.

90. Puklin E, Carlson B, Gouin S, et al. Ideality of pressure-sensitive paint. I. Platinum tetra(pentafluorophenyl)porphine in fluoroacrylic polymer. *J Appl Polym Sci*. 2000;77(13):2795-2804. doi:10.1002/1097-4628(20000923)77.

91. Chu CS, Lo YL. Highly sensitive and linear calibration optical fiber oxygen sensor based on Pt(II) complex embedded in sol-gel matrix. *Sensors Actuators, B Chem*. 2011;155(1):53-57. doi:10.1016/j.snb.2010.11.023.

92. Chu CS, Lo YL. 2D full-field measurement of oxygen concentration based on the phase fluorometry technique that uses the four-frame integrating-bucket method. *Sensors Actuators, B Chem*. 2010;147(1):310-315. doi:10.1016/j.snb.2010.03.032.

93. Amao Y, Asai K, Okura I. Oxygen sensing based on lifetime of photoexcited truplet state of platinum porphyrin-polystyrene film using time resolved spectroscopy. *J Porphyr Phthalocyanines*. 2000;4(3):292-299.

94. Stubenrauch K, Sandholzer M, Niedermair F, et al. Poly(norbornene)s as matrix materials for platinum tetrakis(pentafluorophenyl)porphyrin based optical oxygen sensors. *Eur Polym J*. 2008;44(8):2558-2566. doi:10.1016/j.eurpolymj.2008.06.012.

95. Mayr T, Borisov SM, Abel T, et al. Light harvesting as a simple and versatile way to enhance brightness of luminescent sensors. *Anal Chem*. 2009;81(15):6541-6545. doi:10.1021/ac900662x.

96. Lehner P, Larndorfer C, Garcia-Robledo E, et al. LUMOS - A sensitive and reliable optode system for measuring dissolved oxygen in the nanomolar range. *PLoS One*. 2015;10(6):1-15. doi:10.1371/journal.pone.0128125.

97. Chu C-S, Syu J-J. The Development of a Highly Sensitive Fiber-Optic Oxygen Sensor. *Inventions*. 2016;1(2):9. doi:10.3390/inventions1020009.

98. Chen W-T, Hu R-H, Lou Z-G, Chen H-L. Synthesis and Characterization of meso-Tetra(4-carboxyphenyl)porphyrin complex of Palladium. *Asian J Chem*. 2015;27(2):775-776. doi:10.1093/jae/ejp002.

99. Lo LW, Koch CJ, Wilson DF. Calibration of Oxygen-Dependent Quenching of the Phosphorescence of Pd-meso-tetra (4-Carboxyphenyl) Porphine: A Phosphor with General Application for Measuring Oxygen Concentration in Biological Systems. *Anal Biochem*. 1996;236(1):153-160. doi:10.1006/abio.1996.0144.

100. Stepinac TK, Chamot SR, Rungger-Br??ndle E, et al. Light-induced retinal vascular damage by Pd-porphyrin luminescent oxygen probes. *Investig Ophthalmol Vis Sci*. 2005;46(3):956-966. doi:10.1167/iovs.04-0500.

101. Amao Y, Okura I. An oxygen sensing system based on the phosphorescence quenching of metalloporphyrin thin film on alumina plates. *Analyst*. 2000;125(9):1601-1604. doi:10.1039/b004065g.

102. Hase K, Sakai S, Tsukada K, Sekizuka E, Oshio C, H. Minamitani. Continuous measurement of blood oxygen pressure using a fiber optic sensor based on phosphorescence quenching. *Eng Med Biol 2002 24th Annu Conf Annu Fall Meet Biomed Eng Soc EMBS/BMES Conf 2002 Proc Second Jt*. 2002:1777-1778. http://ieeexplore.ieee.org/xpl/articleDetails.jsp?arnumber=1106648&tag=1.

103. Nowak-Sliwinska P, Käuper P, van den Bergh H, Wagnières G. Study of the pO2-Sensitivity of the Dendrimeric and Free Forms of Pd-meso-tetra(4-carboxyphenyl)porphyrin, Incorporated or not in Chitosan-Based Nanoparticles. *Chim Int J Chem*. 2011;65(9):691-695. doi:10.2533/chimia.2011.691.

104. Yang J, Wang Z, Li Y, Zhuang Q, Gu J. Real-Time Monitoring of Dissolved Oxygen with Inherent Oxygen-Sensitive Centers in Metal-Organic Frameworks. *Chem Mater*. 2016;28(8):2652-2658. doi:10.1021/acs.chemmater.6b00016.

105. Papkovsky DB, Ponomarev G V, Trettnak W, O'Leary P. Phosphorescent Complexes of Porphyrin Ketones: Optical Properties and Application to Oxygen Sensing. *Anal Chem*. 1995;67(22):4112-4117. doi:10.1021/ac00118a013.

106. Trettnak W, Kolle C, Reininger F, Dolezal C, O'Leary P. Miniaturized luminescence lifetime-based oxygen sensor instrumentation utilizing a phase modulation technique. *Sensors Actuators B Chem*. 1996;35-36:506-512. doi:10.1016/S0925-4005(97)80120-7.

107. Kolle C, Gruber W, Trettnak W, et al. Fast optochemical sensor for continuous monitoring of oxygen in breath-gas

analysis. *Sensors Actuators B Chem*. 1997;38:141-149. doi:10.1016/S0925-4005(97)80184-0.

108. Quaranta M, Borisov SM, Klimant I. Indicators for optical oxygen sensors. *Bioanal Rev*. 2012;4(2-4):115-157. doi:10.1007/s12566-012-0032-y.

109. Khalil G, Gouterman M, Ching S, et al. Synthesis and spectroscopic characterization of Ni, Zn, Pd and Pt tetra(pentafluorophenyl)porpholactone with comparisons to Mg, Zn, Y, Pd and Pt metal complexes of tetra(pentafluorophenyl)porphine. *J Porphyr Phthalocyanines*. 2002;06(02):135-145. doi:10.1142/S108842460200018X.

110. Gouterman M, Hall RJ, Khalil G-E, Martin PC, Shankland EG, Cernyt RL. Tetra(pentafluorophenyl)porpholactone. *J Am Chem Soc*. 1989;111(10):3702-3707. doi:10.1021/ja00192a030.

111. Worlinsky JL, Halepas S, Ghandehari M, Khalil G, Brückner C. High pH sensing with water-soluble porpholactone derivatives and their incorporation into a Nafion® optode membrane. *Analyst*. 2015;140(1):190-196. doi:10.1039/C4AN01462F.

112. Rogers JE, Nguyen KA, Hufnagle DC, et al. Observation and Interpretation of Annulated Porphyrins: Studies on the Photophysical Properties of meso-Tetraphenylmetalloporphyrins. *J Phys Chem A*. 2003;107(51):11331-11339. doi:10.1021/jp0354705.

113. Borisov SM, Nuss G, Haas W, Saf R, Schmuck M, Klimant I. New NIR-emitting complexes of platinum(II) and palladium(II) with fluorinated benzoporphyrins. *J Photochem Photobiol A Chem*. 2009;201(2-3):128-135. doi:10.1016/j.jphotochem.2008.10.003.

114. Borisov SM, Nuss G, Klimant I. Red Light-Excitable Oxygen Sensing Materials Based on Platinum (II) and Palladium (II) Benzoporphyrins. *Anal Chem*. 2008;80(24):9435-9442. doi:10.1007/s00604.

115. Napp J, Behnke T, Fischer L, et al. Targeted luminescent near-infrared polymer-nanoprobes for in vivo imaging of tumor hypoxia. *Anal Chem*. 2011;83(23):9039-9046. doi:10.1021/ac201870b.

116. Koren K, Hutter L, Enko B, Pein A, Borisov SM, Klimant I. Tuning the dynamic range and sensitivity of optical oxygen-sensors by employing differently substituted polystyrene-derivatives. *Sensors Actuators, B Chem*. 2013;176:344-350. doi:10.1016/j.snb.2012.09.057.

117. Ehgartner J, Sulzer P, Burger T, et al. Online analysis of oxygen inside silicon-glass microreactors with integrated optical sensors. *Sensors Actuators, B Chem*. 2016;228:748-757. doi:10.1016/j.snb.2016.01.050.

118. Staudinger C, Borisov SM. Long-wavelength analyte-sensitive luminescent probes and optical (bio)sensors. *Methods Appl Fluoresc*. 2015;3(4):042005. doi:10.1088/2050-6120/3/4/042005.

119. Currie MJ, Mapel JK, Heidel TD, Goffri S, Baldo MA. High-Efficiency Organic Solar Concentrators for Photovoltaics. *Science (80-)*. 2008;321(5886):226-228. doi:10.1126/science.1158342.

120. Rozhkov V V., Khajehpour M, Vinogradov SA. Luminescent Zn and Pd tetranaphthaloporphyrins. *Inorg Chem*. 2003;42(14):4253-4255. doi:10.1021/ic034257k.

121. Finikova OS, Cheprakov A V, Vinogradov SA. Synthesis and Luminescence of Soluble meso-Unsubstituted Tetrabenzo- and Tetranaphtho [2,3]porphyrins. *J Org Chem*. 2005;70(23):9562-9572.

122. Kumar R, Ohulchanskyy TY, Roy I, et al. Near-infrared phosphorescent polymeric nanomicelles: Efficient optical probes for tumor imaging and detection. *ACS Appl Mater Interfaces*. 2009;1(7):1474-1481. doi:10.1021/am9001293.

123. Sommer JR, Farley RT, Graham KR, et al. Efficient near-infrared polymer and organic light-emitting diodes based on electrophosphorescence from (tetraphenyltetranaphtho[2,3]porphyrin)platinum(II). *ACS Appl Mater Interfaces*. 2009;1(2):274-278. doi:10.1021/am800236x.

124. Niedermair F, Borisov SM, Zenkl G, et al. Tunable phosphorescent NIR oxygen indicators based on mixed benzo- and naphthoporphyrin complexes. *Inorg Chem*. 2010;49(20):9333-9342. doi:10.1021/ic100955z.

125. Gewehr PM, Delpy DT. Optical oxygen sensor based on phosphorence lifetime quenching and emlpoying a polymer immobilised metalloporphyrin probe. *Med Biol Eng Comput*. 1993;762:11-21.

126. O'Riordan TC, Zhdanov A V., Ponomarev G V., Papkovsky DB. Analysis of intracellular oxygen and metabolic responses of mammalian cells by time-resolved fluorometry. *Anal Chem*. 2007;79(24):9414-9419. doi:10.1021/ac701770b.

127. O'Riordan TC, Fitzgerald K, Ponomarev G V., et al. Sensing intracellular oxygen using near-infrared phosphorescent probes and live-cell fluorescence imaging. *AJP Regul Integr Comp Physiol*. 2006;292(4):R1613-R1620. doi:10.1152/ajpregu.00707.2006.

128. Vanderkooi JM, Maniara G, Green TJ, Wilson DF. An optical method for measurement of dioxygen concentration based upon quenching of phosphorescence. *J Biol Chem*. 1987;262(12):5476-5482.

129. Vasil'ev V V., Borisov SM, Vasil'ev V V., Borisov SM. Optical oxygen sensors based on phosphorescent water-soluble platinum metals porphyrins immobilized in perfluorinated ion-exchange membrane. *Sensors Actuators B Chem*. 2002;82(2-3):272-276. doi:10.1016/S0925-4005(01)01063-2.

130. Čeklovský A, Takagi S. Oxygen sensing materials based on clay/metalloporphyrin hybrid systems. *Cent Eur J Chem*. 2013;11(7):1132-1136. doi:10.2478/s11532-013-0238-z.

131. Dunphy I, Vinogradov SA, Wilson DF. Oxyphor R2 and G2: Phosphors for measuring oxygen by oxygen-dependent quenching of phosphorescence. *Anal Biochem*. 2002;310(2):191-198. doi:10.1016/S0003-2697(02)00384-6.

132. Koo Lee Y-E, Ulbrich EE, Kim G, et al. Near Infrared Luminescent Oxygen Nanosensors with Nanoparticle Matrix Tailored Sensitivity. *Anal Chem*. 2010;82(20):8446-8455. doi:10.1021/ac1015358.

133. OGOSHI H, SETSUNE J-I, YOSHIDA Z-I. SYNTHESES AND REACTIONS OF IRIDIUM COMPLEXES OF OCTAETHYLPORPHYRIN. *J Organomet Chem*. 1978;159:317-328.

134. Koren K, Borisov SM, Saf R, Klimant I. Strongly Phosphorescent Iridium(III)-Porphyrins - New Oxygen Indicators with Tuneable Photophysical Properties and Functionalities. *Eur J Inorg Chem*. 2011;2011(10):1531-1534. doi:10.1002/ejic.201100089.

135. Koren K, Dmitriev RI, Borisov SM, Papkovsky DB, Klimant I. Complexes of IrIII-Octaethylporphyrin with Peptides as Probes for Sensing Cellular O2. *ChemBioChem*. 2012;13(8):1184-1190. doi:10.1002/cbic.201200083.

136. Loredo-Calderón EL, López-Cortina ST, Carranza-Rosales P, Viveros-Valdez E, Hernández-Fernández E, Fernández-Zertuche M. Synthesis and characterization of six nonsymmetric A3B porphyrins with p-chlorophenyl as meso-substituent A or B and determination of their photodynamic activity. *Med Chem Res*. 2016;25(8):1657-1665. doi:10.1007/s00044-016-1600-4.

137. Obata M, Tanaka Y, Araki N, et al. Synthesis of poly(isobutyl-co-2,2,2-trifluoroethyl methacrylate) with 5,10,15,20-tetraphenylporphinato platinum(II) moiety as an oxygen-sensing dye for pressure-sensitive paint. *J Polym Sci Part A Polym Chem*. 2005;43(14):2997-3006. doi:10.1002/pola.20776.

138. Tian Y, Shumway BR, Cody Youngbull A, et al. Dually fluorescent sensing of pH and dissolved oxygen using a membrane made from polymerizable sensing monomers. *Sensors Actuators, B Chem*. 2010;147(2):714-722. doi:10.1016/j.snb.2010.03.029.

139. Tian Y, Shumway BR, Meldrum DR. A new cross-linkable oxygen sensor covalently bonded into poly(2-hydroxyethyl methacrylate)-co-polyacrylamide thin film for dissolved oxygen sensing. *Chem Mater*. 2010;22(6):2069-2078. doi:10.1021/cm903361y.

140. Tian Y, Shumway BR, Gao W, et al. Influence of matrices on oxygen sensing of three sensing films with chemically conjugated platinum porphyrin probes and preliminary application for monitoring of oxygen consumption of Escherichia coli (E. coli). *Sensors Actuators, B Chem*. 2010;150(2):579-587. doi:10.1016/j.snb.2010.08.036.

141. Lu H, Jin Y, Tian Y, Zhang W, Holl MR, Meldrum DR. New ratiometric optical oxygen and pH dual sensors with three emission colors for measuring photosynthetic activity in Cyanobacteria. *J Mater Chem*. 2011;2011(48):19293-192301. doi:10.1039/C1JM13754A.

142. Koren K, Borisov SM, Klimant I. Stable optical oxygen sensing materials based on click-coupling of fluorinated platinum(II) and palladium(II) porphyrins - A convenient way to eliminate dye migration and leaching. *Sensors Actuators, B Chem*. 2012;169:173-181. doi:10.1016/j.snb.2012.04.062.

143. Liu H, Yang H, Hao X, et al. Development of polymeric nanoprobes with improved lifetime dynamic range and stability for intracellular oxygen sensing. *Small*. 2013;9(15):2639-2648. doi:10.1002/smll.201203127.

144. Hutter LH, Müller BJ, Koren K, Borisov SM, Klimant I. Robust optical oxygen sensors based on polymer-bound NIR-emitting platinum(II)–benzoporphyrins. *J Mater Chem C*. 2014;2(36):7589-7598. doi:10.1039/C4TC00983E.

145. Senge MO. Stirring the porphyrin alphabet soup—functionalization reactions for porphyrins. *Chem Commun*. 2011;47(7):1943. doi:10.1039/c0cc03984e.

146. Giuntini F, Chauhan VM, Aylott JW, et al. Conjugatable water-soluble Pt(II) and Pd(II) porphyrin complexes: novel nano- and molecular probes for optical oxygen tension measurement in tissue engineering. *Photochem Photobiol Sci*. 2014;13(7):1039-1051. doi:10.1039/c4pp00026a.

147. Chauhan VM, Giuntini F, Aylott JW. Quadruple labelled dual oxygen and pH-sensitive ratiometric nanosensors. *Sens Bio-Sensing Res*. 2016;8:36-42. doi:10.1016/j.sbsr.2016.03.007.

148. Kadish KM. *The Porphyrin Handbook*.; 1999.

149. Harper D, Buglione DC. "Porphyria". The Online Etymology Dictionar. 2014.

150. Dean ML, Schmink JR, Leadbeater NE, Brückner C. Microwave-promoted insertion of Group 10 metals into free base porphyrins and chlorins: scope and limitations. *Dalton Trans*. 2008;(10):1341-1345. doi:10.1039/b716181f.

151. Weiss C, Kobayashi H, Gouterman M. Spectra of porphyrins: Part III. Self-consistent molecular orbital calculations of porphyrin and related ring systems. *J Mol Spectrosc*. 1965;16(2):415-450. doi:10.1016/0022-2852(65)90132-3.

152. Milani M, Pesce A, Nardini M, et al. Structural bases for heme binding and diatomic ligand recognition in truncated hemoglobins. *J Inorg Biochem*. 2005;99(1):97-109. doi:10.1016/j.jinorgbio.2004.10.035.

153. Rothemund P. Formation of Porphyrins from Pyrrole and Aldehydes. *J Am Chem Soc*. 1935;57(10):2010-2011. doi:10.1021/ja01313a510.

154. Rothemund P. Porphyrin Studies. IV. The Synthesis of α,β,γ,δ-Tetraphenylporphine. *J Am Chem Soc*. 1941;63:267-270. doi:10.1021/ja01846a065.

155. Adler AD, Finarelli JD, R. FL. A simplified synthesis of meso-tetraphenylporphyrin. *J Org Chem*. 1966;32:476.

156. Little RG, Anton JA, Loach PA, Ibers JA. The synthesis of Some Substituted Tetraarylporphyrins. *J Heterocycl Chem*. 1975;12(2):343-349.

157. Lindsey JS, Hsu HC, Schreiman IC. Synthesis of tetraphenylporphyrins under very mild conditions. *Tetrahedron Lett*. 1986;27(41):4969-4970. doi:10.1016/S0040-4039(00)85109-6.

158. Lindsey JS, Schreiman IC, Hsu HC, Kearney PC, Marguerettaz AM. Rothemund and Adler-Longo reactions revisited: synthesis of tetraphenylporphyrins under equilibrium conditions. *J Org Chem*. 1987;52:827-836. doi:10.1021/jo00381a022.

159. Geier GR, Riggs JA, Lindsey JS. Investigation of acid cocatalysis in syntheses of tetraphenylporphyrin. *J Porphyr Phthalocyanines*. 2001;5(9):681-690. doi:10.1002/jpp.380.

160. GUILHERME DSAML, PEREIRA MM. Novel sugar-linked chlorin derivative and process for production thereof. 2009.

161. Nguyen KA, Day PN, Pachter R, Tretiak S, Chernyak V, Mukamel S. Analysis of Absorption Spectra of Zinc Porphyrin, Zincmeso-Tetraphenylporphyrin, and Halogenated Derivatives. *J Phys Chem A*. 2002;106(43):10285-10293. doi:10.1021/jp020053y.

162. Vaz Serra VI, Pires SMG, Alonso CMA, Neves MGPMS, Tome AC, Cavaleiro J. Meso-Tetraarylporphyrins Bearing Nitro or Amino Groups: Synthetic Strategies and Reactivity Profile. *Top Heterocycl Chem*. 2014;33:35-78. doi:10.1007/7081.

163. Johnson AW, Oldfield D. The Nitration and Hydroxylation of Aetioporphyrin. *J Org Chem*. 1965:4303.

164. Vicente MGH, Neves MGPMS, Cavaleiro JAS, Hombrecher HK, Koll D. Electrochemical and Spectroscopic Properties of Cu(ll) beta-Nitro meso- Tetra(pentafluorophenyl)porphyrins. *Tetrahedron Lett*. 1996;37(2):261-262.

165. Bajju GD, Singh N. Synthesis and Characterization of New Meso-Substituted and β-Substituted Unsymmetrical Metalloporphyrins. *Chem Sci Trans*. 2014;3(1):314-322. doi:10.7598/cst2014.583.

166. Catalano MM, Crossley MJ, Harding MM, King LG. Control of reactivity at the porphyrin periphery by metal ion co-ordination: a general method for specific nitration at the β-pyrrolic position of 5,10,15,20-tetra-arylporphyrins. *J Chem Soc, Chem Commun*. 1984;(22):1535-1536. doi:10.1039/C39840001535.

167. Hombrecher HK, Gherdan VM, Ohm S, et al. Synthesis and electrochemical investigation of β-alkyloxy substituted meso-tetraphenylporphyrins. *Tetrahedron*. 1993;49(38):8569-8578. doi:10.1016/S0040-4020(01)96263-5.

168. Song B, Yu BS. Fluorine-19 NMR Spectroscopic Studies of Phenyl-fluorinated Iron Tetraarylporphyrin Complexes. *Bull Korean Chem Soc*. 2003;24(7):981-985.

169. Hogbe MG, Graham WAG, Shifts C. Chemical Shifts and Coupling Constants in Pentafluorophenyl Derivatives. *J Am Chem Soc*. 1968;133(1964):283-291.

170. Birnbaum ER, Hodge JA, Grinstaff MW, et al. 19F NMR Spectra and Structures of Halogenated Porphyrins. *Inorg Chem*. 1995;34(14):3625-3632. doi:10.1021/ic00118a010.

171. Hobbs JD, Majumder SA, Luo L, et al. Structural Heterogeneity and Coordination Chemistry of Nickel(II) Octaethyl-meso-nitroporphyrins. *J Am Chem Soc*. 1994;116(8):3261-3270. doi:10.1021/ja00087a011.

172. Tiwari R, Nath M. Synthesis of 2-nitro-3-(pyrrol-1-yl)-5,10,15,20-tetraarylporphyrins via a Clauson-Kaas reaction and the study of their electronic properties. *New J Chem*. 2015;39(7):5500-5506. doi:10.1039/C5NJ00014A.

173. Baldwin JE, Crossley MJ, DeBernardis J. Efficient peripheral functionalization of porphyrins. *Tetrahedron*. 1982;38(5):685-692. doi:10.1016/0040-4020(82)80211-1.

174. Crossley M, King L, Pyke S. A new and highly efficient synthesis of hydroxyporphyrins. *Tetrahedron*. 1987;43(20):4569-4577. doi:10.1016/S0040-4020(01)86899-X.

175. Giuntini F, Faustino M a. F, Neves MGPMS, Tomé AC, Silva AMS, Cavaleiro J a. S. Synthesis and reactivity of 2-(porphyrin-2-yl)-1,3-dicarbonyl compounds. *Tetrahedron*. 2005;61(44):10454-10461. doi:10.1016/j.tet.2005.08.059.

176. Crossley MJ, Harding MM, Tansey CW. A Convenient Synthesis of 2-Alkyl-5,10,15,20-tetraphenylporphyrins: Reaction of Metallo-2-nitro-5,10,15,20-tetraphenylporphyrins with Grignard and Organolithium Reagents. *J Org Chem*. 1994;59:4433-4437.

177. Crossley MJ, King LG, Newsom IA, Sheehan CS. Investigation of a "reverse" approach to extended porphyrin systems. Synthesis of a 2,3-diaminoporphyrin and its reactions with α-dione. *J Chem Soc, Perkin Trans 1*. 1996:2675-2684.

178. Crossley MJ, King LG. Reaction of metallo-2-nitro-5,10,15,20-tetraphenylporphyrins with oxyanions. Temperature-dependent competition between nucleophilic addition and single-electron transfer processes. *J Chem Soc Perkin Trans 1*. 1996;(11):1251. doi:10.1039/p19960001251.

179. Battersby AR, Jones K, Snow RJ. Novel methods for Demetalating Tetrapyrrolic Metallo-Macrocycles. *Angew chem, Int Ed Eng*. 1983;22:734-735.

180. Watanabe E, Nishimura S, Ogoshi H, Yoshida Z. Orientation of electrophilic meso-substitution in metallooctaethylporphyrins. *Tetrahedron*. 1975;31:1385-1390.

181. With TK. Esterification of porphyrins and hydrolysis of porphyrin esters. *South African J Lab Clin Med*. 1971;(September):218-220. http://www.ncbi.nlm.nih.gov/pubmed/4783910.

182. Tomé JPC, Neves MGPMS, Tomé AC, et al. Synthesis of glycoporphyrin derivatives and their antiviral activity against herpes simplex virus types 1 and 2. *Bioorg Med Chem*. 2005;13(12):3878-3888. doi:10.1016/j.bmc.2005.04.015.

183. Samaroo D, Soll CE, Todaro LJ, Drain CM. Efficient microwave-assisted synthesis of amine-substituted tetrakis(pentafluorophenyl)porphyrin. *Org Lett*. 2006;8(22):4985-4988. doi:10.1021/ol060946z.

184. Lang K, Kral V, Kapusta P, Kubat P, Vasek P. Photoinduced electron transfer within porphyrin-cyclodextrin conjugates. *Tetrahedron Lett*. 2002;43:4919-4922.

185. Costa JIT, Tomé AC, Neves MGPMS, Cavaleiro J a. S. 5,10,15,20-Tetrakis(Pentafluorophenyl)Porphyrin: a Versatile Platform To Novel Porphyrinic Materials. *J Porphyr Phthalocyanines*. 2011;15(11n12):1116-1133. doi:10.1142/S1088424611004294.

186. Dumoulin F, Ahsen V. Click chemistry: the emerging role of the azide-alkyne Huisgen dipolar addition in the preparation of substituted tetrapyrrolic derivatives. *J Porphyr Phthalocyanines*. 2011;15(07n08):481-504. doi:10.1142/S1088424611003434.

187. Kerr RL, Miller SA, Shoemaker RK, Elliott BJ, Gin DL. New type of Li ion conductor with 3D interconnected nanopores via polymerization of a liquid organic electrolyte-filled lyotropic liquid-crystal assembly. *J Am Chem Soc*. 2009;131(44):15972-15973. doi:10.1021/ja905208f.

188. Ienaga K, Nakamura K, Higashiura K, Toyomaki Y, Kimura H. Simple peptides. III: Syntheses and properties of taurine-oligopeptides containing an acidic α-amino acid. *Chem Pharm Bull (Tokyo)*. 1988;36(8):2796-2801. http://cat.inist.fr/?aModele=afficheN&cpsidt=6576532.

189. Ulman A, Frolow F, Manassen J, Rabinovich D. Synthesis and Properties of Tetraphenylporphyrin Molecules Containing Heteroatoms other than Nitrogen. *Inorg Chem*. 1981;(20):1987-1990.

190. A.W. Johnstone R, M. d'A. Rocha Gonsalves A, M. Pereira M, et al. New Procedures for the Synthesis and Analysis of 5,10,15,20-Tetrakis(sulphophenyl)porphyrins and Derivatives through Chlorosulphonation. *Heterocycles*. 1996;43(4):829. doi:10.3987/COM-95-7372.

191. Ye B-H, Naruta Y. A novel method for the synthesis of regiospecifically sulfonated porphyrin monomers and dimers. *Tetrahedron*. 2003;59(20):3593-3601. doi:10.1016/S0040-4020(03)00541-6.

192. Monteiro CJP, Pereira MM, Pinto SM a., et al. Synthesis of amphiphilic sulfonamide halogenated porphyrins: MALDI-TOFMS characterization and evaluation of 1-octanol/water partition coefficients. *Tetrahedron*. 2008;64(22):5132-5138. doi:10.1016/j.tet.2008.03.055.

193. Lupetti A, Paulusma-Annema A, Senesi S, Campa M, Van Dissel JT, Nibbering PH. Internal thiols and reactive oxygen species in candidacidal activity exerted by an N-terminal peptide of human lactoferrin. *Antimicrob Agents Chemother*. 2002;46(6):1634-1639.

194. Baldini L, Hunter CA. Self-assembly of porphyrin arrays. *Adv Inorg Chem*. 2002;53:213-259. doi:10.1016/S0898-8838(02)53006-3.

195. Palacin S, Barraud A. Supermolecular Englneerlng at the Air-Water Interface: Spatially Controlled Formation. *J Phys Chem*. 1991;(95):7438-7447.

196. Vodzinskii S V, MalinoVskii VL, Ishkov Y V., Zhilina ZI, Kirichenzo AM. Synthesis and Properties of 2-nitro-5,10,15,20-tetraheterylporphyrins. *Russ J Org Chem*. 1998;34(6):1-4.

197. Catalano MM, Crossley MJ, Harding MM, King LG. Control of Reactivity at the Porphyrin Periphery by Metal Ion Co-ordination: a General Method for Specific Nitration at the beta-Pyrrolic Position of 5,10,15,20-Tetra-arylporphyrins. *J Chem Soc Chem Commun*. 1984:1535-1536.

198. Hambright P, Gore T, Burton M. Synthesis and characterization of new isomeric water-soluble porphyrins. Tetra(2-N-methylpyridy1)porphine and Tetra(3-N-methylppridy1)porphine. *Inorg Chem*. 1976;15(9):2314-2315.

199. Pasternack RF, Huber PR, Boyd P, et al. Aggregation of meso-substituted water-soluble porphyrins. *J Am Chem Soc*. 1972;94(13):4511-4517. doi:10.1021/ja00768a016.

200. Hambright P, Fleisher EB. Acid-base equilibriums, kinetics of copper ion incorporation, and acid-catalyzed zinc ion displacement from the water-soluble porphyrin alpha,beta,gamma,delta-tetrakis(1-methyl-4-pyridinio)porphine tetraiodide. *Inorg Chem*. 1970;9(7):1757-1761. doi:10.1021/ic50089a030.

201. Giuntini F, Nistri D, Chiti G, Fantetti L, Jori G, Roncucci G. Synthesis of trimethylammoniumphenylthio-substituted phthalocyanines with different pattern of substitution. *Tetrahedron Lett*. 2003;44(3):515-517. doi:10.1016/S0040-4039(02)02597-2.

202. Little RG. The Mixed-Aldehyde Synthesis of Difunctional Tetraarylporphyrins. *J Heterocycl Chem*. 1981;(18):129-133.

203. Fleischer EB. alpha,beta,gamma,delta-Tetra-(4-pyridyl)-porphine and Some of its Metal Complexes. *Inorg Chem*. 1962;1(3):493-495. doi:10.1021/ic50003a010.

204. Kalyanasundaram K. Photochemistry of Water-Soluble Porphyrins: Comparative Study of Isomeric Tetrapyridyl- and Tetrakis(N-Methylpyridiniumyl)Porphyrins. *Inorg Chem*. 1984;23(16):2453-2459. doi:10.1021/ic00184a019.

205. Sirish M, Chertkov VA, Schneider HJ. Porphyrin-based peptide receptors: Syntheses and NMR analysis. *Chem - A Eur J*. 2002;8(5):1181-1188. doi:10.1002/1521-3765(20020301)8:5<1181::AID-CHEM1181>3.0.CO;2-U.

206. Habdas J, Boduszek B. Synthesis of 5-(4'-carboxyphenyl)-10,15,20-tris-(4 pyridyl)-porphyrin and its peptidyl phosphonate derivatives. *J Pept Sci*. 2009;15(4):305-311. doi:10.1002/psc.1117.

207. Klopfenstein WE. On methylation of unsaturated acids using boron trihalide-methanol reagents. *J Lipid Res*. 1971;12(6):773-776.

208. Chouikrat R, Champion A, Vanderesse R, Frochot C, Moussaron A. Microwave-assisted synthesis of zinc 5-(4-carboxyphenyl)-10,15,20-triphenylporphyrin and zinc 5-(4-carboxyphenyl)-10,15,20-triphenylchlorin. *J Porphyr Phthalocyanines*. 2015;19(04):595-600. doi:10.1142/S1088424614500953.

209. Poddutoori PK, Bregles LP, Lim GN, Boland P, Kerr RG, D'Souza F. Modulation of Energy Transfer into Sequential

Electron Transfer upon Axial Coordination of Tetrathiafulvalene in an Aluminum(III) Porphyrin-Free-Base Porphyrin Dyad. *Inorg Chem*. 2015;54(17):8482-8494. doi:10.1021/acs.inorgchem.5b01190.

210.   Li X, Tanasova M, Vasileiou C, Borhan B. Fluorinated Porphyrin Tweezer: A Powerful Reporter of Absolute Configurations for erythro- and threo- Diols, Amino Alcohols and Diamines. *J Am Chem Soc*. 2008;(130):1885-1893.

211.   Iida K, Nango M, Okada K, et al. Synthesis and Characterization of Hybrid Porphyrin Dimers and Halogenated Porphyrin Dimers. *Bull Chem Soc Jpn*. 1995;(68):1959-1968.

212.   Gust D, Moore T a, Moore a L, et al. Long-lived Photoinitiated Charge Separation In Carotene Diporphyrin Triad Molecules. *J Am Chem Soc*. 1991;113(19):3638-3649. doi:10.1021/ja00010a002.

213.   Poddutoori PK, Lim GN, Vassiliev S, D'Souza F. Ultrafast charge separation and charge stabilization in axially linked "tetrathiafulvalene-aluminum(iii) porphyrin-gold(iii) porphyrin" reaction center mimics. *Phys Chem Chem Phys*. 2015;17(39):26346-26358. doi:10.1039/c5cp04818d.

214.   Pasternack RF, Brigandi R a, Abrams MJ, Williams a P, Gibbs EJ. Interactions of Porphyrins and Metalloporphyrins with Single-Stranded Poly(dA). *Inorg Chem*. 1990;29(22):4483-4486. doi:10.1021/ic00347a030.

215.   La T, Richards RA, Lu RS, Bau R, J GMM. Solution Chemistry and Crystal Structure of Nickel Tetrakis(2,3,5,6-tetrafluoro-N,N,N-trimethyl-4-aniliniumyl)porphyrin Trifluoromethanesulfonate (NiTF4TMAP(CF3S03)4). *Inorg Chem*. 1995;(16):5632-5640.

216.   Busby AC, Dinello KR, Dolphin D. A Convenient Preparation of meso-Tetra (4-sulfonatophenyl) porphyrin. *Can J Chem*. 1975;(53):1554.

217.   Fleischer EB, Palmer JM, Srivastava TS, Chatterjee A. Thermodynamic and Kinetic Properties of an Iron-porphyrin System. *J Am Chem Soc*. 1971;93(13):3162-3167.

218.   Srivastava TS, Tsutsui M. Unusual metalloporphyrins. XVI. Preparation and purification of tetrasodium meso-tetra(p-sulfophenyl)porphine. Easy procedure. *J Org Chem*. 1973;38(11):2103. doi:10.1021/jo00951a036.

219.   Dong Z, Scammells PJ. New methodology for the N-demethylation of opiate alkaloids. *J Org Chem*. 2007;72(26):9881-9885. doi:10.1021/jo071171q.

220.   Nicolas I, Maux P Le, Simonneaux G. Synthesis of chiral water-soluble metalloporphyrins (Fe, Ru,): new catalysts for asymmetric carbene transfer in water. *Tetrahedron Lett*. 2008;49(40):5793-5795. doi:10.1016/j.tetlet.2008.07.133.

221.   Gupta C, Singh H. *Uranium Resource Processing*.; 2003.

222.   Gordon AG, Richard JB, William LG. Amine addition salts of steroid-3-monosulfates. 1950. http://www.google.com.gi/patents/US2534121.

223.   Lambert C, Gaschler W, Noll G, et al. Cationic [small pi]-electron systems with high quadratic hyperpolarisability. *J Chem Soc Perkin Trans 2*. 2001;(6):964-974. doi:10.1039/b009664b.

224.   TICE BBP, IKCHOON L, F. H. K. Kinetic Studies of Hydrogen Exchange in Dialkylanilines. *J Am Chem Soc*. 1963;85:329-337.

225.   Kadish KM, Araullo-McAdams C, Han BC, Franzen MM. Syntheses and Spectroscopic Characterization of (T(p-Me2N)F4PP)H2 and (T(p-Me2N)F4PP)M Where T(p-Me2N)F4PP Is the Dianion of porphyrin and M = Co (II), Cu (II), or Ni (II). Structures of (T(p-Me2N)F4PP)Co and (meso-tetrakis(pentafluorophenyl)porphi. *J Am Chem Soc*. 1990;(112):8364-8368.

226.   Richards R, Miskelly GM. Synthesis and Characterization of the Cationic Porphyrin meso-Tetrakis(2,3,5,6-tetrafluoro-N,N,N- trimethyl-4-aniliniumyl) porphyrin. *Inorg Chem*. 1994;(33):3159-3163.

227.   Sun Y-L, Zhou Y, Qing-Lan L, Yang Y-W. Enzyme-Responsive Supramolecular Nanovalves Crafted by Mesoporous Silica Nanoparticles and Choline-Sulfonatocalix[4]arene [2]Pseudorotaxanes for Controlled Cargo Release. *Chem Commun*. 2013;(79):2013.

228.   Tayyari F, Gowda GAN, Gu H, Raftery D. N-Cholamine – A Smart Isotope Smart Tag for Combining NMR- and MS-Based Metabolite Profiling. *Anal Chem*. 2013;85(18):8715-8721. doi:10.1021/ac401712a.

229.   Lamos SM, Shortreed MR, Frey BL, Belshaw PJ, Smith LM. Relative quantification of carboxylic acid metabolites by liquid chromatography-mass spectrometry using isotopic variants of cholamine. *Anal Chem*. 2007;79(14):5143-5149. doi:10.1021/ac062416m.

230. Kvíčala J, Beneš M, Paleta O, Král V. Regiospecific nucleophilic substitution in 2,3,4,5,6-pentafluorobiphenyl as model compound for supramolecular systems. Theoretical study of transition states and energy profiles, evidence for tetrahedral SN2 mechanism. *J Fluor Chem*. 2010;131(12):1327-1337. doi:10.1016/j.jfluchem.2010.09.003.

231. Kra J, Dolensky B, Vas P, et al. Glycol porphyrin derivatives as potent photodynamic inducers of apoptosis in tumor cells. *J Med Chem*. 2008;51(19):5964-5973. doi:10.1021/jm8002119.

232. Hadad CM, Rablen PR, Wiberg KB. C-O and C-S bonds: Stability, bond dissociation energies, and resonance stabilization. *J Org Chem*. 1998;63(24):8668-8681. doi:10.1021/jo972180+.

233. Golf HRA, Reissig HU, Wiehe A. Regioselective nucleophilic aromatic substitution reaction of meso-pentafluorophenyl-substituted porphyrinoids with alcohols. *European J Org Chem*. 2015;2015(7):1548-1568. doi:10.1002/ejoc.201403503.

234. Zakavi S, Omidyan R, Talebzadeh S. The influence of protonation on the structure and spectral properties of porphine: UV-vis, H-1 NMR and ab initio studies. *Rsc Adv*. 2016;6(85):82219-82226. doi:10.1039/c6ra12520d.

235. Meot-Ner M, Adler AD. Substituent effects in noncoplanar .pi. systems. ms-Porphins. *J Am Chem Soc*. 1975;97(18):5107-5111. doi:10.1021/ja00851a014.

236. Kalyanasundaram K. Photochemistry of polypyridine and porphyrin complexes. 1992.

237. Lemon CM, Karnas E, Bawendi MG, Nocera DG. Two-photon oxygen sensing with quantum dot-porphyrin conjugates. *Inorg Chem*. 2013;52:10394-10406. doi:10.1021/ic4011168.

238. Amao Y, Miyakawa K, Okura I, Division A. Novel optical oxygen sensing device: a thin flm of a palladium porphyrin with a long alkyl chain on an alumina plate. *J Mater Chem*. 2000;(10):305-308.

239. Mao YA, Kura IO, Hinohara HS, Ishide HN. An Optical Sensing Material for Trace Analysis of Oxygen . Metalloporphyrin Dispersed in Poly (1-trimethylsilyl-1-propyne) Film. *Polym J*. 2002;34(6):411-417.

240. Tripathi VS, Lakshminarayana G, Nogami M. Optical oxygen sensors based on platinum porphyrin dyes encapsulated in ORMOSILS. *Sensors Actuators, B Chem*. 2010;147(2):741-747. doi:10.1016/j.snb.2010.04.020.

241. Scheicher SR, Kainz B, Köstler S, et al. Optical oxygen sensors based on Pt(II) porphyrin dye immobilized on S-layer protein matrices. *Biosens Bioelectron*. 2009;25:797-802. doi:10.1016/j.bios.2009.08.030.

242. Mills A. Optical Oxygen Sensors: Utilizing the Luminescence of Platinum Metals Complexes. *Platin Met Rev*. 1997;41(Ii):115-127.

243. Amao Y, Asai K, Miyashita T, Okura I. Photophysical and Photochemical Properties of Optical Oxygen Pressure Sensor of Platinum Porphyrin-Isobutylmethacrylate-trifluoroethylmethacrylate Copolymer Film. *Polym J*. 1999;31(12):1267-1269.

244. Gawande MB, Shelke SN, Zboril R, Varma RS. Microwave-assisted chemistry: Synthetic applications for rapid assembly of nanomaterials and organics. *Acc Chem Res*. 2014;47(4):1338-1348. doi:10.1021/ar400309b.

245. Kappe CO, Dallinger D. The impact of microwave synthesis on drug discovery. *Nat Rev Drug Discov*. 2006;5(1):51-63. doi:10.1038/nrd1926.

246. Kappe CO, Dallinger D. Controlled microwave heating in modern organic synthesis: Highlights from the 2004-2008 literature. *Mol Divers*. 2009;13(2):71-193. doi:10.1007/s11030-009-9138-8.

247. Kappe CO, Pieber B, Dallinger D. Microwave effects in organic synthesis: Myth or reality? *Angew Chemie - Int Ed*. 2013;52(4):1088-1094. doi:10.1002/anie.201204103.

248. Chauhan SMS, Sahoo BB, Srinivas K a. Microwave-Assisted Synthesis of 5,10,15,20-Tetraaryl Porphyrins. *Synth Commun*. 2001;31(1):33-37. doi:10.1081/SCC-100000176.

249. Nascimento BFO, Pineiro M, António M, Gonsalves AR. Microwave-assisted synthesis of porphyrins and metallo-porphyrins : a rapid and efficient synthetic method. *J Porphyr Phthalocyanines*. 2007;11:77-84.

250. Liu MO, Hu AT. Microwave-assisted synthesis of phthalocyanine–porphyrin complex and its photoelectric conversion properties. *J Organomet Chem*. 2004;689(15):2450-2455. doi:10.1016/j.jorganchem.2004.05.008.

251. Warner MG, Succaw GL, Hutchison JE. Solventless syntheses of mesotetraphenylporphyrin : new experiments for a greener organic chemistry laboratory curriculum. *Green Chem*. 2001;3:267-270. doi:10.1039/b107999a.

252. Lahiri GK, Summers JS, Stolzenberg AM. A superior method for the metalation of hydroporphyrins. *Inorg Chem*.

1991;30(26):5049-5052.
http://pubs.acs.org/doi/abs/10.1021/ic00026a038%5Cnpapers2://publication/doi/10.1021/ic00026a038.

253. Gunawardhana N, Tabata M. A convenient and eco-friendly way to synthesize Pt(II) and Pd(II) porphyrins in ionic liquids by microwave activation. *Environ Chem Lett*. 2011;9(4):473-477. doi:10.1007/s10311-010-0304-0.

254. Friebolin H. *Basic One- and Two-Dimensional NMR Spectroscopy*.; 2010.

255. Mink LM, Neitzel ML, Bellomy LM, et al. Platinum(II) and platinum(IV) porphyrin complexes: Synthesis, characterization, and electrochemistry. *Polyhedron*. 1997;16(16):2809-2817. doi:10.1016/S0277-5387(97)00026-0.

256. Yamashita K, Katsumata N, Tomita S, et al. Facile and Practical Synthesis of Platinum(II) Porphyrins under Mild Conditions. *Chem Lett*. 2015;44(4):492-494. doi:Doi 10.1246/Cl.141112.

257. Price JH, Birk JP, Wayland BB. Thermal and Photochemical Cis-Trans Isomerization of PtL2C12 (L=Dialkyl Sulfoxide) Complexes. Kinetics and Mechanisms for Thermal Isomerization. *Inorg Chem*. 1978;17(8):2245-2250. doi:10.1021/ic50186a046.

258. Nieto D, González-vadillo AM, Bruña S, Pastor CJ, Kaifer AE, Cuadrado I. Pt (II)-activated coupling of aminoethylferrocene with benzonitrile . A facile access route to a new redox-active bis (ferrocenyl-amidine) anion sensor. *Chem Commun*. 2011;47:10398-10400.

259. Medina-Rodríguez S, Orriach-Fernández FJ, Poole C, et al. Copper(I) complexes as alternatives to iridium(III) complexes for highly efficient oxygen sensing. *Chem Commun*. 2015;51(57):11401-11404. doi:10.1039/C5CC04326C.

260. Koren K, Borisov SM, Saf R, Klimant I. Strongly Phosphorescent Iridium(III)-Porphyrins - New Oxygen Indicators with Tuneable Photophysical Properties and Functionalities. *Eur J Inorg Chem*. 2011;2011(10):1531-1534. doi:10.1002/ejic.201100089.

261. Koren K, Dmitriev RI, Borisov SM, Papkovsky DB. Complexes of Ir III -Octaethylporphyrin with Peptides as Probes for Sensing Cellular O 2. 2012:1184-1190. doi:10.1002/cbic.201200083.

262. Lomova TN, Mozhzhukhina EG. Synthesis, structure, and reactions of iridium(I) complexes with 5,10,15,20-tetraphenyl-21H,23H-porphine and 5,10,15,20-tetraphenyl-21H,23H-porphine dianion. *Russ J Inorg Chem*. 2012;57(2):197-204. doi:10.1134/S0036023612020155.

263. Kadish KM, Deng YJ, Yao CL, Anderson JE. Electrochemical and spectroelectrochemical studies of iridium tetraphenylphorphyrin complex ((TPP)[Ir(CO)3]2) in nonaqueous media. *Organometallics*. 1988;7(9):1979-1983. doi:10.1021/om00099a012.

264. Delgado-Lima A, Fonseca AM, Machado A V. Novel iridium-pentafluorophenyl porphyrin complex. *Mater Lett*. 2017;200(March):6-9. doi:10.1016/j.matlet.2017.03.177.

265. Kanemitsu H, Harada R, Ogo S. A water-soluble iridium(iii) porphyrin. *Chem Commun*. 2010;46(18):3083. doi:10.1039/c000263a.

266. Hambright P. ANION CATALYZED ACID SOLVOLYSIS OF INDIUM(III) PORPHYRINS. *J Coord Chem*. 1983;12(4):297-301. doi:10.1080/00958978308073861.

267. Nakai M, Maeda T, Mashima T, et al. Syntheses and photodynamic properties of glucopyranoside-conjugated indium(III) porphyrins as a bifunctional agent. *J Porphyr Phthalocyanines*. 2013;17(12):1173-1182. doi:10.1142/S1088424613500934.

268. Bedel-Cloutour CH, Mauclaire L, Saux A, Pereyre M. Syntheses of functionalized indium porphyrins for monoclonal antibody labeling. *Bioconjug Chem*. 1996;7(6):617-627. doi:10.1021/bc960045i.

269. Johnson J a, Zhang X, Reeson TC, Chen Y-S, Zhang J. Facile Control of the Charge Density and Photocatalytic Activity of an Anionic Indium Porphyrin Framework via in Situ Metalation. *J Am Chem Soc*. 2014;136(45):15881-15884. doi:10.1021/ja5092672.

270. Bhatti M, Bhatti W, Mast E. Preparation of indium (III) tetraphenylporphine complexes. *Inorg Nucl Chem Lett*. 1972;8(2):133-137.

271. Dammer SJ, Solntsev P V, Sabin JR, Nemykin VN. Synthesis, characterization, and electron-transfer processes in indium ferrocenyl-containing porphyrins and their fullerene adducts. *Inorg Chem*. 2013;52(16):9496-9510. doi:10.1021/ic401163y.

272. Bajju GD, Ahmed A, Gupta D, Kapahi A, Devi G. Synthesis and Spectroscopic Characterization of Some New Axially Ligated Indium (III) Macrocyclic Complexes and Their Biological Activities. 2014;2014.

273. Panda MK, Lazarides T, Charalambidis G, Nikolaou V, Coutsolelos AG. Five-Coordinate Indium(III) Porphyrins with Hydroxy and Carboxy BODIPY as Axial Ligands: Synthesis, Characterization and Photophysical Studies. *Eur J Inorg Chem*. 2015;2015(3):468-477. doi:10.1002/ejic.201402902.

274. Serpe L, Giuntini F. Sonodynamic antimicrobial chemotherapy: First steps towards a sound approach for microbe inactivation. *J Photochem Photobiol B Biol*. 2015;150:44-49. doi:10.1016/j.jphotobiol.2015.05.012.

275. Huang P, Qian X, Chen Y, et al. Metalloporphyrin-encapsulated biodegradable nanosystems for highly efficient magnetic resonance imaging-guided sonodynamic cancer therapy. *J Am Chem Soc*. 2017;139(3):1275-1284. doi:10.1021/jacs.6b11846.

276. Brazzale C, Canaparo R, Racca L, et al. Enhanced selective sonosensitizing efficacy of ultrasound-based anticancer treatment by targeted gold nanoparticles. *Nanomedicine (Lond)*. 2016;11(23):3056-3070. doi:10.2217/nnm-2016-0293.

277. You DG, Deepagan VG, Um W, et al. ROS-generating TiO2 nanoparticles for non-invasive sonodynamic therapy of cancer. *Sci Rep*. 2016;6(1):23200. doi:10.1038/srep23200.

278. Li Y, Zhou Q, Deng Z, et al. IR-780 Dye as a Sonosensitizer for Sonodynamic Therapy of Breast Tumor. *Sci Rep*. 2016;6(1):25968. doi:10.1038/srep25968.

279. Lentacker I, De Cock I, Deckers R, De Smedt SC, Moonen CTW. Understanding ultrasound induced sonoporation: Definitions and underlying mechanisms. *Adv Drug Deliv Rev*. 2014;72:49-64. doi:10.1016/j.addr.2013.11.008.

280. O'Brien WD. Ultrasound-biophysics mechanisms. *Prog Biophys Mol Biol*. 2007;93(1-3):212-255. doi:10.1016/j.pbiomolbio.2006.07.010.

281. Nyborg WL. Biological effects of ultrasound: Development of safety guidelines. Part II: General review. *Ultrasound Med Biol*. 2001;27(3):301-333. doi:10.1016/S0301-5629(00)00333-1.

282. ter Haar G. Heat and sound: focused ultrasound in the clinic. *Int J Hyperth*. 2015;31(3):223-224. doi:10.3109/02656736.2015.1014434.

283. McHale AP, Callan JF, Nomikou N, Fowley C, Callan B. Sonodynamic Therapy: Concept, Mechanism and Application to Cancer Treatment. *Adv Exp Med Biol*. 2016;880:429-450. doi:10.1007/978-3-319-22536-4_22.

284. Wan G-Y, Liu Y, Chen B-W, et al. Recent advances of sonodynamic therapy in cancer treatment. *Cancer Biol Med*. 2016;13(3):325-338. doi:10.20892/j.issn.2095-3941.2016.0068.

285. Leighton TG. What is ultrasound? *Prog Biophys Mol Biol*. 2007;93(1-3):3-83. doi:10.1016/j.pbiomolbio.2006.07.026.

286. Dezhkunov N V., Francescutto A, Ciuti P, Mason TJ, Iernetti G, Kulak AI. Enhancement of sonoluminescence emission from a multibubble cavitation zone. *Ultrason Sonochem*. 2000;7(1):19-24. doi:10.1016/S1350-4177(99)00023-1.

287. Dezhkunov N V., Francescutto A, Serpe L, Canaparo R, Cravotto G. Sonoluminescence and acoustic emission spectra at different stages of cavitation zone development. *Ultrason Sonochem*. 2016. doi:10.1016/j.ultsonch.2017.04.004.

288. McEwan C, Nesbitt H, Nicholas D, et al. Comparing the efficacy of photodynamic and sonodynamic therapy in non-melanoma and melanoma skin cancer. *Bioorganic Med Chem*. 2016;24(13):3023-3028. doi:10.1016/j.bmc.2016.05.015.

289. Pasternack RF, Gibbs EJ, Villafranca JJ, Villafranca JJ. Interactions of Porphyrins with Nucleic Acids. *Biochemistry*. 1983;22(23):5409-5417. doi:10.1021/bi00292a024.

290. Giuntini F, Dumoulin F, Daly R, et al. Orthogonally bifunctionalised polyacrylamide nanoparticles: a support for the assembly of multifunctional nanodevices. *Nanoscale*. 2012;4(6):2034-2045. doi:10.1039/c2nr11947a.

291. Sol V, Chaleix V, Granet R, Krausz P. An efficient route to dimeric porphyrin–RGD peptide conjugates via olefin metathesis. *Tetrahedron*. 2008;64(2):364-371. doi:10.1016/j.tet.2007.10.092.

292. Asayama S, Kawamura E, Nagaoka S, Kawakami H. Design of Manganese Porphyrin Modified with Mitochondrial Signal Peptide for a New Antioxidant. *Mol Pharm*. 2006;3(4):468-470. doi:10.1021/mp0500667.

293.   Rockwood DN, Preda RC, Yücel T, Wang X, Lovett ML, Kaplan DL. Materials fabrication from Bombyx mori silk fibroin. *Nat Protoc*. 2011;6(10):1612-1631. doi:10.1038/nprot.2011.379.

294.   Pillai MM, Gopinathan J, Indumathi B, et al. Silk-PVA Hybrid Nanofibrous Scaffolds for Enhanced Primary Human Meniscal Cell Proliferation. *J Membr Biol*. 2016;249(6):813-822. doi:10.1007/s00232-016-9932-z.

295.   Varkey A, Venugopal E, Sugumaran P, et al. Impact of silk fibroin-based scaffold structures on human osteoblast MG63 cell attachment and proliferation. *Int J Nanomedicine*. 2015;10:43-51. doi:10.2147/IJN.S82209.

296.   Vepari C, Kaplan DL. Silk as a biomaterial. *Prog Polym Sci*. 2007;32(8-9):991-1007. doi:10.1016/j.progpolymsci.2007.05.013.

297.   Altman GH, Diaz F, Jakuba C, et al. Silk-based biomaterials. *Biomaterials*. 2003;24(3):401-416. doi:10.1016/S0142-9612(02)00353-8.

298.   Omenetto FG, Kaplan DL. New Opportunities for an Ancient Material. *Science (80-)*. 2010;329(5991):528-531. doi:10.1126/science.1188936.

299.   Park SH, Gil ES, Shi H, Kim HJ, Lee K, Kaplan DL. Relationships between degradability of silk scaffolds and osteogenesis. *Biomaterials*. 2010;31(24):6162-6172. doi:10.1016/j.biomaterials.2010.04.028.

300.   Murphy AR, Kaplan DL. Biomedical applications of chemically-modified silk fibroin. *J Mater Chem*. 2009;19(36):6443. doi:10.1039/b905802h.

301.   Sugihara A, Sugiura K, Morita H, et al. Promotive effects of a silk film on epidermal recovery from full-thickness skin wounds. *Proc Soc Exp Biol Med*. 2000;225(1):58-64.

302.   Hu K, Lv Q, Cui FZ, et al. Biocompatible Fibroin Blended Films with Recombinant Human-like Collagen for Hepatic Tissue Engineering. *J Bioact Compat Polym*. 2006;21(1):23-37. doi:10.1177/0883911506060455.

303.   Sofia S, McCarthy MB, Gronowicz G, Kaplan DL. Functionalized silk-based biomaterials for bone formation. *J Biomed Mater Res*. 2001;54(1):139-148.

304.   Motta A, Migliaresi C, Faccioni F, Torricelli P, Fini M, Giardino R. Fibroin hydrogels for biomedical applications: preparation, characterization and in vitro cell culture studies. *J Biomater Sci Polym Ed*. 2004;15(7):851-864.

305.   Aoki H, Tomita N, Morita Y, et al. Culture of chondrocytes in fibroin-hydrogel sponge. *Biomed Mater Eng*. 2003;13(4):309-316.

306.   Chen J, Altman GH, Karageorgiou V, et al. Human bone marrow stromal cell and ligament fibroblast responses on RGD-modified silk fibers. *J Biomed Mater Res A*. 2003;67(2):559-570. doi:10.1002/jbm.a.10120.

307.   Kardestuncer T, McCarthy MB, Karageorgiou V, Kaplan D, Gronowicz G. RGD-tethered silk substrate stimulates the differentiation of human tendon cells. *Clin Orthop Relat Res*. 2006;448:234-239. doi:10.1097/01.blo.0000205879.50834.fe.

308.   Dal Pra I, Freddi G, Minic J, Chiarini A, Armato U. De novo engineering of reticular connective tissue in vivo by silk fibroin nonwoven materials. *Biomaterials*. 2005;26(14):1987-1999. doi:10.1016/j.biomaterials.2004.06.036.

309.   Unger RE, Peters K, Wolf M, Motta A, Migliaresi C, Kirkpatrick CJ. Endothelialization of a non-woven silk fibroin net for use in tissue engineering: growth and gene regulation of human endothelial cells. *Biomaterials*. 2004;25(21):5137-5146. doi:10.1016/j.biomaterials.2003.12.040.

310.   Wang X, Yucel T, Lu Q, Hu X, Kaplan DL. Silk nanospheres and microspheres from silk/pva blend films for drug delivery. *Biomaterials*. 2010;31(6):1025-1035. doi:10.1016/j.biomaterials.2009.11.002.

311.   Wang X, Wenk E, Matsumoto A, Meinel L, Li C, Kaplan DL. Silk microspheres for encapsulation and controlled release. *J Control Release*. 2007;117(3):360-370. doi:10.1016/j.jconrel.2006.11.021.

312.   Sionkowska A, Skrzyński S, Śmiechowski K, Kołodziejczak A. The review of versatile application of collagen. *Polym Adv Technol*. 2017;28(1):4-9. doi:10.1002/pat.3842.

313.   Parenteau-Bareil R, Gauvin R, Berthod F. Collagen-Based Biomaterials for Tissue Engineering Applications. *Materials (Basel)*. 2010;3(3):1863-1887. doi:10.3390/ma3031863.

314.   http://www.harbormedtech.com/bridge.

315.   Electrophysiological characterization of embryonic hippocampal neurons cultured in a 3D collagen hydrogel. *Biomaterials*. 2009;30(26):4377-4383. doi:10.1016/J.BIOMATERIALS.2009.04.047.

316. Gingras M, Beaulieu M-M, Gagnon V, Durham HD, Berthod F. In vitro study of axonal migration and myelination of motor neurons in a three-dimensional tissue-engineered model. *Glia*. 2008;56(3):354-364. doi:10.1002/glia.20617.

317. Sabeh F, Shimizu-Hirota R, Weiss SJ. Protease-dependent versus -independent cancer cell invasion programs: three-dimensional amoeboid movement revisited. *J Cell Biol*. 2009;185(1):11-19. doi:10.1083/jcb.200807195.

318. Che ZM, Jung TH, Choi JH, et al. Collagen-based co-culture for invasive study on cancer cells-fibroblasts interaction. *Biochem Biophys Res Commun*. 2006;346(1):268-275. doi:10.1016/j.bbrc.2006.05.111.

319. Shanmugasundaram N, Ravichandran P, Reddy PN, Ramamurty N, Pal S, Rao KP. Collagen-chitosan polymeric scaffolds for the in vitro culture of human epidermoid carcinoma cells. *Biomaterials*. 2001;22(14):1943-1951.

320. Peptide- and collagen-based hydrogel substrates for in vitro culture of chick cochleae. *Biomaterials*. 2008;29(8):1028-1042. doi:10.1016/J.BIOMATERIALS.2007.11.006.

321. Harley BA, Lynn AK, Wissner-Gross Z, Bonfield W, Yannas I V, Gibson LJ. Design of a multiphase osteochondral scaffold. II. Fabrication of a mineralized collagen–glycosaminoglycan scaffold. *J Biomed Mater Res Part A*. 2010;92A(3):1066-1077. doi:10.1002/jbm.a.32361.

322. Tebb TA, Tsai S-W, Glattauer V, White JF, Ramshaw JAM, Werkmeister JA. Development of porous collagen beads for chondrocyte culture. *Cytotechnology*. 2006;52(2):99-106. doi:10.1007/s10616-006-9034-3.

323. Tedder ME, Liao J, Weed B, et al. Stabilized Collagen Scaffolds for Heart Valve Tissue Engineering. *Tissue Eng Part A*. 2008;15(6):1257-1268. doi:10.1089/ten.tea.2008.0263.

324. Yannas I V, Burke JF, Orgill DP, Skrabut EM. Wound tissue can utilize a polymeric template to synthesize a functional extension of skin. *Science*. 1982;215(4529):174-176.

325. Adhirajan N, Shanmugasundaram N, Shanmuganathan S, Babu M. Functionally modified gelatin microspheres impregnated collagen scaffold as novel wound dressing to attenuate the proteases and bacterial growth. *Eur J Pharm Sci*. 2009;36(2-3):235-245. doi:10.1016/j.ejps.2008.09.010.

326. Adhirajan N, Shanmugasundaram N, Shanmuganathan S, Babu M. Collagen-based wound dressing for doxycycline delivery: in-vivo evaluation in an infected excisional wound model in rats. *J Pharm Pharmacol*. 2009;61(12):1617-1623. doi:10.1211/jpp/61.12.0005.

327. Gurney TA, Kim DW. Applications of Porcine Dermal Collagen (ENDURAGen) in Facial Plastic Surgery. *Facial Plast Surg Clin*. 2017;15(1):113-121. doi:10.1016/j.fsc.2006.10.007.

328. Oliveira SM, Ringshia RA, Legeros RZ, et al. An improved collagen scaffold for skeletal regeneration. *J Biomed Mater Res - Part A*. 2010;94(2):371-379. doi:10.1002/jbm.a.32694.

329. Wong JPF, MacRobert AJ, Cheema U, Brown RA. Mechanical anisotropy in compressed collagen produced by localised photodynamic cross-linking. *J Mech Behav Biomed Mater*. 2013;18:132-139. doi:10.1016/j.jmbbm.2012.11.002.

330. Vashist SK. Comparison of 1-Ethyl-3-(3-Dimethylaminopropyl) Carbodiimide Based Strategies to Crosslink Antibodies on Amine-Functionalized Platforms for Immunodiagnostic Applications. *Diagnostics*. 2012;2(4):23-33. doi:10.3390/diagnostics2030023.

331. Amsden B. Solute Diffusion within Hydrogels. Mechanisms and Models. *Macromolecules*. 1998;31(23):8382-8395. doi:10.1021/ma980765f.

332. Lo D, Parris JE, Lawless JL. Laser and Fluorescence Properties of Dye-Doped Sol-Gel Silica from 40 nm to 800 nm. *Appl Phys B*. 1993;56:385-390.

333. ZIMMERMANN N, FREUND S, FREDENHAGEN A, JUNG G. Solution structures of the lantibiotics duramycin B and C. *Eur J Biochem*. 1993;216(2):419-428. doi:10.1111/j.1432-1033.1993.tb18159.x.

334. Hayashi F, Nagashima K, Terui Y, Kawamura Y, Matsumoto K, Itazaki H. The structure of PA48009: the revised structure of duramycin. *J Antibiot (Tokyo)*. 1990;43(11):1421-1430. doi:10.7164/antibiotics.43.1421.

335. Stafford JH, Thorpe PE. Increased Exposure of Phosphatidylethanolamine on the Surface of Tumor Vascular Endothelium. *Neoplasia*. 2011;13(4):299-IN2. doi:10.1593/neo.101366.

336. Zhao M. Lantibiotics as probes for phosphatidylethanolamine. *Amino Acids*. 2011;41(5):1071-1079. doi:10.1007/s00726-009-0386-9.

337. Aoki Y, Uenaka T, Aoki J, Umeda M, Inoue K. A Novel Peptide Probe for Studying the Transbilayer Movement of

Phosphatidylethanolamine. *J Biochem*. 1994;116(2):291-297. http://dx.doi.org/10.1093/oxfordjournals.jbchem.a124522.

338.   Broughton LJ, Giuntini F, Savoie H, et al. Duramycin-porphyrin conjugates for targeting of tumour cells using photodynamic therapy. *J Photochem Photobiol B Biol*. 2016;163:374-384. doi:10.1016/j.jphotobiol.2016.09.001.

339.   Goodwin J, Whitten C. Chelation of ferrous sulphate solutions by desferrioxamine B. *Nature*. 1965;205(4968):281-283. doi:10.1038/205281b0.

340.   Birus M, Gabricevic M, Kronja O, Klaic B. 13C and 1H NMR Line Broadening in Desferrioxamine B Spectra. Kinetics and Mechanism of Siderophore Chemistry. *Inorg Chem*. 1995;34(20):3110-3113. http://pubs.acs.org/doi/pdf/10.1021/ic00115a047.

341.   Edwards DC, Nielsen SB, Jarzecki AA, Spiro TG, Myneni SCB. Experimental and theoretical vibrational spectroscopy studies of acetohydroxamic acid and desferrioxamine B in aqueous solution: Effects of pH and iron complexation. *Geochim Cosmochim Acta*. 2005;69(13):3237-3248. doi:10.1016/j.gca.2005.01.030.

342.   D'Souza F, Krishnan V. Singlet quenching of tetraphenyiporphyrin and its metal derivatives by iron (III) coordination compounds. *Chem Sci*. 1990;102(2):131-146.